High Efficiency Low Cost CO2 Compression Using Supersonic Shock Wave Technology

May 10, 2006 through December 31, 2010

Principle Author: Joe Williams

Report Issued March 2011
DOE Award Number: DE-FC26-06NT42651

Document Number 0800-00220

Submitted by:

Ramgen Power Systems, Inc.
11808 Northup Way, Suite W190
Bellevue, WA 98005
(425) 828-4919

Disclaimer

ABSTRACT

Development and testing results from a supersonic compressor are presented. The compressor achieved record pressure ratio for a fully-supersonic stage and successfully demonstrated the technology potential.

Several tasks were performed in compliance with the DOE award objectives. A high-pressure ratio compressor was retrofitted to improve rotordynamics behavior and successfully tested. An outside review panel confirmed test results and design approach. A computational fluid dynamics code used to analyze the Ramgen supersonic flowpath was extensively and successfully modified to improve use on high-performance computing platforms. A comprehensive R&D implementation plan was developed and used to lay the groundwork for a future full-scale compressor demonstration. Conceptual design for a CO2 demonstration compressor was developed and reviewed.

TABLE OF CONTENTS

Chapter 1

Executive Summary

This report summarizes the results of Ramgen technology development efforts on this contract from 15 May 2006 through 31 December 2010.

Baseline Rampressor (Ram-2) Development

Through an extensive verification procedure, Ramgen demonstrated that its CFD tool was capable of modeling Rampressor flow physics. Verification cases included boundary layer development, separation due to adverse pressure gradients, centrifugal compressor flows, and shock wave/boundary layer interactions. CFD simulations of the inlet flow were found to be in agreement with experiment. Simulations of the rotor flow predicted a total pressure ratio of up to approximately 8.55:1 for a tip gap of 0.001 inch and of approximately 5.81:1 for a tip gap of 0.003 inches. These simulations were found to be in good agreement with test results.

During the test program, Ramgen measured the performance of the annulus-shaped inlet and found the total pressure loss to be approximately 0.5%. IGV losses were also measured and found to be in good agreement with the CFD simulations. During starting tests the rotor was found to start at approximately 100% speed provided that full bleed was available. Performance testing demonstrated a rotor total pressure ratio of 7.8:1 which was in agreement with CFD simulations. A higher pressure ratio is achievable with further development of the supersonic flow path. Testing showed that the Rampressor concept is capable of achieving high total pressure ratios across the rotor.

The Rampressor-2 test program has proven that high total pressure ratio, single stage, supersonic compression is viable, that Ramgen's tools accurately predict test performance, and lay the groundwork for further development and commercial demonstration. During the test program Ramgen achieved a rotor only total pressure ratio of 7.8:1 which is a substantial improvement over the previous Rampressor test program which obtained a total pressure ratio of 2.3:1. Ramgen's commercial targets are a total pressure ratio of 10:1 and a stage efficiency of approximately 85%. More work is required prior to commercial introduction of a Rampressor product, but Ramgen is confident the commercial targets are achievable.

Critical Risk Factor Risk Reduction

Key risk factors, learned during Rampressor-2 testing, have been identified and tracked to manage overall project technical risk. Aerodynamic optimization continues to be a key indicator of technical progress and measure of design success. Tip leakage has been removed as a key risk by adoption of an integral rotor shroud, which eliminates leakage between the flow paths. Rotor mechanical design has made substantial progress and is now evaluated simultaneously with new aero designs to ensure aero design choices can be supported with feasible mechanical configurations. Thrust load has been substantially reduced by selection of a back-to-back or 'double flow' rotor configuration. Aerodynamic starting requirements have been considerably reduced by the new rotor configuration, thus reducing the machine's overall cost and complexity.

A key risk reduction milestone occurred when DOE granted Ramgen a significant amount of CPU time on the Oak Ridge Leadership Computing Facility and a collaboration opportunity with the facility staff. Since that time, Ramgen, Numeca and Oak Ridge have continuously improved performance of our computational fluid dynamics codes to take advantage of the significant resources available. Latest improvements in the parallel code make it now practical for Ramgen to run simulations distributed over more than 1000 CPU cores, providing a major improvement in technology development speed.

Design Reviews

At the conclusion of the risk assessment effort and in light of the Rampressor-2 test results, NETL gathered a qualified team of impartial experts from academia, industry and government to review the technology's current state and the development approach moving forward. The team approved Ramgen's approach and recommended the program proceed into the CO2 compressor demonstration phase.

R&D Implementation Plan

In conjunction with DOE/NETL and industry (Dresser-Rand), Ramgen created a comprehensive plan to demonstrate a full-scale CO2 compressor using Ramgen technology. This plan took the form of a Phase 2 proposal to the DOE which was subsequently awarded and is currently under way. Dresser-Rand has made a significant investment in the program to enable rapid commercialization.

CO2 Compressor Design

After receiving DOE authorization to proceed, Ramgen began design of the CO2 demonstration compressor. Over the course of several months, conceptual designs were created and reviewed to ensure all systems and components had achieved an acceptable level of definition, that open issues had been identified, and that program cost and schedule were on track. Compressor design was subsequently completed under the Phase 2 contract.

Chapter 2

Baseline Rampressor (Ram-2) Development

2.1 Rampressor-2 Report (Task 1.1)

Rampressor-2 testing was successfully completed and documented in a report previously supplied to the DOE. This report was prepared as a standalone document and is included in its entirety as an Appendix to this chapter. Only the page numbers have been changed in the report to reflect its location within this Final Technical Report document – the report begins on page 2A-2.

2.2 Critical Risk Factor Risk Reduction (Task 1.2)

To manage the project technical risk, key risk factors from Rampressor-2 experience have been identified and tracked through development. These factors are typically unique to or at least exaggerated by the fully-supersonic nature of the Rampressor. Each factor needs to be mastered in order to achieve the full technology potential. Factors are listed with a short explanation – substantially more information was developed during the CO2 demonstration compressor preliminary design phase (beyond scope of this contract) and will be reported later.

Substantial progress has been achieved in these risk areas as shown in the DOE design review results later in this chapter.

Aerodynamic Optimization

This is the core of Ramgen's technology and capability. A significant fraction of the company is deployed to improve aerodynamic performance, evaluate new design approaches and optimize efficiency. Ramgen has developed a promising rotor configuration that can achieve the commercial 10:1 pressure ratio performance targets with reduced risk. Some configurations could achieve greater than 10:1 with the same level of technical challenge as originally assumed.

Tip Leakage Mitigation

A major breakthrough in the reduction of this technical risk has been made with the incorporation of a shrouded rotor, which would eliminate the tip leakage aerodynamic and mechanical issue. While a rotating shroud increases boundary layer blockage in the flow path, the trade is heavily in its favor compared to the impact of tip leakage and need to hold very tight tip clearances.

Rotor Mechanical Design Optimization

Significant progress has been achieved with rotor configurations which reduce mechanical stress and enable aero-optimized shapes. The shrouded rotor design is being explored as part of the rotor design optimization. In addition, a configuration that results in lower structural stress as well as reduced parasitic losses has been identified and explored.

Diffusion Loss

We continue to explore refinements in the diffuser design that achieve our performance targets. A significant reduction in the aerodynamics risk has been achieved with the updated rotor configuration and performances estimates and improvements are being made with further design and analyses development.

Thrust Load Mitigation

A back-to-back rotor design has been selected, eliminating this risk with its inherently balanced thrust. This design has being evaluated from the perspectives including rotordynamics, bearing design, manufacturing and structural considerations and has passed all design acceptance criteria.

Aerodynamic Starting

The rotor configuration being considered now has reduced supersonic inlet starting requirements than previous designs. By reducing the starting bleed mass flow requirement, this approach enables substantial knock-on design and cost savings throughout the machine's static structure.

Parasitic Losses

The back-to-back rotor design dramatically reduced the overall parasitic losses and has been selected for future CO2 demonstrator compressor design. Advanced seal configurations have been developed to further reduce losses.

Risk Assessment

At the conclusion of the risk assessment effort, Ramgen worked with industry and the NETL to develop a new work effort to address the risks, successfully demonstrate Ramgen compressor technology in CO2 and enable rapid commercialization of the technology. The resulting contract proposal is contained in a later chapter of this report as documentation of that effort.

Aerodynamic Analysis Tool Development for Use on Supercomputers

This report has been prepared as a standalone document and is included in its entirety as an Appendix to this chapter. Only the page numbers have been changed in the report to reflect its location within this Final Technical Report document – the report begins on page 2A-117.

2.3 Design Review (Task 1.3)

On 10 July 2007, NETL gathered a qualified team of impartial experts from academia, industry and government to review the results from Rampressor-2 testing and the technology development approach moving forward. The design review board included:

- Bill Day (chair, ex-GE and Pratt & Whitney)
- Walt Smith (ex-Pratt & Whitney)
- Ravi Ravindranath (Naval Air Systems Command – NAVAIR)
- Dr. Cengiz Camci (Aero Professor, Penn State)
- Dr. Greg Bloch (AFRL)

Ramgen had initially provided briefing materials for the team's review. After reviewing the material, the team prepared a list of questions and desired information for the on-site review. Following the all-day meeting at Ramgen, the team's questions, conclusions and recommendations were compiled and forwarded to NETL. The team approved of Ramgen's approach and recommended the program proceed into the CO2 compressor demonstration phase. The team's report is attached as an Appendix to this chapter, beginning on page 2A-123.

CHAPTER 2 APPENDIX

Rampressor-2 Report

Aerodynamic Analysis Tool Development for Use on Supercomputers

Design Review

CO_2 Compression Using Supersonic Shock Wave Technology

Scientific/Technical Report

Reporting Period Start Date: May 10, 2006
Reporting Period End Date: May 2, 2007

Principle Authors: Michael J. Aarnio
Allan D. Grosvenor
David A. Taylor
Joseph T. Williams

Report Issue Date: November 9, 2007
DOE Award Number: DE-FC26-06NT42651

Ramgen Document Number 0800-00162

Submitted by:

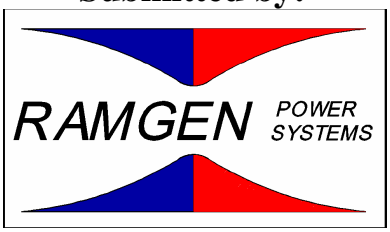

Ramgen Power Systems, Inc.
11808 Northup Way, Suite W190
Bellevue, WA 98005
(425) 828-4919

Disclaimer

This report was prepared as an account of work sponsored by an agency of the United States government. Neither the United States Government nor any agency thereof, nor any of their employees, makes any warranty, express or implied, or assumes any legal liability or responsibility for the accuracy, completeness, or usefulness of any information, apparatus, product, or process disclosed, or represents that its use would not infringe privately owned rights. Reference herein to any specific commercial product, process, or service by trade name, trademark, manufacturer, or otherwise does not necessarily constitute or imply its endorsement, recommendation, or favoring by the United Stated Government or any agency thereof. The view and opinions of authors expressed herein do not necessarily state or reflect those of the United States Government or any agency thereof.

Abstract

Computational performance analyses and experimental performance measurements of a novel supersonic high pressure ratio compressor, the Rampressor, are presented. The performance of the Rampressor was estimated by three-dimensional, viscous, computational fluid dynamics (CFD) simulations. Validation of the CFD scheme was conducted on documented test cases which have similar fluid mechanic physics including boundary layer flow, annular separating diffuser flow, on and off-design centrifugal compressor flows, and shock wave/boundary layer interaction flow. The total pressure and total temperature were measured downstream of the Rampressor rotor using a Kiel probe which was aligned to the flow using nulling ports. The total pressure at the exit of the rotor was estimated by calculating the loss in total pressure between the two locations using three different methods. Compressor speed lines were generated at different rotor speeds and with different tip gaps. The Rampressor tested generated a total pressure ratio of approximately 7.8:1 which was in agreement with CFD analysis.

Table of Contents

List of Figures

List of Tables

Executive Summary

Through an extensive verification procedure, Ramgen demonstrated that its CFD tool was capable of modeling Rampressor flow physics. Verification cases included boundary layer development, separation due to adverse pressure gradients, centrifugal compressor flows, and shock wave/boundary layer interactions. CFD simulations of the flow inlet flow were found to be in agreement with experiment. Simulations of the rotor flow predicted a total pressure ratio of up to approximately 8.55:1 for a tip gap of 0.001 inch and of approximately 5.81:1 for a tip gap of 0.003 inches. These simulations were found to be in good agreement with test results showing that Ramgen has a solid design tool capability.

During the test program, Ramgen measured the performance of the annulus-shaped inlet and found the total pressure loss to be approximately 0.5%. IGV losses were also measured and found to be in good agreement with the CFD simulations. During starting tests the rotor was found to start at approximately 100% speed provided that full bleed was available. Performance testing demonstrated a rotor total pressure ratio of 7.8:1 which was in agreement with CFD simulations. A higher pressure ratio is achievable with further development of the supersonic flow path. Testing showed that the Rampressor concept is capable of achieving high total pressure ratios across the rotor.

The Rampressor-2 test program has proven that high total pressure ratio, single stage, supersonic compression is viable, that Ramgen's tools accurately predict test performance, and lay the groundwork for further development and commercial demonstration. During the test program Ramgen achieved a rotor only total pressure ratio of 7.8:1 which is a substantial improvement over the previous Rampressor test program which obtained a total pressure ratio of 2.3:1. Ramgen's commercial targets are a total pressure ratio of 10:1 and a stage efficiency of approximately 85%. More work is required prior to commercial introduction of a Rampressor product, but since the technology is young and Ramgen has made rapid leaps in progress and performance, Ramgen is confident the commercial targets are achievable.

Chapter 1

Ramgen Compression Technology

Since the sound barrier was broken in the late 1940's, jet and ramjet engines with supersonic inlets have been widely used as a means to propel aerospace vehicles at supersonic speeds. The technology is very well understood and fully characterized.

At supersonic velocities, air is ingested into the engine and flows around a fixed obstructing body in the center of the engine duct, "ramming" the air flow into channels between the center-body and the engine's sidewall. Inside these channels, the airflow is almost instantaneously slowed to subsonic speeds, creating "shock waves". These shock waves are associated with a dramatic increase in pressure, or, in other words, "shock compression."

One well known application of shock compression is its use in the engine inlet of the F-15 fighter jet. Figure 1-1 shows how a supersonic shock compression inlet acts to boost the inlet pressure, while at the same time reducing the air flow to the subsonic velocity required by its engine.

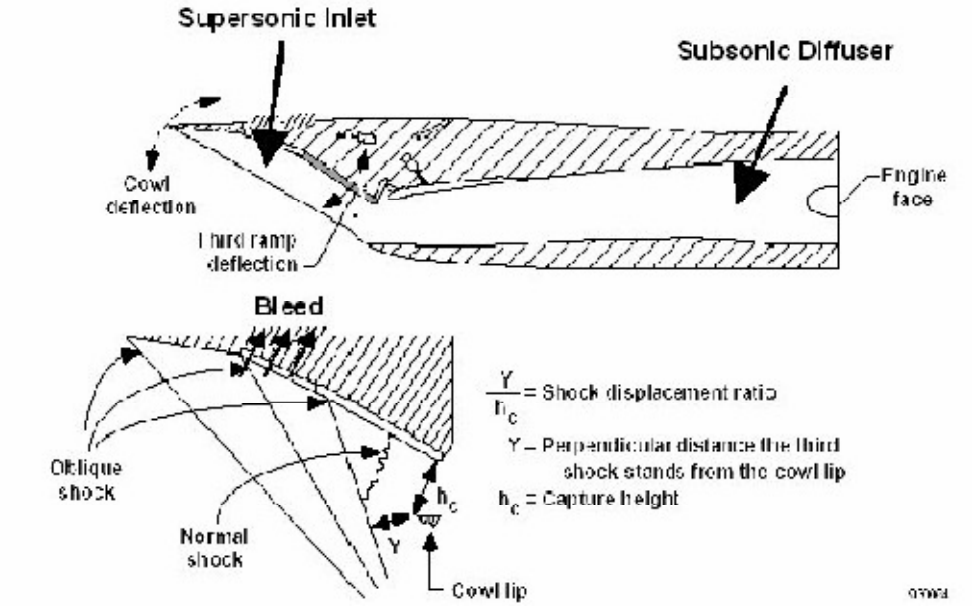

Figure 1-1: F-15 supersonic inlet cross section detail.

Supersonic Compression Process

Ramgen's core compressor design, the Rampressor, is a relatively simple device. It features a disk rotating at the high peripheral speeds necessary to achieve relative supersonic speeds. The rim of the disk has several raised sections and cavities that mimic the ramps in supersonic flight inlets, see Figure 1-2. Air or gas enters through a common duct and is then ingested into the annular space between the supersonically spinning disk and the wall of the stationary casing. When the gas flows into this space, the rim profile creates oblique and normal shocks and therefore compression in a manner completely analogous to supersonic flight inlet systems. The compression process efficiency is very high due to careful design of the oblique and normal shock location and strength, and because the compressor has very few aerodynamic leading edges and minimal drag.

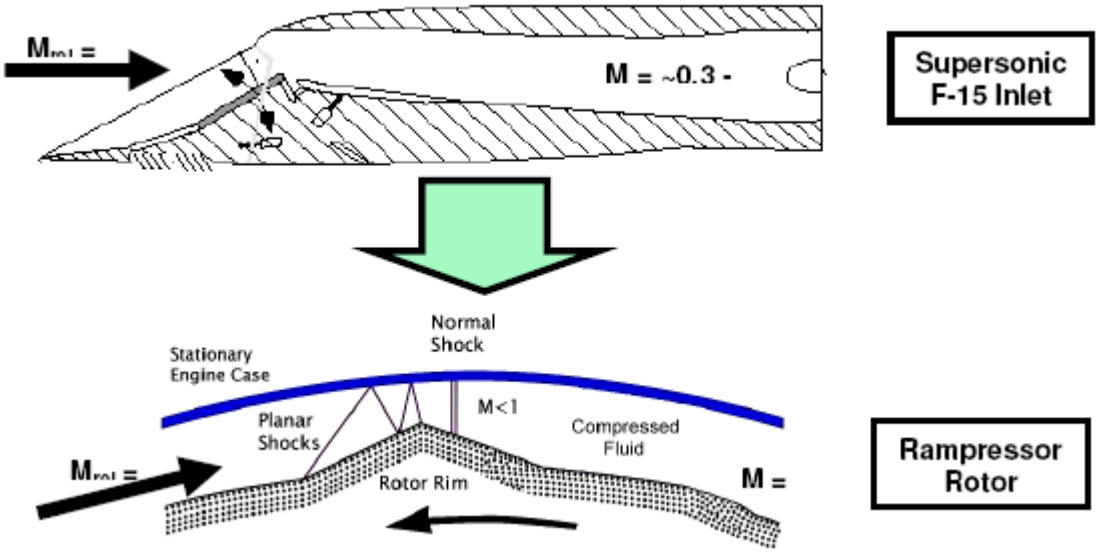

Figure 1-2: Ramgen rotor profile and its relationship to a supersonic flight inlet.

Rampressor Disk

The shock compression flow paths are separated by angled "strakes," as shown in Figure 1-3, to prevent leakage from the high-pressure discharge back into the rotor inlet. Discharge is collected and distributed to an intercooler, aftercooler, or directly to the process depending on the application. The compression process does not use oil for sealing and is thus inherently oil-free.

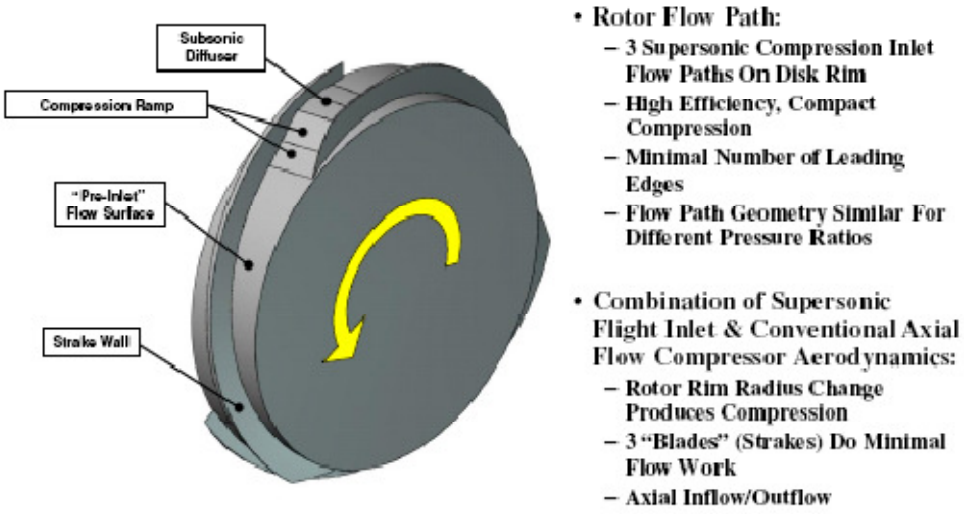

Figure 1-3: Ramgen compressor rotor disk.

Shock waves begin to form at the speed of sound (Mach 1). As speed increases beyond Mach 1 into the supersonic regime, greater compression can be achieved by the shock system. The speed of sound varies depending on the working fluid; a heavier gas will have a lower speed of sound, whereas a lighter gas will have a higher sonic velocity. The pressure ratio achieved by a shock system is therefore dependent on the disk speed in combination with the particular gas and its properties. Ramgen's competitive advantage stems directly from this natural phenomenon.

Designers of conventional compressors limit the flow Mach number to approximately 0.9 to avoid creating shock waves in the flow path – shocks in conventional compressors can produce flow blockages and decrease performance. This is accomplished by adjusting the rotor speed so that the inlet blade tips travel slower than the working fluid's speed of sound. The sonic velocity of a gas is a function of its molecular weight. CO_2 is a relatively heavy gas with a molecular weight of 44 versus air at 28, so traditional compressors must reduce rotational speed and increase size compared to air, with a resulting significant increase in capital cost.

Conversely, Ramgen's compression technology is ideally suited to compressing heavier gases. Heavier gases result in a higher Mach number at the same rotor speed, resulting in a higher pressure ratio. Alternately, the same pressure ratio can be achieved with lower rotor speed – significantly reducing cost and complexity. There is no need to increase size as conventional compressors must. This represents a significant competitive advantage for the Company, particularly as applied to CO_2 compression where the gas is relatively heavy and the design pressure ratio is very high. Reduced to practice, Ramgen's compression technology would allow for a reduction in the number and size of compressor stages, greatly simplifying the design and reducing its cost versus the competition. This benefit is achieved without sacrificing efficiency.

Ramgen Compression Technology Opportunities

There are a substantial number of applications requiring high compression ratio, either dictated by the application or as the result of a de-staging initiative. These include industrial air compressors, gas compressors, turbochargers, and gas turbines of all sizes and designs. Ramgen

compression technology holds unique promise for an economically viable way to compress CO_2 for sequestration at a time when climate change and world security issues have created a critical need for exactly such a technology. Developing a commercial product which can compress CO_2 at a significantly reduced cost is essential to meeting DOE goals for its FutureGen program and for the initiatives to target CO_2 emissions of coal which are gaining momentum around the world.

Chapter 2

Rampressor-2 Mechanical

2.1 Background

Under a previous DOE contract Ramgen designed and constructed a high pressure ratio air compressor termed Rampressor-2 (the second Rampressor test rig constructed by Ramgen). Testing of the inlet guide vanes (IGV) was also conducted under that contract. The details of the design and the results of the IGV tests are detailed in a report by Williams (2007). Testing was conducted at Boeing's Nozzle Test Facility located in Seattle, Washington.

2.2 Failure Analysis and Modification

On February 15, 2006 on the first attempt to reach 20,000 rpm, the rig experienced sudden-onset massive vibration. Despite operator efforts to reduce speed, the turbine controller maintained speed at about 18,000 rpm for approximately 15 seconds. At this point the operator initiated an emergency shutdown. Review of test data indicated the flex coupler failed catastrophically at about the same moment the emergency shutdown was commanded. With the shaft orbiting against static structure, rotating hardware came to a stop less than three seconds later.

The turbine shaft was visibly bent to about 20° from axial. After extensive photography of the failure, the turbine was dismounted and shipped to the OEM for assessment and repair. Upon disassembly, it was found that internal damage was surprisingly light. Although the shaft had to be cut off to remove the turbine wheel, few other components needed replacement. The turbine wheel had touched the diffuser during the vibration event and increased the clearance between the wheel and shroud. The OEM estimated a 6% loss in power from the original rating, which would not be a problem for the expected Rampressor-2 requirements. A new shaft, replacement shaft seals and bearings were the only parts replaced before the turbine was reassembled and shipped back to Ramgen.

2.2.1 Root Cause Investigation

Discussions with a panel of different experts failed to identify a 'smoking gun' root cause for the failure, although a lengthy list of possible candidates was generated. Review of the original DyRoBeS rotordynamics model (provided by the turbine OEM) did not immediately uncover obvious problems. With no firm root cause, and under the guidance of a widely-known turbomachinery design firm, Ramgen began to implement a wide range of fixes, changes, analyses, and tests in an attempt to 'shotgun' solutions to whatever caused the failure.

2.2.2 Fixes and Changes Implemented

Flex Coupling Replaced with Quillshaft

The flex coupling was an obvious focus, considering it was the most obvious failure. A splined quillshaft replacement for the John Crane flex coupling was designed. The principal benefit of this change was a reduction in weight from the John Crane coupling's 7.3 kg (16 lbs) to approximately 2.7 kg (6 lbs). Figure 2-1 shows the DyRoBeS model with the replacement shaft.

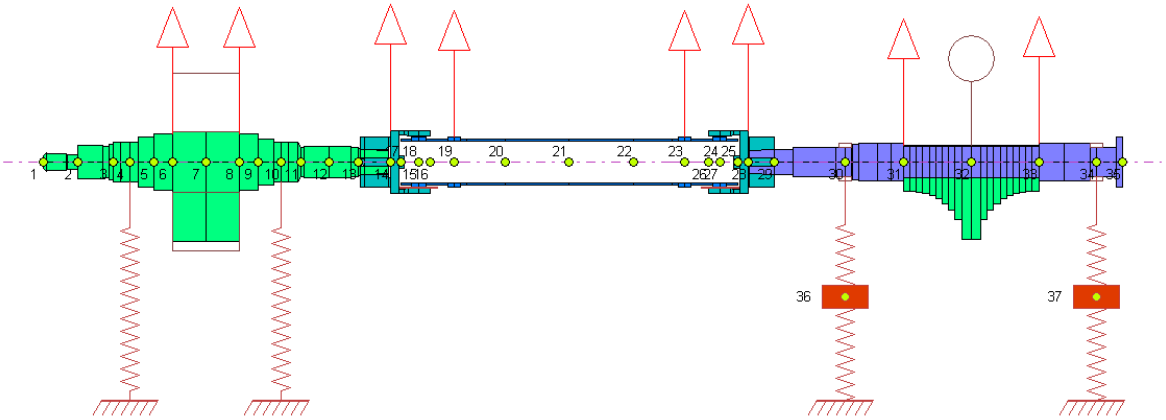

Figure 2-1: DyRoBeS model with the replacement quillshaft.

Rig Stiffness Enhancement

In the absence of a definitive root cause, it was speculated that the static structure might have contributed to the vibration and failure. Finite element analysis of the structure did not indicate a resonant frequency in the vicinity of 18,000 cycles per minute that could have coupled with the shaft rotation and caused the vibration, but did uncover a directional stiffness mismatch. The forward end Rampressor support frame could move left and right more easily than it could up and down. Although no clear path to failure was shown, expert advice indicated that good design practice would have these two stiffness values closer together. Ramgen designed and installed a stiffener which tied the forward end frame more securely and directly to the support skid, as shown in Figure 2-2 and Figure 2-3.

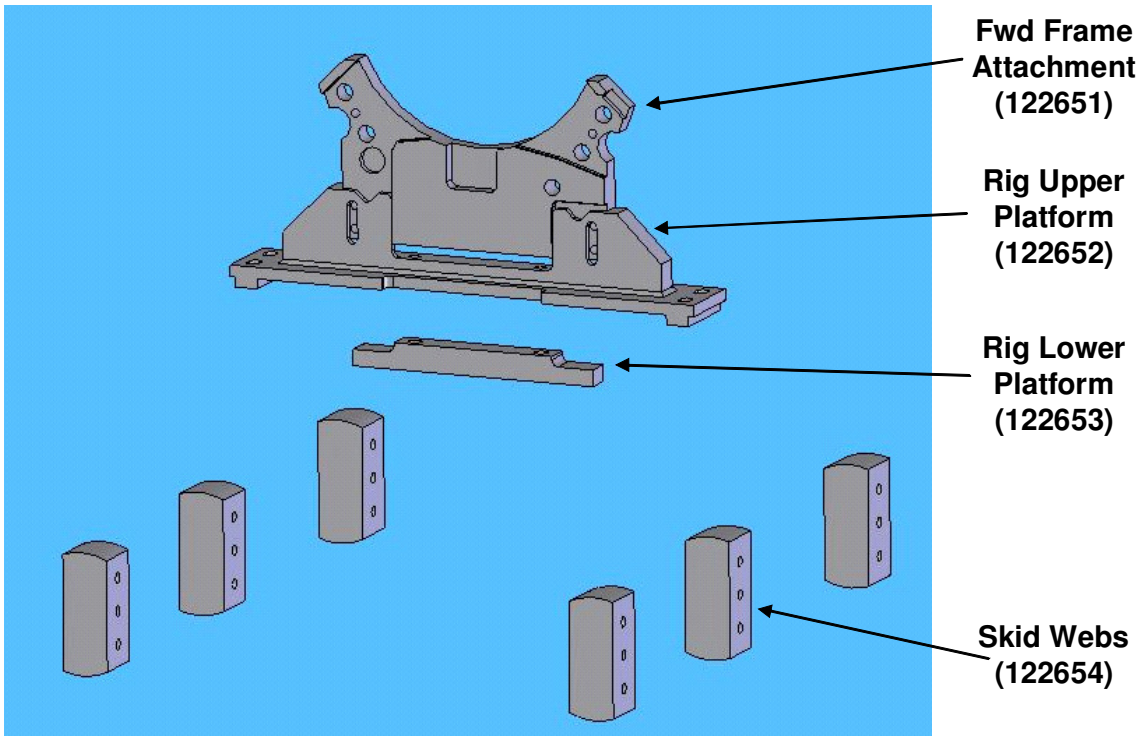

Figure 2-2: Forward end frame stiffness enhancement components.

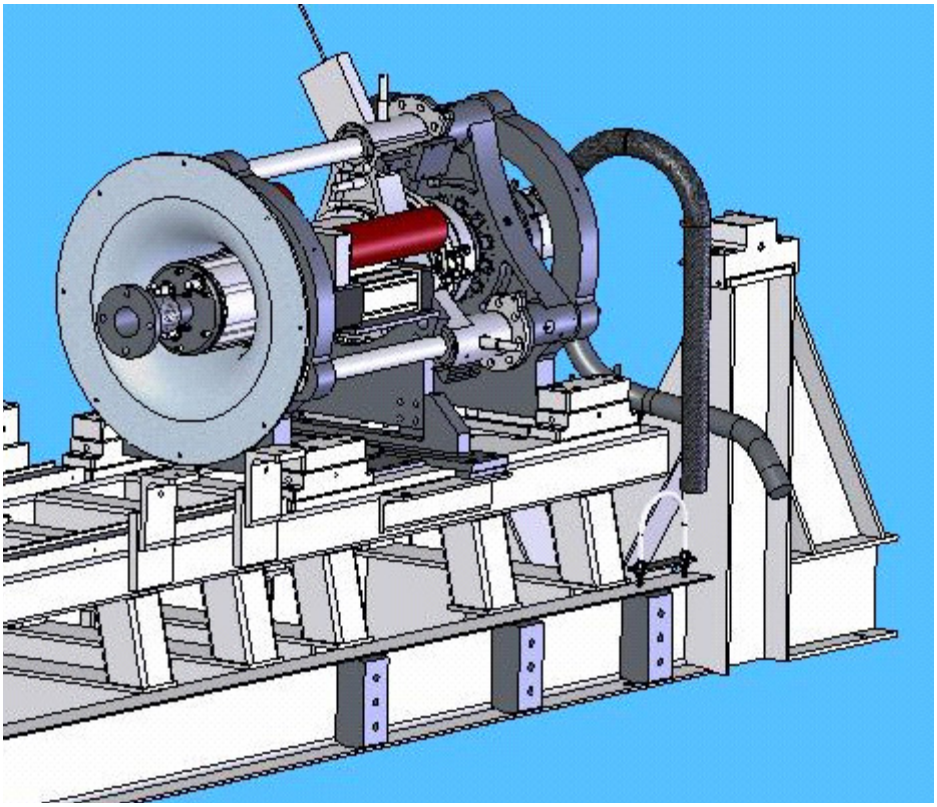

Figure 2-3: Forward end frame stiffness enhancement components as installed.

Ping Test

In addition to extensive finite element analysis of the structure, a physical 'ping' test of the static structure was undertaken. By attaching accelerometers to the structure in strategic locations and impulsively loading the structure with a hammer, a ping test provides actual dynamic response to vibration which is difficult or impossible to accurately model.

Ramgen contracted with a vibration measurement expert to perform an extensive ping test in preparation for the June 2006 test. Data were taken with and without the rig stiffener installed to measure the difference. Although interesting academically, the ping test did not uncover any surprises or unexpected motion that might explain the failure.

Improved Instrumentation

Although Ramgen had an extensive instrumentation suite in place during the failure, the dynamic nature of the event made clear the need for higher speed instrumentation. The vibration measurement expert provided instrumentation, data acquisition, analysis software, and monitoring expertise to prepare for a June 2006 test. All high speed data would now be streamed directly to hard drive storage, enabling later review and analysis of the data. Each test produces 2 to 5 GB of high speed vibration data.

Most important of the added capabilities was real time shaft position monitors. Using eddy current probes at the turbine spline hub and laser proximity probes at the compressor end, test personnel were able to monitor the shaft motion in real time, decompose the data via Fast Fourier Transform (FFT) to identify frequency components, and watch for unexpected rotordynamic behavior. Previously, shaft motion could only be interpreted indirectly by vibration transmitted through the rig. Ramgen could now watch rotordynamic behavior in real-time and abort the test immediately if unexpected behavior occurred.

Dynamic accelerometers were also mounted to strategic points around the rig structure. As with the shaft position sensors, test personnel could look for harmful vibration and frequency content via FFT analysis in real time. Had a static structure resonant vibration caused the failure, these sensors would detect it before another failure could occur.

Lastly, the high speed acquisition monitored the rig's rotational speed sensor. This Hall effect sensor registered a voltage spike every time a shaft feature passed, giving very close tracking of the shaft speed at all times. Data from just prior to the failure appeared to show shaft speed variation; this equipment would allow test personnel to monitor for any unexpected behavior.

Oil Scoop Redesign

Although there was no indication that it caused problems during the January 2006 test, a problem was found and corrected in the lube drain system. Oil 'scoops' are used to prevent the oil from being whirled past the drain by rotating shaft aerodynamic forces. These scoops should open toward the oncoming oil and direct it toward the drain. Due to a design error, the scoops were built facing the wrong direction, away from the oncoming oil. Bearing and lubricant temperatures would have indicated if the scoops were causing unexpected heating in the oil. No such indication was found, but replacement oil scoops were manufactured and installed during the rig retrofit.

Modified Roller Bearing

The contractor bearing designer found a heretofore undiscovered problem with the compressor aft roller bearing design during a review after the failure. At speeds above 25,000 rpm, the bearing could bind on itself, causing a sharp increase in shaft torque and rapid failure of the bearing. The roller bearing was redesigned to increase internal clearances and avoid this problem and three new roller bearings to this specification were produced for further testing. There has been no suggestion or data indicating that roller bearing clearances caused or contributed to the failure.

Pancake Rotor Test

The one of a kind Mach 2.4 compression rotor was installed in the rig during the February 2006 failure. Careful and detailed inspection determined that the rotor was unaffected by the failure, but since a root cause had not yet been identified, a testing change was made to minimize the potential for any future failure to damage this rotor. An inexpensive 'pancake' rotor was built without the intricate (and expensive) aerodynamic surfaces of the compression rotor. This rotor would allow full speed rotordynamic evaluation of the rig without risking the performance rotor. Once rotordynamic issues had been laid to rest the compression rotor would be installed for aerodynamic testing.

2.2.3 Root Cause Discovery

By early June Ramgen had assembled the fixes and changes to the rig and prepared to return to test. There was unease that the 'smoking gun' had not been found, but oversight of the retrofit by the outside expert panel gave some confidence that one of the changes would prevent another failure.

As testing approached, Ramgen contracted the author of DyRoBeS to continue the parallel search for the failure's root cause. A comprehensive audit of the DyRoBeS model, including the turbine internal components, was initiated. In fairly short order, inconsistencies between the turbine configuration and the DyRoBeS model were discovered. The drive turbine OEM had incorrectly modeled a number of turbine components, including two key features which, when corrected, broke open the failure investigation and led to discovery of the real 'smoking gun'. The rotordynamics subcontractor had failed to correctly model rig behavior.

O-ring Damper

The OEM-supplied drive turbine bearings are each supported in a pair of Viton o-rings to provide damping (see Figure 2-4). In DyRoBeS modeling of this configuration, the OEM analysis took credit for damping of 3300 N sec/m (19 lb sec/in) from these o-rings. In reality, the damping value for an o-ring in this configuration should be in the range of 1.8 N sec/m (0.01 lb sec/in). Turbine damping had been overestimated by more than two orders of magnitude.

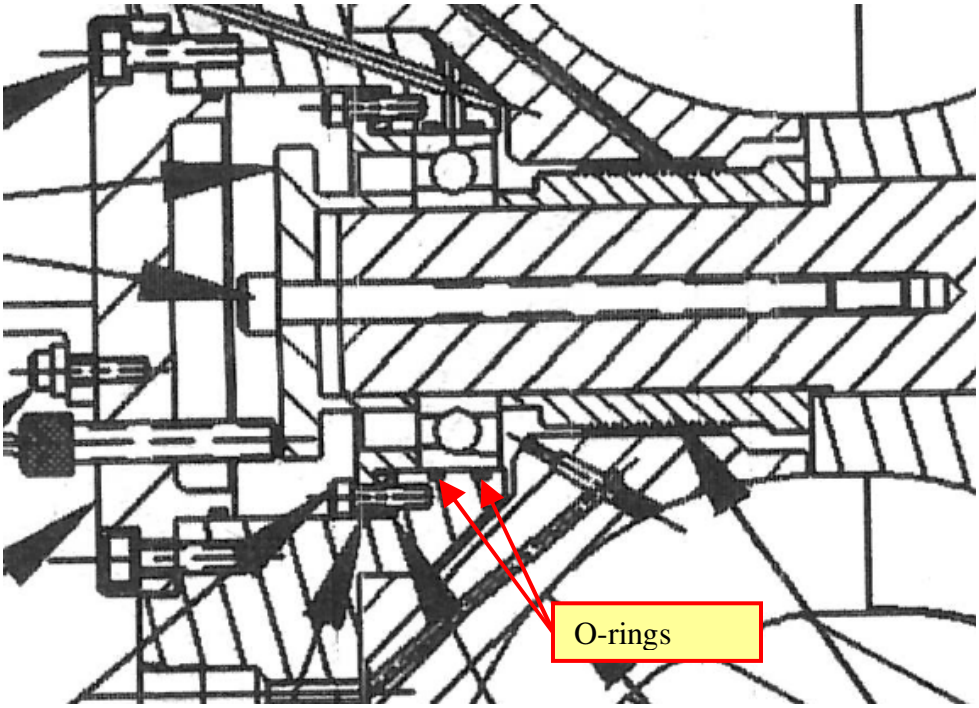

Figure 2-4: Original drive turbine bearing damper configuration.

Damping is used to dissipate the energy of vibration and resonant motion in turbomachinery. Without sufficient damping, a machine can tear itself apart as the vibration energy builds until the metal is stressed to failure. With unrealistic damping values, the original rotordynamics model disguised and covered up vibrational problems by reducing the amplitude and spreading it out over a wider frequency range.

O-ring Nonlinear Stiffness

Magnifying the damping error, the turbine OEM had modeled o-ring radial stiffness as linear. Lateral forces applied to the turbine shaft move it off-center; magnitude of the motion is a function of the o-ring stiffness which is substantially less than the bearing stiffness. The OEM analysis modeled the o-ring stiffness as 3.3×10^6 N/m (19,000 lb/in) of deflection, regardless of deflection amount. This was clearly wrong, as the o-ring can only deflect about 0.064 mm (0.0025 in) before the bearing outer race contacts static structure and the stiffness increases drastically. This is called 'bottoming' the damper and completely changes the rotordynamic response to vibration.

Ramgen performed a lateral pull test on the turbine output shaft to measure the actual o-ring stiffness. As expected, the stiffness was not linear and although the 3.3×10^6 N/m (19,000 lb/in) value from the initial rotordynamic analysis was reasonably correct for the first small amount of motion, the stiffness rapidly increased until the damper bottomed and metal to metal contact sent stiffness sharply higher. Figure 2-5 shows the initial linear model and the actual measured nonlinear stiffness.

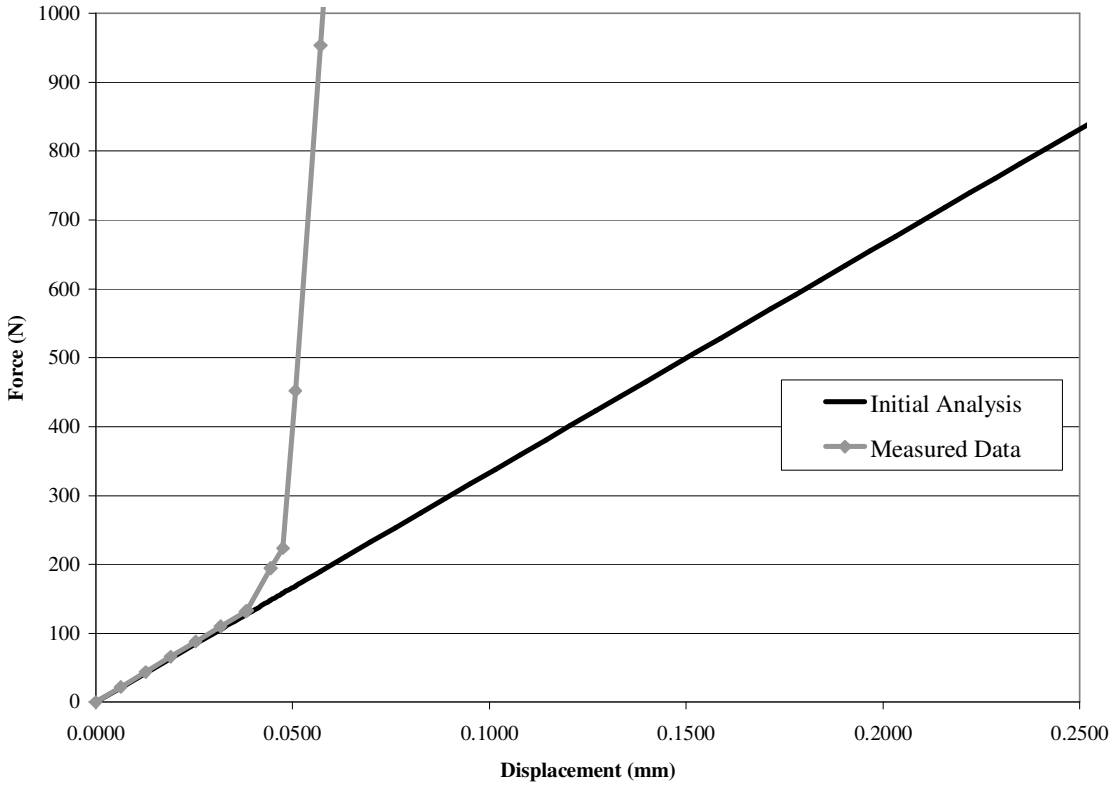

Figure 2-5: Comparison of initial linear o-ring model and measured nonlinear stiffness.

When the DyRoBeS model o-ring stiffness and damping were corrected, the results were striking. A high amplitude rotordynamic mode was now predicted near 20,000 rpm; close enough to possibly explain the February 2006 failure at 18,500 rpm. In addition, DyRoBeS would frequently crash at higher RPM. According to DyRoBeS author Dr. Wen Chen, this indicates highly unstable and difficult to predict rotordynamics. As Figure 2-6 shows, the search for root cause was finished; an underdamped rotordynamic mode had sent the flex coupling into deflections which exceeded its structural strength. As the team struggled with the turbine controller to reduce shaft speed, the flex coupling failed catastrophically and destroyed the turbine shaft.

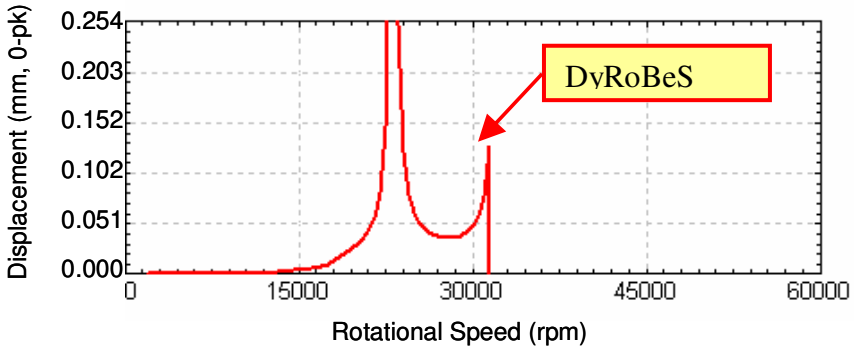

Figure 2-6: Rotordynamic prediction with o-ring stiffness and damping corrected.

Stiffness Added Instead of Damping

Dr. Chen also expressed surprise that the original rotordynamics analyst (also the drive turbine OEM) had suggested increasing bearing stiffness to drive rotordynamic modes beyond the operating range. The accepted industry approach is to add damping, not increase stiffness, particularly for a machine with such a high operating speed. Increased stiffness without damping tends to amplify dynamic/resonant vibration; although a mode peak can be shifted in speed (rpm), the rig is more prone to stability problems.

2.2.4 June Test

In the face of the rotordynamics problem, Ramgen decided to proceed carefully with the rebuilt rig test to verify the audit conclusions without risking another failure. During low speed operation at nearly 13,000 rpm, a sudden increase in shaft vibration was detected by the new high speed instrumentation and the test was quickly aborted without damage. Figure 2-7 and Figure 2-8 show the sudden increase in shaft orbit during this test. Although the new sensors had successfully allowed test personnel to end the test before damage occurred, further testing was deemed too risky and another redesign was undertaken.

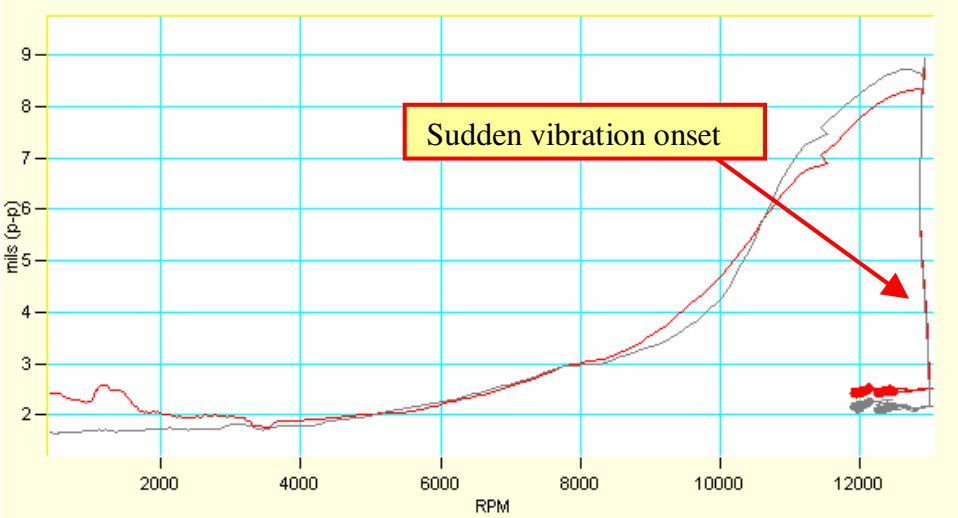

Figure 2-7: Run 65a – Sudden turbine shaft orbit increase and subsequent deceleration.

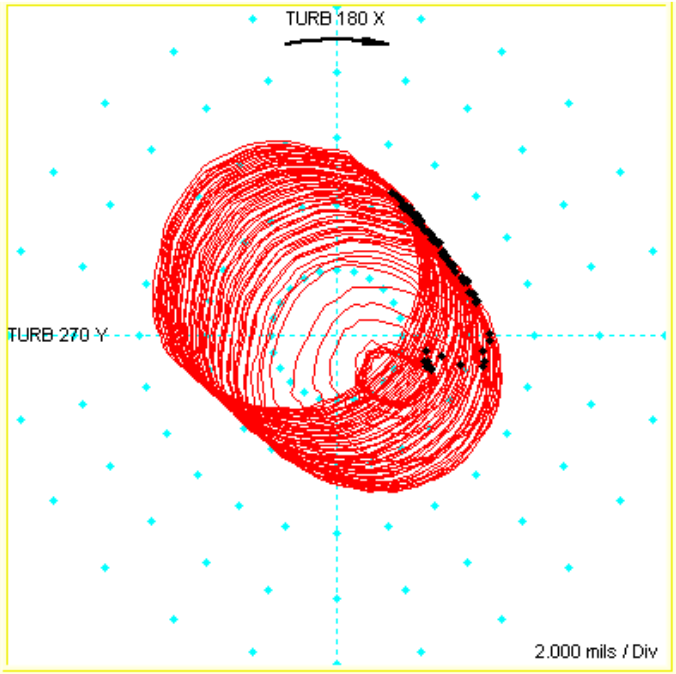

Figure 2-8: Run 65a - Sudden turbine shaft orbit increase.

2.2.5 Final Redesign to Address Root Cause

Over the next months a number of modifications were made to the drive turbine and Rampressor-2 test rig to obtain acceptable rotordynamic characteristics. These modifications were not necessarily made in parallel and resulted from both theoretical analysis and test data analysis. The changes included:

Replacing the Rampressor Aft Bearing

The exceptionally stiff roller bearing, which was designed and built as a direct result of the flawed original rotordynamics analysis, was replaced with a tilting-pad hydrodynamic bearing. Although the drive turbine was the source of the vibration problem, adding compressor damping greatly reduced the vibration amplitude and helped correct the rotordynamics.

Adding Squeeze Film Dampers to the Drive Turbine

Squeeze film dampers were added to both bearings in the OEM-supplied drive turbine. These dampers greatly reduced the vibration caused by the turbine and, with the compressor tilting-pad bearing, produced acceptable vibration levels during operation. Figure 2-9 shows a cross section through the drive turbine prior to modification and Figure 2-10 shows a cross section following modification.

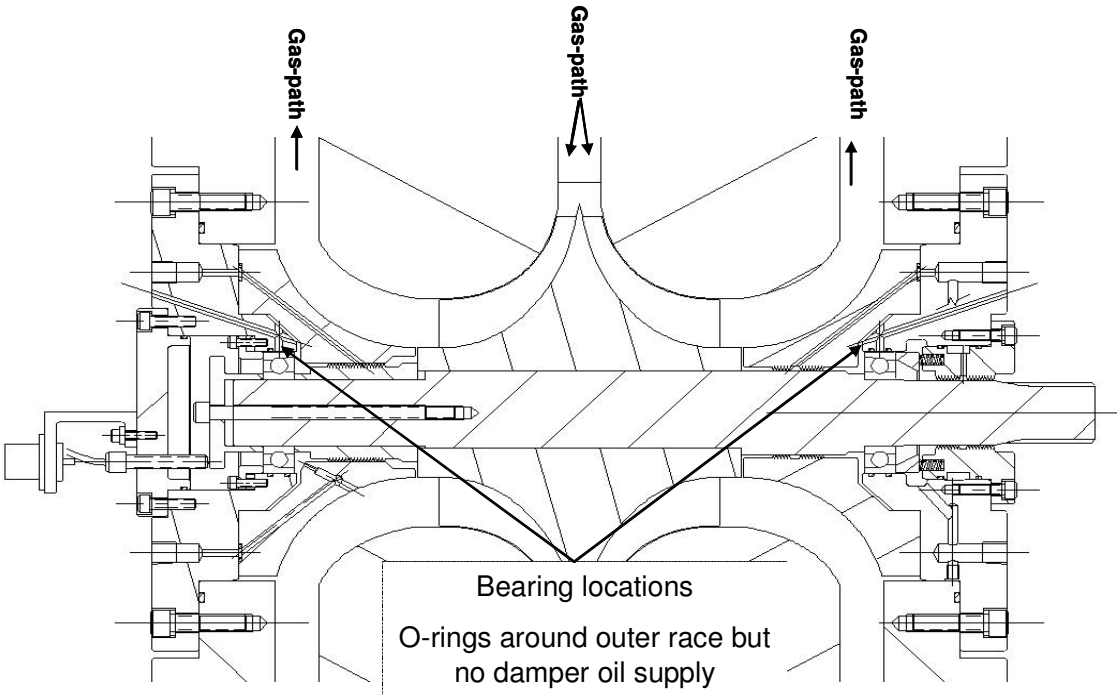

Figure 2-9: Section through the drive turbine original configuration.

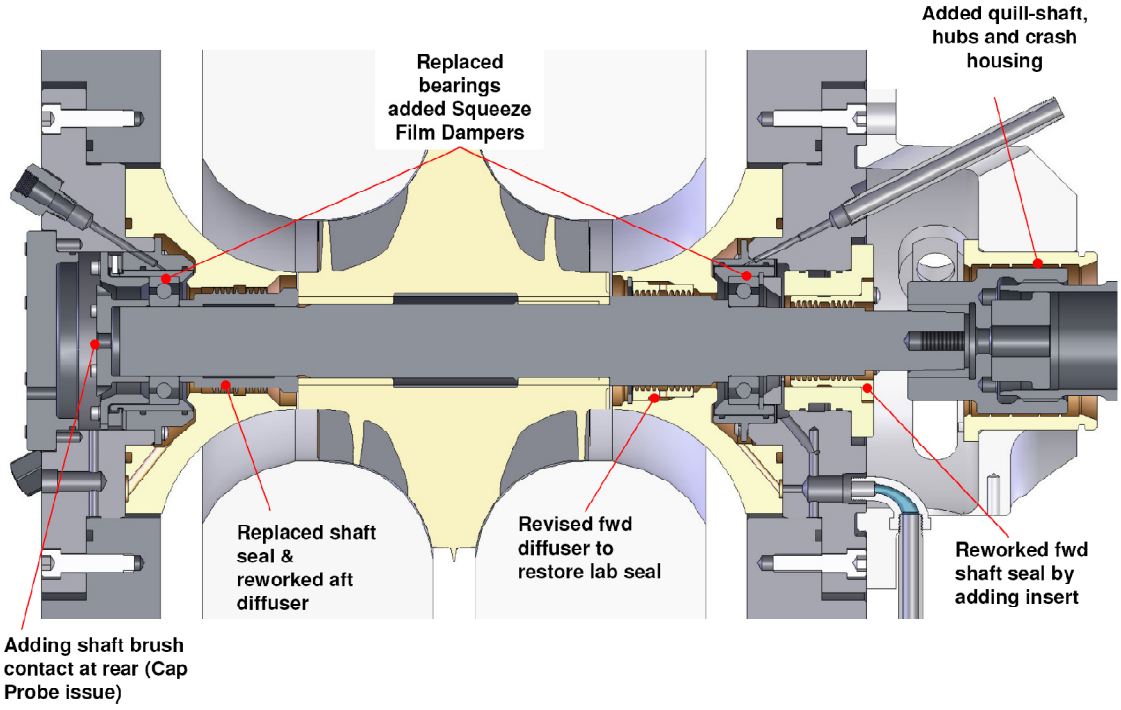

Figure 2-10: Section through the drive turbine final configuration.

Quillshaft Centering Hub

New problems were introduced with the splined quill shaft, relating to the loose fit of the shaft splines in the hub splines. In an effort to limit the off-axis movement of the quillshaft,

centering hubs were added to both ends of the quillshaft. These hubs proved very successful at reducing the relative motion in this joint.

Test rig operation

In addition to the large-scale hardware changes outlined above, changes were also made to some of the secondary flow systems in the drive turbine and rig. These included modifications to the drive turbine lubrication system, adding cooling air jets to the quillshaft hubs, purging seal cavities with the drive turbine, and customizing oil flow rates and pressures to the drive turbine dampers.

2.3 Rig Vibration

Aside from the vibration issues tied to the drive train rotordynamics, the only other vibration issue on the Rampressor-2 test rig related to vibration of the axially translating tip ring. A cross section through the tip ring is presented below in Figure 2-11.

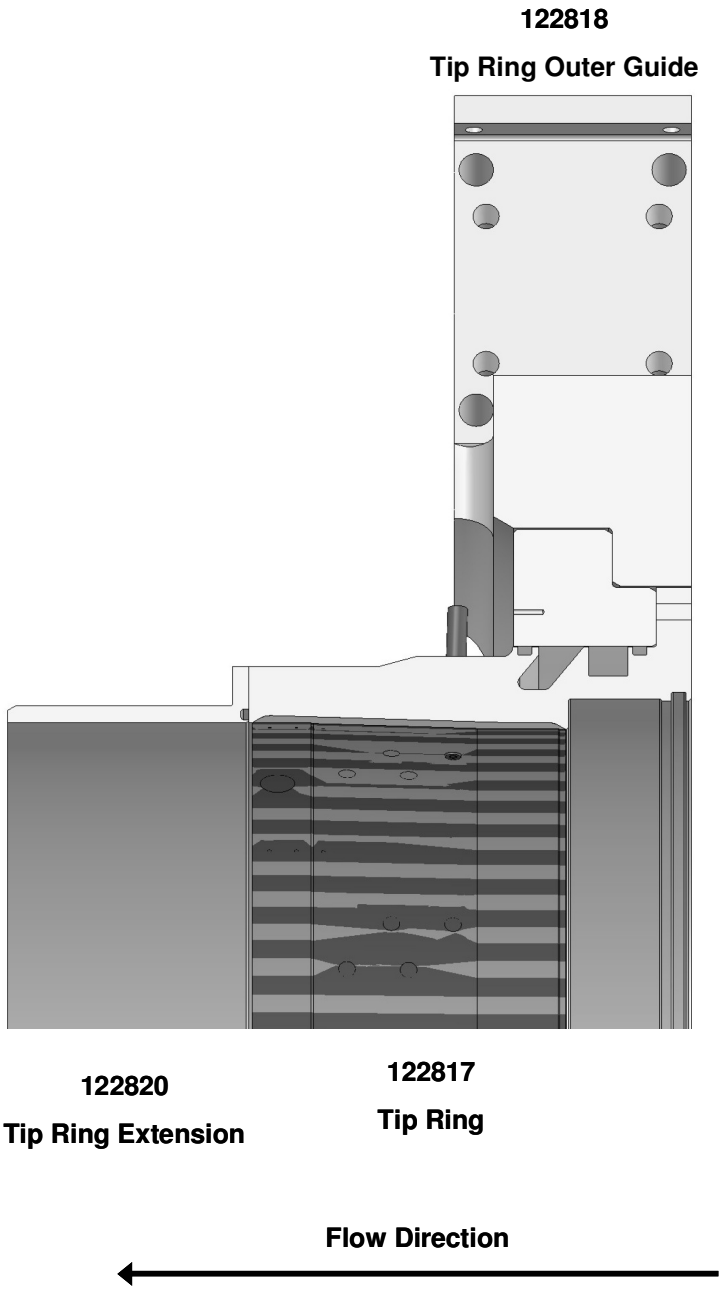

Figure 2-11: Section through tip ring assembly.

During accelerations to high speed, rig instrumentation detected vibration at around 30,000 rpm. Further examination and diagnostic testing revealed the tip ring to be vibrating. Finite element analysis of the tip ring indicated the presence of a tri-lobe resonant harmonic at this rig condition. It appeared this mode was excited by the three flowpaths of the Rampressor-2 rotor. Figure 2-12 shows a typical mode shape plot from this analysis.

Examination of the measured displacement data in conjunction with the finite element analysis determined an upper limit on the tip ring displacements and this; in conjunction with a 'keep-out' zone around 30,000 rpm, avoided the issue becoming more serious.

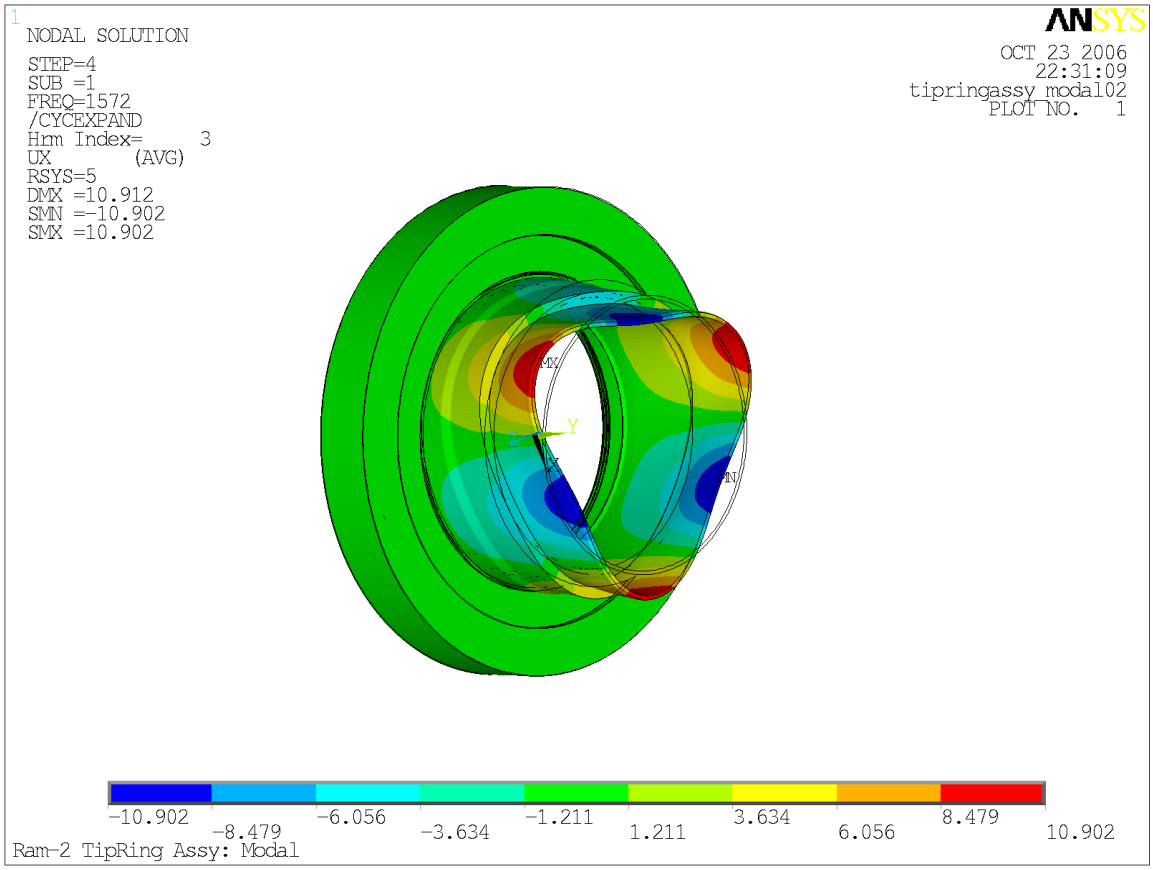

Figure 2-12: Tip ring modal analysis. Third harmonic shown.

Chapter 3

Computational Fluid Dynamics Analysis

Computation fluid dynamic (CFD) simulations were used extensively to analyze flow through the Rampressor test article. Initial CFD runs focused on the inviscid performance of simplified flow paths in order to evaluate a large number of candidate flow paths. After selecting a smaller number of candidate flow paths, full rotor viscous simulations were performed to generate data for final flow path selection. Final simulations included the inlet guide vanes which had previously been modeled separately. Validation of the CFD scheme was also conducted to ensure that it could model the flow physics correctly.

3.1 Description of CFD Scheme and Test Cases

Solution of the Navier-Stokes equations compressible form for the simulations presented herein was conducted using a finite volume, density based scheme that has been modeled after the explicit four stage Runge-Kutta time integration method of Jameson *et al.* (1981). Implementation of this numerical algorithm was conducted in the FINE/Turbo code of Numeca, described by Hakimi (1997). Multigrid acceleration was employed to damp varying error wavelengths efficiently. A cell-centered second order central discretization of space was conducted, employing scalar artificial dissipation through a blend of second and fourth differences to avoid odd/even decoupling and oscillations in the vicinity of high pressure gradients (see equations (3-1) through (3-5)). The particular treatment of dissipation was that of Martinelli and Jameson (1988). Equation (3-1) presents the integral form of the solution and flux vectors of the continuity, momentum and energy equations, along with the source term vector (e.g., turbulence source terms) and artificial dissipation terms.

$$\int_V \left(\underbrace{\underline{Q}_t}_{\substack{vector\,of\\ conserved\\ variables}} + \underbrace{E_x + F_y + G_z}_{flux\,vectors} \right) dV - \int_V \underbrace{\underline{S}}_{\substack{source\\ term\\ vector}} dV - \underbrace{DQ}_{\substack{artificial\\ dissipation\\ terms}} = 0 \tag{3-1}$$

$$D^{(2)}Q = \nabla\left((\lambda)_{i+1/2,j,k} (\varepsilon^{(2)})_{i+1/2,j,k} \right) \Delta Q_{i,j,k} \tag{3-2}$$

$$D^{(4)}Q = \nabla\left((\lambda)_{i+1/2,j,k} (\varepsilon^{(4)})_{i+1/2,j,k} \right) \Delta\nabla\Delta Q_{i,j,k} \tag{3-3}$$

$$\varepsilon^{(2)}_{i+1/2,j,k} = \kappa^{(2)} (\lambda)_{i+1/2,j,k} \max\left(\nu_{i+2,j,k}, \nu_{i+1,j,k}, \nu_{i,j,k}, \nu_{i-1,j,k} \right) \tag{3-4}$$

$$\varepsilon^{(4)}_{i+1/2,j,k} = -\max\left(0, \kappa^{(4)}(\lambda)_{i+1/2,j,k} - (\varepsilon)^{(2)}_{i+1/2,j,k}\right) \tag{3-5}$$

It is not desired to provide full details of the code employed, but it is necessary to discuss a few key features to aid following discussions. The second and fourth differences are laid out in Equations (3-2) through (3-5) where Δ and ∇ are forward and backward difference operators. The spectral radii of the flux Jacobian matrices, denoted by λ, are scaling parameters in the dissipation terms and ν is a pressure gradient sensor employed within the dissipation logic. Within the calculation of first and third order adaptive dissipation coefficients, $\varepsilon^{(2)}$ and $\varepsilon^{(4)}$ respectively, two constants, $\kappa^{(2)}$ and $\kappa^{(4)}$, are available that can be controlled by the user to increase or decrease the amount of dissipation injected into a solution. A delicate balance must be maintained when setting these values to enable reasonable convergence while maximizing solution accuracy. Generally, higher values of these constants can be employed when finer computational grid density is used, and it is instructive to establish sensitivity to these values when testing the dependence of a CFD solution to grid resolution.

Turbulence was modeled using the one-equation closure of Spalart and Allmaras (1992), referred to as S-A. The model has been chosen based on its demonstrated accuracy of predicting boundary layer development (Bardina *et al.*, 1997), separation in diffusing flows (Yaras and Grosvenor, 2003), turbomachinery flows (Heidegger *et al.*, 1999) and shockwave/boundary layer interaction (Mohler, 2005). The model was particularly chosen over other two-equation models that offer similar prediction accuracy, or higher order closures that would require dramatically higher grid resolution and/or CPU time to achieve convergence, due to its numerical robustness, lower sensitivity to grid resolution and computational economy. For example, Hellsten (1996) stated of S-A, "The present model is somewhat more robust than Menter's SST model" and "The CPU time requirement per iteration cycle is some 15-20% less than in the case of two-equation models." Pope (2000) commented on one potential reason for S-A's perceived higher numerical robustness, "The Spalart-Allmaras model is, by design, much simpler and less expensive for near wall aerodynamic flows. This is because, compared with [turbulence kinetic energy and turbulence dissipation rate], the turbulence viscosity [on which S-A is based] behaves benignly in the near-wall region, and is more easily resolved." Yaras and Grosvenor (2003) stated, referring to their studies of three dimensional separating diffuser and vortex generator jet flows, "…the one equation model of Spalart and Allmaras is found to provide the best combination of: minimum resolution requirements of wall boundary layers, consistent prediction accuracy, robustness and computational efficiency."

3.1.2 Flat Plate Boundary Layer

An incompressible turbulent flat plate boundary layer was chosen as the first test case. The goal here was to establish a baseline performance of the scheme in question, and assess its sensitivity to grid resolution, and numerical diffusion. Geometry and operating conditions are listed in Table 3-1. The simulations were conducted with a computational domain, shown schematically in Figure 3-1. A 100 mm (3.937 in) long 'slip wall' boundary was placed upstream of the plate leading edge. Both the upper and aft boundaries of the computational domain were set as outflow boundaries with a fixed, spatially uniform static pressure. All flow variables other than pressure were extrapolated to the outflow boundaries from within the computational domain. At the inflow boundary, uniform distributions of velocity, flow direction and turbulence properties were imposed and static pressure was extrapolated from the interior

nodes. Inflow turbulence intensity was set to 1% but the computational domain was configured with a long enough entry region for turbulence to develop, such that a non-physical turbulence level would not result in the region of interest. Similar approaches were taken with the remaining test cases. The simulations were performed for a few combinations of boundary layer (b.l.) cross stream resolution and y_1^+ values (see Table 3-2) to establish sensitivity to these parameters. Note that sensitivity to grid stretching ratio, cell skew, was not specifically analyzed in this study. Previous tests (Grosvenor, 2000) have determined that the discretization scheme employed is less restrictive than some, but one should try to stay below a stretching ratio of two and maintain a minimum angle between adjacent cell elements of 15^o.

Table 3-1: Flat plate geometry and operating conditions used in simulations.

Plate length x domain height	Freestream velocity	Re_L	Re_θ
2.1 m x 0.15 m (82.7 in x 5.91 in)	33 m/s (108 fps)	4.5×10^6	5.2×10^3

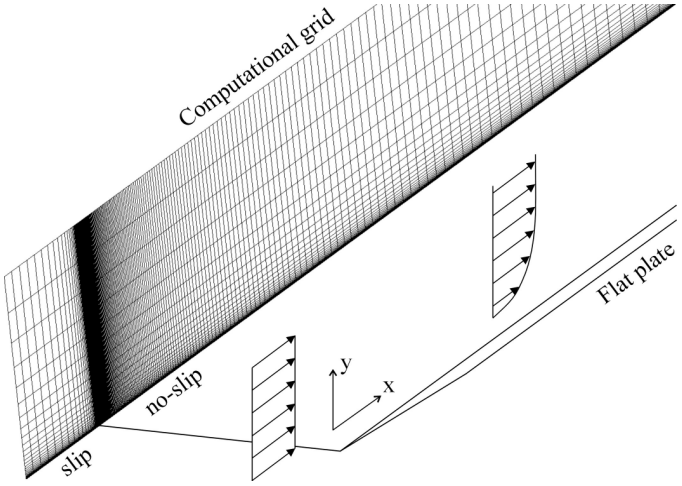

Figure 3-1: Schematic view of flat plate flow and computational grid used in simulations.

Table 3-2: Grid details for flat plate simulations.

# normal	# streamwise	y_1^+	# in boundary layer	$\kappa^{(4)}$
129	273	0.5	47	0.05
41	273	1.0	17	0.05
41	273	5.0	15	0.05
41	273	5.0	15	0.001

Figure 3-2 through Figure 3-4 display predictions of skin friction, velocity profile and shape factor compared with the data of Wieghardt and Tillmann (presented by Coles and Hirst, 1969). Comparison of the three quantities shows consistent trends. The two finest grid resolutions are shown to provide good agreement with the experimental data, while the grid

consisting of a y_1^+ of 5 shows significant differences. However, decreasing the third order artificial dissipation coefficient constant, $\kappa^{(4)}$, established that the discrepancy was due to artificial diffusion rather than sensitivity of the turbulence model. The coarsest grid placed approximately 15 nodes in the boundary layer. It was concluded that the physics of boundary layer development in an incompressible flow could be captured by the employed numerical scheme and turbulence model, but that coarser grids should be checked by either reducing the third order artificial dissipation coefficient constant, or comparing results with a finer grid. In a design cycle analysis, this would mean that several coarser grid simulations could be run, but that a fine grid should be employed periodically to check the validity of conclusions drawn based on coarser resolution.

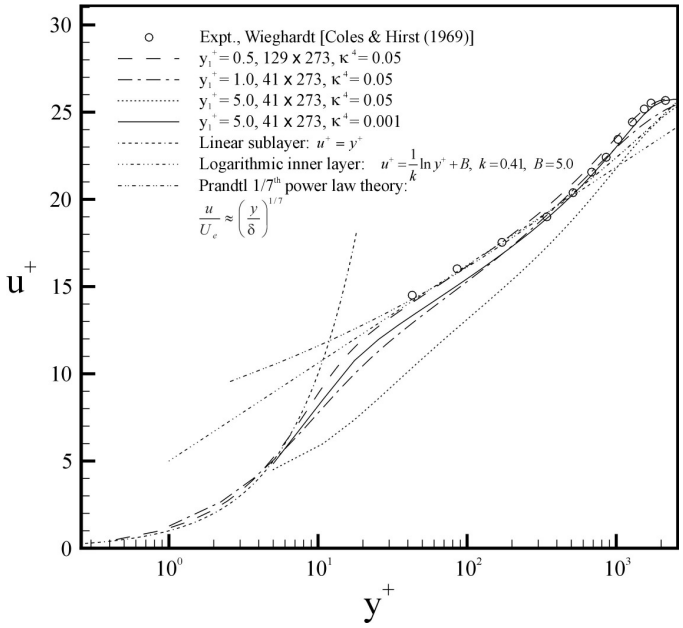

Figure 3-2: Flat plate boundary layer profile prediction at approximately mid-plate location.

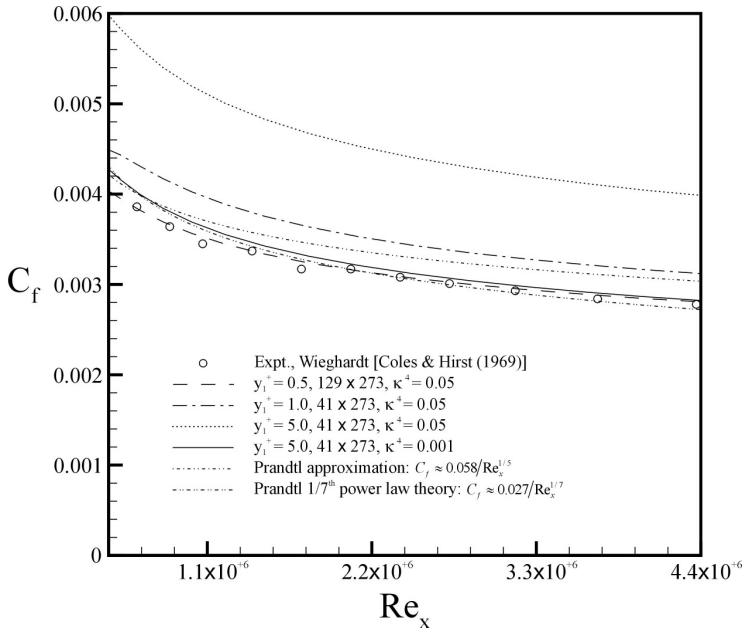

Figure 3-3: Flat plate skin friction prediction.

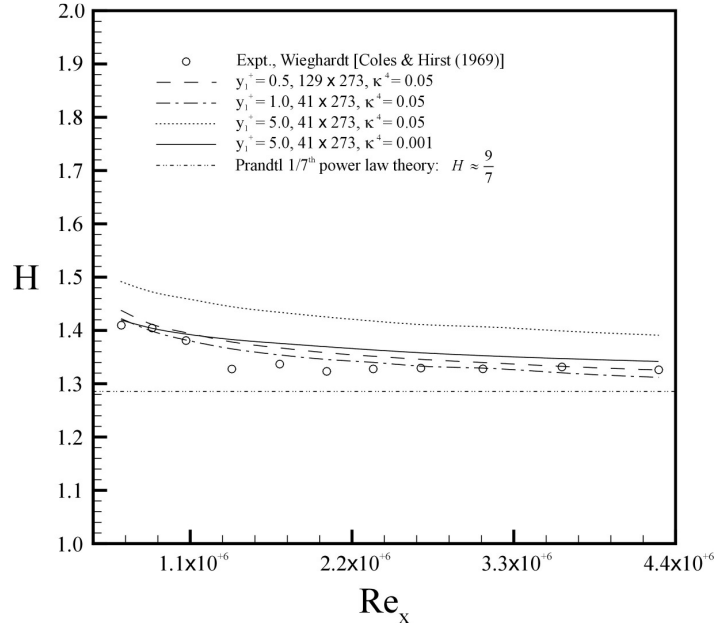

Figure 3-4: Flat plate shape factor prediction.

3.1.3 Annular Separating Diffusing Flow

The axisymmetric, separating, adverse pressure gradient flow identified as Case C.S0 by Driver and Johnston (1990) was studied next. It was chosen to test the ability of the employed numerical scheme and turbulence model to predict incompressible flow separation in the presence of a strong adverse pressure gradient. In this experiment, an annular diffuser was formed by aligning a cylinder longitudinally in a wind tunnel test section with diverging walls. Boundary layer suction was applied at the test section walls such that separation occurred on the cylinder surface only. Note that the suction slots existed outside of the bounding streamlines of

the computational domain employed and were, therefore, unnecessary to include in the simulation. Prediction of the flow in this test case was particularly challenging as the separation bubble is not constrained in the axial direction. Size of the computational domain was minimized by prescribing an outer radius domain boundary that followed a stream tube defined on the basis of mass conservation, see Figure 3-5. This method is consistent with that employed by other authors such as Bardina *et al*. (1997). Geometry and operating conditions are listed in Table 3-3. Three grids were implemented, see Table 3-4, to test sensitivity to spatial resolution. The inflow velocity and turbulence profiles were extracted from zero pressure gradient annulus boundary layer simulations to match the experiment. The outflow static pressure was set to an average (less reflective) condition, and all other flow properties were extrapolated from the interior of the computational domain.

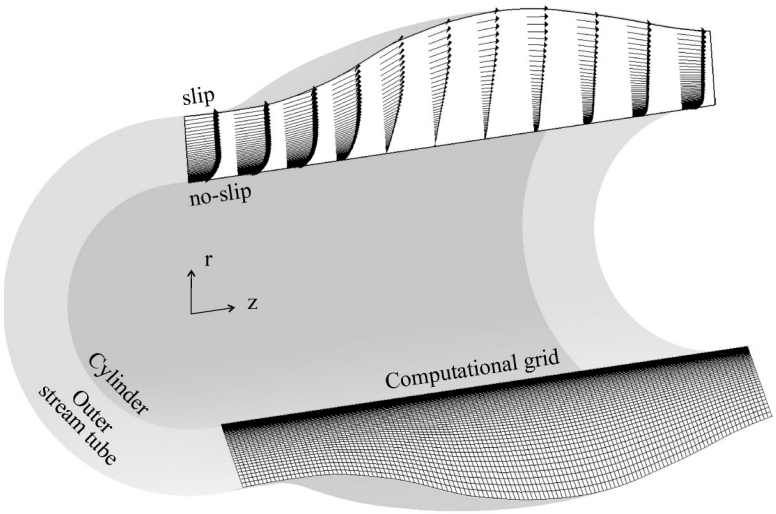

Figure 3-5: Schematic of annular separating diffuser flow and computational grid used in simulations.

Table 3-3: Annular separating diffuser geometry and operating conditions used in simulations.

Annulus length x domain height	Freestream velocity	Re_θ
1.26 m x 0.037-0.071 m (49.6 in x 1.46-2.80 in)	30 m/s (98.4 fps)	3.6×10^3

Table 3-4: Grid details for annular separating diffuser simulations.

# normal	# streamwise	y_1^+	# in boundary layer	$\kappa^{(4)}$
129	321	0.5	97	0.05
65	161	1.0	49	0.05
65	161	1.0	49	0.001
33	81	5.0	24	0.05
33	81	5.0	24	0.001

Comparison of predictions and experiment in Figure 3-6 through Figure 3-10 display a successful reproduction of the boundary layer development through separation and reattachment, and the subsequent impact on pressure recovery. Although Figure 3-8 suggests prediction of separation upstream of the actual separation point based on skin friction, comparison of shape factor distributions are shown to match the experiment well. This discrepancy is due to the locally steeper than realistic velocity profile prediction adjacent to the wall (e.g. position z/R=2.177) shown in Figure 3-6. Skin friction calculation is dependent on this localized behavior, while shape factor is calculated based on an integration of the entire boundary layer. It is therefore suggested here that CFD practitioners can benefit from paying attention to calculated distributions of shape factor when concerned with a flow's potential to separate. Note the incipient detachment shape factor thresholds indicated in Figure 3-10 by previous authors. In this case, it was found that the more recently suggested value of approximately H=2.7 agreed well with the location of separation for this case. It was found that all three grids provided sufficient agreement with the experimental data, but that it was necessary to decrease the third order artificial dissipation coefficient constant, $\kappa^{(4)}$, to achieve similar accuracy to y_1^+=1 with y_1^+=5. It was generally concluded that incompressible flow separation due to a strong adverse pressure gradient could be adequately captured by the employed numerical scheme and turbulence model.

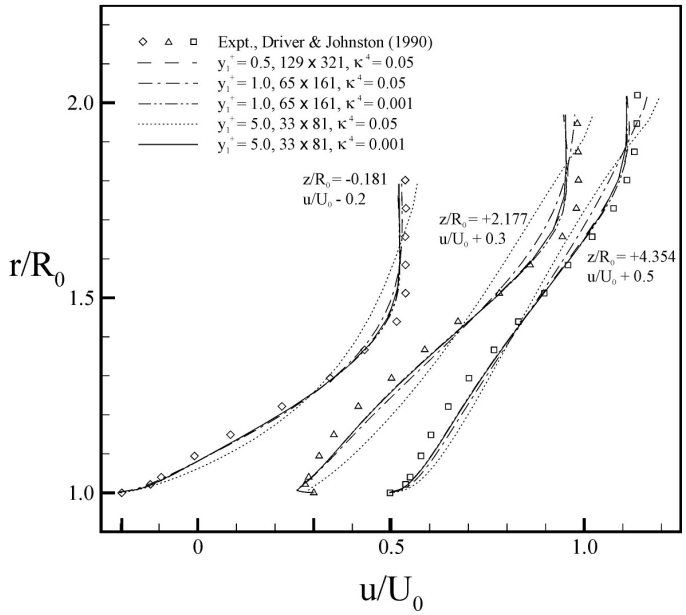

Figure 3-6: Annular separating diffuser boundary layer profile prediction.

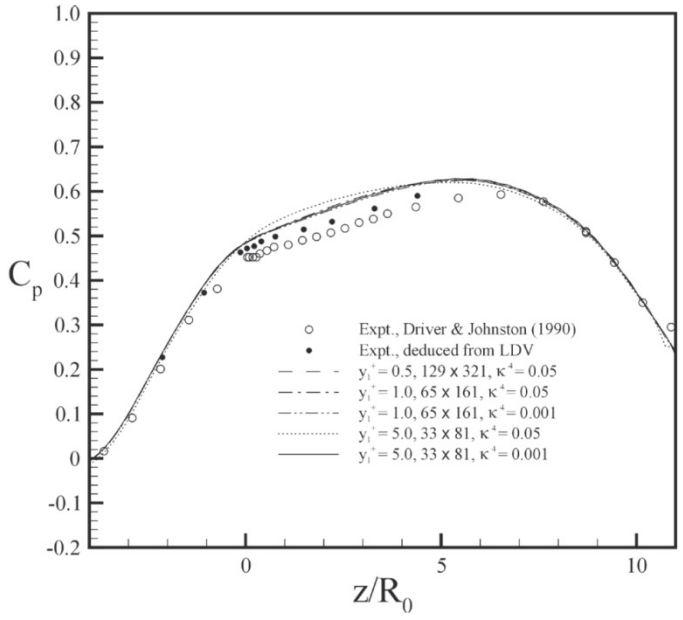

Figure 3-7: Annular separating diffuser static pressure coefficient prediction.

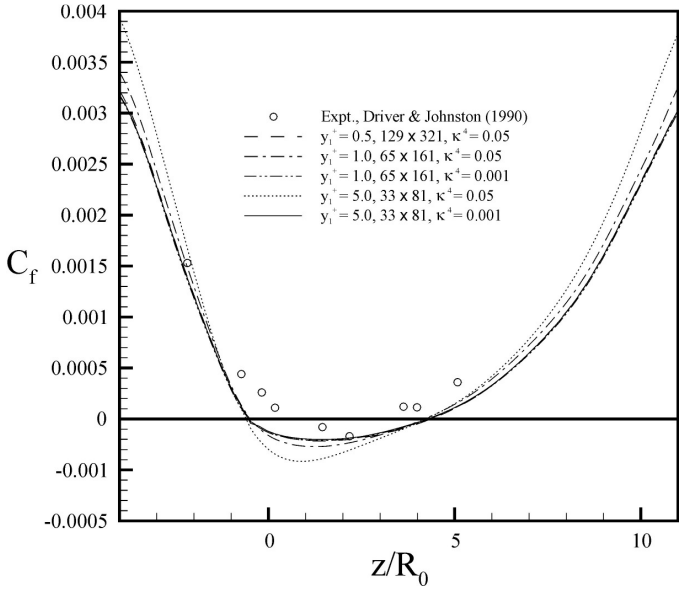

Figure 3-8: Annular separating diffuser skin friction prediction.

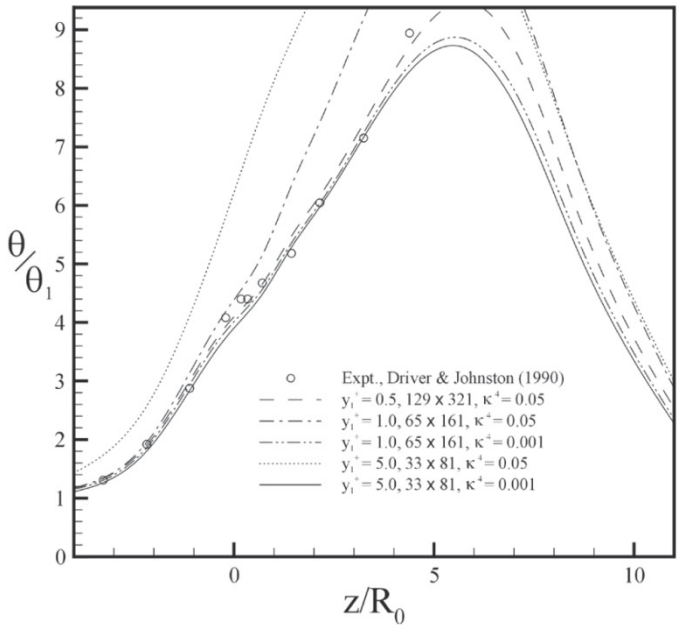

Figure 3-9: Annular separating diffuser momentum thickness prediction.

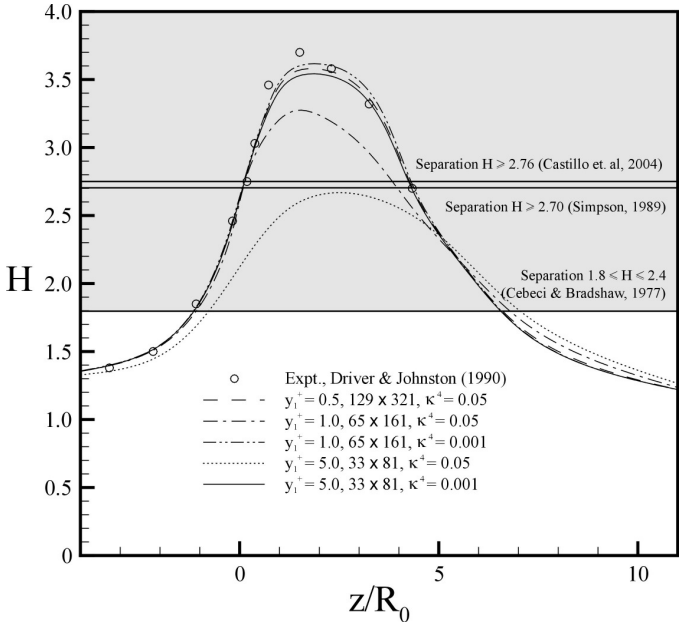

Figure 3-10: Annular separating diffuser shape factor prediction.

3.1.4 4:1 Pressure Ratio Centrifugal Compressor Impeller

The next validation test case run was the centrifugal compressor impeller described by McKain and Holbrook (1997). It was chosen to test the ability of the employed numerical scheme and turbulence model to predict performance of a conventional compressor rotor at on- and off-design conditions. This compressor produces a reasonably high stage total pressure ratio, adequate information is given on the rotor tip clearance, and the quality of data is quite good. Details of the experimental measurements are given by Skoch et al. (1997). The impeller contains 15 main blades with 15 splitter blades, and employs 50 degrees of backsweep from

radial at discharge. The splitter blade leading edge, located at 30% of main blade chord, is offset slightly toward the main blade suction surface in order to produce an even flow split. The inlet tip diameter is 210 mm (8.26 in) and the inlet blade height is 64 mm (2.52 in). The exit diameter is 431 mm (17.0 in), the exit blade height is 17 mm (0.67 in) and the exit tip clearance is 0.203 mm (0.008 in). The stage (impeller with vaned diffuser) was designed to produce a pressure ratio of 4:1 at the design mass flow. The standard day corrected speed for the design flow of 4.54 kg/s (10 lbm/s) was 21,789 rpm. The inlet relative Mach numbers on the suction surface ranged from 0.45 at the hub to 0.90 at the tip.

Figure 3-11 displays four views of the three-dimensional impeller computational grid employed. Note that a single blade and splitter channel was modeled, and periodic boundary conditions were employed to reproduce the 360º impeller. Two grids were tested employing approximately 3.8×10^5 and 3 million nodes, with y_1^+ values ranging from 1 to 5 and 0.1 to 0.5 in the passage respectively. A complex multi-block structure was employed, but the node distributions were approximately 177×49×45 in the streamwise, pitchwise, and spanwise directions for the coarser grid, and 353×97×89 for the finer. Total pressure, total temperature, and 1% turbulence intensity were specified at the inflow boundary based on the experimental measurements. The exit mass flow was set to a range of values to produce a constant speed line, and all other flow properties were extrapolated from the interior of the computational domain. A real gas definition of air was used for the working fluid.

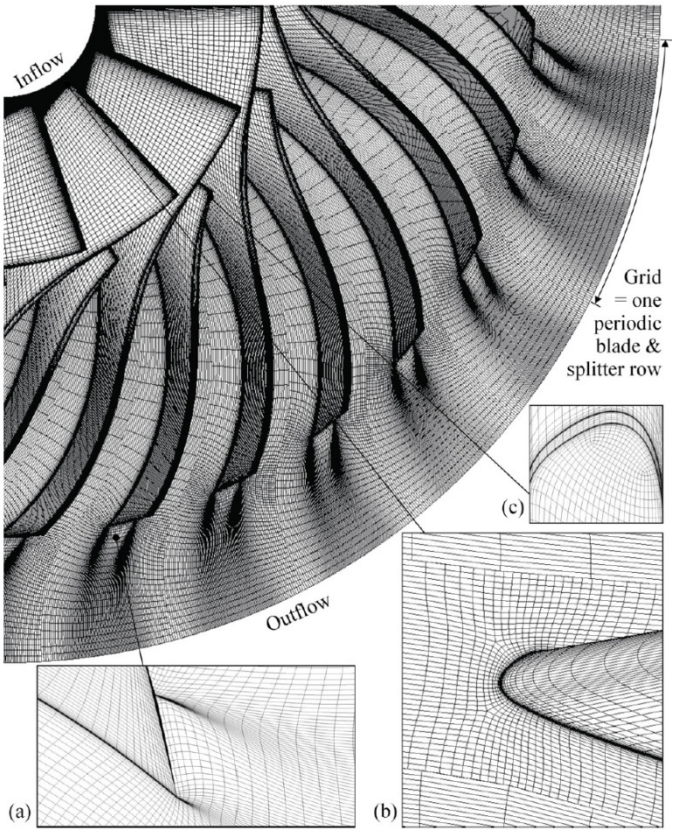

Figure 3-11: Computational grid used for 4:1 centrifugal compressor simulations. The 3 million cell version is shown. Figure (a) shows the trailing edge at the hub. Figure (b) shows the leading edge at the hub. Figure (c) shows the tip clearance at the leading edge.

Comparisons between a predicted constant speed line and experiment are shown in Figure 3-12 and Figure 3-13. Pressure ratio and efficiency at the maximum efficiency point are shown to be predicted quite well by the fine grid, with the predicted accuracy reducing somewhat at off-design. The coarse grid also compared well, when the third-order artificial dissipation coefficient constant, $\kappa^{(4)}$, was reduced to 0.001. Interestingly, at low mass flow the results of both coarse grid simulations matched regardless of the third-order artificial dissipation coefficient constant, $\kappa^{(4)}$. This difference in behavior exists because at this point on the constant speed line, the impeller is near surge, and the lower grid resolution is too coarse to fully capture the boundary layer and tip clearance flow in this condition. The results of the coarse grid with minimized dissipation showed a slight dip in characteristic that could indicate approach of surge. However, convergence was stable at these points and the magnitude of difference between these predicted operating points with the fine grid results and experiment were small. The numerical scheme and turbulence model employed were deemed adequate for the purposes of predicting compressor rotor performance at design and off-design, particularly when comparing with other published predictions (Larosiliere *et al.*, 1997).

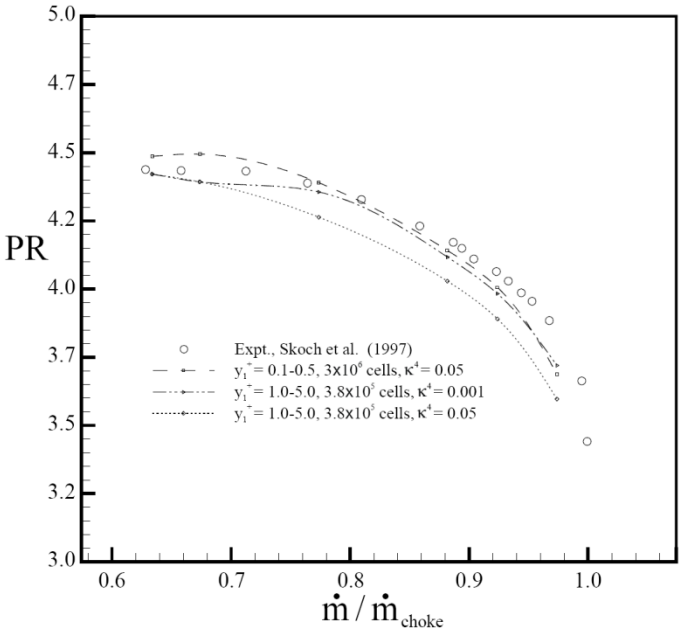

Figure 3-12: Predicted pressure ratio for 4:1 centrifugal impeller at 100% speed.

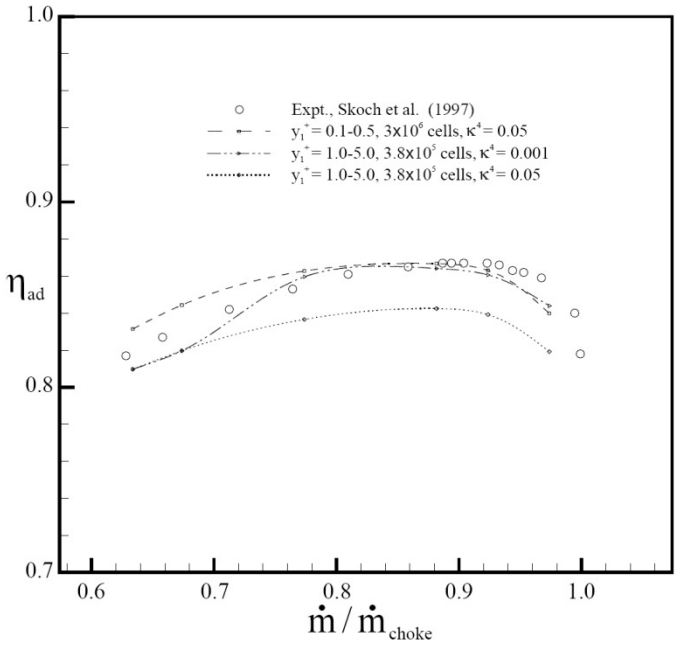

Figure 3-13: Predicted adiabatic efficiency for 4:1 centrifugal impeller at 100% speed.

3.1.5 Transonic Separating Diffuser

The next test case run was the transonic diffuser of Bogar, Sajben and Kroutil (1983). It was chosen to test the ability of the employed numerical scheme and turbulence model to predict flow separation in presence of the strong shock wave/boundary layer interaction produced in this diffuser. The entrance to throat area ratio was 1.4, and the exit to throat area ratio was 1.5. Reasonable two-dimensionality of the flow was produced with a sidewall spacing of approximately four throat heights, and suction slots placed on the side walls of the constant area sections upstream and downstream of the diffuser and along the top corners of the diffuser. The throat height was 44mm (1.7 in) and an exit static pressure to inflow total pressure ratio of 0.72 was applied.

Figure 3-14 displays a schematic of the two-dimensional diffuser geometry, the flow field, and the computational grid employed. Two grids were tested employing 89 nodes in the streamwise direction and 61 in the radial direction, with inlet y_1^+ values of 1 and 5. Total pressure, total temperature, and 1% turbulence intensity were specified at the inflow boundary based on experimental measurements. The outflow static pressure was set to an average (less reflective) condition, and all other flow properties were extrapolated from the interior of the computational domain.

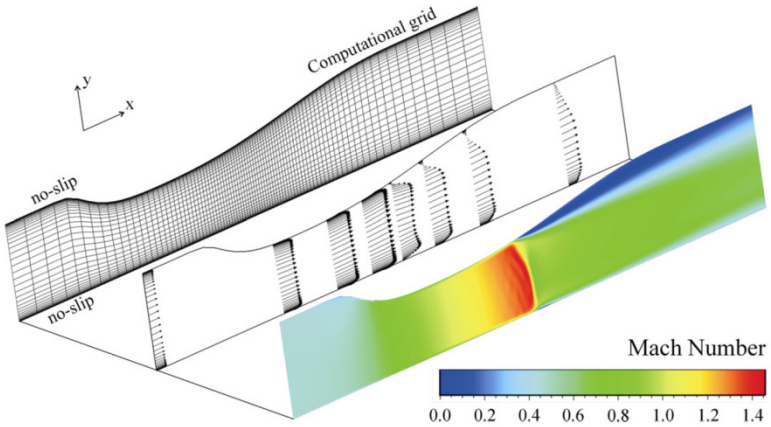

Figure 3-14: Schematic of separating transonic diffuser flow and computational grid used in simulations.

Comparisons between prediction and experiment are shown in Figure 3-15 and Figure 3-16. Flow separation due to the shock wave/boundary layer interaction and subsequent pressure recovery characteristics are shown to be predicted quite well. However, decreasing the third-order artificial dissipation coefficient constant, $\kappa^{(4)}$, produced slightly better boundary layer displacement due to separation and subsequent local reduction in pressure recovery. Note that variation of the first-order artificial dissipation coefficient constant, $\kappa^{(2)}$, was also tested due to its importance in the prediction of strong pressure gradient flows. Values between 0.25 and 0.5 were run, but no appreciable difference in results was observed. It was generally concluded that boundary layer development and flow separation due to a strong shock wave/boundary layer interaction could be adequately captured by the employed numerical scheme and turbulence model.

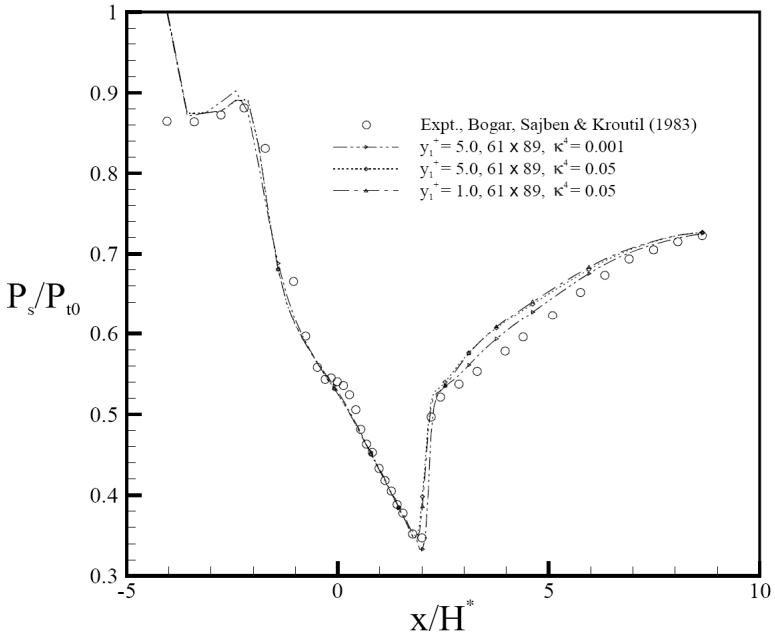

Figure 3-15: Predicted static pressure for separating transonic diffuser.

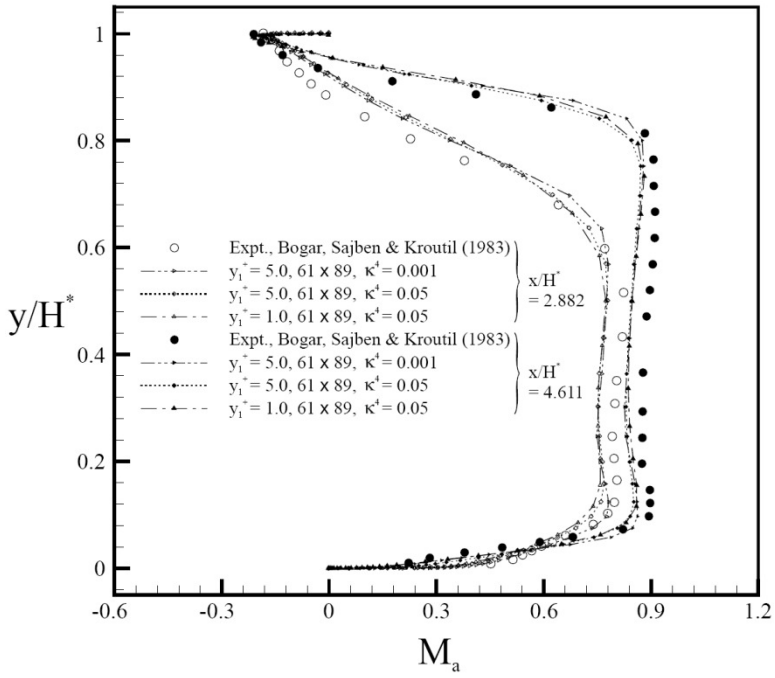

Figure 3-16: Predicted velocity profiles for separating transonic diffuser.

3.1.6 Mach 4 Asymmetric Crossing Shockwave Flow

The Mach 4 asymmetric crossing shockwave flow of Zheltovodov and Maksimov (1998) was studied next. It was chosen to test the ability of the employed numerical scheme and turbulence model to predict flow separation due to a strong high Mach number shockwave/boundary layer interaction. In this experiment, two wedges of dissimilar angle were mounted on a flat plate in a supersonic wind tunnel. Flow separation occurs downstream of the crossing of two strong oblique shockwaves intersecting the plate boundary layer.

Geometry and operating conditions are listed in Table 3-5. Three grids were implemented, Table 3-6, to test sensitivity to spatial resolution. The computational domain was configured to include regions upstream, downstream, and at the sides of the wedges to emulate the configuration of a compressor blade row, see Figure 3-17. Uniform static conditions were set at the inflow boundary, and a turbulent boundary layer was developed upstream of the wedges by a slip wall and flat plate configuration similar to that of the first test case. The outflow boundary was set to a supersonic condition which extrapolates all quantities from the upstream domain. Side and top boundaries were set to inviscid walls.

Table 3-5: Asymmetric crossing shockwave geometry and operating conditions used in simulations.

Upstream plate length	Throat width	Wedge angles	Upstream Mach number	Re_θ
0.21 m (8.27 in)	0.032 m (1.26 in)	7° x 11°	3.89	5.1×10^3

Table 3-6: Grid details for asymmetric crossing shockwave flow simulations.

# streamwise	# pitchwise	# spanwise	y_1^+	# in boundary layer	$\kappa^{(4)}$
369	193	129	0.2-1.8	81	0.05
185	97	65	0.5-3.5	41	0.05
93	49	33	1-7	20	0.05
93	49	33	1-7	20	0.001

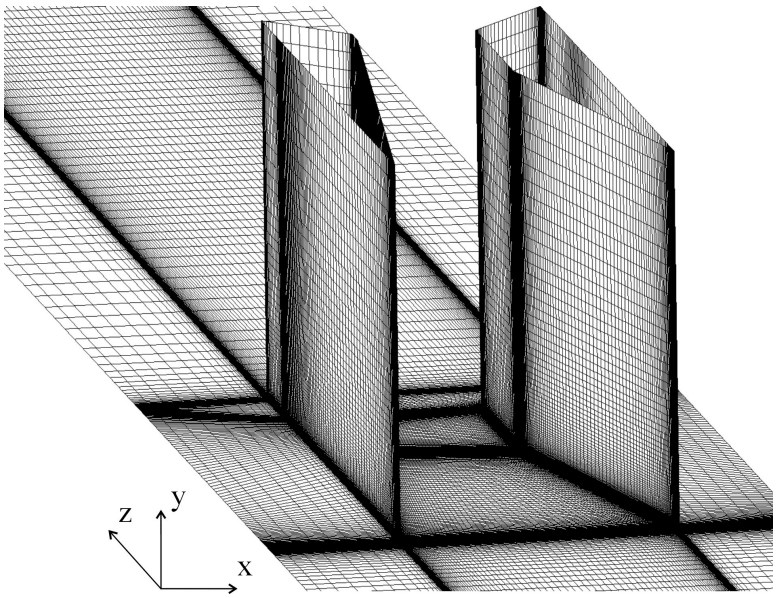

Figure 3-17: Asymmetric crossing shock wave flow computational grid used in simulations. The finest resolution is shown in this image.

Figure 3-18 qualitatively displays the change in prediction as grid density is coarsened. It is evident that the basic physical structure of the shock system is maintained while resolution is decreased. The same is true for predicted streamwise loss generation due to the interaction between these shockwaves and the plate boundary layer. This loss mechanism is illustrated in Figure 3-19 in terms of surfaces of constant streamwise vorticity. A large streamwise vortex is shown to form at the leading edge of the 11° wedge, grow, and then lift off the surface downstream. A smaller streamwise vortex of opposite sense is shown to be generated in the same manner by the 7° wedge. Note that these are displayed separately because the negative sense vortex is wrapped tightly around the other making it difficult to distinguish the two when superimposed. Figure 3-18(b) therefore indicates that the same basic mechanism of boundary layer separation and streamwise vorticity production results from the three grids, but that coarser resolution predicts a somewhat smaller extent of separation. The same trend is observed when comparing limiting plate surface streamlines in Figure 3-20 with that inferred from the experimental oil flow visualization reproduced from Zheltovodov and Maksimov (1998). Following the methods of such researchers as Kelso *et al*. (1996), lines of separation and reattachment are identified as negative and positive bifurcation lines (NBL and PBL), respectively. Separation is seen to occur at the junction of the two oblique shockwaves and the

plate boundary layer (NBLs 1 and 2), followed by a stronger convergence of streamlines downstream nearer to the 7° wedge (NBL3). The largest zone of reattachment exists nearer to the 11° wedge (PBL2), and the next largest occurs adjacent to the 7° wedge (PBL1). These streamline patterns are entirely consistent with the three dimensional vortex structures shown in Figure 3-19, which provides further evidence that the mode of flow separation has been captured in these simulations. It can be seen that the density of streamlines in the separating zones decreases with coarser grid resolution, see Figure 3-20b-d, but the two finest grids produced almost identical results.

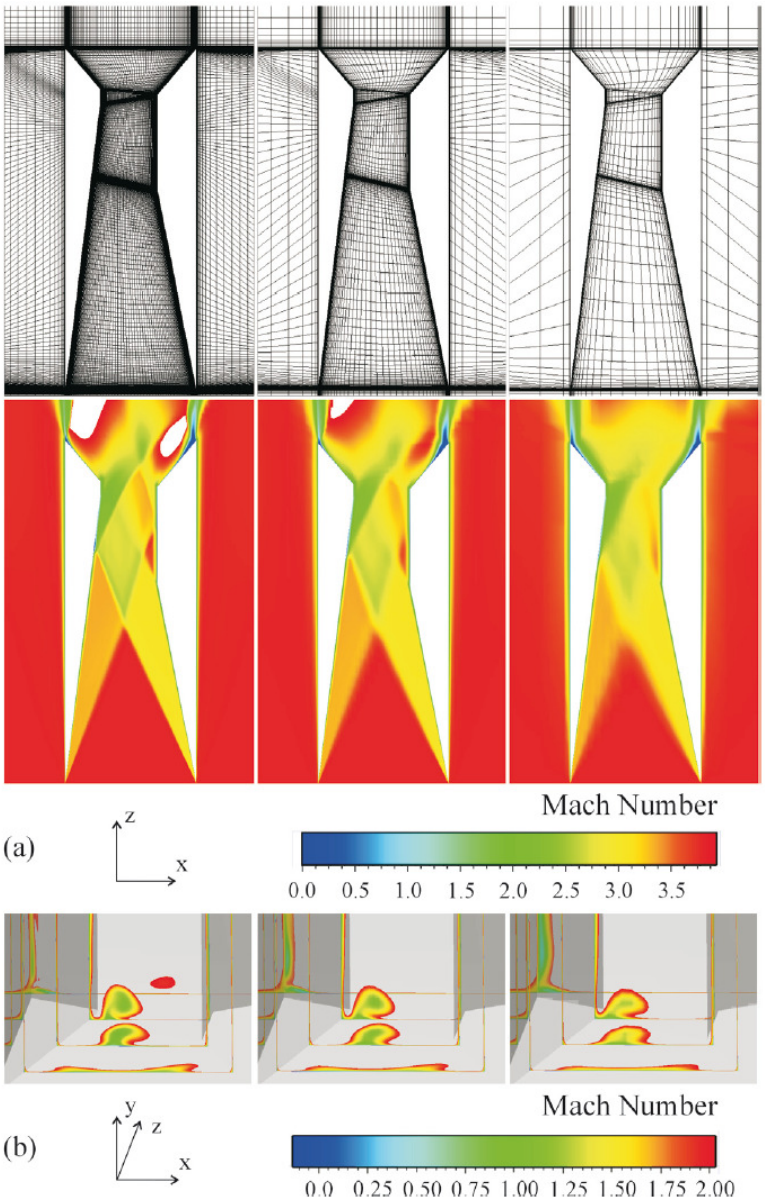

Figure 3-18: Asymmetric crossing shockwave flow sensitivity of shock structure prediction to grid resolution. Figure a shows the Mach number at midspan while figure b indicates streamwise vortex production. The finest to coarsest grids are from left to right.

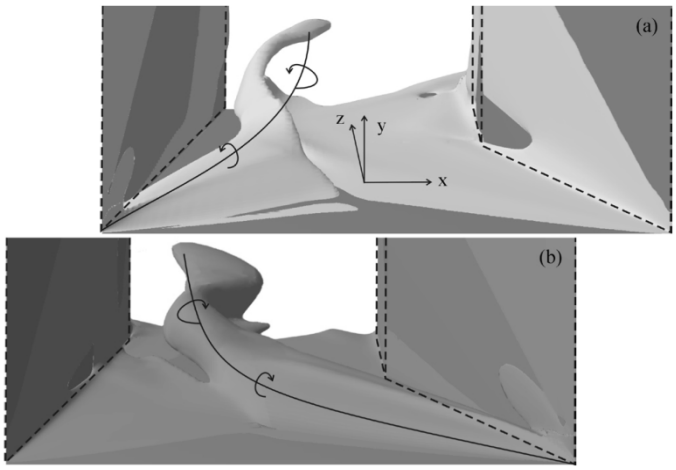

Figure 3-19: Shock induced separation prediction using iso-surfaces of (a) negative vorticity and (b) positive vorticity.

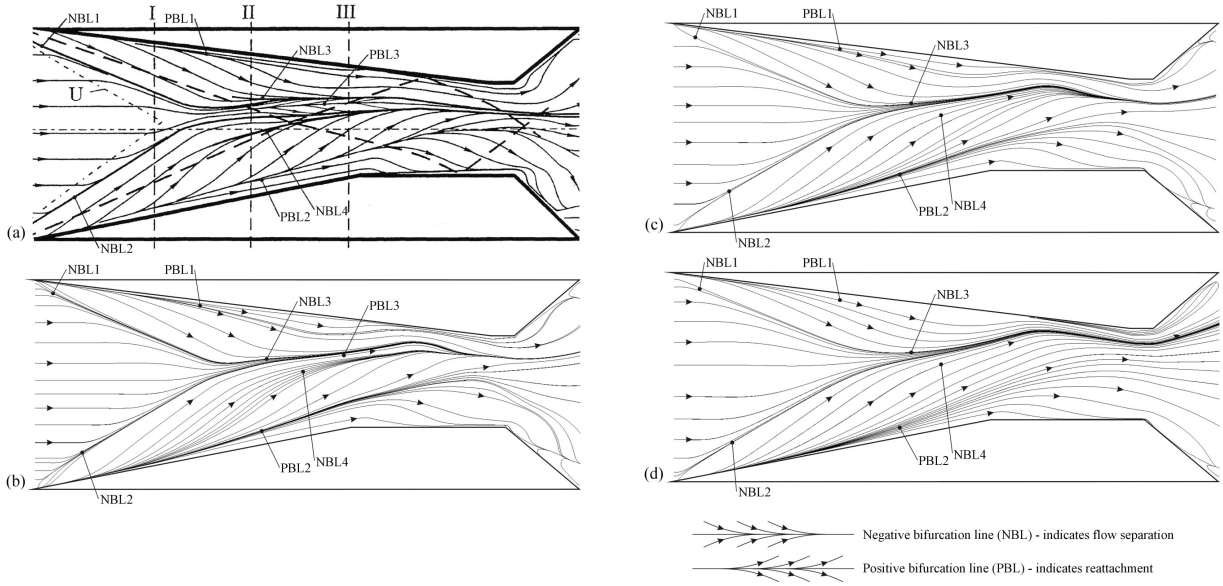

Figure 3-20: Shock induced separation prediction using limiting surface streamlines. Figure (a) shows the experimental results while figures (b)-(d) show the finest to coarsest grids, respectively.

Comparisons between static pressure ratio predictions and experiment are shown in Figure 3-21. The left figure displays streamwise pressure prediction along the plate centerline between the wedges, while the right compares cross stream profiles taken between the leading edge and throat at 24%, 41%, and 58% of wedge length (indicated as I, II, and III in Figure 3-20a). Static pressure measurements were taken in the experiment, while velocity profiles were not. The two finer grid levels result in very good agreement with the measurements, and in a manner consistent with predictions of such authors as Thivet *et al*. (2001). A 'flatter' set of pressure profiles produced from the coarsest level verifies the suggested underprediction of shockwave induced separation by the previous figures. As in the incompressible separation test case, it was found that decreasing the third-order artificial dissipation coefficient constant, $\kappa^{(4)}$, improved prediction accuracy for the coarsest grid. However, this did not result in an identical

solution to the finer grids, thus indicating a necessary threshold of grid resolution one should not go below when simulating shockwave/boundary layer interaction. Note that a range of values were tested for the first-order artificial dissipation coefficient constant, $\kappa^{(2)}$, since it controls the pressure switch that is activated in the presence of shockwaves. However, lower values were not found to make a noticeable improvement in prediction while resulting in lower solution stability. A limitation of the employed spatial discretization scheme is that it reduces to first-order accuracy in the presence of shockwaves. Remedies to such a situation range from employing a high order scheme to employing a grid adaptation method. The grid refinement study performed here is essentially a crude version of the latter. It was generally concluded that flow separation due to a complex interaction of strong oblique shockwaves in high supersonic flow could be adequately captured by the employed numerical scheme and turbulence model, and grid resolution requirements were noted.

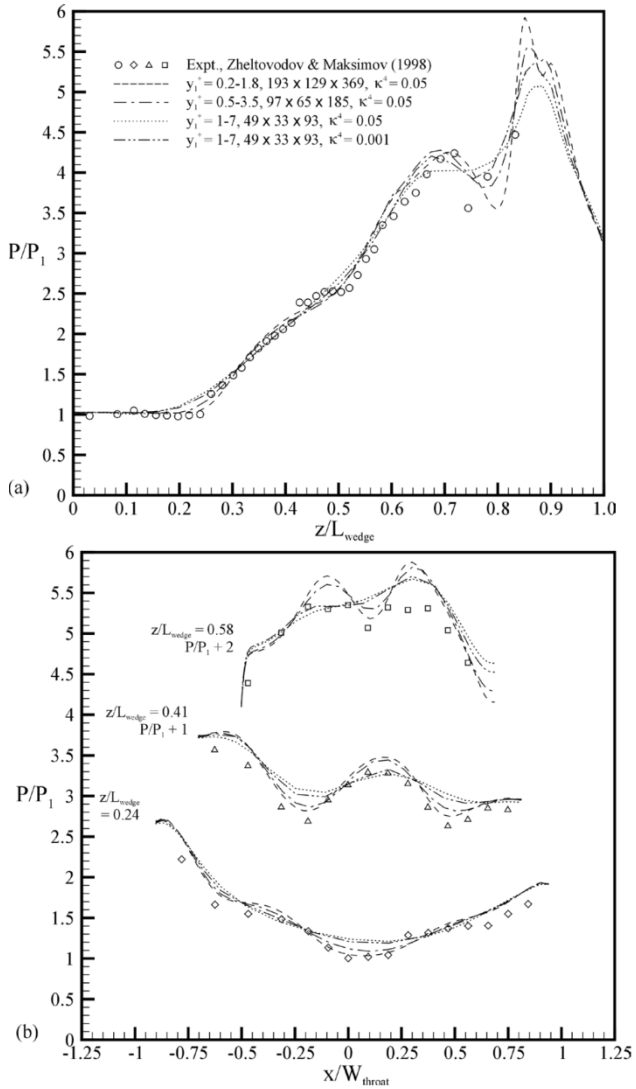

Figure 3-21: Asymmetric crossing shockwave flow prediction of platform static pressure distribution at (a) centerline and (b) cross stream.

3.1.7 Transonic Fan Rotor Flow

The transonic fan rotor flow of Strazisar *et al*. (1989) is presented last. The previous test cases have been studied to individually determine prediction criteria of and ability for a number of phenomena that result in losses in the passage of such a transonic compressive rotor. It was chosen to test the conclusions made above regarding the prediction of boundary layer development, strong adverse pressure gradient and shock induced separation for the case of a transonic compressive rotor. Remaining phenomena that exist in this flow are that of the tip clearance leakage and rotational effects. Considerable study has been previously given of tip clearance flow prediction by such authors as Hah *et al*. (2004) and Van Zante *et al*. (2000). In this experiment, the transonic fan rotor known as Rotor 67 was run from choke to near stall as an isolated rotor. Experimental measurements were first taken for this fan in 1984, and newer ones have since been taken in 2004. It is likely the most thoroughly measured transonic compressive rotor available, and a wealth of CFD predictions of its performance have been published over the last decade and a half since the data was first published. Examples include the earlier work of Chima (1991), Jennions and Turner (1993), Arnone (1994) and more recent studies that concentrate on inverse design and optimization techniques by such authors as Dang *et al*. (2000), Li *et al*. (2004) and Pierret *et al*. (2007). This type of configuration coupled with both the high quantity and quality of measurements taken makes it a particularly good test case to study rotor loss prediction alone, as opposed to that for a stage. Note the distinction of 'near' stall is made, as all simulations described herein were run as steady flows. While many have already performed detailed CFD studies of Rotor 67, most have concentrated on the peak performance condition. The following analysis and discussion focuses on the near stall regime with particular attention given to shockwave/boundary layer interaction and the influence of the casing endwall.

Geometry and operating conditions are listed in

Table 3-7. Note that the tip clearance value has been updated by the authors since this test case was presented in the reference cited above and others such as that of Wood *et al.* (1990). Three grids were implemented, see Table 3-8, to test sensitivity to spatial resolution. Figure 3-22 displays the three-dimensional rotor computational grid employed. Note that a single blade passage was modeled, and periodic boundary conditions were employed to reproduce the 360^{o} row. A complex multi-block structure consisting of an O-type grid surrounding the blade, and H-type grids upstream, downstream, and at either side were employed in order to maximize grid quality (e.g., minimize skew of grid cells).

Table 3-7: Transonic fan rotor geometry and operating conditions used in simulations.

# blades	Tip radius at leading edge	Hub/tip ratio	Tip clearance	Corrected speed	Re_θ
22	25.7 cm (10.1 in)	0.375-0.478	0.61 mm (0.024 in)	16,043 rpm	23×10^3

Table 3-8: Grid details for transonic fan rotor flow used in simulations. The grid numbers listed are approximate due to O-H-H-H-H topology.

# streamwise	# pitchwise	# spanwise	# tip clearance	y_1^+	# boundary layer	$\kappa^{(4)}$
641	81	193	33	0.1-0.5	77	0.05
321	41	97	17	1-5	39	0.05
161	33	49	9	1-5	20	0.05

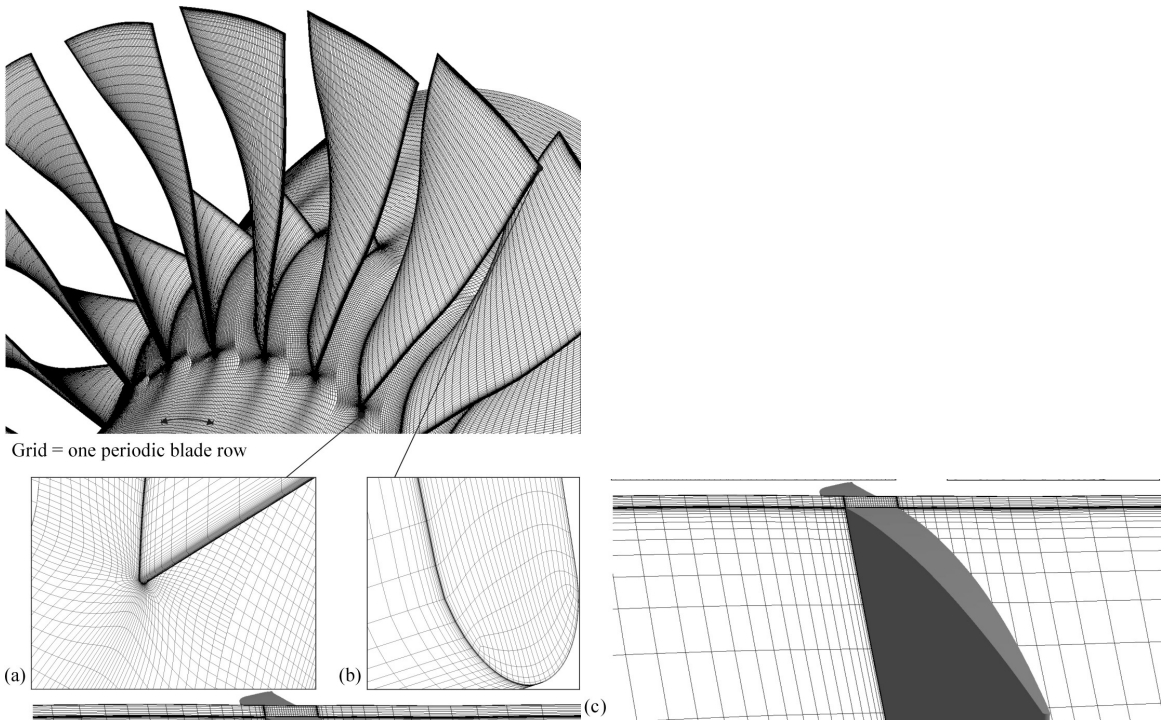

Figure 3-22: Transonic fan rotor flow computational grid used in simulations. The intermediate resolution is shown here. Figure (a) shows the leading edge at the hub. Figure (b) shows the leading edge at the tip. Figure (c) shows the spanwise grid distribution in the tip clearance region.

In constructing the grid, rules of thumb established by previous authors were applied. For instance, Casey (2004) stated that "a minimum of 15 points in the boundary layer is needed to capture details of the boundary layer flow" and that "A minimum of 10 grid points across specific flow details is necessary (tip clearance, local vortices, cooling holes)." Although such guidelines are not often published, these statements are consistent with previous observations (e.g., Yaras and Grosvenor, 2003) and the previous test cases presented herein. The importance

of following such criteria is discussed by Van Zante *et al*. (2000), "The wall-bounded shear layer can have a major impact on the rotor stability depending on its strength. Therefore accurate prediction of stable operating range requires careful attention to grid resolution near the casing." Resolution of the passage shock system is also highly important. However, blade passage grid refinement has been conducted in a non-preferential way. The average CFD practitioner would not spend several iterations of grid generation and simulation to determine where exactly they could cluster grid points to the shock system (unless one were running an automated adaptation procedure in which case the issue of shock refinement would already, by definition, be addressed). It is therefore of interest to know the impact of such an essentially uniform resolution of shockwave(s).

Profiles of total pressure and total temperature were specified at the inflow boundary based on the experimental measurements. The exit mass flow was set to a range of values, approximately 30 to 34.5 kg/s (66 to 76 lbm/s), to produce a constant speed line, and all other flow properties were extrapolated from the interior of the computational domain. A real gas definition of air, defined by a look up table, was used for the working fluid.

Comparisons of Mach number distributions are given in Figure 3-23 and Figure 3-24 at 10% span from the blade tip for two operating points representing maximum efficiency and near stall conditions, respectively. Prediction of leading edge and passage shock structure and spot values of relative Mach number in key areas are shown to be consistent with experiment (Strazisar *et al*., 1989).

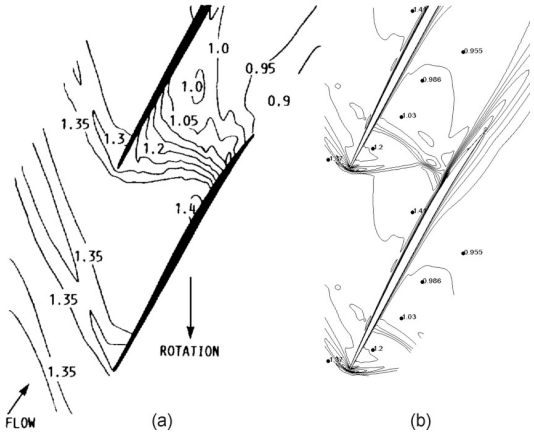

Figure 3-23: Mach number contour prediction near peak efficiency for transonic fan rotor at 10% span from tip. Figure a shows the experimental results while figure b shows the cfd simulation results.

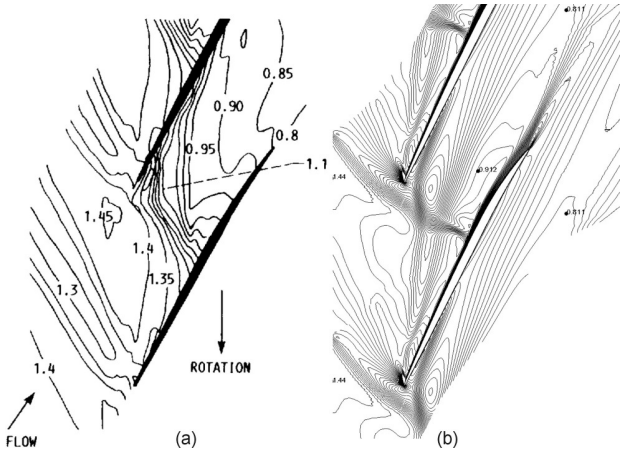

Figure 3-24: Mach number contour prediction near stall for transonic fan rotor at 10% span from tip. Figure a shows the experimental results while figure b shows the cfd simulation results.

Comparisons between predicted and measured constant speed line performance are shown in Figure 3-25 and Figure 3-26. Three different grid resolutions were run at eight mass flows and compared in terms of mass averaged pressure ratio and adiabatic efficiency. Spline fits of these results are presented. Note that only the coarsest grid resolution result was integrated at the experimental rake element locations. No such measurements were taken near the endwalls which would tend to neglect endwall related losses such as the tip clearance leakage flow. It was found that integrating the numerical predictions only at the rake immersions tended to collapse the results of different resolutions closely together. Since it was intended to show the effect of grid resolution on these predictions, annulus mass averaged quantities are compared at the three resolutions, and the coarsest one is shown in terms of rake integration as well in order to demonstrate quantitative prediction. Pressure ratio and efficiency near peak performance are shown to be predicted almost identically by the two finest grid levels, with slight variation observed near stall. The predicted choke point was almost identical for all three grids. The coarsest grid produced a comparable pressure ratio prediction to the finer grids, while the predicted efficiency was notably lower near stall. More importantly, as mass flow was reduced approaching stall, the solution for this coarsest grid began to oscillate sooner than the finer grids. It is not uncommon for CFD practitioners in a compressor group to use such oscillations as an indication of stall. In this case, the indicated stall margin would clearly be less than reality due to the lower grid resolution. The coarse grid result shown in terms of integration at the experimental rake locations exhibits reasonable agreement with measurements at higher flows. From interaction with several gas turbine manufacturers, it is clear that the coarsest grid tested in this study, 240,000 cells, is of the resolution level that would be used for design cycle analysis, or within a shape optimization framework. This is sufficient when the concentration is on peak performance, but resolutions closer to the level of the intermediate grid tested here, 1.2 million cells, should be considered for detailed studies of off-design performance (e.g., studies of endwall boundary layer augmentation for the improvement of compressor stability).

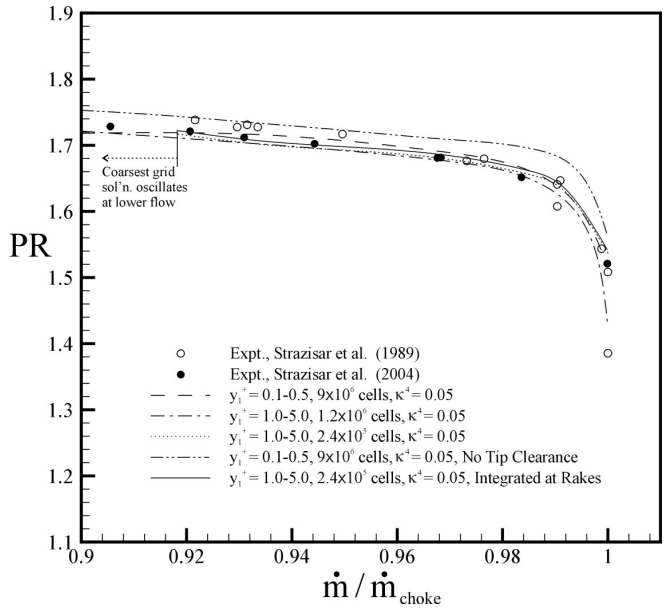

Figure 3-25: Transonic fan rotor flow simulation predicted pressure ratio.

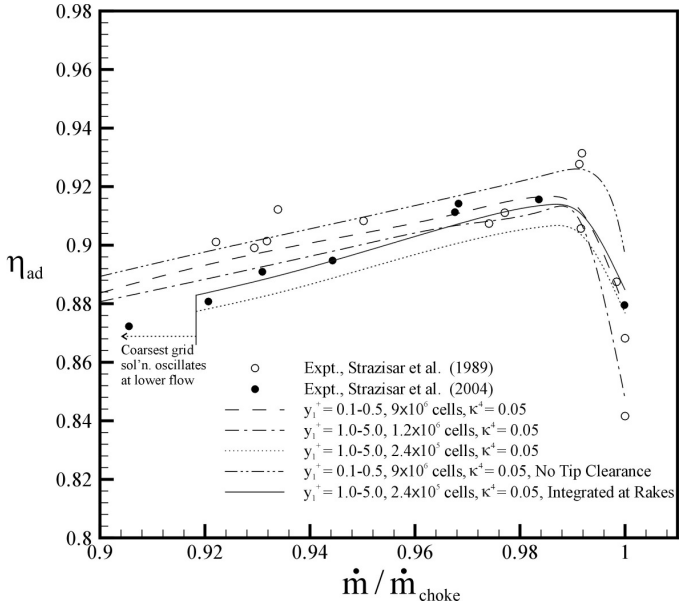

Figure 3-26: Transonic fan rotor flow simulation predicted efficiency.

Note that the speed line plots contain two sets of experimental data. The first is the well known original data (Strazisar *et al*., 1989). Additional experimental measurements have since been taken at NASA Glenn Research Center (Strazisar, 2006). Some differences between the two tests should be noted. The original data was acquired with a non-rotating centerbody upstream of the rotor, and a three strut inlet supporting that centerbody. Thus, there were strut wakes and a relatively thin hub boundary layer feeding into the rotor. In 2003 NASA Glenn Research Center upgraded the Rotor 67 test rig by eliminating the upstream centerbody and struts and installed a nosecone on the rotor which resulted in minimal hub boundary layer (Strazisar, 2006). The numerical prediction results presented herein were produced by simulating the rotor only without a nosecone. Only the section of hub that existed in the blade

passage was set to rotate. However, the hub boundary layer growth upstream of the rotor observed in these simulations was small.

The finest grid run in the present study was used to determine the impact of tip clearance on these results by removing just the grid blocks that existed in the clearance over the blade tip. As shown in the figures, this result over predicts maximum performance quite significantly. In contrast with the other simulations, averaging based only on rake locations was found in this case not to make a large difference in prediction thereby further highlighting the importance of tip clearance. Note that the original speed line measurement data exhibits three peak efficiency points at essentially the same mass flow. Due to this apparent scatter and absence of the higher values in the more recent 2004 data, it is assumed herein that greater confidence should be placed on the low experimental peak values.

Profiles of exit total pressure, total temperature, and flow angle are compared in Figure 3-27 to Figure 3-29. Prediction is shown to be close to the measurements for all grids, with the particular exception of near the endwalls for the coarsest grid. At the near stall condition, shape factor of the shroud boundary layer is plotted along the passage centerline as well as the integrated mass averaged blade passage relative total pressure loss. Impact of the unstarted passage shockwave, see Figure 3-24, is highlighted in these plots by a rapid increase of shroud boundary layer shape factor through separation and an accompanying rapid increase in loss starting just upstream of the leading edge. A striking difference in shape factor prediction is shown between the three grid resolutions with tip clearance and the one without indicating that, with no gap, flow does not separate at the shroud. The difference in loss generated between the configuration with tip clearance and without is consistent with the difference in performance shown in Figure 3-25 and Figure 3-26. Also note from the comparison of loss integrated from the hub to 80% span versus 100% in Figure 3-30 and Figure 3-31 that there is an apparent dominance of the shock system near the blade tip in generating loss. Lastly, note the impact of decreasing resolution shown in Figure 3-31 to produce higher estimation of losses which is consistent with the lower predicted efficiencies displayed for the coarser grid in Figure 3-26.

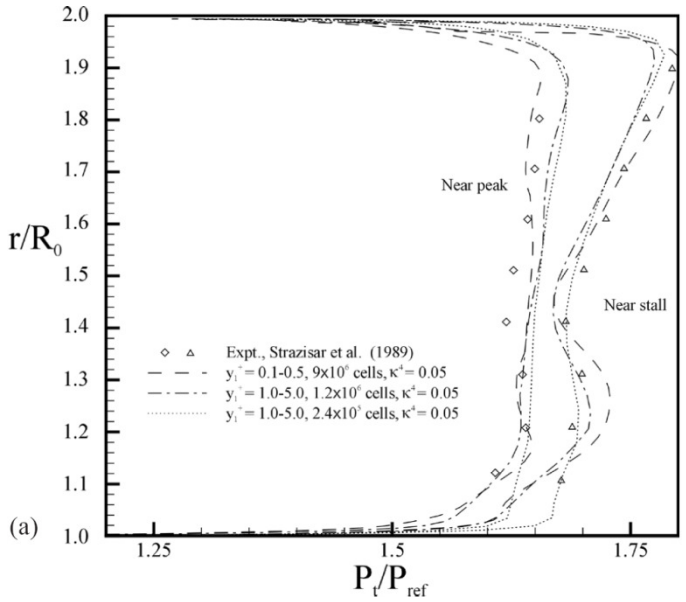

Figure 3-27: Transonic fan rotor flow predicted total pressure ratio profile.

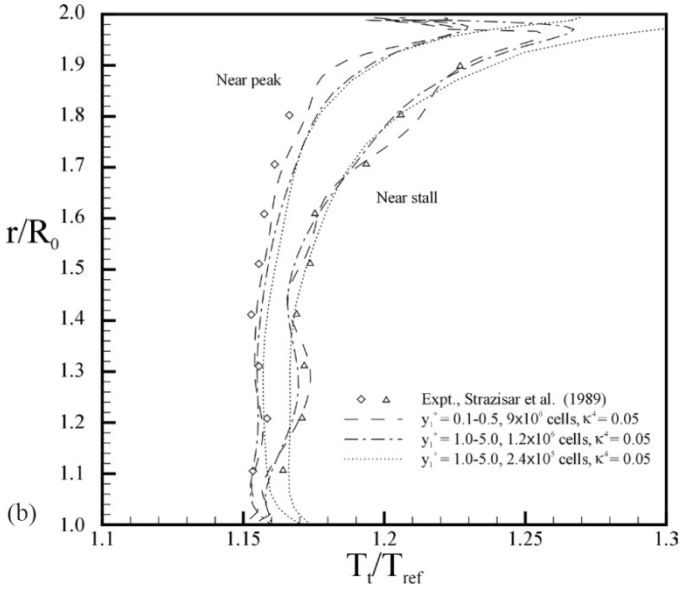

Figure 3-28: Transonic fan rotor flow predicted total temperature ratio profile.

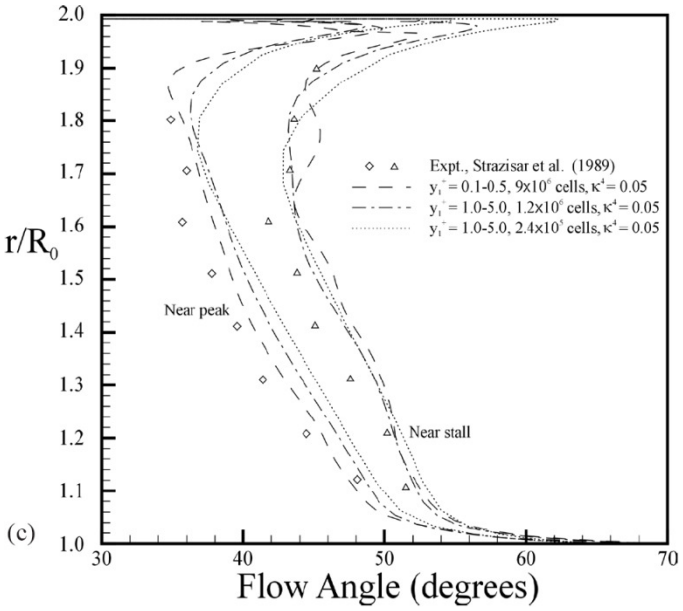

Figure 3-29: Transonic fan rotor flow predicted exit angle profile.

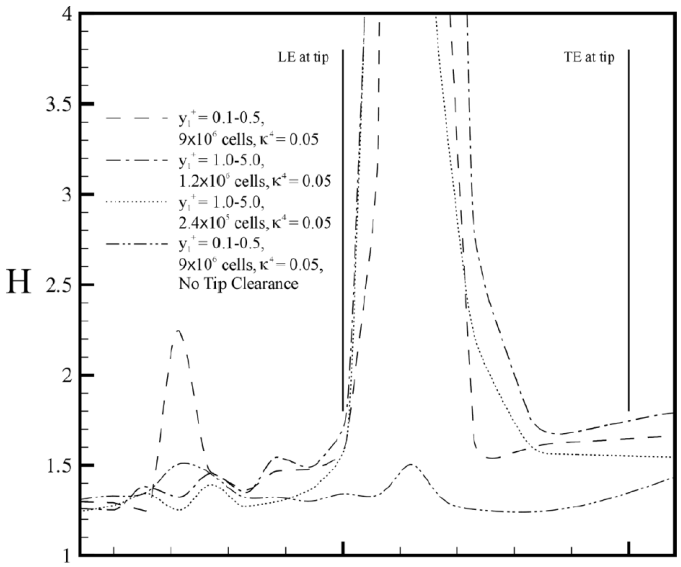

Figure 3-30: Loss generation near stall, shroud boundary layer shape factor along passage centerline.

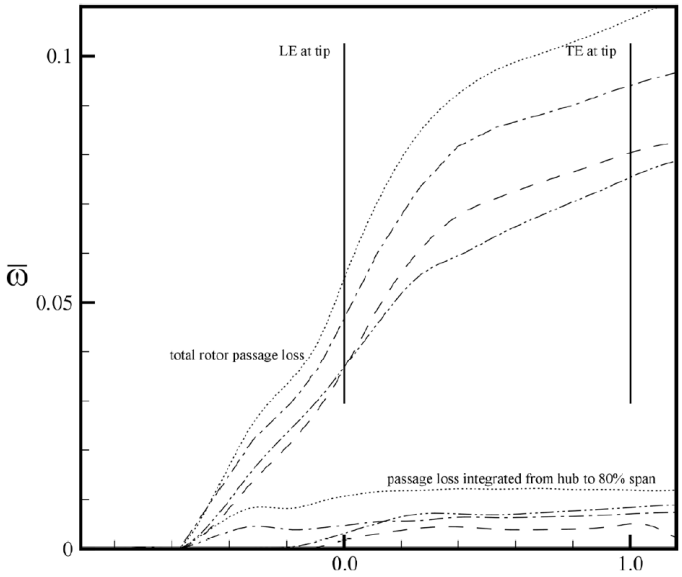

Figure 3-31: Loss generation near stall, mass average relative total pressure loss along passage centerline.

In general, the numerical scheme and turbulence model employed were found to adequately capture the leading edge and passage shock structure of this transonic axial fan rotor. It was found here that resolution requirements of 'building-block' type test cases such as those presented above could be used to guide successful grid generation for such a transonic compressive rotor.

3.1.8 CFD Test Case Conclusions

Test cases have been simulated via RANS CFD to demonstrate the prediction of boundary layer development and separation due to adverse pressure gradient and shockwave/boundary layer interaction that dictate the generation of total pressure losses in

transonic compressor rotors. Particular attention was paid to the near stall condition and the interaction of the passage shock system with the shroud boundary layer and tip clearance leakage fluid. Some important results of this effort have been:

- The Jameson-Schmidt-Turkel type of explicit scheme and Spalart-Allmaras turbulence model have been validated for the fluid physics present in the Rampressor flow path. This turbulence model has shown itself to be an excellent engineering tool for the analysis of such turbomachinery due to its adequate prediction accuracy and numerical robustness.
- The results of this study made it clear that, while the physical mechanisms contributing to losses in a transonic compressor can be adequately predicted by the type of scheme employed, more than one grid should be tested for a given design. While it should not be surprising to the practitioner that grid resolution sensitivity should be tested, the impact of low resolution in such regions as the casing boundary layer and tip clearance was demonstrated. The grid resolution that may be required for a given study is dependent on the type of spatial discretization scheme employed and resultant amount of artificial diffusion imposed on the solution. The coarsest grid tested in this study (240,000 cells including 20 cells in the endwall boundary layer and nine in the tip clearance) is of the level of resolution that would be used for design cycle analysis or within an optimization framework in industry. This is sufficient when the concentration is on peak performance, but resolutions closer to that of the intermediate grid tested (1.2 million cells including 39 cells in the endwall boundary layer and 17 in the tip clearance) should be considered for detailed studies of off-design performance.

3.2 Analysis of the Rampressor Rotor

The potential for one dimensional prediction of losses and ultimate performance of the Rampressor is limited due to the absence of the types of well established correlations and design practices available for conventional turbomachinery design. In fact it is generally accepted that the same is true for any supersonic compressor concept, and that CFD must be relied upon to predict losses in such designs (e.g., Cumpsty and Freeman, 2000).

The numerical scheme and turbulence model described in section 3.1 has been used to verify and refine the Rampressor design described in Williams (2007). Successful prediction of Rampressor rotor performance at design point and off-design requires accurate capture of boundary layer development, diffusing flows and separation, shock wave/boundary layer interaction, and a variety of compressor related phenomena such as tip clearance flow and passage secondary flow vorticity. Validation of the CFD scheme and the Spalart-Allmaras turbulence model presented in the previous section combined with the cited previous validation literature provided reasonable evidence that these features could be adequately captured, and the observations provided direction in what grid resolution should be employed to achieve successful prediction. Using this guidance led to a grid resolution of approximately seven million cells in the Rampressor rotor passage.

3.2.1 Reduced Flow Path Model

Using two dimensional method of characteristics calculations, a number of candidate designs were developed that were intended to capture inflow at an approximate Mach number of

2.4 and use a series of oblique shock waves to compress and decelerate the flow to a low supersonic Mach number at the flow path minimum area or throat. At design pressure ratios, a normal shock would be stabilized downstream of the throat intended to decelerate the flow to subsonic Mach numbers. The flow would then experience additional subsonic diffusion until the desired rotor discharge Mach number was achieved.

In order to compare designs and assess their performance relatively quickly, a reduced model with fewer grid points than the full rotor model was developed that encompassed only the section of flow path between rotor leading edge, and a short distance aft of the trailing edge. Figure 3-32 identifies components of the rotor included in the model, and the location of boundaries. This model was used primarily to evaluate shock structures developed by different flow paths, rather than other phenomena listed above, such as tip clearance and secondary flows. The flow field is based on a geometry where the strake surface used to define the upstream boundary of the flow path has a sharp leading edge and the wall itself has no thickness. This simplification eliminates the generation of a leading edge bow shock. Slip surfaces were applied at the rim, shroud, and strakes. Velocity vectors, static temperature, and low turbulence intensity (~1%) were specified at the inflow boundary to produce Mach 2.4 flow with zero incidence to the strakes, and a radial equilibrium distribution of static pressure was set at the outflow boundary. A real gas definition of air was used for the working fluid.

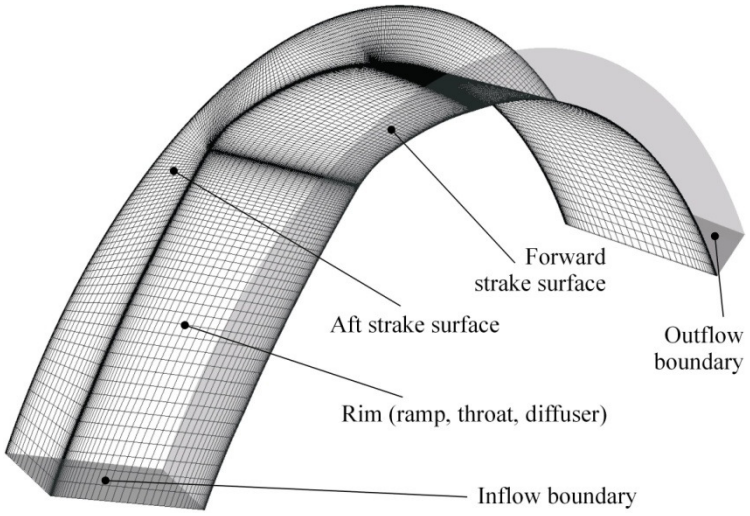

Figure 3-32: Computational grid used for reduced flow path model. Note that all solid surfaces were set as slip surfaces.

The general grid structure used for these reduced model simulations is shown in Figure 3-32. A large number of design variations were considered using the baseline grid resolution displayed in the figure, of approximately 3×10^5 nodes (233 streamwise, 29 spanwise, and 49 pitchwise). However, to obtain a more detailed picture of the compression ramp shock structure, a limited number of simulations were run at a much higher resolution of approximately 11×10^6 nodes (889 streamwise, 113 spanwise, and 113 pitchwise). In this case, the grid distribution was nearly uniform in the pitchwise and spanwise directions with a bias of streamwise resolution toward the ramp section.

Figure 3-33 displays a comparison of focused and defocused rotor designs predicted using the finer grid resolution. The shock systems are highlighted using constant Mach number

lines superimposed on contours of relative Mach number. The oblique shock waves initiated at the compression ramp are clearly visible as well as the reflected wave system that impinges on the shock cancellation throat (minimum area section) of the flow path. Note that the oblique shock waves are curved due to the rotating machine radial pressure gradient as well as the crossing of waves. The difference in oblique shock structure can clearly be seen, as the focused design produces a superposition of generated shock waves at the first reflection point on the shroud, whereas the defocused design produces several discrete weaker shocks that reflect at a series of streamwise positions.

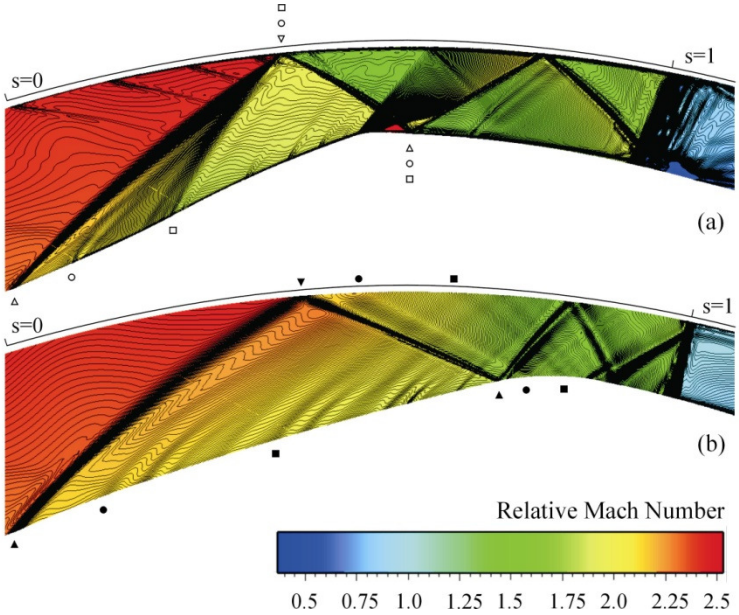

Figure 3-33: Reduced model comparison of the relative Mach number of (a) focused and (b) defocused ramp designs. Symbols indicate three representative oblique shock initiation and reflection points.

The resulting impact on the flow field is indicated in Figure 3-34. The focused design is shown to produce reduction in centerline relative Mach number (and hence increase in pressure) through a series of step changes whereas the defocused design employs a more gradual compression process. Figure 3-35 displays a comparison of centerline absolute total pressure ratio in order to show the impact of different sections of flow path and contrast the ability of the focused and defocused ramp designs to produce pressure ratio. Importance of the terminating normal shock wave in generating pressure ratio is clearly illustrated through a jump in pressure ratio of ~6:1, and it can be seen that the defocused design enables further pressure recovery downstream in the subsonic diffuser.

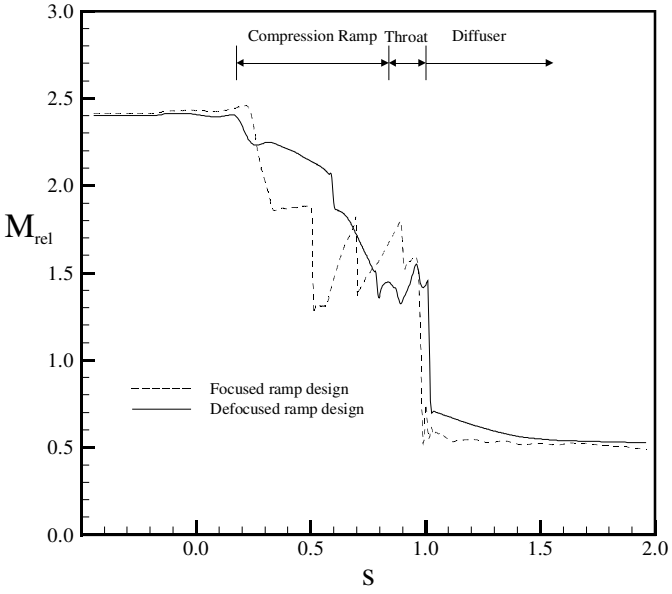

Figure 3-34: Comparison of focused and defocused relative centerline Mach number vs. normalized streamwise distance.

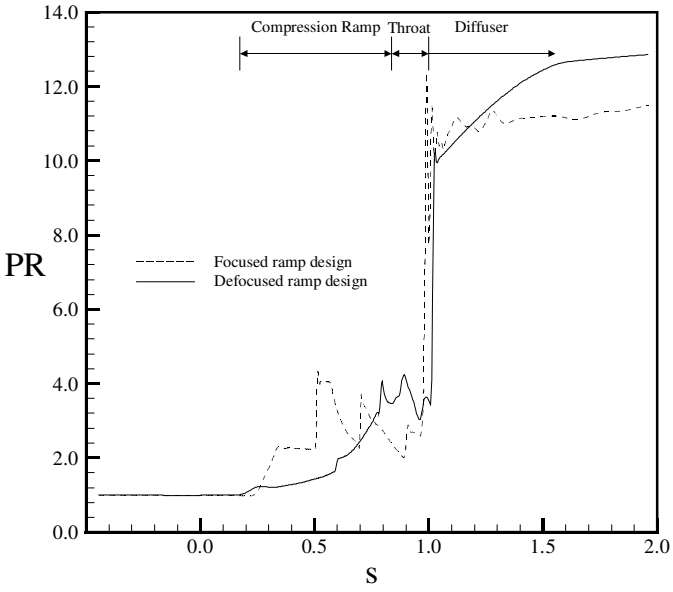

Figure 3-35: Comparison of focused and defocused absolute centerline pressure ratio vs. normalized streamwise distance.

The comparison also illustrates a potential benefit of the defocused shock system for off-design performance. In Figure 3-33(a), the superimposed reflected oblique shocks are shown to intersect the rim at a small distance downstream of the minimum area section (throat) resulting in a local expansion fan and acceleration just upstream of this position. It is much more difficult to design a system that would reflect focused oblique shock waves at an exact desired single location. Another positive feature of the defocused system compared to the focused one is, therefore, a particular suitability to off-design performance, due to the more forgiving distributed system of reflected oblique shocks that do not require an exact intersection point with the rim.

3.2.2 Viscous Rotor Passage Model

The next step of design after reaching an optimum ramp configuration using the reduced flow path was to test the design in presence of boundary layers, leading edge, tip clearance, and other compressor related features. A viscous rotor passage model was constructed. Figure 3-36 displays the computational domain for the rotor flow path and related boundaries. Total pressure, total temperature, flow angle, and low turbulence intensity (~1%) were specified at the inflow boundary to produce Mach 2.4 flow with zero incidence to the strakes, and an average (less reflective) static pressure condition was set at the outflow boundary. All solid surfaces were set as no-slip, with the strake and the axial regions of the rim representative of the rotor width set to design rotation speed. A real gas definition of air was used for the working fluid. Flow control techniques were applied in this design to combat shock wave boundary layer interaction. These devices were included in the present computational model, but they are not described due to their proprietary nature.

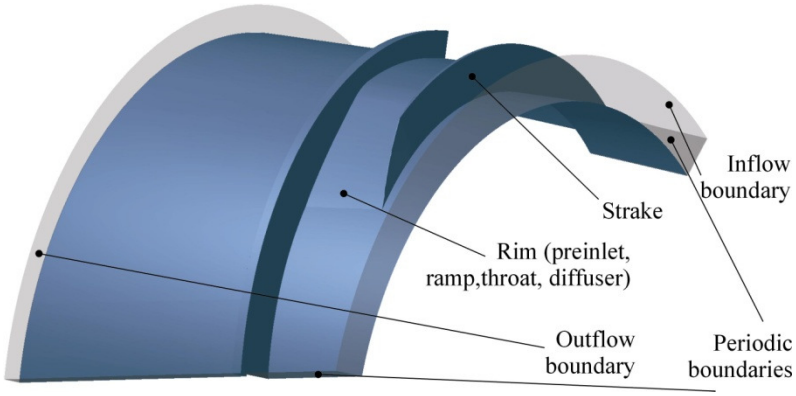

Figure 3-36: Computational domain used for viscous Rampressor rotor simulations.

The computational grid used for the Rampressor rotor defocused flow path simulation is displayed in Figure 3-37, showing rim and strake surfaces. The employed grid resolution was chosen to capture the variety of aerodynamic phenomena discussed earlier, such as passage shock system, secondary, and tip clearance flows. In the rotor passage in between the strakes, 937×65×89 grid nodes were specified in the streamwise, pitchwise, and spanwise directions, respectively. In front of the strakes, 737×33×65 grid nodes were employed, and 297×33×65 grid nodes were set aft of the strakes. The resulting rotor passage grid contained approximately 7.6×10^6 nodes.

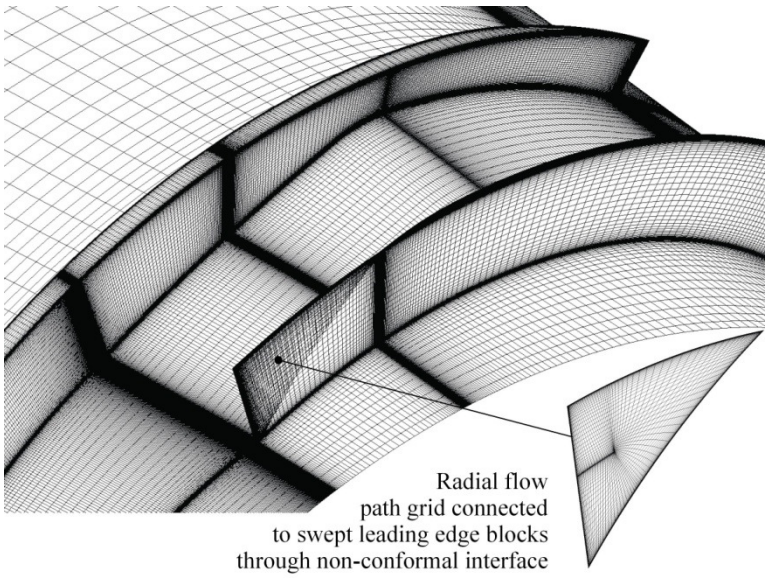

Figure 3-37: Computational grid used for Rampressor rotor simulations.

Clustering of the grid points near solid surfaces in the pitchwise and spanwise directions was prescribed to yield y_1^+ values near to 1. In reality, y_1^+ ranged between 0.1 and 5 in various parts of the passage due to the nature of local acceleration and deceleration of the flow, but it was verified that the grid density and clustering were in line with the findings of the earlier validation studies, such that predictions would not suffer from significant artificial diffusion. The location of the first node from the surface was verified to be in the range needed for the Spalart-Allmaras turbulence model everywhere. In the streamwise direction, clustering was employed to capture the strake leading and trailing edges, as well as the throat curvature.

Note that a non-conformal multi-block grid structure was employed in a few key areas. For instance, grid quality was maximized in the vicinity of the swept leading edge by employing small blocks upstream of the leading edge that were fit to its geometry and interfacing them with the rest of the passage grid that employed radial grid lines in the spanwise direction, as indicated in Figure 3-37. Likewise, the grid structures employed adjacent to each periodic boundary were set up independently of one another, and communication from one to the other was set through non-conformal interfaces. In the case of such interfaces in FINE/Turbo, the connecting surface is decomposed into polygonal elements based on the resolution of mating grid surfaces. The solver calculates fluxes through these elements, and transfers them to corresponding cells on both sides of the connection. Ghost cell values at the interface are then calculated through a weighted averaging procedure to preserve mass conservation (Demeulenaere, 2005).

Viscous rotor passage models of the focused and defocused designs are compared qualitatively in Figure 3-38 in terms of relative Mach number distributions at mid-pitch. Centerline relative Mach number and absolute total pressure distributions are displayed in Figure 3-39 and Figure 3-40. Compared to the reduced flow path model, these simulations incorporated such effects as boundary layers, leading edge shocks, and tip clearance flow. The presence of boundary layers highlighted the importance of minimizing Mach number upstream of the terminating shock to avoid significant flow separation. The leading edge shock was found to be of lower importance for reasons discussed below. Tip clearance, as one would expect in any

kind of rotor with such a high pressure ratio, had a strong influence on performance and produced high levels of blockage at the shroud. Clearances tested ranged from 0.0254 mm (0.001 in) to 0.254 mm (0.01 in). The rotor test rig that has been built employs a translating abradable shroud such that a wide range of clearances can be tested. Tip clearance was identified as a major issue for Rampressor performance at the beginning of the first design program, and ongoing efforts in rotor design and the implementation of flow control techniques are being conducted to minimize its impact, as well as that of other factors such as inflow distortion.

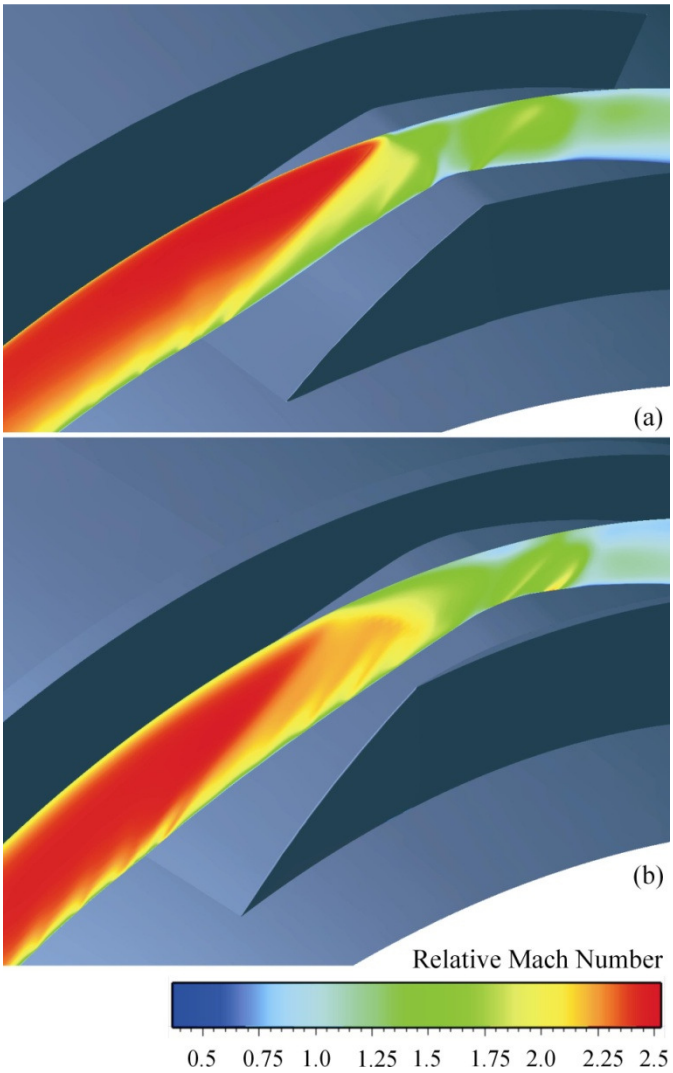

Figure 3-38: Viscous rotor passage model comparison of relative Mach number at mid-pitch for (a) focused (max PR 6:1) and (b) defocused (max PR 8:1) ramp designs.

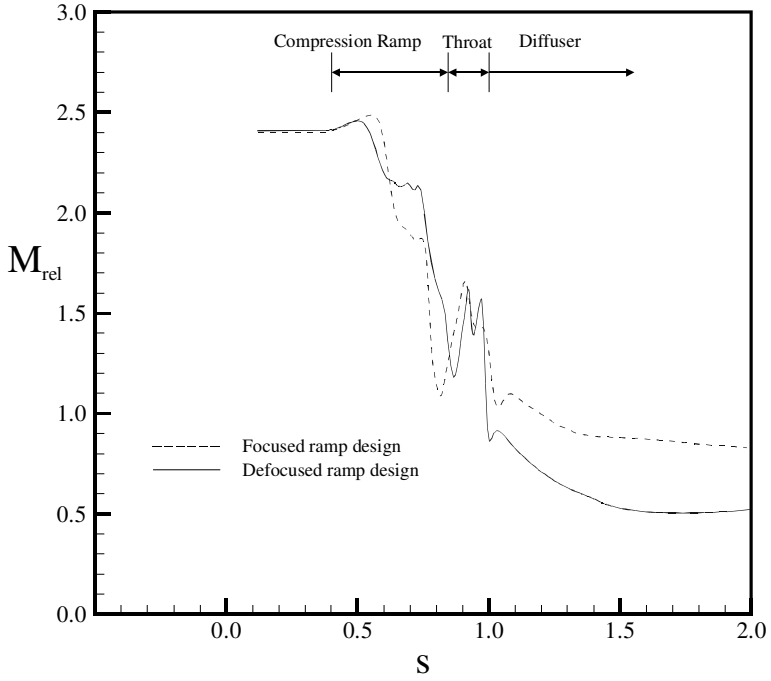

Figure 3-39: Comparison of focused and defocused relative centerline Mach number vs. normalized streamwise distance.

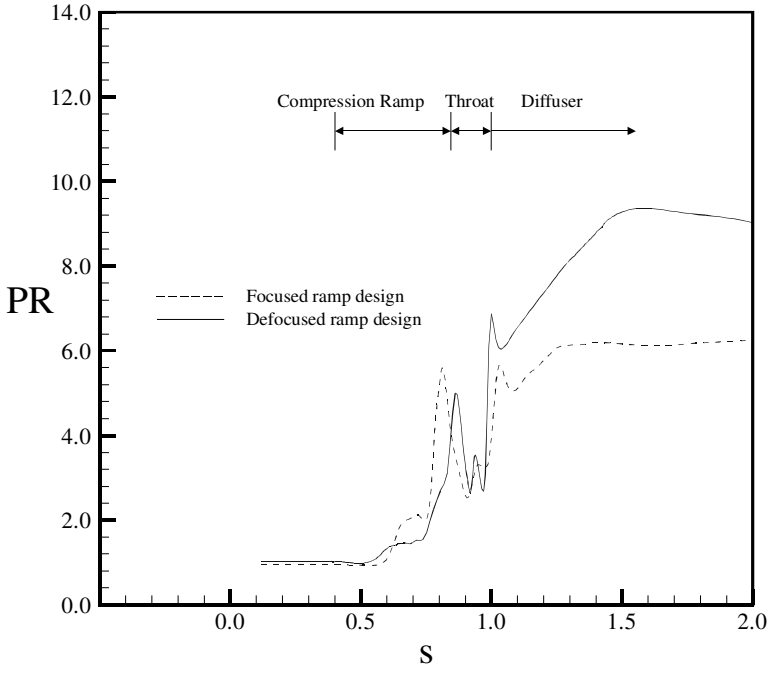

Figure 3-40: Comparison of focused and defocused absolute centerline pressure ratio vs. normalized streamwise distance.

Viscous CFD studies showed intriguing trends regarding boundary layer development in the rotor passage. In contrast to conventional transonic and supersonic rotor designs, the very high hub/tip ratio inherent in the Rampressor design results in essentially no untwist of the strakes due to centrifugal loading which leads to higher flexibility in strake design. A drawback

of the high hub/tip ratio is the resultant close proximity of endwall boundary layers to one another, and a subsequent potential for such a low aspect ratio blade row to suffer from strong secondary flow losses. However, viscous rotor passage CFD studies have shown that the combination of very high stagger and high tip speed results in a shroud that rotates closely aligned to the opposite direction of boundary layer development, and therefore, acts directly to thin the shroud boundary layer. This effect in combination with certain flow control techniques employed in the design tend to compensate for endwall boundary layer development that would otherwise dominate the flow field.

Final selection of ramp design in the present study was made based on the viscous rotor passage simulations. Figure 3-38 shows the focused ramp design produced a stronger set of oblique shocks than the defocused one, as expected from the reduced flow path simulations discussed earlier. The strong impact of boundary layers on the compression process can be seen from a comparison of Figure 3-39 and Figure 3-40 with Figure 3-34 and Figure 3-35. Blockage of the flow path generated by the shock wave/boundary layer interaction decreases the capacity of the normal shock to achieve pressure ratios to 4:1 from a potential 6:1 in the reduced flow path model. With either ramp design, the centerline pre-normal shock relative Mach number was approximately 1.5, which means that further refinement in ramp profile to reduce the value to 1.3 would improve performance of either configuration. Although both Figure 3-39 and Figure 3-40 show an acceleration at the throat for each design, the more gradual compression produced by the defocused ramp resulted in lower boundary layer thickness (i.e., blockage) entering the terminating shock. The result was a stronger interaction with the boundary layers in the focused design compared to the defocused design, which resulted in the development of a series of normal shock waves submerged in high shape factor boundary layer fluid (a shock-train) in the diffuser section of the rotor passage rather than a single terminating shock. The defocused ramp introduced a cleaner flow to the diffuser, leading to the higher pressure recovery shown in Figure 3-40. Results shown for the defocused ramp design result are for a 0.0254 mm (0.001 in) tip clearance. Sensitivity of the focused design to tip gap was so much higher than the defocused, that its performance deteriorated dramatically at any gap height. The focused ramp design result is therefore shown for the no tip clearance case.

Impact of ramp designs was shown to be highly important in terms of achievable pressure ratio. The rotor with the focused ramp design produced a maximum mass averaged exit plane pressure ratio of 6:1, whereas the rotor employing the defocused ramp design reached 8:1.

A series of CFD analyses were performed to characterize performance of the manufactured test hardware. These analyses included studies of the inflow passage length upstream of the inlet guide vanes, impact of struts upstream of the inlet guide vanes (IGV), variation of IGV performance with mass flow, impact of IGV endwall losses on Rampressor rotor performance, and impact of tip clearance on rotor performance. Sensitivity of rotor performance prediction to grid resolution was also tested.

Due to the test rig mechanical design that enabled translation of the rotor shroud to control tip clearance, while enabling access for rotor installation and extraction, the annulus upstream of the inlet guide vanes was overly long. Dimensions are given in Figure 3-41.

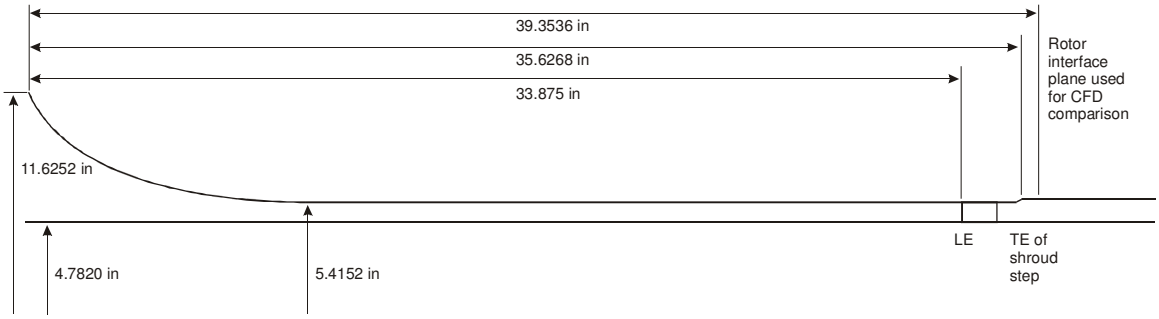

Figure 3-41: Bellmouth and annulus leading to inlet guide vanes.

It was found that the boundary layer growth in this annulus, in conjunction with the particular blade design, led to significant secondary flow losses. Note that a backward facing step existing downstream of the IGV at the junction of the IGV shroud and the translating rotor shroud tended to exacerbate this loss at the shroud. The computational grid employed and, subsequently, predicted flow field is depicted in Figure 3-42 and Figure 3-43, respectively.

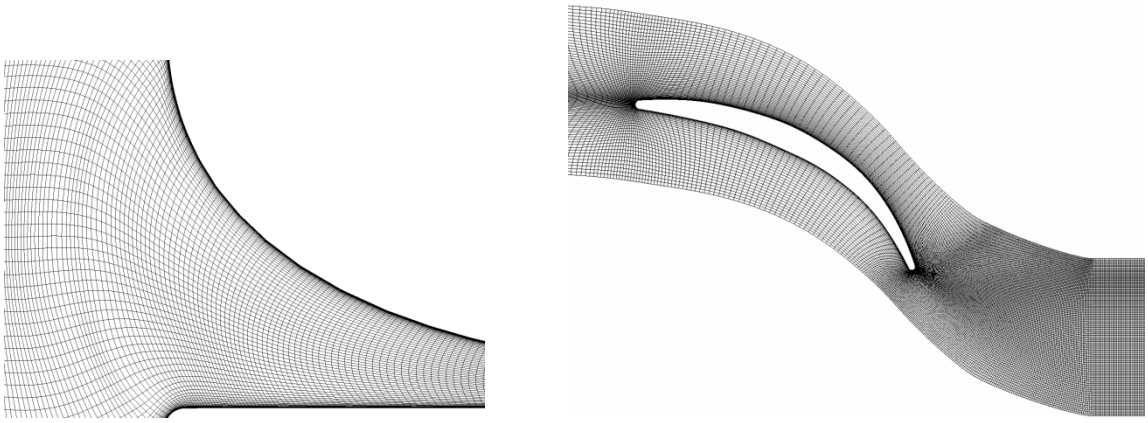

Figure 3-42: Bellmouth and inlet guide vane grid resolution.

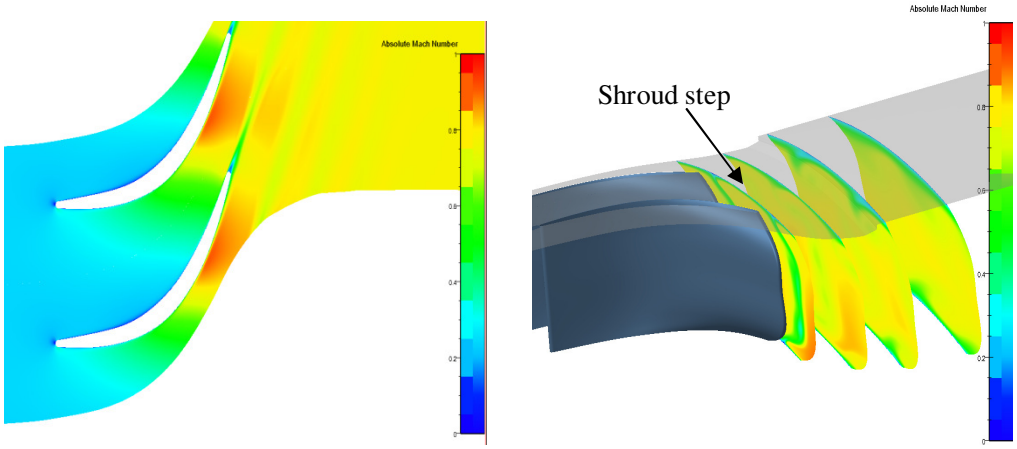

Figure 3-43: Inlet guide vane blade to blade and exit plane Mach number distributions.

Evidence of the IGV secondary flow was plainly seen at the hub from convective heat transfer. The hub existed at a higher temperature than the main flow, due to its proximity to bleed exit channels from the rotor, whose higher temperature tended to conduct and convect

across to the IGV inflow. The imposed temperature distribution was estimated from rig conditions and imposed as a boundary condition on the IGV hub. Subsequent convection of the higher temperature hub surface through the boundary layer and sweeping upward in the secondary flow within the blade row is seen in Figure 3-44.

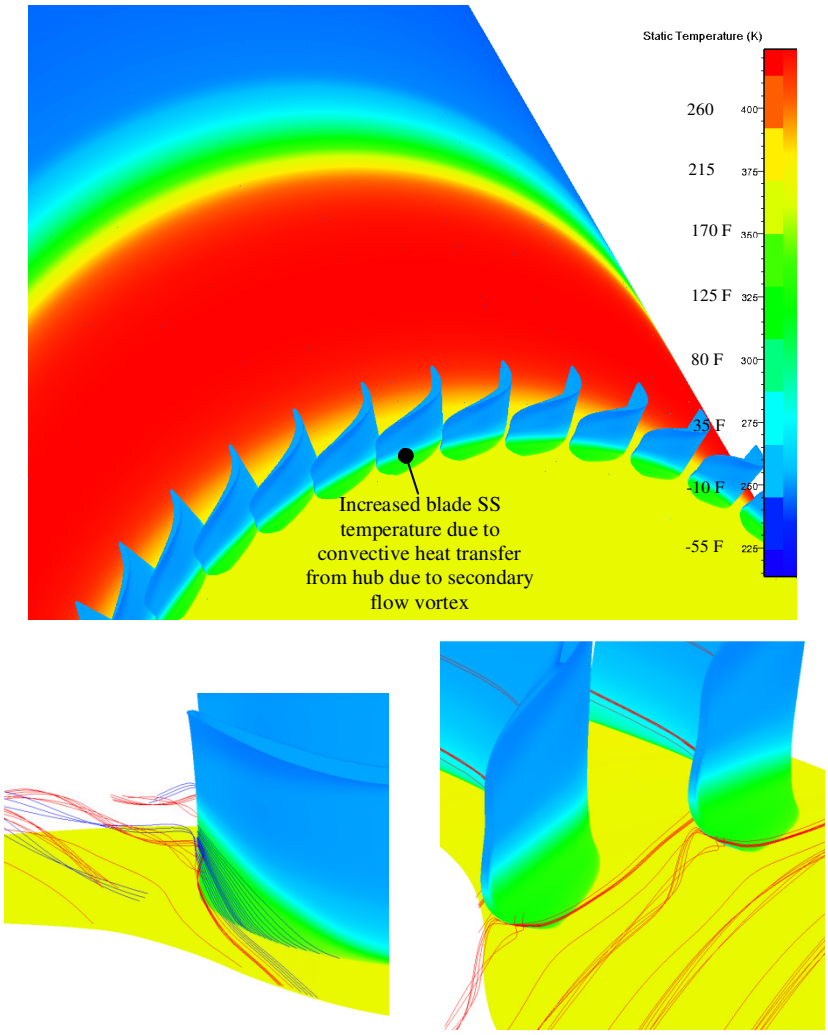

Figure 3-44: Inlet guide vane secondary flow vorticity.

Six struts existed as part of the test rig structure upstream of the IGV row of forty blades. It had been estimated that their impact would be negligible on IGV performance, and this was verified in CFD by connecting one strut passage to seven IGVs. As shown in Figure 3-45 and Figure 3-46, Mach number of flow through the struts remained low (0.2 – 0.3) and resulted in no significant interference.

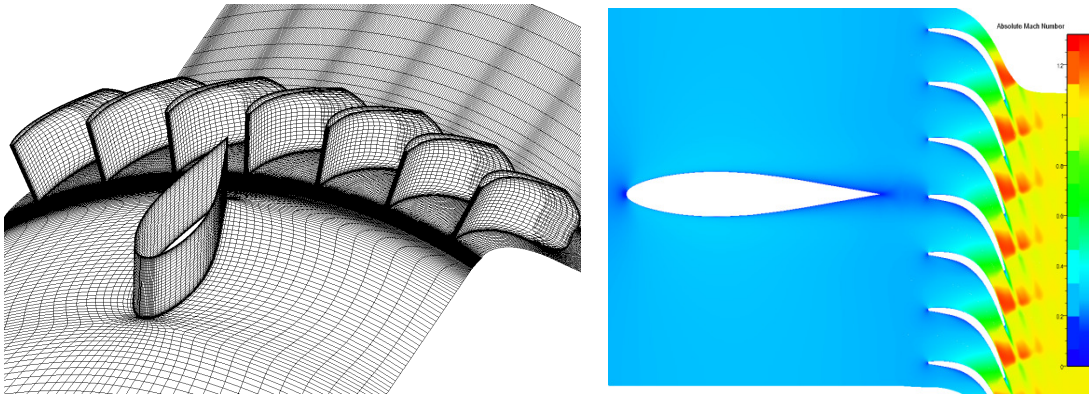

Figure 3-45: Impact of strut on IGV performance. Left) grid used in CFD analysis and right) Mach number of mid-span blade to blade flow.

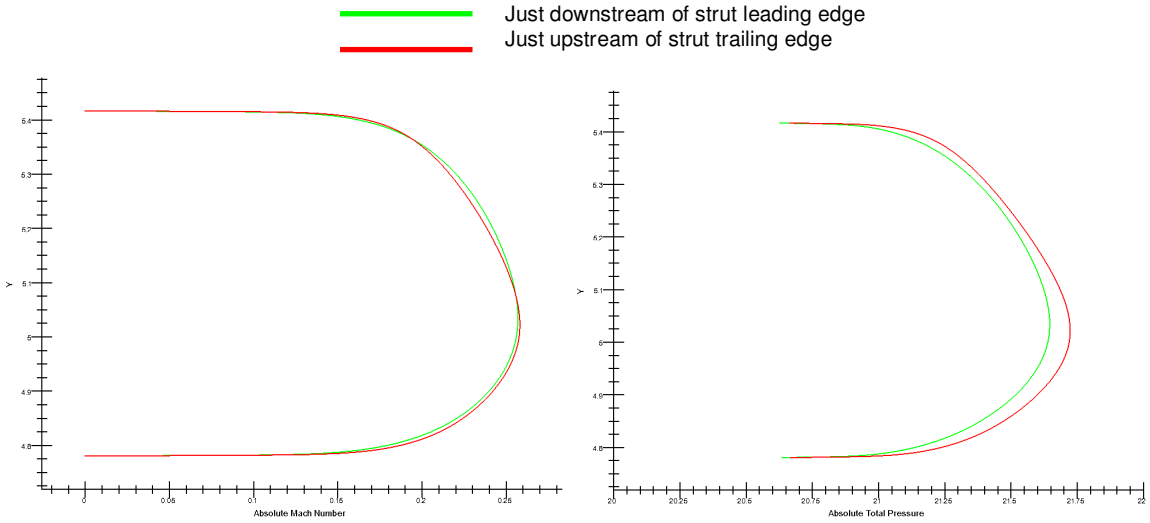

Figure 3-46: Impact of strut on IGV performance. Left) Mach number and right) total pressure pitchwise averaged profiles upstream and downstream of strut.

The predicted total pressure ratio from the inlet of the bellmouth to downstream of the IGV is shown in Figure 3-47. This simulation used conditions from tests to estimate the temperature distribution along the inner wall of the duct between the bellmouth and the IGV. The capture plane curve corresponds to the axial location of the Rampressor rotor inlet. The survey plane curve corresponds to the axial location of total pressure measurements taken during IGV performance characterization tests.

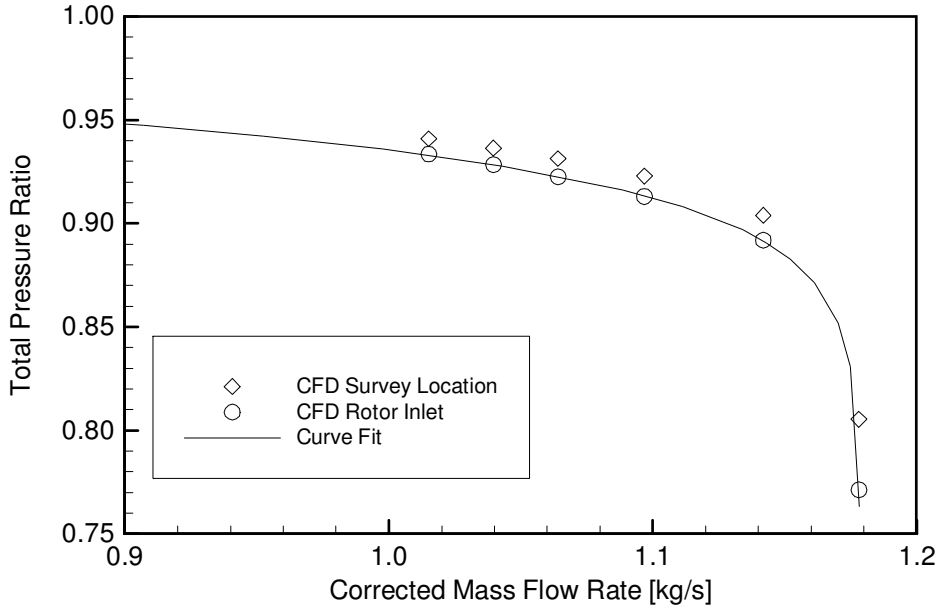

Figure 3-47: CFD prediction of the total pressure loss between the bellmouth inlet and a location downstream of the IGV. The capture plane is at the rotor inlet while the survey plane is upstream at the location where measurements were taken.

Rotor and IGV meshes were coupled via a mixing plane rotor stator interface. Simulations were run on fine grids consisting of 15-20 million grid cells, and coarsened grids consisting of two million grid cells. Performance was first characterized using the coarser grid levels, and verified using the finer at selected intervals. Simulations were run initially containing the long section leading from the bellmouth to the IGV row, see Figure 3-48, and subsequent analyses started at the IGV row, with total pressures extracted from the earlier simulations and appropriate total temperature settings. Table 3-9 lists the conditions used during many of the simulations.

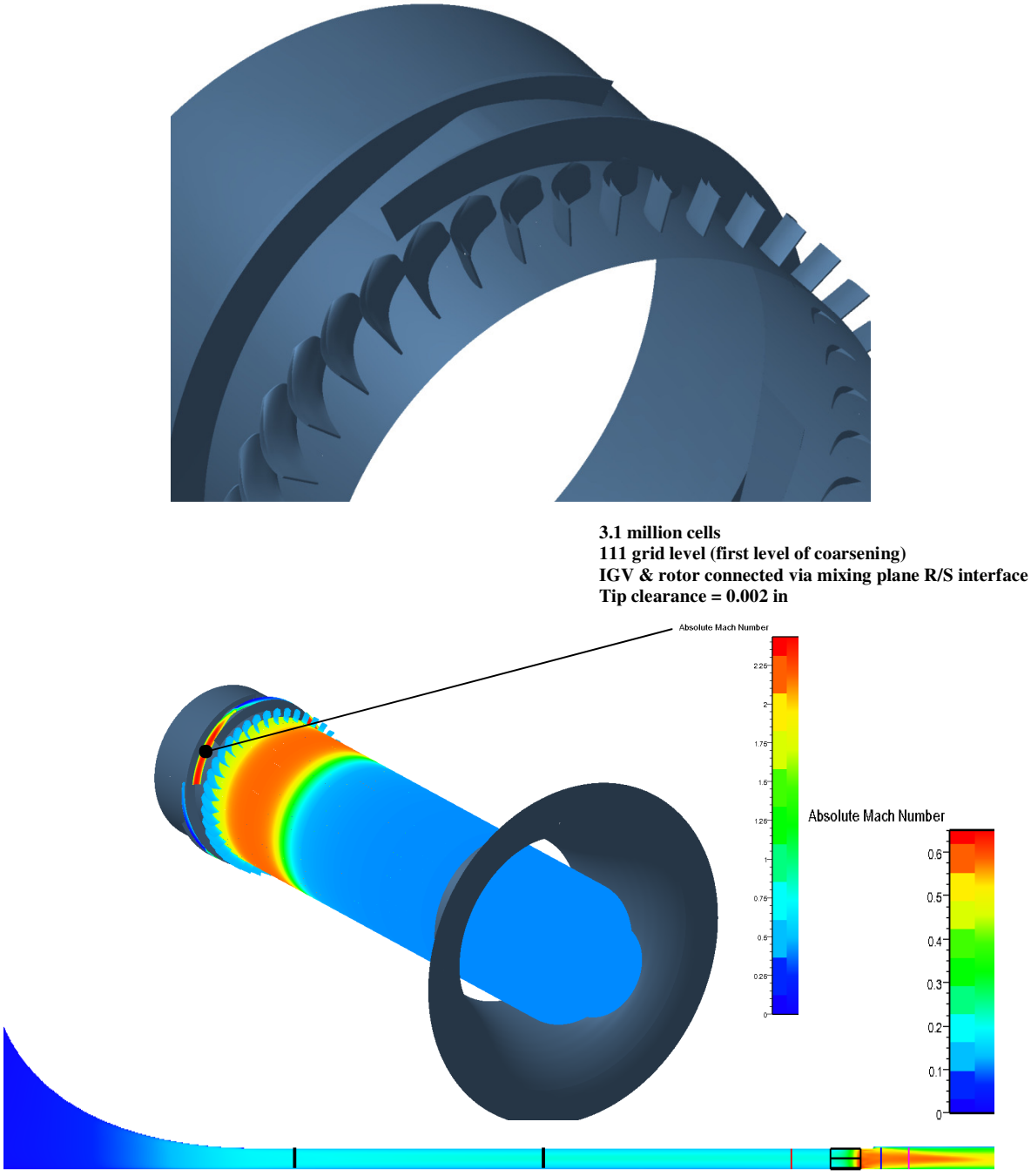

Figure 3-48: IGV and rotor coupled via mixing plane rotor/ stator interface.

Table 3-9: Boundary conditions for IGV and rotor coupled analysis.

Inflow total pressure	95.1 kPa (13.8 psia)
Inflow total temperature	-38°C (-37°F)
Hub wall temperature distribution	Based on forward bleed channel
Inflow corrected mass flow rate	1.06 kg/s (2.33 lbm/s)
Bleed pressure	34.5 kPa (5 psia)
Outflow static pressure	600 kPa (87 psia)

The rotor grids included both the rotor passage, as well as the individual bleed slots, and bleed cavities. These sections of grid were connected through non-conformal interfaces, where fluxes were passed across the boundaries via conservative means. Figure 3-49 shows portions of the grid used during simulations. Earlier grids were generated using the manual Numeca grid generator named IGG. Ramgen later contracted Numeca to enable their automated grid generator AutoGrid to handle Rampressor geometry, which resulted in an order of magnitude increase in the speed of rotor grid generation.

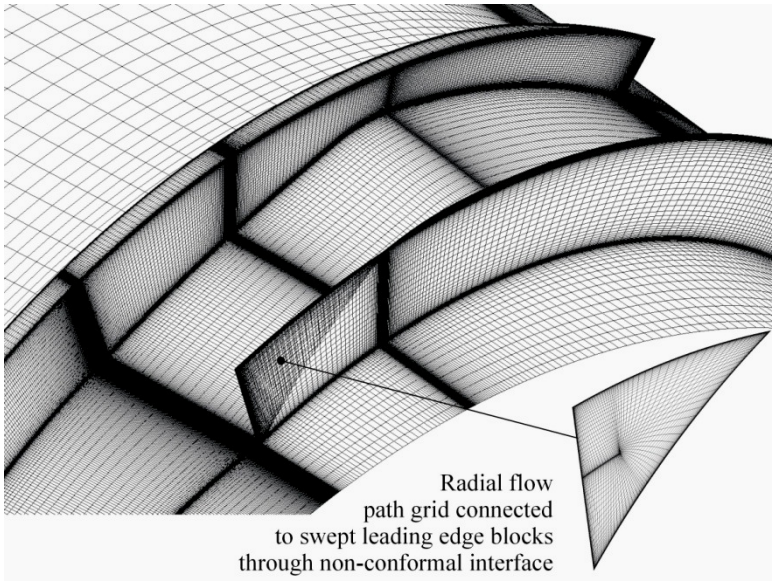

Figure 3-49: Rotor grid generated using IGG.

Figure 3-50 and Figure 3-51 display mid-pitch and mid-span contours of absolute and relative Mach number. Sensitivity to grid generation was tested for rotor simulations over a series of tip clearances. Figure 3-52 shows that coarse and fine grid results agreed well, except at the largest tip clearances. At these clearances, performance that was predicted based on coarser grids tended to be lower than the finer grid prediction so relying primarily on coarse grid results was deemed to be a conservative approach.

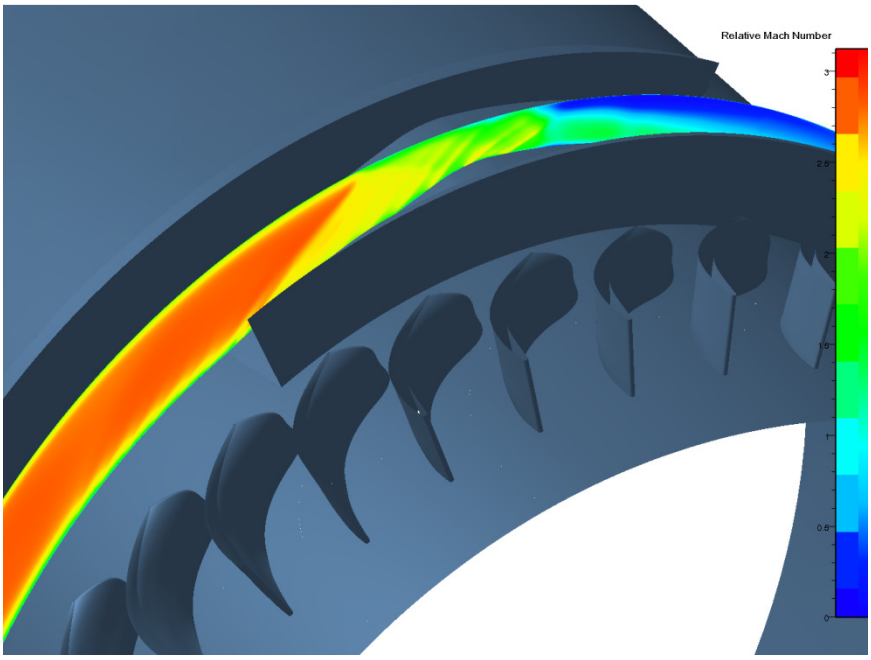

Figure 3-50: Results of IGV and rotor coupled modeling showing relative Mach number at rotor mid-pitch.

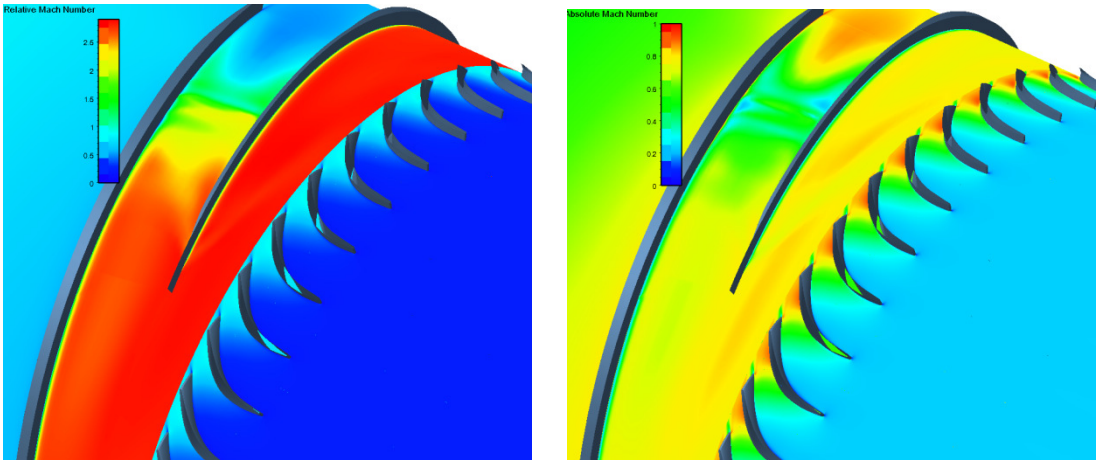

Figure 3-51: Results of IGV and rotor coupled modeling showing left) absolute and right) relative Mach number at rotor mid-span.

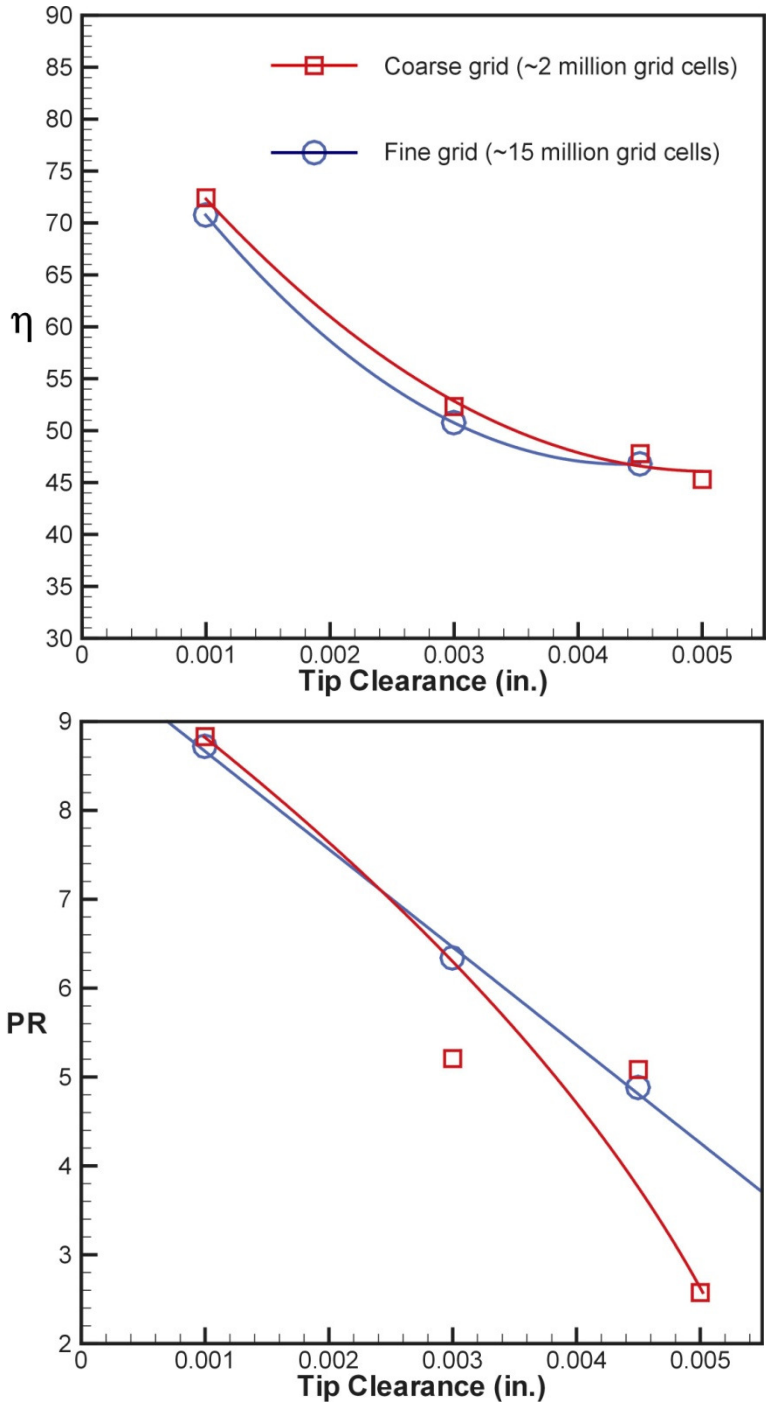

Figure 3-52: Rotor performance prediction sensitivity to grid resolution.

3.2.3 Post-Test Simulation

The values presented in Figure 3-52 resulted from predictions performed prior to experimental testing. Since the boundary conditions in the prediction simulations did not exactly match the conditions of the tests an additional simulation was performed using data obtained in Run 217, which resulted in the highest measured Rampressor performance. The purpose of this simulation was to see how closely the simulation matched the actual test.

The Rampressor-2 stage, consisting of the Rampressor-2 rotor and the IGV, was simulated using the CFD scheme described earlier. At the inlet of the computational domain, total quantities (total pressure, total temperature, and flow angle) were specified using experimental data where possible. During the simulation, the exit static pressure was increased until an unstart of the Rampressor rotor occurred. Rotor speed was matched to the test at 44,500 rpm. The rotor bleed slots were also modeled and the boundary conditions for the bleed slots (static pressure) were taken from the test. Different tip clearances were modeled during the CFD simulations.

With 0.001 inch tip clearance, the simulations indicated a maximum mass averaged total pressure ratio across the rotor of 8.55 at an efficiency of 60.8%. When the tip gap was increased to 0.003 inch, the rotor mass averaged total pressure ratio decreased to 5.81 with an efficiency of 58.9%. The total pressure ratio quoted compares the rotor exit plane to the rotor inlet plane and does not include the other components of the test rig such as the IGV and diffuser. Similarly, the efficiency is for the flow path only between those two axial locations and does not include the effect of bleed. Table 3-10 and Table 3-11 summarize the results of these two simulations. The results are in very good agreement with the experimental data, presented in

Table 3-12. Figure 3-53 depicts the relative Mach number from the rotor inlet to the rotor exit at midpitch (i.e. halfway between the two strakes).

Table 3-10: Run 217 CFD simulation results with a tip gap of 0.001 inch.

Rotor total pressure ratio	8.55
Rotor flow path efficiency	60.8%
Rotor corrected mass flow rate	2.42 lbm/s
Forward bleed mass flow rate fraction	5.1%
Aft bleed mass flow rate fraction	20.1%

Table 3-11: Summary of results of CFD simulation of Run 217 conditions with 0.003 inch tip clearance.

Rotor total pressure ratio	5.81
Rotor flow path efficiency	58.9%
Rotor corrected mass flow rate	2.39 lbm/s
Forward bleed mass flow rate fraction	4.7%
Aft bleed mass flow rate fraction	23.9%

Table 3-12: Summary of run 217 test conditions.

Rotor total pressure ratio	7.76
Rotor flow path efficiency	67.8%
Rotor corrected mass flow rate	2.47 lbm/s
Forward bleed mass flow rate fraction	5.4%
Aft bleed mass flow rate fraction	18.4%

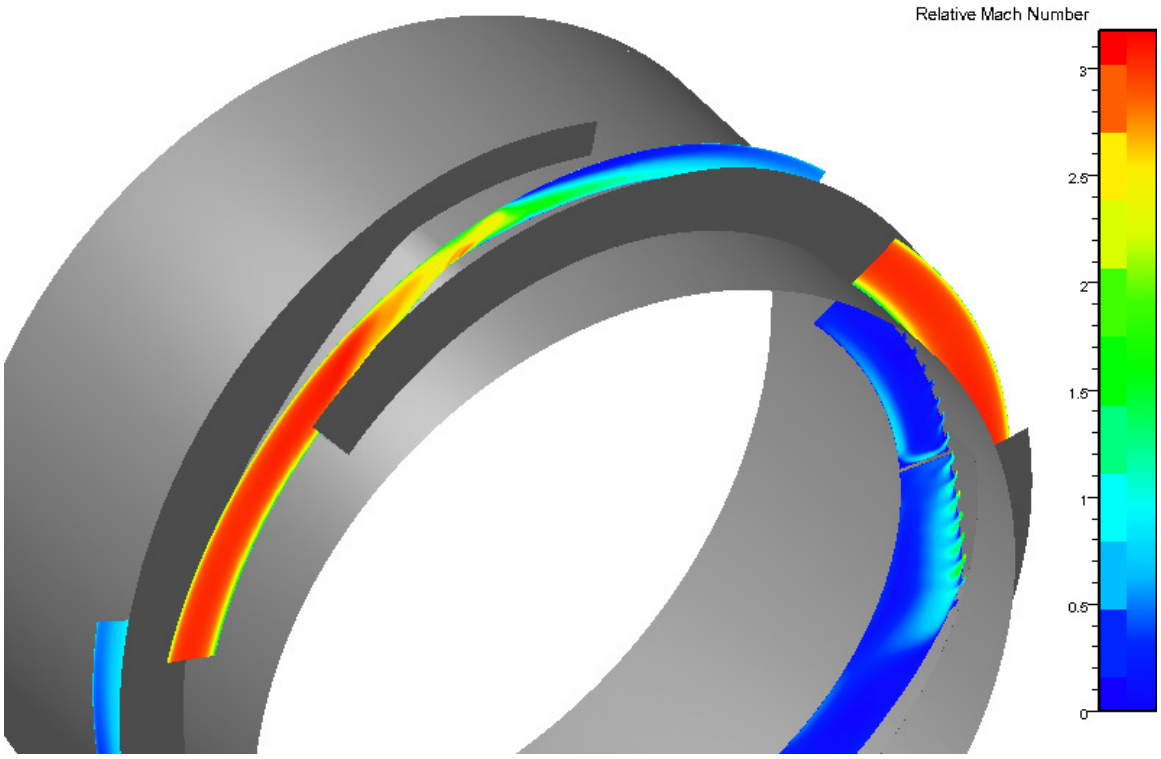

Figure 3-53: Midpitch Mach number from Run 217 CFD simulation with 0.001 inch tip clearance.

Chapter 4

Experimental Results

The Rampressor-2 test program's primary goal was to demonstrate the highest possible rotor total pressure ratio. However, additional testing was also required to fully characterize the performance of the entire Rampressor-2 flow path.

4.1 Facility and Measurements

Testing of the Rampressor-2 test article was conducted at The Boeing Company's Nozzle Test Facility (NTF) located in Seattle, Washington, and described in detail by Bressler (2003). The NTF was chosen as the test location due to its exceptional capabilities and proximity to Ramgen headquarters.

The Rampressor-2 test rig required approximately 200 pressure measurements, over 100 temperature measurements, additional voltage measurements, and processing of the inputs to provide real time measurements of parameters such as mass flow rate. The data acquisition system processor was a Data General MV/18000 SX model 10 connected to a variety of data acquisition hardware. Data were acquired by averaging multiple scans over a period of 9 seconds. Most pressures were acquired using a Scanivalve Corporation HyScan 2000 system although a few, including all differential pressure measurements, were gathered using stand alone transducers connected to a 16 bit analog to digital converter. The expected accuracy of the measurements from the HyScan system was ±0.1% of the full scale (Bressler, 2007). Temperatures were measured using a Hewlett Packard HP3852A data acquisition and control unit configured to read type K thermocouples. Temperature measurements had an accuracy of ±2.8K (±5°) (Bressler, 2007). During testing the system was calibrated twice per day.

The majority of the measurements of the flow field were acquired using a probe which measured both total pressure and total temperature in a Kiel head configuration with nulling channels, see Figure 4-1. Prior to testing the probe was calibrated at The Boeing Company's Flight Test Calibration Laboratory (Seattle, WA). The probe measurement was found to have an error of less than 0.6% for yaw angles between -45° and 45° and Mach numbers between 0.3 and 0.9. At a yaw angle of 0° the error was less than 0.2%. A post-test calibration performed by Aerodyne Engineering (Indianapolis, IN) confirmed the accuracy of the probe.

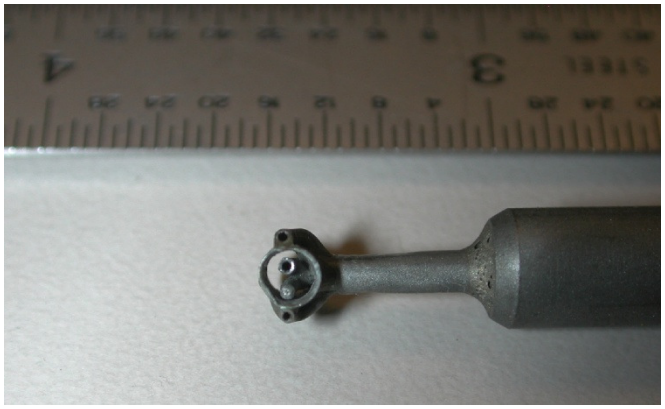

Figure 4-1: Performance probe used to measure inlet performance. The total pressure and total temperature probes are in the shroud and the nulling channels are outside the Kiel shroud. The outside diameter of the Kiel shroud was 3.18 mm (0.125 inches), and the outside diameter of the total pressure probe was 0.82 mm (0.032 inches).

On occasion flow field total pressure measurements were acquired using a pitot probe with nulling channels, see Figure 4-2. Prior to testing the probe was calibrated at The Boeing Company's Flight Test Calibration Laboratory (Seattle, WA). The probe measurement was found to have an error of less than 1% for yaw angles between -30° and 30° and Mach numbers between 0.3 and 0.9. At a yaw angle of 0° the error was less than 0.35%.

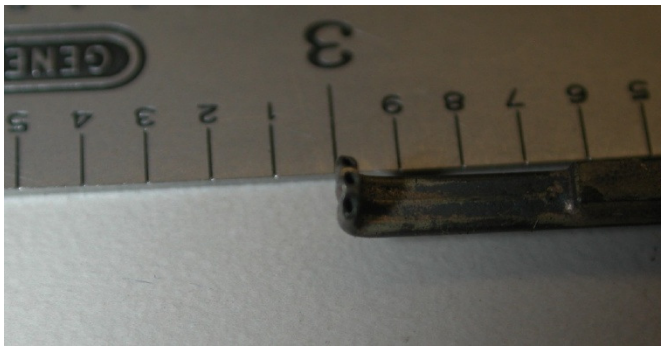

Figure 4-2: Cobra probe used to characterize inlet performance. Total pressure was measured at the center tube while the two side tubes provide nulling channels. The outside diameter of the total pressure probe was 0.82 mm (0.032 inches).

Since the uncertainties of each component of the measurement were independent, the overall uncertainty was calculated with the root sum square method (Taylor, 1997). The resulting uncertainty in the total pressure measurement downstream of the rotor was 0.4-1.0% for the data presented here. The inlet total pressure uncertainty was 1% and the uncertainty of the measured total pressure ratio was 1.1-1.5%.

4.2 Flow Path Starting

The first aero task was to show that the flow path could be started. When discussing supersonic inlets, upon which the Rampressor is based, a started flow path is one where the normal shock at the end of the series of compression waves is downstream of the flow path throat. An unstarted flow path is one with the normal shock upstream of the throat. It is

necessary for the flow path to be started to generate maximum total pressure ratio and therefore efficiency.

4.2.1 Test Procedure

The first step in a typical test was to turn on the secondary flow systems including the forward and aft wheel space air systems, the labyrinth seal purge air systems, and the drive turbine secondary flow systems. These flows provided air pressure across the labyrinth seals to prevent oil from leaking out of the rig or into the bleed or primary flow paths. The next step was to turn on the Rampressor bearing oil system. Then the main air to the Rampressor inlet was turned on and the inlet pressure increased until the Rampressor rotor was spinning, typically at several hundred rpm. Finally, the drive turbine was commanded to 10,000 rpm. While the drive turbine accelerated the main air mass flow rate was manually increased to hold the inlet plenum pressure constant. As the drive turbine approached 10,000 rpm the heater for the drive turbine inflow was turned on. Due to the large amount of work provided by the drive turbine it was necessary to heat the incoming air to avoid ice buildup on the drive turbine exhaust. When heated air entered the drive turbine, the drive turbine was commanded to a higher speed, typically 17,000 rpm. Once at this speed the bleed system was activated with full bleed applied to both the forward and aft bleed cavities. The system was allowed to operate at this speed until the oil temperature in the drive turbine squeeze film dampers warmed to 294°K (70°F) to ensure that the dampers operated properly when passing through the first rotordynamic mode at 24,000 rpm. Finally, the system was accelerated to the desired speed and the test was started. This general procedure was followed throughout the test program.

4.2.2 Starting Tests

When the rotor is spinning at high speed but unstarted the normal shock is strong and located upstream of the throat. Between this normal shock and the throat the flow is subsonic. When the rotor starts the normal shock moves downstream of the throat and the flow upstream of the throat is supersonic. The change from unstarted to started, subsonic to supersonic flow upstream of the throat, results in significant changes in the temperature and pressure in that region of the flow path. These two changes can be used to determine when the rotor starts.

Temperature Effect of Starting

A wall exposed to high speed flow will see the recovery temperature of the flow. In the case of Rampressor-2, the tip ring enclosed the rotor flow, but due to the rotation of the rotor any given part of the tip ring was exposed to many flow path stations. However, the point can be illustrated by assuming the tip ring rotates with the rotor. Following Schlichting, the recovery temperature, T_r, of the flow is given by

$$T_r = T_\infty + \sqrt{\mathrm{Pr}}\,\frac{U_\infty^2}{2C_p}$$

where T_∞ is the freestream temperature, Pr is the Prandtl number, U_∞ is the freestream velocity, and C_p is the specific heat at constant pressure. Assuming the rotor is at Mach 2.4 and 286°K (55°F) inlet air temperature, the recovery temperature of the supersonic flow is 566°K (559°F). To calculate the recovery temperature of the subsonic flow it is necessary to calculate the conditions after the normal shock. If one assumes the normal shock has an upstream Mach

number of 2.4, the recovery temperature downstream of the normal shock is 611°K (640°F). Therefore, as the flow path changes from unstarted to started, the tip ring temperature just downstream of the unstarted normal shock wave would decrease by 45 K° (81 F°).

In the Rampressor-2 test rig, any axial location on the tip ring that was exposed to this change in temperature was also exposed to inlet or exhaust temperatures so less change in tip ring temperature was expected. When the flow path started, less heat was conducted into the tip ring and, since the tip ring was actively cooled, even locations not in close proximity to the starting process were expected to see a decrease in temperature. Figure 4-3 shows the location of the tip ring relative to the rotor during a test along with the location of four thermocouples. Thermocouples tip21 and tip31 were over the flow path and, therefore, were expected to see the largest decrease in temperature. Thermocouple tip11 is closest to the water cooling passage and was expected to see the smallest decrease in temperature.

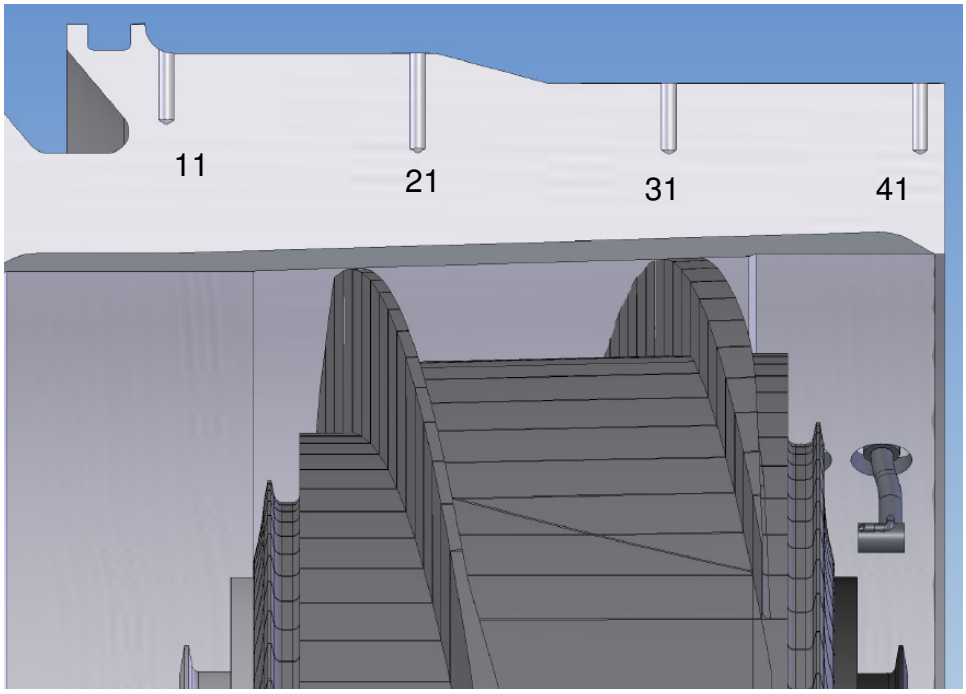

Figure 4-3: Location and numbering convention of tip ring thermocouples. Air flows from left to right. There is a large cooling passage on the upper left end of the tip ring. The dark gray area on the inside diameter of the tip ring is abradable. Tip ring and rotor relative positions match the test configuration for the data shown in Figure 4-4.

Figure 4-4 shows tip ring thermocouple measurements during a test with the configuration shown in Figure 4-3. Between 0 and 10 minutes, the rotor speed was increased from 39,000 rpm to 41,000 rpm. The increase in rotor speed increased the total temperature and wall recovery temperature, resulting in the observed tip ring temperature increase. At 12 minutes, the rotor speed was increased to 42,000 rpm and the flow path started resulting in a decrease in the tip ring temperature. The rotor speed was then increased to 44,000 rpm and, despite the increased recovery temperature, the temperature at thermocouples tip21 and tip 31 decreased by over 18 K° (33 F°). Thermocouple tip41 recorded a temperature decrease of 13 K° (24 F°), while thermocouple tip11 recorded a decrease of over 6 K° (11 F°). At about 20

minutes, all of the tip ring temperatures except tip41 showed a slight increase. At this time the tip ring was gradually moved aft 5 mm (0.2 in) to decrease the tip gap. This motion moved thermocouples tip21 and tip31 farther aft on the flow path, where the average axial temperature is higher. Thermocouple tip41 showed no significant change in temperature because it was downstream of the flow path in the uniform-temperature exhaust region. Thermocouple tip11 showed a slight increase in temperature as it moved closer to the heat flux area over the flow path. At 39 minutes the rotor speed was reduced. As the rotor decelerated from 41,000 rpm to 40,000 rpm the flow path unstarted and the tip ring temperature increased. A second cycle of increasing speed / flow path starting and decreasing speed / unstarting can be seen on the right half of the figure.

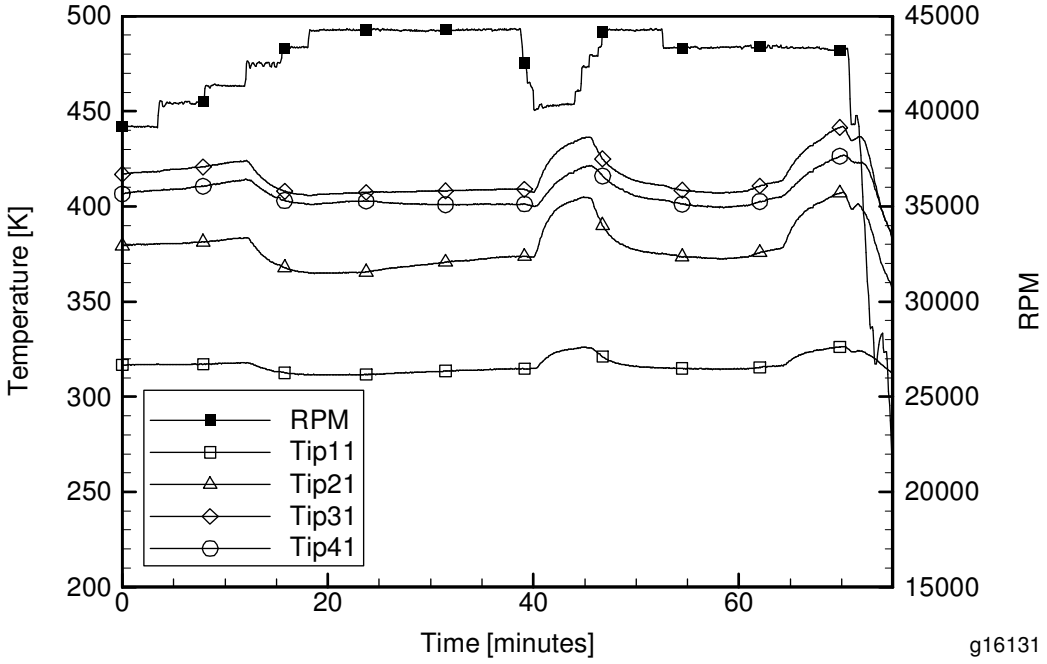

Figure 4-4: Tip ring temperatures detect flow path starting and unstarting with rotor speed variation.

Pressure Effect of Starting

An unstarted flow path will experience higher pressure along the compression surface of the rotor (i.e. the ramp surface upstream of the throat) compared to a started flow path. When the flow path is unstarted, the Mach number on the compression surface is lower resulting in higher static pressure. This pressure increases mass flow through the bleed slots on the compression surface compared to the started flow path. Most of the bleed slots on the compression surface fed into the aft bleed circuit so a large change in flow rate would be expected for this circuit. The forward bleed circuit is primarily fed by bleed slots upstream of the compression surface and would not be expected to change as much as the aft circuit.

Mass flow rates through the bleed systems were measured, but included more than just the rotor bleed flow. Due to the rotor's high speed, non-contact labyrinth seals were used, resulting in wheel space flows mixing with the bleed removal flow. In the test article the forward and aft bleed flows do not mix. An additional labyrinth seal on the forward and aft rotor shafts created additional leak paths for the forward and aft wheel space flows. The main and the

wheel space seals leak into the bleed passages since they have the lowest pressures in the system. The effect of seal leakage on the bleed system measurements needed to be calculated.

Labyrinth seals are a mature technology and leakage flow rates can be calculated with reasonable accuracy provided that the labyrinth seal geometry, labyrinth seal gap, pressure differential across the labyrinth seal, and fluid temperature are known. For the Rampressor-2 test rig the geometry was known and pressure and temperature measurements were taken close to the rotor so that the calculations could be performed. The labyrinth seal gap was not known, however, it was possible to calculate it. The diameters of the static hardware were calculated based upon precision measurements corrected for thermal growth at operating temperatures. Rotor labyrinth teeth were precision measured and corrected for thermal growth and centrifugal growth. The labyrinth seal operating gaps were originally designed for using this method.

Once the seal leakage rates were calculated the measured flow rates were adjusted by adding or subtracting, as necessary, the leakage flow rates. In general, good agreement was found for mass conservation of individual flows. For example, the mass flow into the forward wheel space should be equal to the sum of the mass flow out of the forward wheel space and the leakage past any seal around the forward wheel space. In addition, good agreement was found for mass conservation of all flows into and out of the test rig. Typically, the difference between the sum of the flows into the rig and the sum of the flows out of the rig was less than 4% of the flow entering the rotor.

Figure 4-5 shows the adjusted bleed and rotor exhaust flows as a fraction of the flow onto the rotor (rotor entrance flow). During this test a very tight tip gap was maintained and the rotor exhaust flow was throttled to increase the backpressure. As the backpressure increased the rotor exhaust mass flow rate decreased while the aft bleed mass flow rate increased. The forward bleed mass flow rate also increased during the course of the test. At approximately 48 minutes the backpressure exceeded rotor capability at these conditions and the flow path unstarted. At the moment of unstart the aft bleed mass flow rate increased from approximately 24% of the rotor entrance flow to 35% of the rotor entrance flow. At the same time the rotor exhaust flow decreased from 70% of the rotor entrance flow to 58% of the rotor entrance flow. The started and unstarted mass flow rates are in good agreement with the CFD analysis.

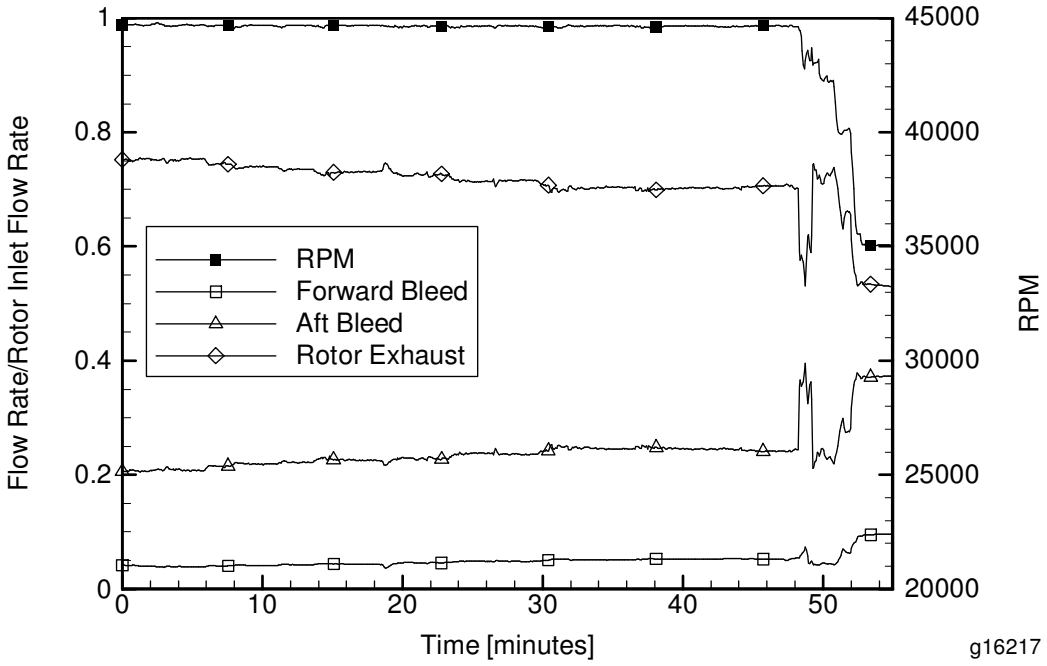

Figure 4-5: Adjusted bleed and exhaust mass flow rates as a fraction of the rotor entrance flow.

4.2.3 Starting Test Conclusions

Analysis of the tip ring temperature data and mass flow rates were used to determine if the flow path started. The observed large changes in tip ring temperature are consistent with a change in the compression surface flow changing from subsonic to supersonic which is indicative of the flow path starting. The observed large changes in aft bleed and rotor exhaust mass flow rates are consistent with supersonic to subsonic transition in the compression surface flow, also indicative of the flow path unstarting. Based on these results it was concluded that the flow path started as desired.

4.3 Inlet Performance

The Rampressor-2 program's major goal was to measure the maximum total pressure ratio across the Rampressor rotor. Unfortunately, it was not possible to make total pressure measurements immediately upstream and downstream of the rotor. The closest upstream total pressure measurement available was in the plenum upstream of the inlet bellmouth and inlet guide vane (IGV). In a previous report (Williams, 2007), the losses associated with the IGV were reported. Due to mechanical constraints, the Rampressor forward frame was connected directly to the bellmouth so the inlet duct was not installed for those tests. Although the pressure loss of the inlet was predicted to be small, the performance of the inlet was measured to verify this prediction.

In order to measure the performance of the inlet, it was necessary to add instrumentation ports to the flow path. As it was not possible to add ports to the Rampressor forward frame, ports were added to the inlet. Ports for total pressure and total temperature surveys were added at three circumferential locations 37.3 mm (14.70 in) downstream of the leading edge of the

inlet. An additional six thermocouple ports were added 39.3 cm (15.49 in) downstream of the inlet leading edge and thermocouples were inserted such that they were located at mid-height of the flow path. The flow path length within the inlet was 42.1 cm (16.56 in).

4.3.1 Total Pressure Loss

Ten point radial surveys of the total pressure were made at each of three survey ports at a corrected speed of 107%. The percent corrected speed was given by

$$\Omega_{\%cor} = \frac{\Omega}{41{,}439}\sqrt{\frac{288}{T_{inlet}}} \tag{4-1}$$

where Ω is the mechanical rotational speed and T_{inlet} is the inlet temperature in Kelvin. 100% corrected speed corresponded to 41,439 rpm and 288°K (59°F) inlet temperature. Surveys were conducted to measure both total pressure and total temperature using the performance probe. An additional survey was conducted at a corrected speed of 121% to determine the effect of mass flow rate. Finally, a cobra probe survey was conducted to determine if the probe had an impact on the measurement. Photographs of the performance and cobra probes are shown in Figure 4-1 and Figure 4-2, respectively.

Figure 4-6 shows survey results at the three different circumferential locations at 107% corrected speed. The locations of the hub and shroud walls are also shown in the figure. The total pressure profile at locations 1 and 3 are nearly identical; the profile at location 2 was of similar shape but showed slightly less total pressure loss. In general the total pressure loss was less than 1%.

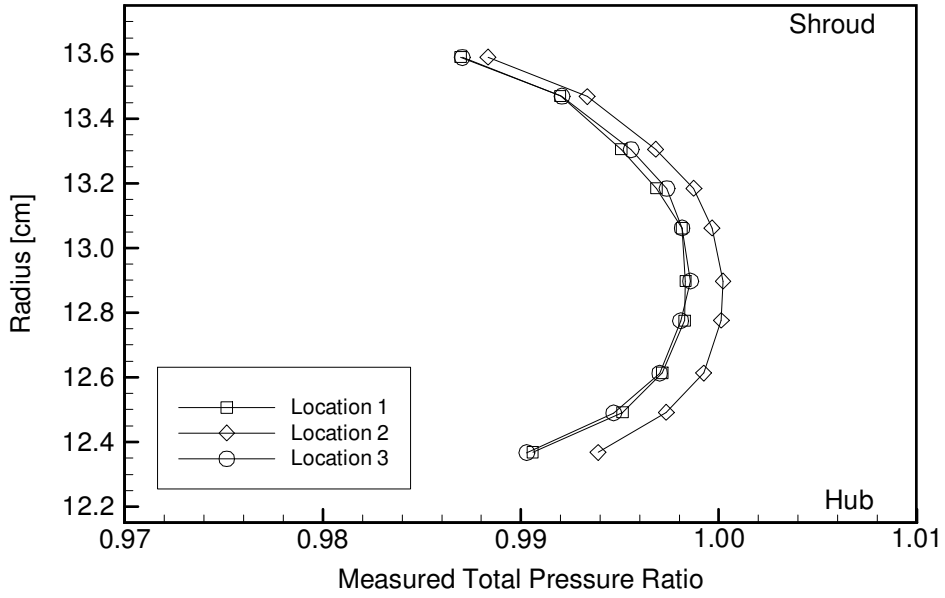

Figure 4-6: Radial surveys of total pressure ratio, plenum to end of inlet, at three different circumferential locations at 107% corrected speed. The shroud and hub are at the top and bottom locations of the plot, respectively.

Figure 4-7 shows the results of the surveys at location 1 at corrected speeds of 107% and 121%. The two profiles were very similar with no apparent decrease in total pressure due to the

higher mass flow rate associated with the higher rotor speed. Note that the 107% curve in Figure 4-7 is the same as the location 1 curve in Figure 4-6.

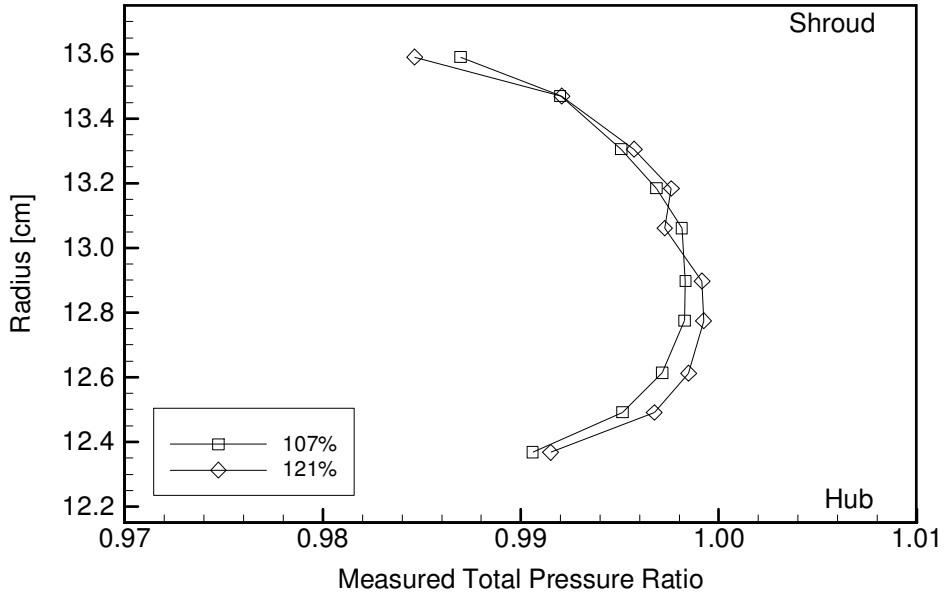

Figure 4-7: Radial surveys of total pressure ratio, plenum to end of inlet, at circumferential location 1 for different rotor corrected speeds.

Figure 4-8 shows the surveys taken with the two different probes. Again, the two surveys were very similar indicating that both probes provided accurate measurements. Due to the smaller size of the cobra probe it was possible to take measurements closer to the hub wall. Note that the performance curve in Figure 4-8 is the same as the 107% curve in Figure 4-7.

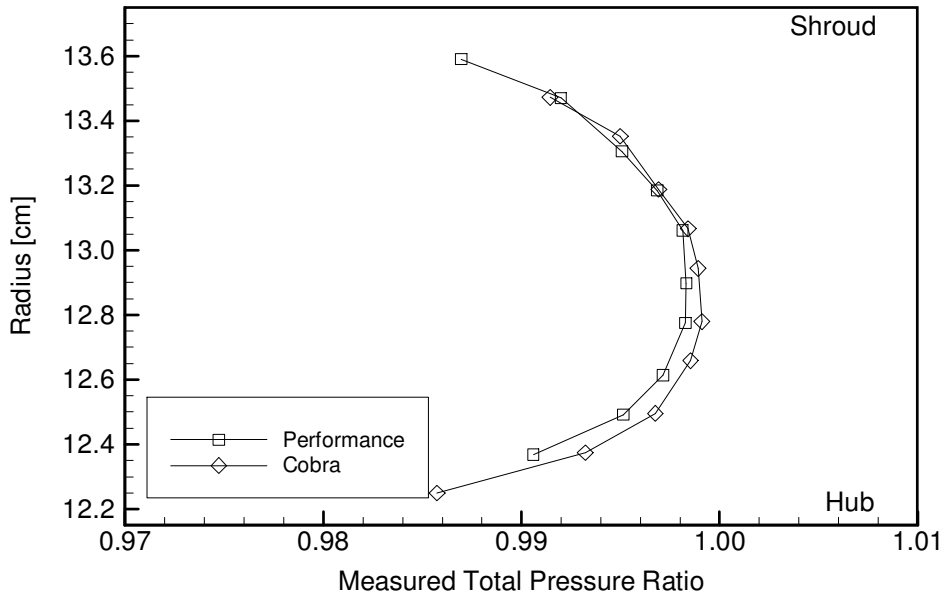

Figure 4-8: Radial surveys of total pressure ratio, plenum to end of inlet, using two different total pressure probes at circumferential location 1 at 107% corrected speed.

Figure 4-9 shows the area averaged total pressure ratio for each of the five surveys plotted against corrected mass flow rate. The area averaged total pressure, π_{Aavg}, is defined by

$$\pi_{Aavg} = \frac{\sum A_{local}\pi_{local}}{\sum A_{local}}$$

where π_{local} is the local total pressure ratio and A_{local} is the local area of the annulus in which the total pressure ratio was calculated. The corrected mass flow rate, $\dot{m}_{corr}$, is defined as

$$\dot{m}_{corr} = \dot{m}\sqrt{\frac{T_{plenum}}{288}}\frac{101{,}325}{P_{plenum}} \qquad (4\text{-}2)$$

where $\dot{m}$ is the measured mass flow rate, T_{plenum} is the inlet plenum temperature in Kelvin, and P_{plenum} is the inlet plenum pressure in Pascals. The area averaged total pressure ratio ranged between 0.994 and 0.996 for the five surveys. In general, the inlet total pressure ratio loss was about 0.5% for speeds of interest to the Rampressor-2 test program.

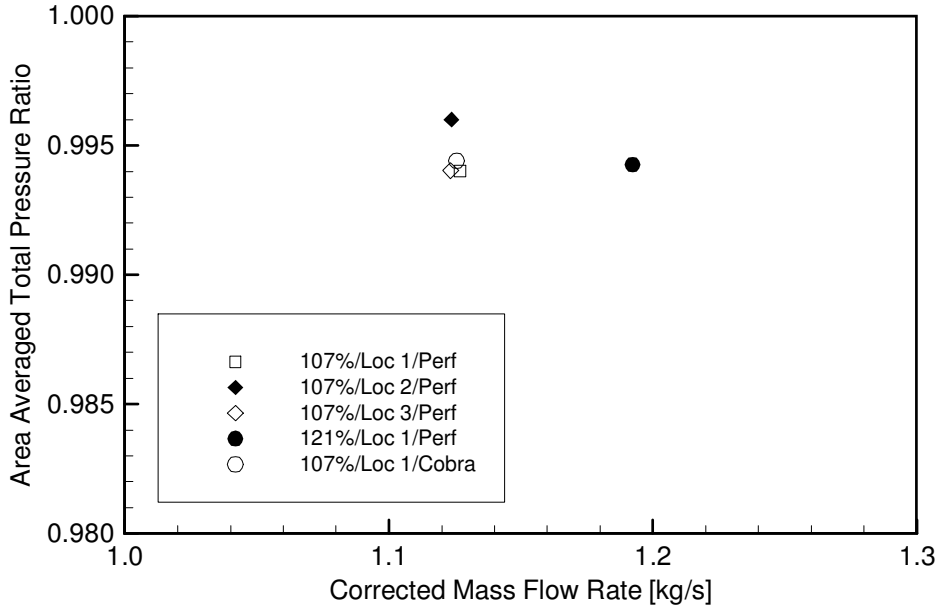

Figure 4-9: Area averaged total pressure ratio, plenum to end of inlet, for each of the surveys presented in the previous three figures.

4.3.2 Total Temperature Change

The Rampressor inlet was designed to minimize heat transfer to the incoming air. Air entered the Rampressor through an annulus shaped inlet. The cylinder which made up the inside diameter of the inlet contained the forward wheel space inlet and exit flows along with the forward bleed flow. The center of the cylinder contained the forward bleed, surrounded by the forward wheel space exit flow, in turn surrounded by the forward wheel space inlet flow. This arrangement kept the coolest flow closest to the main air flow to minimize heat transfer to the main air flow. All three secondary flows entered or exited the test rig through struts in the plenum, see Figure 4-10. Due to the high temperature of the forward bleed flow, its lines were insulated to the extent possible.

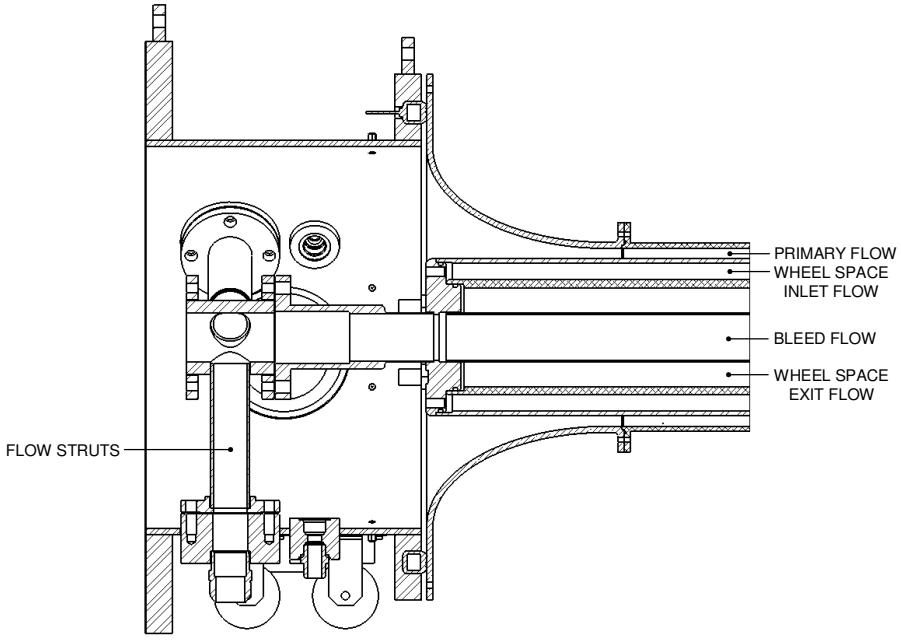

Figure 4-10: Schematic of Rampressor inlet side flow passages.

Initial tests were conducted with the rotor spinning at only 10,000 rpm with no forward bleed flow. Under these conditions, the measurements from the three RTDs located in the plenum were within 0.2 C° (0.4 F°) of each other. At the same conditions, measurements from the six thermocouples located in the inlet were within 0.3 C° (0.5 F°) of each other. For these tests, main air was a few degrees cooler than the secondary flows and the test cell so it was expected that the air would warm slightly between the plenum and the inlet. This was not the case as the inlet thermocouples indicated a temperature 0.9 C° (1.5 F°) cooler than that indicated by the plenum RTDs. The temperature indicated by the RTDs was also higher than that indicated by upstream thermocouples. From this it was concluded that the temperature indicated by the RTDs was higher than that indicated by the thermocouples. Since the difference was within the error of the two measurement systems no attempt was made to reduce the difference.

Once the rotor was brought up to full speed, the heating from the forward bleed flow became apparent. Figure 4-11 shows results from one of the inlet surveys along with the three plenum temperatures. Thermocouple 6c was located directly downstream of one of the struts carrying the forward bleed flow and shows the highest measured temperature. Thermocouple 6a was located approximately halfway between struts and shows the lowest measured temperature. Due to the location of these two thermocouples relative to the struts, they are believed to capture the highest and lowest temperatures within the plenum. Since no total temperature survey of the plenum was performed, the mass averaged total temperature entering the rig was not known, however, it was expected to be within 1 K° of the average temperature of the three RTDs. The fact that the performance probe temperature was lower than the RTDs was cause for concern.

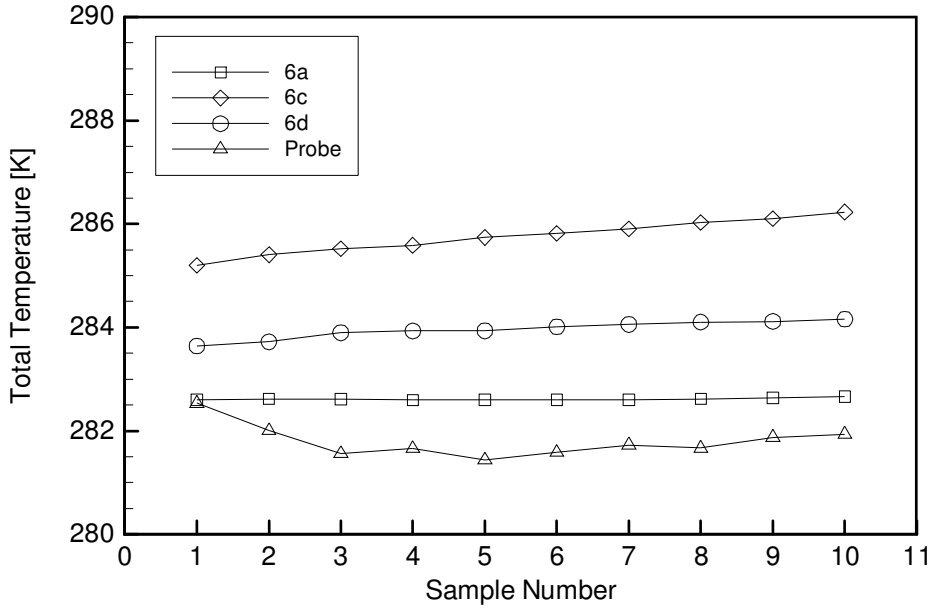

Figure 4-11: Measured plenum total temperature during a typical high speed test with forward bleed. RTD 6c is directly downstream of a strut containing the forward bleed flow. The performance probe temperature is also shown.

The non-uniform temperature distribution seen in the plenum also resulted in a non-uniform temperature distribution in the inlet. Figure 4-12 shows the temperature measurements in the inlet during the course of an inlet survey along with the results of the survey. The data in this figure correspond to the data from Figure 4-11. The temperatures shown in Figure 4-12 are slightly lower than those in Figure 4-11 which was expected due to the previously discussed determination that the plenum RTDs had a slight upward temperature bias.. It can be seen that the difference between minimum and maximum temperatures is consistant although somewhat less than shown in Figure 4-11. This was expected due to mixing which occurred between the plenum and the inlet. It was seen that the temperature from the performance probe was in good agreement with the temperatures from the inlet thermocouples reinforcing the conclusion that the measurements from the RTDs were biased.

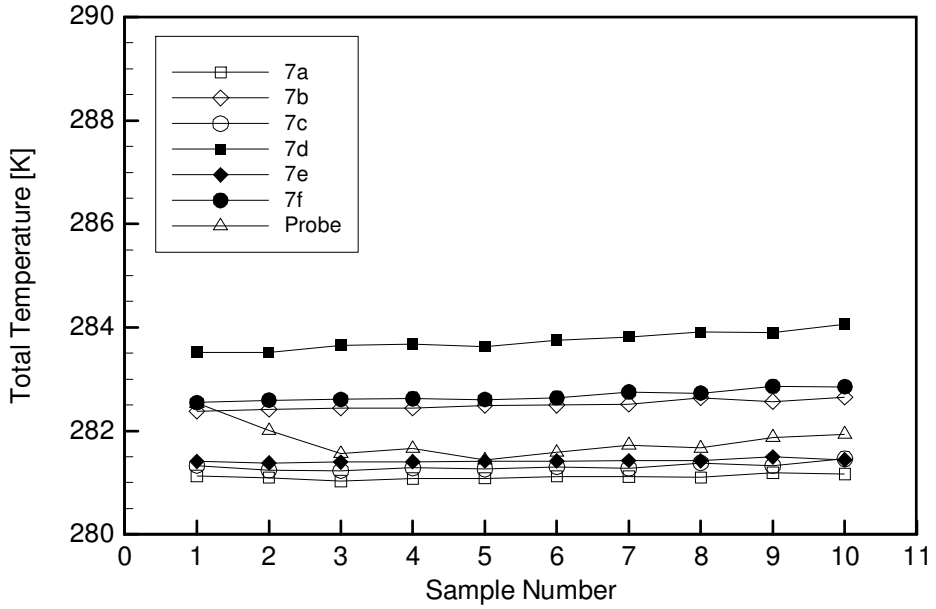

Figure 4-12: Measured inlet total temperature during a typical high speed test with forward bleed. The data are from the same test as those in Figure 4-11.

Figure 4-13 shows the results of the surveys at the three different circumferential locations at 107% corrected speed. The locations of the hub and shroud walls are also shown in the figure. The figure shows the ratio of the temperature measured during the survey to the average temperature of the thermocouples in the inlet. From the figure one sees that the total temperature profiles at the three locations are nearly identical. At the hub the temperature is slightly higher indicative of heat transfer from the forward wheel space supply flow.

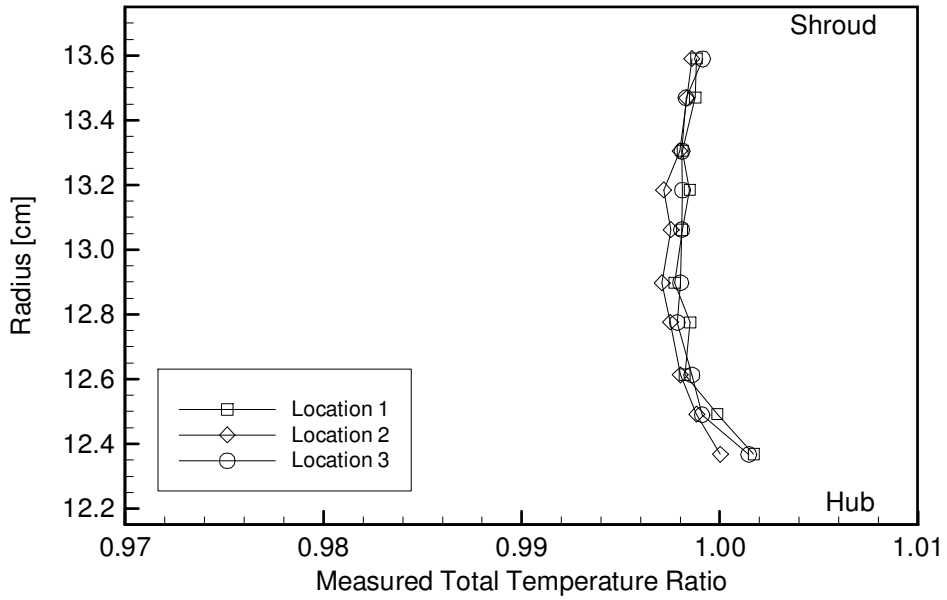

Figure 4-13: Radial surveys of total temperature ratio, bellmouth to end of inlet, at three different circumferential locations with the rotor at 107% corrected speed.

The mechanical speed of the rotor was limited to 107% but it was possible to obtain higher corrected speeds by reducing the main flow temperature. This was accomplished by injecting liquid nitrogen into the main air upstream of the plenum. Figure 4-14 shows the results of the surveys at location 1 for two different corrected speeds. To obtain 121% corrected speed, liquid nitrogen was added to the main air to reduce the plenum temperature to approximately 230°K (-45°F). At 121% speed the heat addition at the hub due to the forward wheel space supply flow is seen as is the heat addition at the shroud. Since the air outside the shroud was stationary the heat transfer was lower and this is seen in the gradient of the temperature near the shroud. It is clear from the data that heat was transferred to the flow so the total temperature ratio must be greater than one and this is seen at the hub.

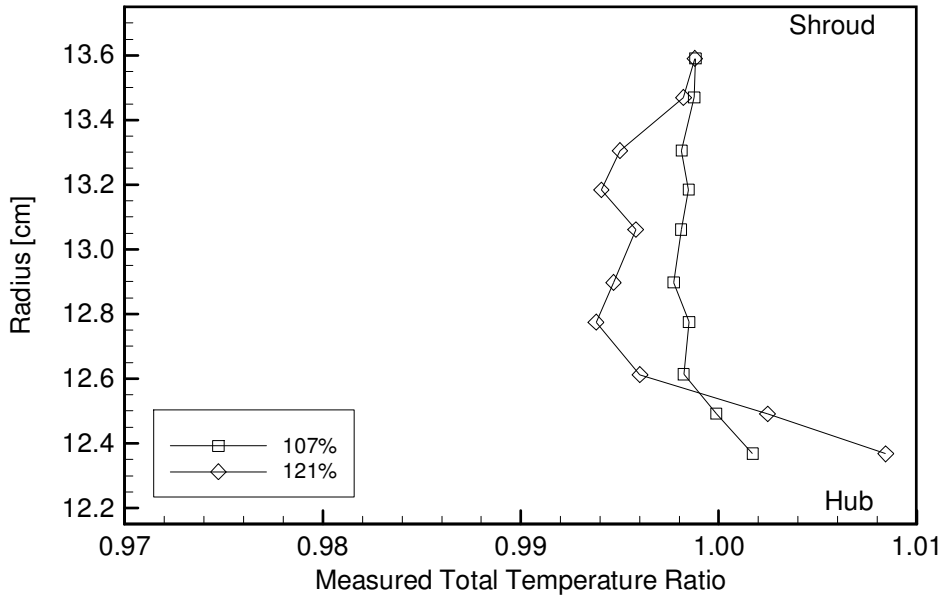

Figure 4-14: Radial surveys of total temperature ratio, bellmouth to end of inlet, at circumferential location 1 for different rotor corrected speeds. In order to obtain 121% speed, liquid nitrogen was introduced into the main air to reduce the plenum temperature to approximately 230°K (-45°F).

Previous data showed that, while not in exact agreement, the plenum and inlet temperature measurements were in general agreement and were mostly likely representative of the mass averaged total temperature. However, with the liquid nitrogen present in the flow, the difference between the indicated temperature from the RTDs in the plenum and the thermocouples in the inlet was not within the measurement error. In this case, the error was attributed to a faulty calibration of the RTDs in the plenum. The RTD's purpose was to provide a total temperature entering the Rampressor. Since the flow Mach number was low in the inlet and the recovery temperature was essentially the total temperature, the inlet thermocouples gave a good measurement of the total temperature entering the Rampressor. For the remainder of the analyses, the inlet temperature measurement was used as the flow total temperature.

4.3.3 Inlet Performance Conclusions

Surveys were conducted at the end of the inlet to measure its performance. These measurements showed fully developed flow at the end of the inlet. The area averaged total

pressure ratio was approximately 0.995, thus, the total pressure loss between the plenum and the end of the inlet was approximately 0.5%.

4.4 Inlet Guide Vane Performance

The losses associated with the inlet guide vane (IGV) were reported in a previous report by Williams (2007). Due to mechanical constraints, the inlet duct was not installed for those tests. In addition, the rotor was removed to provide easy access to the IGV exit flow field. During this test period, additional IGV performance data were gathered for comparison with previous measurements.

4.4.1 IGV Total Pressure Loss

Two survey ports were added to the shroud to enable total pressure measurement downstream of the IGV. Four additional static pressure ports were also added to the tip ring. Each pressure port was located directly opposite a pre-existing hub static pressure port. Unlike previous IGV tests, the rotor was installed and spinning during these tests in an attempt to duplicate the rotor performance test flow field. Due to the design of the test apparatus, it was not possible to move the tip ring during these tests so rotor performance test tip gaps could not be duplicated.

After achieving target rotor speed, the performance probe was moved to the desired radial location and nulled by remotely adjusting its angle until the difference between the left and right channels reached zero. A complete set of data was then taken using the Boeing data acquisition system, including the performance probe angle and total pressure. The rotor speed was then increased or the probe was moved to the next radial location and the process was repeated until all required data had been gathered.

Figure 4-15 shows the IGV exit to plenum total pressure ratio with the performance probe located at the passage centerline. As expected, the total pressure loss increases as the mass flow rate increases. To obtain corrected mass flow rates greater than 2.38 lbm/s, it was necessary to cool the main air with liquid nitrogen. It can be seen that liquid nitrogen had negligible affect on the total pressure loss as the two sets of data are in agreement. Figure 4-16 presents total pressure ratio as a function of corrected speed rather than corrected mass flow rate.

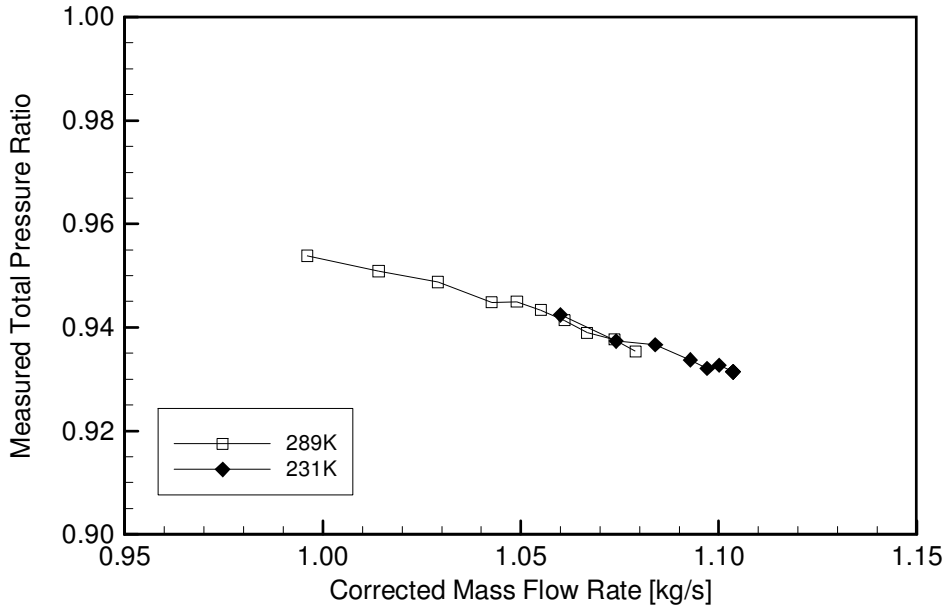

Figure 4-15: Measured centerline total pressure ratio, IGV exit to plenum, at location 1.

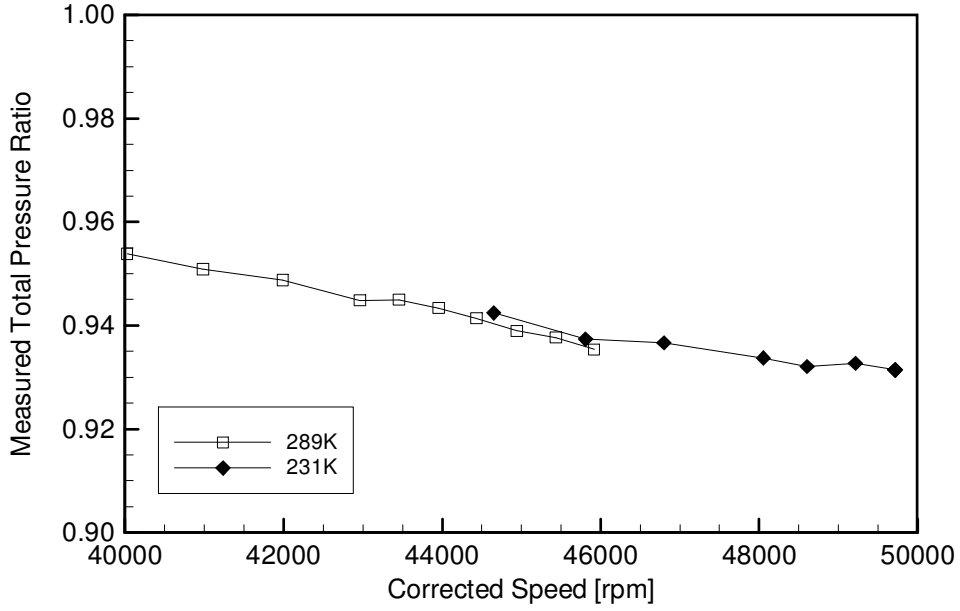

Figure 4-16: Measured centerline total pressure ratio, IGV exit to plenum, at location 1.

Figure 4-17 shows results from the radial surveys conducted downstream of the IGV. The two surveys at location 1 are very similar to each other. The three surveys at location 2 are also very similar. However, the location 1 survey profiles are significantly different than those of location 2. This difference was supported by data taken in the initial IGV measurements. As before, flow profile was independent of corrected speed.

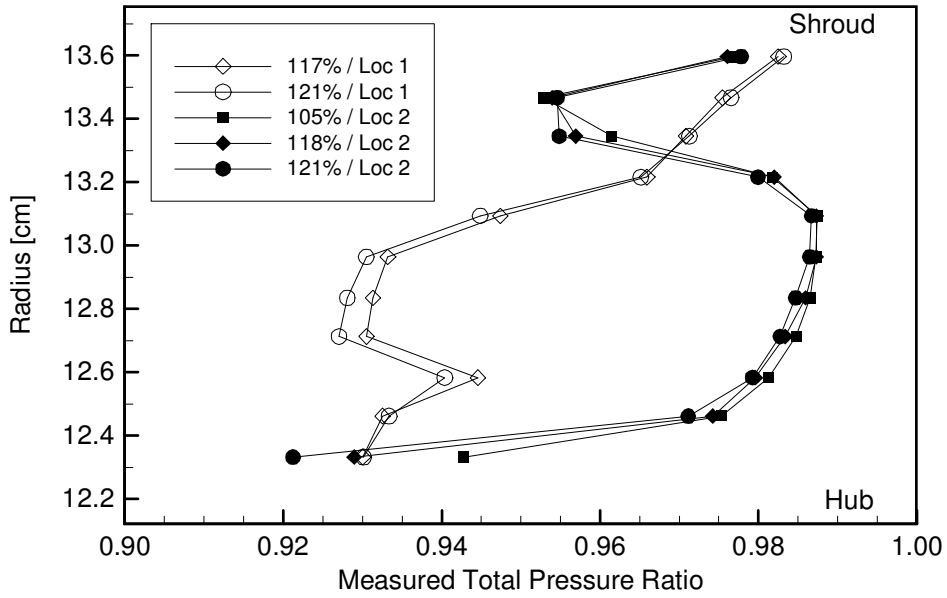

Figure 4-17: Radial surveys of total pressure ratio, IGV exit to plenum. Surveys were conducted at two circumferential locations and at three different corrected speeds.

Figure 4-18 shows the mass averaged total pressure ratio for each of the five surveys presented in Figure 4-17. The mass averaged total pressure ratio, $\pi_{\dot{m}avg}$, is defined by

$$\pi_{\dot{m}avg} = \frac{P_{t,\dot{m}avg,out}}{P_{t,\dot{m}avg,in}} = \frac{\dfrac{\sum_{out} \dot{m}_{local} P_{t,local}}{\sum_{out} \dot{m}_{local}}}{\dfrac{\sum_{in} \dot{m}_{local} P_{t,local}}{\sum_{in} \dot{m}_{local}}} = \frac{\sum_{out} \dot{m}_{local} P_{t,local}}{\sum_{in} \dot{m}_{local} P_{t,local}}$$

where $P_{t,\dot{m}avg,out}$ is the mass averaged outflow total pressure, $P_{t,\dot{m}avg,in}$ is the mass averaged inflow total pressure, $P_{t,local}$ is the local total pressure, $\dot{m}_{local}$ is the mass flow rate in the stream tube associated with $P_{t,local}$, $\sum_{out}$ is a summation over the IGV outflow, and $\sum_{in}$ is a summation over the IGV inflow. The surveys showed that the total pressure ratio at location 2 was greater than that at location 1 with an average pressure loss of approximately 6% for the corrected mass flow rates tested. The variation in total pressure ratio with location was consistent with previous measurements.

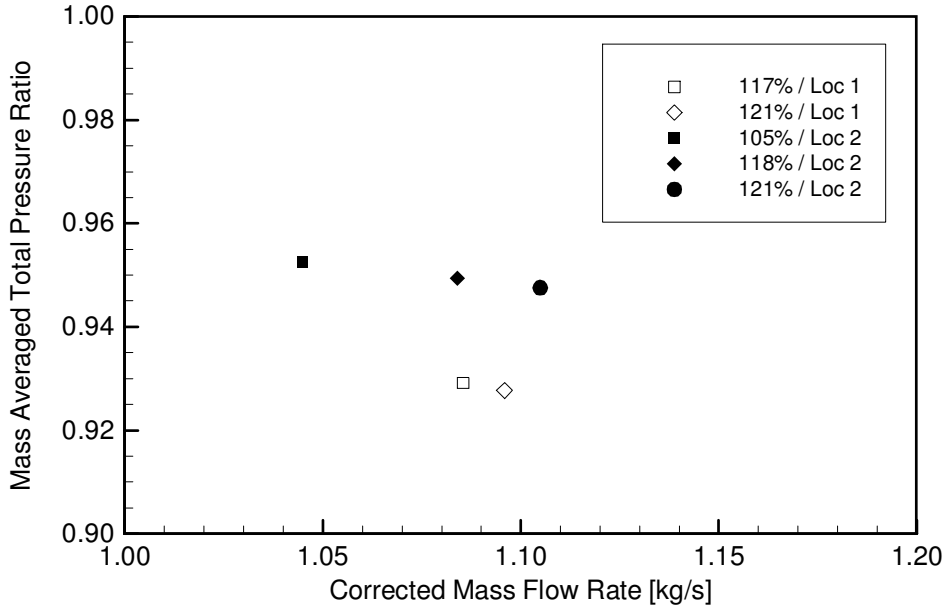

Figure 4-18: Mass averaged total pressure ratio, IGV exit to plenum, for each of the five surveys presented in the previous figure.

When evaluating the above equation the flow area was divided into n+1 stream tubes, where n is the number of radial survey locations. The flow properties in each stream tube were assumed to be the average of the flow properties from the two measurements at the inner and outer radii of the flow tubes. For the innermost and outermost stream tubes, the flow properties at the hub and shroud, respectively, were used. Figure 4-19 shows the results of the survey at 117% speed at location 1 along with the static (total) pressure measurements along the hub and shroud. Also shown are the stream tubes used to calculate the mass averaged values.

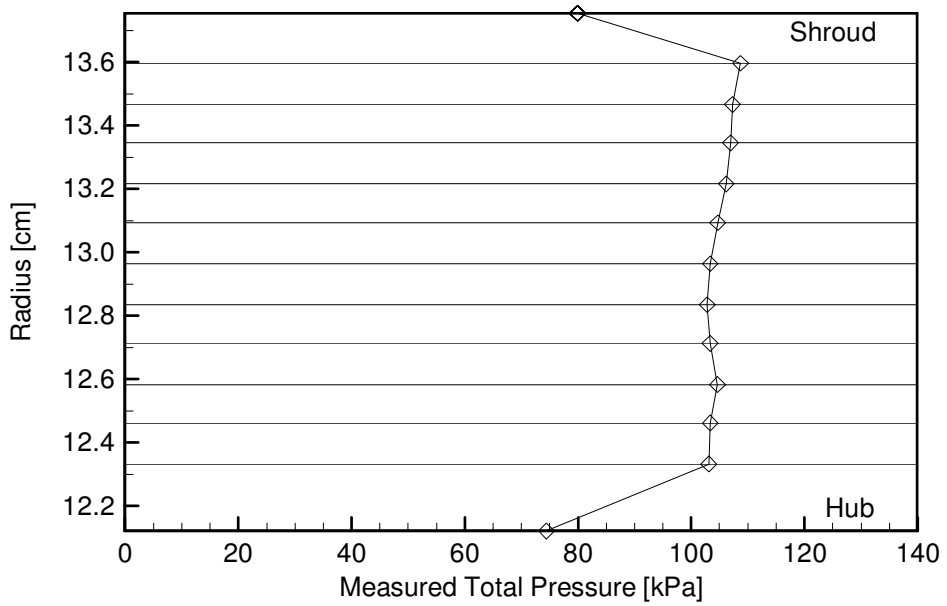

Figure 4-19: Total pressure survey and stream tube boundaries.

4.4.2 IGV Mach Number

The local Mach number of the flow was calculated using the total and static pressure measurements with the assumption of a linear variation in static pressure with radius. Figure 4-20 shows the local Mach number radial profiles at the two different probe locations at different corrected speeds. As one would expect, each local Mach number radial profile was similar to the corresponding total pressure radial profile seen in Figure 4-17.

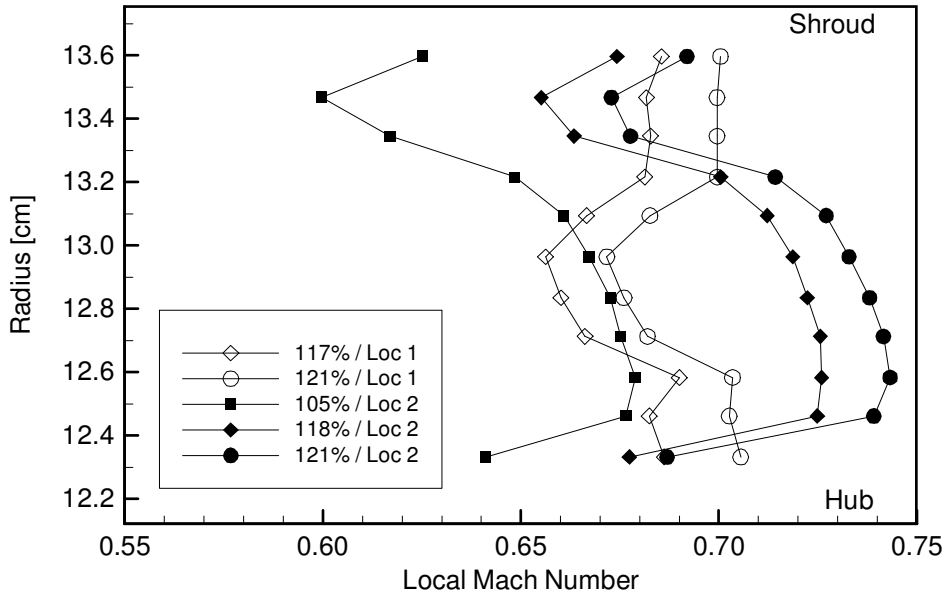

Figure 4-20: Local Mach number radial profiles at different probe locations and different corrected speeds.

Figure 4-21 shows the mass averaged Mach number for each of the five surveys presented in Figure 4-20. The mass averaged Mach number, $M_{\dot{m}avg}$, is defined by

$$M_{\dot{m}avg} = \frac{\sum \dot{m}_{local} M_{local}}{\sum \dot{m}_{local}}$$

where M_{local} is the local Mach number. As expected, the surveys showed that the mass averaged Mach number increased as the corrected mass flow rate was increased.

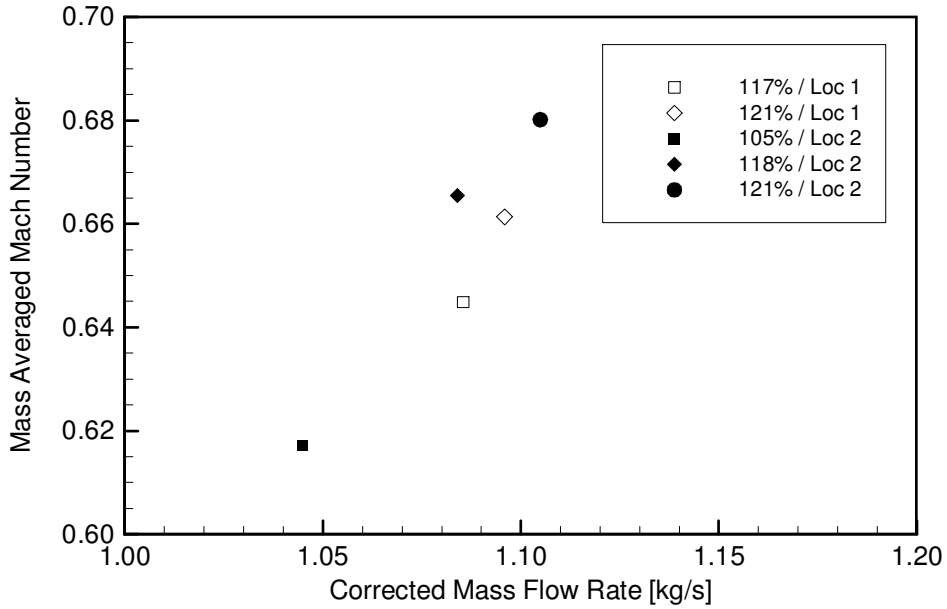

Figure 4-21: Mass averaged Mach number at IGV exit probe location for each of the five surveys presented in the previous figure.

4.4.3 IGV Flow Angle

The flow angle was measured using the performance probe. The mass flow through each stream tube could be calculated with the local density, ρ; area, A; velocity, u, and flow angle, θ.

$$m = \rho A u \cos(\theta)$$

By adding the mass flow rate from all of the tubes, the flow rate through the IGV was calculated. This calculated flow rate was usually slightly different from the measured mass flow rate, $\dot{m}_{meas}$. The continuity corrected flow angle, θ_{cor}, is then defined by

$$\theta_{cor} = \arccos\left(\frac{\dot{m}_{meas}}{\sum \dot{m}_{local}} \cos(\theta_{meas}) \right)$$

where $\sum \dot{m}_{local}$ is the calculated mass flow rate and θ_{meas} is the measured flow angle.

Figure 4-22 shows the continuity corrected flow angle radial profiles at the two different probe locations and different corrected speeds. It is seen that the flow angle at location 2 was typically about 69° in the center of the flow path and lower near the two walls due to boundary layer effects. The flow angle at location 1 peaked at about 70°, similar to that of location 2, but appears to have a large boundary layer influence from the shroud.

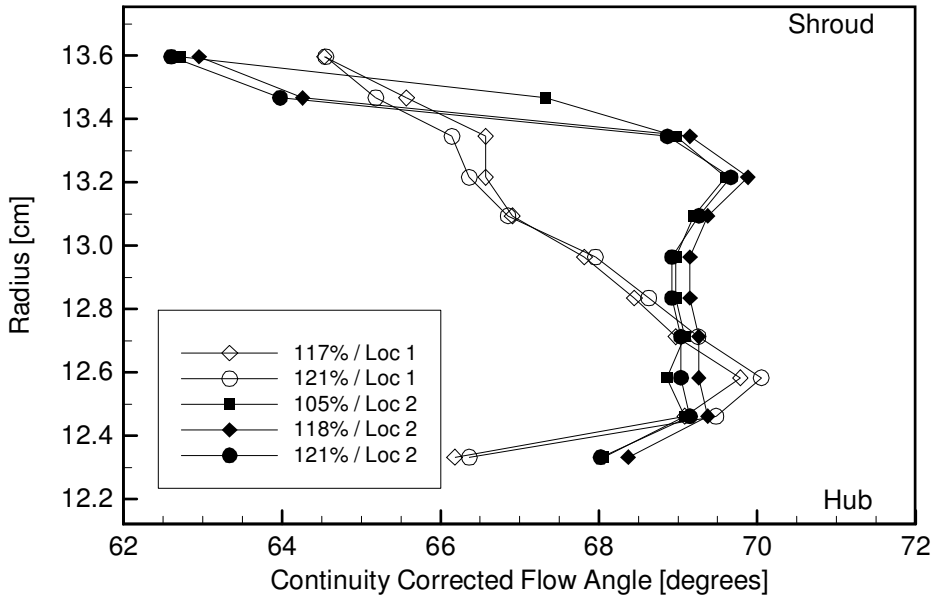

Figure 4-22: Continuity corrected flow angle radial profiles at different probe locations and corrected speeds.

Figure 4-23 shows the mass averaged continuity corrected flow angle for each of the five surveys presented in Figure 4-22. This angle is calculated in a manner similar to the mass averaged Mach number. As expected, the continuity corrected flow angle at location 2 was higher than that of location, although the difference was only about 1°.

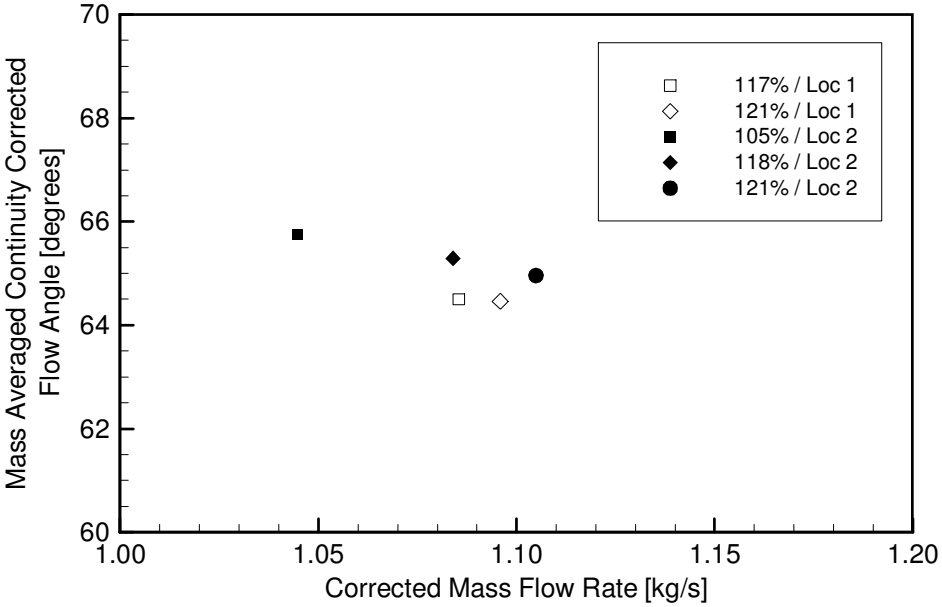

Figure 4-23: Mass averaged continuity corrected flow angle at IGV exit probe location for each of the five surveys presented in the previous figure.

4.4.4 Comparison with Previous Measurements and CFD

Figure 4-24 shows the mass averaged total pressure ratio data from Figure 4-18 plotted with the data reported by Williams (2007). Solid symbols represent new data. Previous data

were gathered at six different circumferential locations. Data were gathered over a wide range of corrected mass flow rates with the probe located at the location labeled C0. For the other five locations, data were gathered at only two corrected mass flow rates. The new data were gathered 9.5 mm (0.37 inches) upstream of the previous measurement location to prevent the rotor from hitting the probe, so one would expect the losses to be slightly lower. However, it can be seen that the new data show significantly more total pressure loss despite being closer to the IGV even when considering the small additional total pressure loss associated with the inlet.

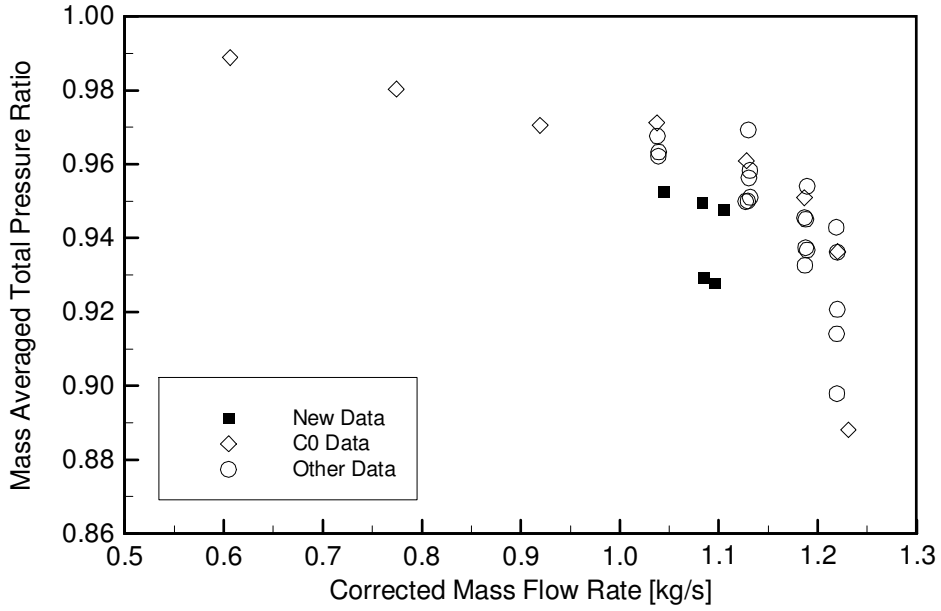

Figure 4-24: Calculated mass averaged total pressure ratio from plenum to post-IGV probe location. The solid symbols represent the new data discussed in this section while the open symbols are the data from previous measurements reported by Williams (2007). The new data are in general agreement with previous measurements.

This additional total pressure loss was also seen in CFD simulations of the inlet flow. The additional total pressure loss was attributed to the fully developed flow profile entering the IGV when the inlet was installed. The fully developed profile resulted in higher centerline velocities, for the same mass flow rate, which produced higher losses in the IGV. Figure 4-25 compares the new experimental data with the CFD simulations plotted in Figure 3-47. The experimental data should be compared with the CFD results at the survey location. The experimental data were in good general agreement with the values of the CFD simulations at the survey plane. The figure also shows a curve fit to the CFD results at the rotor inlet which was used during analysis of the data.

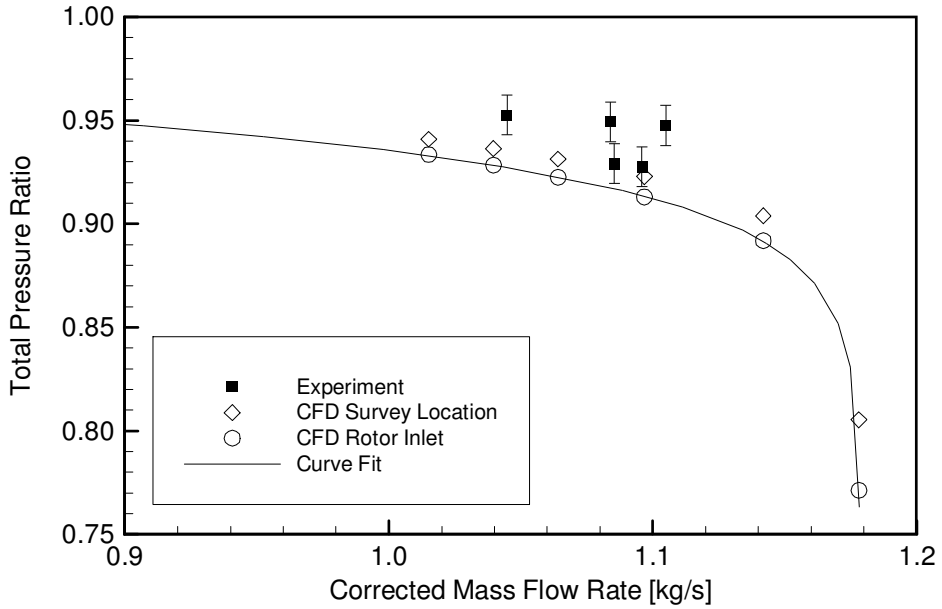

Figure 4-25: Calculated mass averaged total pressure ratio from IGV exit to plenum compared with CFD simulation presented in Figure 3-47. The measurements are in general agreement with the CFD simulations.

Figure 4-26 shows the mass averaged Mach number data from Figure 4-21 plotted with the data reported by Williams (2007). The solid symbols represent the new data. It can be seen that the new data are consistent with the previous measurements.

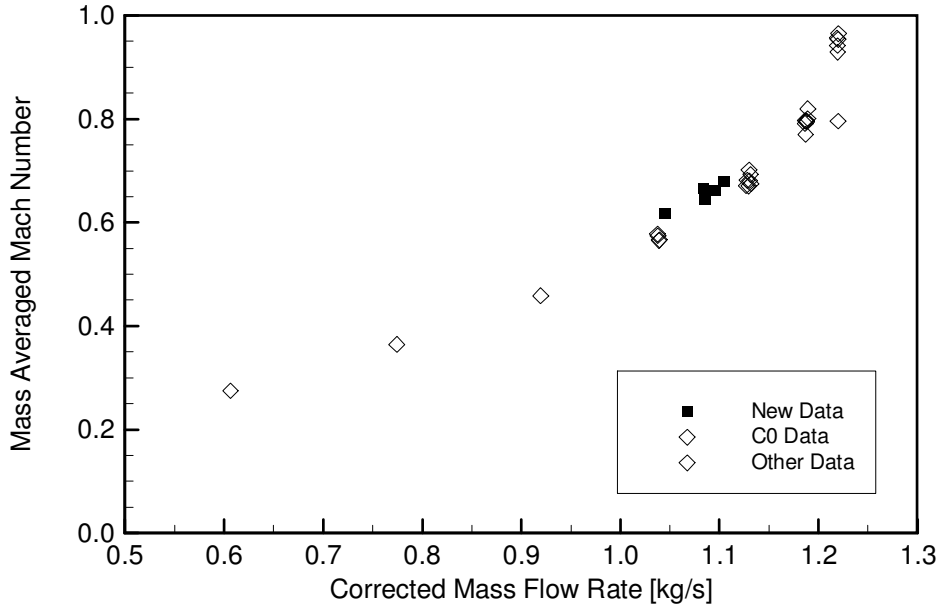

Figure 4-26: Calculated mass averaged Mach number at IGV exit probe location. The solid symbols represent new data discussed in this section while the open symbols are data from previous measurements reported by Williams (2007). The new data are in general agreement with previous measurements.

Figure 4-27 shows the mass averaged continuity corrected flow angle data from Figure 4-23 plotted with the data reported by Williams (2007). The solid symbols represent the new data. It can be seen that the new data are consistent with the previous measurements although the new data may result in a slightly higher flow angle for the same corrected mass flow rate. One possible explanation is the rotor caused the flow to turn slightly more to better align with the rotor strakes.

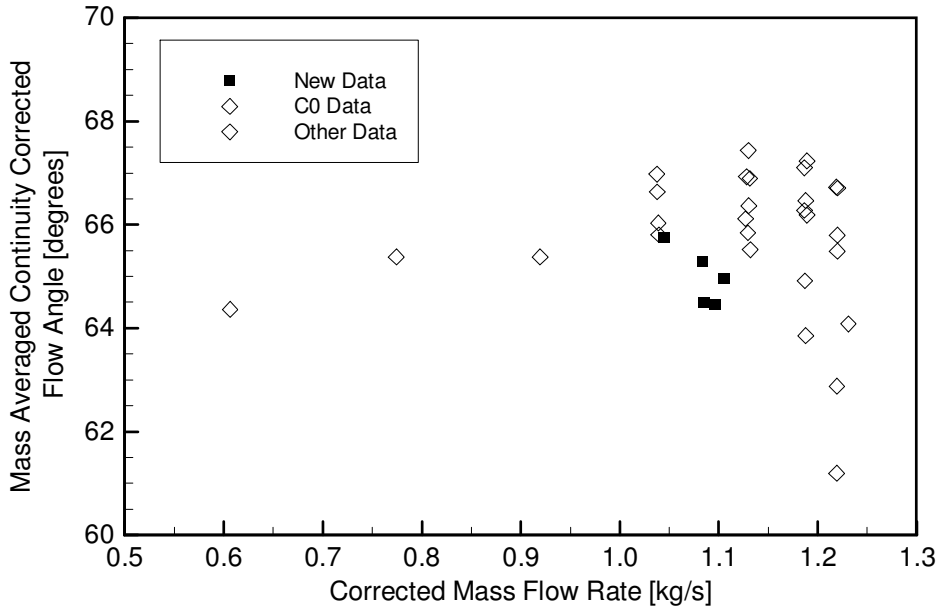

Figure 4-27: Calculated mass averaged continuity corrected flow angle at IGV exit probe location. The solid symbols represent new data discussed in this section while the open symbols are data from previous measurements reported by Williams (2007). The new data are in general agreement with previous measurements.

4.4.5 IGV Performance Conclusions

The Rampressor-2 test rig was modified to make total pressure, static pressure, and flow angle measurements between the IGV and the rotor while the rotor was rotating. Radial surveys were taken at two circumferential locations and three operating speeds. Results of the surveys indicated that the mass averaged total pressure ratio, IGV exit to plenum, were larger than previous measurements reported by Williams (2007) due to the fully developed flow profile. However, the mass averaged Mach number and mass averaged continuity corrected flow angle were in agreement with previous measurements, as anticipated. Due to the large variation in the flow profile with circumferential location it was not possible to determine if the presence of the inlet and rotor affected the flow locally.

4.5 Rotor Performance

As mentioned earlier the purpose of the rotor test was to operate the test rig at the highest possible total pressure ratio. This required operating the rotor so that it was capturing the design point corrected mass flow rate of 1.15 kg/s (2.53 lbm/s). In addition, it was necessary to minimize the tip gap between the rotor and the shroud.

4.5.1 Test procedure

The rotor performance testing followed the test procedure outlined in section 4.2.1 to accelerate the rotor to the desired test speed. Liquid nitrogen was then added to the main air to cool it to approximately 235°K (-37°F) increasing the corrected speed of the rotor and the corrected mass flow rate. Once the desired temperature was obtained, the tip ring was moved in order to reduce the tip gap. In order to obtain the highest total pressure ratio, the tip ring was moved until all of the tip gap measurements indicated a tip gap of under 0.0254 mm (0.001 in). Typically this required rubbing the tip ring against the abradable coating on the inside of the tip ring. When an acceptable tip gap was obtained, the throttle valve was closed incremental amounts until pressure downstream of the rotor had increased a certain amount, typically 34 kPa (5 psig). The increasing back pressure resulted in an increase in temperature which resulted in thermal growth of the rotor and the tip ring. Typically, the thermal growth of the tip ring was larger than the thermal growth of the rotor, so it was necessary to move the tip ring while thermal equilibrium was occurring in order to keep the tip gap constant. Once thermal equilibrium was reached, the throttle valve was closed further and the process was repeated until unstart occurred.

Data for the tests were gathered by two methods. All pressure and temperature measurements were taken by Boeing's data acquisition system. A single data point for each of approximately 100 of the data channels were sent to and stored on a Ramgen computer every 4-5 seconds for the duration of the test. This was called the real time data. When desired, data were gathered, processed, and stored by Boeing's data acquisition system. In this process the data from each channel were averaged over a period of time resulting in higher quality data. Additionally, a larger number of channels could be gathered and more detailed processing could be applied. This was called the set point data.

As mentioned above the design point corrected mass flow rate was 1.15 kg/s (2.53 lbm/s) which occurred at a rotor mechanical speed of 41,439 rpm. Early tests showed that at 42,000 rpm with the rotor started the corrected mass flow was only 1.06 kg/s (2.34 lbm/s). One method of increasing the corrected mass flow rate was to increase the mechanical speed. By increasing the rotor speed to 44,000 rpm the corrected mass flow rate increased to 1.10 kg/s (2.42 lbm/s). The rotor was operated at mechanical speeds as high as 46,000 rpm but at speeds over 44,000 rpm unusual instabilities occurred so rotor performance testing was conducted at speeds of 44,000 rpm and below.

Another way to increase the corrected mass flow rate was to reduce the temperature of the incoming air. Although equation (4-2) seems to indicate that the corrected mass flow rate would decrease by decreasing the temperature, this is not the case. By decreasing the temperature, the density of the main flow increased inversely proportional to the change in temperature. This resulted in an increase in the mass flow rate through the rotor and an overall increase in the corrected mass flow rate. As indicated by equation (4-1) decreasing the inlet temperature also increases the corrected speed. By adding liquid nitrogen to the main flow, the corrected mass flow rate could be increased to the design point condition.

4.5.2 Total Pressure Measurements

The performance probe shown in Figure 4-1 measured the total pressure, total temperature, and flow angle downstream of the rotor. Figure 4-28 shows the total pressure probe in relation to the rotor. The total pressure probe was attached to the tip ring which was moved

during tests to adjust the tip gap. As the tip ring moved, the distance between the performance probe and the tip ring increased. Therefore, in the following plots of total pressure, each data point is taken at a different axial location relative to the rotor. During a typical test the tip ring moved up to 6.4 mm (0.25 in) from the point in which a small tip gap was obtained to the point where unstart occurred. By the end of the test the performance probe could be over 25 mm (1.0 in) from the rotor exit. Total pressure loss between the rotor exit and the performance probe was significant due to the flow's high swirl at the rotor discharge. Swirl angle increased with total pressure, leading to higher total pressure loss at those conditions.

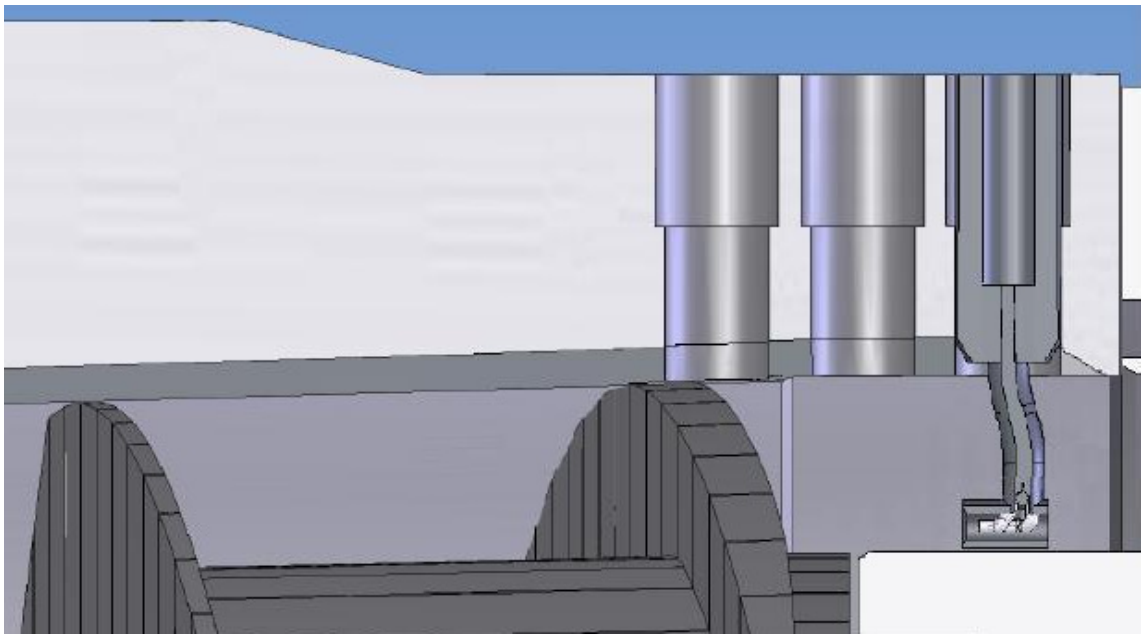

Figure 4-28: Location of the performance probe relative to the rotor. The performance probe could be positioned vertically in the flow path for radial surveys. Here it is shown positioned near the hub. The tip gap was adjusted by sliding the tip ring axially which also moved the performance probe relative to the rotor exit.

4.5.3 Rampressor 2 Rotor Pressure Ratio Post Processing

One of the critical goals of the Rampressor-2 test program was to demonstrate the maximum "rotor-only" total pressure ratio of the Ramgen supersonic shock compression rotor to validate CFD predictions Rotor-only total pressure ratio is defined as follows:

$$PR_{rotor} = \frac{Pt_{rotor\_exit}}{Pt_{rotor\_inflow}}$$

where the rotor exit and rotor inflow total pressures are mass averaged quantities. As in most turbo-machinery tests, it was not possible to measure the mass averaged rotor inflow and exit total pressures directly during the test. As a result these values were calculated based on various quantities that were measured during each test.

Rotor Inflow Total Pressure

In order to determine the mass averaged rotor inflow total pressure, the test rig supply total pressure was measured by multiple total pressure probes immediately upstream of the rig

bellmouth inflow duct. With the multiple measurements and the low velocity at this location, this was considered to be a relatively accurate measurement of average total pressure at that location. Between the bellmouth inflow and the rotor inflow plane, a number of features exist that create total pressure loss including a relatively long constant area annulus, an IGV row, and various surface features, such as steps and gaps, that contribute to the total pressure loss between the bellmouth and the rotor inflow plane. The total pressure loss characteristics of the integrated inflow duct system were characterized as a function of corrected mass flow through the duct using a combination of duct flow measurements and CFD.

The total pressure loss of the inflow annulus and IGV row was determined by comparing the total pressure measured at the bellmouth inflow with total pressure measurements just downstream of the IGV row but some distance upstream of the rotor inflow plane. The total pressure measurements just downstream of the IGV row were performed with the rotor installed and operating at near full speed but at low back pressure levels to simulate the actual flow field that existed during high rotor pressure ratio testing as closely as possible. Radial surveys of total pressure were made for a few corrected mass flow levels at two circumferential locations. These measurements showed good agreement with the mass averaged total pressure loss characteristics predicted by a three dimensional viscous CFD simulation of the entire inflow duct, see Figure 4-25. Having validated the CFD model of the inflow duct, the CFD simulation was then used to characterize the final total pressure loss that occurred between the measurement plane just downstream of the IGV row and the rotor inflow duct. There were additional steps and gaps in the hub and shroud surfaces in this region that contributed additional total pressure loss between the IGV discharge location and the rotor inflow plane. With these losses characterized as a function of corrected mass flow, the total pressure loss between the measured bellmouth inflow plane (measured continuously during every test) and the rotor inflow plane could be calculated for any test case given the corrected mass flow. This approach allowed for the mass averaged rotor inflow total pressure to be calculated for any test condition where bellmouth inflow total pressure and corrected mass flow were known.

Rotor Exit Total Pressure

The total pressure downstream of the rotor was measured using a hybrid three hole nulling Kiel probe mounted in the external shroud. The shroud was translated axially during testing to minimize the gap between the rotor strake tips and the non-rotating shroud itself. With increasing rotor pressure ratios the shroud was moved in the axial direction down stream from the rotor. This had the effect of increasing the distance from the rotor discharge plane to the probe during a test as back pressure and rotor pressure ratio were increased.

The mass average total pressure loss between the rotor discharge plane and the downstream location of the total pressure probe was calculated using a duct loss model developed by Ramgen. The Ramgen model characterized the viscous losses in the highly swirling duct annulus between the rotor discharge plane and the total pressure measurement. This model assumed an exponential decay in swirl angle that is generally accepted for such flow fields (Sparrow and Chaboki, 1984; Uskanar, 1999; Talbot, 1954; Kreith and Sonju, 1965) to calculate the local flow angle variation on the hub and shroud surfaces between the rotor exit plane and the total pressure measurement plane. The local flow angle variation on the hub and shroud surfaces was then used to determine the total path length over which the flow was

exposed to the hub and shroud surfaces as it progressed from the rotor discharge plane to the downstream location of the total pressure measurement.

The shroud internal surface was coated with an abradable material and the roughness of this surface was measured using optical profilometry by Micro Photonics, Inc. (Irvine, CA) and characterized by the mean roughness technique (Taylor *et al.*, 2005). The hub surface was a machined metal surface and the roughness was specified in the manufacturing process. With the effective lengths of hub and shroud surface exposed to the flow as determined from the local flow angle variation and standard correlations for total pressure loss due to surface roughness in pipe and duct flows (Vennard and Street, 1982; Schetz and Street, 1996; Moody, 1944), the total pressure loss between the rotor exit plane and location of the total pressure measurement was calculated.

The model developed by Ramgen was validated using data from two tests (runs 201 and 202) taken at times where the test conditions and rig discharge plenum pressures were highly comparable but the location of the performance probe was shifted. Careful comparison of these data was used to validate the total pressure loss in the discharge duct. This resulted in a generalized correlation for total pressure loss in the duct that accounts for rotor discharge swirl angle, axial distance from rotor discharge plane to performance probe, and rotor discharge flow dynamic pressure.

Results

Processed data from four tests is shown in Figure 4-29. Each line was at constant corrected speed, and as the speed of the rotor was increased the speed lines became steeper and a higher maximum total pressure ratio was achieved. During the two high speed tests the tip clearance was minimized by rubbing the shroud into the rotor after each increase in back pressure. The tip clearance was measured to be less than 0.03±0.05 mm (0.001±0.002 in) during both tests. The resultant speed lines were very steep, with only a small amount of reduction in corrected mass flow rate as pressure ratio across the rotor increased. This reduction was caused by increased tip leakage into the flow path upstream of the throat resulting in increased flow path blockage. The two tests at lower speeds had large tip clearances, approximately 0.38 mm (0.015 in), and the combination of lower speed and larger tip clearance resulted in speed lines with shallower slopes and lower maximum total pressure ratio.

When the back pressure was increased too far, the normal shock wave in each rotor passage moved from its design location downstream of the throat to upstream of the strake leading edge. This resulted in spillage and subsequent reduction in corrected mass flow rate, a process known as unstart. The Rampressor-2 unstart process, although sudden, was benign in that it did not result in excess vibration or other adverse effects. The highest pressure ratio point occurred just prior to unstart and one can observe the slope of the curve decreasing just before unstart. The maximum pressure ratio obtained was $7.76^{+0.93}_{-0.67}$.

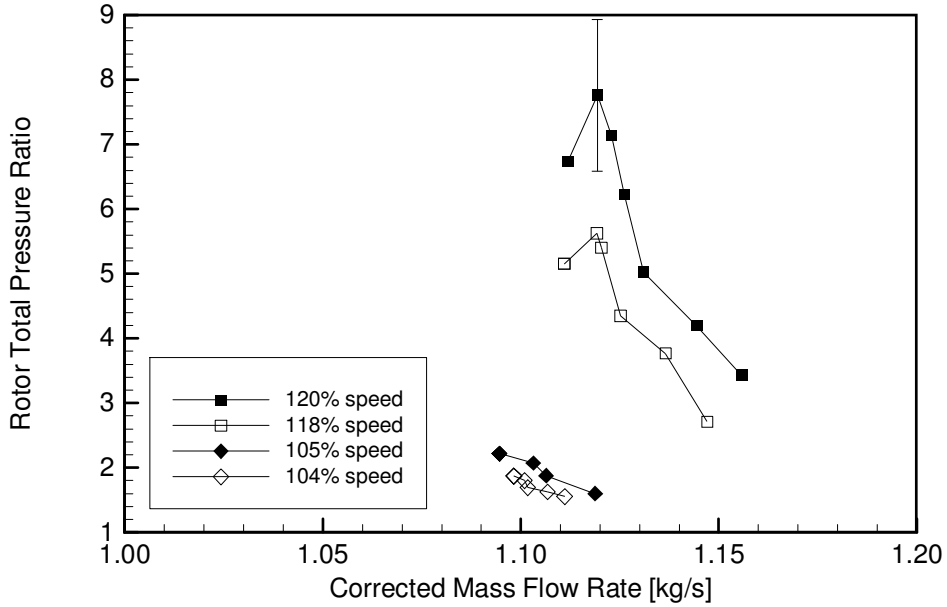

Figure 4-29: Variation of corrected mass flow rate with total pressure ratio and the effect of corrected speed. The drop in total pressure ratio and corrected mass flow rate due to unstart can be seen in the two high speed cases.

The effect of tip clearance is shown in Figure 4-30. The line labeled A was shown in the previous figure and had tip clearance minimized by rubbing into the shroud. The line labeled B was at the same corrected speed but the tip clearance was 0.03-0.05 mm (0.001-0.002 in). The speed line was still steep but had a lower maximum total pressure ratio and lower corrected mass flow rate for a given total pressure ratio. The test at 119% corrected speed had a tip clearance of 0.05-0.08 mm (0.002-0.003 in) and resulted in a speed line whose slope decreased significantly as the back pressure was increased. The final speed line was at 106% and showed a case where a significant change in tip gap was made during the test. At the start of the test the tip gap was approximately 0.38 mm (0.015 in). Midway through the test, the tip gap was reduced to 0.30 mm (0.012 in) resulting in a shift in the speed line to a higher corrected mass flow rate and a higher total pressure ratio.

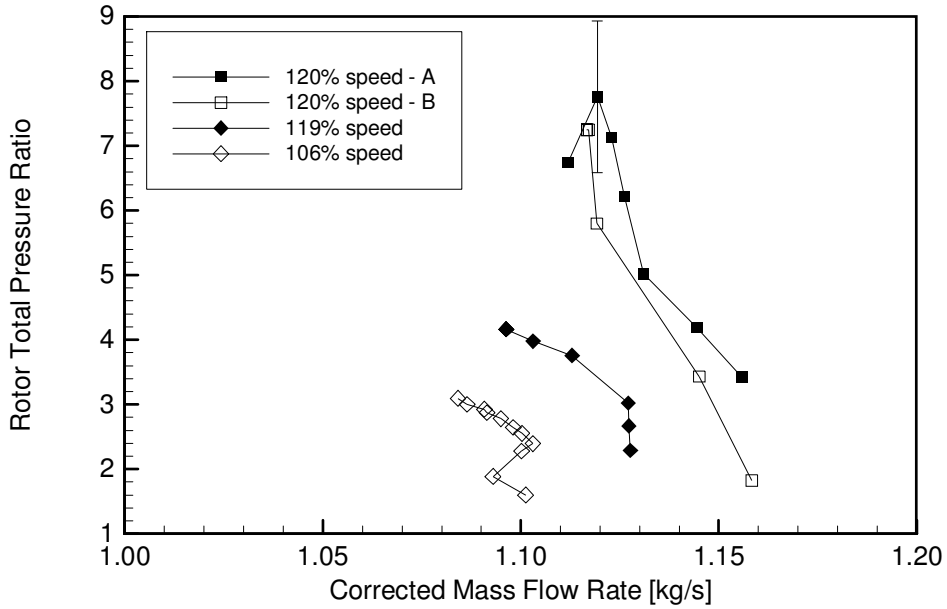

Figure 4-30: Variation of corrected mass flow rate with total pressure ratio and the effect of tip clearance. See text for details on tip clearance for each speed line.

Figure 4-31 shows the radial variation in rotor total pressure ratio for a test at 120% corrected speed. Despite the low radial resolution of the survey, thick boundary layers on both the hub and shroud are resolved. In the core flow, the total pressure ratio increases slightly with radius which was expected since the Mach number in the rotor frame, and, hence, total pressure, increased with radius.

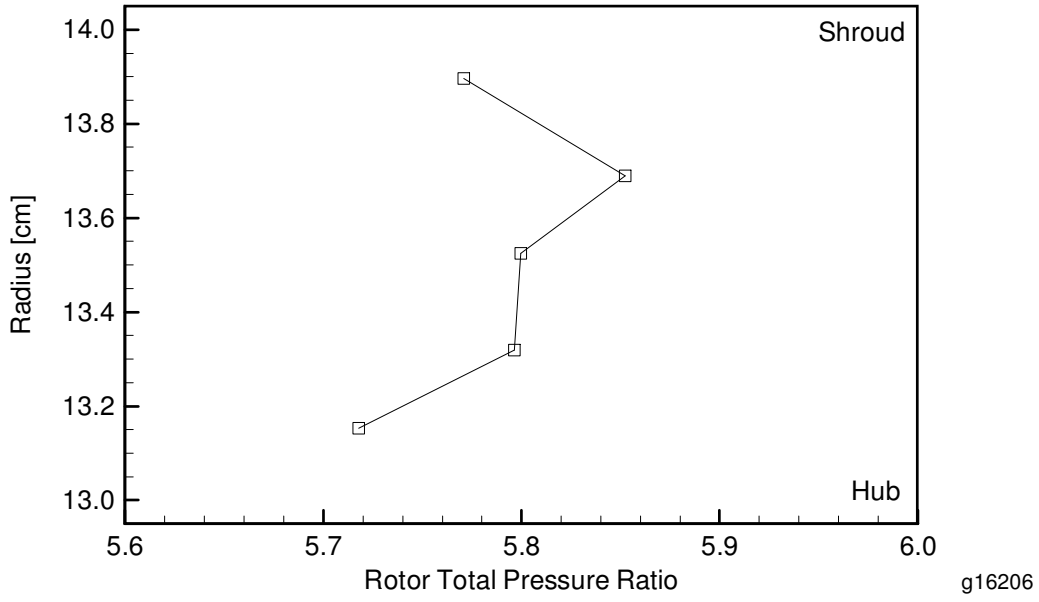

Figure 4-31: Radial variation of rotor total pressure ratio for a test at 120% corrected speed.

4.5.4 Rotor Flow Path Efficiency Calculations

The efficiency of the rotor flow path, η, is given by

$$\eta = \frac{\pi^{(\gamma-1)/\gamma} - 1}{\tau}$$

where π is the rotor total pressure ratio, τ is the rotor total temperature ratio, and γ is the ratio of specific heats of the gas. Using the rotor total pressure ratio results from the previous section and the total temperature ratio measurements the rotor efficiency can be calculated. Due to the proprietary nature of the efficiency calculations, the rotor flow path normalized efficiency, $\tilde{\eta}$, is reported here and is defined as

$$\tilde{\eta} = \frac{\eta}{\eta_{\max}}$$

where $\eta_{\max}$ is the maximum efficiency measured during the test program.

The effect of corrected speed on the normalized efficiency is shown in Figure 4-32. The efficiency speed lines were found to be steep, just like the total pressure ratio speed lines. As the total pressure ratio increases along a speed line the normalized efficiency increases, reaching a maximum at the maximum total pressure ratio. When unstart occurred the efficiency dropped. Increasing the corrected speed shifted the speed lines up and to the right.

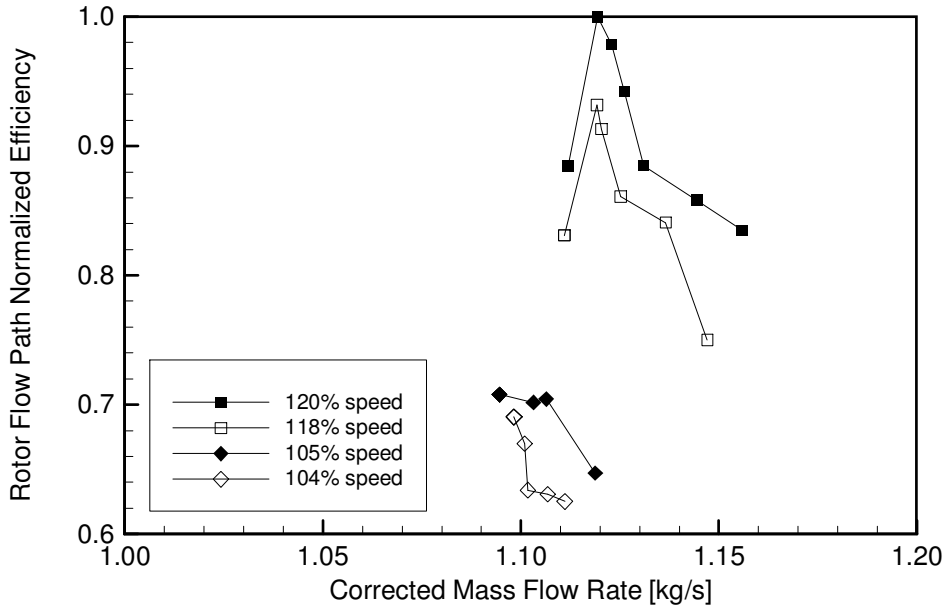

Figure 4-32: Relationship between corrected mass flow rate and normalized efficiency and the effect of corrected speed. The drop in efficiency and corrected mass flow rate due to unstart can be seen in the two high speed cases. The speed lines shown are the same as in Figure 4-29.

The effect of tip clearance on the normalized efficiency is shown in Figure 4-33. The line labeled A was shown in the previous figure and had tip clearance minimized by rubbing into the shroud. The line labeled B was at the same corrected speed but the tip clearance was 0.03-0.05 mm (0.001-0.002 in). The speed line was still steep but had a lower maximum efficiency and lower corrected mass flow rate for a given total pressure ratio. The test at 119% corrected speed had a tip clearance of 0.05-0.08 mm (0.002-0.003 in) and resulted in a speed line which

flattened as the back pressure was increased. The final speed line was at 106% and showed a case where a significant change in tip gap was made during the test. At the start of the test the tip gap was approximately 0.38 mm (0.015 in). Midway through the test, the tip gap was reduced to 0.30 mm (0.012 in) resulting in a shift in the speed line to a higher corrected mass flow rate and a higher efficiency.

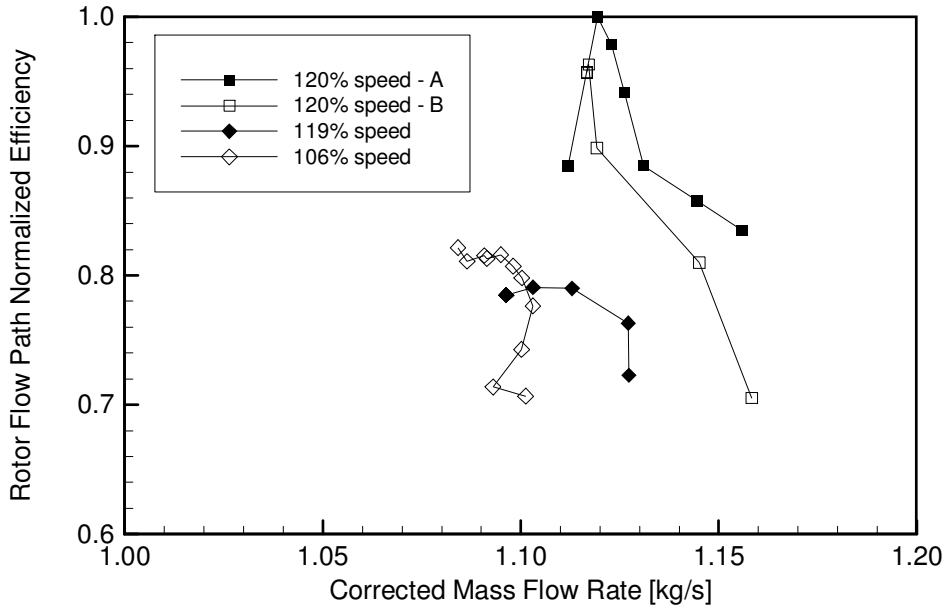

Figure 4-33: Effect of tip gap on normalized efficiency. The speed lines shown are the same as in Figure 4-30. See text for details on tip clearance for each speed line.

Figure 4-34 shows the radial variation in normalized efficiency for a test at 120% corrected speed. The efficiency was nearly uniform across the portion of the flow path surveyed but did decrease slightly with increasing radius.

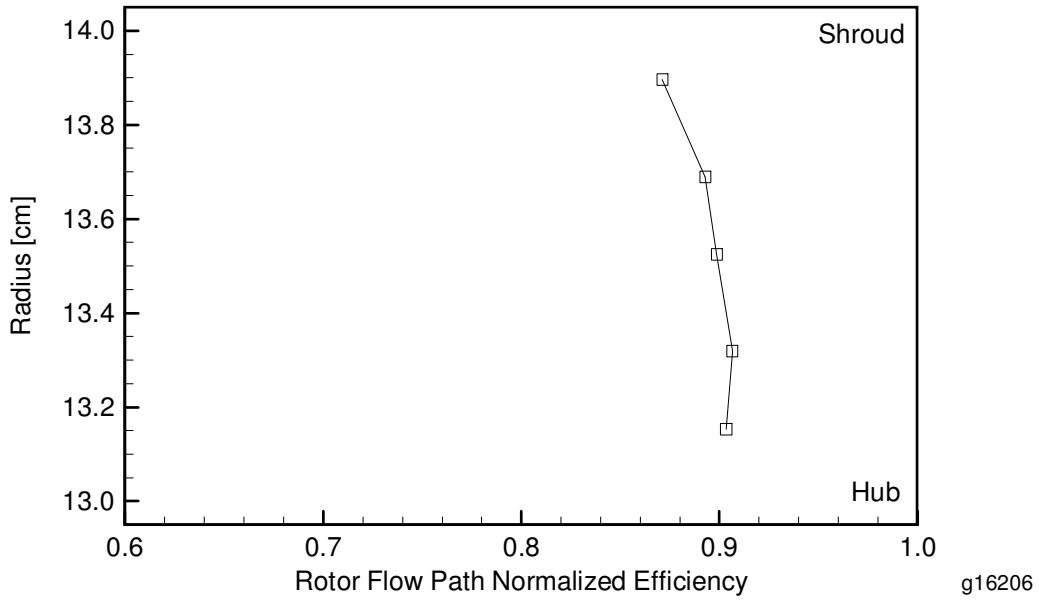

Figure 4-34: Radial variation of normalized efficiency for a test at 120% corrected speed. The survey shown is the same as in Figure 4-31.

4.5.5 Flow Angle Measurements

When making the total pressure measurements, the performance probe was aligned with the flow by adjusting the probe angle until the two nulling ports indicated the same pressure. This process also measured the flow angle. Due to the highly swirling flow, the path length, and hence, total pressure, at the upstream and downstream nulling ports was different resulting in incorrect flow angle measurements. However, the accuracy of the data was improved with a continuity correction. By integrating the local mass flux along the survey the total mass flow rate was calculated. This was not equal to the measured mass flow rate. By applying the appropriate small change of angle to each measurement the correct mass flow rate was obtained. The sum of the measurement and the small change of angle was the continuity corrected flow angle. At low total pressure ratios, when the flow angle was small, the angle correction was typically less than one degree. At the highest total pressure ratios, when the swirl was at a maximum, the angle correction was typically about seven degrees.

Figure 4-35 shows the variation of flow angle with rotor total pressure ratio for the test that generated the highest total pressure ratio. The corrected flow angle was approximately 67° at a moderate total pressure ratio of 3.4, and increased to nearly 84° at the maximum total pressure ratio of 7.76. When unstart occurred the corrected flow angle was nearly unchanged.

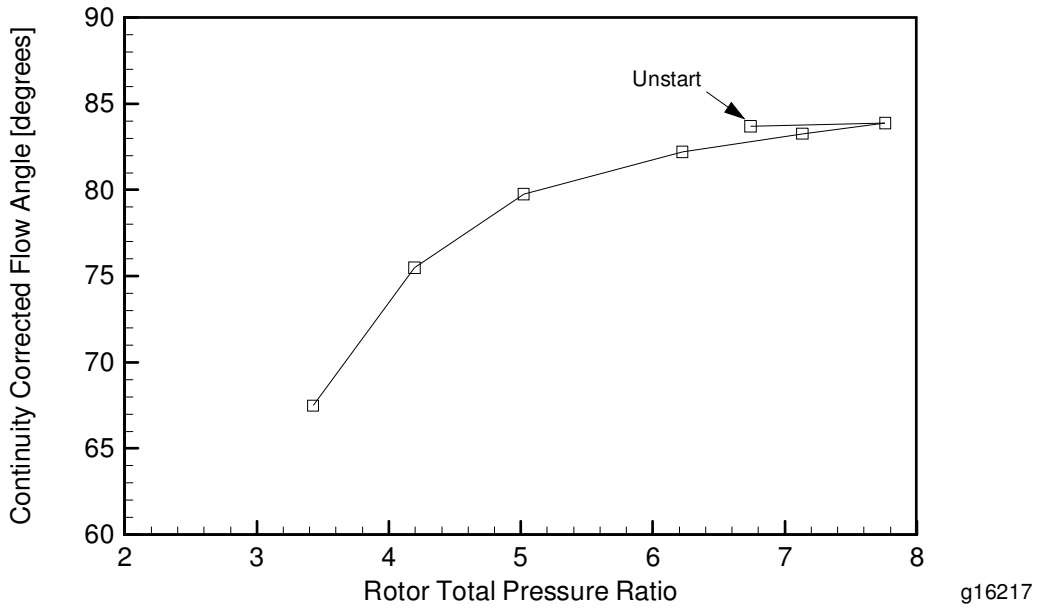

Figure 4-35: Variation of centerline continuity corrected flow angle with total pressure ratio for run which achieved the highest total pressure ratio.

Figure 4-36 shows the radial variation in corrected flow angle for a test at 120% corrected speed. The flow angle is seen to be nearly uniform with only a slight increase with radius.

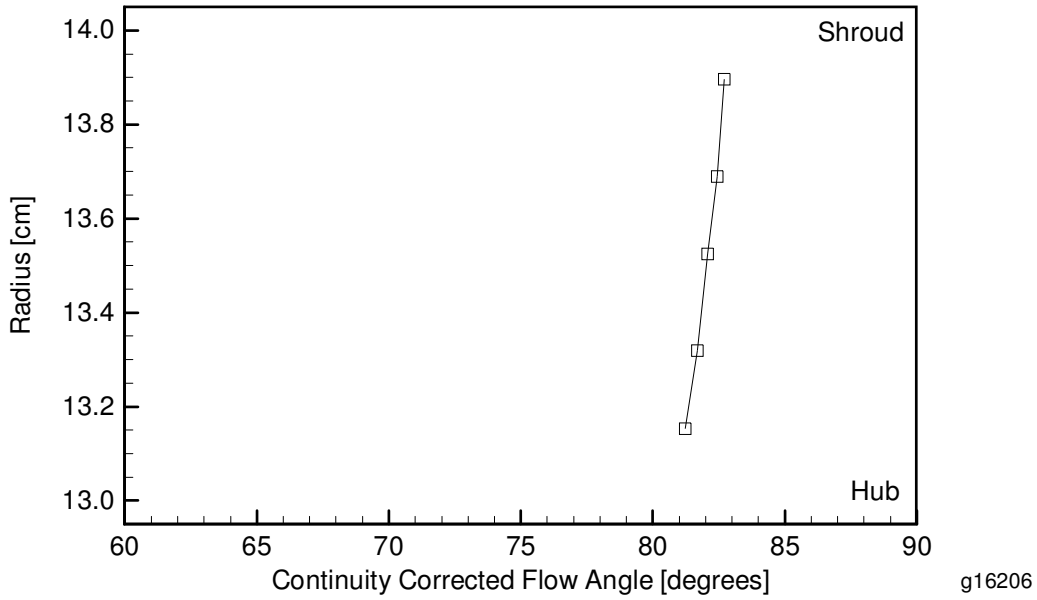

Figure 4-36: Variation of continuity corrected flow angle with radius for the survey shown in Figure 4-31.

4.5.6 Future Testing

Due to the failure of the Rampressor-2 drive train discussed in Williams (2007), Ramgen had limited test time available and was not able to thoroughly test the Rampressor-2 hardware. All of the data presented in this report was from tests conducted with maximum bleed mass flow rates. Future testing should examine the effects of bleed mass flow rate variation on the maximum total pressure ratio and efficiency.

During the test program it was desired to run with a minimum tip gap. Understanding the tip gap measurements and other rig indicators of tip clearance required a significant amount of the limited testing. It was only near the end of the program that Ramgen gained the ability to operate the Rampressor with minimum tip gap. It is desired to understand how the tip gap affects the performance of the rotor so future testing should evaluate this effect. During this program Ramgen obtained measurements at a variety of tip clearances, however, due to physical and operational constraints the gap was not uniform around the rotor nor was it constant along speed lines.

The data presented in this report provide an indication of a Rampressor compressor map. Again, due to limited testing, the number of speed lines presented is limited. Additionally, the tip gap varies along many of the speed lines as well as between speed lines. Future testing should include the generation of complete compressor maps at different tip clearances.

4.5.7 Rotor Performance Conclusions

The testing of the Rampressor-2 rotor showed that it was capable of generating a large pressure ratio in a single stage. With the rotor rubbing into the tip ring, the Rampressor achieved a total pressure ratio of 7.76:1. This was found to be in good agreement with CFD simulations assuming a tip gap on the order of 0.001 to 0.002 inch.

Chapter 5

Conclusions

Detailed analysis of the Rampressor-2 drive train failure discussed in Williams (2007) determined that the failure was due to unexpected rotordynamic vibration. The drive turbine manufacturer had improperly designed turbine dampers, claimed erroneous damping characteristics, and provided inappropriate rotordynamic design guidance for the test rig. With the assistance of an independent rotordynamics expert, Ramgen redesigned the rig drivetrain and was able to complete the test program.

Through an extensive verification procedure, Ramgen demonstrated that its CFD tool was capable of modeling Rampressor flow physics. Verification cases included boundary layer development, separation due to adverse pressure gradients, centrifugal compressor flows, and shock wave/boundary layer interactions. CFD simulations of the flow inlet flow were found to be in agreement with experiment. Simulations of the rotor flow predicted a total pressure ratio of up to approximately 8.55:1 for a tip gap of 0.001 inch and of approximately 5.81:1 for a tip gap of 0.003 inches. These simulations were found to be in good agreement with test results showing that Ramgen has a solid design tool capability.

During the test program, Ramgen measured the performance of the annulus-shaped inlet and found the total pressure loss to be approximately 0.5%. IGV losses were also measured and found to be in good agreement with the CFD simulations. During starting tests the rotor was found to start at approximately 100% speed provided that full bleed was available. Performance testing demonstrated a rotor total pressure ratio of almost 7.8:1 which was in agreement with CFD simulations. A higher total pressure ratio is achievable with further development of the supersonic flow path. Testing showed that the Rampressor concept is capable of achieving high total pressure ratios across the rotor.

The Rampressor-2 test program has proven that high total pressure ratio, single stage, supersonic compression is viable, that Ramgen's tools accurately predict test performance, and lay the groundwork for further development and commercial demonstration. During the test program Ramgen achieved a rotor only total pressure ratio of 7.8:1 which is a substantial improvement over the previous Rampressor test program which obtained a total pressure ratio of 2.3:1. Ramgen's commercial targets are a total pressure ratio of 10:1 and a stage efficiency of approximately 85%. More work is required prior to commercial introduction of a Rampressor product, but since the technology is young and Ramgen has made rapid leaps in progress and performance, Ramgen is confident the commercial targets are achievable.

References

Arnone, A., "Viscous Analysis of Three-Dimensional Rotor Flow Using a Multigrid Method," *ASME J. Turbomachinery*, Vol. 116, pp. 435-445, 1994.

Bardina J.E., Huang P.G., and Coakley T.J., "Turbulence Modeling Validation, Testing, and Development," NASA TM-110446, 1997.

Bogar, T.J., Sajben, M., and Kroutil, J.C., "Characteristic Frequencies of Transonic Diffuser Flow Oscillations," *AIAA J.*, Vol. 21, no. 9; pp. 1232–1240, 1983.

Bressler, T.S., "Nozzle Test Facility at The Boeing Company's Aero/Noise/Propulsion Laboratory," AIAA paper 2003-4454, 2003.

Bressler, T.S., Private communication, 11 October 2007.

Casey, M., "Best Practice Advice for Turbomachinery Flows," in *Proceedings of the 4th QNET-CFD Workshop*, Brussels, Belgium, 2004.

Castillo, L., Wang, X., and George, W.K., "Separation Criterion for Turbulent Boundary Layers Via Similarity Analysis," *ASME J. Fluids Eng*., Vol. 126, pp.297-304, 2004.

Cebeci, T., and Bradshaw, P., *Momentum Transfer in Boundary Layers*, McGraw-Hill, New York, pp. 194, 1977.

Chima, R.V., "Viscous Three-Dimensional Calculations of Transonic Fan Performance," NASA TM 103800, 1991.

Coles, D.E, and Hirst, E.A., "Computation of Turbulent Boundary Layers," 1968 AFOSR-IFP-Stanford Conference, Vol. II, Stanford University, CA, 1969.

Cumpsty, N.A., and Freeman, C., "Comment on 'Shock-Loss Model for Transonic and Supersonic Axial Compressors with Curved Blades,'" *J. Propul. Power*, Vol. 16, pp. 166-167, 2000.

Dang, T., Damle, S., and Qiu, X., "Euler-Based Inverse Method for Turbomachine Blades, Part 2: Three-Dimensional Flows," *AIAA J.*, Vol. 38, pp. 2007-2013, 2000.

Demeulenaere, A., Private communication, 2005.

Driver, D.M., and Johnston, J.P., "Experimental Study of a Three-Dimensional Shear-Driven Turbulent Boundary Layer with Streamwise Adverse Pressure Gradient," NASA TM-102211, 1990.

Grosvenor, A.D., "Numerical Simulations of Diffusing S-Duct and Vortex-Generator-Jet Flows," Master's Thesis, Carleton University, Ottawa, Canada, 2000.

Hah, C., and Rabe, D.C., "Role of Tip-Leakage Vortices and Passage Shock in Stall Inception in a Swept Transonic Compressor Rotor," ASME Paper GT2004-53867, 2004.

Hakimi, N., "Preconditioning Methods for Time Dependent Navier-Stokes Equations – Application to Environmental and Low Speed Flows," Ph.D. Dissertation, Department of Fluid Mechanics, Vrije Universiteit Brussel, Brussels, Belgium, 1997.

Heidegger, N.J., Hall, E.J., and Delaney, R.A., "Follow-on Low Noise Fan Aerodynamic Study, Task 15-Final Report," NASA CR-206599, 1999.

Hellsten, A., "Implementation of a One-Equation Model into the FINFLO Flow Solver," Laboratory of Aerodynamics, Helsinki University of Technology, Report No B-49 Series B, ISBN 951-22-3219-7, 1996.

Jameson, A., Schmidt, W., and Turkel, E., "Numerical Solution of the Euler Equations by Finite Volume Methods Using Runge Kutta Time Stepping Schemes," AIAA Paper 81-1259, 1981.

Jennions, I.K., and Turner, M.G., "Three-Dimensional Navier-Stokes Computations of Transonic Fan Flow Using an Explicit Flow Solver and an Implicit k-epsilon Solver," *ASME J. Turbomachinery*, Vol. 115, pp. 261-272, 1993.

Kelso, R.M., Lim, T.T., and Perry, A.E., "An Experimental Study of Round Jets in Cross-Flow," *J. Fluid Mech.*, Vol. 306, pp. 111-144, 1996.

Kreith, F., and Sonju, O.K., "The Decay of Turbulent Flow in a Pipe," *J. Fluid Mech.*, Vol. 22, part 2, pp. 257-271, 1965.

Larosiliere L., Skoch G., and Prahst P., "Aerodynamic Synthesis of a Centrifugal Impeller Using CFD and Measurements," AIAA Paper 97-2878, 1997.

Li, H-D., He, L., Li, Y-S., and Wells, R., "Blading Aerodynamics Design Optimization with Mechanical and Aeromechanical Constraints," ASME Paper GT2006-90503, 2004.

Martinelli, L., and Jameson, A., "Validation of a Multigrid Method for the Reynolds-Averaged Navier-Stokes Equations," AIAA Paper 88-0414, 1998.

McKain T., and Holbrook G., "Coordinates for a High Performance 4:1 Presure Ratio Centrifugal Compressor," NASA CR-204134, 1997.

Mohler, S.R., "Wind-US Unstructured Flow Solutions for a Transonic Diffuser," NASA CR-213417, 2005.

Moody, L.F., "Friction Factors for Pipe Flow," ASME Transactions, Vol. 66, pp. 671-684, 1944.

Pierret, S., Filomeno Coelho, R., and Kato, H., "Multidisciplinary and Multiple Operating Points Shape Optimization of Three-Dimensional Compressor Blades," *Struct. Multidisc. Optim.*, Vol. 33, pp.61-70, 2007.

Pope, S.B., *Turbulent Flows*, Cambridge University Press, Cambridge, United Kingdom, p. 459, 2000.

Schetz, J.A., and Fuhs, A.E., *Handbook of Fluid Dynamics and Fluid Machinery,* John Wiley and Sons. New York, 1996.

Schlichting, H., *Boundary-Layer Theory*, 7th ed., McGraw-Hill, New York, pp.333-335, 1987.

Simpson, R.L., "Turbulent Boundary-Layer Separation," *Ann. Rev. Fluid Mech.*, Vol. 21, pp. 205-234, 1989.

Skoch G., Prahst P., Wernet M., Wood J., and Strazisar A., "Laser Anemometer Measurements of the Flow Field in a 4:1 Pressure Ratio Centrifugal Impeller," NASA TM-107541, 1997.

Spalart, P.R., and Allmaras, S.R., "A One Equation Turbulence Model for Aerodynamic Flows," AIAA Paper 92-0439, 1992.

Sparrow, E.M., and Chaboki, A., "Swirl-Affected Turbulent Fluid Flow and Heat Transfer in a Circular Tube," J. Heat Transfer, Vol. 106, pp.766-773, 1984.

Strazisar, A.J, Private communication, 2006. Second set of Rotor 67 data presented herein was taken in 2004.

Strazisar, A.J., Wood, J.R., Hathaway, M.D., and Suder, K.L., "Laser Anemometer Measurements in a Transonic Axial-Flow Fan Rotor," NASA TP-2879, 1989.

Talbot, L., "Laminar Swirling Pipe Flow," J. Appl. Mech., pp. 1-7, March, 1954.

Taylor, J.B., Carrano, A.L., and Kandlikar, S.G., "Characterization of the Effects of Surface Roughness and Texture on Fluid Flow – Past, Present, and Future," ASME Paper ICMM2005-75075, 2005.

Taylor, J.R., *An Introduction to Error Analysis*, 2nd ed, University Science Books, Sausalito, CA, 1997.

Thivet, F., Knight, D.D., Zheltovodov, A.A., and Maksimov, A.I., "Insights in Turbulence Modeling for Crossing-Shock-Wave/Boundary-Layer Interactions," *AIAA J.*, Vol. 39, No. 6, pp.985-995, 2001.

Uskanar, Y.A., "Prediction of Heat Transfer in Turbulent Decaying Swirling Flow," ASME Heat Transfer Division, Vol. 1, pp.125-130, 1999.

Van Zante, D.E., Strazisar, A.J., Wood, J.R., Hathaway, M.D., and Okiishi, T.H., "Recommendations for Achieving Accurate Numerical Simulation of Tip Clearance Flows in Transonic Compressor Rotors," *ASME J. Turbomachinery*, Vol. 122, pp.733-742, 2000.

Vennard, J.K., and Street, R.L., *Elementary Fluid Mechanics,* 6th ed, John Wiley and Sons, New York, 1982.

Williams, J., "Design and Fabrication of a 400kW Pre-Prototype Engine; Budget Period 4 Final Report," Ramgen Power Systems Report 0800-00104, Ramgen Power Systems, Inc., Bellevue, WA, 2007.

Wood, J.R., Strazisar, A.J., and Hathaway, M.D., "Test case E/CO-2, Single Transonic Fan Rotor," in *Test Cases for Computation of Internal Flows in Aero Engine Components*, edited by L. Fottner, AGARD AR-275, pp. 165-213, 1990.

Yaras, M.I., and Grosvenor, A.D., "Evaluation of One- and Two-Equation Low-Re Turbulence Models," *Int. J. Numer. Meth. Fluids*, Vol. 42, No. 12, pp.1293-1343, 2003.

Zheltovodov, A.A., and Maksimov, A.I., "Symmetric and Asymmetric Crossing-Shock-Waves/Turbulent Boundary Layer Interactions," EOARD Contract F61708-97-W0136 Final Report, Russian Academy of Sciences, 1998.

Aerodynamic Analysis Tool Development for Use on Supercomputers

Scientific/Technical Report

Principle Authors: Allan D. Grosvenor

Report Issue Date: March 31, 2011
DOE Award Number: DE-FC26-06NT42651

Submitted by:

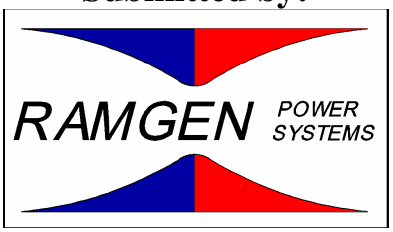

Ramgen Power Systems, Inc.
11808 Northup Way, Suite W190
Bellevue, WA 98005
(425) 828-4919

Aerodynamic Analysis Tool Development for Use on Supercomputers

Having access to, and collaboration with the Oak Ridge Leadership Computing Facility greatly enhances Ramgen's ability to further develop the CO_2 compression technology at a rate consistent with the goals of the Department of Energy. Ramgen is benefitting from OLCF resources in terms of potential to achieve higher quality computational science through increasing the possible spatial and temporal resolution that may be considered using the systems such as Jaguar in addition to our in-house resources, and the expertise offered by Oak Ridge National Laboratory personnel. For example, during 2010 we were able to run a number of simultaneous computations of fine grid CO_2 compressor configurations, each distributed over as many as 500 compute cores. Such a capability enables us to more rapidly assess the impact of different design modifications and operating conditions, while maintaining a high quality CFD solution that enables us to attain better conclusions about the relevant aerodynamics. We are also enabled, through the use of OLCF systems, to run larger stage configuration simulations which include modeling of the time-varying interaction of rotor and stator turbomachine components. Latest improvements in the parallel code make it now practical for us to run simulations distributed over >1,000 cores, and thus enable us to more effectively utilize systems like Jaguar.

Introduction of CFD test case

The test case shown in the figure below has been used for testing the CFD code FINE/Turbo (F/T) at the OLCF in order to have a physically and computationally relevant open science test case. The physics of 3D shock wave / boundary layer interaction (SWBLI) are predicted for two cylindrical bodies aligned in a Mach 4 stream adjacent to a flat plate. Such test cases that can be freely exchanged between vendors and personnel at ORNL have been used to test code developments, and then the improvements have been applied to Ramgen proprietary studies.

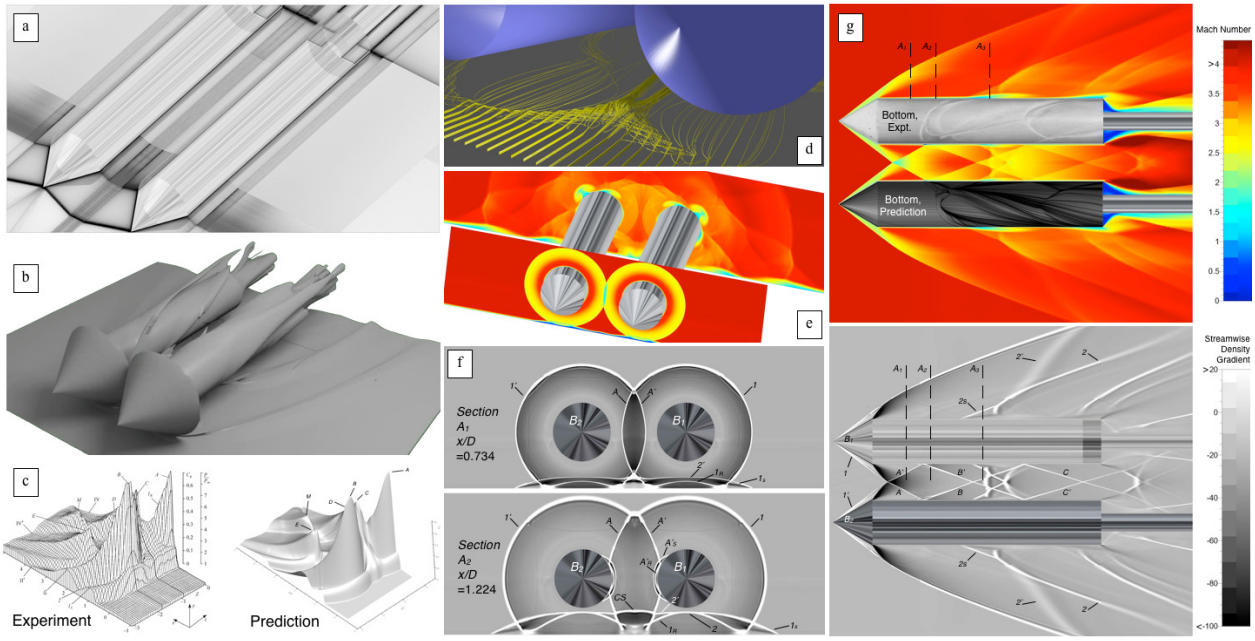

Figure 1: Two-body configuration a) view of 518 million cell computational grid, b) Mach=2.5 iso-surface showing primary bow shock system and displacement effect of separated flow regions in flowfield - visualization provided by Michael Matheson of Oak Ridge National Laboratory, c) comparison of static pressure on plate under bodies between experiment and computation, d) 3D streamlines near plate between bodies - visualization provided by Michael Matheson of Oak Ridge National Laboratory, e-f) streamwise cutting plane views of interacting and reflecting shocks in terms of Mach number and streamwise density gradient, g) view of shock systems cutting through centerlines of bodies

Evolution of Ramgen's utilization of parallel computing

There have been a series of incremental improvements in Ramgen's ability to run the sort of CFD required for development of this technology:

• Originally, the code employed MPICH for parallel communication, there was no version supporting Infiniband interconnects (common in high performance computing), and partitioning had to be performed by manually splitting the computational grid. Through a Ramgen contract between 2005 and 2007, Aeolus Research was hired to test different MPI libraries such as LAM MPI and Scali MPI, and run benchmark tests to identify fundamental bottlenecks in parallel performance, and to prepare versions of FINE/Turbo for alternative interconnects than Numeca's prior default of Gigabit Ethernet (major impact on speed).
• In 2008 and 2009 Ramgen collaborated with SGI to engage Numeca and have SGI technical staff work with Numeca to prepare a version of FINE/Turbo for Infiniband using SGI MPT and tune the parallel implementation for maximum performance of the existing code on a 128 core Intel Nehalem / IB cluster that Ramgen then purchased from SGI in the fall of 2009.
• In late 2009 the present DOE project was initiated to further improve the parallel implementation so that Ramgen could make better use of OLCF resources, and in 2010 Numeca was contracted to implement a new transparent and automated partitioning functionality, to review the parallel and I/O implementations, and to develop improvements that would enable practical parallel computations in the range of hundreds of cores and provide better scalability.
• Prior to 2008 it was common for FINE/Turbo users to be limited to running between 12 and 30 cores per job as a practical maximum. In 2009, as a consequence of working with SGI and Numeca's development of an alternative partitioning technique it became more practical to run a parallel computation distributed over as many as 80 cores. The 2010 Numeca parallel code developments benefitted from detailed testing at the OLCF, and during this time we benefitted from a strong collaboration with OLCF personnel - and particularly our project liaison Michael Matheson. It subsequently became practical to run 128 core jobs during the first quarter, and computations on the order of half a billion grid cells subsequently became possible in FINE/Turbo for the first time during the beginning of 2010. In the summer of 2010 it became possible to run as many as 500 cores per job - although parallel scalability degraded over approximately 256 cores.
• In the winter of 2010, again due to the successful ongoing studies at the OLCF, it was possible to run 1000 core jobs, and reasonable parallel scalability was observed into the range of hundreds of cores depending on total grid size and configuration. Ramgen's ability to run sophisticated CFD models evolved subsequently from 2005 when ten million cells in the computational grids employed for CFD analysis represented a limit to the computation size, to tens of millions of cells between 2006 and 2008, and hundreds of millions of cells between the end of 2009 and beginning of 2010. This process has also enabled us to practically analyze time-varying interactions between stationary and rotating CO_2 compressor components, which is important to the understanding of test rig performance.
• In February 2011 we achieved reasonable parallel scalability performance up to 1,000 cores, which improves our ability to complete jobs on Jaguar without necessitating a very large number of restarts involving many intervening waits in the queue. A major barrier to multiple-thousand core jobs in FINE/Turbo is I/O bottlenecks. The present Phase 2 development work places a strong focus on parallel I/O implementations and discussions with ORNL's ADIOS team have commenced. Each incremental improvement of code scaling improves Ramgen's ability to perform more sophisticated analysis, to turn around more analyses in a given time and to improve simulation boundary conditions.

Latest HPC achievements for Ramgen technology development

In the first quarter of 2010 we began using OLCF facilities and ran F/T there for the first time, reaching parallel simulations running 300 cores. Code performance was measured in terms of I/O and parallel scalability and barriers to efficient large scale computing began to be explored in more detail. We ran the first Ramgen compressor configuration in the first quarter, and through a series of code improvements such computations became more practical in the second quarter. During the second quarter, design-cycle calculations were run and we continued code testing and diagnosis. A number of 500 core simulations were run and a limited number of 1000 core simulations were also run. These tests provided additional data needed to improve our understanding of what code modifications would be needed, and serious additional developments were implemented in F/T during the third and fourth quarters. Successive improvements to the partitioning and load balancing scheme were made, and tracing and debugging of parallel performance and I/O performance was conducted. Some examples of performance improvements are illustrated in the figures below.

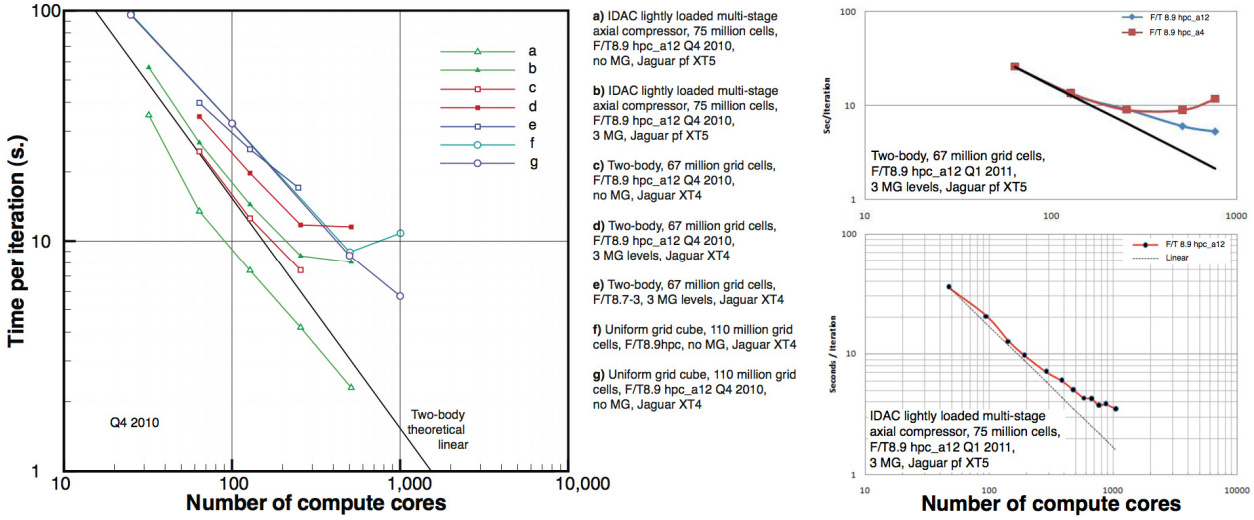

Figure 2: Demonstration of parallel scalability performance measured using a series of test cases. Substantial improvements in the parallel efficiency and practical number of cores that can be run per simulation has been demonstrated over the last year for a series of both linear / stationary, as well as rotating turbomachinery test cases in the 50-100 million grid cell range.

During 2010, Ramgen ran bundles of computations on Jaguar distributed over 256-512 cores per job, and allocating a total of 3,000 cores at a time. It is envisioned that during 2011 it will become possible to extend the scaling of computations and bundling of jobs such that 10,000 cores could be allocated at a time. Numeca has delivered a new version of FINE/Turbo that provides a new transparent automated partitioning capability using a so-called 'metablock' data structure of a virtually partitioned mesh, along with several parallel scalability, and memory scalability improvements that make running several hundred core jobs, and >1000 cores for large jobs, much more practical for Ramgen design-cycle analyses. A training session on this new code version was held at Oak Ridge National Labs in February 2011. This was the third time Ramgen personnel have visited ORNL.

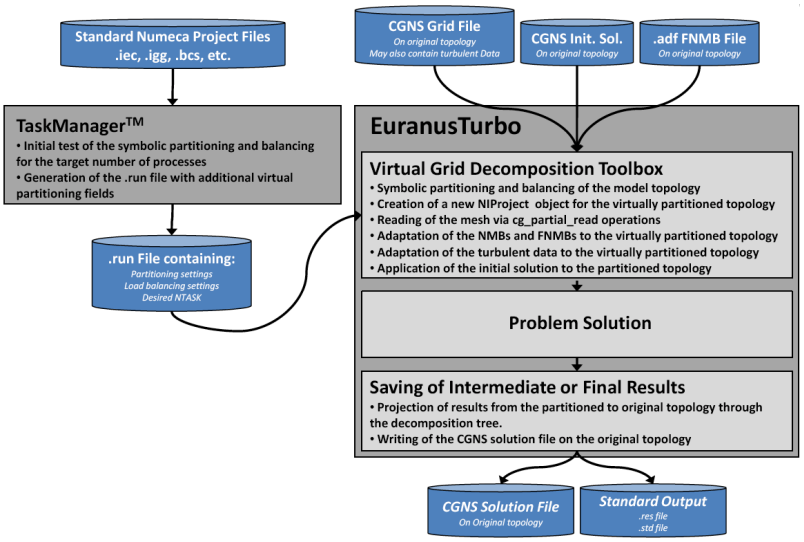

After completion of the project setup, the user may prepare a .run file for a parallel run through the TaskManager interface.

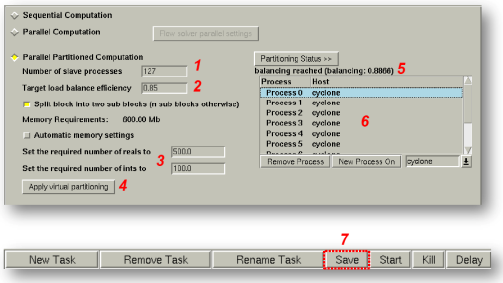

1. The target number of compute processes. With the addition of the host, the total processor utilization will be NTASK+1.
2. The target load balance efficiency. 0.85 or 0.90 are the recommended values .
3. Per-process memory allocation. The memory may be automatically estimated or manually assigned (recommended for runs at ORNL).
4. Clicking the "Apply Virtual Partitioning" button will launch the symbolic partitioning and balancing algorithm.
5. The success or failure of the partitioning algorithm will be displayed. The "Partitioning Status>>" button will display additional debugging information, parroted from the terminal display.
6. Optionally, the contents of the process group file may be defined. This step is not necessary for computations at ORNL.
7. After achieving a satisfactory partition, the "Save" button may be used to write the necessary files to disk.

Figure 3: Description of FINE/Turbo metablock code v. 8.9 hpc_a12 flow chart and interface

Ramgen will make use of these latest gained capabilities in practical use of OLCF resources through design-cycle analysis CFD to expedite development of the Ramgen CO_2 compressor and engine. This will consist of simulations of stage configurations and rig test configurations supporting testing that will begin in 2011 on both the 13,000 HP CO_2 compressor and the proof of concept 1.5 MW engine. Supersonic rotor design studies will be run as well, and studies of specific design concepts will be run in conjunction with parametric design variation studies. Design of Experiments and Optimization techniques are being leveraged where practical, in order to explore vast design spaces efficiently. Non-IP test cases continue to be run for code testing, and we are resolving the aerodynamic phenomena, and studying them, at a level worthy of a series of publications. We have subsequently planned to coauthor such literature with OLCF personnel. Two abstracts, listed below, have been submitted with the intention to co-publish papers on these works with Michael Matheson of Oak Ridge National Laboratory, to the 4th European Conference for Aerospace Sciences, Saint Petersburg, Russia, July 4, 2011 – July 8, 2011. We also intend to submit a paper to the American Society of Mechanical Engineers (ASME) *Turbo Expo*, the premier international conference for gas turbine turbomachinery.

Grosvenor, Zheltovodov, Matheson, Krzysztopic, "Verification for a Series of Calculated 3D Shock Wave / Turbulent Boundary Layer Interaction Flows," *EUCASS* 2011

The last figure clearly demonstrates the substantial improvements of Ramgen's ability to run large parallel computations on systems like Jaguar. Prior to 2009 it was almost impossible to run anything meaningful on OLCF systems, and at the beginning of 2010 we could only run quite small scale parallel jobs. Now we are demonstrating positive speedup on >1,000 cores, there have been significant improvements made to memory efficiency which are necessary to use Jaguar, and we continue to pursue initialization and read/write performance improvements. A dramatic improvement to the ability of Ramgen to use OLCF HPC resources has clearly been made in this program, and the result has been an ability to more productively run Ramgen technology design-cycle analysis, and an ability to run more sophisticated stage and rig configuration analyses.

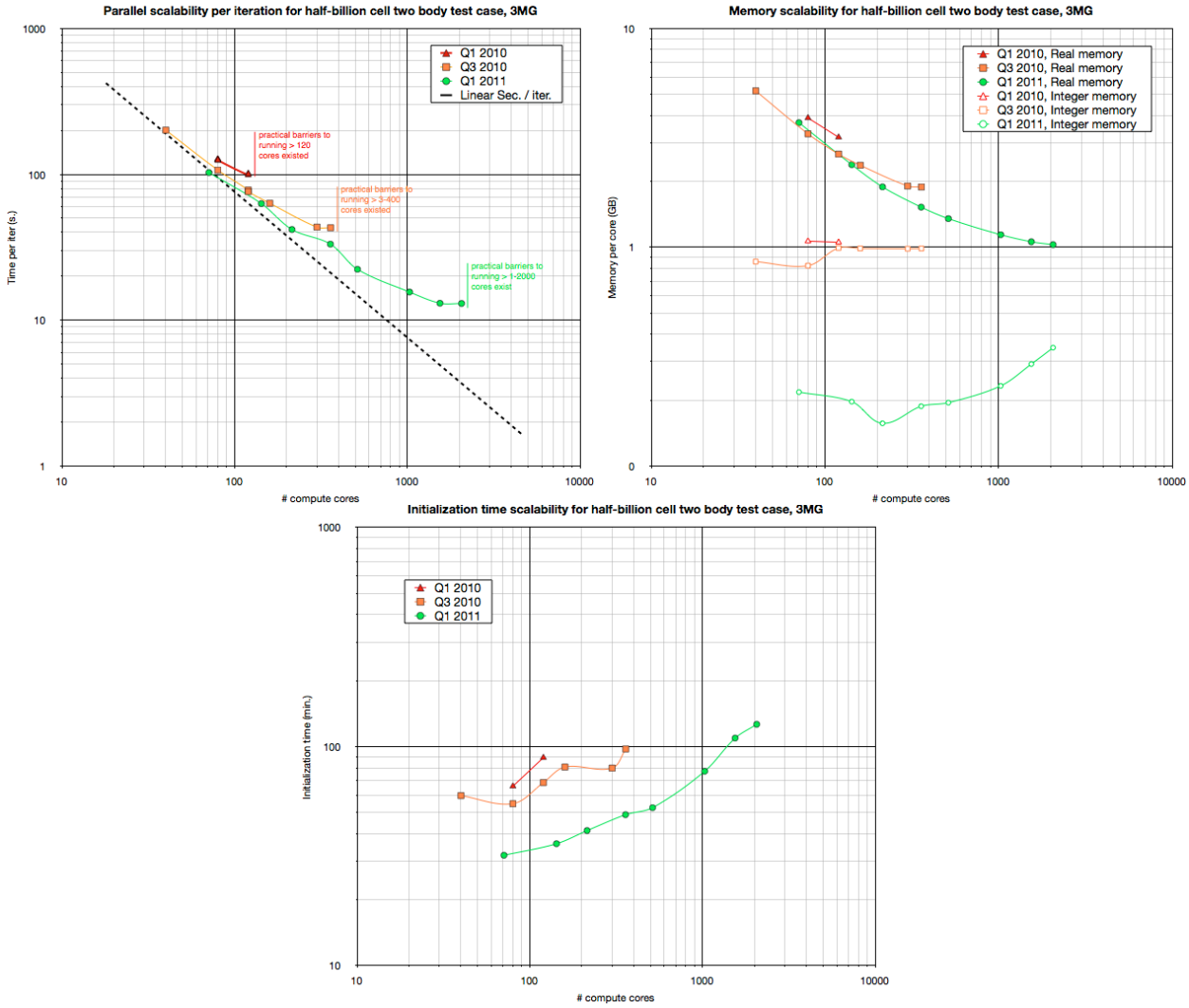

Figure 4: Demonstration of parallel scalability performance measured using two-body configuration 518 million cell test case. Major improvement in parallel computing capability is demonstrated from the state of the code in Q1 2010 to Q1 2011. Substantial improvements in the parallel efficiency and practical number of cores that can be run per simulation have been made over the last year. This half-billion cell model is the largest used for detailed testing. Parallel computing scalability, as well as memory scalability have improved substantially, enabling much more practical use of high performance computing facilities like ORNL's Jaguar for Ramgen design-cycle analysis

DRAFT

PRELIMINARY DESIGN REVIEW FOR THE RAMGEN PROJECT, HELD ON JULY 10, 2007 AT RAMGEN'S FACILITIES IN BELLEVUE, WA: REPORT OF THE DESIGN REVIEW BOARD

By the Design Review Board: Bill Day (chair), Walt Smith, Ravi Ravindranath, Cengiz Camci and Greg Bloch
August 2007

Background / Introduction

Ramgen, in partnership with DOE, has conducted development efforts in the field of shock compression technology. Development efforts have included compressor rig testing of Ramgen's Rampressor concept using a reduced relative Mach Number design (Rampressor-1) to establish proof of concept and testing of a higher relative Mach Number design (Rampressor-2) to validate predicted performance levels at higher stage pressure ratios. These designs and the subsequent rig testing were done for the compression of air. The thrust of future work funded by DOE is aimed at applying this technology to a CO2 compressor as part of the effort to develop technology for the capture and sequestration of CO2 from power plants.

As part of Ramgen's technology development effort, an independent review board was to be convened with the following objectives:

1) Determine the readiness to develop a robust air compressor product using Rampressor technology, and
2) Determine if more air compressor testing is warranted, or if testing to date gives strong enough confidence in shock wave technology to allow a CO2 compressor design effort to commence

This review was done following Ramgen's test of their second, higher relative Mach Number air compressor (Rampressor-2), and at the beginning of work on a CO2 compressor. The review was of the results from Rampressor-2 development to date and of Ramgen's plans for development of a CO2 compressor.

The process for the review was as follows:
1) The Review Board was formed. DOE recruited the Chair, and the Chair selected the other members with final approval by DOE. The process and results of the selection are shown in Appendix 1.
2) Ramgen provided materials about their progress to date and future plans.
3) The Board members developed questions and topics that they would like to see covered in the review which were sent to Ramgen before the review. These are listed in Appendix 2.

4) Ramgen people provided a tour of the Rampressor-2 test rig and then presented results from test and analysis. Handouts of the presentations were provided and were returned to Ramgen after the Board caucused.

5) The Board caucused and developed observations, conclusions, and recommendations which the Chair recorded.

6) The Chair worked with the Board to refine these observations, conclusions, and recommendations to create this final report that represents a consensus.

Executive Summary

1. In answer to the following objectives posed to the board:

   1) Determine the readiness to develop a robust air compressor product using Rampressor technology, and
   2) Determine if more air compressor testing is warranted, or if testing to date gives strong enough confidence in shock wave technology to allow a CO2 compressor design effort to commence.

   Response to Objective number 1):
   Based upon the data presented to the Board, there is significant uncertainty in the performance levels achieved to date, and these data, combined with the analyses presented, do not indicate readiness for the design of a robust air compressor product. In addition, it would not be consistent with current DOE priorities, which are now focused on CO2 compression, to devote more work to the air compressor now unless it would be the best use of resources in starting the development of a CO2 compressor.

   Response to Objective number 2):
   The Board concluded that work on the CO2 compressor should start now, without further tests on an air compressor because a) The cost of more air compressor testing would be high, b) Developing an air compressor is more difficult than developing a CO2 compressor due to the higher wheel speeds necessary for air, and 3) It appears that testing of a rotor designed for CO2 could be done in about the same time as testing of a refurbished air compressor rotor.

2. Development program going forward: Analyses and testing to date have identified tip leakage and shock/boundary layer interaction as the major loss mechanisms requiring resolution for a successful compressor design using Rampressor technology. Ramgen has identified design approaches they believe could be used to address these loss mechanisms, and the lower wheel speeds required for a given relative Mach Number with CO2 make one of these approaches (a shrouded rotor design) much lower risk and could offer lower risk for the mechanical implementation of the second approach (blowing for boundary layer control) as well. The design and development for the CO2 compressor should be conducted in a disciplined, 'gated' process. This process should include the following:
   a. Requirements Review – System level (total power plant) trades for total system acquisition and operating costs should be made to select appropriate requirements for stage pressure ratio (total pressure ratio and number of stages), efficiency, operability (flow range / surge margin), compressor cost, durability, reliability, and maintainability.

b. Concept Design Review- System level trades should be made to justify the concept selected to best meet all requirements. Alternative approaches should be presented with an assessment of benefit vs. risk.
c. Preliminary Design Review- This review should be successfully completed prior to hardware release. Design analyses presented should confirm capability to achieve requirements. Details of the development test plan should be presented along with the risk management plan.
d. Detail Design Review / Test Readiness Review – Detailed design and design analyses should be presented to confirm capability of the rig and test hardware to successfully acquire the data needed to achieve the planned technology readiness.
   Pre-test performance predictions, consistent with meeting product requirements, should be presented for the specific configuration to be built and tested. Book-keeping of performance corrections necessary for instrumentation and test-unique configurations should be presented along with the pre-test predictions.
e. Test Results Review – Results should be used for design verification.

3. Cost trade studies should be conducted at the system (power plant) level to define best configuration for the CO2 compressor design. The impacts upon initial cost and operating cost for alternative CO2 compressor configurations should be established. Specifically, alternatives that increase stage count and the number of intercoolers should be assessed against the current baseline with two compressor stages and one stage of inter-cooling. The reduction in power plant cost ($/kW) should be captured as compressor work is reduced with increased stage count and more intercoolers. This will tend to off-set increases in compressor cost and intercooler costs, and reduced opportunity to use the rejected heat since it would be rejected at a lower temperature. Improvements in efficiency with increased stage count should also be captured.
   Risks should be evaluated as a function of stage count as well. Shroud design options (or tip clearance impacts and control methods) should be assessed for each alternative as wheel speed is lowered with increasing stage count and the risks should be defined for each. Similarly, design options for boundary layer control and the performance impact for each should be assessed for each alternative and the risks defined for each. Selected design requirements should reflect a trade-off between benefits (lower combination of initial cost amortization and operating cost calculated at the system level) and risk based upon these results.

4. A reduced order model (i.e., mean-line model) that captures the effects of all major compressor design variables (wheel speed, aspect ratio, hub/tip ratio, reaction, compression ramp geometry, diffuser geometry, etc.) should be generated and used to select a concept that meets design requirements. Because there is a lack of prior test data for use in creating this model, design-of-experiments methodology should be used to generate the appropriate CFD cases for use in creating this model. This reduced order model should be used to define

the configuration that best meets design requirements with the lowest risk. For example, reaction trades should be used to assess risk in the rotor design compared to risk in the stator (exit diffuser) design.

Observations

These observations formed the basis for the conclusions and recommendations presented in the Executive Summary above. Some observations may seem redundant, but all are presented to capture the specific thoughts of all board members. Where multiple observations relate to the same conclusion or recommendation, they have been grouped together. Some observations and conclusions are presented that are beyond the scope of the Executive Summary.

1. **Move to CO2:** We recognize that DOE's priority has shifted since the emphasis earlier in the program on developing an air compressor. More technology development work would need to be done before readiness is in place to develop a robust air compressor product, and we understand that it would take substantial time and money to refurbish and improve the Rampressor-2 rig to do meaningful testing of the as-is rotor, much less improvements to it. Also, since the cost of continued use of Boeing's test facility would be prohibitive, finding or developing a new facility would also be costly. Thus, we concluded that work on the CO2 compressor should start now, without further tests on an air compressor because a) The cost of more air compressor testing would be high, b) Developing an air compressor is more difficult than developing a CO2 compressor due to the higher wheel speeds necessary for air, and 3) It appears that testing of a rotor designed for CO2 could be done in about the same time as testing of a refurbished air compressor rotor.
2. **Key rotor issues:** The Review Board agrees with Ramgen's conclusion that shock / boundary layer interactions and tip leakage are the key issues that require resolution in order to achieve desired performance levels for the Rampressor design. Resolution of these issues at minimum risk will be key to a successful CO2 compressor design based upon Rampressor technology.
3. **Tip clearance:** The Review Board does not believe it reasonable to expect that the very tight tip clearances (approximately 0.001 inch and certainly less than 0.004 inch; sharp drop off beyond .003 inch) shown to be needed for desired performance levels will be achieved in operation by a production compressor. (We understand that a new bearing technology has recently been identified and a sample delivered to Ramgen, which is a tilting pad bearing wire-EDM'd out of one piece where the pads flex but don't need any additional parts, which can hold tighter clearances. This would be an important breakthrough if it works.) A proper pressure side corner treatment may result in reduced tip clearance penalties, allowing the designer to specify a clearance much larger than 1 mil (perhaps 3- 5 mils).
4. **Shrouded rotor:** The Board agrees with Ramgen's approach to the CO2 compressor rotor design (that it should be shrouded). The Board believes that managing leakages across the seals at the OD of a tip shroud should be much lower risk than attempting to manage tip clearances. Thus, achievement of a low risk shrouded design for the CO2 compressor is very important. Reducing wheel speed sufficiently (with lower pressure ratio) can significantly lower risk for a

shrouded design. Presumably this is possible for the CO2 application due to the lower velocity for a given Mach number than in air, hence lower wheel speed. The shroud should be tested in a computational manner first. One suggestion is that a partial shroud near the tip of the rim should be explored. By designing a proper pressure side extension (similar to a winglet without a suction side extension) this may de-sensitize this flow in terms of the clearance penalties. An issue will be whether a shroud can be done without resorting to unproven materials. Companies like GE or P&W can get the attention of the suppliers of a new material and work with them to develop a design application. It would be a lot riskier for Ramgen to count on doing that. Assuming the shroud can be built in a robust design it will be a lot easier to limit the leakage around the shroud than to hold 1mil clearance (0.001 inches) necessary to meet performance requirements in an unshrouded air compressor design. Some suggestions for sealing at the tip of the shroud are foil seals (They are non contact during operation, like an air bearing), or honeycomb seals which are used widely in gas turbines.

5. **CFD development:** The Review Board was impressed with the CFD development and analyses that has been accomplished to make the design process efficient. The use of design of experiments was good, and the "autogrid" development was quite innovative. We suggest that Ramgen populate the design space selected for the CO2 compressor with enough detailed designs so that reduced order models can be developed to optimize overall compression system performance. Then, with the overall compression system optimum identified, a detailed design for the rotor may commence.
6. **Pressure ratio and efficiency measurement:** From Ramgen's presentation, the Rampressor-2 design was frozen part way through the design optimization process in order to be able to get testing done during the time window available at the Boeing test facility. Analysis of the design that was frozen at this time has indicated that the compressor stage would produce 8:1 pressure ratio . There was a lot of variability and corrections necessary in the test data, but their conclusion was that they achieved 7.92:1. (The actual measured pressure ratio and efficiency prior to the corrections were lower). Corrections built into that performance number included compensating for the impact of a step in the inlet flow path, compensating for the effect of the rough surface of abradable material outside the areas where it is needed, and estimating what some of the pressures were at different places from where the pressure probes were located. These corrections were equivalent to a + or -1 variation in pressure ratio. The Board believes that with a + or - 1 variation on pressure ratio measurement when 8 was the objective, Ramgen doesn't have a good handle on measured performance. They need to test with the probes in the right places to measure performance and make predictions before the test that account for items in the flow path that affect performance, and then have a test that replicates the prediction. If they could do that, it would be a big help to their credibility in being able to predict performance.
7. **Aerodynamic design:** From Ramgen's presentation the biggest problem with the air compressor was separation near the throat which causes an "unstart" at the upper limit of pressure ratio, and that if they could eliminate that, they are

confident that they could get to a pressure ratio of 10 at 85% efficiency. They would do more CFD analysis to develop a design in an attempt to achieve this. Other improvements that they would incorporate are a) Use blowing instead of bleed for boundary layer flow control to address shock wave / boundary layer interaction (The bleed that they used for flow control made a 15% hit to performance; they estimate it would be reduced to 2.5% by blowing.). b) Reduce the area where abradable material is applied (just cover the area over the strakes and no more) in order to reduce losses due to drag on the rough surface, c) Make pitch-wise variation of the strakes and d) Improve the IGV performance. In reference to the separation at the throat causing surge, the Board observed that CFD tools often tend to under-predict separation. So, if designing to prevent separation, you need to be conservative, i.e., have the prediction say that you can get to a higher pressure ratio than you need without surge. Also, when tests show what the surge point is, there needs to be a surge margin compared to the design point. (In gas turbine compressors the surge margin at design point is established to accommodate all de-stabilizing influences identified for the particular installation. Design stall margins typically range from a low of 10% to a high of 35%, although there are some outside this range.) The surge margin needs to be confirmed by test.

8. **Boundary layer blowing:** No one has developed design tools for using BL blowing, and creating them for use inside the rotor is a big challenge. These tools need to be developed and validated. Then, the method of integrating BL blowing mechanically within the rotor seems similar to internal cooling of a turbine airfoil – except that in a turbine airfoil you can cast an intricate set of cooling passages. Here you are presumably limited to starting with a forging and hogging it out, a non-trivial task. Additionally, you must use bleed, not blowing, to get the system started – another complication. Per Ramgen, you need to bleed about 35% of the air to get the system started.
9. **Pitch-wise geometry changes:** Ramgen presented techniques that might be used to better manage flow separation risks by the use of pitch-wise geometry changes (among many alternatives). Use of these alternatives, in combination with reduced pressure ratio per stage, should be pursued to minimize or eliminate the need for blowing on surfaces other than the inner flow-path. This offers Ramgen an advantage over conventional systems attempting to pursue high pressure ratio per stage by achieving separation-free flow with boundary layer control only on the surfaces where it is mechanically easier to accomplish (the inner wall).
10. **Diffuser:** The diffuser inlet conditions for the Rampressor-2 design are M =0 .77 @ 85 degree swirl. The Board would observe that this is a lot of swirl based upon gas turbine experience. The design presented to address this high swirl uses two sets of airfoils in tandem. It was stated that this concept has been tested in a different application. The Board notes that there is very little industry experience with tandem airfoils. The only instance that the Board members know of is the engine (by Rolls-Royce) for the T45 trainer aircraft. Tandem vane technology had limited success in low speed, low angles (45^o – 50^o) and the application to high speed and high angles has not been tried before in turbomachinery industry. The present tandem airfoil shape design for the second set of airfoils does not

look acceptable. The magnitude of velocity contours showed strong diffusion / recirculation in the second half of the second airfoil. The re-circulatory flow zone with reduced momentum could easily be eliminated by the improved shape design of the second airfoil. Due to the unknowns for this concept, the combination of high Mach number and high swirl, and the supercritical properties for CO2 at that point in the final stage of compression, the Board believes this to be high risk, even considering the testing cited for the concept. It should be tested very thoroughly, at conditions from start-up through the entire load range, in the static tests on air which are planned early in the program to simulate the CO2 application. It would be worthwhile to have alternate designs of the overall system that don't work the diffuser so hard and do more of the diffusion in the rotor, so trade-offs can be done for the overall system design.

11. **Outside help in CFD analysis:** There are so many things to do in optimizing the overall system, consider getting some outside help for specific CFD analyses. The details of the geometry for multiple configurations can soak up a lot of man hours, and with limited resources, getting outside help to could enable an aggressive schedule. People skilled at CFD who could work under the direction of Ramgen's designers may enable Ramgen to speed up the pace of analyzing and evaluating different configurations. A risk in this approach is that Rampressor rotor design is the "new invention" that is RAMGEN's key intellectual property and forms the basis of their future products, so they would need to be careful on who they select for help.

    Conventional turbomachinery, while required for a successful RAMGEN product, is not the "new invention" that RAMGEN is developing and conventional turbomachinery expertise may not be indigenous at RAMGEN. RAMGEN has already purchased some external expertise, for example by retaining Byron Roberts to do the IGV and stator designs. Hiring additional external expertise outside the rotor design may or may not be helpful to maintain schedule.

12. **Outside help in mechanical systems analysis:** When designing the overall mechanical system, get help from industry and government experts in identifying sources for outside support. Avoiding problems like critical speed issues can save a lot of grief. It may be possible for the Air Force to assist DOE partner Ramgen under the auspices of the Propulsion and Power Systems Alliance. POC for mechanical systems would be Nelson Forster (Nelson.Forster@wpafb.af.mil; 937-255-5568).
13. **Shake test:** When the whole prototype system is made, run a shake table test to see vibration modes. Better to identify them here and make changes, than in the test stand. It may be possible for the Air Force to assist DOE partner Ramgen under the auspices of the Propulsion and Power Systems Alliance. POC for this activity would be Dr. Tommy George (Tommy.George@wpafb.af.mil; 937-986-5531).
14. **Technology Readiness Level:** For aircraft turbine engine compressors, AFRL considers a ***successful*** demonstration by either CFD or a cascade test to be TRL=3; a single-stage high-speed compressor rig test is TRL=4 (assuming the

design requires a multi-stage compressor); a multi-stage high-speed compressor rig test is TRL=5. Furthermore, a TRL assessment must include the intended performance parameters such as stage pressure ratio and efficiency. For example, a successful TRL=4 demonstration of some particular loading and efficiency levels implies the technology is TRL=4 for any loading and efficiency values ***at or below the demonstrated values***; the TRL would be less than 4 for a similar product with loading and efficiency goals higher than the previously-demonstrated values (because those higher goals have not yet been demonstrated).

Based on discussions with Ramgen prior to the review the board had asked Ramgen to assess themselves, and they did so as part of their technology development path charts (provided us as hand-outs) where they used a TRL calculator available online to assess themselves at TRL-3 (green level) with some progress to TRL-4 (yellow level). They then presented how they viewed the TRL progression from 3-4 to 7 at the completion of field testing.

The Board agrees with Ramgen's self-assessment of the RP-2 compressor as TRL=3 with some progress toward 4 for the ***demonstrated*** loading and efficiency levels (not the CO2 product design goals). We based our assessment upon the fact that RP-1 demonstrated proof of concept at a inlet relative Mach Number of 1.6, achieving a pressure ratio of 2.3 and validating design tools for this pressure ratio range. This demonstrated that flight inlet performance levels can be achieved in a shock compression system with very tight clearances and the use of flight inlet design practices for this level of pressure ratio. RP-2 targeted a much higher inlet relative Mach Number and much higher stage pressure ratio. Because the test schedule resulted in release of the rotor aero design for RP-2 prior to design optimization, this design had a lower pressure ratio and efficiency potential than the stated technology goal, but it achieved "approximately" the pressure ratio and efficiency values that were predicted for that design iteration. (The significant measurement uncertainties from the RP-2 test prevents the Board from stating that these goals were clearly demonstrated.) Knowledge gained from work done on RP-1 and RP-2 identified control of shock / boundary layer interaction as being critical to achieving target performance levels, and identified techniques to further reduce losses. Validation of a design that uses these approaches to achieve technology goals in a single stage will result in TRL=4.

Because the increased stage pressure ratio and efficiency goals for the notional CO2 compressor exceed even the best CFD predictions that Ramgen has achieved to date, the Board assesses the TRL of the notional CO2 product as 2 with some progress toward 3.

15. **Risk matrix:** Do a risk matrix of each component, i.e. if this component fails in this way, these are the consequences- see Appendix 3. This highlights the relative importance of risks and helps show where you should put most of your development money.

16. **Pressure ratio per stage:** Why is it necessary to achieve 10:1 in one stage? It may make better economics to do less than that before inter-cooling. It still could be better than what can be done with reciprocating or radial compressors. For example, do the 100:1 requirement in 3 steps instead of 2. Recognizing that lower pressure ratio means that the compressor discharge temperature would be less useful (or not at all useful) for power recovery, it seems better to reduce the work put into compression in the first place. Per Ramgen's presentation, conventional compressors can't get beyond a pressure ratio of about 2.5 and still have a range of 30%, which customers want. If Ramgen can achieve 30% range at say 6:1, they would seem to have a considerable competitive advantage – as long as they can do that 6:1 at as least as high an efficiency as the recips or the centrifugals.

    The U.S. Air Force has access to compressor performance data from all of the major aircraft gas turbine engine manufacturers, and these data can be used to identify the trade space between stage loading and efficiency as shown in the following figure, see figure1. The abscissa is the arithmetic average isentropic work input per stage normalized by the square of the tip speed for the first rotor, and the ordinate is polytropic efficiency (which accounts for the fact that the number of compressor stages varies among the machines). Many more data are available than are shown in the figure (because this plot has been sanitized for public release), but the dotted black line identifies the approximate state-of-the-art today. There is no derived equation that defines this line; rather the line is fit to the (unplotted) data.

    It is clear from this figure that high stage loading and good efficiency tend to be mutually exclusive. You can trade loading for efficiency, but you can't have both without advancing the state-of-the-art. An improvement to SOA will likely change the slope of the line, but the maximum low-loading efficiency is unlikely to improve significantly. Although not apparent from this figure, increasing stage loading reduces operability (flow range between choke and stall). The important point here is that, for any fixed technology level, reducing stage loading will increase efficiency and operability. As an added benefit, a lower pressure-ratio design can be achieved with a lower inlet relative Mach number, thereby reducing the shock strengths and reducing the likelihood of shock-induced boundary layer separation; this increases the likelihood that the CFD tools used to design the rotor will accurately predict the rotor flow and not under-predict a separation.

    On chart #46 in the package that Ramgen sent to us before the meeting, they claim to have demonstrated tip speeds "up to ~2200ft/s" (~670m/s). A PR=10 stage would have a loading coefficient of 0.60 with this wheel speed. A PR=8 stage (e.g., Rampressor 2) would have a stage loading coefficient of 0.52. A reduced stage loading of PR=5/stage (3 stages = 125OPR) with the same 2200ft/s tip speed results in a 0.38 loading coefficient. The SOA curve suggests reducing the stage PR from 10 to 5 will result in a roughly a 4% improvement in polytropic efficiency (and roughly 2.5% better than was demonstrated for Rampressor 2). Please keep in mind the dotted black SOA line represents the very mature state of

axial fan/compressor aerodynamics. The (unplotted) line that corresponds to the relatively immature rampressor technology is likely to have a steeper slope, which implies the efficiency benefit of reduced stage loading will likely be even greater.

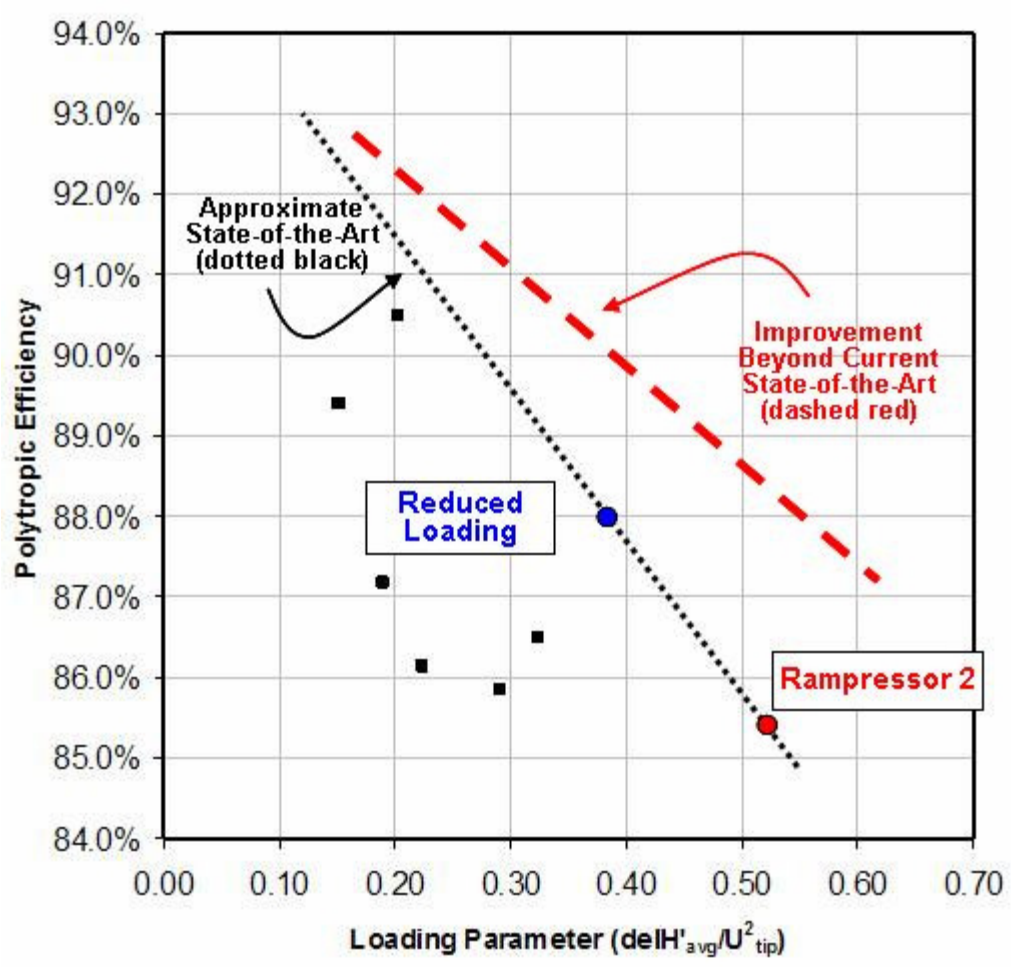

Figure 1: Compressor efficiency vs. stage loading

17. **Trade studies:** System level trades, including total power plant cost impacts, need to be accomplished. There was no evidence that these had been used in setting design requirements (such as number of stages and hence pressure ratio per stage). An example of such a study is provided in appendix 4. While the ground-rules and assumptions used for this simplified example may differ substantially from those validated for use in the overall system trades recommended in the executive summary, this example serves to illustrate that the impact of the compression system on overall power plant size requirements can be more significant than the cost increase associated with a stage count increase.
18. **Response to questions submitted prior to the review:** Most though not all of the topics and questions were addressed. Given the time available Ramgen did address the most important issues. Their emphasis on which issues to address was appropriate.

Appendix 1: Selection of the Review Board members

Candidates for the Review Board were identified by The Chair, DOE and Ramgen. Candidates were contacted by the Chair to determine their interest in serving on the Board. In some cases the person contacted was not interested but suggested someone else who may be and seemed to have the requisite skills. Criteria for selection to the board were a) Have considerable skills and experience in compressor development and / or in supersonic flow and analysis of same, and b) Not have worked for Ramgen so as to avoid the possibility of conflict of interest. The size of the Board was to be limited to 5 members to keep costs under control. Also it was desired to have two members whose background was from industry, two from government and one from academia.

The candidates considered and those selected are listed in the following table. Contact information for the Board members is also included in the table.

Candidates for the Ramgen Preliminary Design Review Board: Selected candidates are in bold.

0	AREA	Consultant	Service or Expertise	Contact Info	Recommended by	Status, lm= voice mail	Comments
1	Academia	MIT - Dr. Ed Greitzer C17	Shock wave technology development	business: (617) 253-2128 fax: (617) 258-7566 Massachusetts Institute of Technology Dept. Aeronautics & Astronautics Cambridge, MA 02139 greitzer@MIT.EDU	Gregory Bloch	4/13 lm	
2	Academia	MIT - Dr. Alan Epstein	Compressor aerodynamics	name: Epstein, Alan H email: epstein@MIT.EDU <mailto:epstein@MIT.EDU> phone: (617) 253 2485 address: 31 265 department: Department of Aeronautics and Astronautics title: Professor	Gregory Bloch	4/16 Bio received	
3	Academia	U. of Washington - Bob Briedenthal	Mixing, fluid mechanics, fluid dynamics	(206) 685-1098 breidenthal@aa.washington.edu	Ramgen	4/13 bio received	Bob consulted for Ramgen in fuel / air mixing of the combustor
4	Academia	U. of Washington - Dave Pratt	Thermodynamic analysis of supersonic shock compression engine	Prof. Emeritus, U. of Washington pratt@combustion.com 360-588-1647	Ramgen	4/17 bio received	Has done consulting for Ramgen, in combustion
5	Academia	U. Michigan - Dr. Werner Dahm	Over 20 years of experience in turbomachinery, gas turbines, compression, and power generation. His research focuses on fluid dynamics, turbulence, and mixing.	Professor of Aerospace Engineering University of Michigan Ann Arbor, MI 48109-2140 Ph: 734-764-4318 Email: wdahm@umich.edu	Ramgen	4/16 Werner is not interested: a) Too much on his plate, b) He consults for another organization doing sililar work	
6	**Academia**	**Penn State - Cengiz Camci**	**Aerodynamics and unsteady flow with application to compressors**	**PROF AERO ENGR, 0223 HAMMOND BLDG, UNIVERSITY PARK, PA 16802 Phone 814 865 9871 e-mail cxc11@psu.edu**	**Karen Thole**	**Selected for the board**	
7	**Government, AFRL**	**Gregory S. Bloch**	**AFRL**	**gregory.bloch@wpafb.af.mil Voice: (937)255-7373 fax (937)656-4232 Dr. Gregory S. Bloch U.S. Air Force AFRL/PRTF Bldg 18 Room A005 1950 Fifth St. Wright-Patterson AFB, OH 45433-7251**	**Tom George**	**Selected for the board**	**He is familiar with Ramgen; was part of 2002 review.**
8	Government, AFRL	William E. Koop	AFRL	William.Koop@WPAFB.AF.MIL	Ron Harp	4/17 exchanged e-mails; expect he will recommend someone else at AFRL	
9	Government NASA	Tony Strazisar - NASA Glenn	compressor aerodynamics	216-433-5881 Anthony.J.Strazisar@grc.nasa.gov	Ramgen	4/13 lm 4/25 He called back; I told him we already have filled the slots.	
10	Government NAVY	Mike Osborne		Navy Department, 202-781-3800, michael.e.osborne@navy.mil	Tom George	4/13 talked to Mike; 4/17 bio received	
11	**Government NAVY**	**Ravi Ravindranath**	**Nval Air Systems Command (NAVAIR)**	**301-757-0472 ravi.ravindranath@navy.mil CIV NAVAIR AIR 4.4.3.3 B106 Room 202A 22195 Elmer Road, Patuxent River, MD 20670**	**Mike Osborne**	**Selected for the board**	**4/17 lm Rob Leitner; do you know him? (No, but it's a good organization for candidates.)**
12	Industry	Aubrey Stone	Axial compressor and turbine aero review		Ramgen	4/12 sent e-mail	
13	Industry	Colin Rodgers	General compressor design.Internationally recognized expert in centrifugal compressor and turbine designs. Over 50 years of experience with turbomachinery technologies.	phone: (619) 296-3807 fax: (619) 296-3807 crodgers@4dcomm.com 3010 N Arroya Dr. San Diego, CA 92103	Ramgen	4/12 lm	
14	Industry	George Schaefer	Pre-swirl nozzle design	George Schaefer - Dir. Aero. Equip. & Tech. Sales phone: +1 (802) 296-2321 ext 152 fax: +1 (802) 296-2325 gjs@conceptsnrec.com http://www.conceptseti.com Concepts NREC Corporate Headquarters 217 Billings Farm Road White River Junction, VT 05001-9486	Ramgen	4/12 lm	
15	Industry	Florida Turbine Technologies, Inc	Turbomachinery design, internal aerodynamics, rotordynamics, bearing design, static structure design	Contracts Manager - Lloyd Mazer phone: (561) 746-3317 x337 fax: (561) 746-3356 LMazer@fttinc.com http://www.fttinc.com 140 Intracoastal Pointe Drive Jupiter, FL, USA 33477 Mr. P. Dean Johnson 561-427-6332 djohnson@fttinc.com	Ramgen	4/18 Dean Johnson will send bio on Jack Wilson, mech design expertise at FTT. 4/19 bio received for Jack Wilson.	FTT worked with Ramgen on ramcompressor rig
16	Industry	Rose Engineering - Bill Rose	Supersonic aerodynamic design, analysis and CFD	P.O. Box 5146 Incline Village, NV 89450 Phone: 775.831.5094 Fax: 775.831.9150+E16 http://www.rose-engineering.com/	Ramgen	4/13 Bill Rose called to decline the opportunity; too many other things on his plate.	4/13 Bill Rose called to decline the opportunity; too many other things on his plate.
17	Industry	Walter (Chip) Gallagher	Over 30 years of service at Air Products in the area of rotating equipment. Is responsible for the safe, efficient, reliable operation of rotating equipment throughout the world. Evaluates new turbomachinery equipment for the	Manager, Machinery Engineering Air Products & Chemicals, Inc. 7201 Hamilton Blvd. Alle+E17ntown, PA 18195 Ph: 610-481-4723 Cell: 610-390-2543 Email: gallagwf@apci.com	Ramgen	4/17 talked to Chip; 4/17 bio received	
18	**Industry**	**Walt Smith**	**36 years experience at Pratt & Whitney in compressor design & development and system design & integration**	**J. Walter Smith 158 Kokomo Way, Seneca, SC - 29672 Phone: (864) 638-7723 e-mail: smithjessew@hughes.net**	**Bill Day**	**Selected for the board**	
19	Industry	Harry Miller		Dresser-Rand, paul Clark Drive, Olean, NY 14760-0560; 716-375-3316; cell_716-378-9123, harry_f_miller@dresser-rand.com	Tom George	4/13 lm 4/20 he left message that his legal dept said it would be a conflict of interest for him to serve, since Ramgen is considered a compatitor.	
20	**Industry**	**Bill Day**	**42 years experience at GE and P&W developing and leading the development of advanced gas turbines**	**25 Longview Road, Avon, CT 06001 billday3@comcast.net 860-404-0759**	**Tom George**	**Recruited to chair the board**	

Appendix 2: Topics and Questions developed by the Review Board and submitted to Ramgen prior to the review

PRELIMINARY DESIGN REVIEW FOR THE RAMGEN PROJECT: TOPICS AND QUESTIONS PRIOR TO THE DESIGN REVIEW

June 27, 2007

Bill Day, Tom George, Walt Smith, Ravi Ravindranath, Cengiz Camci and Greg Bloch

Approach to this document -- Bill Day, Chair of the Design Review Board

I was originally planning to create an integrated document from the inputs of the design review board members, but having gotten their inputs I think it more productive to show each set of inputs independently. The reasons are that a) It would take a significant effort to develop such a report and to be sure I covered everything and b) I figured that it wasn't worth the effort, since it should be more productive for both Ramgen and the board members if everyone knows who asked what questions. I saw no point in keeping the questions secret. After all, you would know who asked what questions if they were spontaneous at the meeting, so why not the same beforehand?

So, though it may seem disjointed, the following are the topics and questions, identified by the authors.

Outline of Topics – Walt Smith

I. Summary of Industrial Conceptual Design Initiation Process Supported by Ramgen Technology Development Effort

A. Identification of Need / Requirement

B. Selection of Alternative Concepts
C. Figures of merit for comparison of alternatives
D. System level figure of merit for comparison of alternatives
E. Optimization technique to select best system for each alternative being compared
F. Selection of preferred concept for each alternative
G. Identification of strategic technologies for each alternative

II. Results of Concept Initiation Process

A. Potential benefits for selected concept (system level)
B. Strategic technologies to enable selected concept
C. Comparison of major figures of merit to optimized alternative (best alternative)

III. Technology Development Plan for Strategic Technologies Enabling Selected Concept
   A. Current Technology Readiness Levels
      1. Aerodynamics
      2. Structures
      3. Materials
      4. Manufacturing Technology
      5. Component Integration
      6. Systems Integration
   B. Plan to achieve TRL-6 for each strategic technology

IV. Design Review / Development Plans for Demonstrations Supporting Technology Development Plans
   A. Design Process for Demonstrator Rigs
   B. Current Status Within Demonstrator Rig Design Process
   C. Review Standards / Success Criteria

Examples of What Walt Would Expect to See For the Above Items

I. A flowchart showing the overall concept initiation process for the requirement (need) in question
   A. Need for CO2 Sequestration Defined
   B. Alternative Concepts for CO2 Sequestration Identified
   C. Figures of merit including efficiency and initial cost comparison for selected alternatives
   D. System level figure of merit comparison that combines operating cost impact of efficiency with amortization of initial cost
   E. Alternatives Making Use of High Pressure Compressors and Inter-cooling Selected
      1. Centrifugal Compressors / Inter-cooling
      2. Axial Compressors / Inter-cooling
      3. Screw Compressors / Inter-cooling
      4. Ramgen Concept / Inter-cooling
   F. Conceptual level design optimization results for each alternative
      1. Number of Stages (Wheel Speed and Loading vs. Efficiency)
      2. Number of Intercoolers and Limits on Temperature Reduction (Size and Cost of Intercoolers vs. Reduction in Work of Compression)
   G. Strategic Technologies for Each Alternative
      1. Centrifugal Compression System

a. Materials / bonding for high impeller speeds
b. BLC for diffusion process

2. Axial Compression System
   a. Improved Aero Design Techniques to Minimize Shock / BL Interaction at Tip
   b. Improved Clearance Control Techniques
3. Screw Compressor System (For example see the website: **Power Engineering - High Pressure Fuel Gas Boosting Compressors)**
   a. Improved Aero Design Techniques to Increase Specific Flow
   b. Manufacturing Technology to Reduce Cost
4. Ramgen Concept
   a. Improved Structural Design Techniques to Manage Rotor / Strake Stresses
   b. Improved Clearance Control Techniques
   c. BLC for diffusion process

II. Benefits for Selected Concept
   A. Comparison of System Level FOM to Current Practice
   B. Strategic Technologies Required to Achieve Benefit
   C. Comparison of System Level FOM to Best Alternative and Comparison of Required Strategic Technologies (RISK)

III. Technology Development Plans Taking Each Discipline from Current TRL to TRL – 6. For one of many definitions of TRL see http://esto.nasa.gov/files/TRL_definitions.pdf
   A. Clear definition of steps needed to take each discipline from current TRL to TRL-6
   B. Relationship of needed steps in technology readiness to planned demo / rig testing

IV. Design Reviews for Demonstrator Hardware to Achieve TRL-6
   A. Limited design process for rig hardware assuring structural adequacy for intended demonstration / test and functionality to acquire desired data to provide planned progression in technology readiness
   B. Detailed design data for rig hardware illustrating its capability to deliver desired data
   C. Success criteria that requires establishment of benefit for selected concept, clear definition of the technology development required to deliver this benefit, and design data showing the planned component /

rig demonstrations will provide progress in the development of the required technologies

Topics and Questions – Bill Day and Tom George

1 Performance Assessment (Meets or exceeds the competition).

1.1 Performance Targets/Goals Are Reasonable

1.1.1 Efficiency across the load range vs. competition.
1.1.2 Surge margin across the operating range.
1.1.3 Other?

1.2 Clearances (Ability to hold and consequence when not held)
1.3 Engineering Codes (What key engineering codes or standards will frame the developmental process and how will they be used to set the design and quality processes)?

2 Technical Risk Assessment

2.1 Describe the configuration, including materials and manufacturing processes.
2.2 How are failures contained, from safety perspective (ex., failure modes & effects analysis or FMEA)
2.3 How are clearances controlled, considering transients and changes in ambient temperature?
2.4 What happens to clearances vs. bearing wear and airfoil wear?
2.5 What happens to performance with likely wear?
2.6 What inlet filtration requirements vs. those of competition are needed to keep clearances and wear acceptable?
2.7 How is the compressor maintained (ex. airfoil repair)?
2.8 What is the expected time between overhauls? What determines the need for overhaul?
2.9 Scale-up: What are the risks in scaling the compressor up so that it will compress the CO2 from the type of large frame-type gas turbine that is used in an IGCC?

3 Developmental Plan

3.1 What is the program management structure and process for carrying out the development program?
3.2 Does the development schedule mesh with DOE's programmatic requirements? (Testing / reviews / decision points)
3.3 What is the estimated development cost by phase, including the scale-up needed for an IGCC?

3.4 Are the required facilities and people available?

4 Production Assessment (What are cost and production requirements)

4.1 What is the estimated production cost of the design vs. that of the industry leading existing product design? (Assumes the use of available methodologies that enable one to predict production costs of a product based on its design, independent of who sells it). See http://www.pricesystems.com/ This system is used by P&W and others in the aerospace business
4.2 How will required number of compressors be produced? Are facilities/people available for both small industrial size and large IGCC size compressors?
4.3 How will product support be provided (facilities/hardware/people)?

5 Technology Readiness. Considering the above assessments, what is Ramgen's Technology Readiness Level? For definitions see http://en.wikipedia.org/wiki/Technology_Readiness_Level

6 Business Plan. Considering estimated performance and production cost vs. competition, will end users have adequate incentive to buy the Ramgen design?

Questions from Ravi Ravindranath

1. Though shock/BL control has been demonstrated in inlet applications, not sure it has been demonstrated in rotating machinery. Could be a challenge and would like see some substantiating data.

2. Rampressor produces the pressure ratio through shock compression and shock compression is good to develop pressure ratios beyond SOA compared to conventional turbomachinery. But the compression process is very inefficient. Not clear whether the quoted numbers for efficiency are test data or by analysis.

3. Rotor exit angle of 75 - 85 Deg. Looks extremely tangential. Recovery in the stationary plane would be very lossy. Overall stage efficiency could be low.

4. CFD for real gases work differently compared to ideal gases due to changes in the gas constant. Has this been addressed?

5. CFD run for real gases may give erroneous results due to choice of choice of constant gamma assumption. Is there a correction applied for the predicted performance?

6. How is the stall margin/surge margin predicted in the CFD programs?

7. The best performance match is at 0.004' tip gap, while the worst efficiency is at this tip gap also (compared to 0.001" and 0.002") Is this a reflection of the CFD fidelity? If the compressor performance is this much dependent on clearance, how is clearance measured in the compressor and maintained over the life of the compressor.

8. "Prediction assume that the design intent is met in all the components" - Can this assumption be true? How good is the prediction and has the predictive tools been validated/calibrated against available data?

9. May be I am confused here. They talk about oil-free compressor as-well-as Co2 compressor. From the looks of it, looks like the bearing is conventional, which would need lubrication. Is this true or is the bearing system magnetic?

Questions from Cengiz Camci

Aero-thermal flow measurements/physics :

They displayed tip clearance measurements in a range from 0.001 inch to 0.004 inch in a rotating machine with a tip speed of more than 2000 ft/second. I need to know more about the way they measure this clearance. I also need to hear about the operational character of this extremely tight clearance (compared to conventional transonic/axial compressors). A more specific item could be the specific casing surface design in case an unexpected rub incidence.

I am also interested in knowing more about the influence of heat transfer to the rampressor rotor flow especially from the hot end in case of a radial turbine driving the rampressor. Is there any estimate of efficiency degradation due to heat addition to the rotor from a possible heat source in the system ? (turbine driver..)

How does the surface roughness character play a role in this suggested compression system.

Since the compression passage heights are much shorter than the aspect ratios of modern transonic compressors, I would like to know more about the types of secondary flows that may develop from the momentum deficit fields (turning along the entrance region) before and during a typical compression sequence.

I would like to see a better uncertainty quantification for all aero-thermal measurements they are presenting.

Performance related Aero-thermal computations:

Any attempt to resolve shock waves in a more realistic way by using adaptive gridding ? A few computational results suggested that shock waves are smeared from the lack of grid resolution near the shock systems.

The reports do not include any grid-independency results.

I understand/appreciate the choice of a simplistic and time efficient turbulence model (Spalart_Alm. model). This is totally understandable. However, due to specific flow physics in this compression system, shock boundary layer interactions will always exist. Any future plan to be more conscious around shock boundary layer interaction regions ?

Unsteady deterministic oscillations in this rotor may significantly enhance momentum and heat transfer in the passages of this rotor.

One expects to see information about how clearance flows are handled and their influence on local total pressure drop characteristics at the exit.

I also expect to see a more detailed account of secondary flow development in this specific compression system. What is getting into this specific rotor as far as the momentum deficits are concerned in inlet channels/ducts.

Pressure ratio of 50 to 100 appears in the reports. In a PR=100 system where 10,000 HP is provided to the rotor it is likely that there will be significant convective heat transfer to the rotor/bearings. Any heat transfer related comments/suggestions/designs will be useful. At PR=100 an isentropic compression approximately generates 1554 F which is not a negligible temperature for a rotor with a tip speed of 2000+ feet/second .

Questions from Greg Bloch

My input comes in two forms: generic (tailored to the process) and specific (tailored to the Rampressor). The generic segment comes by way of DoD best practices for program reviews and risk mitigation, which may duplicate processes already in place at either DoE or Ramgen. I include these not because I think they are a priori better than anyone else's best practices (which I obviously couldn't assess unless I compared them both), but rather to ensure that at least one set of best practices is available and used.

In the following website see a somewhat generic outline that DoD uses regarding the various technical reviews that occur throughout the life of a product:

https://learn.dau.mil/CourseWare/800860_2/scopage_dir/tr/trs.html

Sections pertinent to a PDR are on pages 10-11; some reference is made to previous reviews (which may or may not have already occurred for the Rampressor) that are discussed earlier in the document. The generic "are we ready to proceed?" questions that I would ask are included in the list on page 11. These effectively ask the question, "Show me your plan and convince me that you can execute it with the resources available".

The following two charts are a somewhat generic risk assessment template that DoD uses for identifying, assessing, and mitigating risk items. The criteria for various levels of

probability and consequence can be customized as required for a particular program as long as they still capture the varying levels of probability (from "not gonna happen" to "virtual certainty") and consequence (from "who cares?" to "this kills the program") and as long as the same criteria are applied consistently across the entire program. These risks are typically phrased in the form, "if A happens, then B will be the consequence" to enable easier assessment of both probability and consequence. Again, these are not intended to duplicate or replace any existing risk mitigation processes, but simply to ensure that at least one appropriately-defined process is available and used.

Details on Risk Matrix

Level	Likelihood	Probability of Occurrence
1	Not Likely	~10%
2	Low Likelihood	~30%
3	Likely	~50%
4	Highly Likely	~70%
5	Near Certainty	~90%.

Likelihood

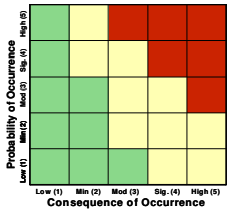

Consequence

Level	Technical	Schedule	Cost
1	Minimal or no impact	Minimal or no impact	Minimal or no impact
2	Minor technical shortfall, no impact to high level technical requirements	Additional activities required, able to meet key dates. Subsystem slip < 3 months	Budget increase < 1%
3	Moderate technical shortfall but workaround available which will eliminate impact to high level technical requirements	Minor schedule slip, no impact to key milestones. Subsystem slip < 6 months. Critical path slip < 3 months.	Budget increase < 5%
4	Unacceptable, workarounds available which will eliminate impact to high level technical requirement	Program critical path affected, all schedule float associated with key milestone exhausted. Critical path slip 3 to 6 months	Budget increase 5% to 10%
5	Unacceptable, no alternative exist	Cannot achieve key program milestones	Budget increase > 10%

If A happens, then B will be the consequence.

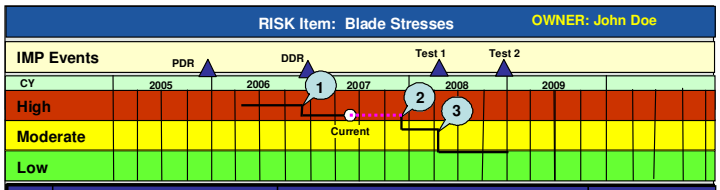

ID	Mitigation Activity	Exit Criteria	Completion
1	• Do some analysis	• All Blades Successfully Pass Dynamic and HCF Design Criteria	PDR Complete (month/year)
2	• Do some bench testing	• Any Responses Identified and Lie Outside Steady State Operating Range	DDR Complete (month/year)
3	•Run a rig test	• Successful demonstration of operability and acceptable stresses	Rig test Complete (month/year)

My specific questions are shown below; I have attempted to minimize the overlap between my specific questions and those asked by the rest of the review team.

- Have you considered the APNASA code for your CFD studies? This code is widely used in gas turbine engine design (fans, compressors, turbines) and includes multi-stage effects. POC is Ken Suder at NASA Glenn Research Center (Kenneth.L.Suder@grc.nasa.gov (216) 433-5899). You may have a challenging time gridding the features on the blades, but if you can, this code is likely to give a fairly reliable prediction. This code is America's Favorite Price (free). Another free alternative if APNASA is unsuitable is MSUTurbo. I can provide contact information for the keeper of this code separately (if Ramgen is interested).
- Have you optimized the IGV design as thoroughly as the rotor geometry? Are the IGVs variable stagger for throttling, or are they split-flap designs?
- To whom is the IGV and de-swirler design subcontracted? How is the intellectual property protected?
- What are the design-point performance parameters (e.g., mass flow, pressure ratio, efficiency)? Does this machine always run at a single-point condition, or is throttling (i.e., operation at reduced mass flow) required? What happens to the pressure ratio requirements when operated at lower mass flow?
- What are the Mach numbers relative to rotors 1 and 2 at design and off-design conditions?

- What happens when the Rampressor stalls? Will extended operation in stall damage the machine? How is stall identified and how is recovery initiated?
- How are the aeromechanics of the Rampressor addressed? Please show that steady state stresses are within the materials limits, that the natural modes of the rotor blades and disk have been identified, and that these modes are not excited by any known drivers in the anticipated operating range (or identify issues that are known to exist).
- A compressor with a 10:1 or 100:1 pressure ratio will generate a significant thrust load. How are the bearing thrust loads modulated or controlled (or are the bearings simply designed to tolerate them)?
- How are the various cost, schedule, and performance risks mitigated? Please provide a complete list of the various risk items and a risk mitigation waterfall chart for each yellow and red risk.

- Is Ramgen paying for the testing mentioned on chart 48? If the US Government is funding this task (even partially), it is typical for the testing to be done within the US.
- Will you measure tip clearance during the test? At how many axial and circumferential locations? (I would expect the aft end of the rotor to be much hotter than the front, with thermally induced radial growth to match.)
- How will you control the tip clearance down to only 0.001"?
- On chart 53, why is there no time between the single-stage and two-stage tests? What is the perceived value of doing the single-stage test separately (and at the same time as the two-stage)?
- Are the motor and drive system costs (including controls) backed up by industry quotes? Are these quotes for single-unit purchase, or do they require multiple-unit sales to reach a discounted price? If multiple units were assumed in the pricing, how many units were assumed and what happens to the price if you only purchase one?

Appendix 3: Risk Analysis

Details on Risk Matrix

Level	Likelihood	Probability of Occurrence
1	Not Likely	~10%
2	Low Likelihood	~30%
3	Likely	~50%
4	Highly Likely	~70%
5	Near Certainty	~90%.

Likelihood

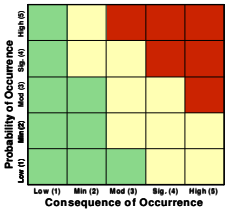

Consequence

Level	Technical	Schedule	Cost
1	Minimal or no impact	Minimal or no impact	Minimal or no impact
2	Minor technical shortfall, no impact to high level technical requirements	Additional activities required, able to meet key dates. Subsystem slip < 3 months	Budget increase < 1%
3	Moderate technical shortfall but workaround available which will eliminate impact to high level technical requirements	Minor schedule slip, no impact to key milestones. Subsystem slip < 6 months. Critical path slip < 3 months.	Budget increase < 5%
4	Unacceptable, workarounds available which will eliminate impact to high level technical requirement	Program critical path affected, all schedule float associated with key milestone exhausted. Critical path slip 3 to 6 months	Budget increase 5% to 10%
5	Unacceptable, no alternative exist	Cannot achieve key program milestones	Budget increase > 10%

If A happens, then B will be the consequence.

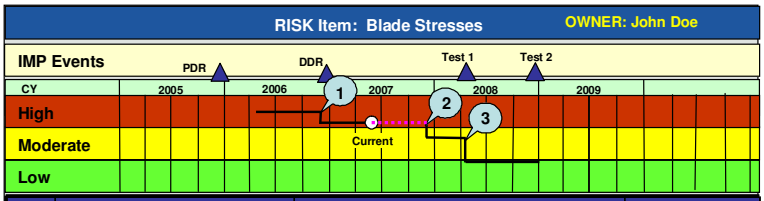

ID	Mitigation Activity	Exit Criteria	Completion
1	• Do some analysis	• All Blades Successfully Pass Dynamic and HCF Design Criteria	PDR Complete (month/year)
2	• Do some bench testing	• Any Responses Identified and Lie Outside Steady State Operating Range	DDR Complete (month/year)
3	•Run a rig test	• Successful demonstration of operability and acceptable stresses	Rig test Complete (month/year)

Appendix 4 – Example of System Level Cost Trade Study

System Level Cost Comparison for Stage Count

Assumptions: Design Pressure Ratio = 100
Intercooler Effectiveness = 0.98
Intercooler Pressure Loss = 0.04
Polytropic Efficiency = Constant = 0.9
Power Plant Cost = 2.3 Billion Dollars (630 MW IGCC)
Power Plant Cost Scales to the 0.7 power
Power Plant Scales as a func of comp work, and frac of output consumed by comp (5%)

Number of Stages		2	3	4	5
Compressor Cost	Base		$290,837.65	$608,755.13	$933,220.31
Intercooler Cost	Base		$211,051.24	$331,703.15	$412,619.41
Motor / Drive Cost	Base		-$124,697.88	-$174,836.82	-$198,564.05
Total Compression System Cost	Base		$377,191.01	$765,621.46	$1,147,275.67
Business Plan Adjustment			$554,093.59	$1,124,697.92	$1,685,347.96
Work of Compression	Base		-8.210%	-11.507%	-13.069%
Power Plant Size	Base		99.5895%	99.4247%	99.3466%
Power Plant Cost	Base		-$6,613,126.78	-$9,271,068.68	-$10,530,482.99
Operating Cost	Base		-0.41%	-0.75%	-0.86%

Note: This is only an example of the type of system cost trade that needs to be made to establish requirements. Assumptions for scaling power plant to achieve same overall capability and cost due to scaling should be reviewed and assumption for constant efficiency should be refined. This serves to illustrate that the impact upon total system cost caused by reductions in compressor work can be significant.

Chapter 3

R&D Implementation Plan

In conjunction with DOE/NETL and industry (Dresser-Rand), Ramgen created a comprehensive plan to demonstrate a full-scale CO2 compressor using Ramgen technology. This plan took the form of a Phase 2 proposal to the DOE which was subsequently awarded and is currently under way. This proposal is included as an Appendix to this report to document the background, foundational work performed, R&D requirements, cost, schedule and ideal setting determined by this effort.

CHAPTER 3 APPENDIX

Phase 2 Proposal

Revised Project Plan

CO_2 Compression Using Super-Sonic Shock Wave Technology

March 10, 2009

WORK PERFORMED UNDER AGREEMENT

DE-FC26-06NT42651

SUBMITTED BY

Ramgen Power Systems, LLC.
11808 Northup Way, Suite W190
Bellevue, WA 98005

PRINCIPAL INVESTIGATOR

POC: Karen Belshaw
(425) 828-4919 ext. 289
Fax: (425) 828-7756
email: kbelshaw@ramgen.com

SUBMITTED TO

U. S. Department of Energy
National Energy Technology Laboratory

Charles Alsup
CHARLES.ALSUP@NETL.DOE.GOV

TABLE OF CONTENTS

1 EXECUTIVE SUMMARY

As a direct result of NETL's leadership and support for developing Ramgen's advanced CO_2 compression technology, Ramgen is pleased to report that all project Phase 1 objectives have been met and the key objectives exceeded. This technical progress, combined with Dresser-Rand bringing very significant additional resources as a new participant with Ramgen and NETL in the development process, makes it possible to substitute a test of a 13,000 hp CO_2 compressor for the originally planned 3000 hp unit. This improvement is within the current project scope, described in Section 2.1, and substantially reduces the time and cost of full development while increasing the probability of meeting performance requirements.

The current DOE cooperative agreement instructs that, as part of Phase 1 of the cooperative agreement, the work completed is to be reviewed and the overall plan improved based on results. As required by this instruction, Ramgen and Dresser-Rand have together reviewed the completed work results and identified a number of opportunities to improve the Phase 2 and Phase 3 plans. In order to meet this cooperative agreement requirement, Ramgen is submitting an improved work plan that is a within scope change to achieve the current cooperative agreement objective to develop an advanced CO2 compressor.

Dresser-Rand has made an independent and comprehensive review of the rapid progress with the technology development detailed in this proposal and of the tremendous and unique benefits to the nation of the eventual, after development, widespread commercial deployment of this CO_2 compressor. At the end of their review, this acknowledged global leader in compression technology and CO_2 related systems has joined with Ramgen and NETL to complete the development of this technology.

CCS on the massive scale required for greenhouse gases is exploring new territory and the many variables have to be clarified by conducting demonstrations to build the factual record. Substituting the 13,000 hp compressor will advance this process by having Advanced Compression available earlier for inclusion in the large scale CCS demonstrations to obtain empirical data on projected reduction of CCS costs. Ramgen has done an analysis of the potential for this advanced CO_2 compressor to significantly contribute to reducing the cost of CCS which is submitted for NETL review in Section 3.1.2 of this cooperative agreement modification. As is the case with all early analysis of new CCS systems, it is subject to the accuracy of multiple inputs.

This improved Phase 2 and Phase 3 plan modification which is within the scope of the current cooperative agreement will result in saving two years of development time and reducing full development costs by at least $15 million (see Section 3.1.4.). Design advances have been achieved based on test results and configuration breakthroughs (see description in Section 2.3 Phase 1 Key Objectives and Status). In addition, Dresser-Rand, which joined with Ramgen and NETL in November of 2008, brings investment combined with unique resources to the development process. In order to fully meet the current work scope objectives and take advantage of the rapid progress made to date, Dresser-Rand will: provide $22 million in cash; collaborate fully with Ramgen using its 60 years of engineering experience compressing CO_2; and adapt an existing closed loop CO_2 test facility capable of testing a 13,000 hp unit (a test facility of this size would otherwise have been unaffordable to the program). The Dresser-Rand

facility is one of three in the world with gas mixing capabilities that will enable important controlled tests on CO_2 with different contaminant content.

Dresser-Rand's participation at this level will permit moving directly to the 13,000 hp compressor and support meeting the cooperative agreement requirement of an option to provide testing of Advanced Compression at this scale at a DOE project in the 2012-2015 time frame. The larger size will eliminate scaling questions and enable factual determinations of impact on plant costs, both capital and operational. The larger unit is projected to have better overall efficiency and reduced capital cost per capacity. Additionally, the larger size matches up well with the needs of utilities planning CCS demonstrations. Over the past year Ramgen has had extensive discussions with utilities planning CCS demonstrations and several have stated their need for an advanced CO_2 compressor in the 13,000 hp size range as quickly as possible and preferably in the 2012-13 timeframe.

Scale-up steps that will be eliminated by substituting the larger compressor are described in Section 3.1.4 Speed of Development. The goal remains exactly the same to develop and test Advanced Compression of CO_2.

Substituting the larger size compressor to accomplish the original work scope and objectives will ultimately accelerate the wide spread application of the technology to obtain reductions in greenhouse gases. The more rapid completion of the original work scope for this technology will provide NETL with a valuable tool two years earlier to assist in reducing the cost of CCS in new and existing coal plants and in retaining affordable electricity. While CCS systems at this scale are new with many uncertainties that must be tested to make final determinations, Ramgen has done estimates that over a twenty year period reducing development time by these two years could save US ratepayers as much as $34 billion. These savings derive from several advantages including: lower capital costs; lower installation costs; much smaller footprint (space requirements are a serious complication for many retrofits, as noted in a CCS study conducted by AEP and Alstom; DOE/NETL-401/110907); lower maintenance costs; and using the Ramgen compressor's high heat deltas to reduce the parasitic energy load on the coal plants.

The estimated $34 billion in savings number will be influenced by the capture system or systems which emerge as preferred options for utilities and the willingness of the capture technology developers to integrate their technology with advanced CO_2 compressor to optimize the total efficiency of capture/compressor technology. It assumes maximizing the heat that can be captured and used given the high single stage pressure ratios unique to the Ramgen compressor. As noted earlier, the Ramgen analysis that CO_2 compressors represent a significant fraction of the capital and operating cost penalties of CCS systems is set forth in Section 3.1.2, and Figure 3.5 represents a summary of Ramgen's assumptions and calculations). Also as noted earlier, achieving Advanced Compression of CO_2 at the 13,000 hp size enables this larger unit to be available for testing in the critically important CCS demonstrations in the 2012-15 period required by the DOE Solicitation.

National and world leaders are increasingly emphasizing the importance of conducting large scale demonstrations of CCS in the shortest feasible timeframe. Given its predominance in the oil and gas industry, Dresser-Rand can rightfully claim to be the world's leading CO_2 compressor company. The Ramgen compressor is the only option Dresser-Rand has identified in the world for including Advanced Compression at lower capital and operating costs in

demonstrations of CCS. The Ramgen/Dresser-Rand timeline proposed in this within scope modification is dependent on the requested NETL funding. Importantly, Dresser-Rand considers the innovative Ramgen technology a means by which a US company can continue to lead the world with high technology, patent protected compressor products made in the US using US made components. This will add jobs to the US work force and will help meet the DOE jobs objective stated in the solicitation that resulted in Ramgen's cooperative agreement.

As noted above, the improved work plan presented in this requested cooperative agreement modification results from a series of major technological breakthroughs achieved as part of the successful completion of Phase 1. One important achievement was a substantial reduction in the technical risk remaining for product development. The major objectives completed during Phase 1 included:

1) World record pressure ratio obtained for a single stage axial compressor – Ram 2
2) Significant risk reduction in the critical technology areas of aerodynamic and mechanical design including early validation testing
3) DOE sponsored technology review and evaluation
4) Improved R&D Implementation plan with technical and industrial input
5) CO_2 compressor conceptual design

As instructed by the DOE cooperative agreement, the Phase 1 R&D plan of the current agreement includes a review of the work completed in Phase 1 to identify ways to improve the overall plan. The achievements in Phase 1 have been incorporated into the modified work plan in this proposal in order to deliver sooner to the DOE a significantly larger and more efficient demonstration unit. The improved plan is the basis for the Phase 2 and Phase 3 work in this within scope agreement modification. The major features of the improved plan include:

1) Larger demonstration unit to reduce "scale-up" and ultimate customer acceptance risk while increasing performance and reducing capital costs per unit of CO_2 processed (see description in Section 2.3, Phase 1, Key Milestones of how exceeding major objectives in Phase 1 enables substitution of 13,000 hp compressor)
2) CO_2 testing sooner
3) Additional performance verification check points – static testing, CFD validation, rotating CO_2 testing, retrofit rotor
4) Single stage configuration that integrates well with broader range of available capture technologies i.e. chilled ammonia, aqueous ammonia
5) Acceleration of Commercial availability by ~2 years and reduction of cost to commercialization by ~ $15 million (see Section 3.1.4.).
6) Plan that has been screened by a number of utilities and developers planning CCS demonstration; manufacturers, and Dresser-Rand
7) Larger demonstration unit made possible by use of modified Dresser-Rand test facilities
8) Dresser-Rand technical contributions and expertise accumulated over 60 years of compressing CO_2 and becoming the world leader for Enhanced Oil Recovery
9) Dresser-Rand financial contribution in excess of the project's cost-share requirements

Ramgen's improved plan takes advantage of the opportunities created by the Phase 1 work and will result in comprehensive Phase 2 and Phase 3 work periods within the original scope. This proposal identifies tasks that will deliver an all-inclusive feasibility design review with a more

mature commercial design layout based on the advanced rotor configuration. We project performance validation for all critical parts of the flowpath, including: IGVs; supersonic flow-path; radial diffuser; and stationary diffuser. We have also identified the Dresser-Rand test facility in Olean NY as the site for the rotating test and demonstration facility. To complete the full Phase 2 requirements Ramgen is proposing a within scope modification at a total cost of $42.4 million for the FY2009 through FY2012 period with $20.4 million of this from NETL. The NETL funding request by DOE fiscal year is $5.4M for FY2009, $8M for FY2010 and $7M for FY2011. The $22 million of private match does not include in-kind contributions.

2 BACKGROUND

2.1 Objective - A Novel CO_2 Compressor

Ramgen has based this development program on the scope and requirements of the original DOE Funding Opportunity Announcement; Enabling Turbine Technologies for High-Hydrogen Fuels; CFDA Number 81.089 Fossil Energy Research and Development; Topic 4: Novel Concepts for the Compression of Large Volumes of Carbon Dioxide (DOE Solicitation).

Ramgen Power Systems, LLC. (Ramgen) is currently developing a novel CO_2 compressor concept capable of providing the required pressure ratio (PR) to convert to supercritical the CO_2 outflow from any kind of capture system. Ramgen's concept is projected to be more efficient and cost less than other options available in the foreseeable future. The DOE Solicitation also requires an option for testing the technology in the DOE FutureGen project in the 2012-2015 timeframe.

The supersonic compressor concept will work efficiently with a variety of capture systems. Capture system pressure ratio requirements range from 10:1 pressure ratio in a single rotor stage unit to 100:1 pressure ratio in 2 single-stage units. For example, advanced MEA requires 100:1 PR while Solexsol can require 2 or 3 different PR stages. The Alstom chilled ammonia system requires < 10:1 PR. The Powerspan aqueous ammonia system can be either a 10:1 or 100:1 PR system. Ramgen's single stage and discreet drive approach provides great flexibility in adapting to a variety of plant and capture system requirements, while holding down production costs. The development work currently being done is suitable to AEP's Alstom chilled ammonia capture process, and the advanced compressor technology is broadly applicable to most capture systems. Ramgen will develop and test a 10:1 single stage compressor delivering supercritical CO_2 on the order of 1500 psia. The CO_2 compressor delivery condition is specified in Section Part I - D. Topic 4 of the DOE Solicitation. This work will additionally provide the foundation for multi-stage systems capable of 100:1, or greater pressure ratio, depending on the application. This development work is preparing for a demonstration unit equivalent to that sized for use in a 250 MW PC coal plant (equivalent to approximately 2 million tons of CO_2 per year).

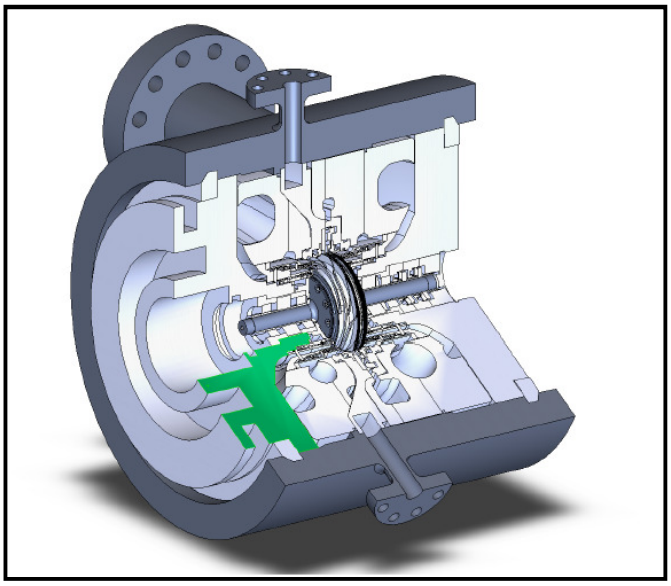

Figure 1.1. Ramgen's Super-Sonic Shock Wave CO_2 Compressor Concept

Nominal Specifications:

- Capacity 75 lbs/sec
- Gas Composition TBD
- Inlet Pressure 15 psia to 275 psia
- Inlet Temperature 70°F
- Discharge Pressure 1500 to 2700 psia
- Power 13,000 bhp
- Dimensions:
  - Length 12 ft (with drive motor)
  - Width 4.5 ft
  - Height 5.0 ft
- Motor options
  - Direct Drive variable speed motor
  - Steam turbine
  - Induction motor with gearbox

2.2 Larger Compressor Substituted in Proposal to Improve Program Scope Achievement

The original DOE Solicitation requires the demonstration of a CO_2 compressor capable of compressing large volumes of CO_2, more efficiently and at less cost than current options. Ramgen's original plan developed a 3000 hp unit for sub-scale testing. The requested within scope adjustment to our Development Plan will facilitate achieving the scope, goals and objectives of the DOE Solicitation by demonstrating a 13,000 hp compressor unit. Substituting this 13,000 hp development unit will result in providing units for major CCS demonstration projects approximately 2 years sooner than the original Ramgen plan. The substitution of the 13,000 hp compressor for the 3000 hp unit in the current cooperative agreement was made possible by unexpected technical risk reduction in Phase 1 and by the resources committed to the project through the engagement of Dresser-Rand.

Dresser-Rand – A Key Industrial Partner
Ramgen's original development plan was proposed in 2005 and was based on Ramgen supporting development through Phase 3 without the partnership of a major OEM.

In November, 2008, after more than 6 months of intensive technology review, Ramgen and Dresser Rand entered into a comprehensive agreement to support development of Ramgen CO_2 compressor technology. The plan entered into is dependent on continued DOE support for the development, but it provided critical matching funds and additional resources. Dresser-Rand is a world class compressor manufacturer with a global reach and experience base. They have extensive experience with CO_2 in the field, and are the principle world-wide suppliers of compressors for Enhanced Oil Recovery. Dresser-Rand will contribute $22 million of matching funds to developing this CO_2 compressor program. In addition, the testing will be done at a modified existing Dresser-Rand closed loop CO_2 testing facility in Olean, New York. It is important that following the development of the CO_2 compressor Dresser-Rand has the proven capability to manufacture, distribute and service the technology in the US and worldwide on the scale required to make a significant contribution to reducing greenhouses gases and maintaining affordable electricity. This support will greatly enhance the DOE goal described in the original solicitation to move into commercial applications in the earliest feasible timeframe.

CO_2 Compressor Ready for Major Demonstration Project in 2012-2013 Period
The substitution of the larger compressor in the development plan will reduce the time required for making advanced compression part of major CO_2 demonstration projects. Dresser-Rand's involvement will bring industrial experience to bear on the design of the CO_2 compressor, thus reducing the time, technology and money gap between demonstrator unit and ultimate product. Dresser-Rand will also allow Ramgen to test the CO_2 compressor in a world class test facility owned by Dresser-Rand, located in Olean, New York. This test facility will allow Ramgen to test the demonstration unit with far greater control and up-time than in a field demo scenario. The Dresser-Rand test facility will eliminate the risk of disruptions due to the plant itself, the carbon capture machinery, and the storage availability. It will also permit demonstration on a variety of CO_2 gas mixtures that can be created in the facility. Finally, the larger size demonstration unit is directly applicable to a unit capable of servicing a 250MW coal plant without the need to scale up or down. The larger unit permits higher efficiency by reducing size constrictions of the aero-flow through the compressor. The larger size also lowers the cost per unit of CO_2 compressed.

2.3 Project Goals and Results

Ramgen is using lessons learned from our Rampressor 1 and Rampressor 2 design process and test results as well as recommendations from Dresser-Rand to execute improvements in the development plan for a novel CO_2 compression technology.

Phase 1 - Complete

Cooperative agreement Objectives

The objectives of Phase 1 as defined by the DOE Solicitation were to 1) identify and define the proposed components or systems, (2) establish expected performance of the proposed system, (3) identify and provide plans to resolve barrier issues, (4) develop a

conceptual design, and (5) develop an R&D Implementation Plan with a cost estimate that takes the proposed component or system through all three phases of the project.

Key Objectives (3) Resolve Barrier Issues and (5) R&D Implementation Plan above were exceeded during Phase 1 and this achievement made the improvements now being proposed for this cooperative agreement possible.

Schedules: Phase 1 was started in May, 2006 and ended February, 2008.

Key Objectives and Status

The unexpected achievement during Phase 1 was a configuration breakthrough that simultaneously resolved a number of aerodynamic, mechanical, and manufacturing challenges or barrier issues.

Ramgen investigated several critical technical challenges in the Task activity called Critical Success Factors Risk Reduction. In May of 2007 Ramgen completed the high pressure ratio (8:1) Rampressor 2 testing with the results from this test directly applicable to a single stage high pressure ratio (10:1) or two stage (100:1) CO_2 compressor. At the completion of the test the key challenge areas were assigned a risk value. At the conclusion of Phase 1 the configuration breakthrough was achieved and the technical risks were reevaluated in consideration of this major advancement, see Figure 2.1.

Phase 1 objectives also included completing the conceptual design of a select number of CO_2 compression demonstrator candidates. These candidates have been evaluated and final configurations for the scaled demonstration unit were selected at the Conceptual Design Review. The breakthrough configuration analysis identified the technical merits of building a larger vs. smaller machine. A larger unit comes with reduced technical risk. The size of the aerodynamic flow paths for the 3000 hp unit are at the probable small end of the continuum of offerable units. The smaller units have more aero challenges in reaching performance targets than their bigger embodiments.

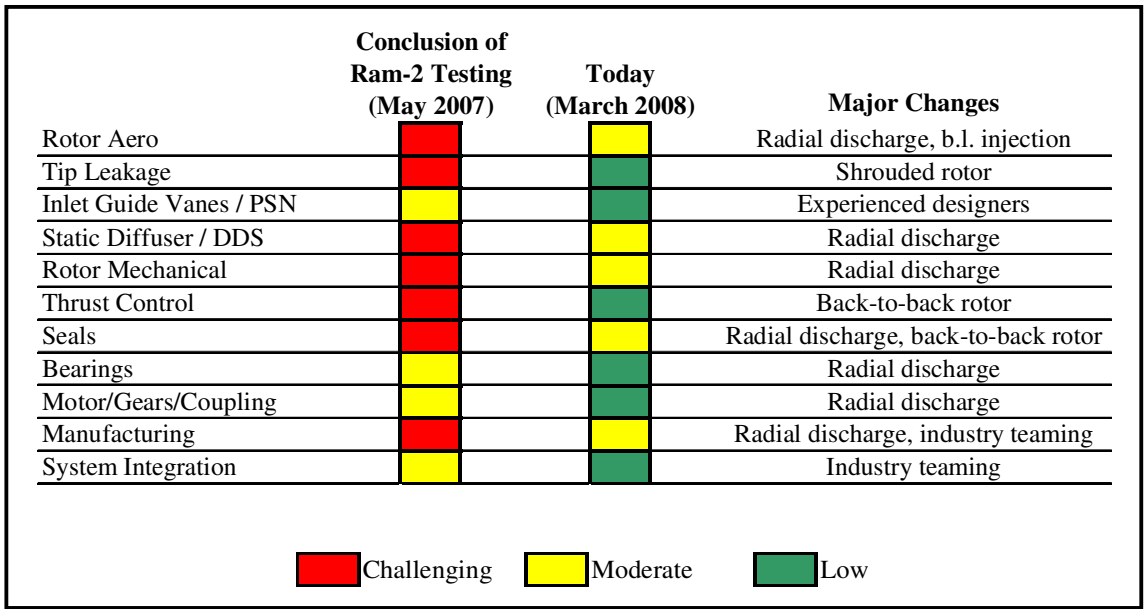

Figure 2.1 Ramgen Risk Assessment Before and After Configuration Breakthrough

Figure 2.1 summarizes the technical risk areas before and after the configuration breakthrough was achieved. The configuration breakthrough is confidential and has been presented to the DOE during 2008.

The final major objective of Phase 1 was to develop an R&D Implementation Plan describing the path and cost to develop the CO_2 compressor through commercialization. Ramgen completed this task and started communicating with the DOE about a new Phase 2 proposal in November, 2007. ***This new proposal conceived of an improved development plan that would complete the development of the technology about 2.5 years sooner.*** However, the demonstration unit was a 3000 hp size, and the track from demo unit to CCS offering would still require a post Phase 3 full-scale pre-commercial test step. This additional step was recognized in the original DOE Solicitation as being supported through other competitive initiatives.

Phase 2

Cooperative agreement Objectives

The objectives of Phase 2 are to develop a detailed design and validation test program. Ramgen has pursued the detailed design in Phase 2. Today, the Ramgen CO_2 compressor represents a design in which all of the significant technical issues identified in Phase 1 have been addressed.

Schedules: Phase 2 started in March, 2008 and is projected to end in June of 2010.

Cost Summary: Ramgen is proposing that an additional $13.2 million dollars of DOE and $8.8 million dollars of private funding be allocated to complete the Phase 2 tasks, which exceeds the minimum 30% Phase 2 cost-share requirement in the original solicitation.

Key Objectives and Status

At the conclusion of Phase 1 Ramgen presented a revised Implementation Plan for the DOE's consideration. The improved plan was being reviewed within the DOE as Phase 1 was being completed. As required by the original cooperative agreement award, Ramgen proceeded with Phase 2 after the DOE granted it authority to do so in March of 2008. Ramgen proceeded with the detailed design of the CO_2 compressor, while also negotiating with Dresser-Rand to become a significant financial and technical partner in developing technology. Ramgen is now at the point in Phase 2 at which we must obtain DOE approval for our improved development plan proposal.

Phase 3

Cooperative Agreement Objectives

The objectives of Phase 3 are to fabricate a pre-commercial prototype CO_2 compressor and conduct longer term testing using actual or simulated coal derived CO_2 gas. This project includes provisions for the development of preliminary test plans for full-scale testing at the DOE's FutureGen project, as required in the cooperative agreement. Ramgen's original proposal conceived of a 3000 hp, ¼ scale unit, which is capable of processing the volume of CO_2 produced by a 50 MW coal plant. While this is a meaningful unit for testing, there is a sizable step from this 50MW coal-plant-scale-unit

to a unit capable of servicing a 250MW coal plant. Our proposal now includes a 13,000hp full-scale demonstration unit capable of processing the volume of CO_2 coming from a 250MW coal plant (approximately 2 million tons annually).

Schedules: The original Phase 3 plan was scheduled from July, 2009 to the end of 2010 with approximately 4 months of testing. The current proposal will conclude in mid 2012, with the added improvements of approximately 17 months of testing and two iterations to hit target performance goals. The timing of the development plan completion aligns with the dates required in the cooperative agreement for the FutureGen option. In addition these dates coincide with the need for CCPI projects to select CO_2 compressors for their DOE funded demonstrations.

Cost Summary: Ramgen has estimated the cost of the proposed Phase 3 work at approximately $7.2 million dollars and approximately $13.2 million dollars from private cost share, which exceeds the minimum 50% Phase 3 cost-share requirement in the original solicitation.

Key Objectives and Status

During Phase 3, procurement of all hardware will be completed and the CO_2 compression demonstrator will be assembled. The unit will be tested at the Dresser-Rand facility in Olean, New York. The state-of-the-art Olean test facility will allow us to conduct development type testing as well as run the unit under typical field conditions. With the ability of the Dresser-Rand facility to test a variety of CO_2 gas compositions the CO_2 compressor can be tested in a variety of conditions. Additionally, most field demo sites are commercial plant operators, with low tolerance for test machinery that has never been tested. With a Ramgen controlled test facility capability we will be able to test when the unit is ready, without dependency on the power plant, developing capture systems or having successful sequestration systems. Ramgen will also be able to check-out the demonstration unit in a test friendly environment with all the proper access to diagnostic instrumentation and engineering personnel with extensive experience with CO_2.

Following Phase 3 testing, the Ramgen CO_2 compressor will be well positioned to be included in a number of suitable demonstration sites with one of the DOE Sequestration Partnerships such as PCOR in North Dakota, or with a potential CCPI participant like AEP and their Mountaineer demonstration of the Alstom chilled ammonia capture process.

2.4 Ramgen Compression Technology – What Is It?

Ramgen Innovation Using Well Understood Technology

Since the sound barrier was broken in the late 1940's, ramjet engines have been widely used as a means to propel aerospace vehicles at supersonic speeds. The underlying supersonic shock theories and aerodynamic technologies are very well understood and fully characterized. Ramgen's primary innovation has been to apply ramjet engine concepts as a stationary "shock" compressor. The principal advantage of shock compression is that it can achieve exceptionally high compression efficiency, at very high compression ratios.

The Rampressor™

All conventional, subsonic jet engines feature discrete compression, combustion and expansion sections to create the thrust used to propel an aircraft. In operation, hot pressurized exhaust gas expands through the turbine to drive the compressor, and then further expands through a nozzle, creating forward thrust.

Ramjet engines feature these same discrete compression, combustion and expansion sections. The significant difference in ramjet engines is that the compressor section does not rotate and the turbine section is therefore eliminated. There are no rotating components in the engine. At supersonic velocities, air is ingested into the engine and flows around a fixed obstructing body in the center of the engine duct, "ramming" the air flow into channels between the center-body and the engine's sidewall. Inside these channels, the airflow is almost instantaneously slowed to subsonic speeds, creating "shock waves." These shock waves are associated with a dramatic increase in pressure, or, in other words, "shock compression." As with conventional subsonic turbine engines, fuel is then added and the hot, pressurized exhaust gas expands through a nozzle to create forward thrust, see Figure 2.4.1.

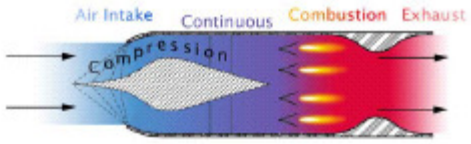

Figure 2.4.1. Ramjet Engine

Ramjets are simple, with no moving parts, but the aircraft has to be moving at supersonic speeds to initiate the shock necessary for effective operation. As a result, all ramjet experience has been in the context of supersonic planes and missiles.

One well-known application of shock compression is its use in the F-15 fighter jet. The pictures and illustrations in Figure 2.4.2 show how a supersonic shock compression inlet acts to boost the inlet pressure, while at the same time reducing the air flow to the subsonic velocity required by the combustor.

Ramgen's Technology Breakthrough

Ramgen's primary technical innovation has been to apply ramjet engine concepts in a stationary compressor application as illustrated in Figure 2.4.3.

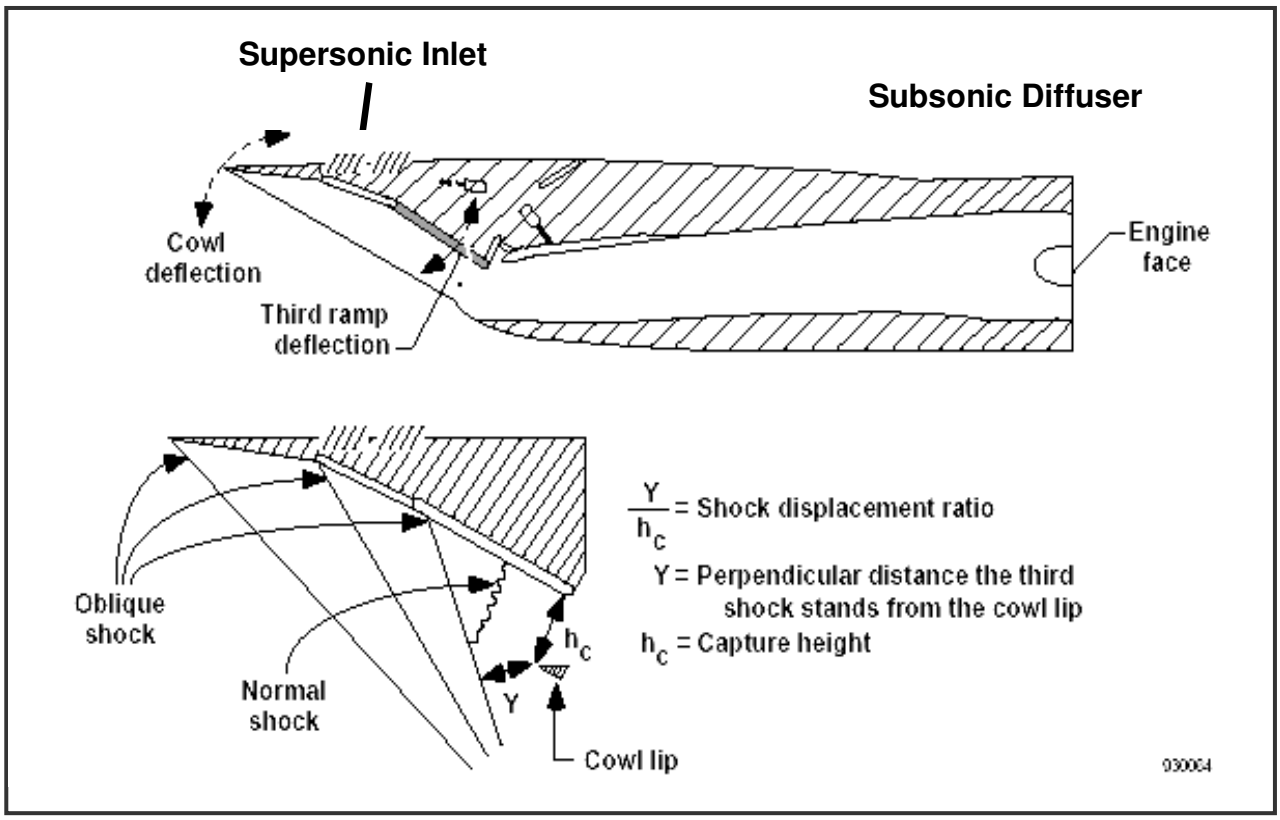

Figure 2.4.2 F-15 Supersonic Inlet Cross Section Detail

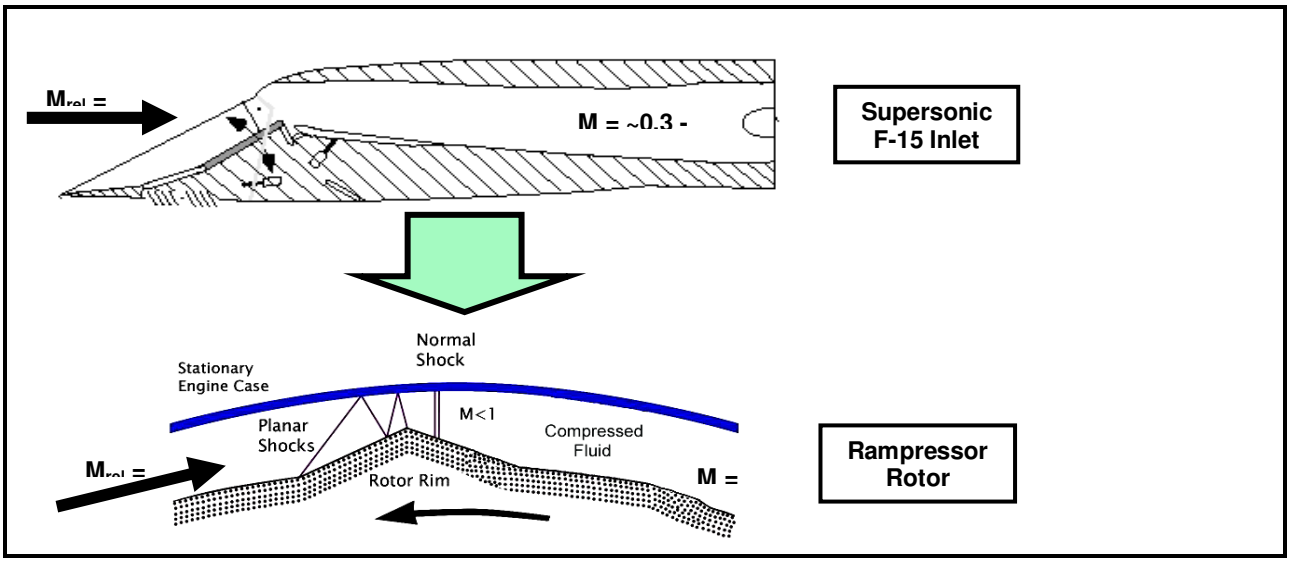

Figure 2.4.3 Rampressor Rotor Profile

Ramgen's core design, the Rampressor, is a relatively simple device, see Figure 2.4.4. It features a rotating disk, which operates at the high peripheral speeds necessary to achieve supersonic effect in a stationary environment. The rim of the disk has raised sections and cavities that mimic the effect of the center-body and channels of a conventional ramjet inlet. Air enters through a common inlet and is then ingested into the annular space between the supersonically spinning disk and the outer edge of the casing. When the flow of air enters this space, the raised sections of the disk rim create a "ramming" effect, generating shock waves and air compression in a manner completely analogous to ramjet inlets on supersonic aerospace vehicles. The

efficiency of this compression process is very high because the compressor has very few aerodynamic leading edges, and minimal drag.

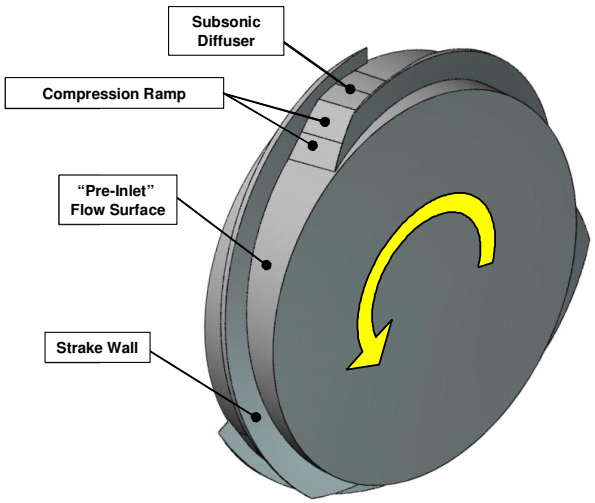

- **Rotor Flow Path:**
  - **3 Supersonic Compression Inlet Flow Paths On Disk Rim**
  - **High Efficiency, Compact Compression**
  - **Minimal Number of Leading Edges**
  - **Flow Path Geometry Similar For Different Pressure Ratios**
- **Combination of Supersonic Flight Inlet & Conventional Axial Flow Compressor Aerodynamics:**
  - **Rotor Rim Radius Change Produces Compression**
  - **3 "Blades" (Strakes) Do Minimal Flow Work**
  - **Axial Inflow/Outflow**

Figure 2.4.4 Ramgen Compressor Rotor Disk

The disk chambers or "strakes" are angled, so the compressed air is "augured" via rotation into a collector and then on to the compressed air system. The compression process is inherently oil-free, requiring no oil for lubrication and/or sealing.

The strength of the shock wave, hence the amount of compression, increases exponentially with the relative Mach number. For example, in air at Mach 1.6 a compression ratio of 3.5:1 is achieved, while at Mach 2.4 it is approximately 15:1. The higher Mach number is achieved by spinning the disc faster. Similarly, the heavier the gas, the lower the speed required to achieve a given Mach number.

3 PROPOSED WORK RATIONALE

3.1. Value of the Technology

Ramgen's shock compression technology represents a significant advancement in the state of the art for all compressor applications and specifically for CO_2 compression. The principal advantages of Ramgen's shock compression is that it can achieve exceptionally high compression efficiency at very high single-stage compression ratios, and this results in a product simplicity and size that will lower both manufacturing and operating costs. The high single-stage compression ratios also produce heated gas with a useable temperature delta rather than requiring expensive and energy consuming multi-stage intercoolers to maintain compression efficiency. The heat capture from the gas can then be used to off-set parasitic heat loads required for capture technology or to produce steam.

The Rampressor CO_2 compressor system should be capable of meeting the needs of any capture system pressure and flow requirements with improved efficiencies and dramatic reductions in package size, weight, and cost compared with existing technologies.

The novel Ramgen technology concept addresses the two greatest objectives identified by the Department of Energy for the Capture and Storage of CO_2**: lower capital and operating costs, and better overall system efficiency.**

3.1.1 Cost

Conventional centrifugal and axial compressor design practice typically limits the inlet Mach number to 0.90 to prevent disruptive shock effects from occurring within the blade flow path. Mach number is inversely proportional to molecular weight. In practice, this limits the achievable pressure ratio per stage of compression in a state of the art turbo-machinery compressor to approximately 1.8:1. Consequently, a conventional "high performance" integrally-geared centrifugal compressor processing CO_2 to the specified pressure ratio of 10:1 will likely require 4 stages of compression (1.8 x 1.8 x 1.8 x1.8) with an intercooler between stages one and two, two and three, and three and four, and possibly an aftercooler. These intercoolers would waste their heat out to the atmosphere because the gas temperature delta per stage would only be about 90 degrees Fahrenheit and thus has no value. To achieve compression from one atmosphere to one hundred atmospheres (100:1), eight (8) stages of compression would be required along with a corresponding number of stainless steel intercoolers between each stage, and possibly an aftercooler, again wasting the heat to the atmosphere.

Ramgen, on the other hand, designs its rotors to create, manage and use these shock structures and can realize the full effect of their ability to efficiently generate substantial pressure ratios. The proposed Ramgen CO_2 product will achieve the required pressure ratio in one or two stages of compression, each rated at 10:1 (10 x 10 = 100). Each stage of compression, instead of warming the gas by 90 degrees Fahrenheit would warm it nearly 400 degrees Fahrenheit. Instead of the heat of compression being waste heat that has to be disposed of using even more energy and expensive capital equipment, the heat in the hot gas produced by the Ramgen CO_2 compressor is useable heat. That valuable heat can be applied to the capture system or steam generation.

Again, importantly, the advantage of the Ramgen Compressor is not that it makes more heat than a conventional compressor. If it did this it would be less efficient and require more shaft power. The advantage is that the heat is in useable form. Instead of being spread out over multiple stages, the heat is captured in a single jump that creates a highly useable temperature delta. In this way, instead of wasting 100% of the heat created by compression, using a Ramgen Compressor you can recapture and use 70-80% of the heat. The energy savings this makes possible are enormous and unequivocal.

3.1.2 Cost of Electricity

Providing information useful to NETL on the projected impact of Advanced Compression on the DOE goals for Cost of Electricity with CCS is important. Ramgen has developed a cost model based on DOE and MIT calculations for Levelized COE and $\$/MtCO_2$. This model closely duplicates the results published in the 2007 DOE report for the Alstom/AEP retrofit plant study, and the 2007 MIT comparisons of various plant and CCS scenarios. Figure 3.1 shows a comparative analysis in terms of Cost of Electricity (COE).

Case 1 is a baseline COE for a PC coal plant without CCS. Case 3 is a DOE documented configuration of the same baseline coal plant with CCS. Ramgen has studied the analysis and found input assumptions that yield a compressor power consumption and cost impact that is too low, a view shared by Dresser-Rand and AEP. Therefore, we have calculated a Revised Case 3 based on our analysis of available industrial compressors. The Revised Case 3 CCS COE penalty would be reduced by 18% if the MANTurbo CO_2 compressors were replaced by Ramgen CO_2 compressors.

After establishing a Revised Case 3 CCS baseline with and without Ramgen CO_2 compressors, we analyzed a number of CCS configurations. Our goal was to determine if we could identify a configuration that yielded an overall COE penalty of 35% or less to achieve the DOE's goal of a 35% COE penalty for combustion based power plants. For gasification based power plants the DOE goal is a COE penalty of 10%. When combined and optimized with advanced capture technology, advanced Ramgen CO_2 compressors reduce the COE penalty by 23% over an integrated MANTurbo installation.

In summary, our analysis is that Advanced Compression is required to achieve that DOE COE penalty goals. The opportunity to reduce the impact to COE in one single component yields a huge "bang for the buck" contributed by Ramgen's CO_2 compressor development.

Stated in terms of capital savings, one 554 MW Pulverized Coal plant CO_2 compressor installation using Ramgen technology instead of conventional technology would save approximately $150 million, or about 18% of the complete CCS system capital cost.

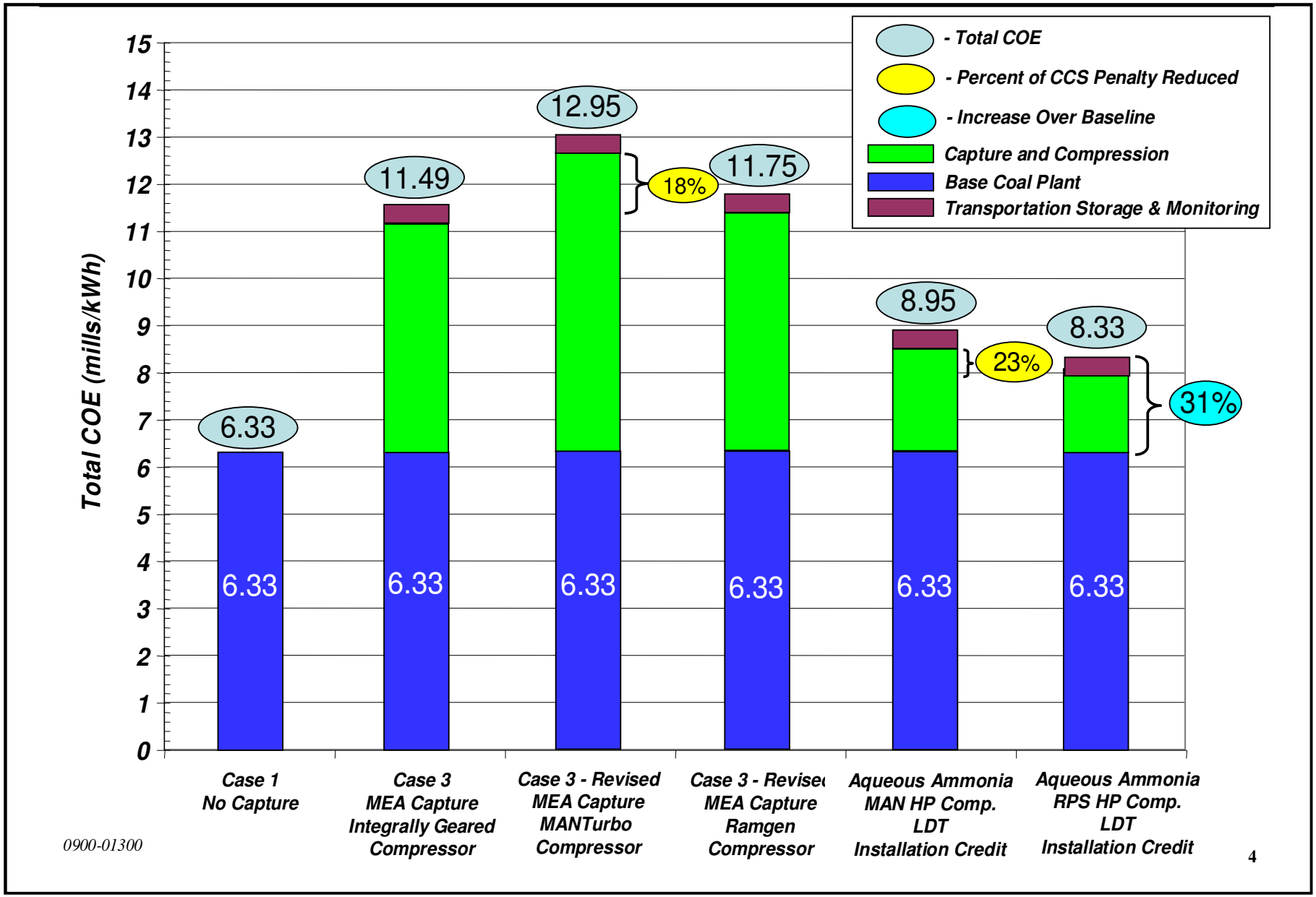

Table 3.1 Cost of CCS

Figure 3.2 is a picture of a conventional 10-stage, 200:1 pressure ratio "high performance" integrally geared CO_2 compressor as manufactured by MAN-Turbo in Germany. The pressure ratio per stage is 1.7:1, ($200^{1/10}$ = 1.698). There may be two fewer stages at the nominal specified 100:1 pressure ratio, but the limitations of the conventional approach are obvious. This particular unit has an inlet capacity of 13,800 icfm with dimensions estimated at 18 ft long, 12 ft wide and 18 ft high. If you look closely you can see a person on the machinery to fully appreciate the size of these machines. Six or seven of these sized units would be required to deliver the 600,000 – 700,000 lbm/hr suggested by the specification, and this would not include the one to two back-up spare units, which is common industry practice. These highly complicated engineering configurations seem very much misapplied for the CO_2 compression service as they significantly add to the overall cost and complexity of carbon capture and sequestration.

It should be noted this MAN Turbo machine is a 6000hp unit, which processes approximately half of the CO_2 the proposed 13,000 hp Ramgen CO_2 compressor will process. At a conservative size estimate of 12 ft long, by 9ft wide and 9 ft high, the Ramgen CO_2 compressor will be 8 times smaller volume and 4 times smaller footprint.

Figure 3.2 – MAN Turbo 10-stage 200:1 CO_2 Compressor

The other conventional approach for large volume CO_2 compression would be to use a conventional inline process compressor train. This type of design uses aero components typically limited to 13,000 ft-lbf/lbm per stage and is projected to require a 3-casing, 12-stage; two-intercooler compressor similar to the two casing design shown in Figure 3.3, below. The unit shown below is an Elliott Turbo, two casing unit. A third, barrel-type casing would be required to achieve the 1500 psia discharge pressure. Dresser-Rand

manufactures similar units and fully understands the expense and limitations of using such units on CCS.

Figure 3.3 – Elliott Turbo Process Compressor Train

3.1.3 Efficiency

Current large scale CO_2 turbo-compressors are generally offered with adiabatic stage efficiencies ranging from 75-83%, depending on flow. These designs can be configured as an 8-stage integrally-geared and intercooled design, or as a 12-stage, 3-casing, 3-intercooler, process compressor train. The proposed two-stage Ramgen CO_2 concept would achieve the required pressure ratio in one to two stages of compression, and do so with comparable input power, but with increased plant efficiency due to recovered heat of compression.

In addition, and as a direct result of the Rampressor being able to achieve single-stage compression ratios of 10:1, stage discharge temperatures are estimated to range between 450-500°F, depending on inlet gas and cooling water temperatures. This offers the potential for significant waste heat recovery, without compromising the compressor performance. This combined compressor and heat recovery creates an even more impressive energy efficiency advantage by recovering up to 80% of the electrical input energy in the form of useful heat. The heat can be used to regenerate amine solutions or heat boiler feedwater.

Conventional CO_2 turbo-compressor designs, with their limited pressure ratio per stage, are therefore also limited to approximately a 90°F stage temperature rise per stage. This eliminates any possibility to recover the heat of compression and necessitates an incremental heat exchanger and cooling tower capital expenditure.

Both the input power and the combined heat recovery impacts are summarized in Table 3.1. below for the Ramgen technology as well as the theorized conventional integrally geared and inline process configurations. This analysis assumes that heat of compression can be recovered down to 250°F. The average stage discharge temperature is shown to make the point, but the heat recovery effect is based upon actual stage by stage discharge temperature projections.

	Ramgen	Intergrally Geared Turbo	Inline Process Turbo
lbm/h	150000	150000	150000
icfm	21411	21411	21411
Stages	2	8	12
Intercoolers	1	7	2
Casings	1	1	3
kW	7333	7382	8312
hp	9830	9899	11147
bhp/100	45.9	46.2	52.1
Isothermal Efficiency	65.8%	64.0%	56.9%
Approx. Avg Stage/Casing Discharge Temp. - F	470	210	380
Max Thermal Recovery Temperature - F	250	250	250
kW	5263	554	4172
% Recoverable	71.8%	7.5%	50.2%
Net kW	2070	6828	4141

Table 3.1. Comparison of Ramgen CO_2 Compressor to Conventional Machines

As can be seen, the input power requirement for the Ramgen CO2 compressor and the conventional integrally geared design are similar, while the process turbo suffers from relatively poor aero efficiency. The heat recovery impact suggests that the net effect of successfully recovering the heat of compression can reduce the input power requirements from 1/3 to 1/2 that of the conventional designs.

3.1.4 Speed of Development

The proposed work plan is within the current cooperative agreement's scope but allows Ramgen, in conjunction with Dresser-Rand, to complete the overall development of the technology in time to provide units at the scale required for CCS demonstrations. The 13,000 hp demonstration unit shortens the time between development and CCS project offering. Figure 3.4 shows a summary schedule of the development of a small machine, like the originally proposed 3000 hp demonstration unit, and a large machine, like the proposed 13,000 hp unit. The ability to eliminate development steps on the way to offering units for CCS saves approximately 2 years and at least $15M.

The steps eliminated by the Large Machine Plan include:

- Aerodynamic flow path scale-up
- Mechanical scale-up
- Fabrication from scratch and maintenance of 13,000 hp capable test facility
- Manufacturing second not-for-sale demonstration unit
- Negotiating with a demonstration-friendly coal plant owner

The larger unit also comes with reduced technical risk. The size of the aerodynamic flow paths for the 3000 hp unit are at the probable small end of the continuum of offerable units. The smaller units have more aero challenges in reaching performance targets than their bigger embodiments. Ramgen's original small machine development plan accounted for these challenges, but if a larger size increases the probability of successful development, the speed of development will also benefit.

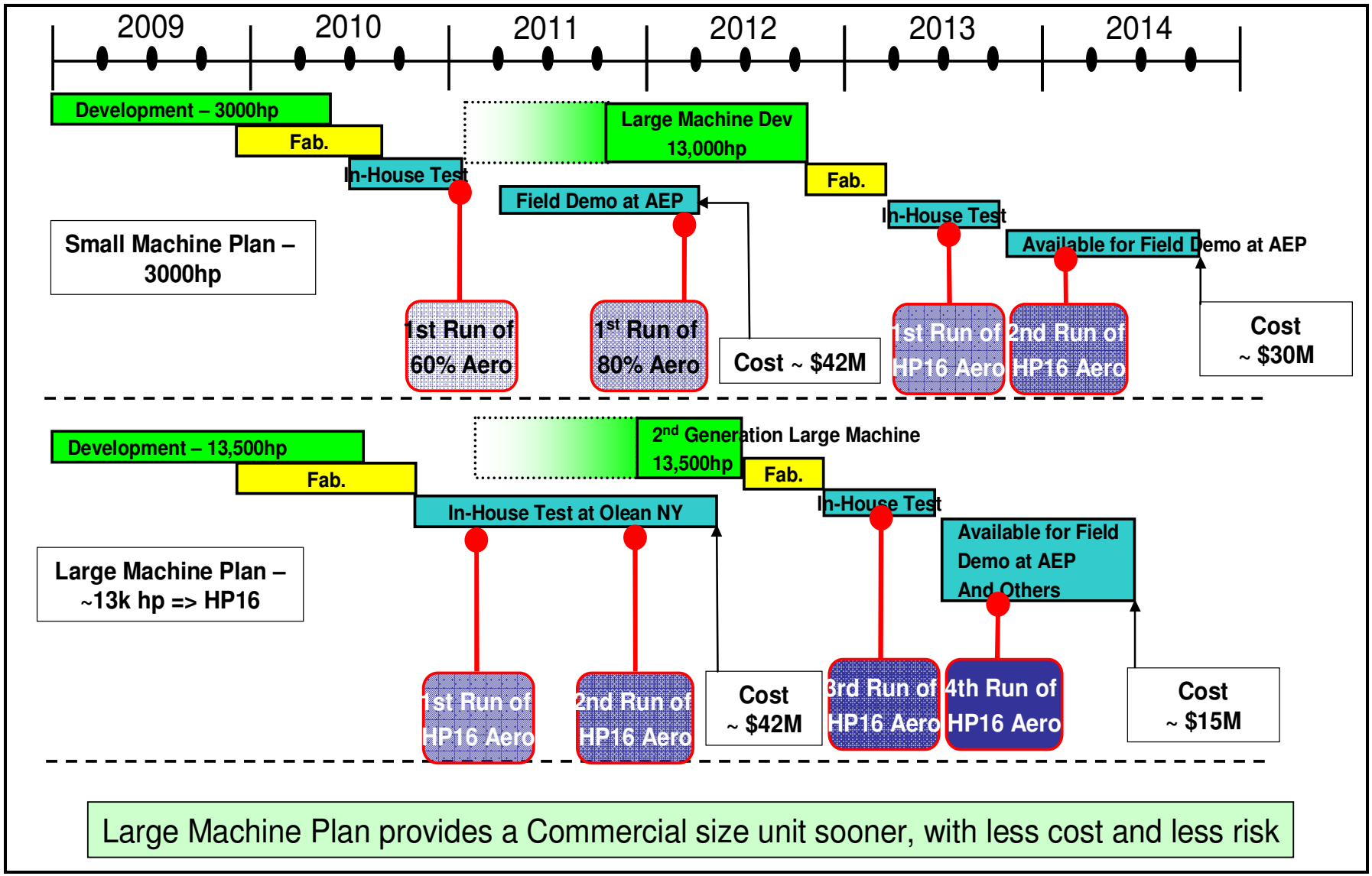

Figure 3.4 Comparison of Large vs. Small Development Plan

3.1.5 Greater Confidence in Success

The unexpected Phase 1 technical breakthroughs allowed Ramgen to consider substituting a larger size unit for testing in the development process. However, doing so was limited by funding and test facility capability. The 3000 hp machine was proposed as the largest machine our funded program could afford to build. Ramgen's technical team recognized from very early on that a bigger machine would give us greater technical confidence in success.

Our engagement with Dresser-Rand addresses the building of the 13,000 hp unit in three key ways. Dresser-Rand will bring their 70 years of experience in turbo-machinery and 60 years of specific CO_2 compressor experience, to this development. Second, additional Dresser-Rand financial support will help with the higher immediate costs of the 13,000 hp unit. Third, Dresser-Rand has a test facility capable of testing a larger demonstration unit. Without their test capability it would be impossible to substitute the 13,000 hp unit in the current cooperative agreement. Additionally, we will be in a closed loop test facility capable of premixing different gas combinations. This will increase the speed with which the technology can be adopted around the world.

3.1.6 Lower Overall Development Cost

As shown in Figure 3.4, the development of the small machine will yield the proof-of-concept prototype as required by the original DOE Solicitation Part I – C. Funding Opportunity Objectives. The DOE solicitation also recognizes a follow-on step that will require more government funding to go from proof-of-concept prototype to pre-production unit. Figure 3.4 shows that the follow-on development step ends in the 2014 timeframe for the 3000 hp size unit. Ramgen believes the 13,000 hp program will achieve the same level of proof-of-concept in 2012 that the 3000 hp program would otherwise achieve in 2014.

In the 13,000 hp scenario, Ramgen CO_2 compressors can begin to be offered in the 2012 timeframe, 2 years earlier than in the 3000 hp scenario. Ramgen is planning on providing large machines to demonstration projects, like those in proposals for the DOE regional partnerships and CCPI. This would save millions of dollars in development support and potentially $34 billion dollars over the next 20 years in CCS implementation costs. See Figure 3.5.

This analysis is provided with the assumption that CCS systems at this scale are new with many uncertainties that must be tested to make final determinations. These estimates by Ramgen can be influenced by, for example, the capture system or systems which emerge as preferred options by utilities. While this advance compression has advantages with most capture systems, the amount it will reduce cost will vary from one system to another and with the degree of system integration.. Ramgen believes there are major opportunities to maximize the efficiency of integrated capture/compression systems given the unique heat benefits of the Ramgen advanced compressor. See Figure 3.5 for a summary of Ramgen's assumptions and calculations.

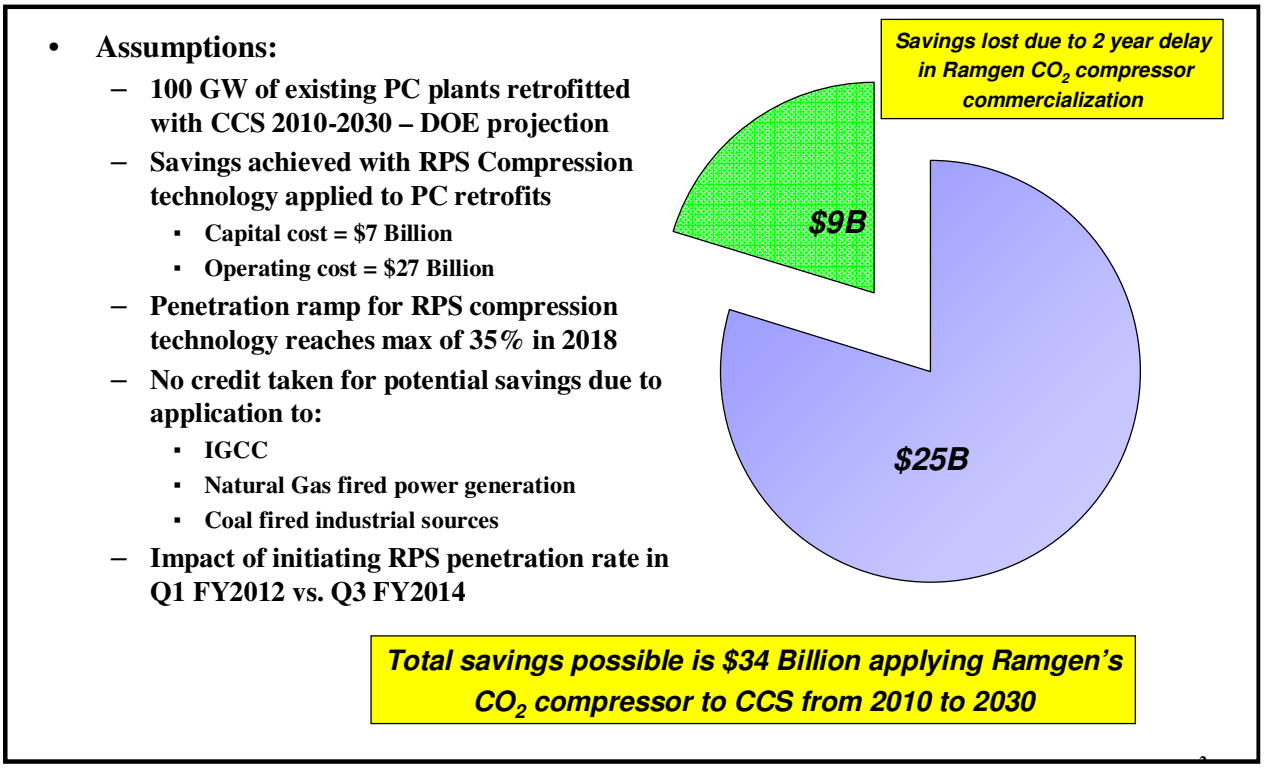

Figure 3.5 Estimated Costs of Implementation Delay

4 NATIONAL BENEFITS

The DOE Solicitation Part I – B. Background Information, Benefits from this Solicitation lists a number of benefits the development of turbine technologies will provide:

a) lower energy consumption
b) fuel cost savings
c) electricity cost savings
d) emissions reduction
e) US equipment exports
f) Re-powering of older fossil plants
g) Use of coal, our nation's most abundant fossil fuel
h) Creation of US jobs
i) Keeping US businesses competitive

The Innovation of the Ramgen Compressor

Historically, the most important breakthroughs in technology result from new combinations of well known technologies from diverse fields. The Ramgen compressor combines Aero based shock wave compression with Mechanical technology to create a revolutionary product that has enormous advantages, particularly with heavier gases such as CO_2. Dresser-Rand, the leading compressor manufacturer in the world, recently described this Ramgen technology as "game changing".

This innovation is particularly important because of the fundamental limitations which conventional compressors have with CO_2. A revolutionary breakthrough of the significance

promised by the Ramgen technology is required to reduce the cost of compressing CO_2 to achieve affordable CCS.

A principal advantage of Ramgen's shock compression is that it can achieve exceptionally high compression efficiency at very high single-stage compression ratios, resulting in a product simplicity and size that will lower both manufacturing and operating costs.

.

Unique

To the best of our knowledge, Ramgen is the only company in the world which is developing a fundamentally new approach to the compression of heavy molecular weight gases such as CO_2. Additionally, shock wave based compression appears to be the only way to produce heat in the compressed gas at high enough temperature to recover and use the heat in an integrated capture and compressor configuration.

In addition to the cost advantages and as a direct result of the Rampressor being able to achieve single-stage compression ratios of 10:1, stage discharge temperatures are estimated to range between 450-500°F, depending on inlet gas and cooling water temperatures. This offers the potential for significant heat integration, without compromising compressor performance. The combined compressor and heat recovery creates an energy efficiency advantage by recovering 70-80% of the electrical input energy in the form of useful heat. Potential uses for the available heat are to regenerate amine solutions or pre-heat boiler feedwater.

Anticipated Benefits of Ramgen Compression Technology Development

The major benefit of the proposed work will be a significantly lower capital, space and maintenance costs and significantly lower power requirement for CO_2 compression in support of Clean Coal, FutureGen, and CCS. The successful development of the Ramgen CO_2 Compressor will also serve to save and expand a compressor manufacturing and technology base in the US, creating economic opportunity and jobs. Today there are no large scale integrally geared CO_2 turbo-compressors manufactured in the US.

In addition to meeting the basic objective of CO_2 compression at lower capital and operating costs with higher system efficiencies, the development of the Ramgen CO_2 compressor will also provide an advanced technology platform to support other IGCC and FutureGen needs as follows:

<u>A CO_2 working Fluid Turbine</u>

The DOE Funding Opportunity Announcement notes that one way to mitigate the Green House Gas (GHG) emissions is by deploying an Oxy-fuel Combustion concept in a CO_2 working fluid gas turbine cycle. There will likely be many configuration concepts for such a system, but in all of these configurations the gas turbine compressor section will be subject to the same Mach number limitations of current conventional air and gas compressors.

The Ramgen CO_2 compressor would, however, offer an outstanding configuration platform for such an engine. Two stages of compression at pressure ratio from "35:1 or higher" as the solicitation requires, is a pressure ratio of only 6:1 per stage, well within the range currently proposed for the Ramgen CO_2 Compressor. In fact, this configuration and its ability to increase pressure ratio without having to add stages, offers enormous flexibility to increase turbine inlet

temperatures as material limits are increased, without imposing significant modifications on the compressor.

In addition to the stage pressure ratio advantages, Ramgen's unique subsonic exit velocities can easily accommodate a matched set of counter-rotating stages that could eliminate a significant fraction of the flow turning losses that represent 40-60% of the losses in conventional turbine designs.

A Derivative ASU Feed Air Compressor

The development of a 100:1 two-stage CO_2 compressor will offer the opportunity to take further advantage of the development of an advanced Ramgen air compression technology. This could improve the cost and performance of either cryogenic or Ion Transport Membrane based Air Separation Unit (ASU) components.

A two-stage, 100:1 pressure ratio CO_2 compressor will require rotor tip speeds of approximately 1500-1600 ft/s, as indicated in Figure 4.1, below. If this tip speed were applied in an air compressor configuration, as is required for the air separation unit feed air, it would produce an approximate 4.5:1 pressure ratio per stage, based upon the difference in molecular weight between air and CO_2. At a 4.5:1 pressure ratio per stage, a two-stage, intercooled air compressor configuration would closely match the current ASU operating pressure of 20 bar or 300 psia. (4.5 x 4.5 = 20.25).

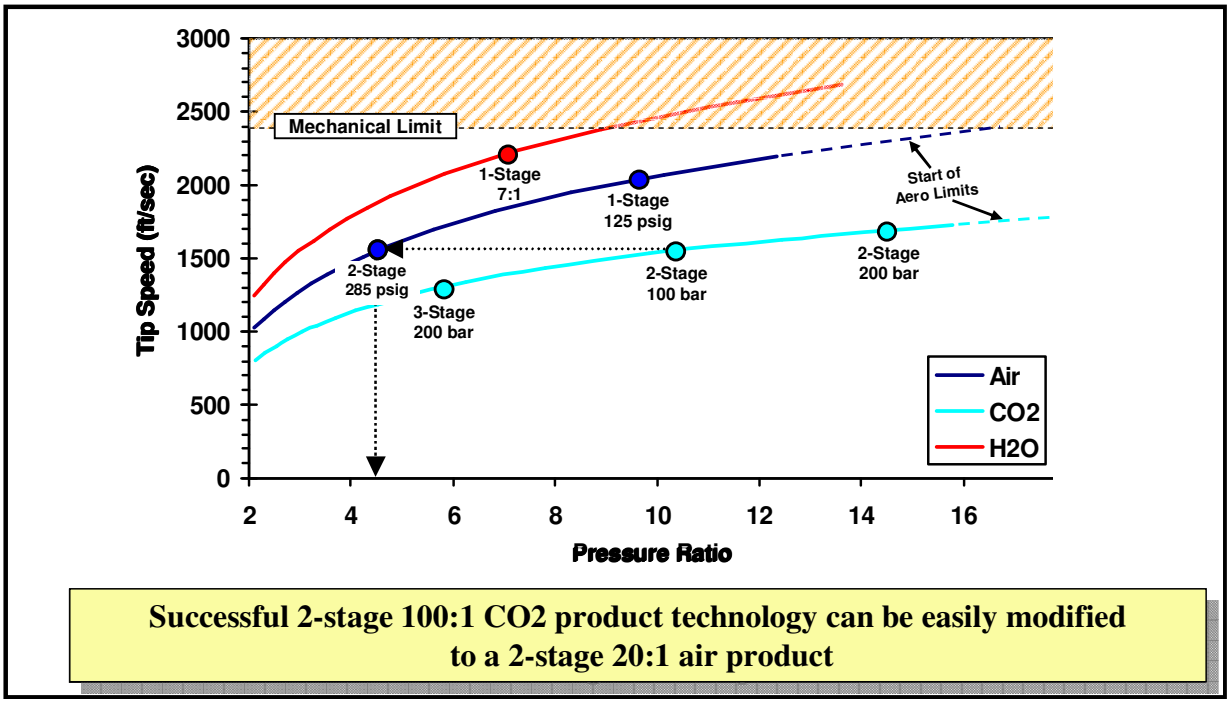

Figure 4.1 – Tip Speed vs. Pressure Ratio for Three Gases

The conventional technology designed for 300 psia would be a large scale 4-stage integrally geared design, while the Rampressor would remain as a two-stage unit. Ramgen's ability to recover the heat of compression would remain as a significant advantage. These large scale integrally geared designs are currently foreign sourced.

A 40+% Efficient Simple Cycle Gas Turbine - ASCE

The counter rotating two-rotor Ramgen configuration can also be applied to the compressor and turbine, respectively, in a conventional Brayton Cycle gas turbine utilizing air as the working fluid. This results in exceptionally high component efficiencies and minimal flow turning losses.

The Ramgen Fuel-fired Air Compressor – Matching ITM & IGCC

The ASCE gas turbine described above can also be configured as a bleed air compressor to work in conjunction with a large scale Ion Transport Membrane (ITM) system and within an IGCC plant. We are currently in discussions with a major Membrane System Developer on this concept and expect continued interest.

The fuel-fired configuration benefits from the reduced cost of fuel to drive the compressor vs. the higher cost of electricity to provide the same drive power. The operating cost of the fuel-fired configuration can be approximately ½ that of an electric drive. In addition, the output of the ITM is approximately twice that of the current configuration. The current configuration requires the ITM feed air to be heated to approximately 800°C and a supplemental duct burner is applied. Unfortunately, this depletes the oxygen content, lowering its partial pressure, and in so doing, lowering the amount of oxygen that can be extracted from a given size ITM. The Ramgen Fuel-fired Compressor/ITM hybrid already has excess oxygen by virtue of the "excess air" turbine cycle and could extract approximately twice the amount of oxygen from the comparably sized ITM. In addition, heat can be recovered from the turbine exhaust and used elsewhere in the facility or process.

The fuel-fired option can also relieve the need to bleed air from the main gas turbine, maintaining output power and not requiring special turbine modifications which can be a problem for some manufacturers. This should allow for a more competitive environment and lower plant cost.

General IGCC Plant Opportunities

IGCC plants require an inordinate amount of electric power to drive the air and other gas compressors. The air separation unit at the Polk power station in Tampa, Florida requires 56 MW to drive the main air compressor and the oxygen and nitrogen boost compressors, and represents an 18% parasitic loss to the IGCC plant. Similarly the air, oxygen, and nitrogen compressors in a NETL model [Advanced Power Systems Comparison Study, Final Report, U.S. DOE-NETL, December, 2002] require over 25 MW of power.

Ramgen reviewed the information from the report and concluded that many design options exist for Rampressor technology based compressors that offer considerable flexibility in further optimizing the IGCC cycle and overall system efficiency. A Ramgen assessment indicates as high as a 2% improvement in overall plant efficiency can be achieved in combination with the potential for significant cost reduction and improved compressor and system reliability. This scenario does not take advantage of the significant opportunity for heat recovery by utilizing the high pressure single-stage compression capability of the Rampressor technology, or the impact that the bleed air concept could have on the ASU used in conjunction with an ITM.

5 STATEMENT OF PROJECT OBJECTIVES

Title of Work to be Performed
High Efficiency Low Cost CO_2 Compression Using Supersonic Shock Wave Technology

Objectives
This project demonstrates a novel concept for CO_2 compression using supersonic shock wave compression technology. Ramgen will demonstrate the simultaneous potential of shock wave compression to achieve high compression efficiency and high stage pressure capability. The high stage pressure capability will allow Ramgen to use a single stage configuration which will offer significant cost savings over conventional designs.

Phase 1 is completed. The progress and closeout of the task have been provided to the COR as part of the Phase 2 Continuation application per the cooperative agreement instructions. The Phase 1 objectives included demonstrating the feasibility of high pressure shock wave compression by completing Ram 2 testing of a high pressure ratio (8:1) air compressor rotor and evaluating a number of candidate conceptual configurations for the CO_2 Compressor demonstrator. Ramgen has also developed and proposed a viable path as part of its R&D Implementation Plan under review with the DOE.

The Phase 2 objectives are to identify and reduce technical risk areas through the execution of a Critical Success Factors Risk Reduction validation and test program. The CO_2 Compressor Preliminary and Final Design phases will also be completed.

The Phase 3 objective is to demonstrate at a suitable demonstration site a proof-of-concept, supersonic shock wave CO_2 Compressor producing supercritical CO_2 at a pressure on the order of 1500psia.

Scope of Work
Ramgen will employ classic engineering strategies to execute a successful CO_2 Compressor demonstration program. Ramgen's technical team will design and analyze the CO_2 compressor demonstration rig in deterministic steps, Conceptual Design Review (CDR), Preliminary Design Review (PDR) and Final Design Review (FDR) with an increasing level of detail at each step. The design process incorporates a number of decision gates along with risk assessment and risk reduction tasks. The program is also intended to produce early stage preliminary aero flow path validation data. Ramgen's effort will feature several risk reduction efforts including: Critical Factor Investigation for designing a supersonic CO_2 compressor; Performance Model Update; and, a Risk Closure Plan. Upon completion of the engineering design, the CO_2 compressor demonstration test rig will be fabricated and assembled. The final demonstration step will be a CO_2 compressor rig operating at a suitable site.

Tasks To Be Performed
The following task descriptions summarize the work to be executed for this program. The tasks are shown on the Figure 6.1 schedule.

PHASE 2

Task 2.1 – Requirements and Large Machine Feasibility

To address new variables introduced by the change in compressor size from approximately 3,000 hp to approximately 13,000 hp, a feasibility study will be conducted for the large machine to ensure the program meets budget, schedule, and technical feasibility requirements. This study will be conducted in concert with Dresser-Rand, utilizing Dresser-Rand's extensive design, manufacturing, and test expertise to ensure accurate projections. This task will be complete when the compressor, facility, and supporting equipment have passed a Feasibility Review.

Aerodynamic development will continue during the feasibility study, including:

- Evaluate inlet guide vane performance
- Evaluate various stationary diffuser configurations
- Perform studies to understand the trade-offs between optimizing for inlet starting requirements and optimizing for design point performance

Task 2.2 – CFD Comparison / SWBLI Investigation

To ensure Ramgen's CFD tools have the most accurate performance prediction capability possible and to advance the understanding of shock wave boundary layer interaction (SWBLI), a sequence of tests, benchmarks, and validations will be undertaken. The tests would occur under direct-connect static test conditions to reduce cost and improve instrumentation access. A low-cost facility using air as the working fluid is envisioned. The leading candidate facility is the Naval Postgraduate School in Monterey, CA where Ramgen has performed a number of successful static tests. The test and comparison sequence would include:

- Build and test supersonic nozzles with representative Mach numbers and boundary layers. Obtain detailed Schlieren measurement of boundary layer and shock formation.
- Add shock generating geometry. Obtain detailed measurements of shock-boundary layer interaction.
- Compare results to CFD prediction and adjust CFD or test instrumentation until results are in alignment.
- Validate and improve alternate boundary layer control techniques and approaches.

At the conclusion of this effort a Risk Closure Plan will be prepared as a deliverable.

Task 2.3 – Inlet Guide Vane Characterization

Aerodynamic performance of the compressor inlet guide vanes (IGVs) is crucial to overall stage performance. A dedicated development and test program will be performed to demonstrate performance of this system prior to start of a rotating test.

Ramgen has contracted with an expert blade designer to design and analyze IGVs for the CO_2 compressor. 2D and 3D viscous CFD simulations will be used to optimize the vane shape and correct for boundary layers introduced in the inlet duct. On and off design performance will be analyzed and the design iterated until required performance levels are indicated.

A cascade test will be performed to experimentally measure IGV flow characteristics and performance. Flow characteristics including exit Mach number, pressure loss, and flow angle

will be measured across the IGV actuation angle range. This data will then be compared to the CFD-predicted performance to ensure the vanes meet performance expectations.

A static test using air as the working fluid is envisioned, likely at the Naval Postgraduate School in Monterey, CA where Ramgen has performed a number of successful static tests. Due to aerodynamic coupling between the rotor and IGVs, it may prove necessary to test the IGVs in concert with the rotating compressor rotor. In this case, the compressor itself will be instrumented to characterize the IGV flow and data will be collected during the early phases of the compressor test program.

Task 2.4 – Stationary Diffuser Characterization

Compressor discharge diffuser performance is equally crucial to overall stage performance. A dedicated development and test program will also be performed to demonstrate performance of this system prior to the start of a rotating test.

Viscous CFD simulations will be used to optimize the diffuser shape and correct for boundary layers in the rotor discharge. On and off design performance will be analyzed and the design iterated until required performance levels are indicated.

A cascade test using air as a working fluid also will be performed to experimentally measure diffuser flow characteristics and performance. Flow characteristics including exit Mach number, pressure loss, and flow angle will be recorded. This data will then be compared to the CFD-predicted performance to ensure the diffusers meet performance expectations.

As with the IGVs, aerodynamic coupling between the rotor and diffusers may require testing the diffusers in concert with the rotating compressor rotor. In this case, the compressor itself will be instrumented to characterize the diffuser characteristics and data will be collected during the early phases of the compressor test program.

Task 2.5 – CO_2 Compressor Design

Task 2.5.1 - Preliminary Design Phase

A preliminary design phase will proceed in parallel with the component development and test efforts, which would:

1. Finalize the aerodynamic requirements for the CO_2 compressor rig
2. Extensive rotor aerodynamics development will occur, including:
    - Explore aerodynamic sensitivity to boundary layer jet location and configuration
    - Evaluate alternative boundary layer control strategies
    - Evaluate starting bleed requirements for different rotor configurations
    - Explore static diffuser design options; estimate performance
    - Evaluate various flowpath configurations including different strake counts, strake angles, capture plane width-to-height ratios, and specific speeds
    - Evaluate alternate boundary layer control techniques and approaches
    - Evaluate different ramp and diffuser geometries
    - Evaluate various aerodynamic configurations to help understand their impact on peripheral/parasitic losses of the overall system

- Evaluate and analyze methods to minimize the losses to the overall system due to routing boundary layer fluid from/to the main rotor flow path

3. Extensive rotor mechanical development will also occur, including:
   - Evaluate the mechanical/structural impact of new rotor features developed during Conceptual Design phase. These features significantly reduce mechanical stress levels and increase rotor performance but need further analyses
   - Explore alternate rotor construction techniques to reduce mechanical stress
   - Explore boundary layer injection jet supply routing and techniques
   - Evaluate rotor material choices for strength allowables and manufacturing capability
4. Down-select conceptual configuration candidates to a single configuration
5. Verify the proposed rig design is capable of achieving functional requirements for the final design
6. Confirm the design meets the program goals and objectives
7. Identify any issues which must be addressed before proceeding to the Final Design Phase of the program
8. Culminate in the identification of a specific rig layout and list of action items to pursue during the final design of the demonstration rig

Task 2.5.2 – Preliminary Design Review

A Preliminary Design Review (PDR) will be conducted at the completion of this phase. A summary of the PDR will be provided to the DOE. Once the PDR is completed, work will begin on the rig's final design, including:

1. Address action items remaining from PDR
2. Complete analysis and engineering design activities required to the point where experimental data from the IGV and diffuser static tests are available to finalize the rotor final design
3. Order certain long lead hardware, e.g. castings, forgings, drivetrain, etc.

Task 2.6 – Test Facility Preparation

The test cell effort, which will continue into Phase 3, will:

1. Support Dresser-Rand facility design efforts through requirements definition, preparation of an Interface Control Document (ICD), and mutual design reviews
2. Design and build auxiliary equipment needed to interface between the facility and the compression demonstrator
3. Oversee construction at Dresser-Rand's Olean facility and ensure all required capabilities and interfaces are built per the ICD
4. Assist and oversee system check out and debug prior to onset of compressor testing

Task 2.7 – Aero Tool Development

Ramgen will work continuously through Phase 2 and Phase 3 to improve our understanding of the supersonic aerodynamics necessary to achieve product performance levels in the CO_2 compressor. Through development of in-house analytical tools, expansion and customization of

commercial CFD codes, and detailed CFD validation experimentation, this task will provide the tools needed for fast, accurate evaluation of compressor aerodynamics. These tools and techniques will be used to explore alternate configurations, design techniques, and geometries to determine the optimal rotor aerodynamic design approach.

1. Customization of Numeca FINE/Turbo mesh generator to accommodate Rampressor-specific flowpath geometry
2. Customization of WIND-US CFD code to accommodate Rampressor-specific geometry
3. Customization of WIND-US CFD code to accommodate correct rotor-stator interface for coupled rotating/stationary component simulations
4. Customization of Numeca FINE/Turbo mesh generator to accommodate various strake leading edge geometries
5. Develop tools to streamline post-processing for WIND-US and FINE/Turbo
6. Upgrade Ramgen's meanline code (CADRE) to model boundary layer control schemes and their effect on supersonic aerophysics
7. Upgrade CADRE to allow parametric analysis of performance
8. Improve CFD modeling accuracy for supercritical CO_2
9. Begin accessing DOE supercomputers to significantly increase the amount of CFD runs available during the detailed design phase

Task 2.8 – Product Traceability

A product-oriented task will monitor the demonstration compressor design and provide input to ensure the resulting test unit reflects CO_2 sequestration market requirements and can be adapted to sequestration applications with a minimum of product design effort.

PHASE 3

Task 3.5 – Test Facility Preparation

The test cell effort will continue into Phase 3 and will primarily be focused on final check-out and debug of all systems prior to the start of compressor testing.

Task 3.6 – Aero Tool Development

Ramgen will work continuously through Phase 3 to improve our understanding of the supersonic aerodynamics necessary to achieve product performance levels in the CO_2 compressor. In Phase 3 the primary focus is to improve CFD modeling accuracy for supercritical CO_2 through the development of the models and anchoring of the models with the actual test results.

Task 3.7 – Product Traceability

A product-oriented task will monitor the demonstration compressor design and provide input to ensure the resulting test unit reflects CO_2 sequestration market requirements and can be adapted to any number of sequestration applications with a minimum of product design effort.

Task 3.1 – CO_2 Compressor Design and Test

Experimental data from the static tests will enable completion of the compressor demonstrator final design and procurement of long lead items.

Task 3.1.1 – Detailed Design & Fabrication

The final demonstrator design will be completed in this task, including:

1. Incorporate experimental data from the static tests into the rotor final design
2. Finalize design of the rotor and all other rig components and systems
3. Conduct a Final Design Review (FDR) and provide a summary to the DOE

Ramgen will produce detailed manufacturing drawings that include but are not limited to the following: rotors; bearing supports; exhaust casing and ducting; flexible coupling; intake casing and ducting; pressure case; instrumentation; rig support; and, adaptors for test installation. During the detailed design phase some longer lead procurement operations will be released for manufacture such as material procurement and forging inspections.

Ramgen will utilize its in-house system to procure the CO_2 Compressor demonstration rig. Additional testing or design activities required to address any gap between the predicted demonstration rig performance characteristics and the identified product performance characteristics will be identified and documented. An updated product performance model will be submitted to the DOE.

Task 3.1.2 - Testing

The CO_2 compressor demonstrator will be installed and tested at Dresser-Rand's facility in Olean, NY. Ramgen will install and provide test support for the demonstrator at the cell.

Test objectives include, but are not limited to, the following: starting data regarding ramp rate; overspeed techniques; and, bleed requirements vs. RPM for the supersonic inlet. Overall compression performance across the rotor would be measured by instrumentation and methods traceable to industry standards for compressor efficiency. Rampressor performance with turndown will be investigated with varying mass flow at the inlet. Task 3.2 will be complete when the rig has demonstrated performance equivalent to CFD prediction. Test results will be summarized and submitted to the DOE for review.

Task 3.1.2 – Update to Performance Model

At the conclusion of this effort an update to the CO_2 compressor Performance Model will be prepared as a deliverable.

Task 3.2 - IGV Retrofit

Due to the developmental nature of Ramgen's supersonic compression technology, a risk reduction program will be implemented. This program will continue to advance supersonic compression state-of-the-art while the compressor is being built and assembled. Compressor test results will enable further refinement of the IGV design. The highest performance IGV design available will be drawn, fabricated, and flow tested in the same manner as shown in Phase 2. This IGV will be available for the compressor retrofit described in Task 3.4.

Task 3.3 – Diffuser Retrofit
As with the IGV retrofit, diffuser design and analysis work will continue while the demonstrator is built and tested. Test results will be used to iterate and improve the diffuser design. This upgraded performance diffuser will be available for the compressor retrofit described in Task 3.4.

Task 3.4 - CO_2 Compressor Retrofit
In concert with the IGV and diffuser redesign, an improved-performance rotor will be developed. Based on the lessons learned during demonstrator test and the ongoing CFD design and analysis program, the new rotor will benefit from all the advances in supersonic compression technology made since the first rotor design was frozen for manufacturing. This second set of aero will be released to drawings, manufactured, and installed in the demonstrator for a comprehensive test program.

At the conclusion of this effort Ramgen will provide a summary of the results. The final deliverable will be a validated CO_2 compressor of sufficient scale to be included in future commercial demonstration projects.

D. DELIVERABLES

Ramgen will submit periodic, topical and final reports in accordance with the "Federal Assistance Reporting Checklist". In addition, the following deliverables shall also be provided:

1. Task 2.1.3 – Feasibility Review Summary – Requirements and Large Machine Feasibility
2. Task 2.2.5 – Risk Closure Plan – CFD Comparison / SWBLI Investigation
3. Task 2.5.2 – Preliminary Design Review Summary - CO_2 Compressor rig
4. Task 2.5.3 – End of Phase 2 Review Summary including Performance predictions
5. Task 3.1.1.1 – Final Design Review Summary - CO_2 Compressor rig
6. Task 3.1.3 – Updated CO_2 Compressor Product Performance Model
7. Task 3.4.4 – Presentation of Results and Validated CO_2 Compressor Unit

6 PROJECT TIMELINE

Table 6.1 shows the timeline for Ramgen's CO_2 compressor project. The tasks and subtasks are described in detail in the Statement of Project Objectives. The timeline also shows interdependencies. The Milestone Log is cross-referenced with the task numbers and titles used in the timeline. A diamond symbol is used in the timeline to denote Milestone events listed in the Log.

Attachments 1, 2 & 3 provide summaries and details for the project task costs for Phase 2 and Phase 3.

Exhibit 4.1 of the attachments show the participating team members by Group (Aero, Mechanical), Name, and Skill (performance, analysis, CFD, design, rotordynamics, etc.) for Phase 2 and Phase 3.

Figure 6.1 – Project Timeline Phase 2

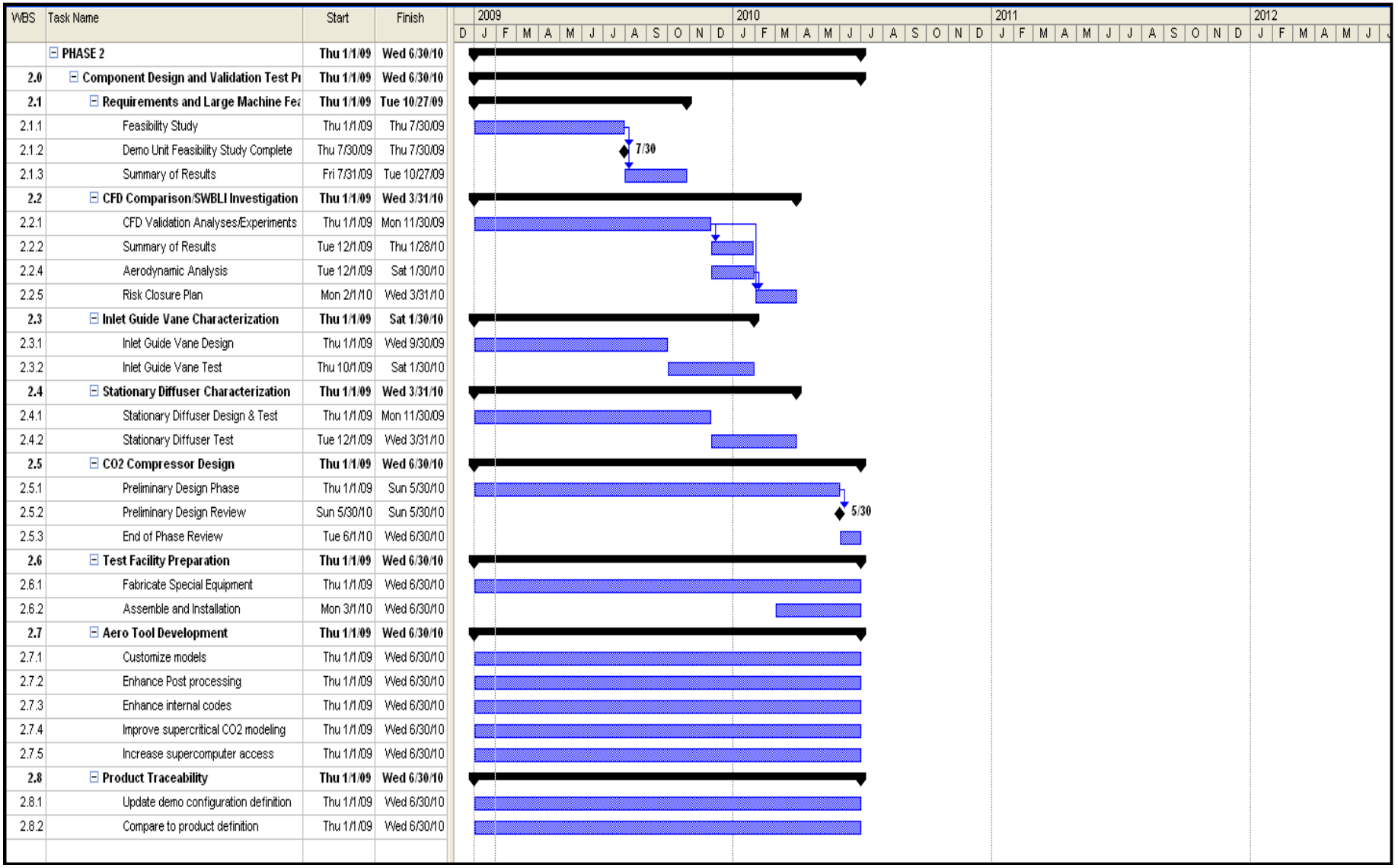

WBS	Task Name	Start	Finish
	PHASE 2	**Thu 1/1/09**	**Wed 6/30/10**
2.0	**Component Design and Validation Test Pl**	**Thu 1/1/09**	**Wed 6/30/10**
2.1	**Requirements and Large Machine Fea**	**Thu 1/1/09**	**Tue 10/27/09**
2.1.1	Feasibility Study	Thu 1/1/09	Thu 7/30/09
2.1.2	Demo Unit Feasibility Study Complete	Thu 7/30/09	Thu 7/30/09
2.1.3	Summary of Results	Fri 7/31/09	Tue 10/27/09
2.2	**CFD Comparison/SWBLI Investigation**	**Thu 1/1/09**	**Wed 3/31/10**
2.2.1	CFD Validation Analyses/Experiments	Thu 1/1/09	Mon 11/30/09
2.2.2	Summary of Results	Tue 12/1/09	Thu 1/28/10
2.2.4	Aerodynamic Analysis	Tue 12/1/09	Sat 1/30/10
2.2.5	Risk Closure Plan	Mon 2/1/10	Wed 3/31/10
2.3	**Inlet Guide Vane Characterization**	**Thu 1/1/09**	**Sat 1/30/10**
2.3.1	Inlet Guide Vane Design	Thu 1/1/09	Wed 9/30/09
2.3.2	Inlet Guide Vane Test	Thu 10/1/09	Sat 1/30/10
2.4	**Stationary Diffuser Characterization**	**Thu 1/1/09**	**Wed 3/31/10**
2.4.1	Stationary Diffuser Design & Test	Thu 1/1/09	Mon 11/30/09
2.4.2	Stationary Diffuser Test	Tue 12/1/09	Wed 3/31/10
2.5	**CO2 Compressor Design**	**Thu 1/1/09**	**Wed 6/30/10**
2.5.1	Preliminary Design Phase	Thu 1/1/09	Sun 5/30/10
2.5.2	Preliminary Design Review	Sun 5/30/10	Sun 5/30/10
2.5.3	End of Phase Review	Tue 6/1/10	Wed 6/30/10
2.6	**Test Facility Preparation**	**Thu 1/1/09**	**Wed 6/30/10**
2.6.1	Fabricate Special Equipment	Thu 1/1/09	Wed 6/30/10
2.6.2	Assemble and Installation	Mon 3/1/10	Wed 6/30/10
2.7	**Aero Tool Development**	**Thu 1/1/09**	**Wed 6/30/10**
2.7.1	Customize models	Thu 1/1/09	Wed 6/30/10
2.7.2	Enhance Post processing	Thu 1/1/09	Wed 6/30/10
2.7.3	Enhance internal codes	Thu 1/1/09	Wed 6/30/10
2.7.4	Improve supercritical CO2 modeling	Thu 1/1/09	Wed 6/30/10
2.7.5	Increase supercomputer access	Thu 1/1/09	Wed 6/30/10
2.8	**Product Traceability**	**Thu 1/1/09**	**Wed 6/30/10**
2.8.1	Update demo configuration definition	Thu 1/1/09	Wed 6/30/10
2.8.2	Compare to product definition	Thu 1/1/09	Wed 6/30/10

Figure 6.2 – Project Timeline Phase 3

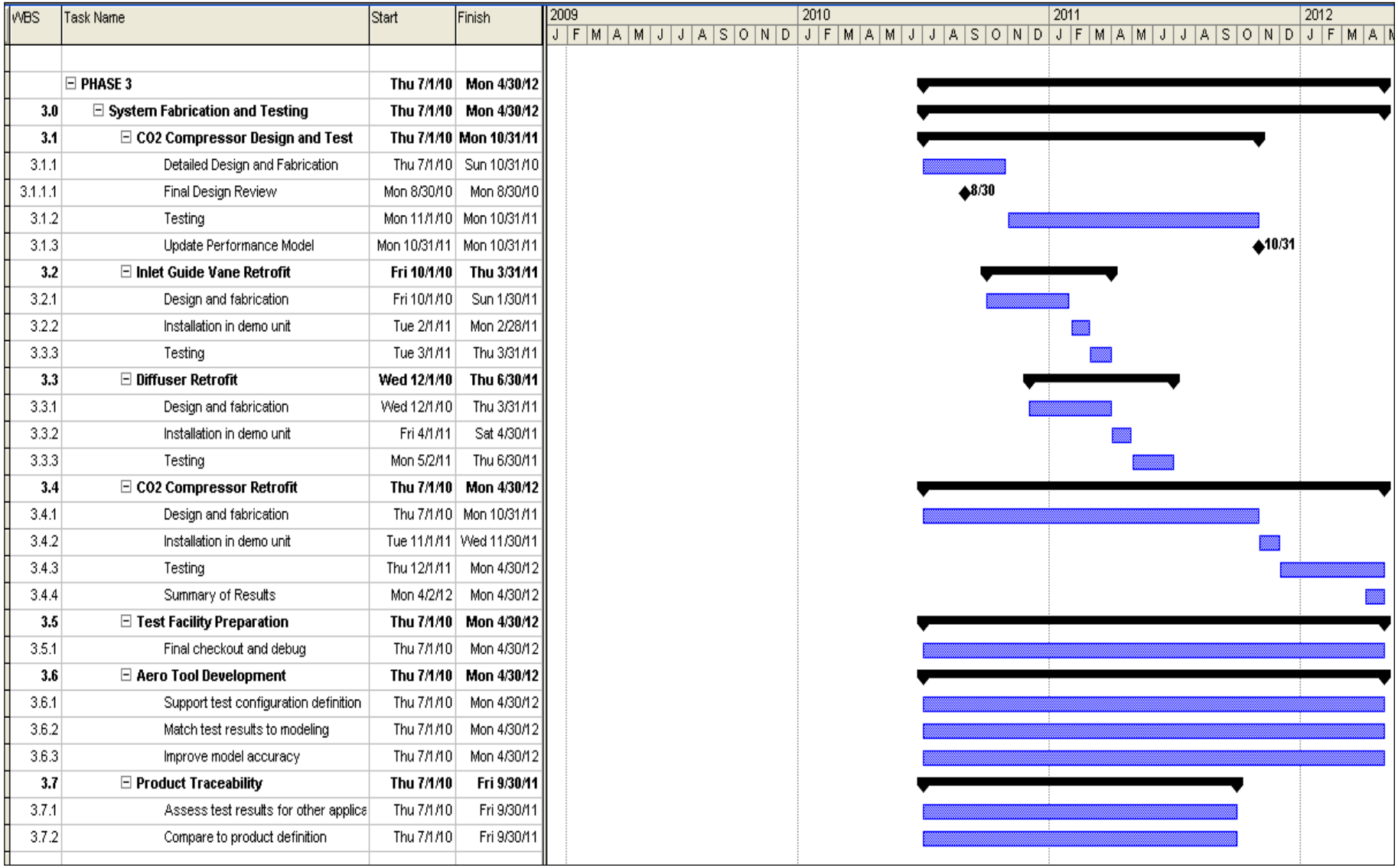

WBS	Task Name	Start	Finish
	PHASE 3	**Thu 7/1/10**	**Mon 4/30/12**
3.0	**System Fabrication and Testing**	**Thu 7/1/10**	**Mon 4/30/12**
3.1	**CO2 Compressor Design and Test**	**Thu 7/1/10**	**Mon 10/31/11**
3.1.1	Detailed Design and Fabrication	Thu 7/1/10	Sun 10/31/10
3.1.1.1	Final Design Review	Mon 8/30/10	Mon 8/30/10
3.1.2	Testing	Mon 11/1/10	Mon 10/31/11
3.1.3	Update Performance Model	Mon 10/31/11	Mon 10/31/11
3.2	**Inlet Guide Vane Retrofit**	**Fri 10/1/10**	**Thu 3/31/11**
3.2.1	Design and fabrication	Fri 10/1/10	Sun 1/30/11
3.2.2	Installation in demo unit	Tue 2/1/11	Mon 2/28/11
3.3.3	Testing	Tue 3/1/11	Thu 3/31/11
3.3	**Diffuser Retrofit**	**Wed 12/1/10**	**Thu 6/30/11**
3.3.1	Design and fabrication	Wed 12/1/10	Thu 3/31/11
3.3.2	Installation in demo unit	Fri 4/1/11	Sat 4/30/11
3.3.3	Testing	Mon 5/2/11	Thu 6/30/11
3.4	**CO2 Compressor Retrofit**	**Thu 7/1/10**	**Mon 4/30/12**
3.4.1	Design and fabrication	Thu 7/1/10	Mon 10/31/11
3.4.2	Installation in demo unit	Tue 11/1/11	Wed 11/30/11
3.4.3	Testing	Thu 12/1/11	Mon 4/30/12
3.4.4	Summary of Results	Mon 4/2/12	Mon 4/30/12
3.5	**Test Facility Preparation**	**Thu 7/1/10**	**Mon 4/30/12**
3.5.1	Final checkout and debug	Thu 7/1/10	Mon 4/30/12
3.6	**Aero Tool Development**	**Thu 7/1/10**	**Mon 4/30/12**
3.6.1	Support test configuration definition	Thu 7/1/10	Mon 4/30/12
3.6.2	Match test results to modeling	Thu 7/1/10	Mon 4/30/12
3.6.3	Improve model accuracy	Thu 7/1/10	Mon 4/30/12
3.7	**Product Traceability**	**Thu 7/1/10**	**Fri 9/30/11**
3.7.1	Assess test results for other applica	Thu 7/1/10	Fri 9/30/11
3.7.2	Compare to product definition	Thu 7/1/10	Fri 9/30/11

7 MILESTONE LOG

The following milestones are linked to the tasks found in the Project Timeline Figure 7.1. When the tasks are complete the milestone verification will be provided to the COR.

PHASE 2

Title: Demo Unit Feasibility Study Complete
Planned Completion: July 31, 2009
Verification Method: A summary report of the internal review on technical risk areas before completing Preliminary Design

Title: Static Testing/Test Readiness Review
Planned Completion: September 30, 2009
Verification Method: A summary report of the internal technical review will be available for COR review

Title: CFD Validation Testing Complete
Planned Completion: December 30, 2009
Verification Method: A summary report of the technical results will be available for COR review

Title: Risk Closure Plan Review
Planned Completion: March 31, 2010
Verification Method: A summary report of the internal technical review will be available for COR review

Title: Preliminary Design Review
Planned Completion: May 30, 2010
Verification Method: A summary report of the internal technical review materials presented at the review will be available for COR review

Title: End of Phase Summary of Results – Analysis/Test/Performance Update
Planned Completion: June 30, 2010
Verification Method: A summary report of the technical results will be available for COR review

PHASE 3

Title: Final Design Review
Planned Completion: August 30, 2010
Verification Method: A summary report of the technical review materials presented at the review will be available for COR review.

Title: Detailed Drawings Complete
Planned Completion: October 31, 2010
Verification Method: A summary report of the technical review materials presented at the review will be available for COR review

Title: CO_2 compressorTest Readiness Review
Planned Completion: December 31, 2010
Verification Method: A summary report of the internal technical review will be available for COR review

Title: Inlet Guide Vane Retrofit Testing Complete
Planned Completion: March 31, 2011
Verification Method: A summary report of the technical results will be available for COR review

Title: Diffuser Retrofit Testing Complete
Planned Completion: June 30, 2011
Verification Method: A summary report of the technical results will be available for COR review

Title: Updated Performance Model
Planned Completion: October 31, 2011
Verification Method: A summary report of the internal technical review will be available for COR review

Title: CO_2 Compressor Retrofit Test Readiness Review
Planned Completion: November 30, 2011
Verification Method: A summary report of the internal technical review will be available for COR review

Title: Presentation of Testing Results
Planned Completion: April 30, 2012
Verification Method: A summary report of the technical results will be available for COR review

8 RISK MANAGEMENT

Technical Risk Evaluation/Reduction Tasks

The evaluation of risk is just as important to the success of a program as the evaluation of program status. A key to success in research and development programs is to identify critical technology risk areas, identify plans to reduce or eliminate those risks, and track progress on those factors critical to program success.

Ramgen's CO_2 compressor development schedule Figure 6.1 shows a number of these risk evaluation tasks. A complete CO_2 compressor package will include compressor stage(s), a drive system and peripherals. Ramgen addressed factors that are critical to completing the CO_2 stage

design and package design activities in Phase 1, while testing on the Ram 2 rig was being conducted.

The generic Critical Success Factors Risk Reduction for a Ramgen technology compressor include: boundary layer control optimization, tip clearance optimization; mechanical design for production, diffuser optimization, and thrust balance. At the conclusion of the Ram 2 testing Ramgen reassessed the technical risks of the Rampressor technology compressor. This evaluation has shaped the CO_2 compressor risk reduction efforts and tests planned for Tasks 2.1 Requirements and Large Machine Feasibility and Task 2.2 CFD Comparison. SWBLI Investigation. At the conclusion of Task 2.2, the technology risks will be reassessed and a Risk Closure Plan will be prepared. At the end of Phase 2 Ramgen will prepare an end-of-phase review. As part the review, performance predictions for the demonstrator will be presented. These predictions will incorporate the sub-component performance levels and loss estimates as well as any appropriate component performance characteristics generated throughout the program thus far in Task 2.5 - CO_2 Compressor Design**.**

Progress Risk Evaluation/Reduction Tasks

Ramgen's definition of a successful project is one that meets schedule, budget and program objectives. To that end Ramgen incorporates a number of different activities to monitor and assess our progress as well as minimize risk.

Critical Task Reviews

Ramgen's design philosophy manages risk by incorporating comprehensive reviews at every critical stage of a development program. During the design phase of a program Ramgen conducts detailed reviews of program status at the Conceptual Design Review (CDR), Preliminary Design Review (PDR) and Final Design Review (FDR).

During the Critical Factors investigations there are Critical Design Reviews (CDR) after design of the experiments are completed.

During each of these reviews the following attributes are examined:

- Program goals
- CDR/PDR/FDR objectives as appropriate
- Performance to program schedule
- Hardware cost update
- Comparison to budget

Upon completion of each review, action items are distributed and tracked to closure. If the project team has successfully met the Review objectives, we will proceed into the next phase of development. A resolution plan will be implemented to track and close any objective shortfalls. Ramgen's CO_2 compressor development plan has several of these reviews scheduled. A table of evaluation criteria for each review is listed in Table 8.1.

Table 8.1 – Design Review Evaluation Criteria

Conceptual Design Review Objectives	Review program goals and objectives Select an overall rig layout(s) from candidates to pursue in preliminary design phase that meets all program goals and objectives Review conceptual design of all systems – Review requirements and present supporting analyses and verify they are complete and in line with program goals and objectives – Present conceptual design approach – Review criteria and assumptions used for designs – Identify required analyses and discuss approach – Verify that design will be able to meet all requirements – Identify any unresolved issues, challenges, or risks and discuss solution approach – Verify designs have progressed satisfactorily and are ready to proceed to preliminary design stage Review Program Schedule and Budget Targets
Preliminary Design Review Objectives	Review program goals and objectives Review preliminary design of all systems – Review requirements and verify they are complete and in line with program goals and objectives – Review design approach and decisions – Review criteria and assumptions used for designs – Review analyses that have been performed – Identify remaining analyses to be performed and discuss approach – Verify that design will be able to meet all requirements – Verify designs have progressed satisfactorily and are ready to proceed to detailed design stage – Verify all significant risk areas have been addressed so that no major design revisions will occur during the detailed design phase Review Program Schedule and Budget Targets
Final Design Review Objectives	Review program goals and objectives Review detailed design of all systems – Review requirements and verify they are complete and in line with program goals and objectives – Review design approach and decisions – Verify designs are complete and team is ready to proceed to drawing preparation – Verify appropriate criteria and assumptions used for designs – Verify all required analyses have been performed – Verify that design meets all requirements Review Program Schedule and Budget Targets

9 SUCCESS CRITERIA AND DECISION POINTS

Program Success Criteria

The success of Ramgen's novel CO_2 compression will be dependent on demonstrating the potential for substantial capital and operating cost reduction without sacrificing efficiency. At the same time, the design must also demonstrate the potential for product-like reliability and operability.

Cost Targets

Currently the commercial cost target for a 100:1 pressure ratio (PR) compressor is approximately $400/hp. The "state of the art" compressor offerings today, such as the 100:1 PR MAN-Turbo, are at $1000/hp or higher.

Efficiency Targets

Ramgen is currently targeting a commercial stage efficiency of 85%. That target does not include the potential benefit to increase the efficiency of the machine, the sequestration process, or the overall plant efficiency by utilizing the useful heat generated by the Ramgen compression process. Today's machines use intercooling between as many as 8 stages to achieve approximately 85% overall stage efficiency. Simply stated, the overall power requirement for a Ramgen compressor product will be comparable to the MANTurbo. However, the potential for heat recovery to increase the effective efficiency of the process is critical. By one conservative estimate, if half the compressor input power is recovered as heat and used to regenerate the CO_2 sorbent, it will result in a 20% reduction in the COE penalty. Ramgen believes that 70-80% of the input power can be recovered as heat.

Evaluation

The performance predictions for the CO_2 compressor will be updated in Task 2.5, and the CO_2 compressor testing will serve as the final validation of the Ramgen technology CO_2 compressor at a demonstration scale. Throughout the process Ramgen will be constantly assessing the impact of design decisions and test results on the product cost.

Chapter 4

CO2 Compressor Design

4.1 Initial CO2 Compressor Characterization (Task 3.1)

Ramgen conducted a comprehensive Configuration/Feasibility Review in the last week of October and first week of November, 2009. After closing out action items from this review, the Demo Unit design was declared Feasible and internal authorization was given for Engineering to proceed into Preliminary Design. All critical areas were reviewed and approved. Some immediate actions were assigned; these were quickly answered and closed out.

In conjunction with the review, Ramgen selected a rotor configuration family known as SE 01 for the demonstration compressor. In a typical phased Feasibility, Conceptual, Preliminary, and Detailed design process, design down selection would be performed during the Preliminary phase. Ramgen chose to complete the aero and mechanical analyses necessary to perform the down selection during the configuration/feasibility portion of the program to reduce program risk and focus the remainder of the program effort on a single rotor family which has been shown capable of meeting our requirements.

To accomplish the design down selection, significantly more detailed work was required than usually expected in a feasibility study. A rotor feasibility study would typically include 1D meanline aero design analysis, 2D rotor aero geometry analysis using method of characteristics, general location and quantity estimates for boundary layer features, and mechanical rotor analyses using general stress formula with stress concentration scalars applied. In contrast, the recently-concluded effort also included 3D viscous, real gas CFD of each rotor flowpath component, detailed rotordynamic analyses, bearing and damper designs, full finite-element analyses of the rotor included detailed boundary layer control features, and other analyses focused on ferreting out any problems with the configurations being considered.

By performing this level of evaluation and selecting a single rotor configuration family early in the program, the program's technical risk was significantly reduced. Dresser-Rand personnel were involved in the critical mechanical design and analyses efforts and provided valuable input regarding best commercial and corporate practice. Ramgen and D-R have developed a very good working relationship enabling full access to the design and analysis expertise contained within D-R Engineering.

The SE 01 rotor family was selected because it represents the best balance of performance capability and design challenge. Ramgen will now proceed into the Preliminary and Detailed design phases with significantly improved models, analysis techniques, and design tools developed during this effort.

The Feasibility/Configuration Review agenda is included in this summary to indicate the breadth of material covered.

Mechanical

The Mechanical team presented design and analyses showing how the individual systems for the ~13,400 HP CO2 demonstration compressor are feasible. The remaining design work is significant but achievable in the program schedule and budget. The critical issues have been identified and are being carefully tracked.

Among the concerns for scaling the compressor to 13,400 HP from 3,000 HP were the affordability of the electric motor and variable-frequency drive and the availability of a gearbox at the required speed and power. Working closely with D-R Supply Chain Management personnel, Ramgen was able to show that multiple options were available that met our budget and schedule requirements. Offerings from Siemens, ABB, GE/Mitsubishi, Direct Drive Services, and Converteam were evaluated. Down selection to the ABB team (ABB and Laurence Scott) occurred shortly after the review.

Development contracts with multiple gearbox vendors produced feasible solutions for parallel-shaft and compound epicyclic gearbox approaches. Down selection to Allen Gears' compound epicyclic design occurred shortly after the review.

The Mechanical agenda is presented to show the extent of issues and level of detail presented. After reviewing each system and resulting action items, each system was deemed feasible and ready to proceed into the conceptual design phase.

Mechanical Agenda

Rotor Structure
- Stress results from SE 01 analysis, including pressure and CF loads
- Thermal analysis results
- Status of composite manufacturing development program and all-metal rotor effort
- Rotor start/stop, life, and safety margin pedigree to be used for design

Rotordynamics
- Results from SE 01 lateral rotordynamics and stability
- Critical factors in achieving satisfactory SE 01 rotordynamics

Seals
- Shaft seal configuration for SE 01 and resulting leakage rates
- Rotor seal configuration for SE 01 and resulting leakage rates

Static Structure Layout
- Journal and thrust bearing configuration for SE 01
- Pressure case, inlet ducting, and outlet ducting
- Variable IGV mounting and actuation, including subcontract approach
- Starting bleed removal path
- Performance bleed removal path

Facility
- Overview of facility FEED results and plant layout
- Overview of CO2 closed-loop and PFD
- Overview of CO2 makeup system
- Overview of bleed vent/capture
- Overview of leakage capture & recompression requirements and approach
- Overview of lubrication system

Drivetrain
- Overview of Motor & VFD specifications, incl. power curve
- Overview of gearbox requirements, development status, fallback plans
- High-speed coupling configuration

Controls & Instrumentation
- Overview of compressor control approach
- Overview of performance instrumentation
- Overview of diagnostic instrumentation

Maintenance and Access
- Estimate time to access rotor after installation

Aero

The Aero team presented design and analyses showing how the aero components were feasible. The remaining design work is significant but achievable in the program schedule and budget. The critical issues have been identified and are being carefully tracked. After reviewing each system and resulting action items, each system was deemed feasible and ready to proceed into Preliminary design.

The Aero agenda is presented to show the extent of issues and level of detail presented. The IGV component showed reasonable performance, although the presentation lacked a complete picture of real geometry effects on performance (e.g. fillets, trailing edge thickness, upstream boundary layer, gaps between hub and shroud, rotor interaction, etc.). Specific action items for the Preliminary Design phase were assigned to analyze these effects. We believe the IGV can achieve necessary performance levels.

Current supersonic ramp CFD models have advanced sufficiently to give confidence the design will achieve the necessary flow quality. More work is necessary to reduce flow distortion, control separation and minimize bleed but Feasibility goals have been met - further work is appropriate for the Preliminary and Final design phases.

Current diffuser CFD models appear to show sufficient performance to meet our goals. These models will be enhanced in future work as the detailed design progresses.

Aero Agenda

IGV
- Show 3D real gas CFD for SE.01 IGV (and others) with realistic inflow conditions

Rotor Performance
- 3D real gas CFD for shock compression, exducer, boundary layer features
- Current bleed feature size, location, mass flow
- Describe future optimization approach for SE.01 family

Exducer and Diffuser
- 3D real gas CFD for SE.01 exducer and diffuser with realistic inflow conditions
- Describe MSU development/test plan

SPIT (System Performance Integration Tool)
- High-level overview of SPIT function and approach
- Current results for SE 01 and others

Starting
- Analytical starting simulations and results/limitations
- 2D CFD starting simulations and results

Update Demonstrator Spec
- Present Demonstrator Spec with any updates available for Mechanical guidance

Lessons Learned for CFD Workflow Improvement
- Workflow description, identify bottlenecks, plans for overcoming or reducing impact

4.2 CO2 Compressor Rig Conceptual Design (Task 3.2)

After completion of the initial CO2 compressor characterization, conceptual designs were developed for each system and component. Conceptual design reviews were held over the course of several months, corresponding to the need-by dates to maintain production and delivery. Per Ramgen's established design review process, each presentation listed important interfaces, system requirements, work approach, design concepts, budget and schedule. These presentations have been compiled as an Appendix to this chapter to communicate the conceptual approaches taken.

CHAPTER 4 APPENDIX

CO2 Compressor Rig Conceptual Design

Conceptual Design Review

Compressor Skid System

System owner(s):

John Beers

Jill Roulo

January 22, 2010

System Definition and Scope

- **This system encompasses the mounting skid for the compressor, gearbox and other ancillary equipment that will be mounted near the compressor.**

Functional Requirements/Design Goals

1. **Provide a rigid mounting base for the compressor and gearbox with an estimated combined weight of 30,000 lbs**
2. **Keep total weight of the skid/compressor/gearbox assembly under 60,000 lbs to enable lifting by the facility bridge crane OR keep total weight under XX,XXX lbs as limited by shipping requirements, whichever is less.**
3. **Limit total width to 96”**
4. **Serve as a platform for local assembly and cross-country shipment of the compressor/gearbox unit**
5. **Provide lifting features to enable lifting of the skid/compressor/gearbox assembly in a single lift**
6. **Support the compressor/gearbox assembly so that it is aligned with the centerline of the motor**

Functional Requirements/Design Goals cont.

6. Provide for adjustment of vertical, horizontal and angular location of skid and/or compressor/gearbox assembly for final alignment to motor/low speed coupling
7. Withstand torsion, thermal and axial loads with minimal displacement and appropriate dynamic response
8. Provide for anchoring of skid to facility pedestal
9. Support the assembly tooling for insertion of the bundle into the pressure case (bundle cradle and tooling that is TBD)
10. Accommodate oil drains, instrumentation, electrical, secondary flows (starting bleed, performance bleed, HP seal leakage, isolation flow, diffuser bypass, shaft seal leakages, WS recirculation circuits, etc.)

Important Interfaces

- **Electrical**
  - **The baseplate will support all wiring needed for the controls and instrumentation.**
  - **The baseplate will support an on skid control panel.**
- **Mechanical**
  - **The baseplate will support the compressor and integrally mounted gear which will align with the motor shaft.**
  - **Provide for additional support of the gearbox if needed.**
  - **The baseplate will support the compressor internals (bundle) cradle which will align with the bore of the pressure case.**
- **Fluid**
  - **Any piping that is connected to the bottom of the pressure case may need to exit through the baseplate**

Test Stand Layout

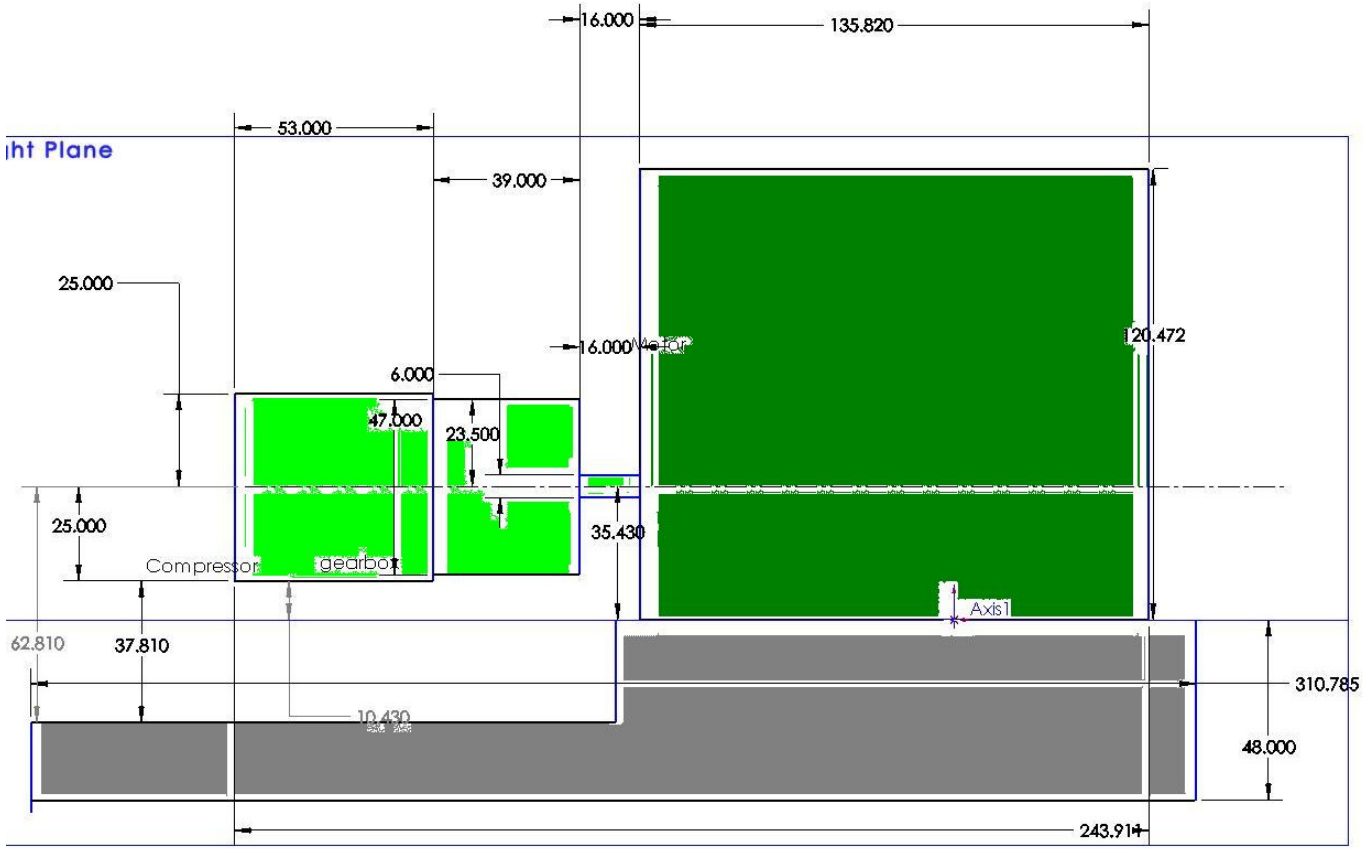

Design Concept #1

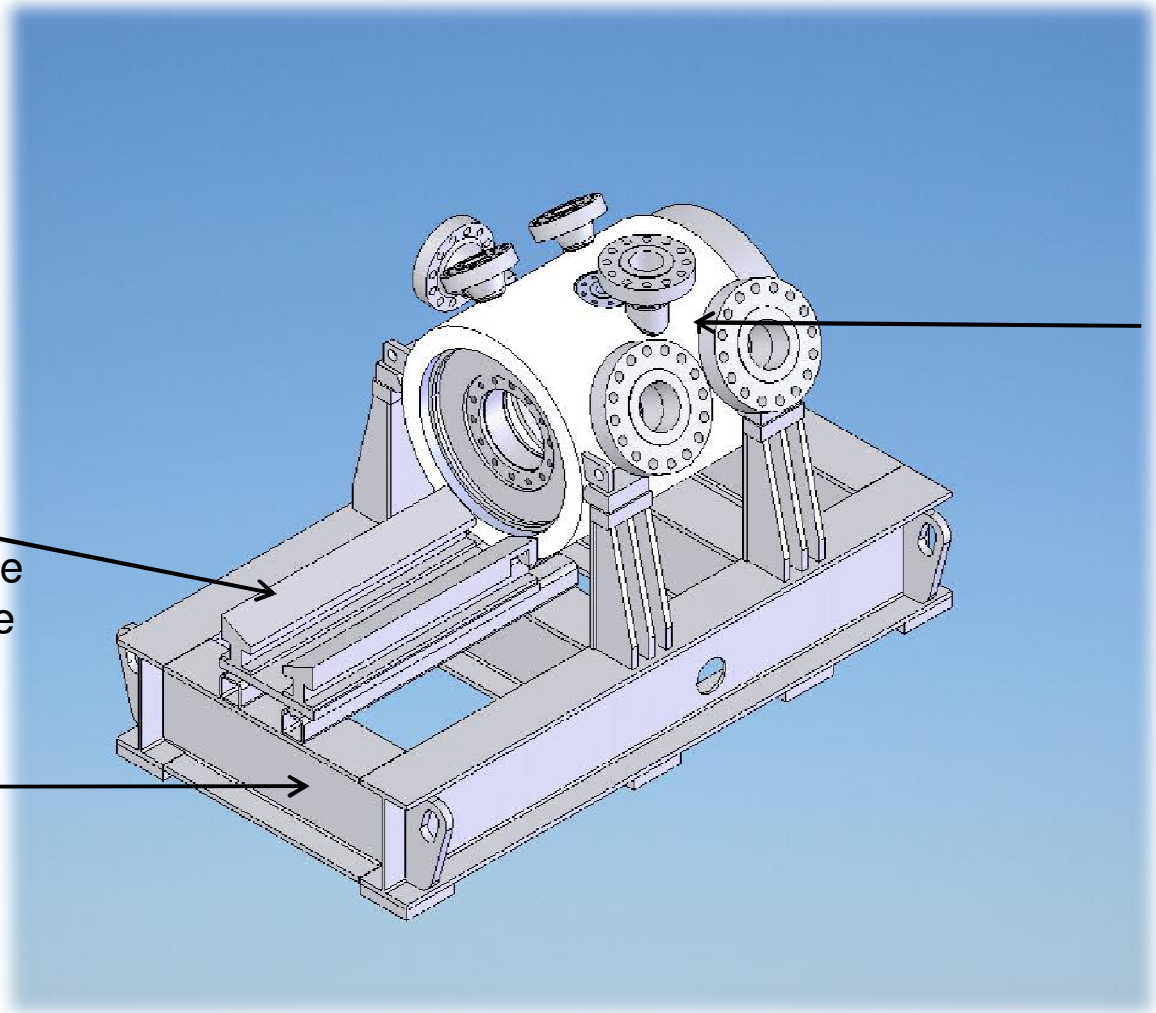

Design Concept #1

- **General description**
  - **Made from 24 inch I-beam with a weight of 162 lbs per ft.**
  - **The I-beam has a moment of inertia of 5170 in^4**
- **Pros/cons**
  - **There is a great deal of experience with using I-beam to form baseplates by D-R.**
  - **The strength of the I-beam section lends itself to this design**
  - **Any piping that needed to be routed through the side of the base would need to have holes cut in the web**
  - **The baseplate would weigh approximately 11060 lbs.**
- **Preliminary analysis results, etc.**

Design Concept #2

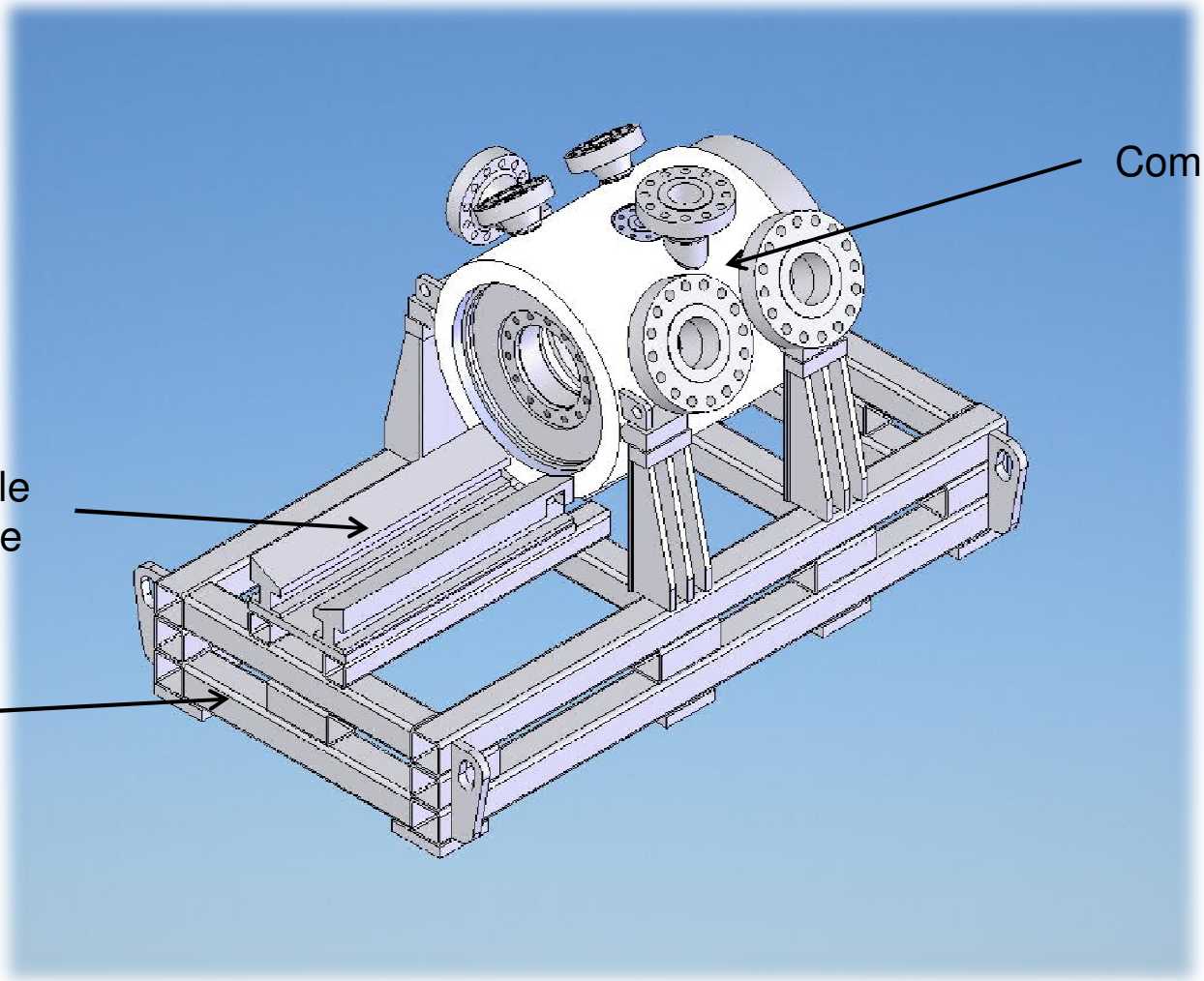

Design Concept #2

- **General description**
  - **Fabricated from eight inch square tubing with a wall thickness of .625 inch. (Max. available wall thickness for eight inch square tubing.**
- **Pros/cons**
  - **The weight of the baseplate is approximately 9370 lbs.**
  - **The design can allow for exiting piping to pass through the design without cutting holes in the tubing.**
  - **Not experienced with the welding of tubing. May need to analyze the welds.**
  - **The tubing is not as strong in bending.**
- **Preliminary analysis results, etc.**

Design Overview

- **I-Beam design**

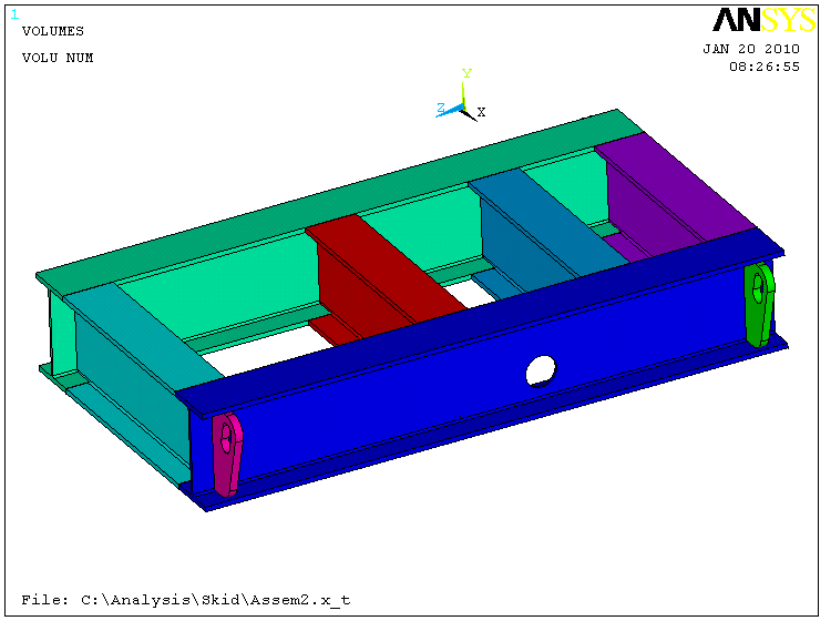

- **Tube-Design**

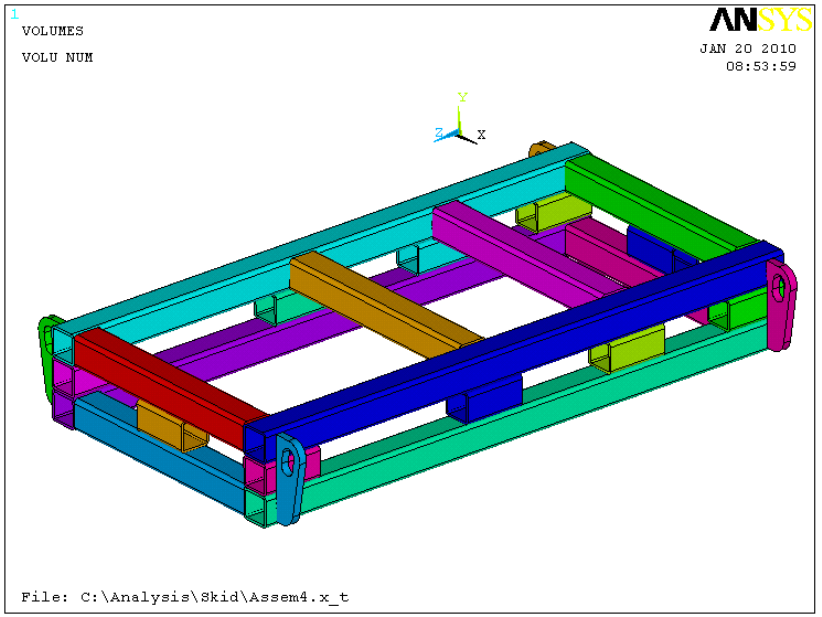

Assumption – spreader bar is being used so that loads are mostly vertical on the lifting lugs

Bending Checks

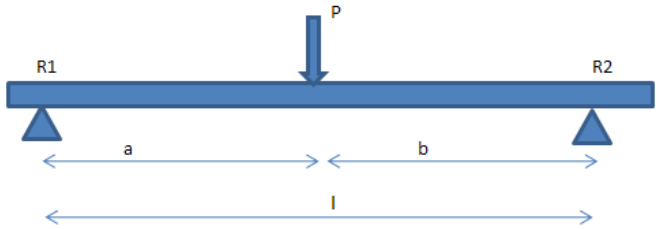

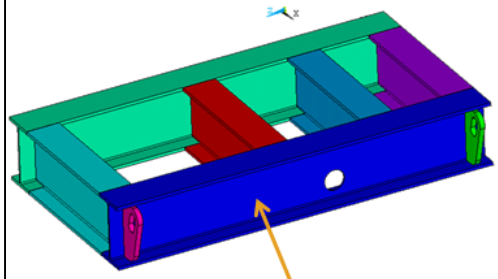

			Comments
P	21523.85	Lbf	Total load/2
a	90	in	
b	60	in	
l	150	in	
R1	8609.54	Lbf	Pb/l
R2	12914.31	Lbf	Pa/l
Max Moment	774858.6	Lbf-in	Pab/l
c	12.5	in	24x162 Beam
I	5170	in4	
Bending Stress	1873.449	psi	

Check for I-Beam cross section

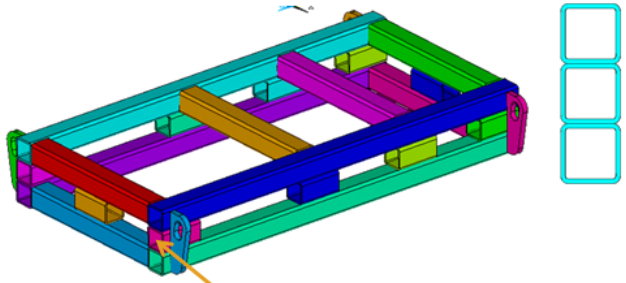

			Comments
P	20677.85	Lbf	Total load/2
a	88.5	in	
b	64	in	
l	152.5	in	
R1	8677.917	Lbf	Pb/l
R2	11999.93	Lbf	Pa/l
Max Moment	767995.7	Lbf-in	Pab/l
c	12.2	in	24x162 Beam
I	2924.8	in4	
Bending Stress	3203.483	psi	

Check for Tube cross section assuming 3 of them in parallel

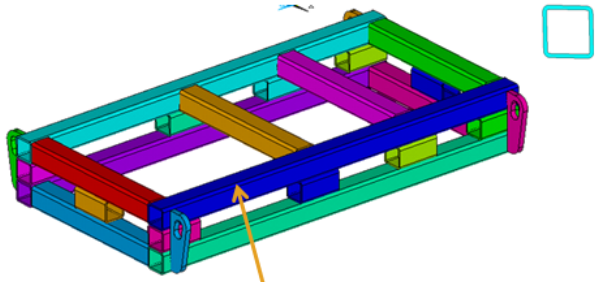

			Comments
P	20677.85	Lbf	Total load/2
a	88.5	in	
b	64	in	
l	152.5	in	
R1	8677.917	Lbf	Pb/l
R2	11999.93	Lbf	Pa/l
Max Moment	767995.7	Lbf-in	Pab/l
c	4	in	24x162 Beam
I	153	in4	
Bending Stress	20078.32	psi	

Check for Tube cross section assuming one of them carries the load

Bending Stresses

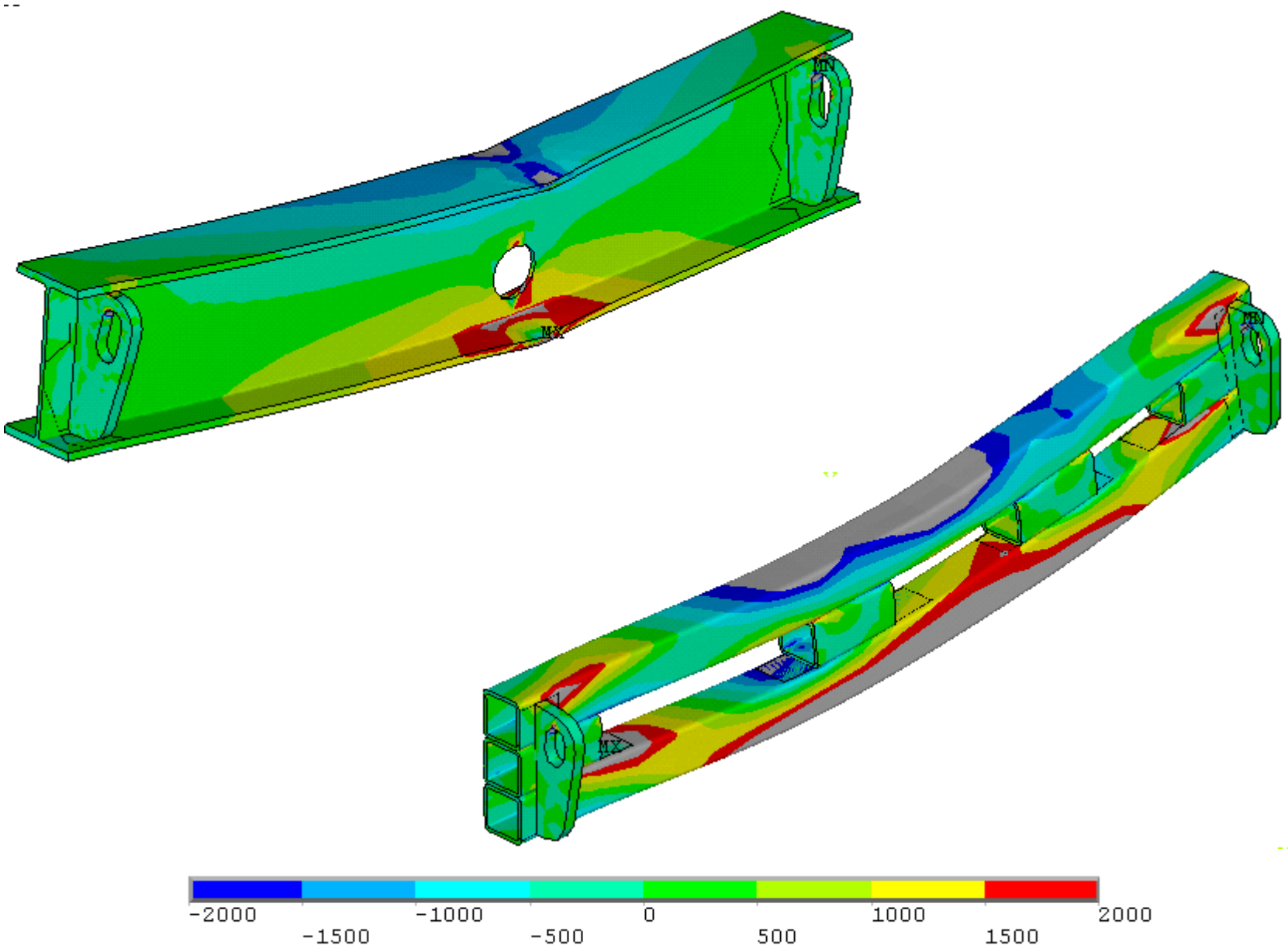

Lug Analysis

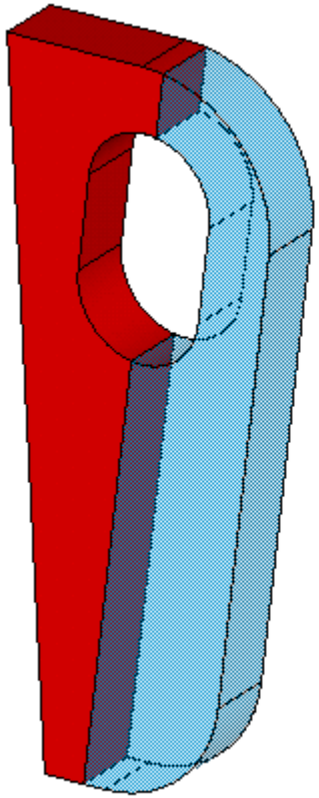

Hole to edge distance	2 in	
Lug thickness	2 in	
Shear Pullout Area	4 in^2	
Shear Force	10761.93 Lbf	assuming lugs share the weight
Shear Stress	1345.241 psi	

Shear Pullout check

Further Analysis required

- Analysis of compressor pedestal design including thermal growth effects
- ~~Analysis of harmonic coupling of the compressor/skid~~
- Static analysis of compressor weight and operational loads.
- Modal analysis of the compressor /skid assembly
- Compressor/skid “ping” test
- Analysis of the lifting loads
- Analysis of the spreader bar/box
- Others-TBD

Further Design Questions

- **Will we add deck plate to the top of the baseplate?**
- **How much space is needed for the on skid control panel?**
- **Is a separate spreader bar needed for lifting the skid?**
- **Will the bundle cradle remain in place or be removed during operation?**
- **Is additional bracing needed for the pedestals?**
- **Will the gearbox require additional support?**
- **What are the standard lengths of structural shapes?**

Budget and Schedule

- PDR date – Feb 17th
- FDR date – May 5th
- Drawing Release date
- Estimated Manufacturing Time/Delivery date
  - Concrete pad design interface to ATSI by February 22, 2010
  - Seattle arrival August 20, 2010
- Any differences from master schedule? Yes supports assembly in Sept 10
- Is schedule achievable? Yes

- Current budget
  - Hardware: $107,000
  - ODC's: $0
- Is current budget adequate?
  - Yes

Conceptual Design Review
Controls and DAQ

John Beers

Jerome Mullins

06/14/2010

Controls and DAQ Scope

- I/O System excluding Sensors and Facility I/O
- Control System PLC and Programming Software
- Local Touchscreen and Programming Software
- Vibration System Rack and Cards
- Vibration System Analysis Software
- DAQ Software with
  - I/O Servers
  - Historian
  - Trend/Plotting Package
  - Data Analysis Package
- Protocol Gateways if required
- Additional IGV and Bypass Positioners
- Specification of VFD interface requirements
- Specification of any Control Room PC Special Requirements

Control and DAQ Conceptual Design

- **Use a common set of I/O Transmitters/Converters for DAQ and PLC**
  - **Duplication is eliminated**
  - **Easy to expand or reduce the set of points used for control as needs change**
  - **DAQ can log "everything" to a single database**
  - **Fewer enclosures to mount and wire**
- **Provide I/O mounted on the skid**
  - **Eliminate the "rats nest" of a centralized control panel**
  - **Keep field wiring/piping runs short**
  - **Allow wiring/piping to be completed earlier in assembly process**
- **Provide additional DAQ access to**
  - **PLC processor (setpoints, limits, calculated values, etc.)**
  - **Vibration System (overall, gap, X-amplitude, Y-amplitude, acceleration, etc.)**
  - **VFD (power, motor and drive temperatures, speed, etc.)**
  - **IGV/Bypass Actuators (position, speed, etc.)**
  - **Facility PLC and I/O (via Control PLC)**

Architecture

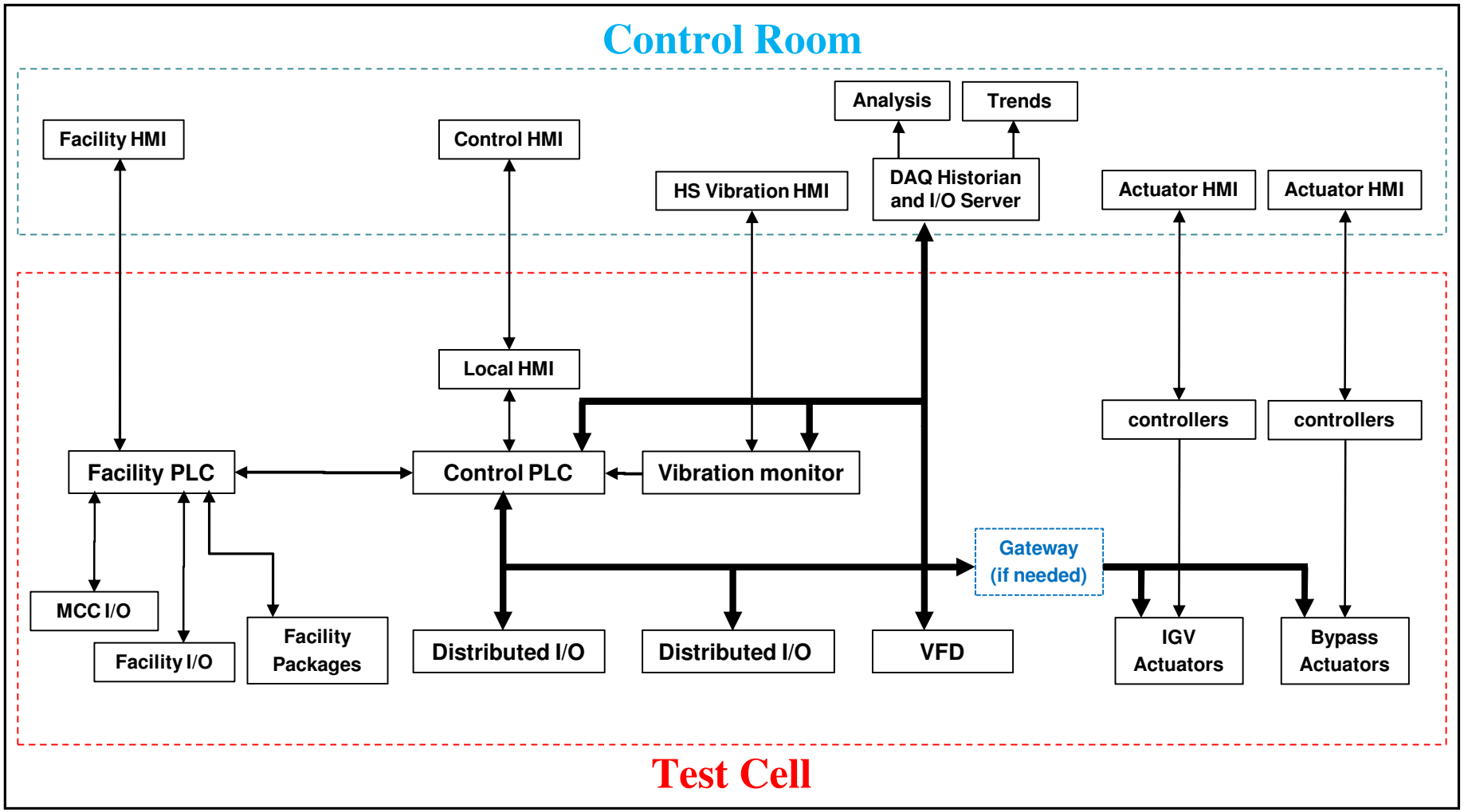

Rampressor Control and DAQ Conceptual Design

- **Dedicated Data Historian to create log files**
  - **SQL Access to Database**
  - **OPC Access to Real-Time Data**
  - **Mirror database in Bellevue**
- **Trending and Plotting software to display Real-Time and Historical Data**
  - **Multiple clients**
  - **Multiple plots per client**
  - **Ad-hoc selection of plotted variables, scales, and timebases**
- **Analysis Software to verify calculations and models**
  - **MatLab has both OPC and SQL Toolsets available for real-time and post-process analysis**
- **Communication Protocols**
  - **HS Vibration Systems support Modbus/TCP**
  - **Parker IGV/Bypass Actuators support Ethernet/IP**
  - **VFD supports Profibus, Modbus, DeviceNet, and Modbus/TCP**
  - **Facility PLC and Control PLC support Modbus/TCP or Ethernet/IP and Profibus or DeviceNet, depending upon the manufacturer**

Rampressor Control and DAQ Conceptual Design

- **PLC features**
  - **24 Vdc for digital I/O – safety, low noise**
  - **4-20 ma. for analog I/O except temperatures**
  - **3-wire Pt100 RTC or Type K T/C for temperatures**
- **Trending and Plotting software to display Real-Time and Historical Data**
  - **Multiple clients**
  - **Multiple plots per client**
  - **Ad-hoc selection of plotted variables, scales, and timebases**
- **Analysis Software to verify calculations and models**
  - **MatLab has both OPC and SQL Toolsets available for real-time and post-process analysis**
- **Communication Protocols**
  - **Bently-Nevada and Shinkawa HS Vibration Systems support Modbus/TCP**
  - **Parker IGV/Bypass Actuators support Ethernet/IP**
  - **VFD supports Profibus, Modbus, DeviceNet, and Modbus/TCP**
  - **Facility PLC and Control PLC support Modbus/TCP or Ethernet/IP and Profibus or DeviceNet, depending upon the manufacturer**

Control Loops

- **Valves**

V-1	**Controls Rampressor Inlet Pressure**
V-2a/ b	**Controls Rampressor Discharge Pressure, Manually Set, Operate as a single valve**
	optional - Programmable Automatic Cycle or Pressure or Flow control
V-4	**Controls HP Seal leakage pressure to approximate Aft bleed pressure**
V-5, V-22	**Controls Aft Bleed Pressure, Separate Start/Unstart Setpoints**
V-6 ,V-23	**Controls Fwd Bleed Pressure, Separate Start/Unstart Setpoints**
V-7	**Controls Bleed/Suction Pressure, Maintain a fixed ΔP below the calculated or measured pressure downstream of the inlet guide vanes**
V41,51,61,71	**Balances DE and NDE pressures or flows for 4, 5, 6, and 7**
V-8	**Controls NDE Thrust Pressure, Adjust to balance and/or bias DE and NDE Thrust Pressures**
V-9	**Controls DE Thrust Pressure, Adjust to match IGV exit pressure**
V-18	**Regulates Dry Gas Seal Supply pressure to a fixed setpoint or a deltaP over WSD cavity pressure**
V-26	**Isolation Valve, Open during operation, fail in place, Closed overnight**
V-28	**Regulates Inlet Pressure of CP-6**
V-20	**Facility, Lowers Plenum Pressure as needed**
V-21	**Facility, Raises Plenum Pressure as needed**
IGVs	**Parker or other Actuators, Manual Positioning**
Bypass Valves	**Existing Parker Actuators, Manual Positioning**

- **Speeds**

VFD	**Manually Entered Setpoint, Controlled Ramp Rates**

- **Temperatures** **controlled in Facility PLC**

Control Suppliers

- **PLC Suppliers**

1. ~~ABB Compact 800 or 800xA~~ - Poor Support
2. Allen-Bradley ~~CompactLogix or~~ ControlLogix – CompactLogix is too small/slow
3. ~~CCC Vanguard Series 5~~ - Poor Support, Communications
4. GE ~~RX3i, 90-30, or~~ 90-70 – 90-30 is too small/slow
5. ~~Koyo Productivity 3000~~ - Poor Support, Communications
6. ~~Modicon M340, Quantum, or Premium~~ - Poor Support
7. Siemens ~~S7-1200,~~ S7-300~~, or S7-400~~ – S7-1200 has no remote I/O yet, S7-400 is overkill

- **Local HMI Suppliers** - match selected PLC

1. ~~ABB Panel 800 PP865~~
2. Allen-Bradley PanelView Plus CE
3. GE QuickPanel View
4. ~~Koyo Productivity 3000~~
5. ~~Modicon Magelis XBT GTW~~
6. ~~Red Lion G315~~
7. Siemens MP377
8. ~~Wonderware Compact Panel Computer~~

Control Suppliers

- **Vibration System Suppliers**

1. ~~Allen-Bradley XM Series~~ - Poor Software, Communications
2. Bently-Nevada 3500 ~~or 1900~~ – 1900 is too small, 3500 is fastest with best software
3. ~~CCC Vibrant Series 5~~ - Poor Support, Slow
4. ~~IOTech ZonicBook or 600~~ - Poor Support (aquired by NI), Communications
5. Shinkawa ~~VM-5~~ or VM-7 – VM-5 is previous generation, B-N has better support

DAQ Suppliers

- **DAQ I/O Suppliers**

1. **Acromag BusWorks 900 ~~or EtherSTAX~~ – EtherSTAX is not for skid mounting, ProfiBus version is an old design that is slow, ~$50 per point**
2. **Allen-Bradley 1794 Flex I/O – Use if PLC is an Allen-Bradley, supports Ethernet/IP, DeviceNet, and Profibus ~$100 per point**
3. **~~Beckhoff EtherCAT~~ – EtherCAT is too proprietary, no access from PLC**
4. **~~Hi-Techniques Win600E~~ – Oscilloscope type, for Lab use w/small point count**
5. **~~iba AG ibaPadu, ibaNet750~~ – Expensive, no access from PLC**
6. **~~Measurement Computing IOTech 6000~~ - Poor Support (aquired by NI), Communications**
7. **~~NI CompactRIO or PXI~~ – Poor communications, no access from PLC**
8. **Scanivalve ~~DTS/~~DSA 3200 Series – Only applicable to dry non-differential pressures < 850 psig, includes built-in Calibration and Purge valves, Scanivalve may want RamGen to fund the development of Modbus/TCP for access from the PLC ~$600 per point with sensor, calibration source, and valves**
9. **~~HBM QuantumX or MGCplus~~ – no access from PLC**
10. **Siemens ET200M – Suports ProfiBus and ProfiNet ~$100 per point**

DAQ Suppliers

- **DAQ Software Suppliers**

1. ~~Agilent VPro 9.2~~ – No OPC or industrial I/O support
2. ~~DSP Development DADiSP~~ – No OPC or industrial I/O support
3. iba AG ibaPDA - Excellent speed, OPC, Profibus, Modbus/TCP, Ethernet/IP
4. ~~MCC DASYLab~~ – No OPC or industrial I/O support
5. ~~NI LabView~~ – Difficult to deal with programming for > 100 I/O
6. Rockwell FactoryTalk Historian ME – Hardware solution works with Allen-Bradley PLC
7. ~~Schneider Electric Vijeo Historian~~ – Poor Support
8. Siemens WinCC – Works with OPC servers, most major PLCs and networks.
9. Wonderware Intouch Historian – Works with everyone, max logging rate of 30K/sec (1,000 points at 10 per second is 10K/sec)
10. MathWorks MatLab – No historian, use in conjunction with another product
11. ~~HBM catman Enterprise or Professional~~ - No OPC or industrial I/O support, Enterprise only supports MGCplus I/O system, Professional supports ProfiBus only, poor Support.

Budget

- **Available Budget**
  - **Control hardware $141,814**
  - **DAQ and instrumentation hardware $500,000**
  - **Programming $111,251**

- **Budgetary costs:**
  - **Vibration System, $50k to $75k**
  - **PLC (w/o I/O) and Control HMI, $30 to $50k**
  - **I/O System (PLC + DAQ), $390k (650 channels at $600/channel average)**
  - **DAQ Software, $25k to $50k**
  - **Control Room PCs, $35k to $50k**
- **Total $530k to $615k**
  - **Programming ($111k) not included**
  - **On-skid installation, wiring, valves, raceways, mounting frames, etc. not included**

Schedule

- **PDR target Will be set by Quotes (August?)**
- **FDR target Will be set by Quotes (October?)**

- **All Hardware in Seattle, Nov 1, 2010**

Instrumentation CDR

Bryan Jilka

5/28/10

Goals

- **Review requirements from SRR**
- **Discuss remaining undecided requirements:**
  - **Purge/Cal**
  - **TC vs. RTD**
  - **Accuracy**
- **Discuss impacts on DAQ and control systems**
- **Review possible equipment**
- **Review schedule and budget**
  - **Review measurement list**

Instrumentation Requirements

- **Provide instrumentation sufficient in scope, accuracy, and redundancy for Ramgen to debug, troubleshoot, and measure performance of demo rig compressor.**

- **Provide instrumentation sufficient in scope, accuracy, and redundancy for Ramgen to monitor health of compressor drive train components**

- **Coordinate measurement requirements of facility from ATSI**

- **Provide instrumentation sufficient in scope and traceable to required specifications to meet D-R option agreement requirements for:**
  - **Performance (PTC-10)**
  - **Vibration (API, D-R spec, others?)**

- ***Complete Measurement list compliant with PTC-10 Requirements is currently being reviewed individually.***

Instrumentation Requirements Concept (cont.)

- **Repeatability:**
  - **< 0.5% of FS**
- **Accuracy targets:**
  - ***Assume Control/Monitoring/Performance measurements don't require separate accuracies unless otherwise specified.***
  - **Static pressure and Differential Pressure:**
    - **< 0.5% of FS (PTC-10 requires 1% of reading agreement)**
  - **Total Temperature:**
    - **< 4°F ~= 2°C @ FS (PTC – 10 requires 0.5% of absolute temperature agreement)**
  - **Accelerometers:**
    - **100 mV/g sensitivity or better**
  - **Proximity Probes:**
    - **200mV/mill sensitivity or better (Bentley Nevada ProxPac)**
  - **Mass Flow:**
    - **Performance: < 1% of Design Point, appropriate range to cover relevant operating space.**
    - **Monitoring: +/- 15% of Design Point, <=0.1% Repeatability**
  - **Others:**
    - **Velocimeters, Key Phasers, Gas Composition meters I need input on.**
- **All information on this slide are assumptions pending review**

Instrument Requirements Concept (cont.)

- **Resulting Accuracies:**
  - **Enthalpy:**
    - **~= 0.25% of Value (Depends on range of Pressure and Temperature meters)**
  - **Density:**
    - **~= 1% of Value (Depends on range of Pressure and Temperature meters)**
  - **Efficiency:**
    - **~= 1.5 - 2 percentage point (i.e. 0.80 +/- 0.02)**
- **A/D Conversion:**
  - **0.1% minimum (from DAQ and Control System Requirements)**
- **Calibration:**
  - **Requires calibration no less than every 12 months**
  - **PTC requires before test and check afterwards**
- **Reliability:**
  - **Have scheme for dealing with blocked lines.**
  - **Design instrument to minimize blockage potential**
- **Connections:**
  - **Possibly G1/4 or G1/8, No requirement has been levied**
  - **Maintain easy access to facilitate purge ability**
  - **No NPT connections.**

- **All information on this slide are assumptions pending review**

Instrument Requirements Concept (cont.)

- **Frequency Response (Electronics):**
  - **<1 sec (250ms target) for all DAQ only measurements**
  - **50ms response for control measurements (From Control Requirements)**
- **Signal:**
  - **Avoid voltage signals if possible**
- **Redundancies:**
  - **4x for all PTC -10/Performance Measurements**
  - **Most others 4x or less as cost and space allow unless otherwise requested**

Efficiency Control Volume

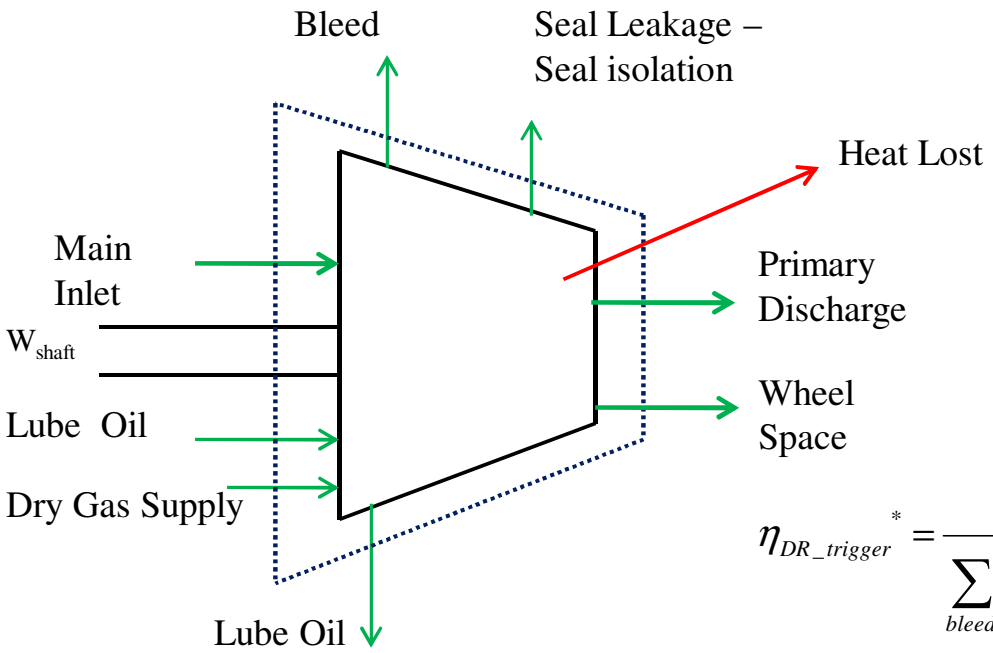

Compressor Package Performance:
-Rampressor only
-Shaft power after gearbox losses

$$P_{parasitic} = \sum Q + \sum_{\text{sec\_flows}} \dot{m} \Delta H_{total}$$

$$P_{mech} = \sum \dot{m}_{oil} Cp(\Delta T)$$

$$\eta_{DR\_trigger}{}^{*} = \frac{(\dot{m}_{out} + m_{bleed})(Ht_{ideal} - Ht_{Inlet\_Flange})_{Inlet\_Flange}^{Exit\_Flange}}{\sum_{bleed} \dot{m}_{bleed}(Ht_{bleed} - Ht_{in}) + (\dot{m}_{out})(Ht_{exit\_flange} - Ht_{in})}$$

$$\eta_{Flow\_Path} = \frac{\dot{m}_{delivered}(Ht_{ideal} - Ht_{Inlet\_Flange})_{Inlet\_Flange}^{Exit\_Flange}}{\sum_{bleed} \dot{m}_{bleed}(Ht_{bleed}) + \sum_{shroud\_cav} \dot{m}_{shroud\_cav}(Ht_{cav}) + \sum_{WS} \dot{m}_{WS}(Ht_{WS}) + \dot{m}_{delivered}(Ht_{delivered}) - (\dot{m}_{in})(Ht_{in})}$$

$$\eta_{Flange} = \frac{\dot{m}_{delivered}(Ht_{ideal} - Ht_{Inlet\_Flange})_{Inlet\_Flange}^{Exit\_Flange}}{\sum_{flanges} \dot{m}_{flange}(\Delta Ht_{flange}) + Q_r + P_{mech}}$$

Includes all flows > 1% of Design delivered mass

* - Contractually Ignores all Mechanical, Seal, and Windage losses

Inlet Flanges

- 4x Pressure Measurements
  - Total by DR Contract flows
  - Static on all others
- 2 Total Pressure Probe for Suction Flow
- 4x Temperature Measurements
- Mass Flow Measurement
  - 2x Delta Pressure (2 Transducers – 1 Tap)
  - 2x Static Pressure (2 Transducers – 1Tap)
  - 1x Temperature (1 Well)
- Iterate on static temperature to solve entire static and total state

ASME PTC 10–1997

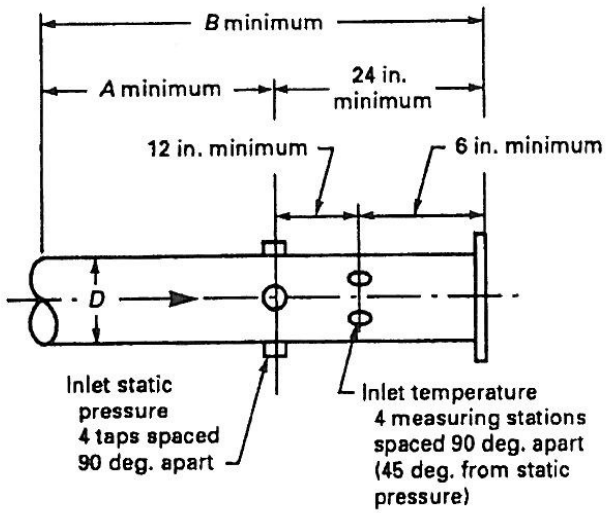

Inlet Opening Preceded By	Minimum Dimension	
	A	B
Straight run	2D	3D
Elbow	2D	3D
Reducer	3D	5D
Valve	8D	10D
Flow device	3D	5D

For open inlet, see Fig. 4.2.

For vortex producing axial inlet, see Fig. 4.3.

Inlet Configuration

Inlet Flanges (cont.)

- **Critical to follow PTC-10:**
  - **Suction (x2) (INND07, INDE07)**
    - **10" Pipe – 10' Long (4D minimum for P,T and ~6D for Flow meter)**
  - **Oil Supply (COLSND, COLSDE,TOLSDE)**
    - **Required for Mechanical loss**

- **Less Critical:**
  - **Dry Gas Seal Supply (BSSUND,BSSUDE) ~=2% Core Flow**
  - **Coupling supply (pressure measurement)**
  - **Location is to be where ever is mechanically convienent**
  - **Same Redundancy as Critical flows.**

Discharge Flanges

- 4x Pressure Measurements
  - Total by DR Contract flows
  - Static on all others
- Total pressure probe for main discharge and bleed flow
- 4x Temperature Measurements
- Mass Flow Measurement
  - 2x Delta Pressure See suction slide
  - 2x Static Pressure
  - 2x Temperature
- Iterate on static temperature to solve entire static and total state

COMPRESSORS AND EXHAUSTERS

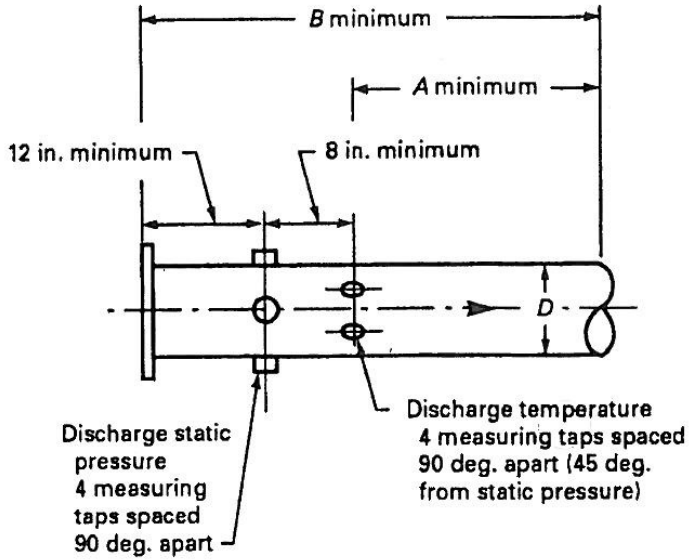

Discharge Opening Followed By	Minimum Dimension A	B
Straight run	2D	3D
Elbow	2D	3D
Reducer	3D	5D
Valve	3D	5D
Flow device	8D	10D

For open discharge, see Fig. 4.4.

For diffusing volute with unsymmetrical flow, see Fig. 4.5.

Discharge Flanges (cont.)

- **Critical to PTC 10**
  - **Primary Discharge** (STEX99)
  - **Aft Bleed (x2)** (BLAFDE, BLAFND)
  - **Fwd Bleed (x2)** (BLFWDE, BLFWND)

- **Performance**
  - **HP Seal Leakage (x2)** (HSFLDE, HSFLND)
  - **Isolation (x2)** (ISFLDE, ISFLND) ~=3%
  - **Wheel Space (x2)** (WSFLDE,WSFLND) ~=1-2%
  - **Oil Drain (x2)** (COLEDE,COLEND)

- **Less Critical:**
  - **Dry gas seal leakage (mixed leakage)** (BSLKDE, BSLKND) ~=.1%
  - **Location is to be where ever is mechanically convenient**

IGV Performance

3 Ps Taps

3 Ps Taps

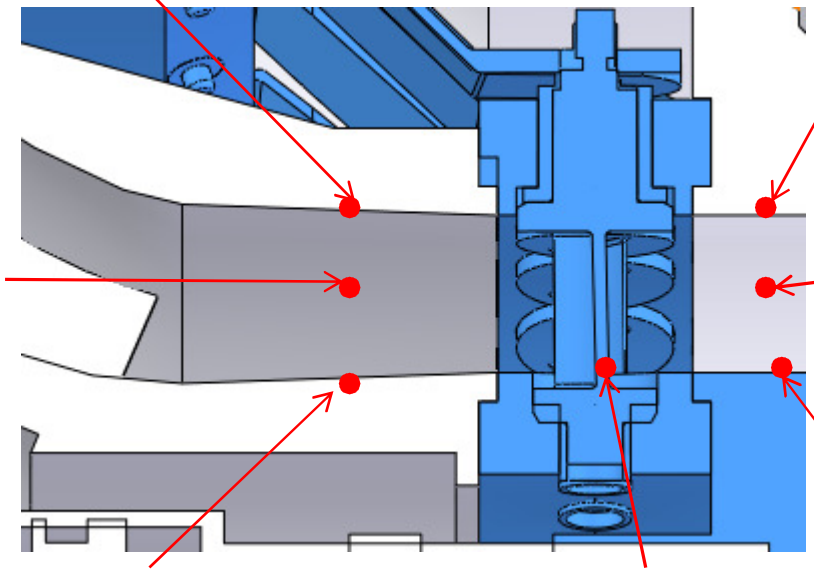

6 Permanent Rakes
3 Total Temperature
-3 Total Pressure
-3 holes each

1 Kulite port
3 Cobra Survey Probes
-Total Pressure Only

3 Ps Taps

3 Ps Taps

IGV Blade Angle*
(via actuator position)

Critical Performance equations:

$$\bar{\omega} = \frac{P_{total\_in} - P_{total\_exit}}{P_{total\_in} - P_{static\_in}} \qquad PR_{total} = \frac{P_{total\_exit}}{P_{total\_in}}$$

Critical parameters: $\theta_{IGV\_exit}, M_{IGV\_exit}$

Diffuser

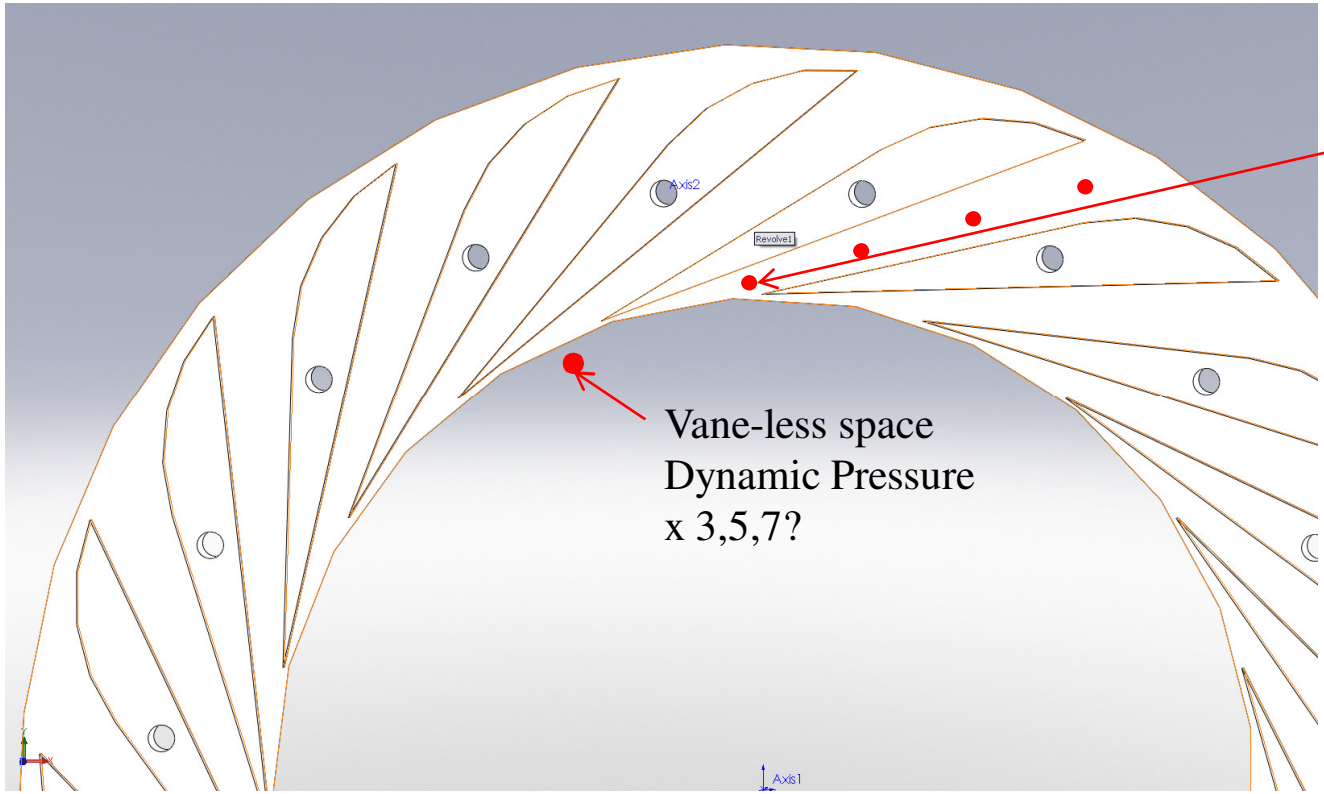

Vane-less space
Dynamic Pressure
x 3,5,7?

3 passages x4 Hub Ps Ports (PSDDSN40-50 & PSDDST40-50)

Aero Requested as many as can fit clustered around LE Throat Region.

Lube Oil

- Pressure x1
- Temperature x1
- Mass Flow
- Pressure Differential

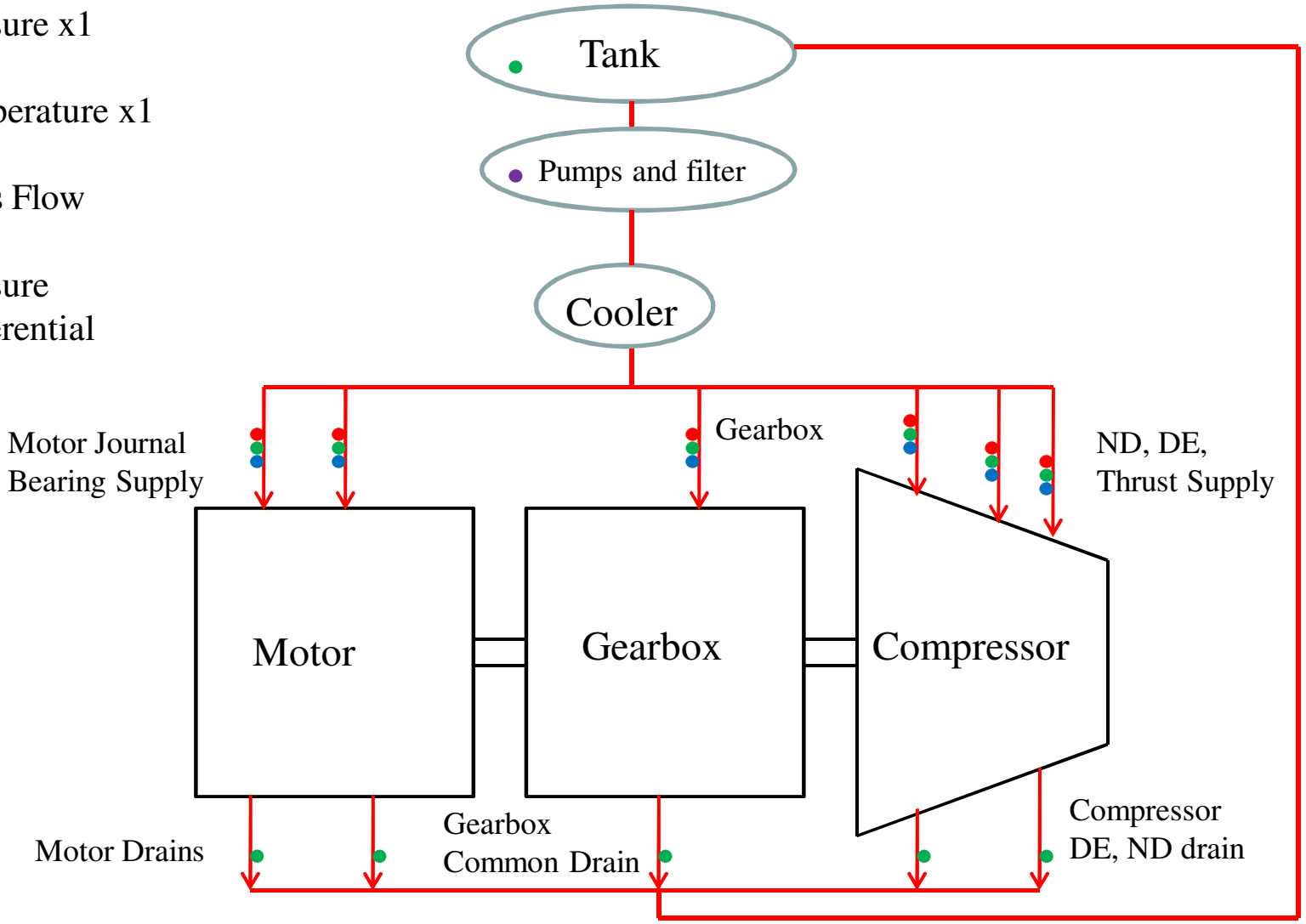

NDE/DE Journal Bearings

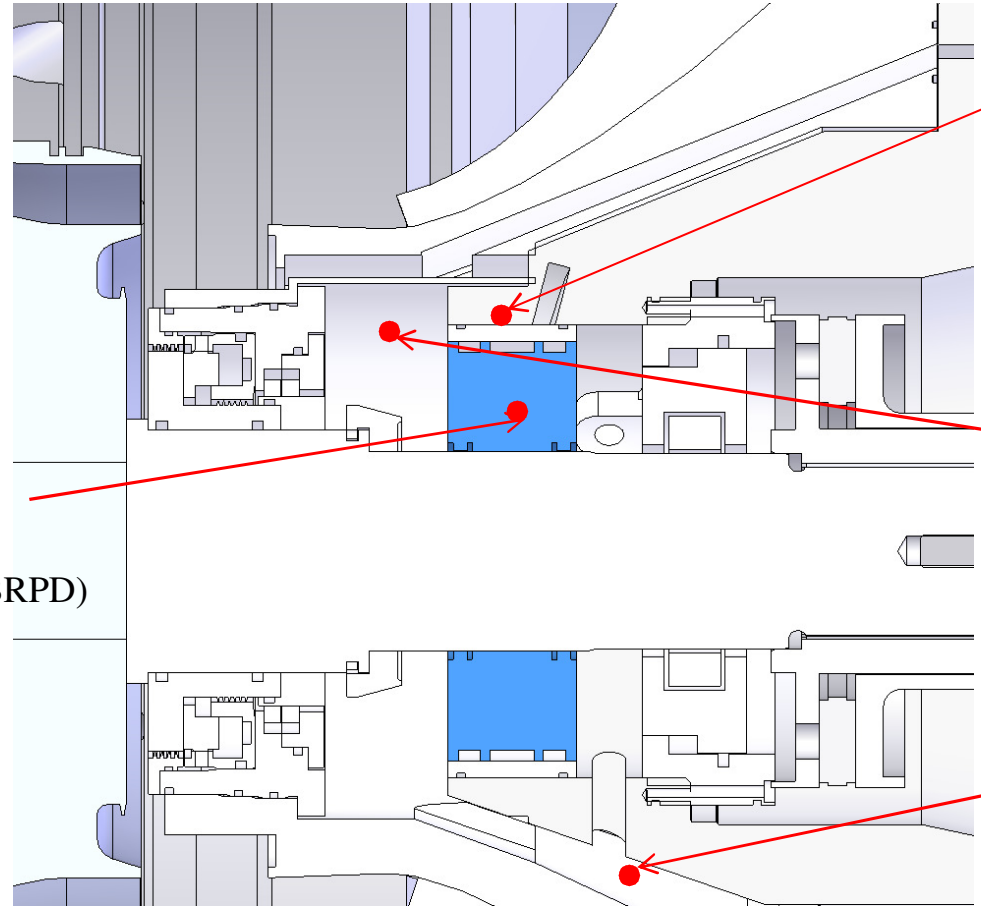

Bearing Frame Metal Temperature x3-4? (TTBSMT)

Bearing Cavity Pressure x3-4? (PSBCAV)

Bearing Pad Temperature x3-4? (TMBRPD)

Bearing Oil Exit Temperature x3-4? (TSBOLE)

* PTC-10

Oil Measurements – See Lube oil Slide

Shaft Seals/Wheel Space

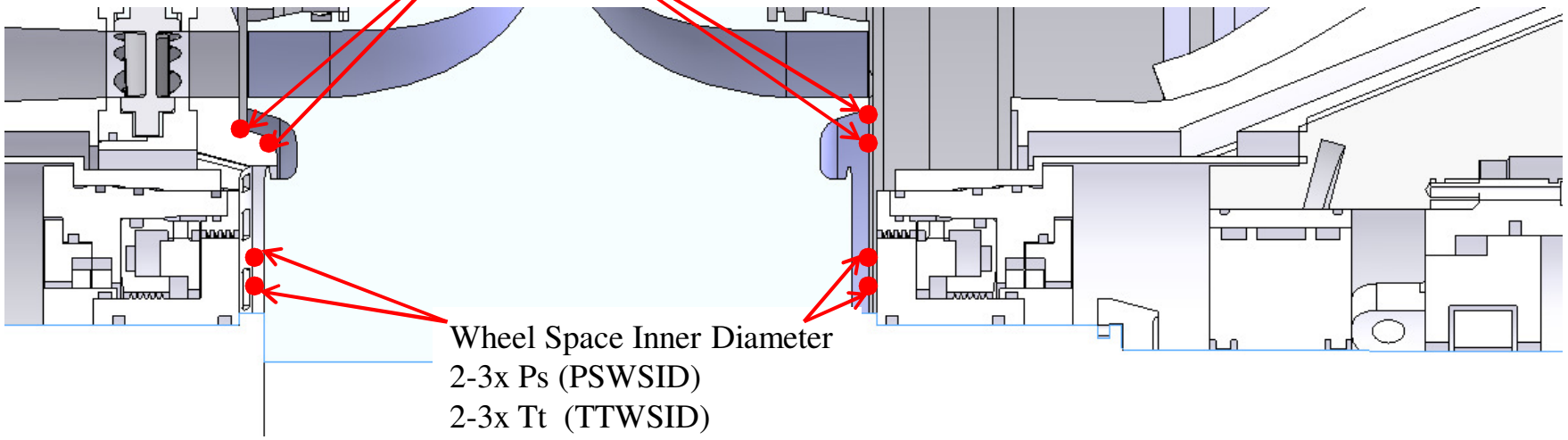

NDE Barrier Seals @ Flange
3x Barrier Seal Supply (PSBSND)
3x Vent Gas (PSVGND)
3x Seal Gas (PSSGND)

DE Barrier Seals @ Flange
3x Barrier Seal Supply (PSBSDE)
3x Vent Gas (PSVGDE)
3x Seal Gas (PSSGDE)

Flow meter options

	length	Accuracy	Pressure loss	rangeability
Orifice plate	15-30d	1-4%	High	4:1
Venturi	30+d	1%	Low	4:1
Nozzle	30d	1-2%	med	4:1
Cone	4	From 0.5%	Med	10:1
Multi hole plate	4	0.7%	Med	8:1
Pitot/Annubar	12-34d	0.8-1.5%	med	8:1

All operate on delta pressure-Pitot measures total pressure directly, others measure static pressure

High accuracy requires high Beta and proportional loss except with Pitot

Wide flow range reduces signal/error ratio at low flow

Range required is 2.4:1 (40 lbm/s to 95 lbm/s) discharge

Range required is 1.6:1 (60 lbm/s to 95 lbm/s) suction

Range required is 4:1 (2% to 8%) performance bleed

V-Cone Mass Flow Meter

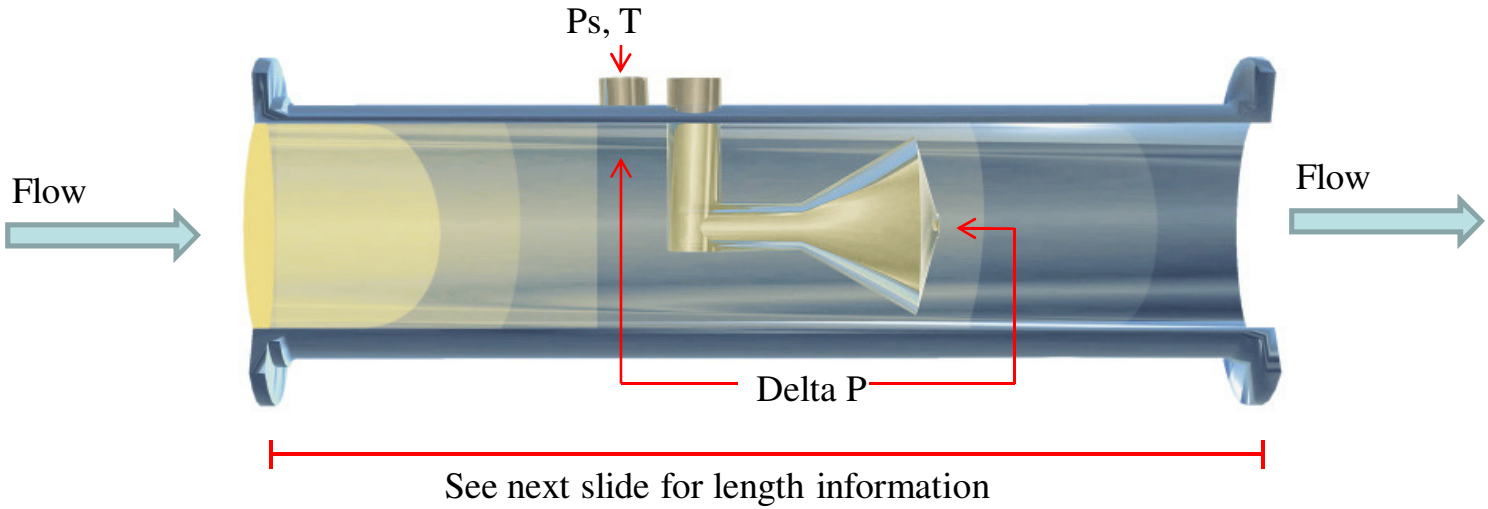

- **Schematic of McCrometer V-Cone Flow meter (recommended by DR)**
  - **Offers high range and accuracy with a medium pressure loss**

- **Conventional Differential pressure flow meter use (Eqn 3-1.1 PTC 19.5):**

$$w = \tfrac{\pi}{4} D_{actual}^2 \beta^2 C \varepsilon \sqrt{\frac{2\rho(\Delta P)}{1-\beta_{actual}^4}} \qquad \beta = \sqrt{1-\frac{d^2}{D^2}}$$

$$\%P_{loss} = (1.3 - 1.25\beta) * 100$$

* Depending on design and DR study results

V-Cone (cont.)

- Accuracy: up to ±0.5% of rate
- Repeatability: ±0.1%
- Turndown: 10:1
- Standard Betas: 0.45 through 0.85
- Headloss: Percentage of differential pressure produced varies with beta ratio.
- Installation: Typically 0-3 diameters upstream and 0-1 diameters downstream.

Model VW Bulletins
ANSI B16.5 Weld Neck, RF Flanges
24509-35 Class 150 or 300
24509-36 Class 600 or 900
24509-37 Class 125 or 250

The V-Cone is manufactured under a quality management system that is certified to ISO 9001:2000.

* Each V-Cone is sized for the intended application. Specific performance ratings must be obtained through the sizing process.

MODEL VW(L) DIMENSIONS

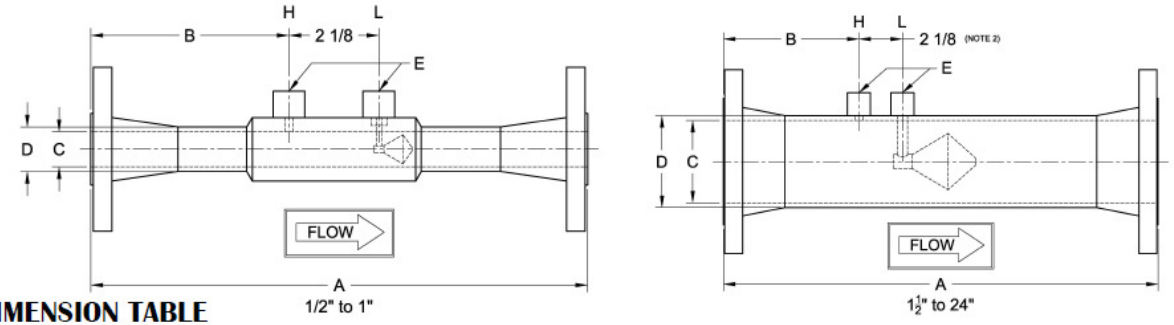

DIMENSION TABLE

Size	ANSI B16.5 Class 150				ANSI B16.5 Class 300				Stainless		Carbon		D		E (Note 2)
	A (Note 1)		B		A (Note 1)		B		C (Note 2)		C (Note 2)				
inch	inch	mm	inch	mm	inch	mm	inch	mm	inch	mm	inch	mm	inch	mm	NPT
½	11.38	289.1	4.63	118	11.75	298.5	4.82	122	0.622	15.8	-	-	0.84	21.3	¼
¾	11.75	298.5	4.81	122	12.13	308.1	5.00	127	0.824	20.9	-	-	1.05	26.7	¼
1	12.00	304.8	4.94	125	12.50	317.5	5.19	132	1.049	26.64	-	-	1.31	33.4	¼
1½	14.38	365.3	5.19	132	14.88	378.0	5.44	138	1.645	41.78	-	-	1.9	48.3	¼
2	16.38	416.1	5.69	145	16.88	428.8	5.94	151	2.104	53.44	-	-	2.37	60.3	½
2½	16.75	425.5	5.88	149	17.25	438.2	6.13	156	2.504	63.60	-	-	2.87	73.0	½
3	18.75	476.3	5.88	149	19.50	495.3	6.25	159	3.104	78.84	-	-	3.5	88.9	½
4	21.25	539.8	6.63	168	22.00	558.8	7.00	178	4.090	103.8	-	-	4.5	114	½
6	28.25	717.6	7.38	187	29.00	736.6	7.75	197	6.065	154.1	6.065	154.1	6.62	168	½
8	33.00	838.2	8.51	216	33.75	857.3	8.88	226	7.981	202.7	7.981	202.7	8.62	219	½
10	35.00	889.0	8.51	216	36.25	920.8	9.13	232	10.02	254.5	10.02	254.5	10.7	273	½
12	38.00	965.2	9.26	235	39.25	997.0	9.88	251	12.00	304.8	11.94	303.3	12.7	323	½

Entire flow meter (Flange to Flange) is ~ 3ft or less

A+ FlowTek Orfice Plate

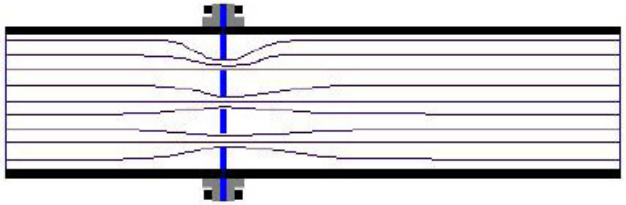

A+ FlowTek Balanced Flow Meter - A Cost Effective Solution

TECHNOLOGY

Testing and measurement were conducted by NASA personnel and technology validated through Texas A&M University - Kingsville. The A+ FlowTek Balanced Flow Meter provides balanced kinetic energy and momentum across the fluid flow region. The A+ FlowTek technology significantly reduces turbulent shear, fluid flow stresses and associated eddy formations.

PRESSURE LOSS

The A+ Balanced Flow Meter provides a 50% reduction in pressure loss, saving substantial energy costs.

A+ FlowTek Balanced Flow Meter *Standard Orifice*

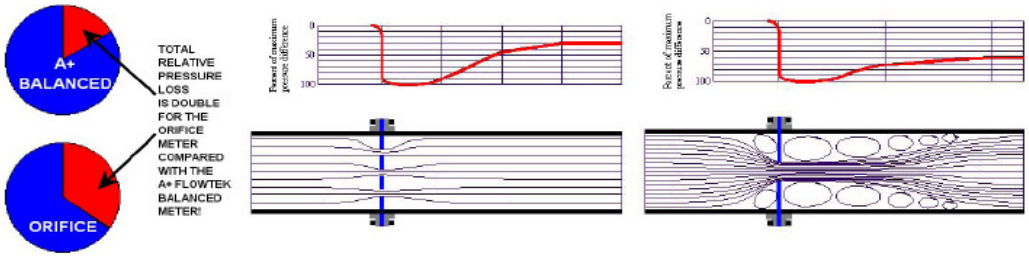

BENEFITS

This new A+ FlowTek balanced metering technology provides many benefits when compared to orifice plate design.

- Reduced pressure loss
- Improved accuracy
- Enhanced repeatability
- Increased rangeability
- Self venting & Draining
- Lower vibration
- Reduced noise
- Straightens flow

- Cost effective
- Reduces pipe erosion
- Improved solids handling
- Direct orifice replacement
- No piping changes
- No instrumentation changes
- Same calculation method
- Reduced installation length

Allegedly offers:

-10:1 range

-Low pressure loss

-Better accuracy then ASME Nozzle

-As little as 0.5D up/down stream straight run requirements

Coriolis Flow meter

- **Mass flow accuracy**
  - **+/-0.10% of flow rate**
- **Repeatability**
  - **+/- 0.20% of rate**
- **Temperature rating**
  - **-400 to 662°F (-240 to 350°C)**
- **Pressure rating**
  - **1480 psi (102 bar)**
- **Range:**
  - **20:1**

- **Benefits:**
  - **Direct inline measurement of mass flow, density and volume flow and temperature from a single device**
  - **Unique design delivers unparalleled measurement sensitivity and stability to ensure consistent, reliable performance over the widest flow range**
  - **Immune to fluid, process, or environmental effects for superb measurement confidence**
  - **Install anywhere with no flow conditioning or straight pipe run required**
  - **No moving internal parts results in no maintenance or repair**
  - **Compliant, custody transfer accuracy that delivers sustainable measurement performance**
  - **Real-time flow data for pipeline operations, supervisory control and data acquisition systems**

- **Information directly from website.**

Pressure Transducer options

- **GE UNIK 5000, Sensotec, NoShock 100 Series, PCB Instruments**
  - **Up to 15ksi and 257°F, 5kHZ**
  - **Accuracy: 0.2%-0.5% of FS; Repeatability: 0.05% of FS**
- **Differential: Omega PX650 Series, PCB Instruments, GE UNIK 5000**
  - **Up to 50in H20, 800psi, 350°F, 1MHz**
  - **Accuracy 0.5% of FS, Repeatability: 0.05% of FS**

- **High Speed Kulite Probe Transducers / Entran**
- **Scanivalve DS3217 (CHECK CO2 CAPABILITY)**
  - **Up to 750psia, 140°F, 500hz**
  - **Accuracy: 0.3-0.5% of FS**

- **Daily sanity check with transducers in power up sequence**
  - **While system is at settle out pressure before start up, check transducers.**
  - **If a transducer doesn't agree within 2%, transducer needs checked.**
  - **If any line becomes a regular check point, a block valve will be added to make that process easier**
  - **Differential Pressure sanity check:**
    - **Block Valve on one end closed prior to opening isolation**
    - **Attach valve to vent to atmosphere to read a DP.**
    - **Increase redundancy in case on fails**
- **1/8" Stainless tubing to transducer rack.**

Temperature Measurements

- **Most Temperature Measurements will be in thermo wells**
  - **Except for a few being used by control or in a pipe less than 4”D**
  - **Size is likely to be around ¼”D by 1” long (Analysis to be done to determine exact size but are expected to be stock wells).**
  - **Wet or Dry Thermowells?**

- **RTD vs. TC**
  - **RTD’s are generally more accurate and drift less however are more expensive.**
  - **TC’s are generally faster, sensitive and cheaper.**
  - **All purchased equipment contains RTD’s**

  - **Suggested Scheme:**
    - **RTD is thermowells**
    - **RTD’s on all external case DAQ measurements, metal/bearing temperatures, and purchased equipment.**
    - **TC’s All internal case CO2 measurements and control measurements**

Blockage scheme

- **Mount pressure ports and transducers above centerline:**
  - **Let gravity keep blockages out**

- **Install two valves per hose to allow CO2 to be blown into the line and relieve blockages once per day**

- **Increase redundancy such that we can still operate a test even with a blocked line**

More Equipment

- **Proximity Probes/ Keyphaser by Bently Nevada**
  - **Up to 10kHz, 350°F, 200mV/mil**

- **Accelerometers / Velocimeters**
  - **PCB Accelerometer: Model 352C33**
    - **Up to 10kHZ, 200°F, 100mV/mil**
  - **Omega: ACC310**
    - **Up to 10kHZ, 250°F, 100mV/mil**
  - **No data yet on Velocimeters**

- **Humidity- Omega HX15 Series**
  - **Up to 1kHz, 356°F**
  - **Accuracy: +/-2% of reading**

- **Gas Composition**
  - **Spectrograph or Chromatograph (PTC-10)**

Schedule and Budget

- PDR Scheduled for week of June 21st
- FDR Scheduled for week of August 2nd

- Local Assembly to begin November 1st

- DAQ and instrumentation hardware budget $500,000

- Rough estimates: $500/Channel Pressure- $400/Channel Temperature
- Current channel count is ~ 300/Pressure -200/Temps -200/others
- Implies cost of $230,000 roughly for all P and T (instrument and transmitter, wells)
  - Doesn't include valves
- Flow meters (depends on Size of pipe)
  - A+ orfice plate – $50,000 for all CO2 flow meters
  - McCrometer - $90,000 for all CO2 flow meters (estimate based on first quote)

Suggested Removal of Measurements

- **Reduce Redundancy of non PTC-10 Flows**
  - **Seal Flows x2**
  - **HP Seal Flange x2**
  - **Isolation Flange x2**
  - **Wheel Space Flange x2**
- **Remove Total Pressure Probes**
- **2 differential pressures on flow meters**

LUBE SYSTEM

CDR/PDR

3/19/2010

John Beers

Requirements

- Motor---3.9 GPM at 30 PSI
- Gearbox---75 GPM at 30 PSI
- Compressor---125 GPM at 30 PSI
- Operating temperature at ~ 120 degrees F supply
- ISO VG 32 oil
- Minimum temperature of 59 degrees F supply
- Alarm temperature of 131 degrees F (gear box alarm)
- Trip Temperature of 140 degress F (gear box limit)
- Ten minute rundown time (Ramgen calculated)
- Must have a “power loss” system
- Appropriate instrumentation
- Tank heater
- Cooler
- System must gather and return oil
- 8 x full flow for settle out time and resulting tank volume (D-R design guideline)

Run-down Compressor Calculations

Rotor Deceleration Analysis											
Speed Ratios											
	Low		9.8393	Electric motor							
	Intermedi		3.1071	Intermediate speed gearbox components							
	High		1	Rotor							
Moments of Inertia											
Low speed section		[lbm ft^2]		4747.412							
	Motor	[lbm ft^2]	4510		from ABB (Bruce Ingram) 1/13/2010						
	Gearbox	[lbm ft^2]	237.412		from Allen Gear Stiffness & Inertia Calc 12/21/2009						
Intermediate speed		[lbm ft^2]		65.382							
	Gearbox	[lbm ft^2]	65.382		from Allen Gear Stiffness & Inertia Calc 12/21/2009						
High speed section		[lbm ft^2]		3.415							
	Gearbox	[lbm ft^2]	0.415		from Allen Gear Stiffness & Inertia Calc 12/21/2009						
	Rampress	[lbm ft^2]	3.00		from Dave Taylor 432 lb in^2 1/8/2010						
Total moment of inertia											
	High-Equi	[lbm ft^2]	506.95								
Analysis											
	Δt	[s]	5								

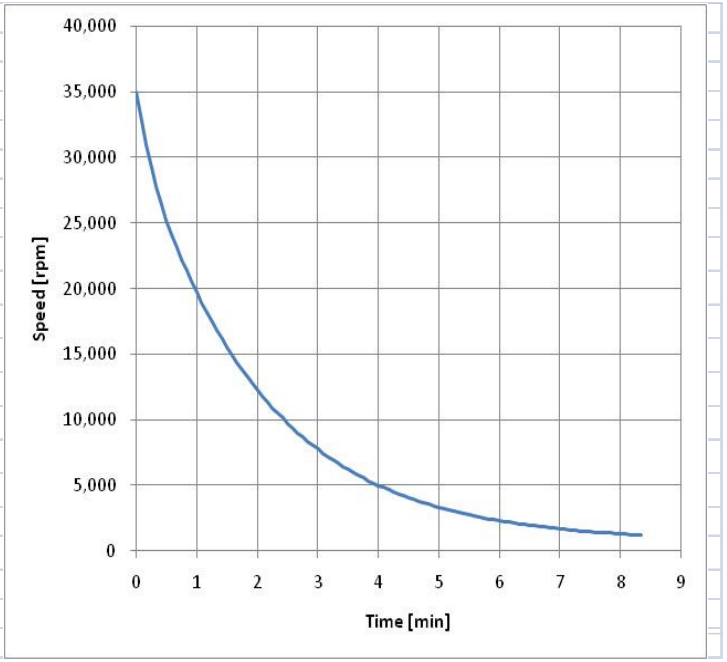

Due to high rotational speeds, ~10 minute rundown predicted for motor/gearbox/compressor

Gearbox Rundown oil flow

Ramgen Rundown Oil Flow Requirement

Date:	**21/01/2010**
Contract No:	**22244**
Contract Name:	**Ramgen**
Key Reference:	**Rundown Oil Flow Requirement**

Values in this box indicate oil flow variation of sprays due to inlet

	Oil Flow			
Supply Pressure (psi)	30	10	7.5	5
Total Mesh Flow (igpm)	26.8	15.5	13.4	10.9
HS Cplg Teeth Flow (igpm)	1.5	0.9	0.8	0.6

HS End Star Brg Load (lb)	8123
LS End Star Brg Load (lb)	5653

10 PSI

Time	0 - 1 Min	1 -2 Min	2 - 3 Min	3 - 4 Min	4 -5 Min	5 - 6 Min	6 - 7 Min	7 -8 Min	8 - 9 Min	9 -10 Min
Compressor Speed	36306	20000	12000	7500	5000	3000	2500	2000	1500	1500
Speed Decrease (%)	0	45	67	79	86	92	93	94	96	96
Comp Starwheel Speed	11685	6437	3862	2414	1609	966	805	644	483	483
Starwheel Brg Load (%)	50	15	5	2	1	0.3	0.2	0.2	0.1	0.1
Starwheel Brg Load (lb)	2827	858	309	121	54	19	13	9	5	5
Spindle Brg Oil Flow (igpm)	2.8	1.2	0.7	0.5	0.3	0.2	0.2	0.1	0.1	0.1
LS Shaft Speed	3690	2033	1220	762	508	305	254	203	152	152
Ø3.0" LS Brg Oil Flow	1.1	0.6	0.4	0.4	0.3	0.2	0.2	0.2	0.1	0.1
Ø6.5" LS Brg Oil Flow	8.1	6	5	4.5	3.7	2.6	2.3	2.1	1.8	1.8
Tooth Mesh Oil Flow	15.5	15.5	15.5	15.5	15.5	15.5	15.5	15.5	15.5	15.5
HS Cplg Teeth Oil Flow	0.9	0.9	0.9	0.9	0.9	0.9	0.9	0.9	0.9	0.9
Total Flows (igpm)	42.3	30.1	25.9	24.2	22.1	20.3	20.0	19.2	18.8	18.8

Total Vol.	**242**	**Gallons (imp)**
	291	**Gallons (US)**
	1100	**litres**

Legend

Bearing oil flows (predominantly speed dependent)

Spray nozzle oil flows (predominantly pressure dependent)

291 gallon drop tank capacity required for gearbox alone with 10 minute rundown assumption

Option 1: Power Loss Rundown – Gravity Drop Tank

- **Calculated rundown time of ten minutes**
  - **Gearbox: 291 gallons over ten minutes**
  - **Motor: XX gallons over ten minutes (conservative assumption, local oil rings)**
  - **Compressor: XXX gallons over ten minutes**
- **Cobey, Inc calculated system requirements 45 gal/min for the ten minute run down time**
  - **500 gallon drop tank**
  - **Main reservoir ~2300 gallons**

Option 2: Power Loss Rundown – DC Back Up Motor

- Same rundown time requirements as Option 1
- 2 HP 180 volt D-C motor
  - Loss of power detected by transfer switch and automatically starts DC motor
  - Loss of flow detection by control system commands DC motor to start
- Main reservoir tank reduced to ~1800 gallons

Drop tank vs. DC back up

Drop tank

- **Pro**
  - **Inexpensive**
  - **No controls –one line operation**
- **Con**
  - **Because of our rundown time – we require an unusually large tank~500 gallon -space is an issue**
  - **Increased size of the main reservoir due to rundown tank size-space is an issue**

DC backup

- **Pro**
  - **Small main reservoir**
  - **System is tunable for rundown time –add or subtract batteries**
- **Con**
  - **More expensive**
  - **Additional equipment required –batteries, transfer switch and charger cabling etc.**

Rundown recommendation

- **D-C rundown system**
  - **Will fit into current design for main reservoir and keep civil on schedule**
  - **System is tunable**
  - **Often used in industrial applications**
  - **Additional expense of ~$10K**

Lube system arrangement

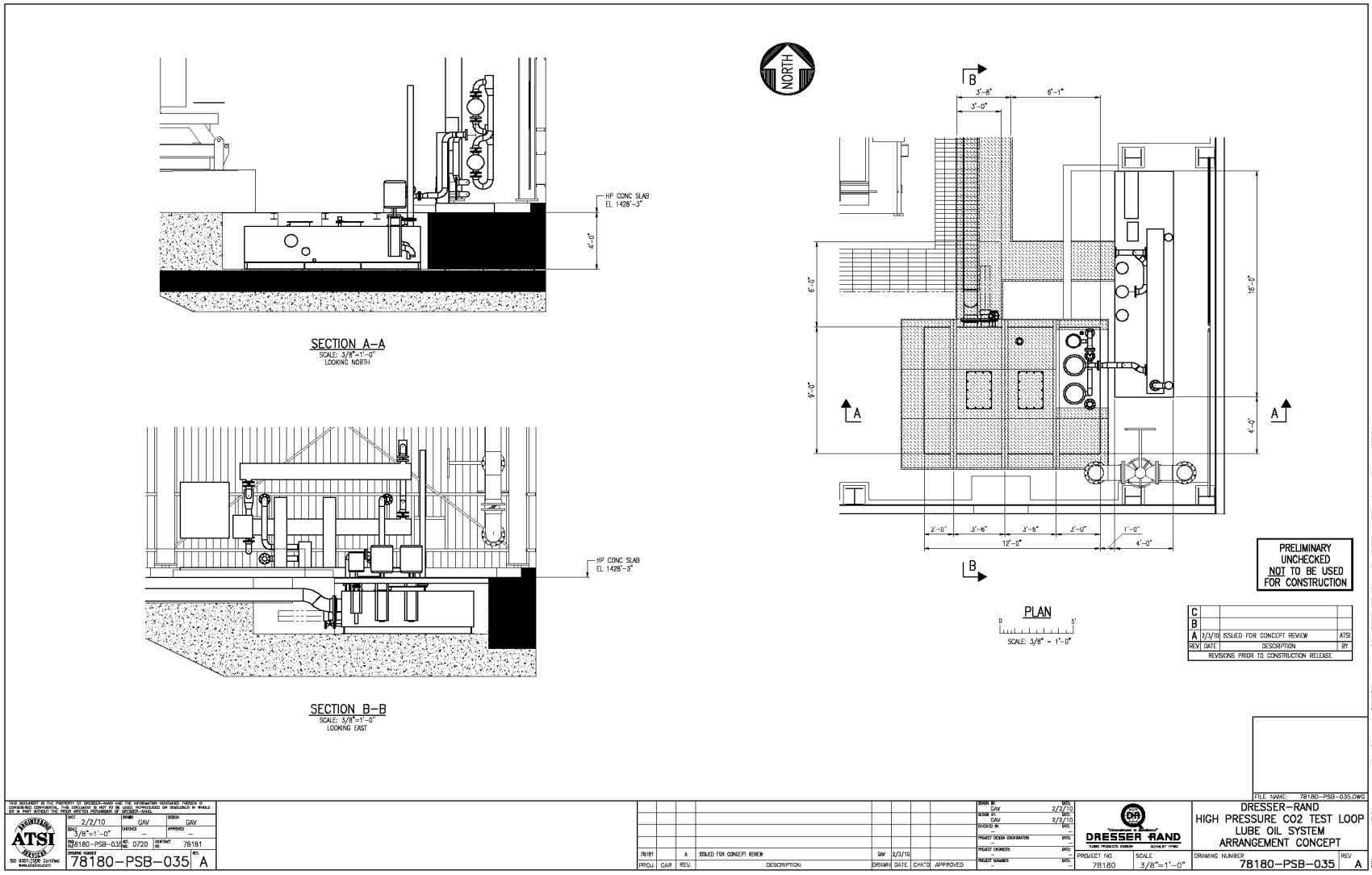

Oil reservoir layout

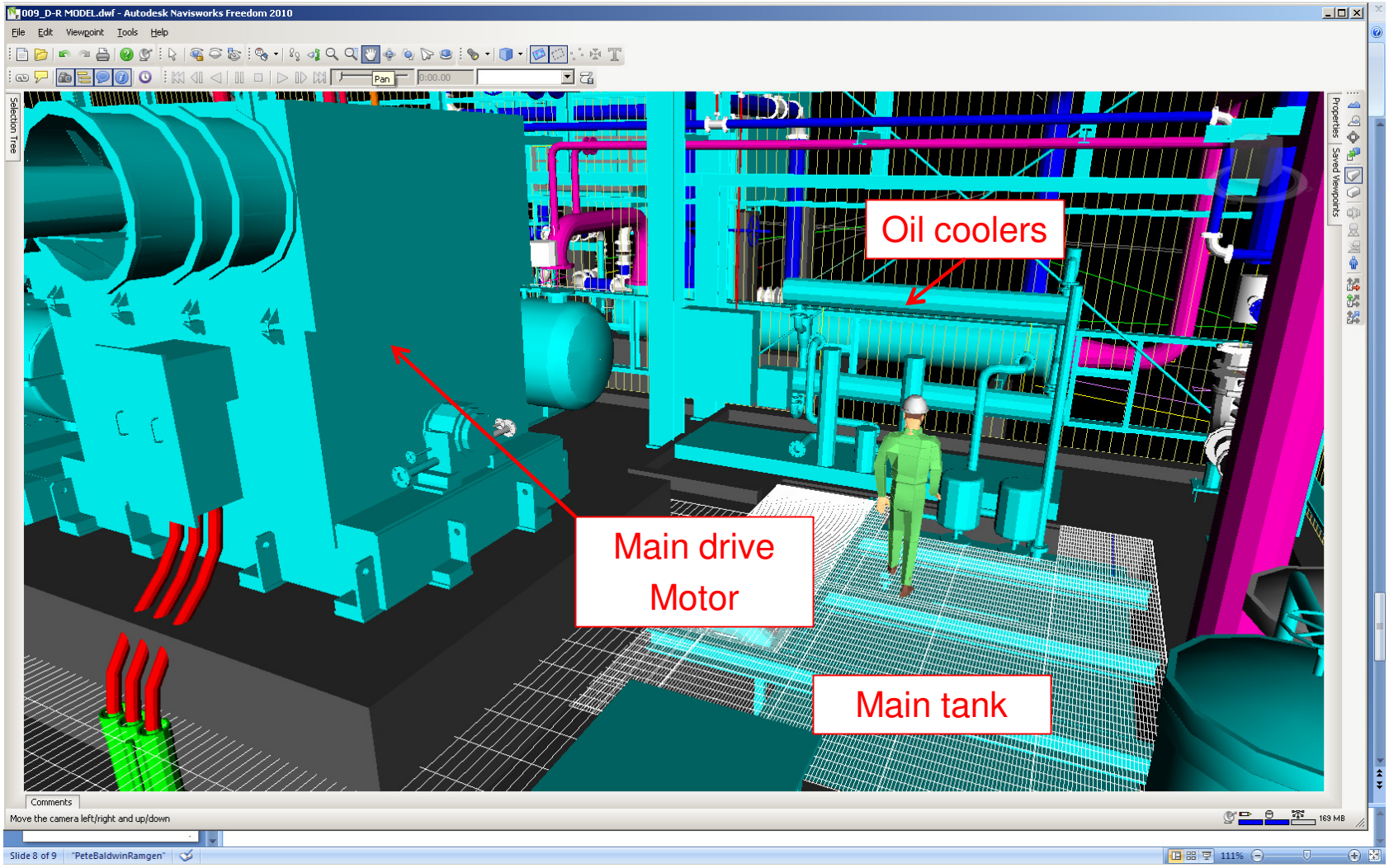

Layout

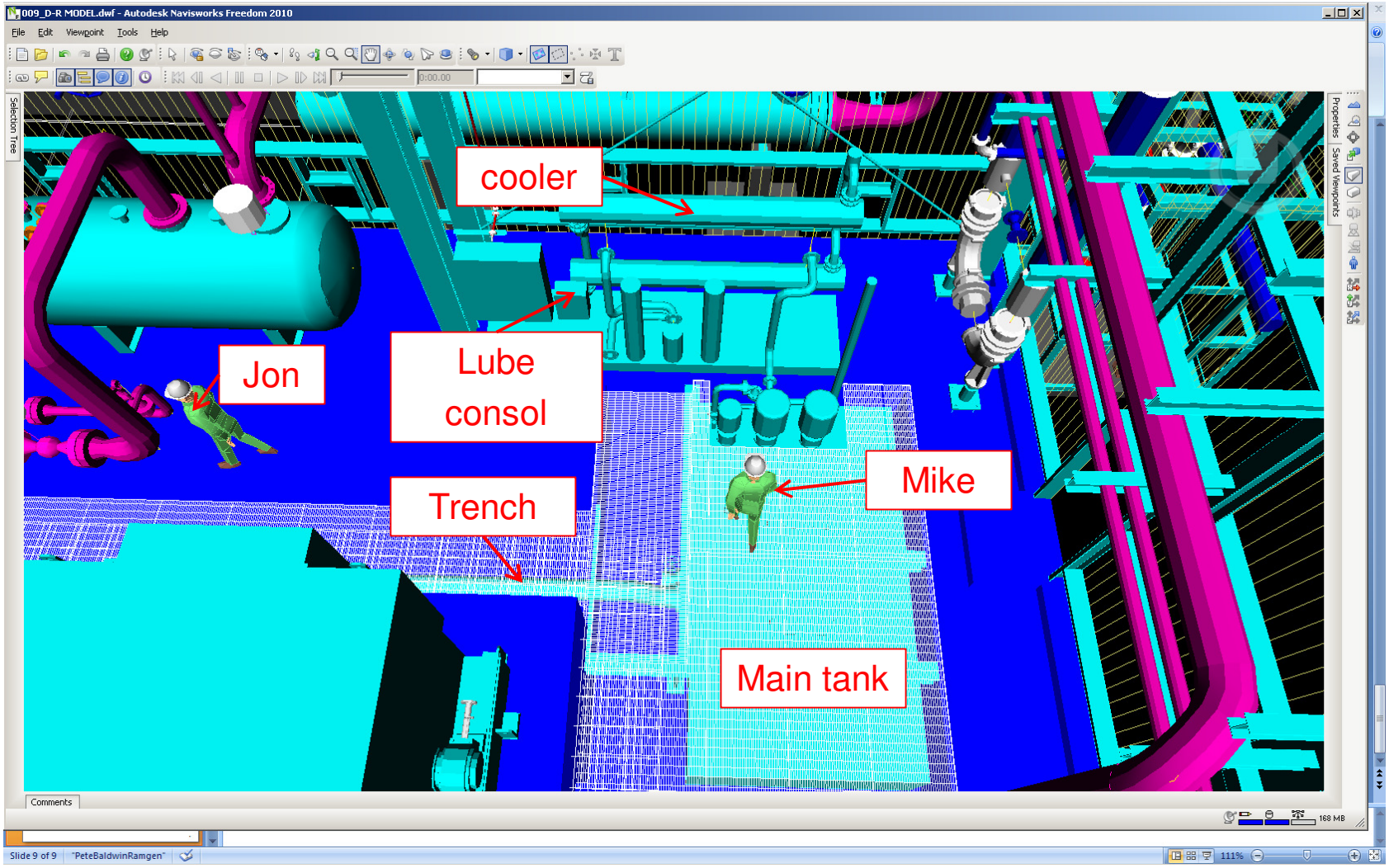
009_D-R MODEL.dwf - Autodesk Navisworks Freedom 2010
File Edit Viewpoint Tools Help
cooler
Jon
Lube consol
Mike
Trench
Main tank
Comments
Slide 9 of 9
"PeteBaldwinRamgen"

Budget and schedule

- **Current budget - $175,000**
  - **Cobey quote - $168,000 (DC back up option) + ~$10,000 additional facility electrical equipment for DC motor**
  - **Oilquip – still waiting for quote**
  - **Trola – no quote**

- **Delivery is ~16 weeks after order –August delivery to facility fits in schedule**

Conceptual Design Review

CO2 Flow Loop

System owner(s):

Karl Guntheroth

John Beers

2/4/2010

Rev 3/2/2010

System Definition and Scope

- **This system encompasses the valves, pipes, heat exchangers and other equipment which handle CO2 outside the Rampressor in a closed loop.**
- **Interfaces are typically Rampressor Case flanges. See ..\Pressure Case - CDR.pptx and ..\Secondary Flows_CDR2.pptx for sizes and locations.**

Summary of function

1. The function of the core closed loop is to take the Rampressor discharge gas and reduce the temperature and pressure so that it can be returned to the Rampressor suction side. Core loop is in black on PFD.
2. Secondary flows from the Rampressor are also returned to the core loop after cooling and compressing where required. Secondary flows are in red and green on PFD.
3. CO2 is stored as liquid supplied to the closed loop as vapor by a make up system, shown in blue on PFD.
4. Measurements of pressure, temperature and mass flow are taken in accordance with PCT-10.

Missing Requirements/Design Goals

1. **Fwd and Aft performance bleed pressure and flow tabulated for operating point.**
2. **Discharge pressures available for ejector tabulated for operating point.**
3. **Leakage estimates based on latest model tabulated for operating point.**
4. **Final Case port arrangement and sizes**
5. **Starting bleed flows and pressures. Delete aft starting bleed?**
6. **PCT-10 owner has not defined instrumentation requirements.**

Functional Requirements/Design Goals (cont.)

1. **Shaft leakage is up to date.**
2. **Rim leakage cascade is from November 2009. Worst case only.**
3. **Bleed requirements are sketchy, and only for design pioint.**
4. **Discharge pressure schedule is from “Injection Era”.**

Functional Requirements/Design Goals (cont.)

1. **Operations requirements:** ..\..\..\Demo Unit Mechanical Systems\Controls & Instrumentation\process control revD 20100127.doc

Functional Requirements/Design Goals (cont.)

1. **A 3-5 micron gas filter is to be placed in the suction line of the test loop to protect the compressor from foreign object damage.**
2. **Both compressor suction lines' mass flow, temperature and pressure shall be measured independently. The accuracy of these measurements shall be within 1% of measured variable and according to ASME PTC-10 guidelines. Discharge and secondary flows noted in the PFD shall also be measured within the greater of +/-1% or +/-0.05 lbm/s. Measurement of starting bleed is desired but not required.**
3. **Control of the suction pressure shall be maintained to a remotely adjusted set point of nominally 220 psi within +/-2% of the measured value and according to ASME PTC-10 guidelines. The suction pressure in this line may change up to 10% for up to one minute in response to a change in mass flow between 86 and 69 lbm/s caused by rotor start or unstart.**
4. **The suction gas temperature shall be controlled to a remotely adjusted nominal setpoint of 100 ^{o}F +/- 1 ^{o}F and according to ASME PTC-10 guidelines. Thermostat arrangement shall avoid boiling coolant in heat exchangers with CO2 at 650 ^{o}F.**
5. **The pressure drop (flow resistance) with discharge valves open shall produce discharge pressure less than 135% of suction pressure for the *un-started condition*.**
6. **The flow resistance with discharge valves open shall produce discharge pressure less than 170% of suction pressure for the *design point condition.***

Functional Requirements/Design Goals (cont.)

7. The compressor discharge valve(s) position shall be controlled remotely to produce +/- 2% resolution at the minimum flow according to ASME PTC-10 guidelines (2,420 psia, 500 ^{o}F, 76 lbm/s). This is expected to require a minimum of two valves in parallel to achieve required control resolution.
8. The suction side piping system shall provide enough gas volume in the loop and make up gas necessary to ensure stable operation. The volume shall take into account starting bleed, and discharge density changes. This requirement is estimated to be met with a 300 cubic ft Plenum Tank operating between 220 and 300 psia.
9. The bleed piping shall be capable of removing TBD lb/s of gas during Starting Bleed. This will be accomplished from two (2) compressor connections with maximum static pressure at connection of 60 psia.
10. A vent header around the building and a small stack running up the side of the building shall be included to vent CO2 to a safe location.
11. The test loop shall include a provision to bleed gas from the system and measure charge purity. Manual sample collection may be acceptable.
12. The CO2 delivery system shall supply a steady make up flow as required to compensate for CO2 leakage - see table 2.
13. The CO2 delivery system shall provide short term (<1 minute) make up CO2 to compensate for starting bleed- see table 2. This requirement is estimated to be met with a 600 cubic feet tank operating between 500 and 220 psia.

Functional Requirements/Design Goals (cont.)

14. **A make up CO2 evaporator heat exchanger to maintain a CO2 vapor feed must be able to operate on fuel or steam (not dependent on ambient temperature).**
15. **Liquid pumped from the liquid CO2 tank shall be replaced with vapor regulated to maintain the lesser of 250 psi or 50 psi below relief valve pressure. Excess vapor due to evaporation from the tank shall be vented to maintain maximum pressure as required by tank manufacturer.**
16. **A CO2 system shall be included to reduce CO2 release. This system may pump the loop down at the end of each test and recover the CO2 into a vessel where it can be re-used during the next test cycle, or employ other methods that are safe and economical.**
17. **Critical performance measurements will be redundant and in accordance with ASME PTC-10 guidelines.**
18. **The accuracy, quantity, and locations of measurement instrumentation shall meet the requirements by the latest version ASME Performance Test Code 10 - Compressors and Exhausters, and additionally as defined by the Company.**
19. **Permissible fluctuation requirements for the test loop controls are specified in ASME Performance Test Code 10.**
20. **Like branches of pipe shall be constructed to have equal flow characteristics.**
21. **Auxiliary compressors and controls shall be able to handle the full range of flows noted in Table 2.**
22. **Vendor shall demonstrate that variations in secondary flows and compressor outputs do not disrupt suction conditions, or propose a design that produces better control.**
23. **A safety pressure relief device must be included on the compressor discharge piping upstream of valve V-2.**

Baseline PFD

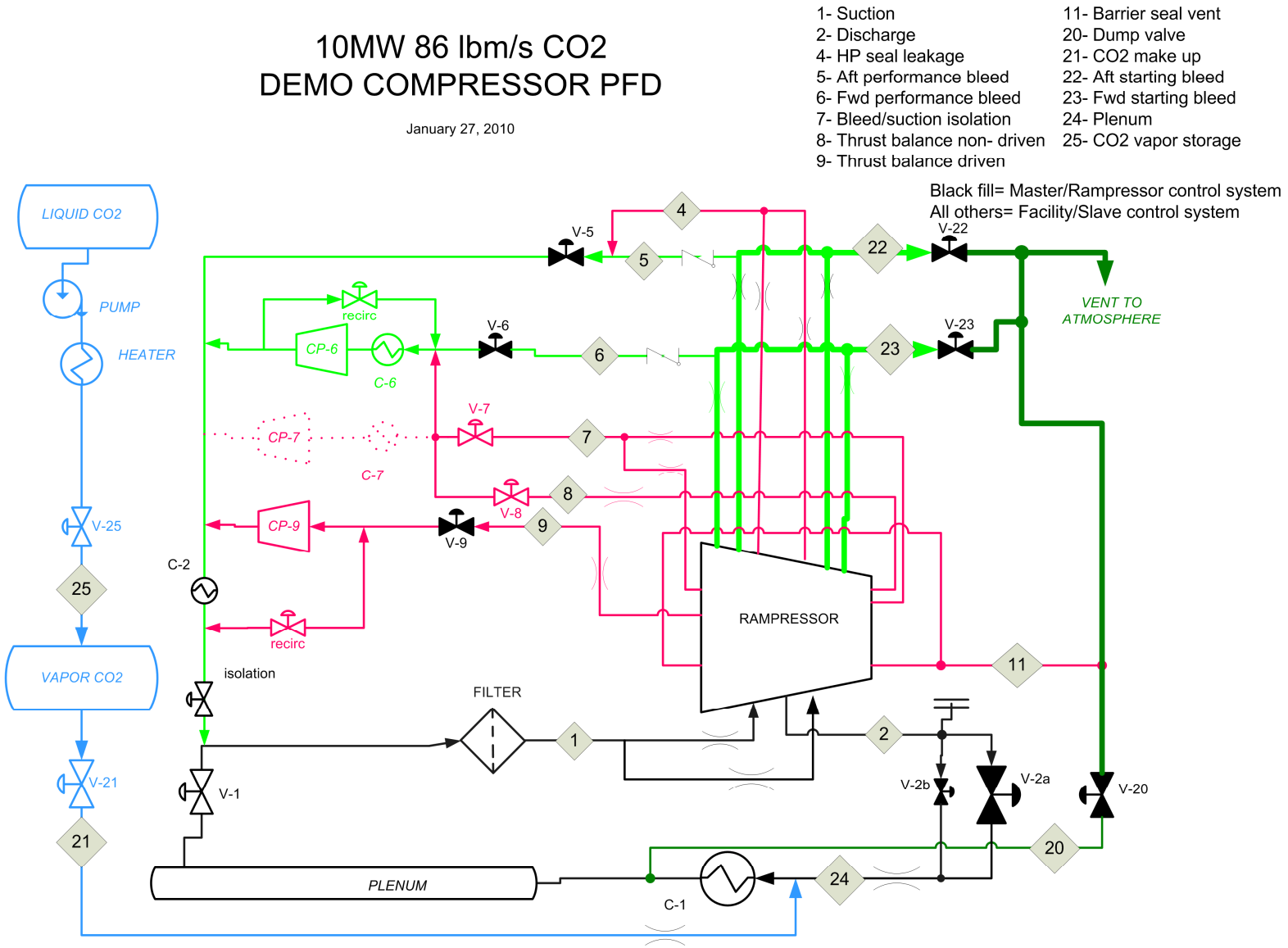

PFD option 1

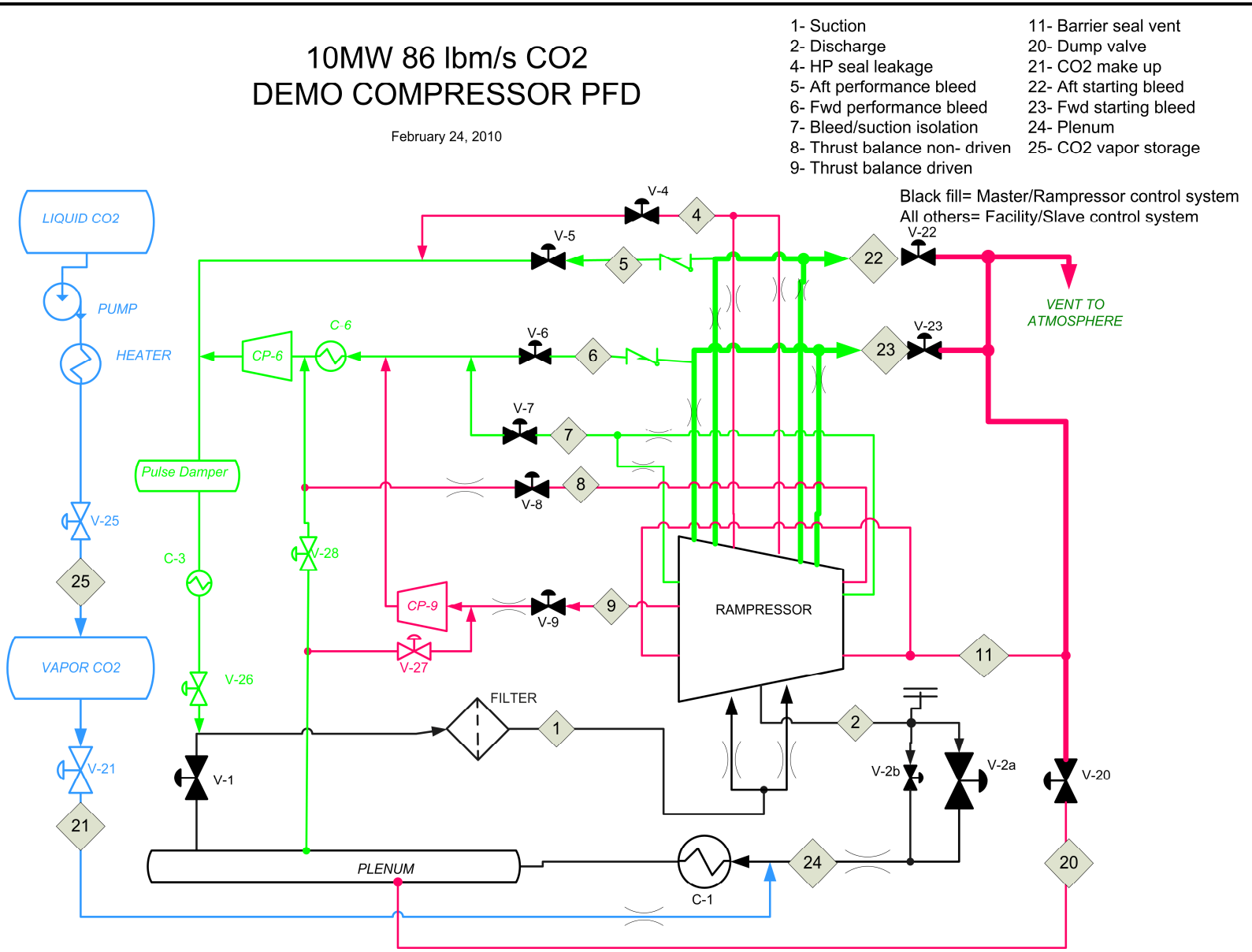
10MW 86 lbm/s CO2
DEMO COMPRESSOR PFD
February 24, 2010
1- Suction
2- Discharge
4- HP seal leakage
5- Aft performance bleed
6- Fwd performance bleed
7- Bleed/suction isolation
8- Thrust balance non- driven
9- Thrust balance driven
11- Barrier seal vent
20- Dump valve
21- CO2 make up
22- Aft starting bleed
23- Fwd starting bleed
24- Plenum
25- CO2 vapor storage
Black fill= Master/Rampressor control system
All others= Facility/Slave control system
LIQUID CO2
PUMP
HEATER
VAPOR CO2
CP-6
C-6
Pulse Damper
C-3
CP-9
V-4
V-5
V-6
V-7
V-8
V-9
V-22
V-23
V-25
V-26
V-27
V-28
V-21
V-1
V-2a
V-2b
V-20
FILTER
RAMPRESSOR
PLENUM
C-1
VENT TO ATMOSPHERE
1
2
4
5
6
7
8
9
11
20
21
22
23
24
25

PFD Option 2

10MW 86 lbm/s CO2
DEMO COMPRESSOR PFD
Secondary compressor discharge to plenum

February 26, 2010

1- Suction
2- Discharge
4- HP seal leakage
5- Aft performance bleed
6- Fwd performance bleed
7- Bleed/suction isolation
8- Thrust balance non- driven
9- Thrust balance driven
11- Barrier seal vent
20- Dump valve
21- CO2 make up
22- Aft starting bleed
23- Fwd starting bleed
24- Plenum
25- CO2 vapor storage

Black fill= Master/Rampressor control system
All others= Facility/Slave control system

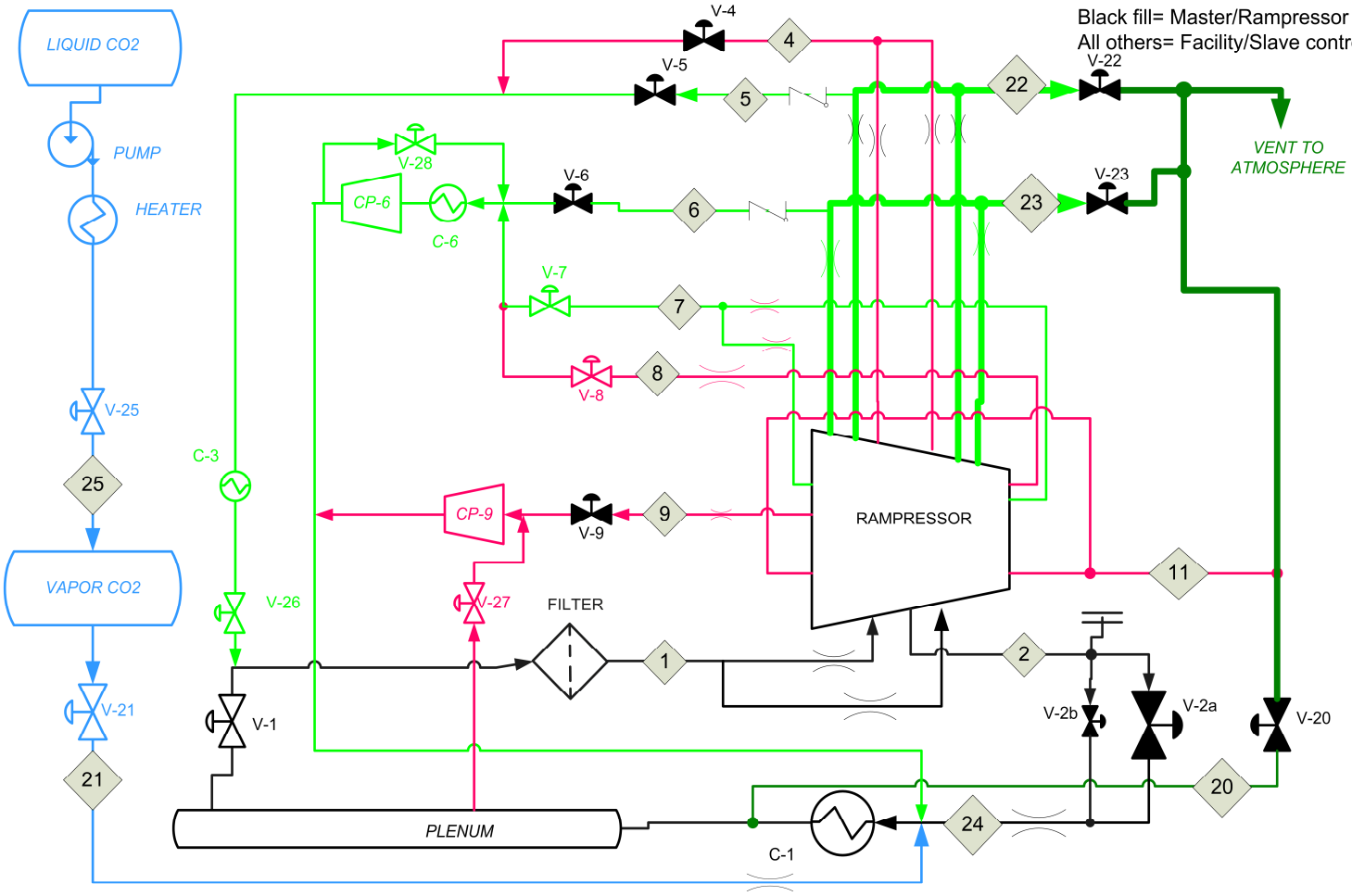

Comparison continued

RAMGEN POWER SYSTEMS ™

- Option 2 could use VFD to save power at reduced load, but at full load uses 50% more power and $100,000 capital cost. At half load saves 25%. VFD adds $125,000. At full power for 1000 hours uses $1800 more electricity, at half power saves $9000.
- Option 2 reduces the plenum capacity. The plenum pressure cannot exceed the discharge pressure of the auxillary compressors. In option 1 and Baseline, the plenum can fluctuate between 250 and 500 psia to damp out disturbances such as starting bleed.
- Cost of discharging 1 lbm/s @ $.12/lb for 900 hours is $390,000. It is cheaper to buy a conservative compressor than to risk to venting excess.
- Option 3 is same as 2 except it adds a 140 hp compressor for Aft bleed discharging to the plenum.

Changes to PFD option 1

RAMGEN POWER SYSTEMS ™

- V-28 and V-27 provide recirculation to the secondary compressors. These valves are set to control the compressor suction pressures. These valves are supplied from the plenum, which allows the secondary compressor discharge mass flows to be constant even if the secondary flows vary, allowing more stable control of Rampressor suction pressure.
- V-26 represents a requirement that the secondary flows be isolated from the Rampressor, but the valve location is optional.
- CP-9 is shown as feeding into CP-6. This is optional. In this configuration CP-9 is a single stage using C-6 as an intercooler and CP-6 as the second stage. This is intended to be simpler than CP-9 being two stages with it's own intercooler. Total power is not changed.
- "leakage" flows are shown in pink.
- Bleed flows are shown in green.
- A volume was added as a pulse damper to prevent discharge pulses from CP-6 from affecting Rampressor suction.

Optional PFD with Ejectors

10MW 86 lbm/s CO2
DEMO COMPRESSOR PFD

January 27, 2010

1- Suction
2- Discharge
4- HP seal leakage
5- Aft performance bleed
6- Fwd performance bleed
7- Bleed/suction isolation
8- Thrust balance non-driven end
9- Thrust balance driven end
11- Barrier seal vent
20- Dump valve
21- CO2 make up
22- Aft starting bleed
23- Fwd starting bleed
24- Plenum
25- CO2 vapor storage

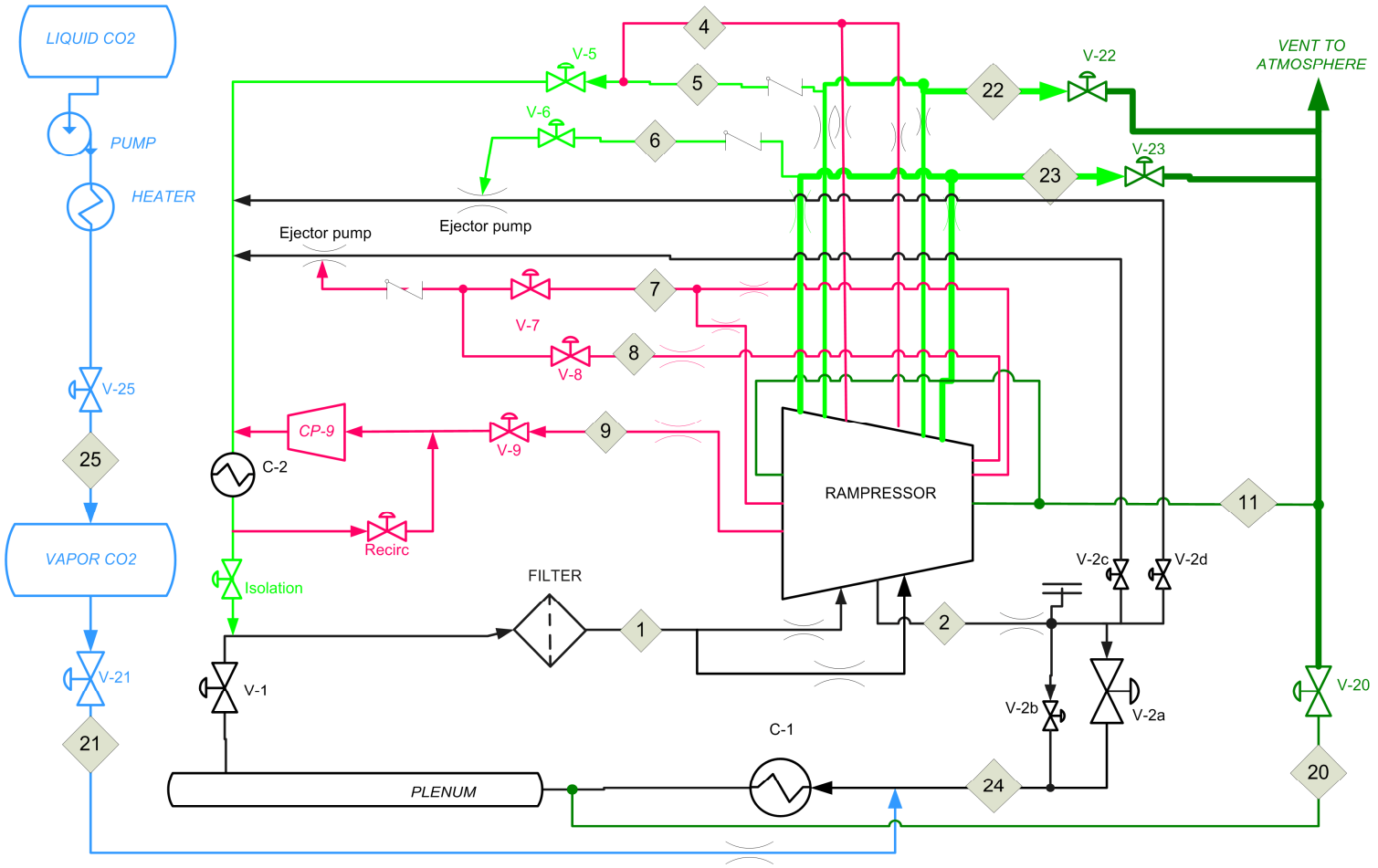

Estimated Ejector Performance

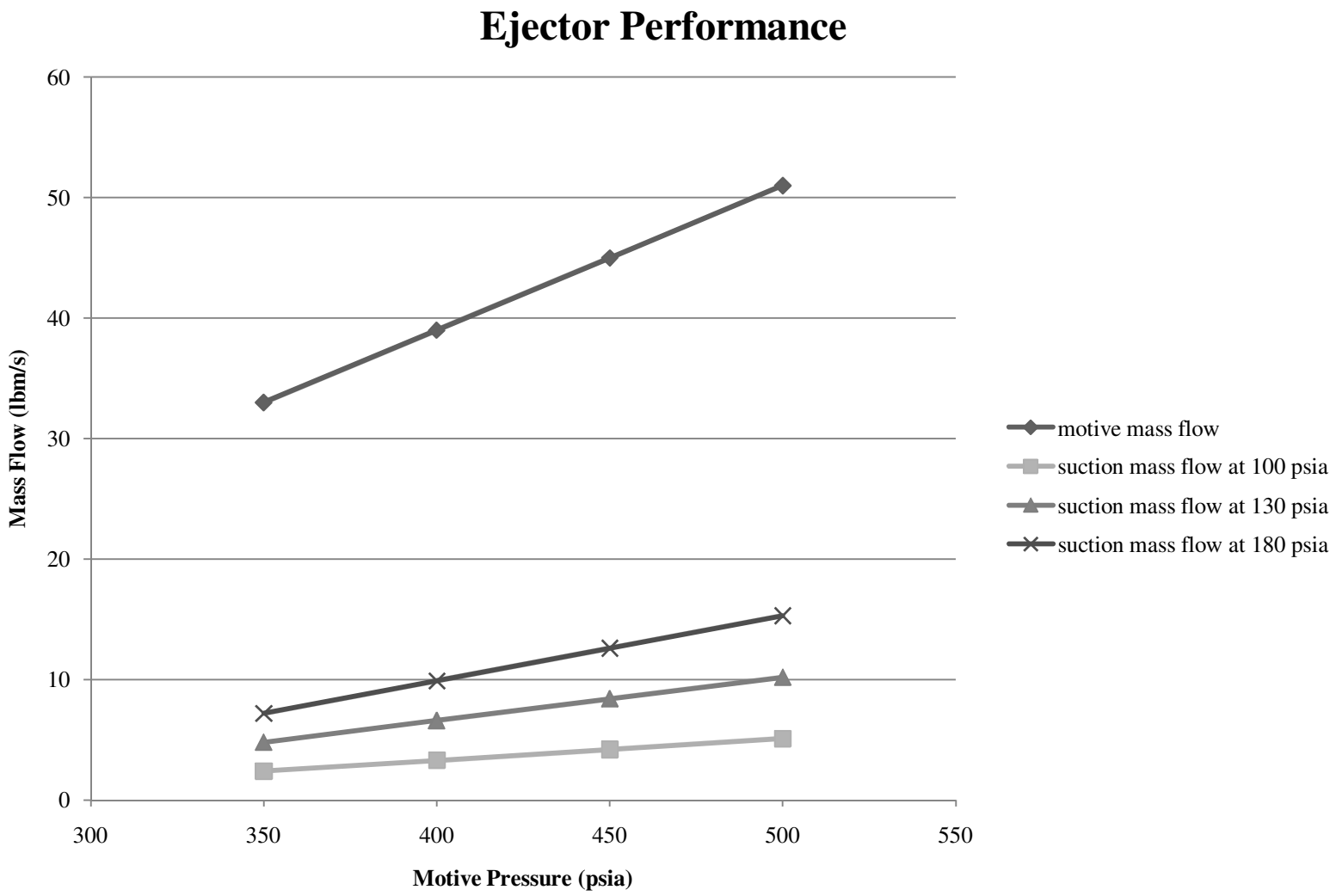

Ejector Vs Compressor

- **Ejectors require at least 400 psia discharge to operate. Aero has only committed to 300 psia.**
- **Operation with ejector "off" may be acceptable at low back pressure. Low suction on fwd performance bleed.**
- **Ejectors bypass 1/3 of Co2 around suction pressure control valve, reducing control leverage.**
- **Two Ejectors are <$50,000, 3-4 month lead time**
- **Compressor is $250,000, 4 month lead time, adds to heat load, adds to electric load, guess $50,000 additional.**
- **Thrust balance by compressor functions at any speed. Compressor Only 30 hp.**

Design pressure

1. **Design for Discharge pressure 2685 psig (2700 psia) @ 650F for 22% margin. This is standard for class 1500 flanges.**
2. **ASME Relief valves provide +/-3% tolerance UG-126 (d).**
3. **Rampressor Case is being designed to higher pressure.**
4. **Will increase to 2940 psig if cost impact is small. Valves appear to be available, but flanges have not been located.**
5. **Could change to 2735 psig (2750 psia) @ 600F with same materials for 25% margin. Relief valves (not rupture disk) provide +/-3% accuracy and will reseat.**
6. **Most of system is designed for settle out pressure, expected to be 450 psi. OK for class 300 flanges rated 550 psia @ 600 F.**

Impact of water in CO2

- **Cost wise, ATSI answered that in the FEED. D-R also answered it in the ICS and would not fund the difference. I found that stainless adds about 1/3 to valve costs, but with higher class it might be 1/2. Pipe material cost is about 4 times, higher class might make that 6 times.**
- **PTC 10 does not require simulating corrosion conditions. PTC 10 only requires that the mole weight of the gas be the same in test as in the application (unless you want to do math to prove similarity- then even mole weight is up to you). Separate corrosion tests would reduce risk to the rig and allow multiple materials to be evaluated.**
- **Suction gas saturated with water was studied for AEP. We planned to use a drier to remove enough water that condensation could not form at IGV discharge conditions to protect the rotor from erosion. Mike may be able to add more, but John and I did not see much discussion in the AEP final report.**
- **You can't be saturated without liquid water being present/possible. I don't think there are any places in the pipe where water will tend to drop out in operation as it would in a high pressure after-cooler. Water would tend to stay vapor as pressure drops durring venting/leakdown, but would condense cooling off. We would want to look carefully at the temperature of gas in any choked valves. I think all low points should have drains anyway, but they would be operated more. The filter will remove 99+% oil or water droplets and has a drain. Heat exchangers use stainless tubes already since they are wet on at least one side. Valves and compressors must be specified for humidity, but they use a lot of stainless on parts where surface finish is critical. Stainless may require switching to higher flange classes, because it is weaker. Higher class and stainless both add to cost and lead time for valves and pipe**

Design Work Plan

- **Design by ATSI**
- **Dynamic pipe analysis by Norm Samurin, PE**

Budget and Schedule

- SSR – Not scheduled- see FEED
- CDR – February 4, 2010
- PDR - March 4, 2010
- FDR - March 25, 2010
- Need by dates
  - Component purchase orders for Valves, Compressors, Heat exchangers
  - Release to pipe fitters
  - Validation test November 1, 2011
- Other dates
  - Firm design of Rampressor interfaces and leakage rates TBD
  - Firm Aero requirements for bleed and other operations TBD
- Current budget
  - Hardware: Part of Facility
  - ODC's: $30,000 (QMC)

RAMGEN POWER SYSTEMS

Conceptual Design Review

Pressure Case System

System owner(s):

Jill Roulo

01-25-10

System Definition and Scope

- **The pressure case is the outer shell of the compressor that provides pressure containment, support of the inner bundle and through the heads and bearings ultimately support of the rotor. The case must allow for numerous connections including one discharge, two inlets and two six inch bleeds.**
- **The system includes the forged barrel, the nozzles, the shear ring and the retaining ring. The heads, non-drive end bearing housing and hydro plugs are also part of the pressure containing vessel and will need to be tested during hydro-testing.**

Design Goals

- A pressure vessel design that meets the ASME Pressure Vessel Code Section VIII Division 1 or Division 2.
- The case design approved by a Professional Engineer per ASME Pressure Vessel Code.
- Manufacturing of the pressure case such that it could be stamped as a coded pressure vessel.

Functional Requirements

- **The case must support the bundle.**
- **The different pressures between the inlet plenum and discharge volute must be separated by a seal against the case bore.**
- **The case will provide drainage for any liquids that collect in the bottom of the case.**
- **The case will be supported by feet that are near the centerline height of the compressor to reduce the amount of thermal growth in the vertical direction.**
- **The case will support the gearbox which will be integrally mounted to the case.**
- **The case will have provision for lifting the case with the bundle installed and the gear box as a unit.**

Functional Requirements continued

- The openings/nozzles will need to align with the openings in the internals and many will need to be sealed with bayonets.
- The case needs to allow the bundle to be installed though the non-drive end and held in place with a segmented shear ring and retaining ring.
- The case must be designed for the pressure and temperature expected during operation in a CO2 environment which could potentially be wet.
- The case will be bolted to the bundle cradle.
- The case will need an anti-rotation dowel to prevent the internals from rotating in the case.
- The case will need to provide planar and concentric alignment and adjustment for the gearbox mounting.

Important Interfaces

- **Electrical**
  - **The case must allow for the sealed exit of all instrumentation wiring and actuator linkages.**
- **Mechanical**
  - **The integrally mounted gear will have a low speed shaft end that must be aligned with and coupled to the motor.**
  - **The base plate will have pedestals that support the pressure case by its feet.**
- **Fluid**
  - **The nozzles and openings in the case must line up with the openings in the inner bundle.**
  - **Drains must be present on the bottom of the case.**

Design Concept #1

- **General description**
  - **Forged barrel with welded on nozzles.**

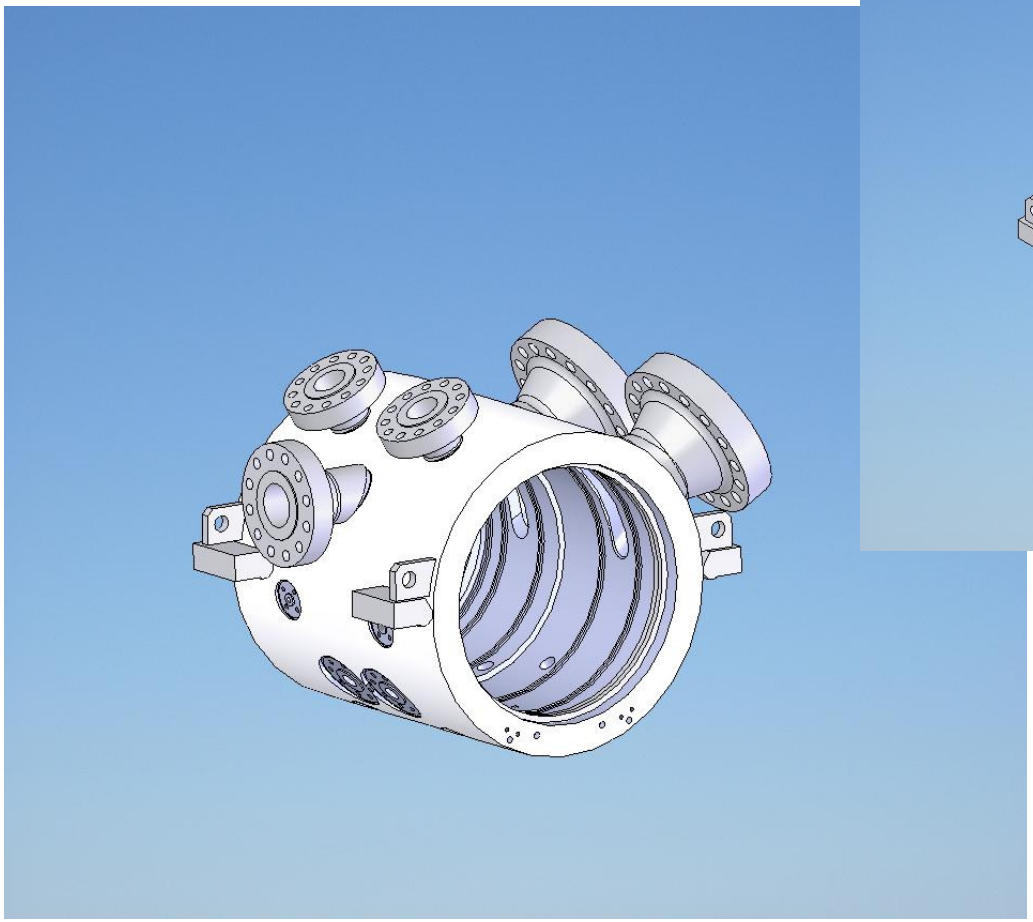

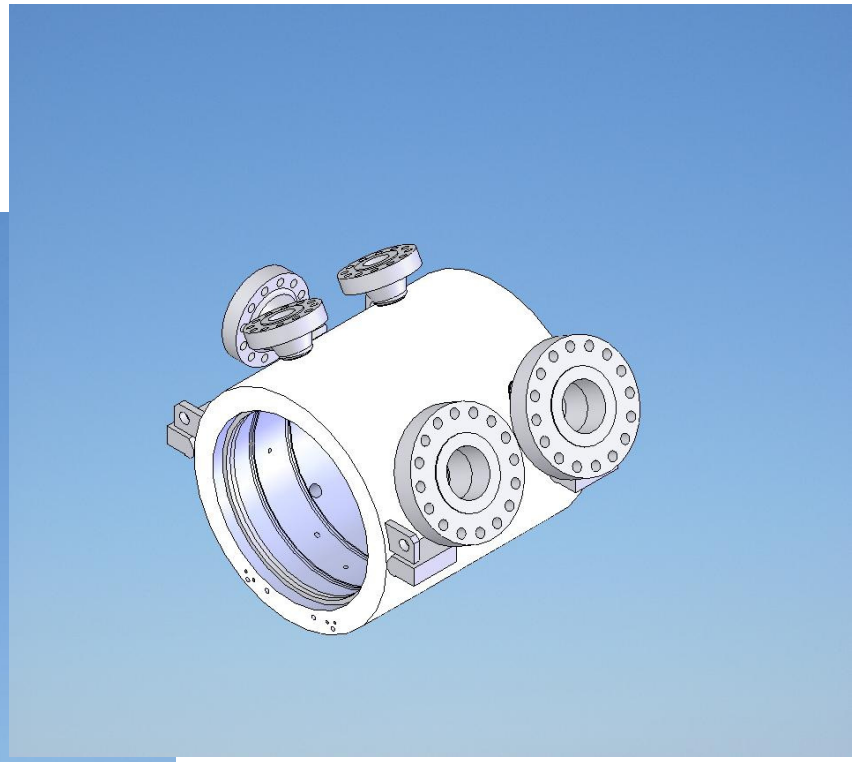

Design Concept #1

- **Pros**
  - **Reduced amount of steel needed compared to design concept #2**
  - **Proven design. (Similar to many of D-R's DATUM cases.)**
  - **Can use a combination of welded on and machined flats connections.**
- **Cons**
  - **Increased amount of welding compared to design concept #2**
  - **Castings are required for the complicated transitions for the inlets.**
- **Preliminary analysis results, etc.**
  - **Initial hand calculations suggest that the case barrel section must be at least 3.50 inches thick plus 1/8 inch for corrosion allowance.**
  - **Initial hand calculations suggest that the head must be 4.5 inches thick.**

Design Concept #2

- General description
  - Entire case made thick enough to accommodate all connections as machined flats on the case.
- Pros
  - The forging could be ordered early without concern for meeting the minimum thickness.
  - The amount of welding would be reduced from design concept #1.
  - No castings/patterns would be needed.
- Cons
  - The weight of the case would be considerably more than design concept #1.
  - The transition from oval to round for the inlets would have to be machined entirely into the case.
- Preliminary analysis results, etc.
  - Decided not to pursue this design.

Work Plan / Analysis Tasks

- **Outside contract support**
  - **We are planning to engage Becht Engineering in the analysis of the case. They will provide us with a design approved by a Professional Engineer. A technical specification of requirements has been written and a proposal has been submitted by Becht Engineering.**
- **FEA**
  - **The FEA analysis needed for the nozzles and the shear ring design will be performed by Becht Engineering.**
- **CAD**
  - **The Solidworks model will be the basis for all analysis performed.**
- **We are going to meet with Seattle Boiler and discuss their manufacturing capabilities and our design requirements**

Budget and Schedule

- PDR date – before February 12th
- FDR date – before April 14th
- Drawing Release date April 15th
- Estimated Manufacturing Time/Delivery date September 1st
- Any differences from master schedule?
- Is schedule achievable? Yes

- Current budget
  - Hardware - $450,000 including case, heads, shear rings and hydro tooling
  - ODC - $13,500
- Is current budget adequate?

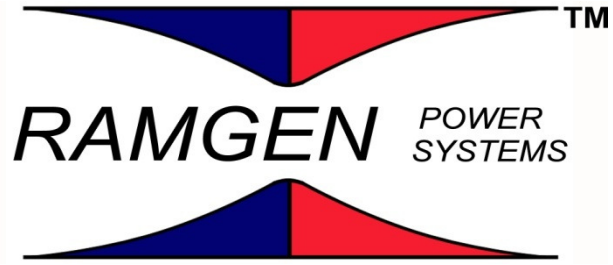

CO2 Demo Rig Assembly
Conceptual Design

June 2, 2010

Review Outline

- **Requirements**
- **Sub-assembly assembly and instrumentation**
  - **IGV**
  - **Diffuser bypass**
  - **Non-driven-end (NDE) shaft**
  - **Driven-end (DE) shaft**
- **Bundle assembly**
- **Bundle installation**
- **Thermal management**
- **Split rotor changes**
- **Assembly location**
- **Schedule**

Review Outline

RAMGEN POWER SYSTEMS™

Requirements

- **Allow for acceptable operation under all anticipated loading (pressure and temperature) conditions.**
- **Provide access for component inspection and replacement.**
  1. **Rotor inspection**
  2. **Diagnostic instrumentation**
  3. **Bearings**
  4. **Stationary diffuser replacement**
- **Minimize assembly complexity and time.**
- **Provide features to ensure alignment and avoid improper installations**
- **Maximize aerodynamic design flexibility (vs. layout optimization)**

IGV Cartridge Assembly

1. **Attach interior (717405) and exterior (717406) IGV shroud supports**
2. **Insert linkage pivot pins (717412) into linkage arms (717407 (NDE) or 717408 (DE)) and install into IGV unison ring (717411).**
3. **With unison ring and exterior IGV shroud support concentric, insert IGV (717401(NDE) or 717402 (DE)) and OD bushing into IGV shroud support and linkage end. Install IGV nut.**
4. **Sandwich IGV post and ID bushing between IGV hub supports (717404 (exterior) and 717403 (interior)).**
5. **Attach Hub seal land, if applicable.**

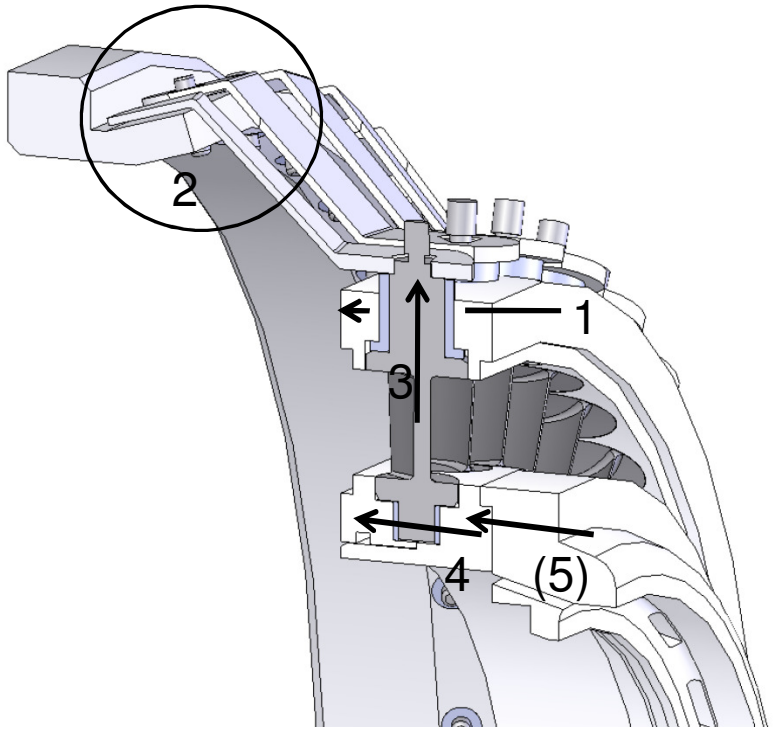

Instrumentation

1. **PE173N (PE171D); 8 channels**
2. **TE174N (TE172D); 8 channels**
3. **PE165N (PE163D); 8 channels**
4. **TE166N (TE164D); 8 channels**
5. **PE113N PE111D); 8 channels**
6. **TE114N (TE112D); 8 channels**
7. **PE244N (PE237D); 8 channels**
8. **TE245N (TE238D); 8 channels**
9. **PE248N (PE246D); 6 channels**
10. **TE249N (TE247D); 6 channels**

*** #6 and #8 may move to discharge assembly**

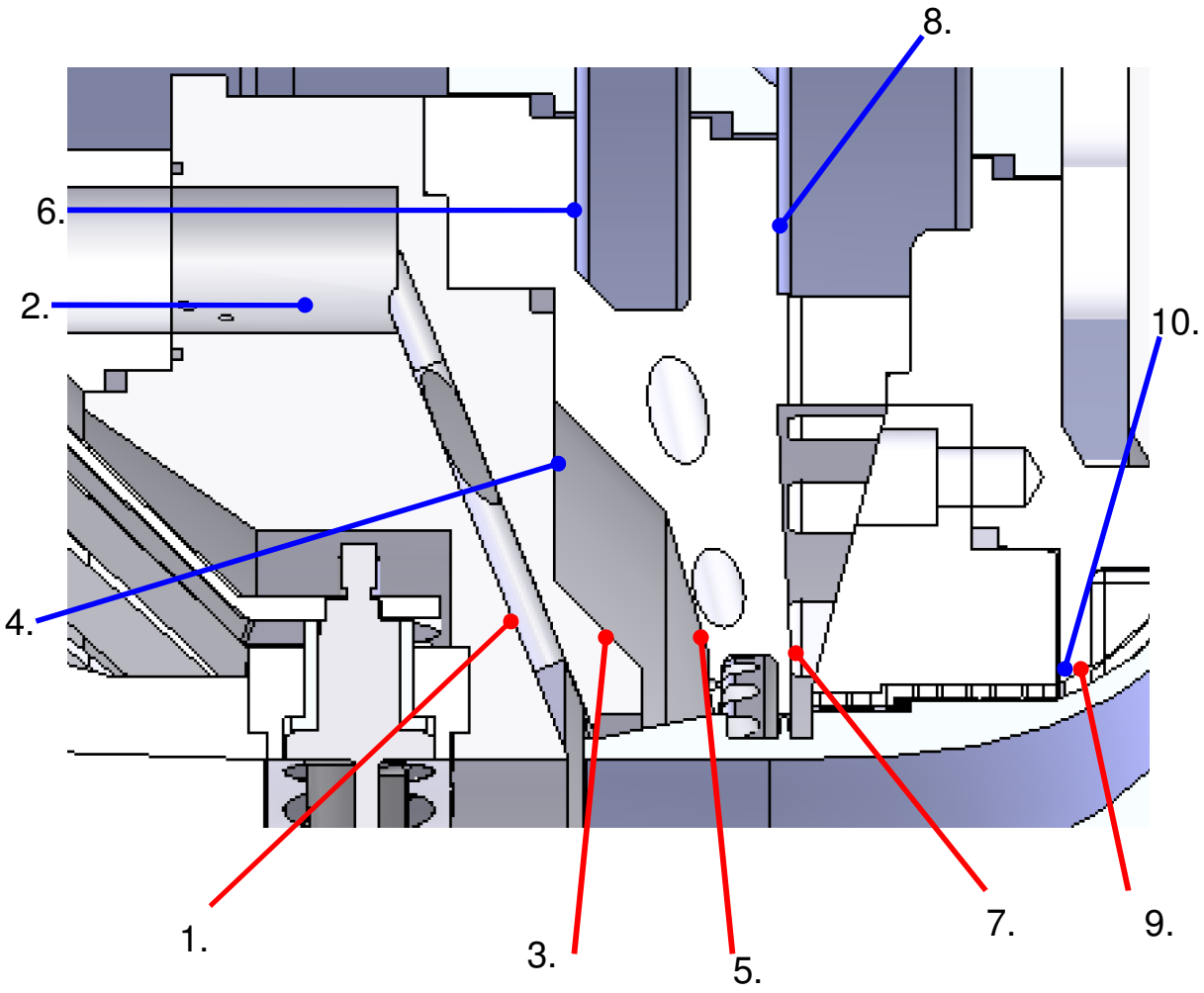

#. Non-Driven End (Driven End)

0900-01341

IGV cartridge instrumentation

- **IGV cartridge instrumentation**

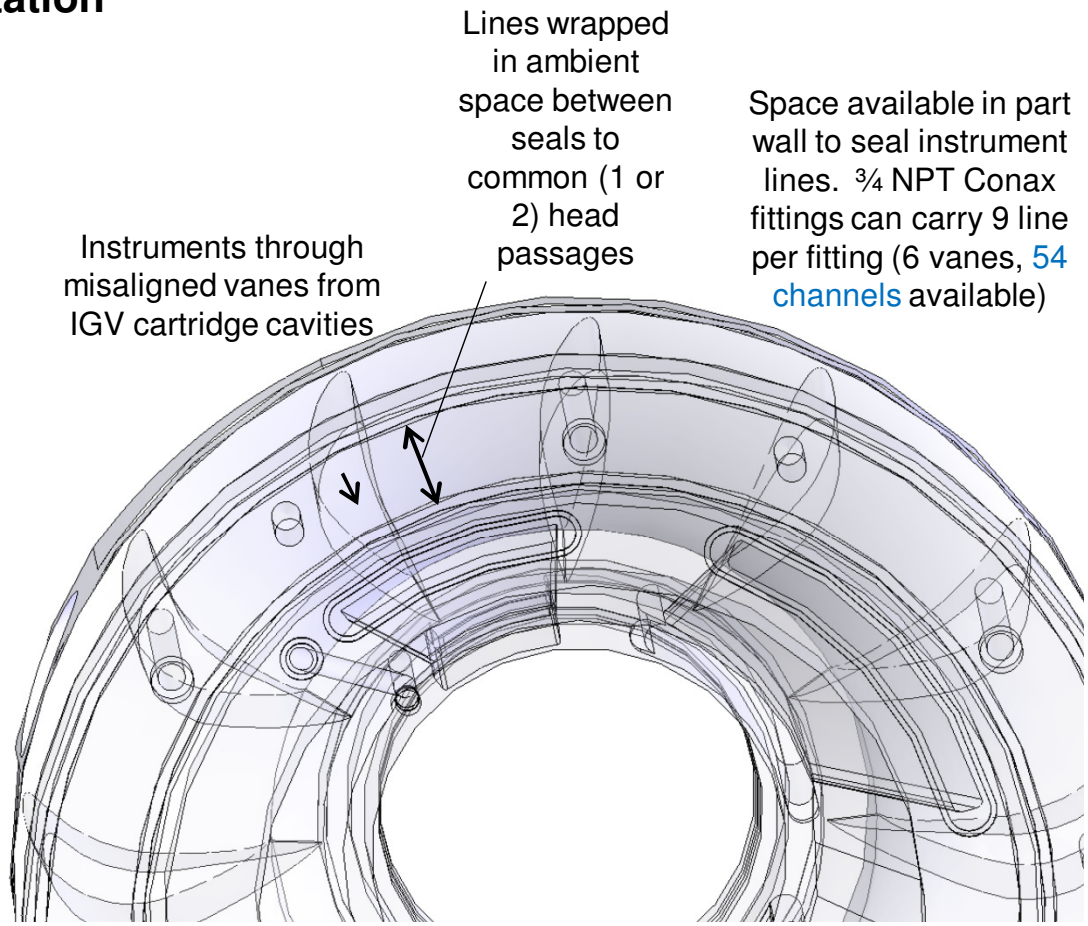

Bypass valve installation

1. **Install bypass dowel (717505), actuation rollers, pins, and thrust rollers into bypass actuator ring (717504 (or mirror)).**
2. **Assemble internal portions of actuation ring rod assembly.**
3. **Install bypass actuator ring into discharge volute (717603 (NDE) or 717605 (DE)). Then engage the bypass actuation ring rod end (717512).**
4. **Attach bypass plate (717503) (with dynamic pressure transducer, if possible) to bypass dowel.**
5. **Install bypass actuation coverplate (not shown)**

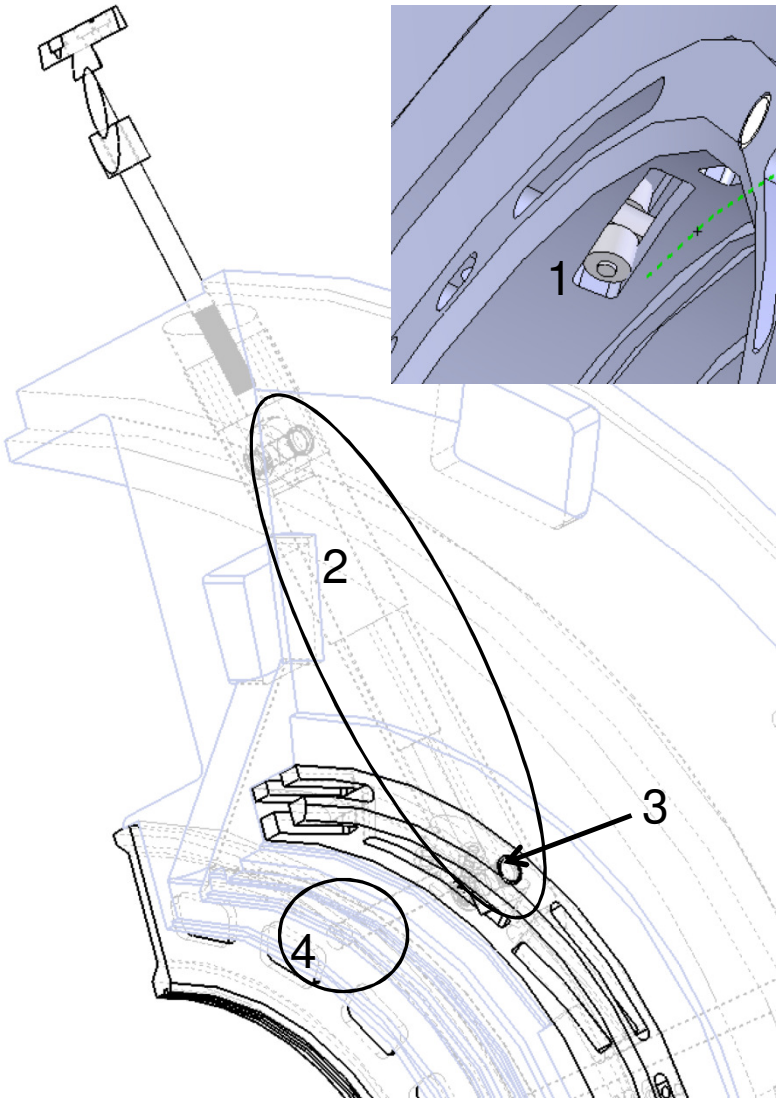

Static diffuser instrumentation

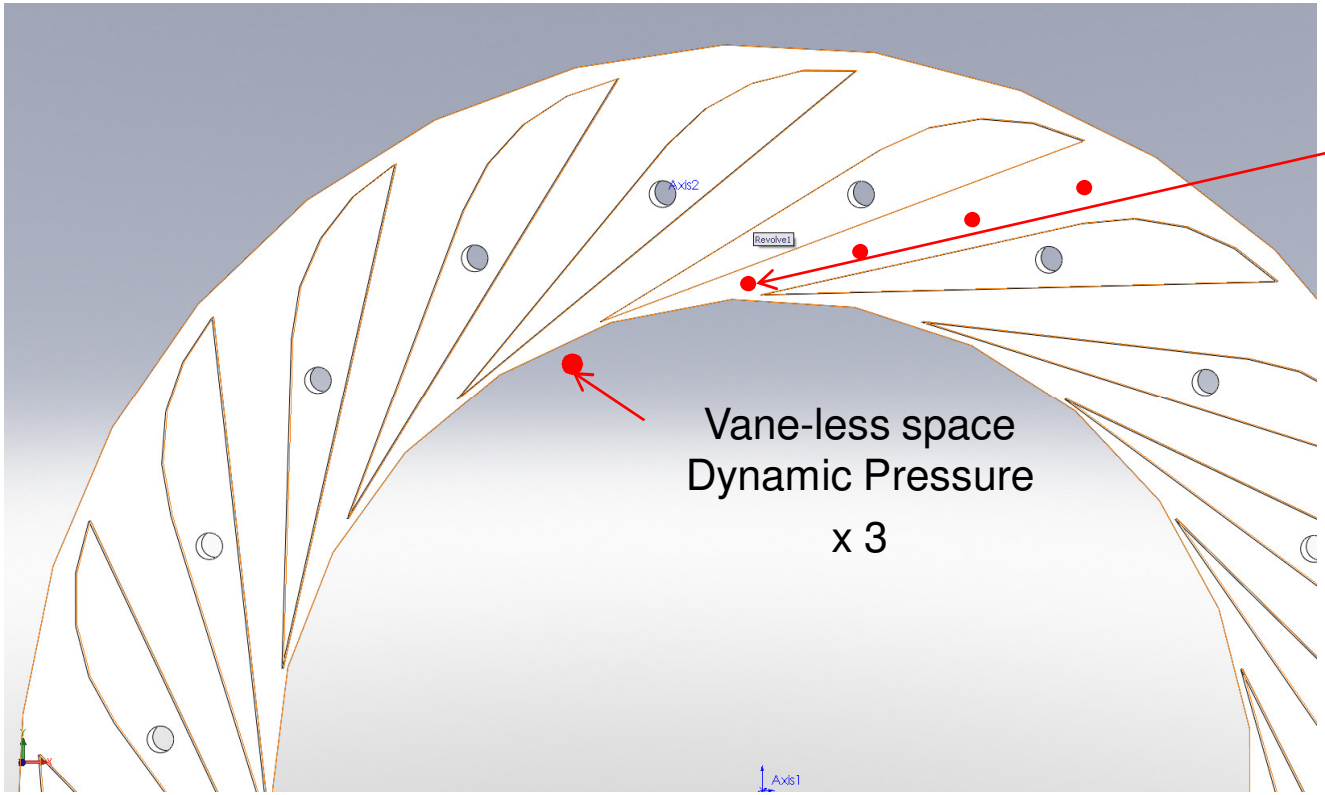

3 passages x4 Hub Ps Ports (PSDDSN40-50 & PSDDST40-50)

Aero Requested as many as can fit clustered around LE Throat Region. Note this region is currently inboard of the face seal and is in a region of thinning wall thickness.

Routing may include HP leakage and aft bleed cavity temperatures.

Embed pressure lines in back side of plate and route to a single location (at thickest part of vane accessible through boss cutout).

Static diffuser installation

1. **Attach vaned diffuser (717501) and stationary diffuser backing plate (717502) (as individual parts or as assembly) to the DE volute section (717605).**
2. **Route instrument lines (30-36 channels) to NDE side of rig (through diffuser vane).**
3. **Install centering keys and pressure rings as required for volute position control.**

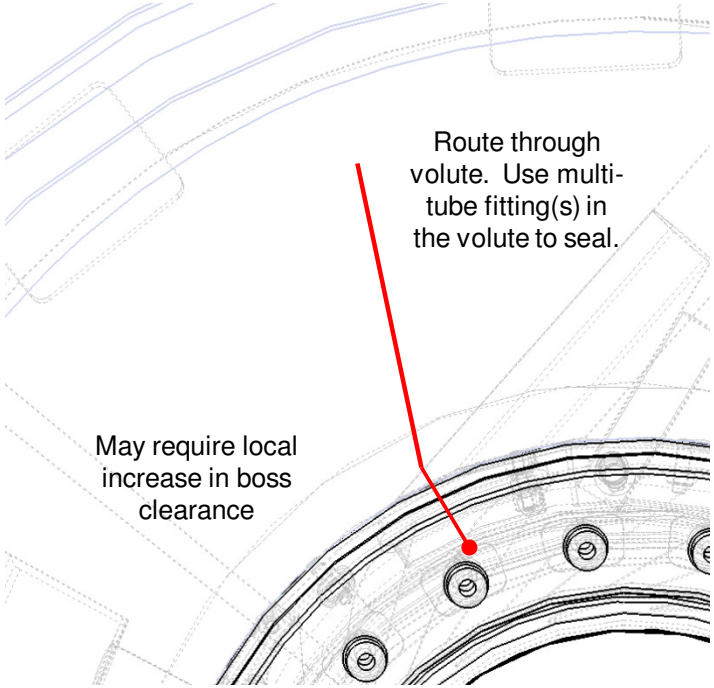

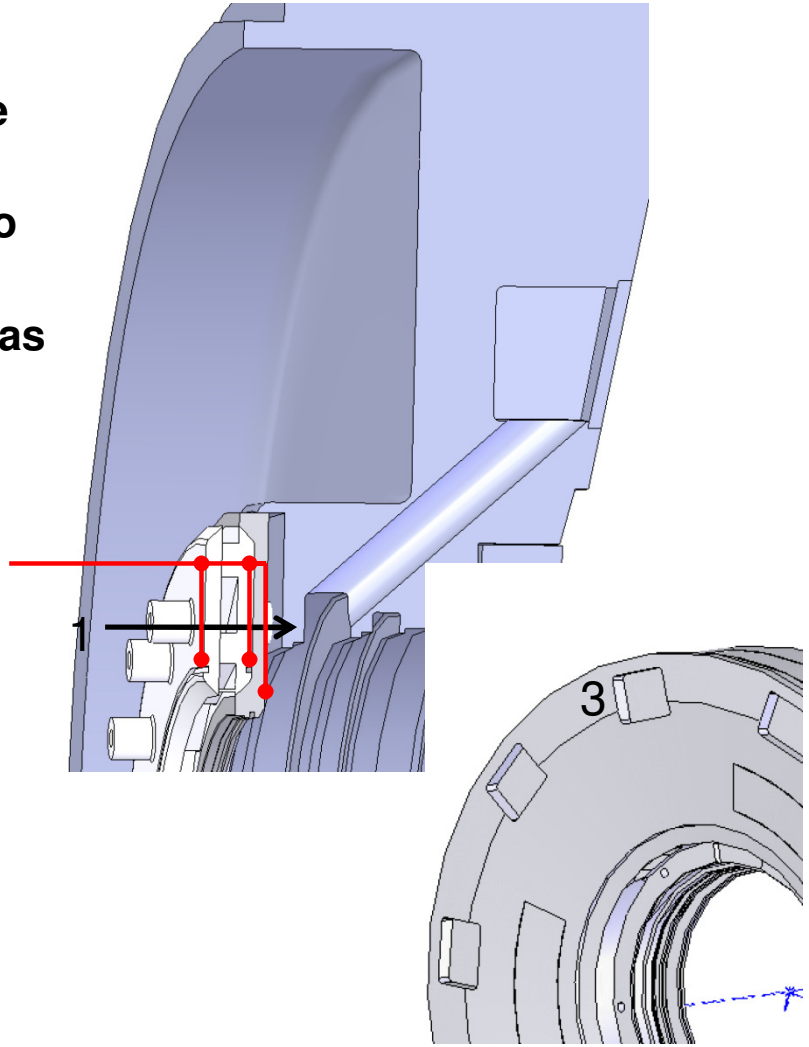

0900-01341

Non-driven-end Bearings

1. **Install dry gas seal onto shaft.**
2. **Install thrust collar and lock nuts (special tooling required).**
3. **Install journal and thrust bearings on shaft, then capture with split housing. Damper provisions may not be possible to incorporate.**
4. **Attach dry gas seal to split housing.**
5. **Install bearing cartridge into IGV hub shroud. Requires cartridge to be smaller or include wheel space laby seal land.**
6. **Attach bearing retension cartridge (717703) to split housing.**

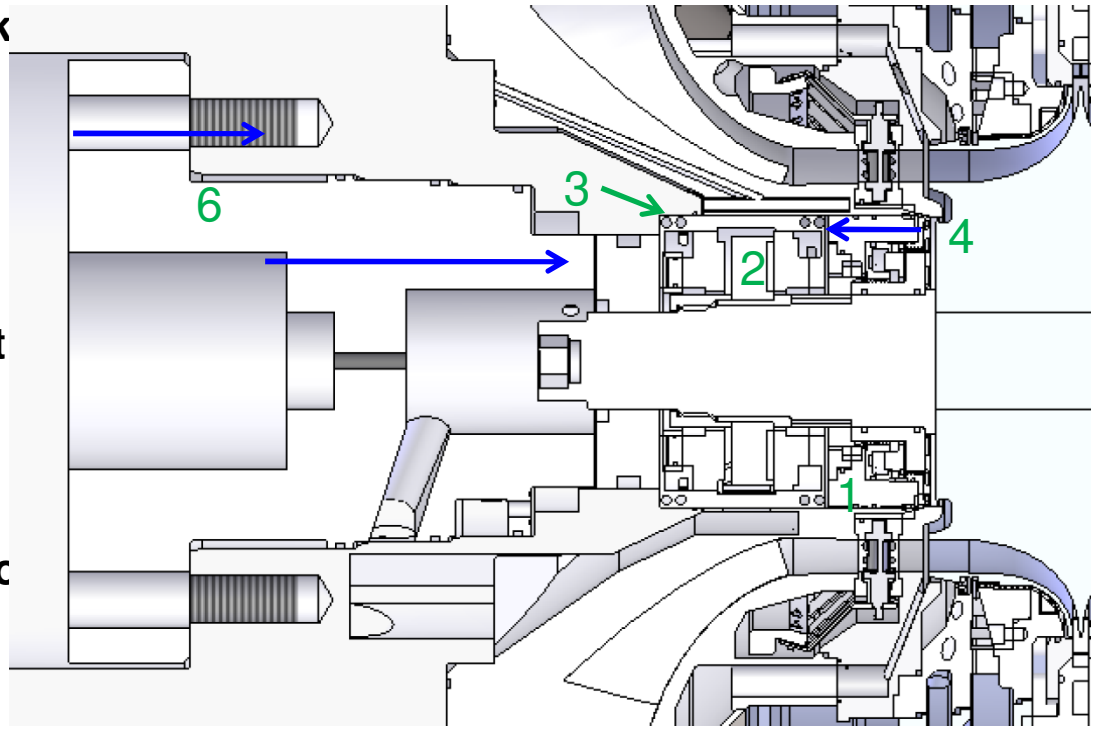

Driven-end Bearings

Stationary components

1. **Install stationary portion of the dry gas seal into the driven-end head.**
2. **Stack spacers, journal bearing, prox probes, and barrier seal behind dry gas seal cartridge. Fasten to driven- end head.**

Shaft

1. **Install dry gas seal onto shaft. Secure with lock nut**

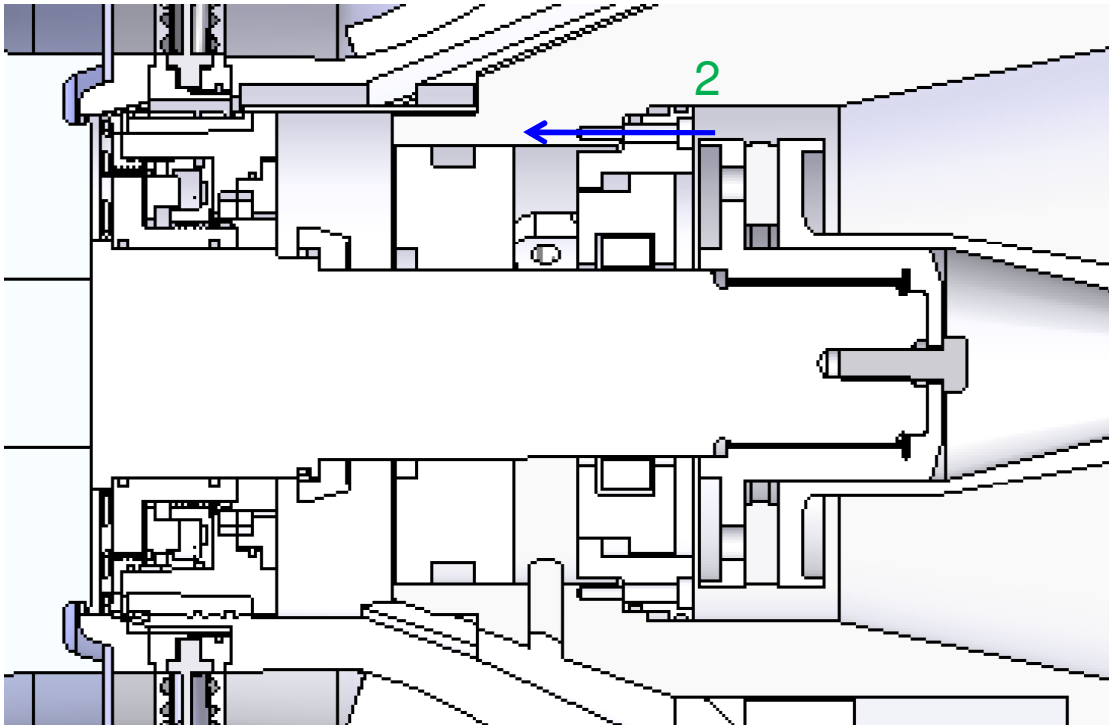

Driven-end Bearings

All instruments routed to space between head and star carrier.

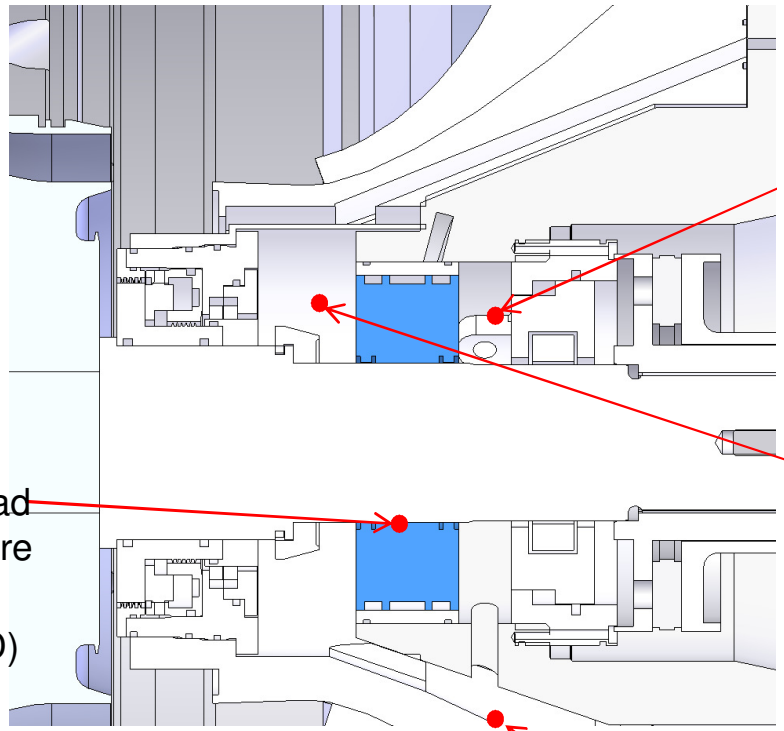

2

Instrumentation

1. **ZT192F**
2. **ZT191F**
3. **NDE Bypass valve feedback position,**
4. **NDE Bypass valve feedback position,**
5. **ZR192S**
6. **ZZ192S**
7. **ZR191S**
8. **ZZ192S**

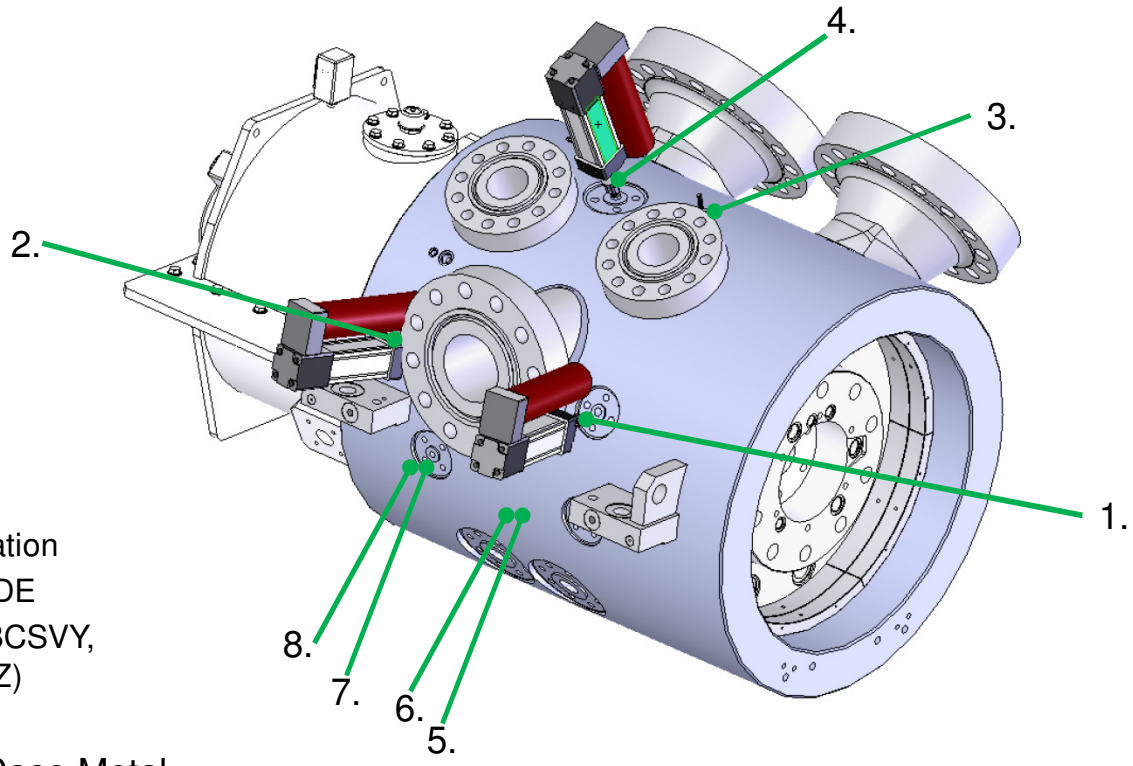

Case Vibration
x2- ND&DE
(VBCSVX,VBCSVY,
VBCSVZ)

4x Pressure Case Metal Temperature

Thermal Management

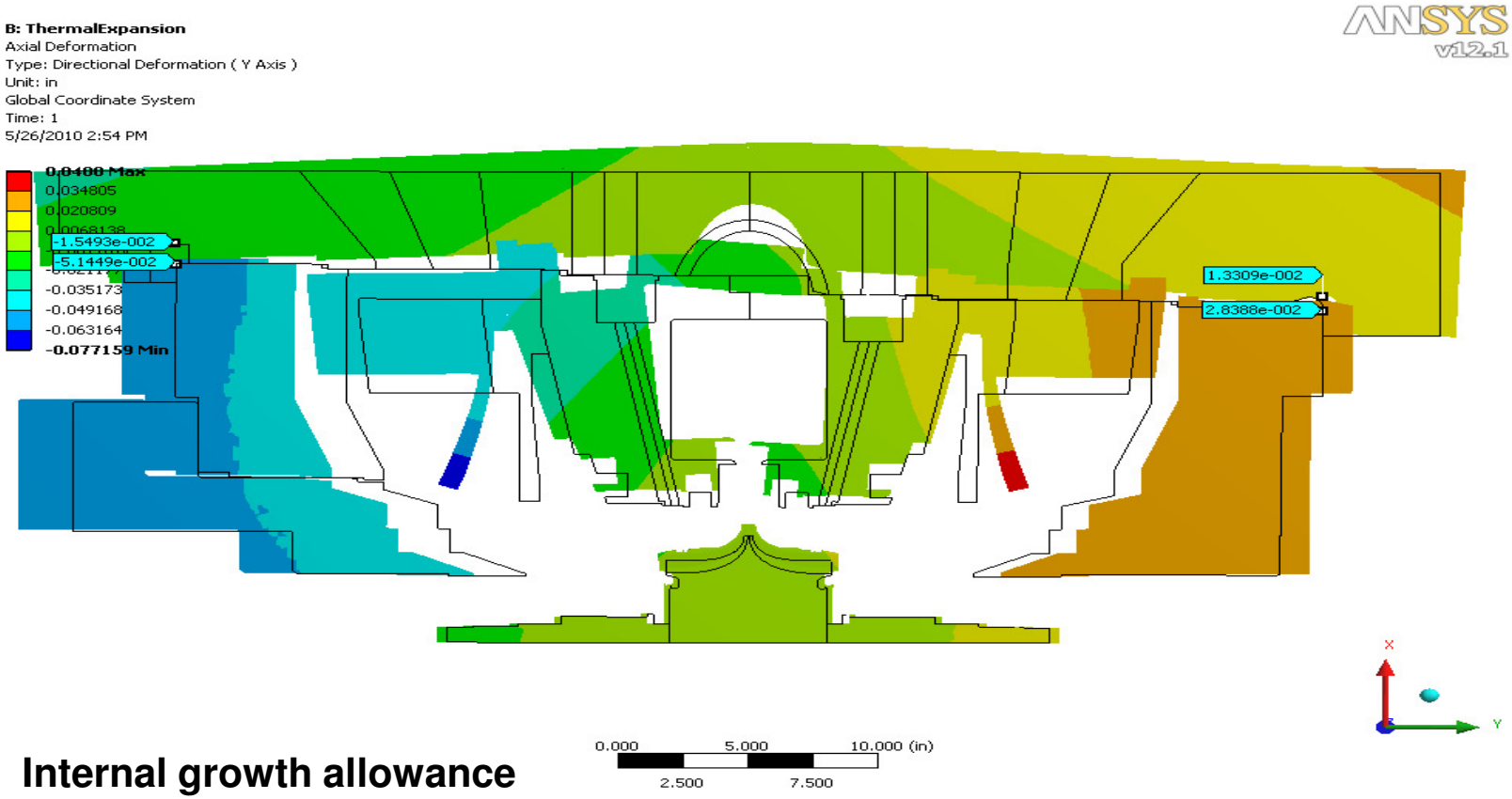

Internal growth allowance required to accommodate bundle growth in excess of pressure case growth (shear ring overload concern).

Bundle Assembly

1. **Install driven-end IGV cartridge.**
2. **Connect pressure heads, keys, radial inlets and volute using bundle, outside diameter pockets and studs.**
3. **Install IGV actuator, internal bayonets.**

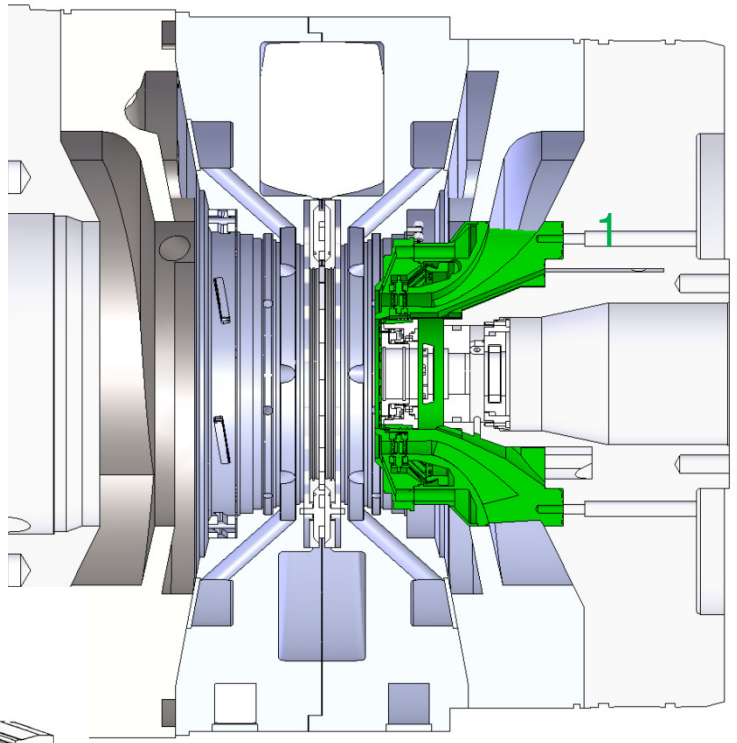

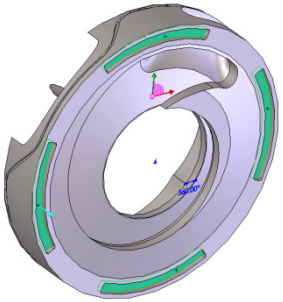

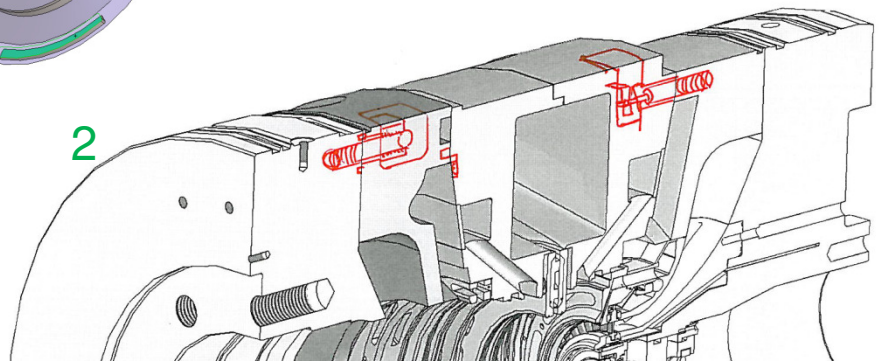

Bundle Installation

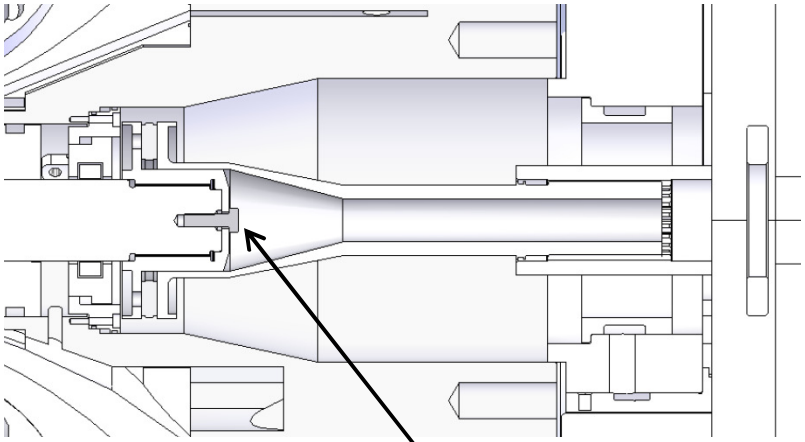

HS coupling hub retension bolt. Accessed through coupling bore.

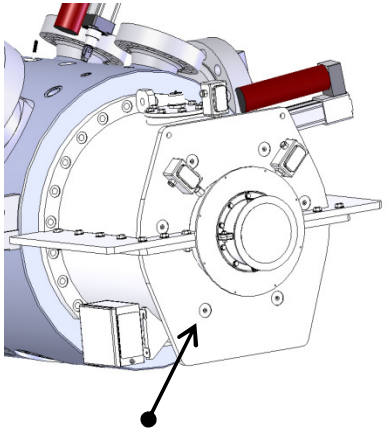

Gearbox draw bolts (6)

Thermal Management

RAMGEN POWER SYSTEMS™

650 degF discharge temp

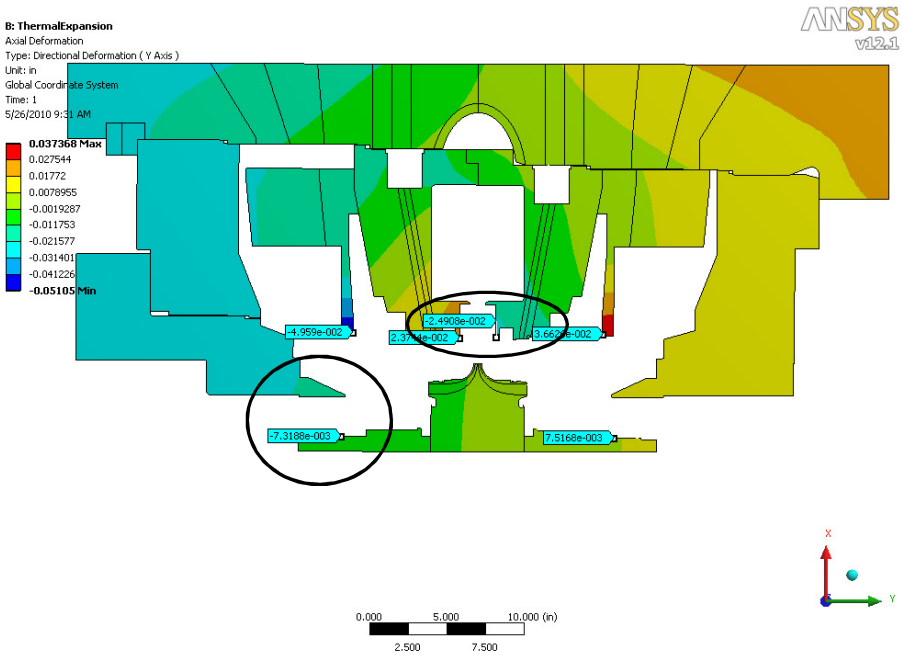

400 degF discharge temp

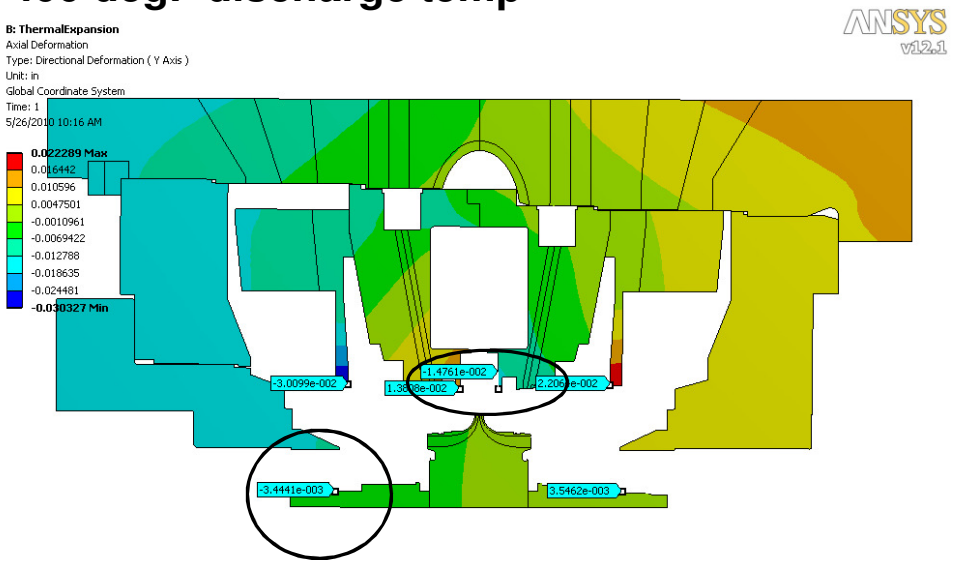

Temperature only effects tend to offset, over the discharge temperature range , with diffuser attachment point moving toward the midplane (-2.49e-002 and -1.48e-002) and case and shaft growth (-2.2e-002 + 0.73e-002 and -1.28e-002+0.34e-002).

Cold build offset .0075 (avg of .0102 and .0054) toward drive.

Internal step used to mitigate thermal growth impact from the DE of the pressure case. Step location may be moved to minimize cold build offset.

Thermal Management

Separation loads will likely need to be carried in the volute in order to prevent overloading of the positioning step.

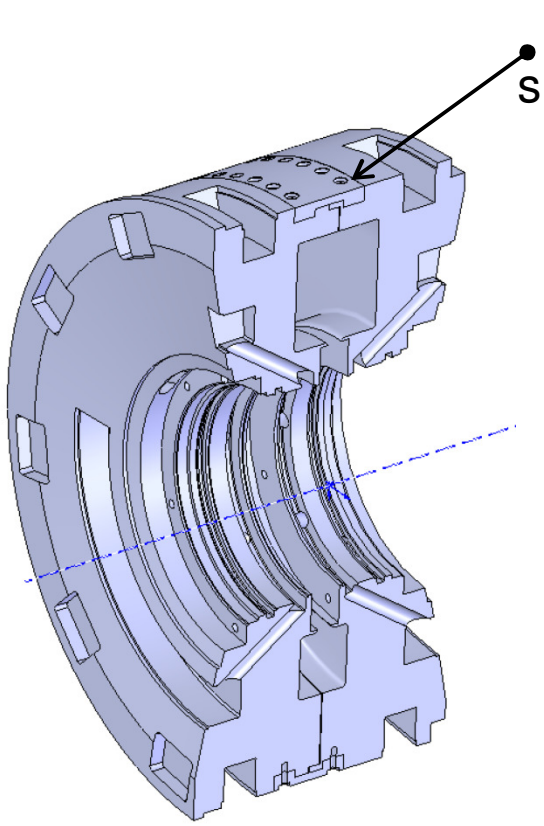

Position Management

400 psia discharge

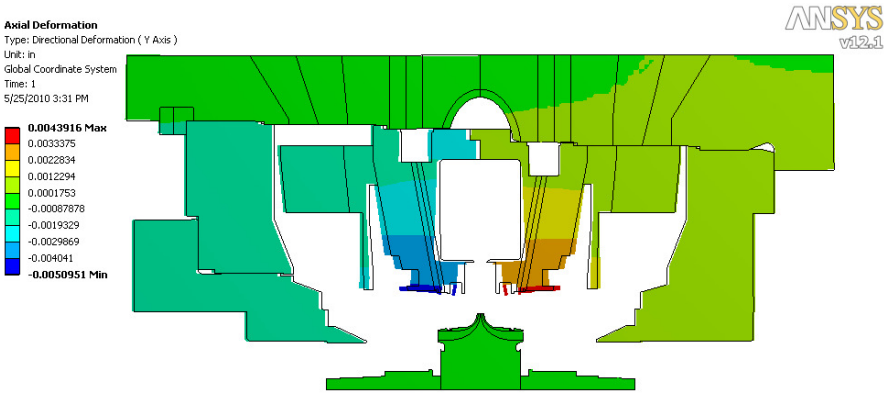

2200 psia discharge

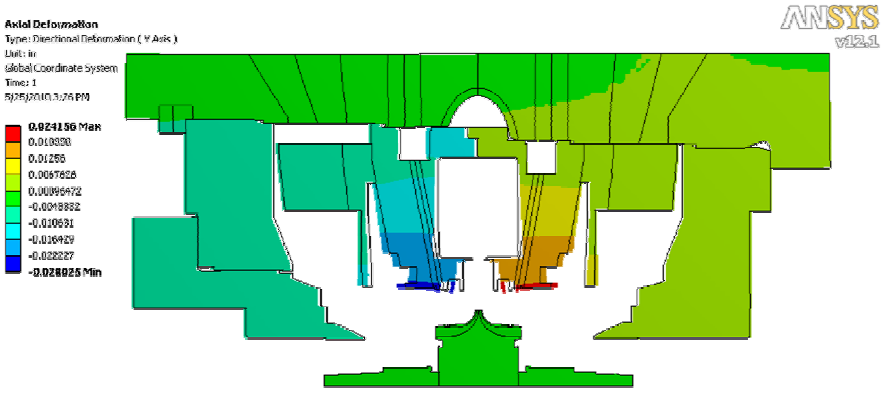

DE diffuser attachment shows .020 in. of pressure generated variation.

.008 in. of thrust collar

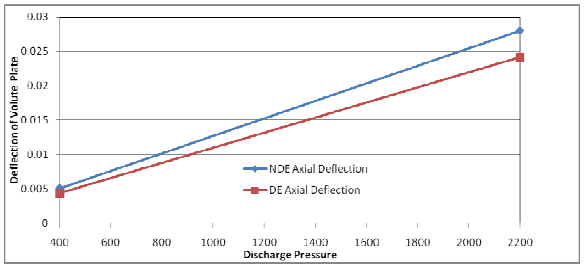

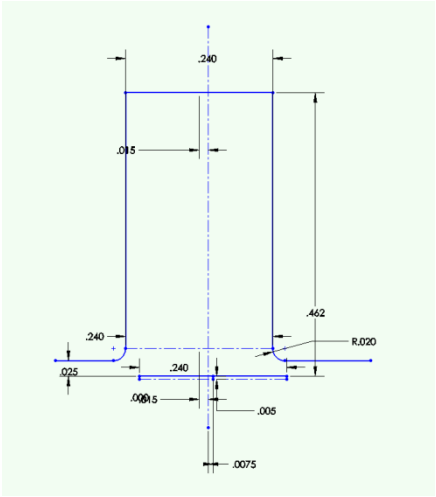

cold build/start-up

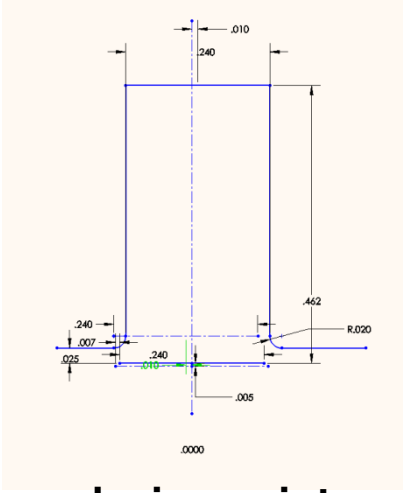

design point

Assembly location

Local Assembly Facility Requirements

Building

1500-2000 sq. ft.

Minimum 200 sq. ft. “office” space

Minimum 20 ft x 60 ft assembly bay with 20 ft ceiling

10 ft min. wide x 14 ft min. high roll up door with flatbed truck access (truck should be able to back a full 40 ft trailer into the space and leave it there)

Floor load rating (xxxx lb/ft^2)

Heating system to maintain at least 60 F in winter in assembly bay

Overhead hoist (permanent or temporary) with 20,000 lb minimum capacity (50,000 lb preferred) and hook height of at least 15 ft (see estimated component weights).

Case – 18,300 lb

Bundle – 10,400 lb

Baseplate – 12,500 lb

Shear / Retaining Ring – 1,200 lb

As close to current office as possible to minimize travel time (~10 minute max one-way travel time preferred)

Accessible by bus or bike

Electrical/Communications

Internet connectivity (reasonable speed)

Phone that can be heard throughout building

Security system

4x 110V electrical outlets 20 ft apart, or 2x outlets 10 ft apart

220 V electrical available in multiple locations preferred

Good uniform task lighting (skylights preferred)

Water and utility sink in shop

Parking for 4+ cars

Candidates

South Park

MI warehouse space

TBD alternate eastside location

Schedule

RAMGEN POWER SYSTEMS™

Assembly approach

• modularize internal components into sub-assemblies for bench assembly and instrumentation.

• Minimize instrument routing complexity and count through large components

Ideal assembly release condition

- All components in pressure case installed (rotor removed after fit check)
- Pressure case installed on baseplate.
- Instruments routed to terminations at junction boxes or patch panels, mounted on the baseplate.
- End-end checkout of installed instrumentation (mechanical and electrical)
- Secondary flows plumbed to the boundaries of the baseplate
- Survey and actuator, functional and control checkouts performed.
- Gearbox mounted.
- Bundle removed and installation tooling validated

Schedule

RAMGEN POWER SYSTEMS™

Schedule challenges

- Internal components require the most fabrication operations and are the last to be defined.
- Mitigation efforts
  - Rough machine parts in advance of final release
  - Utilize assembly approach which allows driveline test without IGV assembly and which allows for minimal IGV installation effort.

Budget

- $27,000 assembly budget
- $116,000 subscale, assembly-testing budget can be available
- Adequate as understood today. But does not account for additional assembly space lease.

RAMGEN POWER SYSTEMS ™

Conceptual Design Review

Rotordynamics

System owner(s):

Jonathan Bucher

1/19/09

System Definition and Scope

- **This system encompasses the bearings, thrust system, shafting, drive, gearbox, couplings, shaft sealing and shroud sealing components as they pertain to operational displacements and forces, to bearing operating temperatures and to stable operation of the demonstration unit at all anticipated running speeds.**

Functional Requirements/Design Goals

1. **Provide acceptable lateral imbalance response per API standards. Where possible provide acceptable lateral imbalance repsonse to D-R standards.**
   - **Rotor vibration amplitude at each radial bearing will be within API-617 7th edition limits (the lesser of 1 mil or < SQRT (12000/MCOS)**
   - **Rotor subsynchronous vibration amplitudes will be less than 20% of the allowable limit**
2. **Provide acceptable stability margin to API standards. Where possible provide acceptable stability margin to D-R standards.**
3. **Provide acceptable torsional characteristics per API 617**
4. **Utilize a bearing design acceptable for product life**
   - **Radial bearing metal temperatures to be <220 F**
5. **Utilize shroud sealing with acceptable leakage**
6. **Utilize shroud seal consistant with available shroud space**
7. **Utilize components which will accommodate axial bundle extraction (permanent placement of the pressure housing, minimal teardown to remove bundle)**
8. **Componets must carry full load torque**
9. **Minimze system parasitic losses**
10. **Utilize common oil and lubrication system for compressor and gearbox**

D-R option agreement criteria shown in red

Design Work Plan

- ETI turbo to develop baseline geometry (complete)
- D-R lateral and torsional design support and criteria
- Dynatech to validate D-R seal inputs
- RMT to validate and fabricate bearings
- CFD modeling of leakage flows in the shroud/static stucture cavity
- CFD validation of applied cross-couping?
- TBD additional modeling validation as required (shroud seals, etc.)

Important Interfaces

- **Electrical - none**
- **Mechanical**
  - **Rotating**
    - **Drive, gearbox and compressor shaft to coupling interfaces**
    - **Bearing journal diameters**
    - **Bearing and gearbox rotational axis alignment**
    - **Motor and gearbox rotional axis alignment**
    - **Shaft diameters: journal bearings, thrust collar, shaft seal, shroud seal**
    - **Diffuser width and diameter**
  - **Rotating to static**
    - **Shroud seal geometry inputs (hole pattern, tooth shape)**
    - **Swirl break interface and geometry**
    - **Bearing to housing fits**
    - **Bearing bore alignment**
    - **Gearbox alignment/centering**

Important Interfaces

- Static interfaces
  - Drive / gearbox hot and cold alignment
  - Compressor / gearbox hot and cold alignment/axial growth
  - Pressure case / head fits
  - Shaft clearance
  - Oil drains

- **Fluid**
  - CO2 at discharge interaction with rotor (discharge stiffness and cross coupling strength)
  - Lubrication supply conditions
  - HS coupling cooling

- **Instrumentation**
  - Compressor
    - High frequency shaft proximitors, 5x (90 deg at each bearing, 1 axial on NDE)
    - High frequency pressure case accelerometers, 6x (2x tri-axial)
    - Vibration transmiters, 3x (1x tri-axial), low freqency
    - Oil supply and drain temperatures, 7x(8x) TCs (1 ea. thrust and journal oil supply, 2 ea. NDE and DE oil drains)
    - Oil supply pressure, 3x(4x)

Important Interfaces

- Gearbox
  - Per manufacturer
- Drive
  - Shaft proximity probes, 5x (90 deg at bearings + axial)
  - Oil supply and discharge temperature, 4x
- Oil cooler
  - Upstream static temperature/leakage temperature: 1x, 2 plcs (8x placement locations)
  - Upstream static pressure: 1x, 2 plcs (8x placement locations)
  - Downstream static differential pressure: 1x, 2 plcs (8x placement locations)

- Control parameters
  - Leakage capture cavity static pressure
    - Pressure control to match aft bleed static pressure (zero separation tooth differential)
  - HS coupling cooling flow supply pressure (manual)
  - Oil flow rates (manual)
  - Supply oil temperature (manual)

Rotordynamic Design Areas

- Basic architecture
- Journal bearings
  - Shaft sizing
  - Bearing properties
- HS Coupling
- Thrust management system
- Thrust bearings
- Oil service sizing
- Shaft sealing
- Shroud sealing

Basic Architecture

Overhung

- **Pros**
  - **Improved service access**
  - **Reduced shaft sealing**
- **Cons**
  - **Baseline instability appears unmanageable**

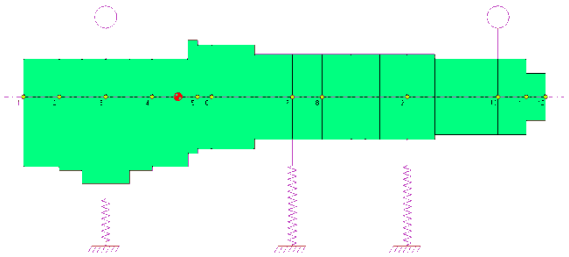

Precessional Mode Shape - UNSTABLE FORWARD Precession
Shaft Rotational Speed = 37300 rpm, Mode No.= 2
Whirl Speed (Damped Natural Freq.) = 9897 rpm, Log. Decrement = -2.9090

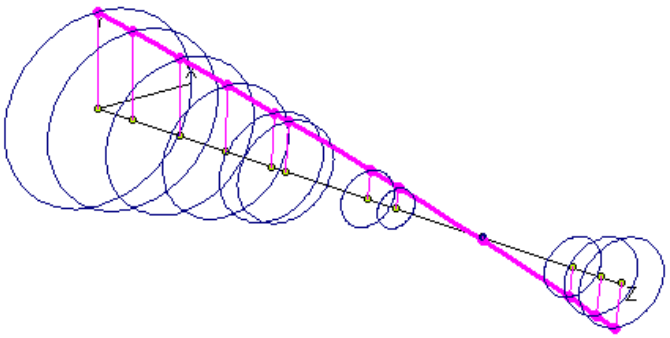

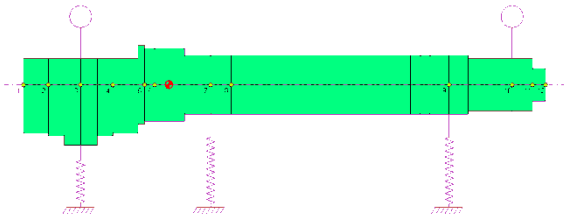

Precessional Mode Shape - UNSTABLE FORWARD Precession
Shaft Rotational Speed = 37300 rpm, Mode No.= 2
Whirl Speed (Damped Natural Freq.) = 10503 rpm, Log. Decrement = -2.2979

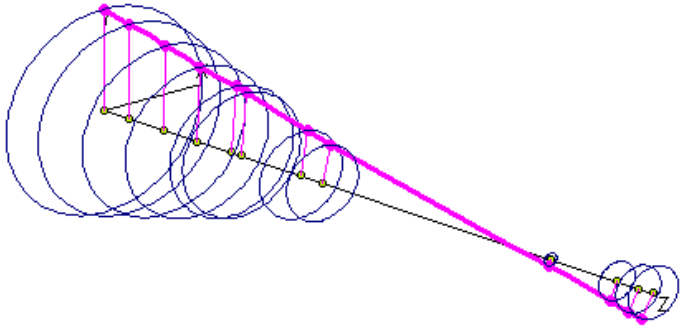

Basic Architecture

Simply Supported (Beam compressor)

- **Pros**
  - **Improved stability (1/10th neg. log dec. of overhung)**
- **Cons**
  - **Additional shaft sealing**
  - **Additional lubrication services on non-driven-end**

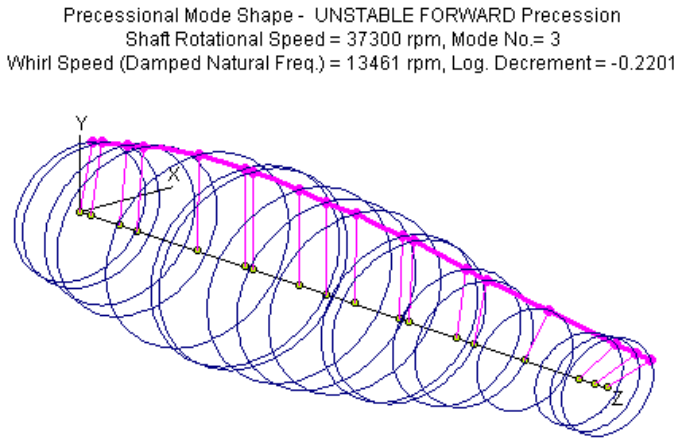

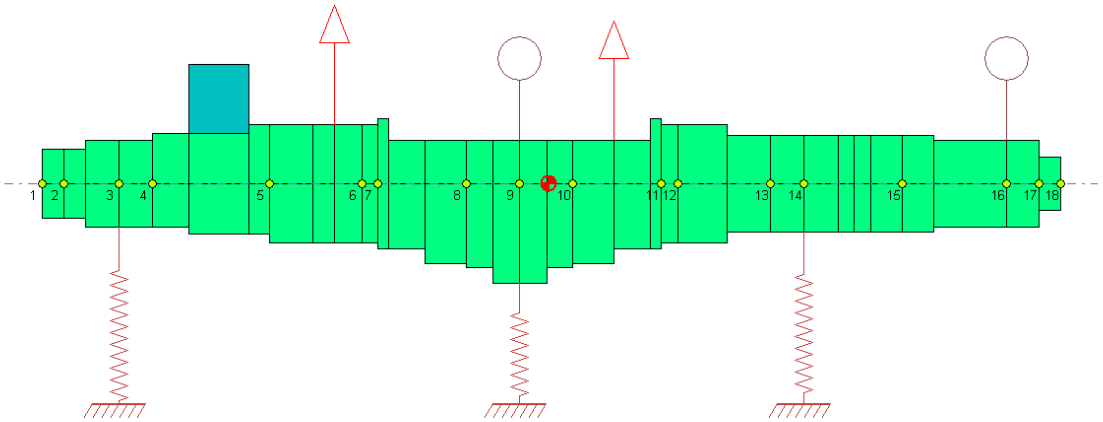

Journal Bearing Type

Conventional rolling element

- ***Pros***
  - ***High stiffness***
  - ***Comparatively low lubrication requirements***
- ***Cons***
  - ***Limited load carrying capacity***
  - ***Minimal natural damping (can be combined with squeeze film dampers)***

Hybrid/Ceramic rolling element

- ***Pros***
  - ***50% life increase over conventional rolling element bearings***
- ***Cons***
  - ***Cost***

Gas film bearings

- ***Pros***
  - ***No external lubrication***
- ***Cons***
  - ***Additional sealing requirements***
  - ***Low stiffness results in instability***

Journal Bearing Type

Tilt pad hydrodynamic

- ***Pros***
  - ***Most stable bearing type***
  - ***Industry expectation***
- ***Cons***
  - ***Large oil consumption***

Flex pad hydrodynamic

- ***Pros***
  - ***Reduced cost and complexity over tilt-pad bearings (for sizes >1.5 in.)***
- ***Cons***
  - ***Lower inherent stability than tilt pad bearings***

Magnetic

- ***Pros***
  - ***50% life increase over conventional rolling element bearings***
- ***Cons***
  - ***Cost***
  - ***Implementation challenging as a result of large shaft and static components***

Journal Bearing Size

Shaft torque capacity

1.65 conceptual shaft dia. does not support use of rolling element bearings

Conceptual Shaft Sizing Criteria

		design point check	min op speed check
shaft power	hp	13,500	13,500
dp shaft speed	rpm	34,728	29,172
max cont. speed	rpm	34,728	29,172
max angular velocity	rad/sec	3,637	3,055
allowable torque at max speed	ft*lbf	2,042	2,431
allowable torque at max speed	in*lbf	24,500	29,166
stress allowable, min UTS	ksi	130	130
matl comment		room temp Ti 6-2-4-2 per Aerospace Structural Metals Handbook, 1998 edition, Vol 4, code 3718, pg 45, Table 3.011	room temp Ti 6-2-4-2 per Aerospace Structural Metals Handbook, 1998 edition, Vol 4, code 3718, pg 45, Table 3.011
req'd safety factor	#	4	4
allowable stress	ksi	32.5	32.5
surface speed	ft/sec	237.2735809	211.2386956
shaft dia (min. to carry torque)	in.	1.565857495	1.659548297
shaft radius	in.	0.782928748	0.829774148
polar moment of inertia	in^4	0.590213089	0.74466249
torsional shear stress	ksi	32.5	32.5
torsional stress minus allowable stress	ksi	0.0	0.0

Preliminary Design Shaft Sizing Criteria

1.1.1.1. General Stress Criteria (Yield, Burst, Creep)

All hubs, shafts, and spacers shall be capable of withstanding 115% of the design speed according to the following criteria:

Stresses shall be less than 0.2% yield strength in the axial and hoop components.

Stresses shall be less than 1.2 times the 0.2% yield strength in the maximum radial bending and maximum hoop bending components.

1.1.1.2. Low Cycle Fatigue (LCF)

No credit for LCF shall be taken. Fracture life of an assumed preexisting flaw of the minimum detectable flaw size shall be used instead.

1.1.1.3. Fracture Life

Minimum life of engine required at all locations. Initial surface flaw size assumed shall be the minimum size detectable by FPI or MPI as appropriate. Surface flaw sizes detectable by other than FPI or MPI (such as eddy current) shall require approval by the Ramgen Power Systems Director of Mechanical Design. Initial subsurface flaw size assumed shall be the minimum size detectable by UI or radiographic inspection as appropriate. No credit shall be taken for shot peening.

1.1.1.4. Creep Life

Minimum life of engine required at all locations. Stresses shall be less than the 48,000 hour 0.5% creep strength, and less than the 100,000 hours creep rupture strength in the radial and hoop components.

Stresses shall be less than 1.2 times the 48,000 hour 0.5% creep strength, and less than 1.2 times the 100,000 hour creep rupture strength, in the maximum radial bending and maximum hoop bending components.

1.1.1.5. Rotor Seizure

No torsional shear or buckling permissible from rotor seizure loads, assuming deceleration from design speed to static in 2.5 seconds for the ramjet rotor, and 1.0 seconds for the impulse turbine rotor. For designs mechanically joined between the ramjet rotor and the impulse turbine rotor (designs utilizing a reversing speed reducer), the quill shaft between the ramjet rotor and the speed reducer is permitted to fail in torsion under rotor seizure conditions. The quill shaft fragments shall be contained within the engine.

Journal Bearing Size

Bearing surface speed limts

Hydrodynamic bearing manufacturers recommendation for 250 ft/sec max surface speed

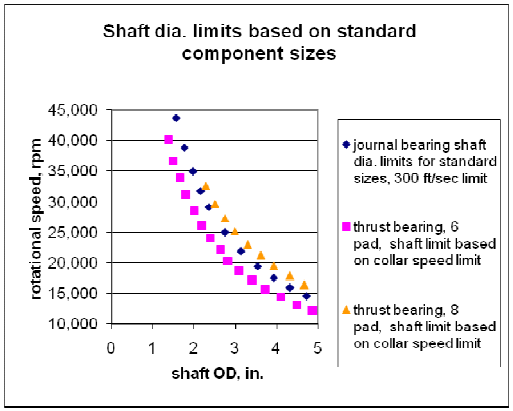

DE bearing initial size

surface speed limit	ft/sec	317.4972
cylinder OD	in	2.25
max rotational speed	rpm	32,340

NDE bearing initial size

surface speed limit	ft/sec	282.2197
cylinder OD	in	2
max rotational speed	rpm	32,340

Installations of higher surface speeds have been implemented on a limited production basis, primarily in performance gearbox applications (RMT data shown).

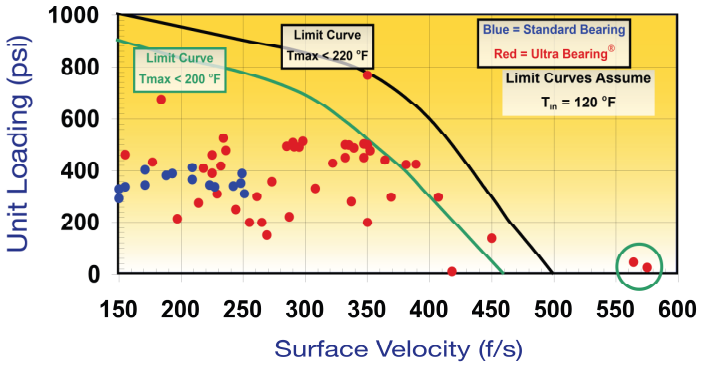

Journal Bearing Size

Rotordynamic implication of bearing/shaft size

Increased stability corresponds to increased shaft size

2.25 in reduction results in 2 in.

Level 1 analysis Log dec. under 1x Wachel @ max clearance: +0.046 to -0.151

Increased shaft size results in:

- ***higher surface speed (operating temp)***
- ***lighter film unit load (film stability), 200 psi is industry target***
- ***lower eccentricity ratio (stability)***

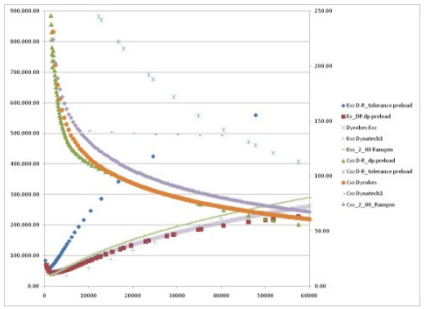

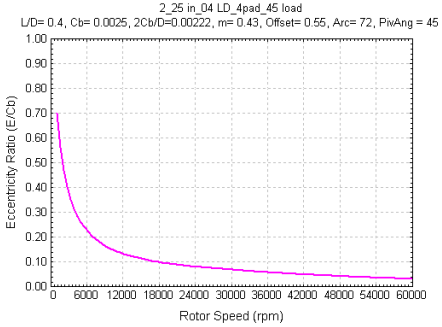

HS coupling

Dual element flex coupling

- *Pros*
  - *Long life design*
  - *Provides isolation from gearbox subsynchronous inputs*
- *Cons*
  - *Cost*
  - *Increased wight (vs. gear coupling)*
  - *requires radial assembly access*

Gear coupling

- *Pros*
  - *Light weight*
  - *Cost*
- *Cons*
  - *Wear component*
  - *Potential for torque or misalignment lock-up*
  - *Transmits gearbox subsynchronous inputs*

Hybrid coupling

- *Pros*
  - *Enables installation for our configuration*
  - *Provides isolation from gearbox subsynchronous inputs*
- *Cons*
  - *Higher weight resulting from requirement for steel components*

HS couplings – Thrust management

- **Impeller generated thrust loads**
  - **Few surge conditions can be managed by a reasonably sized thrust system. Single sided surge is considered outside the design scope**

single-side-surge thrust potential			
suction total pressure @ max fluctuation	psia	231	
discharge plenum pressure @ max suction fluctuation	psia	2310	
rotor exit static pressure	psia	1500	
IGV discharge pressure	psia	150	
simple scenerios			
max possible thrust load	lbf	123,373	flowpath and WS at Pt_discharge to Ps_IGV exit
max flowpath generated thrust load (possible to bleed WS)	lbf	37,103	flowpath only at Pt_discharge to Ps_IGV exit
exit static generated thrust load	lbf	77,108	flowpath and WS at Ps_discharge to Ps_IGV exit
exit static generated thrust load, flowpath only	lbf	23,190	flowpath only at Ps_discharge to Ps_IGV exit
single WS decompression	lbf	5,404	WS decompression to Ps_IGV exit
Single side unstart to zero mass flow	lbf	4,627	flowpath and WS at Pt_suction to Ps_IGV exit
Single side unstart to zero mass flow, flowpath only	lbf	1,391	flowpath only at Pt_suction to Ps_IGV exit

HS couplings – Thrust management

- **Coupling generated thrust loads**
  - **Full torque lock-up requires 2000 lbf to overcome (Allen Gear estimate)**
  - **With anti-friction coating and run-in lock-up load can be reduced to 1110 lb (Balinit C Star coating)**
  - **Thrust system should provide a thrust preload which nominally exceeds the lock-up load, i.e. shaft thermal growth/alignment cannot overcome thrust bearing for rotor position control.**

HS couplings – Thrust systems

RAMGEN POWER SYSTEMS™

Concepts

- **Hydrodynamic bearing system with dedicated thrust collar carrying thrust loads**
  - **Pros**
    - **Adequate system capacity for design point operation**
  - **Cons**
    - **WS preloading results in large leakage flows for required loads**
    - **Single side surge loading is unmanageable**
    - **Large oil flows required**
- **Angular contact ball bearings with mechanical preload**
  - **Pros**
    - **Does not require WS preloading**
  - **Cons**
    - **Configuration is unlikely to provide adequate driveline life at design point loading**

HS couplings – Thrust management

- **Gearbox selection/attachment resulted in elimination of Kop-flex element option with paired elements, each with .050 in. travel potential**

14 inch shaft separation:

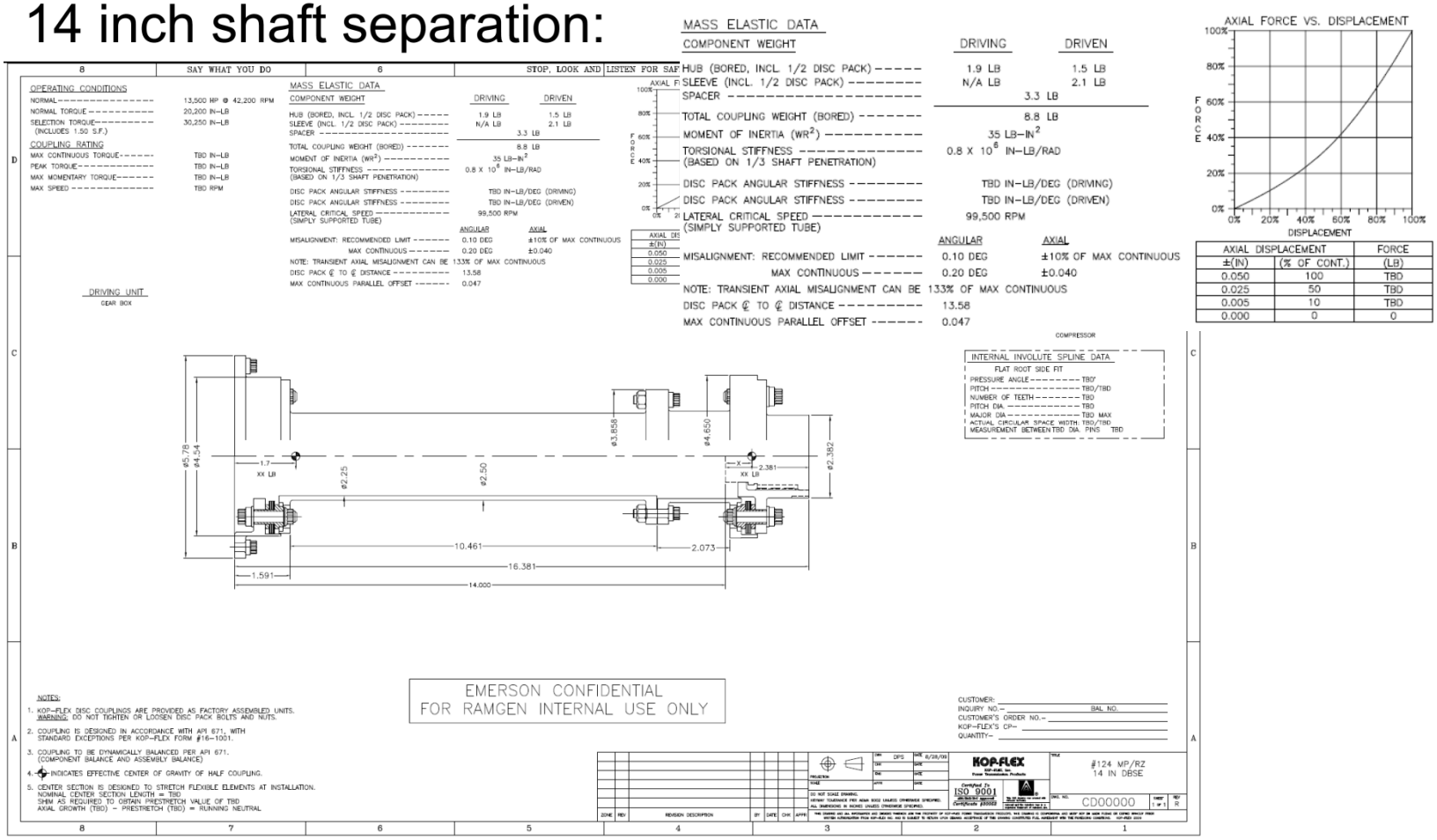

HS couplings – Thrust management

- **Bibby and Allen coupled to provide a replacement element option**
- **Travel/misalignment for this element is limited to 0.025 in.**

Bibby 10HS-10-110 coupling element

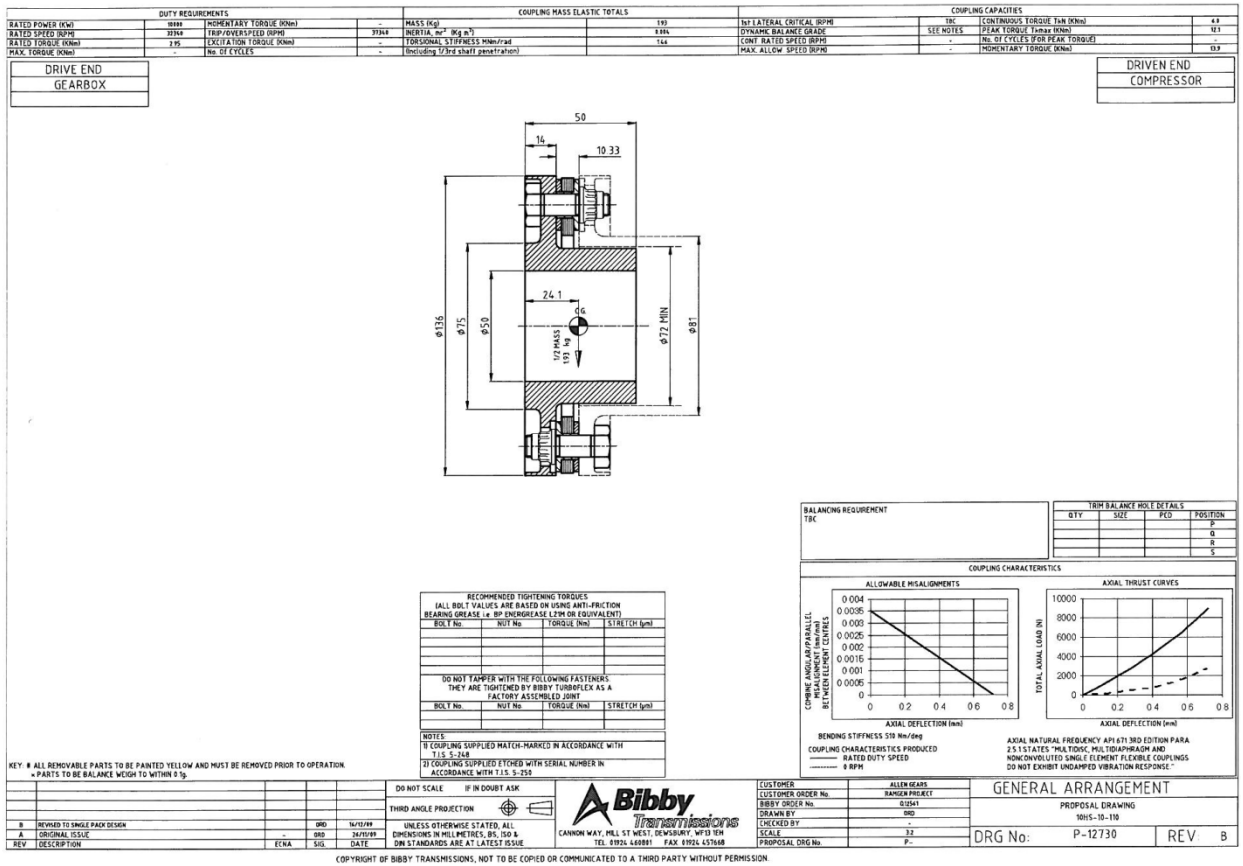

HS couplings – Thrust management

- **Coupling generated thrust loads**

Bibby 10HS-10-110 coupling element requires tight alignment control to generate split from the full-load torque-lock-up condition

torque lock-up with coated spline	lbf	1100
safety margin on lock-up		1.25
required min. thrust load	lbf	1375

		Permissible parallel offset							Bending load	
		coupling length	in.				curve fit, zero speed, axial load, lbf	curve fit, full speed, axial load, lbf	allowable combined angular/parallel offset, deg	bending load at max allowable offset, ft-lbf
		6	7	8	9	10				
axial deflection	0.0050	0.0172	0.0201	0.0229	0.0258	0.0286	67	279	0.1642	61.7467
in.	0.0100	0.0134	0.0156	0.0178	0.0201	0.0223	109	579	0.1278	48.0611
	0.0150	0.0096	0.0112	0.0128	0.0144	0.0159	164	894	0.0914	34.3755
	0.0200	0.0058	0.0067	0.0077	0.0086	0.0096	273	1253	0.0550	20.6899
	0.0215	0.0046	0.0054	0.0062	0.0070	0.0077	321	1375	0.0443	16.6690
	0.0250	0.0019	0.0023	0.0026	0.0029	0.0032	475	1717	0.0186	7.0043

HS couplings – Thrust management

Wheelspace generated thrust loads, 2000 lbf design point selected to

- providing margin on coated slip load
- providing residual preload at slip
- accomodating WS decompression in thrust bearing overload condition

Total thrust preload desired	lbf	2000
Shaft seal contribution	lbf	300
other contribution	lbf	0
WS expected contribution	lbf	1700
load side (NDE) ID	in.	3.25
soft side ID	in.	3
common OD (max.)	in.	6.743
load side (NDE) pressure	psia	144

OD side seal dia, in.	required differential pressure, psid
6.743	59.4
6.5	65.1
6	80.2
5.5	101.9
5	135.3
4.5	192.4
4	309.2

6.75 in. dia. seal leakage potential, sealflow.xls
estimate at .005 in. radial clearance for single tooth

seal DP, psid	leakage, lbm/sec
10	0.01377
20	0.2219
30	0.2702
40	0.2969
50	0.3117
60	0.3208
70	0.326
80	0.3264
90	0.3264
100	0.3264
110	0.3264

HS couplings – Thrust management

- **Impeller ½ mass and response has not dramatically changed as a function of a 10% coupling mass change**
  - ***Level 1 analysis Log dec. under 1x Wachel: +0.046 increased to +.0722 with increase of coupling mass and inertia***
  - ***Displacement of .00034 in. (AF=2.24) effectively unchanged***

Thrust Bearings

Concepts

Rolling element-angular contact with spring preload

- *Pros*
  - *Mechanical rather than aero preload*
- *Cons*
  - *Configuration life is short*
  - *Overload potential is minimal*

Hydrodynamic

- *Pros*
  - *Highest load capacity*
  - *3x dp load over-capacity*
- *Cons*
  - *High oil consumption*
  - *High parasitic loss*
  - *Require additional bearing span*

***Tapered land –** minimal axial space, 200 psi max loading*

***Tilt-pad – moderate axial space,** 350 psi loading possible*

***Tilt-pad with self leveling features –** most required axial space, highest loading*

Magnetic bearings and thrust collar

- *Pros*
  - *Variable load capacity*
- *Cons*
  - *Large spacial requirement*
  - *Defining characteristics requires detailed inputs and significant development effort*

Thrust Bearings

- **Thrust bearing size is non-standard, but standard sizing rules can be applied**

Standard Thrust Bearings

		surf speed	656	200 psi load	mid line arc length	radial heigl	arc/rad hgt
size	Collar OD, in.	max rpm	Collar ID, in.				
6103	3.740	40,197	1.378	1,899	1.340	1.181	1.134
6112	4.094	36,719	1.496	2,282	1.464	1.299	1.127
6123	4.449	33,794	1.654	2,679	1.598	1.398	1.143
6134	4.843	31,047	1.811	3,168	1.742	1.516	1.149
6146	5.276	28,498	2.008	3,739	1.907	1.634	1.167
6159	5.748	26,156	2.205	4,426	2.082	1.772	1.175
6174	6.260	24,017	2.402	5,249	2.268	1.929	1.175
6190	6.811	22,074	2.638	6,194	2.474	2.087	1.186
6207	7.402	20,313	2.835	7,343	2.680	2.283	1.174
6225	8.071	18,628	3.110	8,712	2.927	2.480	1.180
6246	8.780	17,124	3.425	10,265	3.195	2.677	1.193
6269	9.567	15,715	3.740	12,179	3.484	2.913	1.196
6293	10.433	14,410	4.094	14,464	3.803	3.169	1.200
6320	11.378	13,214	4.488	17,171	4.154	3.445	1.206
6348	12.402	12,123	4.882	20,415	4.525	3.760	1.203
6380	13.543	11,101	5.354	24,308	4.947	4.094	1.208
6415	14.724	10,211	5.866	28,651	5.391	4.429	1.217
8103	4.606	32,639	2.283	2,514	1.353	1.161	1.165
8112	5.079	29,603	2.520	3,054	1.492	1.280	1.166
8123	5.512	27,277	2.756	3,579	1.623	1.378	1.178
8134	5.984	25,123	2.992	4,219	1.763	1.496	1.178
8146	6.535	23,005	3.307	4,991	1.933	1.614	1.197
8159	7.087	21,215	3.622	5,828	2.103	1.732	1.214
8174	7.717	19,483	3.937	6,919	2.288	1.890	1.211
8190	8.425	17,845	4.331	8,204	2.505	2.047	1.223
8207	9.173	16,389	4.685	9,770	2.721	2.244	1.213
8225	10.000	15,034	5.118	11,593	2.968	2.441	1.216
8246	10.905	13,786	5.591	13,772	3.239	2.657	1.219
8269	11.890	12,645	6.142	16,281	3.540	2.874	1.232
8293	12.913	11,643	6.693	19,157	3.850	3.110	1.238
8320	14.094	10,667	7.323	22,781	4.205	3.386	1.242
8348	15.394	9,767	7.992	27,189	4.592	3.701	1.241
8380	16.772	8,964	8.740	32,185	5.009	4.016	1.247
8415	18.307	8,212	9.567	38,268	5.473	4.370	1.252
alternate designs							
10	5.25	28,637	3	2,916	1.29590697	1.125	1.152

Designed tilt-pad thrust bearing

DyRoBeS-Beperf

Number of Pads = 10
Inner Diameter ID (in) = 3.00000
Outer Diameter OD (in) = 5.00000
Circumferential
Length of Pad (in) = 1.10000

Operating Condition
Rotor Speed (rpm) = 37300.
Thrust Load (Lbf) = 2000.00
Oil Inlet Pressure (psi) = 30.00
Inlet Temperature (F) = 120.00

Lubricant Properties
Amokon ISO-VG 32
Specific Gravity at 60 F= .86300
Coefficient of Expansion= .43776E-03
Viscosity 1 (cSt) @ F = 32.6000 @ 104.
Viscosity 2 (cSt) @ F = 5.6100 @ 212.
Specific Heat Coeff (Cp)= .41785 .48462E-03 .00000 .00000

Program Converged, The converged results:

Radial Pad Width (in) = 1.0000
Circumf Pad Length (in) = 1.1000
Pitch Line Velocity (ft/min) = 39060.
Brg Unit Pressure (psi) = 181.82

Actual Oil Flow (gpm) = 61.772
Orifice Diameter (in) = .2411

Operating Temperature (deg.F) = 132.27
Temperature Rise (deg.F) = 12.26
Minimum Film Thickness (mil) = 2.68
Frictional Power Loss (HP) = 60.03

Shaft Sealing

Labyrinth seals (nominal loss .092 lbm/sec (47 SCFM))

- *Pros*
  - *Reduced cost and complexity*
  - *Not surface speed limited*
- *Cons*
  - *Increased shaft leakage (unrecoverable CO2 loss)*

Pocket damper seals (nominal loss .129 lbm/sec (66 SCFM))

- *Pros*
  - *Can add system damping between bearings*
- *Cons*
  - *Increased shaft leakage over labyrinth (unrecoverable CO2 loss)*
  - *Requires large gas density and pressure to operate*

Carbon ring seals (<.020 lbm/sec (<10 SCFM))

- *Pros*
  - *Reduced leakage*
  - *Minimal axial space required*
- *Cons*
  - *Surge/discharge pressure will fail seals*

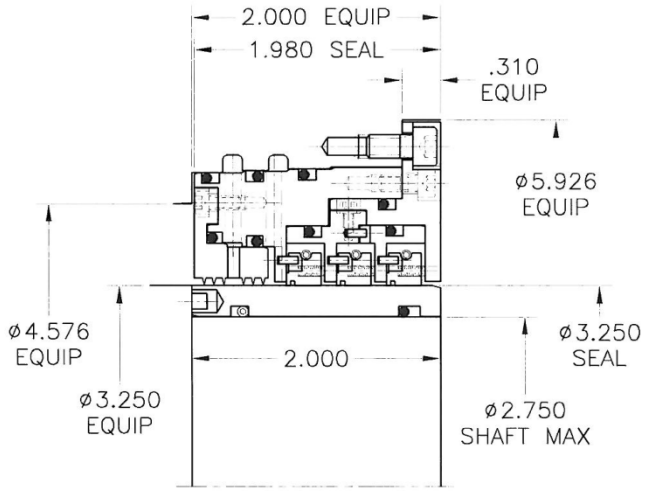

Shaft Sealing

Dry Gas seals (<.002 lbm/sec (<1 SCFM))

Tandem

- ***Pros***
  - ***Commercial leakage levels***
  - ***Can handle surge lvel pressure differential***
  - ***Can handle single seal failure without increased gas release***
- ***Cons***
  - ***Relatively large axial space requirement***
  - ***Expensive***

Single

- ***Pros***
  - ***Commercial leakage levels***
  - ***Can handle surge level pressure differential***
  - ***Can be installed in minimal axial space***
  - ***Can generate small scale thrust load with dynamic seal placement***
- ***Cons***
  - ***Expensive***
  - ***Failure leakage set by vent passage size***

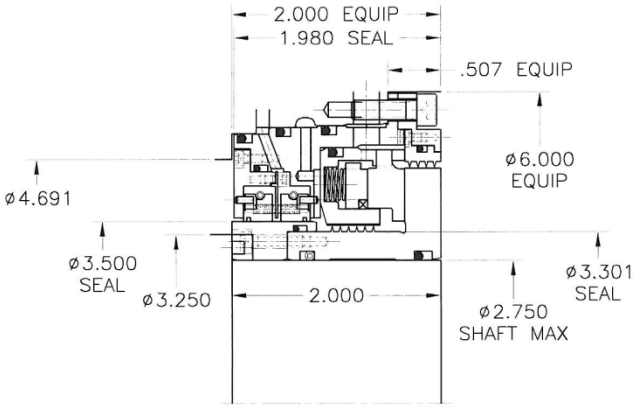

Shroud Sealing

Labyrinth seals

Pocket damper seals

Film riding seals

(See Shroud seal CDR for details)

This seal has expanded importance in light of the fact it is likely to be used to stabilize the rotor

Current Configuration

Simply supported

2.25 in. and 2 in. journal diameters

5-5.5 in. dia., interior thrust plate with hydraulicly fit collar

Mixed carbon ring and single, dry gas shaft sealing

Wheelspace generated thrust load

Narrow shroud seal (laby or pocket damper)

Hybrid coupling

Level 1 analysis Log dec. under 1x Wachel: +0.046 to +.780

Level 1 analysis Log dec. under 2x Wachel: -0.965 to -.345

Displacements <.0003, max AF: 2.70 – 4.16

36-40k mode emerging as shaft length is reduced to increase stability

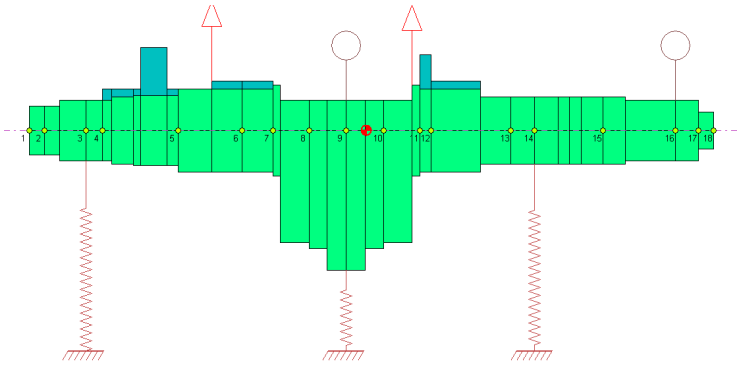

Influences

Rotor width increase for 1.25 in. shroud seals (shroud seal, span implications)

Level 1 analysis Log dec. under 1x Wachel: -.098 to +.476

Displacements <.0003, max AF: 2.76 – 4.37

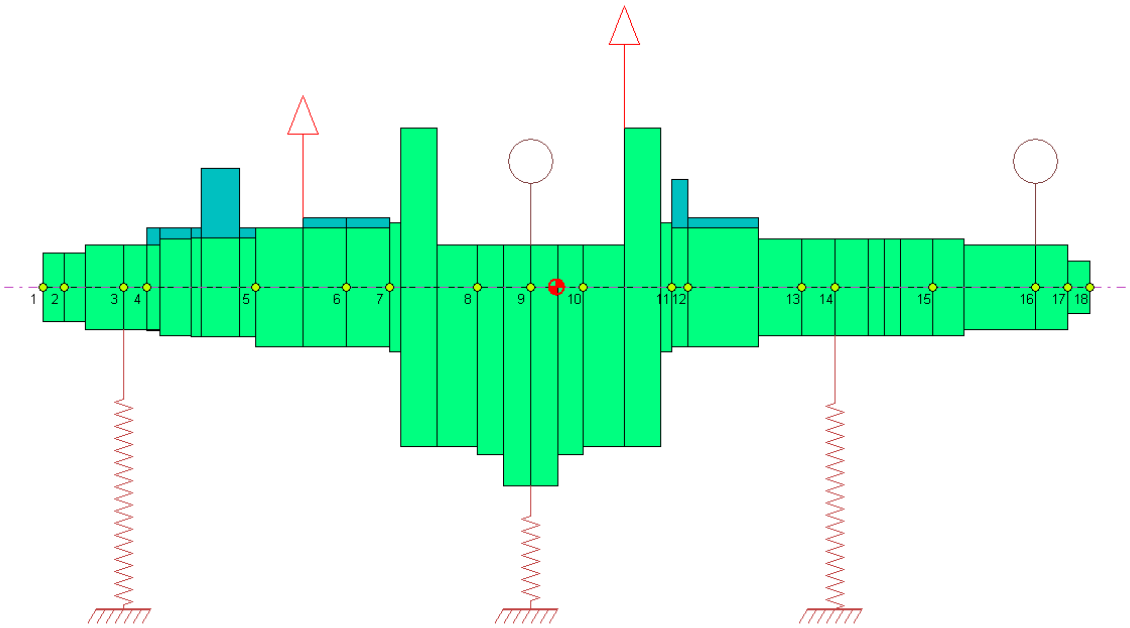

Influences

Fit thrust collar implications

Level 1 analysis Log dec. under 1x Wachel @ max clearance: +0.046 to +.125

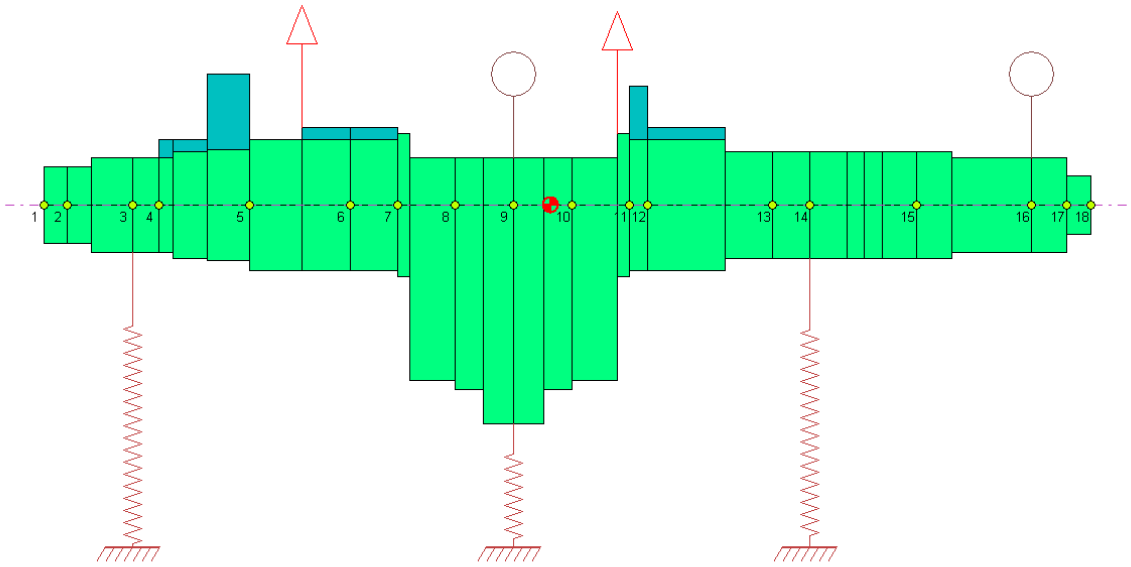

Influences

Removal of NDE exterior barrier seal

Level 1 analysis Log dec. under 1x Wachel @ max clearance: +0.046 to -.006

Displacements <.0003, max AF: 2.70 still at 18K, but 35K peak moved above operating range

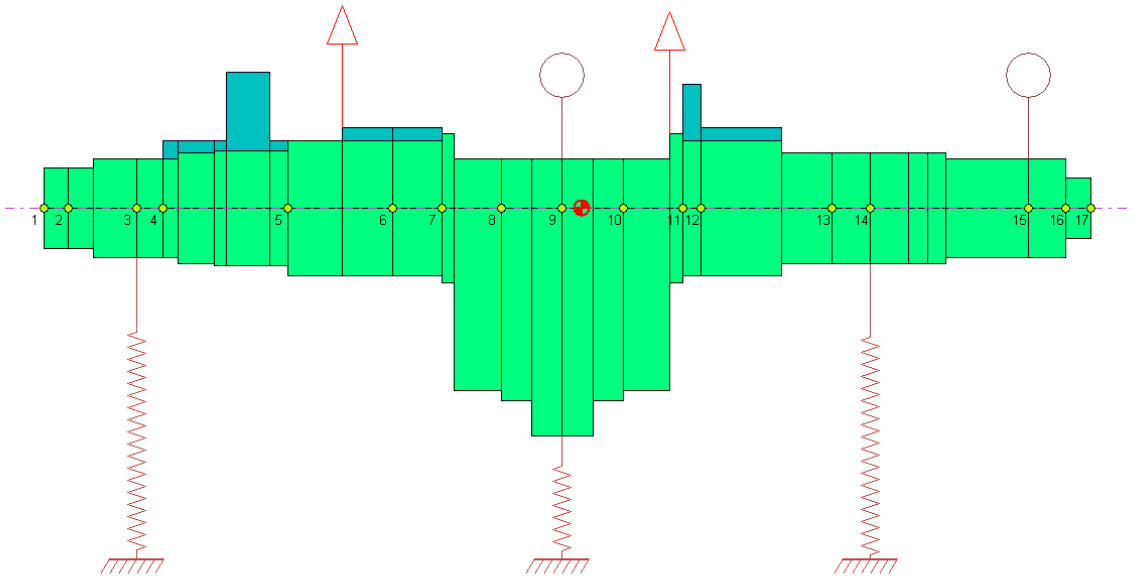

Influences

Diffuser width implications

Diffuser width assumption increased from 0.253 to 0.4, Wachel number reduced from 116,000 in-lbf Kxy to 73,000 in-lbf

Level 1 analysis Log dec. under 1x Wachel @ max clearance: +0.046 to +.452

Level 1 analysis Log dec. under 1x Wachel @ max clearance: +0.046 to +.452

Level 1 analysis Log dec. under 2x Wachel @ max clearance: -0.965 to -.230

Influences

Shroud seal influence characteristics

Baseline Level 1 analysis Log dec. under 1x Wachel @ max clearance: +0.046

1-1.25 pocket damper seal (D-R mock estimate): Log dec. +.431
(Kxx (1/3 bearing stiffness) 82,000 lbf/in, Kxy +/-82000, Cxx 21)
(Eccentricity effects are required to cahracterize this concept

1.25 Carbon ring seal: Log dec.: -.129
(Kxx 36370 lbf/in, Kxy 97510/-63270, Cxx 29.82 lbf-s/in, Cxy 1.93)

0.5 Laby: Log dec.
(TBD)

Torsional

Preliminary data on Allen gearbox, coupling and compressor provided to Dresser-Rand for preliminary evaluation

D-R input is required since ETI generate rules for coupling stiffness have been violated, i.e. coupling stiffness exceeds compressor shaft stiffness (vs. 80% rule of thumb for coupling stiffness to shaft stiffness)

Ramgen model generated for comparison to D-R results is complete. Potential to engage ETI on modelling and results

Budget and Schedule

- **PDR, driveline – last week of February 2010**
- **PDR, compressor rotordynamics – First week of March 2010**
- **FDR - May 7, 2010**
- **Estimated drawing release date – TBD**
- **Shedule issues**
  - **None noted at this time**
  - **Uncertainty on shroud seal property estimates presents the potential for schedule risk**

- **Current budget**
  - **Hardware: All harware is considered in part cost estimates**
  - **ODC's: $35,881 – external rotordynamics review**
    $17,940 – external bearing design
- **Budget issues:**
  - **Uncertainty of shroud seal modelling present potential additions**

RAMGEN POWER SYSTEMS ™

Conceptual Design Review

Rotor Shroud High Pressure Seal

System owner(s):

Jonathan Bucher

1/12/09

System Definition and Scope

- **This system encompasses the high pressure seal around the rotor shroud that will seal the discharge flow from the bleed and/or inlet flows**
- **Secondary leakage take-offs may be included as part of the system depending on seal type selected**

Functional Requirements/Design Goals

1. **Provide a mechanical seal between the discharge (Pt = 2400 psi, Tt = 520F) and inlet (Pt = 215, Tt = 99 F (IGV discharge)) of the compressor rotor on the external side of the rotor shroud**
2. **Operate in the region between the fixed static structure and the rotating shroud with relative surface speeds**
3. **Withstand rotor displacement and vibration due to start-up/shut-down tranients and supersonic start events**
4. **Avoid overheating rotor and/or seal due to direct mechanical contact (friction) or fluid shearing**
5. **Seal life design target must exceed total estimated run time of demo unit compressor**
6. **Maintain gas state through seal at all conditions, avoid liquifaction**

Functional Requirements/Design Goals

7. Rotating seal features and location must be designed within acceptable shroud stress limits
8. Provide adequate rotordynamic stability improvement
9. Allow axial disassembly
10. Allow maximum accuracy measurement of the aft bleed flow (minimal mass transfer to/from aft bleed cavity)
11. Tolerant to variable downstream pressure associated with aft bleed cavity pressure control
12. Routing should return leakage flow to suction while maintaining compressor suction temperature
13. Allow measurement of HP seal cavity flow and seal inlet and discharge static pressures
14. Aero input for diffuser performance impact?
15. Seal must be field serviceable

Design Work Plan

- Shapiro design study report (complete)
- Labyrinth seal flow modeling using internal, NASA and DR design rules
- Dynatech and D-R pocket damper modelling tools
- CFD modeling of leakage flows in the shroud/static stucture cavity
- ATG development of hybrid leaf seal

Important Interfaces

- Electrical - none
- Mechanical
  - Rotating to static surface interface
    - Shroud geometry inputs
    - Heat transfer to support target design clearance
    - Minimized axial seal width
  - Static interfaces
    - Swirl brake support
    - Diffuser bypass sealing
    - Radial assembly interfaces for Non-Driven-End
  - Leakage flow take offs as required
    - Static diffusion for suction return at low aft bleed pressure (cooler approach pressure)?
- Fluid
  - CO2 at discharge pressure (Pt = 2200) and temperature (Tmax = 650 F)
    - CO2 may reach higher temperatures due to shearing of flow between rotating and static components
  - CO2 at aft bleed flow pressure and temperature

Important Interfaces

- Instrumentation
  - Leakage capture cavity static pressure
    - 3x wall static, 2x plcs. (DE and NDE cavities)
  - Discharge vaneless space/seal entrance conditions
    - 4x wall static, 2x plcs. (DE and NDE cavities)
  - Leakage circuit flow metering
    - Upstream static temperature/leakage temperature: 1x, 2 plcs (8x placement locations)
    - Upstream static pressure: 1x, 2 plcs (8x placement locations)
    - Downstream static differential pressure: 1x, 2 plcs (8x placement locations)
  - Circuit cooling
  - Circuit recompression (not currently incorporated)

- Control parameters
  - Leakage capture cavity static pressure
    - Pressure control to match aft bleed static pressure (zero separation tooth differential)

Design Concept #1

RAMGEN POWER SYSTEMS™

Straight or stepped multi-tooth labyrinth seal, tooth on rotor

- **Pros**
  - **non-contact seal able to function at high surface speeds**
  - **can be designed for minimal axial length**
  - **can tolerate large differential pressures to tooth**
- **Cons**
  - **challenging fabrication/assembly issues to achieve seal gaps required for reasonable seal performance (nominally 0.005 clearance)**
  - **seal is not inherently compliant; seal rubs could result in decreased seal performance, overheating of seal and/or rotor**
    - **abradable material at seal interface may be required; could be source of particulate causing rotor erosion**
  - **Seal leakage (even at nominal operating conditions) will require significant flow removal (approx. 5.0 lb/s) to avoid impacting bleed flow removals and/or leakage to inlet**
  - **Seal type has very low inherent damping**
  - **External design tools have not consistantly predicted seal characteristics**
  - **Has highest shroud mass to incorporate features**

Design Concept #1

RAMGEN POWER SYSTEMS™

Straight or stepped multi-tooth labyrinth seal, tooth on rotor

NASA KTK code results for teeth of varying height (assuming 5 mil clearance)

Straight laby seals

	seal OD	length	number teeth	tooth height	leakage per seal	leakage, total shroud HP seal	circumference fraction of case1 circ.	leakage/baseline leakage	fraction of core flow
	in.	in.	#	in.	lbm/sec/seal	lbm/sec			86%
case 1, baseline/Shapiro tooth geom.	9.85	0.65	4	0.5	2.669	5.338	1	1	6.21%
case 4, case 1 dia. with 0.4 tall teeth	9.85	0.65	4	0.4	2.646	5.292	1	0.991383	6.15%
case 2, same as 1 expect 0.4 tall teeth	9.65	0.65	4	0.4	2.592	5.184	0.979695	0.97115	6.03%
case 3, same as 1 expect 0.3 tall teeth	9.45	0.65	4	0.3	2.51	5.02	0.959391	0.940427	5.84%
case 5, same as 1 expect 0.2 tall teeth	9.25	0.65	4	0.2	2.418	4.836	0.939086	0.905957	5.62%
case 6, same as 1 expect 0.125 tall teeth	9.1	0.65	4	0.125	2.336	4.672	0.923858	0.875234	5.43%
case7, same as 6 with smaller tooth tip thickness (.016 vs. 0.04)	9.1	0.65	4	0.125	2.24	4.48	0.923858	0.839266	5.21%
case 8, same as 1 expect 0.05 tall teeth	8.95	0.65	4	0.05	2.224	4.448	0.908629	0.833271	5.17%
case 9, same as 8 expect baseline dia. 9.85 used	9.85	0.65	4	0.125	2.448	4.896	1	0.917197	5.69%
case 10, case 6 with 5 teeth	9.1	0.65	5	0.125	2.364	4.728	0.923858	0.885725	5.50%

Design Concept #1

RAMGEN POWER SYSTEMS ™

Straight or stepped multi-tooth labyrinth seal, tooth on rotor

NASA KTK code results for case6 (KT modified to be in data range)

```
K N I F E -- T O -- K N I F E  S E A L  D E S I G N  M O D E L

 STRAIGHT LABYRINTH SEAL SAMPLE DATASET ( # 1 )

        I N P U T  D A T A  R A N G E  C H E C K
KNIFE  1
      VARIABLE     MIN    VALUE    MAX
        THETA     30.     90.0     90.
        KT/CL      .0     3.000    3.3
      (E-30)/D     .0     2000.0  27000.
KNIFE  2
      VARIABLE     MIN    VALUE    MAX
        THETA     30.     90.0     90.
        KT/CL      .0     3.000    3.3
     (KP-KT)/KH    .54    1.256    4.
      (E-30)/D     .0     2000.0  27000.
KNIFE  3
      VARIABLE     MIN    VALUE    MAX
        THETA     30.     90.0     90.
        KT/CL      .0     3.000    3.3
     (KP-KT)/KH    .54    1.256    4.
      (E-30)/D     .0     2000.0  27000.
KNIFE  4
      VARIABLE     MIN    VALUE    MAX
        THETA     30.     90.0     90.
        KT/CL      .0     3.000    3.3
      (E-30)/D     .0     2000.0  27000.

 K N I F E -- T O -- K N I F E  S E A L  D E S I G N  M O D E L

 STRAIGHT LABYRINTH SEAL SAMPLE DATASET ( # 1 )


SPECIFIC HEAT RATIO  (GAMMA) =  1.3600
MOLECULAR WEIGHT          =  44.0100
NUMBER OF KNIVES          =  4
SEAL TYPE                 =  STRAIGHT
FLOW DIRECTION            =
SEAL LENGTH (2-D SEAL)    =  .0000 (INCHES)
AVG. KNIFE DIAMETER (3-D SEAL) =  9.1000 (INCHES)
INLET TOTAL PRESSURE      =  1473.0000 (PSIA)
```

K KNIFE NO.	N CL (IN)	I KR (IN)	F KT (IN)	E KP (IN)	G KH (IN)	E SH (IN)	O DTC (IN)	M THETA (DEG)	E BETA (DEG)	T DIA (IN)	R ROUGH (RMS)	Y TEMP (DEGR)	D KCCO (IN)	A KECO (IN)	T 4FL/D MULT	A DEL (DEG)	C	DEL	E	AREA	ALPHA
1	0.005	0.001	0.015	0.172	0.125	0	0	90	20.9	9.1	50	960	-1	1	0	0	0.0115		1		
2	0.005	0.001	0.015	0.172	0.125	0	0	90	20.9	9.1	50	960	1	1	0	0.0115	0.0115		1	4.248	
3	0.005	0.001	0.015	0.172	0.125	0	0	90	20.9	9.1	50	960	1	1	0	0.0115	0.0115		1	4.248	
4	0.005	0.001	0.015	0.172	0.125	0	0	90	20.9	9.1	50	960	1	-1	0	0.0115	0		1	4.248	

F (W STN NO.	L = KNIFE NO.	O 2.22315 AREA (IN**2)	W LB/SEC TEMP (DEG | R ITERATION WRT/PTA R)	E != WRT/PSA TYPE	S 25) 4FL/D (PSIA)	U KFACT (PSIA)	L KFACT LOSS METHOD	T PT (IN**2)	S PS	A MN	T KFACT	C PARM	H AMUL	O ADDER	K XKUNC	E MOD	P AREA	O	I	N	T
1	0.143	960	0.3237	0.3449	1473.0001	0.306	0.144														
2	1	0.143	960	0.3304	0.353	0	0.337	CONTR	1443.241	1350.738	0.313	Q	0.2	0.854	0	0.395	0.144				
3	1	0.143	960	0.3541	0.3827	0	1.072	LHOLE	1346.481	1246.086	0.339	Q	3	0.697	0.798	0.394	0.144				
4	1	0.143	960	0.3675	0.3998	0	0.486	EXPND	1297.704	1192.741	0.354	PT-PS	0	0.486	0	1	0.144				
5	2	0.143	960	0.3754	0.4102	0	0.269	CONTR	1270.323	1162.587	0.363	Q	0.2	0.595	0	0.452	0.144				
6	2	0.143	960	0.4096	0.4567	0	1.017	LHOLE	1164.312	1044.076	0.403	Q	3	0.582	0.798	0.377	0.144				
7	2	0.143	960	0.4312	0.488	0	0.486	EXPND	1105.896	977.223	0.43	PT-PS	0	0.486	0	1	0.144				
8	3	0.143	960	0.4467	0.5114	0	0.313	CONTR	1067.467	932.438	0.45	Q	0.2	0.595	0	0.525	0.144				
9	3	0.143	960	0.5083	0.6157	0	1.007	LHOLE	938.165	774.546	0.538	Q	3	0.582	0.798	0.36	0.144				
10	3	0.143	960	0.5553	0.7145	0	0.486	EXPND	858.672	667.406	0.619	PT-PS	0	0.486	0	1	0.144				
11	4	0.143	960	0.6006	0.8425	0	0.372	CONTR	793.987	565.976	0.722	Q	0.2	0.595	0	0.625	0.144				
12	4	0.143	960	0.6489	1.2117	0	0.295	LHOLE	734.862	393.534	0.999	Q	3	0.835	0.07	0.27	0.144				
13	4	0.143	960	1.2117	0	1	EXPND	393.534	PT-PS	0	1	0	1	0.144							

F PHI I	L = W	O *	W *	C SQRT(TIN)	U /	R (PT	V UP	E *	WHERE AREF)	PR (WHERE	= AREF=	PT .143)	UP	/	PT	DOWN	AND
1	2	3	4	5	6	7	8	9	10	11	12	13	14				
1.-1./PR**;	0	0.00674	0.03527	0.0846	0.15182	0.23344	0.32569	0.42402	0.5239	0.62151	0.71412	0.79246	0.87339	0.92862			
PHI**2	0	0.00129	0.00616	0.01386	0.02362	0.03473	0.04657	0.05854	0.07014	0.08092	0.09049	0.09853	0.10478	0.10691			
R/G * PHI**2	0	0.00141	0.00672	0.01512	0.02577	0.03791	0.05082	0.06389	0.07655	0.08831	0.09875	0.10752	0.11435	0.11667			

Design Concept #2

RAMGEN POWER SYSTEMS™

Pocket Damper/Hole Pattern Damper Seals

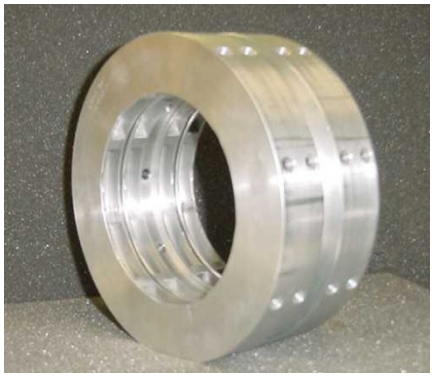

- **Pros**
  - **non-contact seal able to function at high surface speeds**
  - **Can provide useful amounts of rotor damping**
- **Cons**
  - **Operating conditions (L/D is outside of the conventional design envelope); design characteristics are exptrapolated**
  - **challenging fabrication/assembly issues to achieve seal gaps required for reasonable seal performance (nominally 0.005 clearance)**
  - **Operable clearances are 20-40% greater than those for labyrinth seals**
  - **Required seal width for useful damping is estimated at 1.25 in.**
  - **seal is not inherently compliant; seal rubs could result in decreased seal performance, overheating of seal and/or rotor**

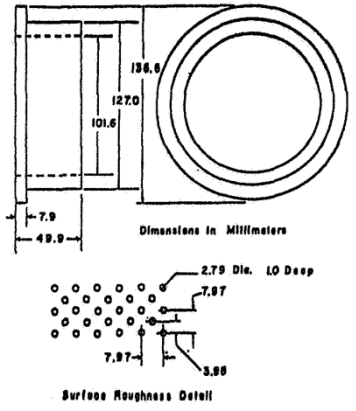

Figure 6(c). Round-hole pattern stator insert.

Design Concept #3

Floating Ring Seal as proposed by Shapiro

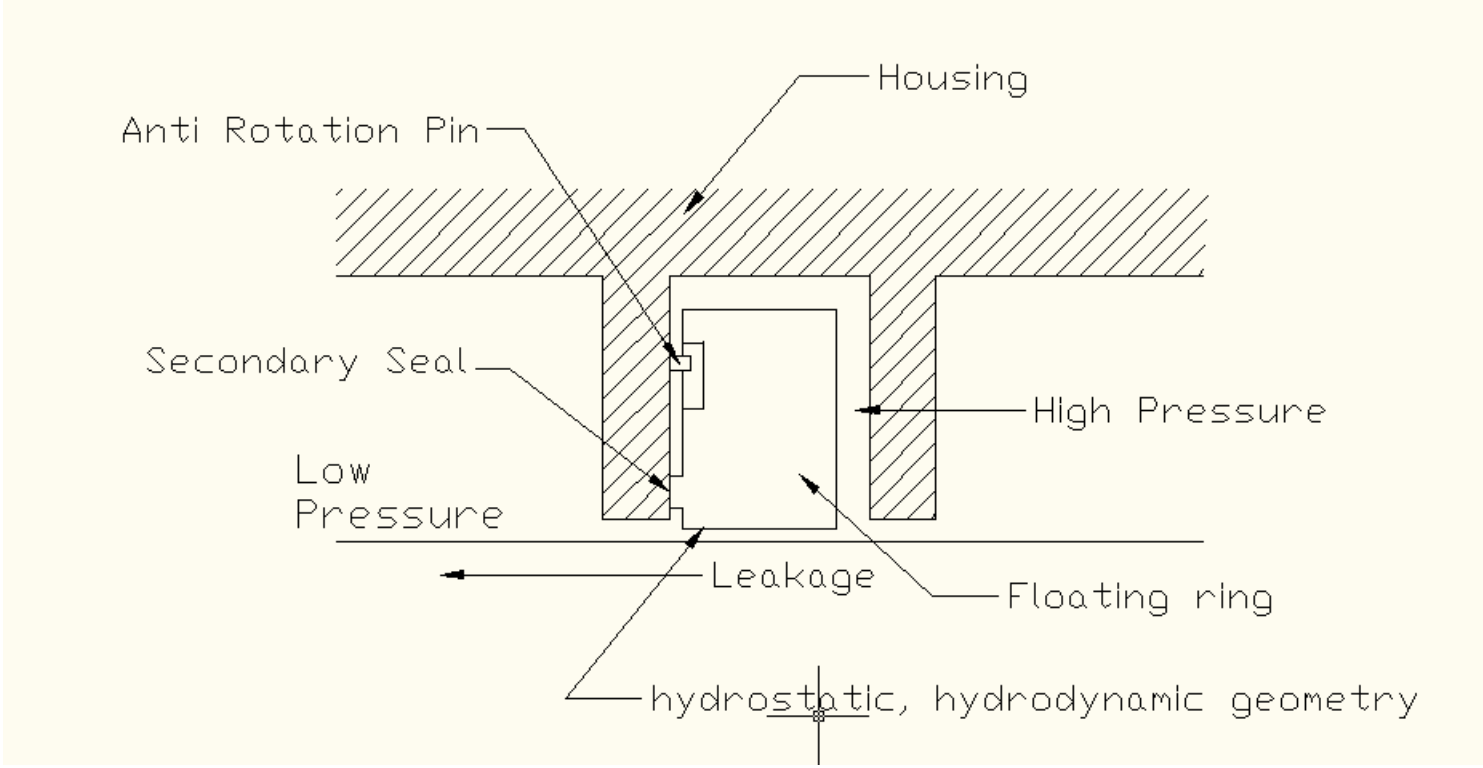

Design Concept #3

1 in. length, floating ring seal characteristics

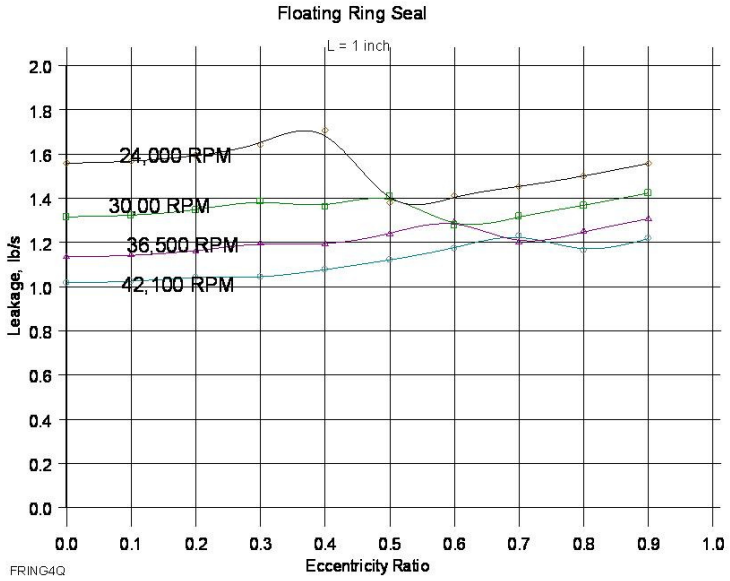

ECC	KXX	KXY	KYX	KYY	DXX	DXY	DYX	DYY
0.000	0.2130E+05	0.4657E+05	-.4657E+05	0.2130E+05	21.15	-.5175	0.5175	21.15
0.1000	0.2148E+05	0.4773E+05	-.4698E+05	0.2155E+05	21.33	-.5400	0.5309	21.67
0.2000	0.2201E+05	0.5144E+05	-.4824E+05	0.2237E+05	21.92	-.6128	0.5753	23.35
0.3000	0.3090E+05	0.6532E+05	-.5204E+05	0.3548E+05	24.96	-.4851	1.119	28.35
0.4000	0.3373E+05	0.7758E+05	-.5657E+05	0.4034E+05	26.99	-.8634	1.207	33.99
0.5000	0.3637E+05	0.9751E+05	-.6327E+05	0.4657E+05	29.82	-1.542	1.385	43.37
0.6000	0.3984E+05	0.1342E+06	-.7230E+05	0.5992E+05	34.02	-2.795	1.921	60.23
0.7000	0.4532E+05	0.2086E+06	-.8530E+05	0.1017E+06	40.62	-5.314	3.869	94.29
0.8000	0.6158E+05	0.3897E+06	-.1065E+06	0.3026E+06	52.73	-12.56	11.69	178.3
0.9000	0.1491E+06	0.9882E+06	-.7294E+05	0.2568E+07	74.37	-39.20	64.45	442.9

Design Concept #3 (cont.)

Floating Ring Seal as proposed by Shapiro

- **Pros**
  - **Non-contacting**
  - **Contact tolerant through carbon abrasion**
  - **Reduced leakage relative to labyrinth seals**
- **Cons**
  - **Requires 1 in. min. (1.25 in.) axial shroud length**
  - **Thermal expansion mismatch will increase wear with rotor thermal growth** *
  - **Single dia. requires accurate thermal modelling of operating conditions for diameter over the length of the seal**

Coefficients of Thermal Expansion for Selected Materials

material	linear α (10^{-6} K^{-1})
aluminium	23.1
barium ferrite	10
brass	20.3
carbon, diamond	1.18
carbon, graphite ∥	6.5
carbon, graphite ⊥	0.5
chromium	4.9
concrete	8 ~ 12
copper	16.5
germanium	6.1
glass	8.5
gold	14.2
iron	11.8
lead	28.9
nickel	13.3
platinum	8.8
plutonium	54
silicon	4.68
silver	18.9
solder, lead-tin	25
steel, stainless	17.3
steel, structural	12
tin	22
titanium	8.5
tungsten	4.5
uranium	13.9
water, ice (0 °C)	51
zinc	30.2

material	volume β (10^{-6} K^{-1})
alcohol, ethyl	1120
gasoline	950
jet fuel, kerosene	990
mercury	181
water, liquid (1 °C)	−50
water, liquid (4 °C)	0
water, liquid (10 °C)	88
water, liquid (20 °C)	207
water, liquid (30 °C)	303
water, liquid (40 °C)	385
water, liquid (50 °C)	457
water, liquid (60 °C)	522
water, liquid (70 °C)	582
water, liquid (80 °C)	640
water, liquid (90 °C)	695

Design Concept #5

Foil Seal as proposed by Shapiro

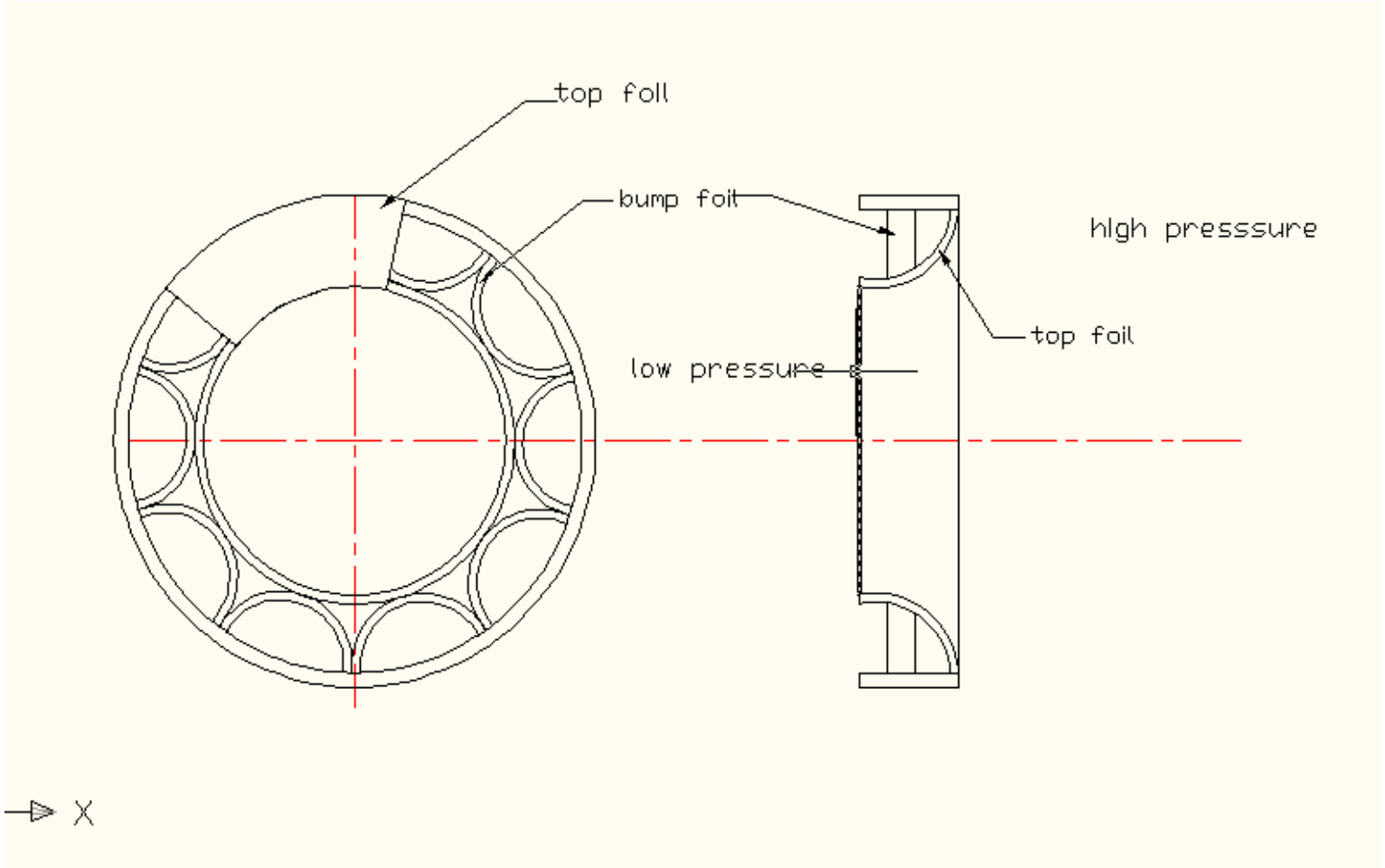

Budget and Schedule

- **PDR – February 18, 2010**
- **FDR - May 13, 2010**
- **Estimated drawing release date – TBD**
- **Shedule issues**
  - **Rotordynamics not mature enough today to select a concept**

- **Current budget**
  - **Hardware: $minimal, all harware is currently considered in part cost estimates or in development money**
  - **ODC's: $80,731**
- **Budget issues:**
  - **ODC budget restricts development to a single design concept (in addition to baseline hole pattern/labyrinth design)**

Conceptual Design Review

Rotor Manufacturing Development Program

Dave Taylor

2nd Feb 2010

System Definition and Scope

- **This system encompasses the Rotor, comprising:**
  - **Impeller (aka Rampressor)**
  - **Shafts (whether integral to impeller or not)**
  - **Impeller Shroud (aka cover)**
  - **Composite Ring (Hybrid Rotor)**
  - **Retainer Ring (Hybrid Rotor)**

Functional Requirements/Design Goals

- **The Rotor Manufacturing Development Program is intended to address 3 main areas. They are shown below along with the specific goals:**

- **Composite Ring**
  1. **Verify the material properties for the composite ring**
  2. **Validate the use of the composite material in CO2 environment**
  3. **Demonstrate the ability to fabricate a composite ring of representative dimensions**
  4. **Static test of representative ring to confirm behavior (See Geenes slides)**

- **Shroud Attachment**
  1. **Demonstrate the ability to attach/fabricate shroud using test specimens**
  2. **Investigate the resultant joint properties for each process**
  3. **Down-select process(es) for further assessment using representative rotor geometry.**
  4. **Confirm joint behavior on representative rotor geometry via spin pit testing**

Functional Requirements/Design Goals

- **Impeller Manufacturing**
  1. **Create virtual machining model for early feedback on machining challenges**
  2. **Create fully-featured rotor for further understanding of manufacturing challenges not addressed in 1 above.**
     - **Impeller**
     - **Down-selected shroud attachment method**
  3. **Demonstrate ability to install composite shroud ring**
     - **See separate slide presentation**
  4. **Test rotor in Spin pit to confirm deflections, shroud integrity etc**
     - **Details still TBD. Eg**
       - » **Spin to failure?**
         - – **What failure – shroud failure, disc burst or what?**
       - » **Room temp or elevated**
       - » **What parameters to measure?**
         - – **Shroud deflection at inlet, mid and exit ?**
       - » **Other**

Manufacturing Development Plan - Old

- **Prior to last couple of weeks, the rotor manufacturing development program was looking reasonable.**
  - **Composite ring on track for post cure**
  - **Shroud attachment test specimens running later than planned but did not appear to be schedule impact.**
  - **Mold fabrication proceeding at Howmet.**
  - **See schedule in this folder 'RotorDesign&Dev_2010-01-13.mpp'**
- **Then things went awry…..**

Manufacturing Development Plan - Issues

In the last couple of weeks the following events have occurred that impact the rotor manufacturing development program

- **Composite Ring**
  1. **Composite ring post cure not performed correctly**
     - **4th ring unacceptable**
       - » **Recovery plan being put in place. New SOW. Not critical path (yet)**

- **Shroud Attachment**
  1. **NDA agreement not obtained with Howmet so PCC selected**
     - **PCC then balked at producing mold for alternate process**
       - » **Test specimen mold being hand-worked (ECD 2/3)**

  2. **Discussion with D-R on some details of the proprietary attachment process resulted in the feedback from D-R that back-to-back impeller is not possible using this process.**
     - » **Looking at 2-piece impeller options now.**

  3. **Strong urging from D-R to consider Steel rather than Ti**
     - » **Looking at alternative materials now, in both single and 2-piece configurations.**
     - » **Steel was considered long time back and dismissed. Exducer design may be more open to steel**

Manufacturing Development Plan - Issues

4. **Shroud Attachment Specimen testing ECD went from mid Feb to early March**

- **Rotor configuration**
  1. **Analysis indicated splitters required in exducer**
     - **Settled on 11 flowpath + 11 splitter configuration as baseline design**
     - **Work ongoing to assess revised configuration and feed results -> Manufacturing Development Rotors.**

Work Plan

For discussion of plan to address the aforementioned issues, see the following file located in the same directory as this file:

'*RotorIssues_Jan2010.docx*'

See individual separate powerpoint files in this directory for discussion of:

1. **Composite ring hydrostatic test**
2. **Composite ring retention development**
3. **Status of composite material testing**

Schedule

- **PDR date: 4th week of Feb**
  - **Probably at risk due to current issues**
- **FDR date: 4th week of March**
  - **Possible at Risk due to current issues**
- **Drawing Release date – TBD**
- **Schedule**
  - **See next slide for overview**
  - **See this file (*RotorDesign&Dev_2010-02-02.mpp*) located in same dir as this file for details**

Conceptual Design Review

Inducer Mechanical

Rob Draper / Geene Cevrero / Dave Taylor

21st July 2010

Agenda

- System Definition and Scope (**Dave**)
- Review action items from prior design review (**Dave**)
- Requirements (**Dave**)
- Design Concepts
  - Summary of discarded options (**Dave**)
  - GS35 Segmented (**Rob**)
    - Brief summary of final configuration & conclusions
  - GS35 Blisk (**Dave**)
    - Baseline
    - Changes for mechanically acceptable configuration
  - Rotor 257, 257b (**Dave**)
- Rotor Assembly - How will Inducer & Exducer be attached - (**Geene**)
  - Summary of all options considered
  - More detailed discussion of non-central bolted & shaft locknut configurations
  - Further work
- Program (**Dave**)
  - Manufacturing
  - Schedule
  - Budget

The Rotor Assy will be covered in a supplemental CDR the week of Aug 2nd

System Definition and Scope

- **The Inducer is the axial flow component of the rotor assembly. The rotor assembly comprises 2 Inducers (Axial Flow) components, one at each inlet plus the dual entry Exducer.**

- **The Inducer includes an integrated shroud which encompasses the flowpath.**

- **The Inducer interfaces with:**
  - **The static structure via 2 -3 seals on the shroud.**
  - **The static structure in the wheelspace via a seal arm lab tooth**
  - **The Exducer via a radial pilot, axial bolts and shear pins**

Agenda

- System Definition and Scope (**Dave**)
- Review action items from prior design review (**Dave**)
- Requirements (**Dave**)
- Design Concepts
  - Summary of discarded options (**Dave**)
  - GS35 Segmented (**Rob**)
    - Brief summary of final configuration & conclusions
  - GS35 Blisk (**Dave**)
    - Baseline
    - Changes for mechanically acceptable configuration
  - Rotor 257, 257b (**Dave**)
- Rotor Assembly - How will Inducer & Exducer be attached - (**Geene**)
  - Summary of all options considered
  - More detailed discussion of non-central bolted & shaft locknut configurations
  - Further work
- Program (**Dave**)
  - Manufacturing
  - Schedule
  - Budget

Action Items from previous Rotor CDR

1. Dave to prepare a proposed fatigue/life design requirement for aero/mechanical review and approval
   - Incomplete

2. Aero needs to determine extent of 'supersonic' surface finish requirements (supersonic region changes with back-pressure)
   - 4 micro inches throughout ? Now have split rotor so 'supersonic' applies to Inducer only.

3. Need to show manufacturing ability to meet aero surface finish requirements. If it's impossible to meet these requirements, then aero needs to revisit them
   - Plan in place – see discussion in manufacturing section

4. Need to determine flowpath geometric matching requirements for split rotor configuration
   - This applied to close-coupled split rotor. Now that Inducer & Exducer are split by approx ¾" of vaneless space, this does not apply, other than normal flowpath step requirements.

5. Have not shown ability to meet aero-requested profile requirements. If it's impossible to meet these requirements, then aero needs to revisit them.
   - Inducer fabrication can meet aero-requirements. Confirm via Praewest Manufacturing trial

6. Ensure seal analysis and conjugate heat transfer analysis use appropriate exducer leakage conditions (probably not CFD results)
   - In-progress.

7. Need to reconcile which types of bleed geometry mechanical can implement and aero can tolerate
   - In progress.

Action Items

1. Assess fillet / fillet scoop bleed in more detail now that aero have more interest. Use split rotor inducer model as vehicle. Consider hole size, angle, streamwise location and scoop size.
   - Work completed by Rob. See summary \\Rp-file\engineering\CO2Program\Demo Unit Mechanical Systems\Rotor\BLEED\CornerBleedFEA.ppt

2. A note that under-rim 'scalloping' is permissible if a coverplate is used
   - Noted

3. Update Budget to reflect split rotor configuration
   - Done & communicated to Joe.

4. Refine schedule with split rotor specific manufacturing input (this is an on-going item anyway)
   - Done & communicated to Aaron et al

Program Actions (Kirk, Mike, and Joe)

1. Discussed yesterday

Agenda

- System Definition and Scope (**Dave**)
- Review action items from prior design review (**Dave**)
- Requirements (**Dave**)
- Design Concepts
  - Summary of discarded options (**Dave**)
  - GS35 Segmented (**Rob**)
    - Brief summary of final configuration & conclusions
  - GS35 Blisk (**Dave**)
    - Baseline
    - Changes for mechanically acceptable configuration
  - Rotor 257, 257b (**Dave**)
- Rotor Assembly - How will Inducer & Exducer be attached - (**Geene**)
  - Summary of all options considered
  - More detailed discussion of non-central bolted & shaft locknut configurations
  - Further work
- Program (**Dave**)
  - Manufacturing
  - Schedule
  - Budget

Inducer Functional Requirements / Design Goals

- **Provide structure to carry the flowpath at the required location**
- **Provide a shroud (cover) on the OD of the flowpath.**
- **Provide structure on the outer surface of the shroud to facilitate leakage flow sealing.**
- **Provide routing for flow removal from the main flowpath**
- **Minimize steps in flowpath between rotating and static components**
- **Provide size / mass / stiffness commensurate with rotordynamic requirements**

Inducer Functional Requirements / Design Goals

RAMGEN POWER SYSTEMS™

Inlet & Exit conditions

Item	Revised Assumption (4/19/10)	note
Suction flange conditions	Nominal mass flow rate: 86 lbm/sec (@ 220 psia and 100 F) Maximum mass flow rate: 97 lbm/sec (@ 220 psia and 100 F) Unstarted mass flow rate: 69 lbm/sec (@ 220 psia and 100 F) Nominal suction pressure: 220 psia ±1% Fluctuation during performance test (max - min): 2% Suction pressure may vary ±10% at other conditions Minimum suction pressure: 55 psia Nominal suction temperature: 100°F ± 2° Fluctuations during performance test (max - min): 0.5%	These are the anticipated suction conditions with flow path started. Mass flow may be less at lower rotor speeds. The closed loop system may be operated with lower suction pressures and temperatures with an unstarted rotor.
Discharge flange conditions	Nominal discharge pressure: 2200 psia Fluctuation during performance test (max - min): 2% Maximum discharge pressure: Margin over 2200 psia is required ~2400 psia is a reasonable TARGET Minimum discharge pressure at design speed: 330 psia (prior to starting) Nominal discharge temperature: 535°F Maximum discharge temperature: 625°F Minimum discharge temperature at design speed: 200 F (prior to starting)	Aero does not have a maximum pressure requirement Piping temperature limit is 650 F

Extract from \\Rp-file\engineering\CO2Program\Requirements\2010.06.22 Aero Spec for Mech Preliminary Design.xlsx

Inducer Functional Requirements / Design Goals

- **Rotor will rotate clockwise as viewed from the driven end looking forward**
  - **Same as Rampressor-2**

- **Capable of carrying full speed (36,306 rpm), Power (10MW) and torque load (2209 ft.lb)**

- **Life Requirement** (Needs Confirming – See Action Item 1)
  - Cycles: Min 400 start cycles
    - Start stop cycle to MCOS
    - See requirements document (extract on later slide)
  - Hours: Min 900 hrs of testing
    - See requirements document (extract on later slide)

- **Disc Burst Margin > 125% MCOS**

- **Inspection**
  - Ultrasonic After HIP
  - LPI after machining

- **Balancing**
  - Major components individually balanced to ISO 1940 grade G1 or better
  - Rotor Assy multiplane dynamically balanced to Umax=4W/N

Inducer Functional Requirements / Design Goals

- **Acceptance Testing**
  - Overspeed to >=115% MCOS for 1 minute
    - API 617 Chapter 1 Section 4.3.3.1
    - Spin Pit
    - Pre and Post test dimensional inspection required
    - Pre & Post test NDI (not in API spec but would seem prudent)

- **Marking**
  - Marked with unique ID number

- **Rotor Acceleration Limits**
  - Ramp rate limit to avoid excessive accel loads and/or thermal transients

- **Corrosion Resistance (goal)**
  - API Standard 617, 7th edition, July 2002
    - NACE MR0175 materials shall be used in sour gas applications as described in the specification (2.2.1.6)

Agenda

- System Definition and Scope (**Dave**)
- Review action items from prior design review (**Dave**)
- Requirements (**Dave**)
- Design Concepts
  - Summary of discarded options (**Dave**)
  - GS35 Segmented (**Rob**)
    - Brief summary of final configuration & conclusions
  - GS35 Blisk (**Dave**)
    - Baseline
    - Changes for mechanically acceptable configuration
  - Rotor 257, 257b (**Dave**)
- Rotor Assembly - How will Inducer & Exducer be attached - (**Geene**)
  - Summary of all options considered
  - More detailed discussion of non-central bolted & shaft locknut configurations
  - Further work
- Program (**Dave**)
  - Manufacturing
  - Schedule
  - Budget

Inducer Options

Option	Description	Feasibility			Score
		Manufacturing	Mechanical	Aero	
0	Current GS35 rev2-5	Promising (1 vendor only)	Some Issues. Looks promising	Aero preferred	6
1	Split inducer	Promising	Does not appear feasible		0
2	Strakes as full length inserts	Promising	Does not appear feasible		0
3	Unshrouded Inducer	Feasible	Some Issues. Looks promising	Needs much work	6
4	Separate shroud	Feasible	Some issues - needs more work		3
5	Circumferential attachment slot	Feasible	Early Promise	Similar to option 0	3
6	Axial Segments	Feasible	Promising		3
7	Setback (Partially) shrouded	Promising	Not feasible		0
8	Reduced Flowpath length	Promising	Promising		4
9	Short Sidewall	Feasible	Appears Feasible	?	6

Green = 3, Yellow = 2, Orange = 1, Red = 0

The following slides show options 5, 0 and 9. The remainder are shown in the appendix

Agenda

- System Definition and Scope (**Dave**)
- Review action items from prior design review (**Dave**)
- Requirements (**Dave**)
- Design Concepts
  - Summary of discarded options (**Dave**)
  - GS35 Segmented (**Rob**)
    - Brief summary of final configuration & conclusions
  - GS35 Blisk (**Dave**)
    - Baseline
    - Changes for mechanically acceptable configuration
  - Rotor 257, 257b (**Dave**)
- Rotor Assembly - How will Inducer & Exducer be attached - (**Geene**)
  - Summary of all options considered
  - More detailed discussion of non-central bolted & shaft locknut configurations
  - Further work
- Program (**Dave**)
  - Manufacturing
  - Schedule
  - Budget

GS35 Blisk

The following slides show the results of a structural analysis of the Inducer supplied as GS35

Analysis Details

Material: Ti-5553
Analysis Speeds: 36,306 rpm
Analysis temp: Elevated

Cyclic symmetry
Frictionless restraint on rear of disc
Circumferential restraint at single location on front of disc
Radial displacement of 0.0075” on pilot dia based on Exducer analysis

Ramgen Power Systems Proprietary

Agenda

- System Definition and Scope (**Dave**)
- Review action items from prior design review (**Dave**)
- Requirements (**Dave**)
- Design Concepts
  - Summary of discarded options (**Dave**)
  - GS35 Segmented (**Rob**)
    - Brief summary of final configuration & conclusions
  - GS35 Blisk (**Dave**)
    - Baseline
    - Changes for mechanically acceptable configuration
  - Rotor 257, 257b (**Dave**)
- Rotor Assembly - How will Inducer & Exducer be attached - (**Geene**)
  - Summary of all options considered
  - More detailed discussion of non-central bolted & shaft locknut configurations
  - Further work
- Program (**Dave**)
  - Manufacturing
  - Schedule
  - Budget

Rotor 257b

Views on CAD model

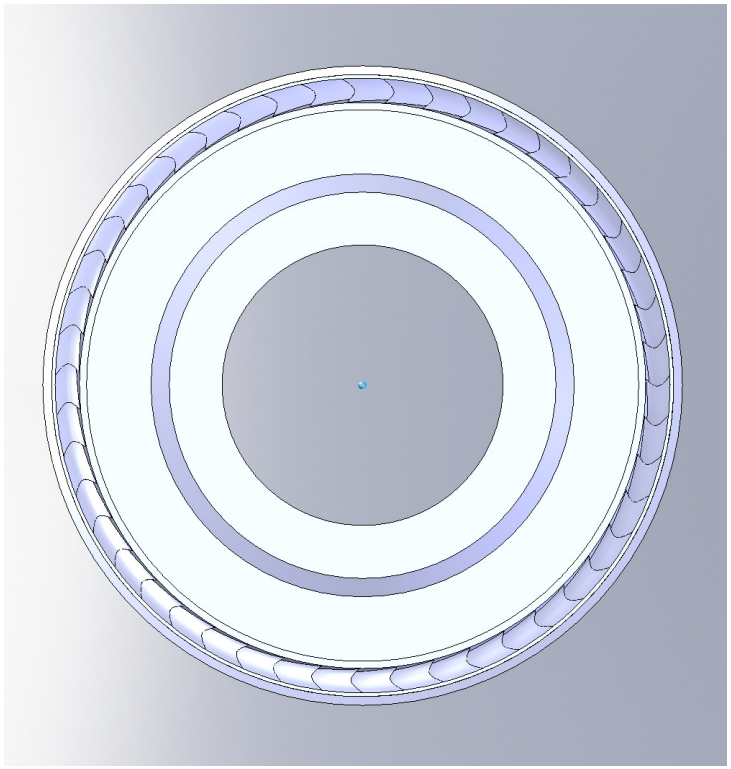

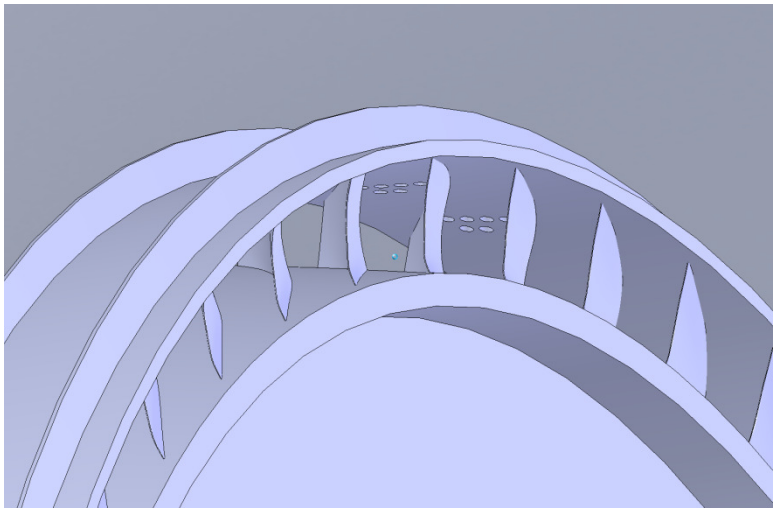

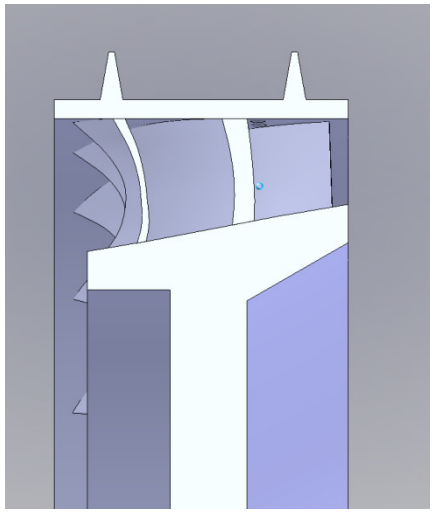

Rotor257b Machining Access

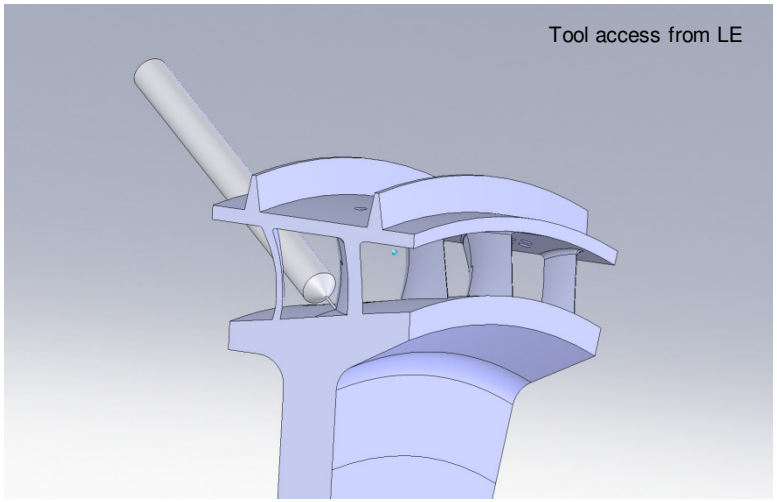

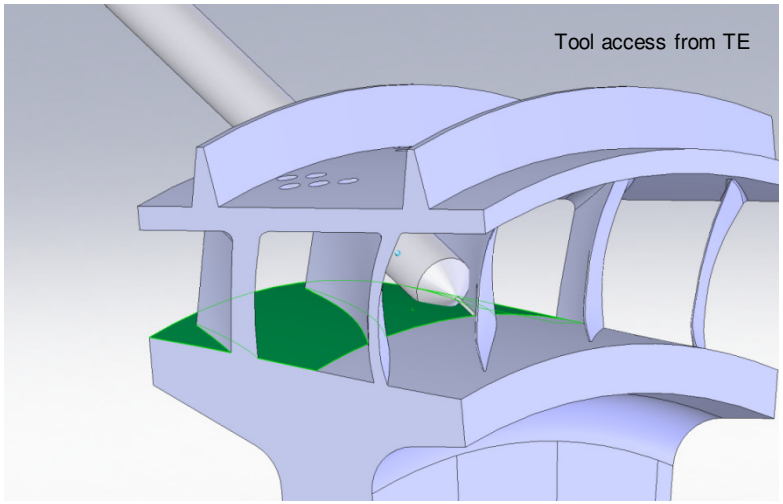

MINIATURE END MILLS

BALL

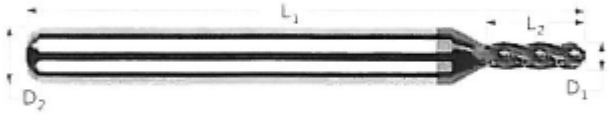

Length of Cut = 3 x Diameter Micro Grain Carbide

CUTTER DIA.	LOC	SHANK DIA.	OAL	UNCOATED			ALTiN COAT
D_1 +.0005" -.0005"	L_2 +.010" -.000"	D_2	L_1	2 FL	4 FL	PRICE	4 FL
.005	.015	1/8	1-1/2	74005		35.60	

Extract from Harvey tools catalog. Very similar to data received from Finecast.

Machining access is tight.
Needs review by machine shop

Rotor 257b

Analysis Model

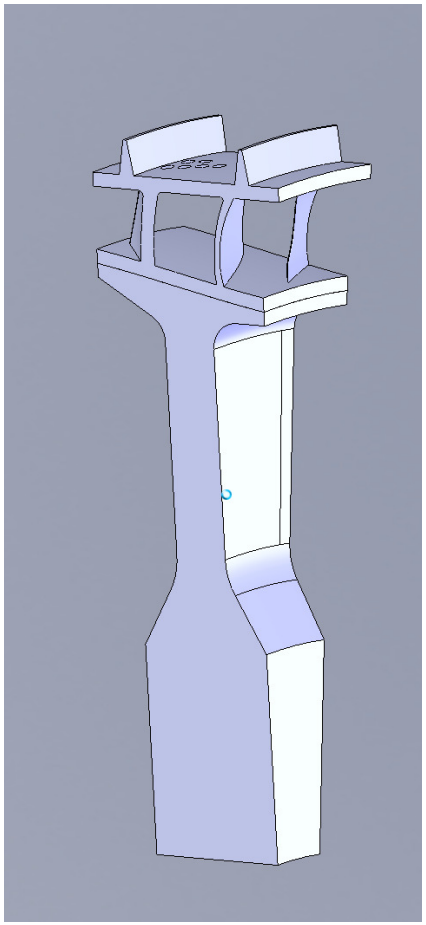

- Took Rotor 257 geometry and moved out to 4.374” shroud radius. maintained blade thickness, LE & TE Profiles etc
- Rotor 257 blade geometry supplied as IGES file with LE and TE features included
    - Leading edge scalloped & elliptical
        - Appears to be approx 0.005 - 0.010” thick
    - Trailing edge radial with full round
        - Appears to be 0.005 – 0.010” thick
- Strake to rim fillet not possible – vagaries of model after moving.
- Strake to shroud fillet:
    - 0.005” rad in LE region, increasing to 0.020” at TE
- Bleed features added to shroud only
    - Added from 50% chord and downstream only
- Aero design point 27,206 rpm
- Structural Analysis at 33,743 rpm (MCOS)

Rotor257b.SLDPRT<-.004>
Rotor257b_Run01.wbpj

Agenda

- System Definition and Scope (**Dave**)
- Review action items from prior design review (**Dave**)
- Requirements (**Dave**)
- Design Concepts
  - Summary of discarded options (**Dave**)
  - GS35 Segmented (**Rob**)
    - Brief summary of final configuration & conclusions
  - GS35 Blisk (**Dave**)
    - Baseline
    - Changes for mechanically acceptable configuration
  - Rotor 257, 257b (**Dave**)
- Rotor Assembly - How will Inducer & Exducer be attached - (**Geene**)
  - Summary of all options considered
  - More detailed discussion of non-central bolted & shaft locknut configurations
  - Further work
- Program (**Dave**)
  - Manufacturing
  - Schedule
  - Budget

Inducer Manufacturing

- **Baseline**
  1. Create Ti-5553 HIP Compact
  2. Heat Treat
  3. 5-axis machine Blisk, EDM bleed features where required
  4. Abrasive flow to remove EDM re-cast layer
  5. Surface Finish Treatment (MicroTek) to improve surface finish
  6. Inspect
  7. Balance
  8. Spin Pit Proof Test

Conceptual Design Review

Exhaust & Discharge Systems

System owner(s):

Ryan Edmonds, Brian Massey

Date

1/22/2010

System Definition and Scope

- **Provide for Exhaust of rotor core flow, aft bleed flow, and high pressure seal leakage.**
- **The system additionally includes diffuser vane bypass capability around the stationary diffuser vanes.**

Functional Requirements/Design Goals

- Transition core exhaust flow from stationary diffuser to discharge piping
  - Fit exhaust volute into current pressure vessel envelope
- Manifold aft bleed & HP seal leakage for discharge through pressure vessel
  - Minimize number of takeoffs
- Provide for flow exhaust during rotor low back pressure started operation
  - Bypass the diffuser vanes
  - Movable diffuser vanes
- Provide for IGV discharge survey
- Maintain diffuser & rotor alignment
- Minimize heat transfer into the pressure case
- Accommodate alignment and core bundle extraction
- Acceptable total pressure loss

Important Interfaces

- **Electrical**
  - **Anticipating electrical motor driven actuators on bypass valve outside of pressure vessel**
- **Mechanical**
  - **Pressure Vessel**
    - **Qty. 2 c-seals planned at interface with pressure vessel**
  - **Radial Inlet**
    - **Axial load path thru radial inlet plenum**
  - **Rim Seal Cartridge**
    - **C-seal on OD interface to volute discharge plate**
  - **HP Seal Leakage Plate**
    - **C-seal on OD interface of volute discharge plate**
    - **Sliding c-seal on bypass valve plate interface to seal leakage plate**
  - **Diffuser Vane Cartridge**
    - **Bolted connection to volute discharge plates**

Important Interfaces Cont'd

- **Fluid**
  - **Main Exhaust, currently modeling**
    - » **10" sch. 160 connection thru pressure vessel**
    - » **0.955" at diffuser discharge**
      - – **Assume no diffusion with maximum space utilized**
    - » **P=2200 psia, T = 650 deg. F**
  - **Aft Bleed,**
    - » **2X 3" sch. 160 connections thru pressure vessel**
    - » **7X R0.375" takeoffs thru volute plate**
    - » **P=220 psia, T=520 deg. F**
  - **HP leakage, 2X 3" sch. 160 connections thru pressure vessel**
    - » **6X R0.65" takeoff thru volute plate**
    - » **P=220 psia, T=520 deg. F**

Instrumentation

- **IGV survey probe (qty. 2) fed through discharge volute both NDE & DE**
- **Diffuser**
  - **Propose 3 Ps measurement locations in diffuser**
    - **4 Ps ports along endwall, both sides of passage, 3 locations (24 total)**
  - **Single Pt measurement location with 3 ports on vane LE (3 total)**
  - **27 measurements in all**

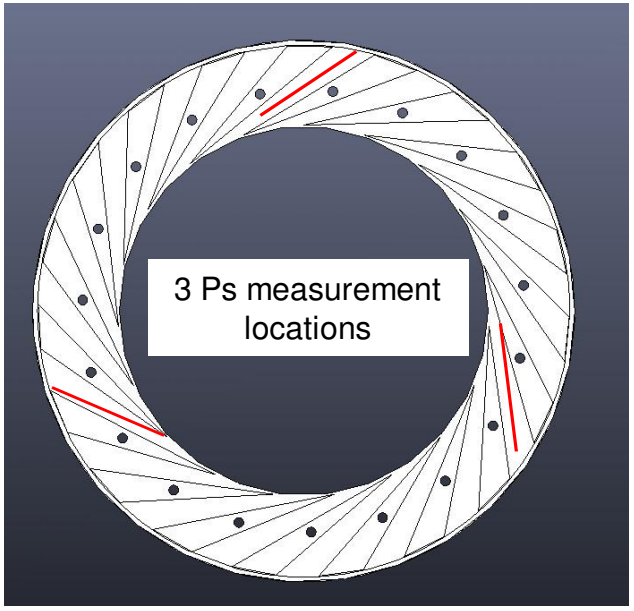

At each Ps location:

•8 Ps ports in passage (4 each side)

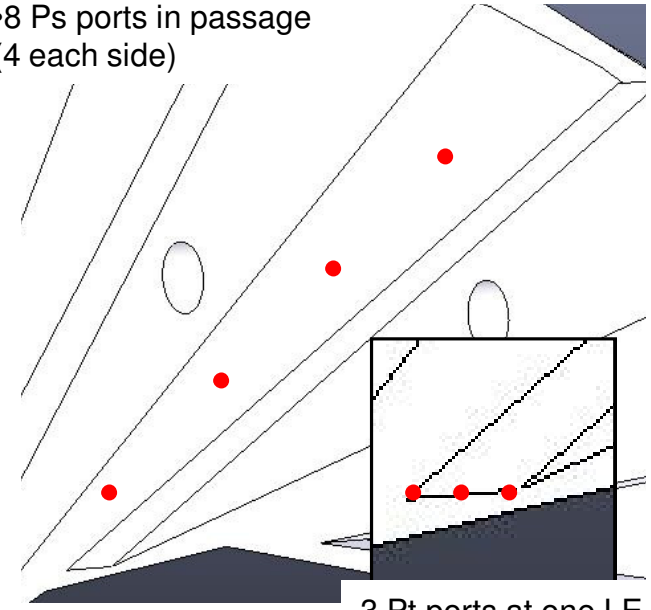

3 Pt ports at one LE vane location

Future Analyses

- **Volute Analyses Required**
  - **Aero definition of volute geometry**
  - **Aero CFD of volute geometry**
  - **Aero CFD of bypass passage and return**
  - **Heat transfer & structural modeling at volute/pressure vessel interface**
  - **Seal design for HP leakage cavity & aft bleed cavity**
- **Actuator Analyses required:**
  - **Detailed actuator pin stresses due to pressure differentials across plate**
  - **Definition of actuator requirements – strength and movement**
  - **Deflection/displacement of actuator pushrod, check for interference with passage walls during movement**
  - **Separation forces between vanes and backplate depending on seal arrangement**
  - **Detailed seal designs**

Schedule

- **Schedule**
  - **PDR date**
    - **3rd week of March**
  - **FDR date**
    - **Last week of May**
  - **Drawing Start**
    - **May 7th, 2009 (~5 weeks)**
  - **Drawing release**
    - **June 15th, 2009**
  - **Manufacturing start**
    - **Jul. 1st, 2009 (~8 weeks)**
  - **Delivery date**
    - **Sept. 1st, 2009**

Schedule and Budget

- **Is schedule achievable?**
  - **Exducer and diffuser follow core aero flowpath design, if supersonic flowpath does not freeze well before May 31st exducer, diffuser, and volute final design will slip current schedule**
  - **More overlap than desired between final design and drawing creation for Sept. 1st, 2009 delivery**
- **Current budget**
  - **$280,000 for hardware**
- **Is current budget adequate?**
  - **No anticipated ODC costs**

Conceptual Design Review

Secondary Systems

System owner(s):

Jonathan Bucher

Date

2/4/2010

System Definition and Scope

Flow rates and losses for annuli and routing passages supporting fluid transfer from the primary flowpath and within the supporting systems. Secondary systems includes instrumentation egress internal to the pressure case.

Functional Requirements/Design Goals

- **Route fluids from desired flowpath or driveline location to or from the exterior of the pressure housing with acceptable mass and pressure losses.**
- **Interface with facility flow loops and controls**

Primary and Secondary Systems

- **Primary systems**
  1. **Suction nozzles**
  2. **Discharge nozzle**
- **Flowpath secondary systems**
  4. **High pressure seal leakge flow**
  5. **Aft/performance bleed**
  6. **Forward/starting bleed**
  7. **Suction isolation flow (rotor)**
- **Shaft sealing, secondary systems**
  8. **Non-driven-end, wheelspace pressure control circuit discharge**
  8. **Driven-end, wheelspace pressure control circuit discharge**
  10. **Non-driven-end, barrier seal supply gas**
  10. **Driven-end, interior, barrier seal, supply gas**
  10. **Driven-end, exterior, barrier seal, supply gas**
  11. **Non-driven-end, shaft seal, mixed gas discharge**
  11. **Driven-end, shaft seal, mixed gas discharge**
  18. **Driven-end, shaft seal purge gas supply**

Numbering consistent with previously released Prelim SE01a flows and passage sizes.ppt

Primary and Secondary Systems

- **Driveline secondary systems**
  - **12. Non-driven-end, journal bearing lubrication supply**
  - **12. Non-driven-end, thrust bearing lubrication supply**
  - **13. Non-driven-end, oil drain (supply oil , barrier seals)**
  - **14. Driven-end, journal bearing lubrication supply**
  - **15. Driven-end, oil drain (supply oil , barrier seals)**
  - **– Driven-end, gearbox drain (star oil, HS coupling purge return)**
  - **20. High speed coupling, cavity purge supply**
  - **– Driven-end coupling borescope access**
  - **– Driven-end vision/light access**
  - **16. Non-driven-end damper supply**
  - **16. Driven-end damper supply**
  - **17. Non-driven-end damper return**
  - **17. Driven-end damper return**

Primary and Secondary Systems

- **Actuators**
  - **33. NDE, IGV actuator**
  - **33. DE, IGV actuator**
  - **32. NDE, diffuser bypass actuator**
  - **32. DE, diffuser bypass actuator**
  - **31. NDE, survey plane actuator**
  - **31. DE, survey plane actuator**
- **Case drains**
  - **35. Discharge drain**
  - **35. NDE, suction drain**
  - **35. DE, suction drain**

Primary and Secondary Systems

- **Instrumentation**
  - **34. Driven-end, IGV hub/shroud**
  - **34. Driven-end, wheelspace; proximeters; oil drain temps**
  - **34. Non-driven-end, IGV hub/shroud**
  - **34. Non-driven-end, wheelspace; proximeters; oil drain temps**
  - **34. Non-driven-end, diffuser**

Important Interfaces

- **Electrical**
  - **No direct electrical interface for secondary flow connections**
- **Mechanical**

Mechanical Interfaces

- **Suction nozzles (2 plcs.)**
  - **Connection size: 12 in., ASME B16.5-2009, 1500 # class, material group 1.2 (A 352 Gr. LCC/LC2), RTJ, flange**
  - **Location**
    - **Radial: 50 deg CW from TDC (viewed toward the drive end)**
    - **Axial: Centerline 12.213 in. from rotor mid-plane**

fluid co2
units e

system		DP nominal inflow plenum, per side	DP nominal inflow plenum, per side	DP nominal inflow plenum, per side	DP nominal inflow plenum, per side	DP nominal inflow plenum, per side	DP nominal inflow plenum, per side	DP nominal inflow plenum, per side
core flow	lbm/sec	43	43	43	43	43	43	43
duct flow % core flow	%	100	100	100	100	100	100	100
sizing mass flow	lbm/sec	43	43	43	43	43	43	43
sizing pressure	psia	220	220	220	220	210	210	220
sizing temp	degF	100	100	100	100	110	110	100
density	lbm/ft^3	1.73065772	1.730658	1.730658	1.730658	1.61046	1.6104601	1.7306577
local SOS	ft/sec	865.953829	865.9538	865.9538	865.9538	876.6657	876.66566	865.95383
Duct Mach number		0.1	0.113331	0.07	0.07281	0.05	0.0544604	0.0513095
inflow velocity	ft/sec	86.5953829	98.13901	60.61677	63.04978	43.83328	47.743569	44.431649
required area	ft^2	0.28692113	0.253172	0.409887	0.39407	0.609136	0.5592469	0.559197
equiv. dia.	in.	7.25299825	6.81309	8.668991	8.500083	10.56802	10.126004	10.125552
nom pipe size/dia.			8		10		12	12

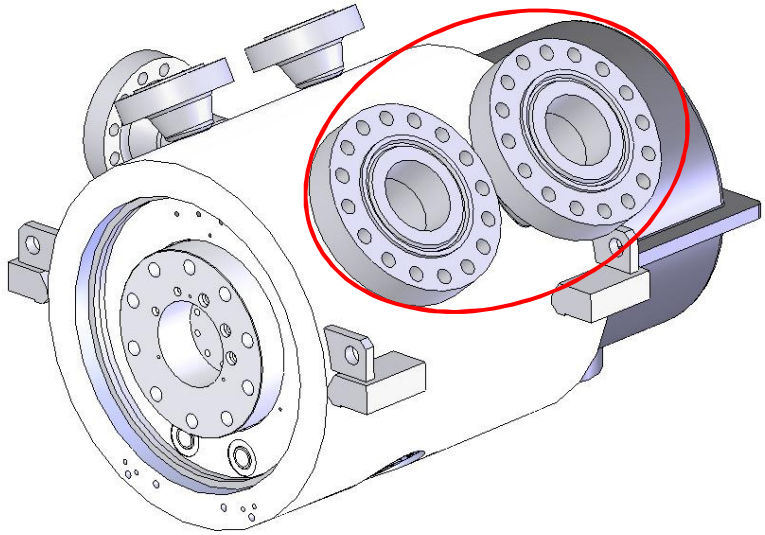

Mechanical Interfaces

- **Discharge nozzle (2 plcs.)**
  - **Connection size: 10 in. (8 in. possible), ASME B16.5-2009, 1500 # class, material group 1.2 (A 352 Gr. LCC/LC2), RTJ, flange**
  - **Location**
    - **Horizontal: tangentially oriented ≈30 CCW of TDC (viewed toward the drive end), TBD offset from horizontal**
    - **Axial: Rotor mid-plane**

system		exhaust nominal, single discharge	exhaust nominal, single discharge	exhaust nominal, single discharge	exhaust nominal, single discharge
core flow	lbm/sec	86	86	86	86
duct flow % core flow	%	100	100	100	100
sizing mass flow	lbm/sec	86	86	86	86
sizing pressure	psia	2200	450	2200	450
sizing temp	degF	525	525	525	525
density	lbm/ft^3	9.6457658	1.9004454	9.64576584	1.90044536
local SOS	ft/sec	1185.3458	1162.7335	1185.34579	1162.73351
Duct Mach number		0.0297096	0.1536956	0.01908902	0.09874158
required area	ft^2	0.2531748	0.2532219	0.39403336	0.39415117
equiv. dia.	in.	6.8131282	6.813762	8.49968444	8.50095496
nom pipe size/dia.		8 in., sched 160	8 in., sched 160	10 in., sched 160	10 in., sched 160

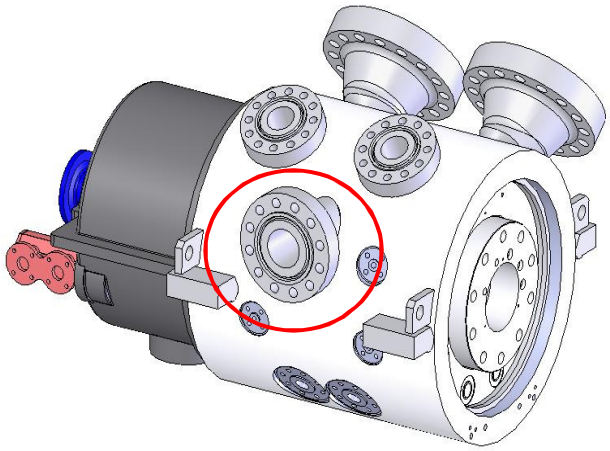

Mechanical Interfaces

- **High Pressure Seal Leakage Flow (2 plcs.)**
  - **Connection size: 3 in., ASME B16.5-2009, 1500 # class, case integral, raised face, flange**
  - **Location**
    - **Radial: 150- 200 deg CCW (viewed toward the drive end)**
    - **Axial: Centerline 5.625 in. from rotor mid-plane**

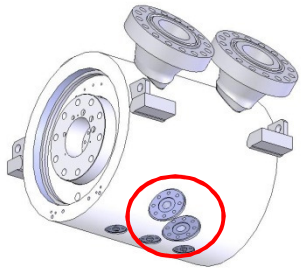

fluid co2
units e

HP seal leakage System

system		design point post rub leakage	design point post rub leakage
core flow	lbm/sec	43	43
duct flow % core flow	%	0	0
2x clearance seal leakage, design point	lbm/sec	5	5
sizing mass flow	lbm/sec	5	5
sizing pressure	psia	220	220
sizing temp	degF	520	520
density	lbm/ft^3	0.927588	0.927588
local SOS	ft/sec	1160.783	1160.783
Duct Mach number		0.123405	0.298443
required area	ft^2	0.03763	0.01556
equiv. dia.	in.	2.626651	1.689032
nom pipe size/dia.		3 in.	2 in.

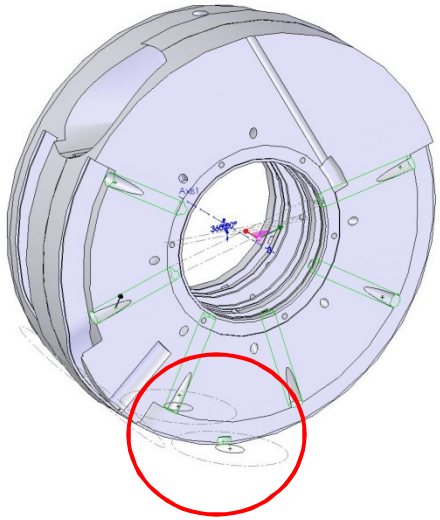

HP leakage

- Target area is 5.42 in^2
- Rotor shroud takeoff holes
  - 36 X 0.438" dia
  - Holes to be angled to compliment rotor shroud induced swirl
  - 1D Mach ~ 0.12
- Lower collection annulus
  - Cross section sized based on 2/7 of total flow
    - 7 takeoffs, 2X for conservatism → 2/7 of total flow
  - 1D Mach ~ 0.19
- Volute plate takeoff holes
  - R0.5" X 7 holes, 5.49in^2
  - 1D Mach ~ 0.12

Aft Bleed

- Target area is 2.24 in^2
- Rotor shroud takeoff holes
  - 0.2" dia. at shroud tapered to ~0.280" dia. X 36 holes
  - Holes planned to be angled by TBD deg. to compliment rotor bleed swirl
  - 1D Mach ~ 0.15
- Lower collection annulus
  - Cross section sized based on 1/3 of total flow
    - 6 takeoffs, 2X for conservatism → 1/3 of total flow
  - 1D Mach ~ 0.18
- Volute plate takeoff holes
  - R0.375" X 6 holes, 2.65 in^2
  - 1D Mach ~ 0.15

Mechanical Interfaces

- **Suction isolation flow (2 plcs.)**
  - **Connection size: 1 in., ASME B16.5-2009, 1500 # class, case integral, rasied face, flange**
  - **Location**
    - **Radial: 95-120 deg CCW (viewed toward the drive end)**
    - **Axial: Centerline ≈12.213 in. from rotor mid-plane**

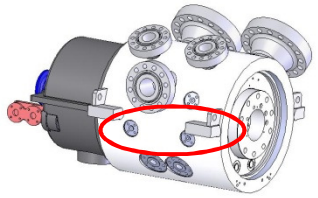

system		
core flow	lbm/sec	43
duct flow % core flow	%	0
2x clearance seal leakage, design point	lbm/sec	1.1
sizing mass flow	lbm/sec	1.1
sizing pressure	psia	220
sizing temp	degF	520
density	lbm/ft^3	0.927588
local SOS	ft/sec	1160.783
Duct Mach number		0.139217
required area	ft^2	0.007338
equiv. dia.	in.	1.159935
nom pipe size/dia.		1 in.

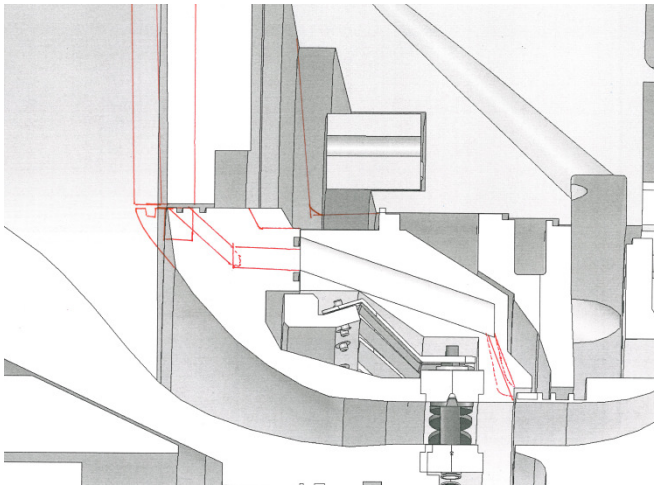

Mechanical Interfaces

- **Wheelspace flow extraction, NDE (non-driven-end)**
  - **0.73 lbm/sec flow extraction, assumes choked flow from .010 clr at 6.7in ID**
  - **Connection size: 1 in., ASME B16.5-2009, 1500 # class, head integral, raised face, flange**
  - **Location**
    - **Radial: TBD deg CCW (viewed toward the drive end)**
    - **Axial: Bearing housing**

fluid	CO2		
units	e		
Mid seal take-off (leakage returned to inflow plenum)			
system		**WS vent, LP side, max flow (2x clearance), stationary frame, per side**	**WS vent, HP side, max flow (2x clearance), stationary frame, both sides**
core flow	lbm/sec	43	43
duct flow % core flow	%	1.697674419	1.697674419
sizing mass flow	lbm/sec	0.73	0.73
sizing pressure	psia	60	140
sizing temp	degF	50	50
density	lbm/ft^3	0.495045496	1.197614717
local SOS	ft/sec	851.4731821	834.3676182
Duct Mach number		0.25	0.25
required area	ft^2	0.006927344	0.002922189
equiv. dia.	in.	1.126989026	0.731965225
nom pipe size/dia.			
number of internal plenum holes	#	6	6
req'd hole area	in.^2	0.16625626	0.070132534
req'd hole dia. for area match	in.	0.460091343	0.298823552

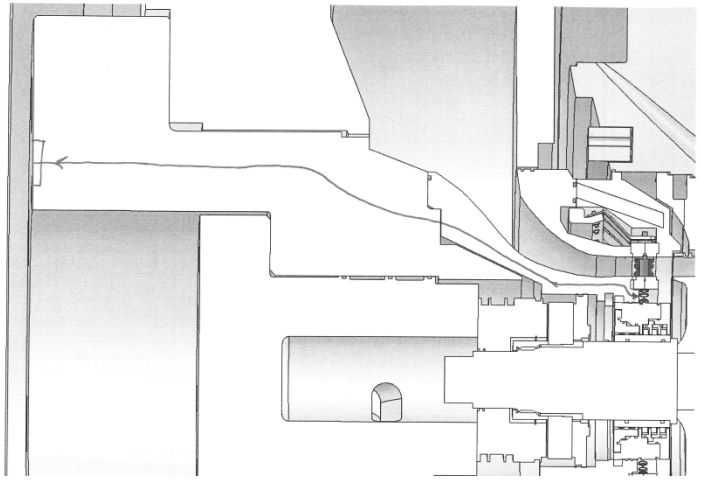

Mechanical Interfaces

- **Wheelspace flow extraction, DE (driven-end)**
  - **0.73 lbm/sec flow extraction, assumes choked flow from .010 clr**
  - **Connection size: 1 in., ASME B16.5-2009, 1500 # class, head integral, raised face, flange**
  - **Location**
    - **Radial: TBD deg CCW (viewed toward the drive end)**
    - **Axial: DE case end, ≈19.0 in. from rotor mid-plane**

fluid CO2
units e

Mid seal take-off (leakage returned to inflow plenum)

system		WS vent, LP side, max flow (2x clearance), stationary frame, per side	WS vent, HP side, max flow (2x clearance), stationary frame, both sides
core flow	lbm/sec	43	43
duct flow % core flow	%	1.697674419	1.697674419
sizing mass flow	lbm/sec	0.73	0.73
sizing pressure	psia	60	140
sizing temp	degF	50	50
density	lbm/ft^3	0.495045496	1.197614717
local SOS	ft/sec	851.4731821	834.3676182
Duct Mach number		0.25	0.25
required area	ft^2	0.006927344	0.002922189
equiv. dia.	in.	1.126989026	0.731965225
nom pipe size/dia.			

number of internal plenum holes	#	6	6
req'd hole area	in.^2	0.16625626	0.070132534
req'd hole dia. for area match	in.	0.460091343	0.298823552

No model

Mechanical Interfaces

- **Barrier seal supply gas, NDE**
  - **10 SCFM design point leakage per seal**
  - **Connection size: .765 dia. hole, TBD connection (1 in., MS fitting)**
  - **Location**
    - **Radial: 100 deg CCW (viewed toward the drive end)**
    - **Axial: DE case end, ≈19.0 in. from rotor mid-plane**

Air		
gas temp	degF	100
	degR	559.67
purge gas pressure	psia	85
air density	lbm/ft^3	0.410162408
local speed of sound	ft/sec	1162.572655
stnd pressure	psia	14.7
stnd temp	degF	59
air standard density	lbm/ft^3	0.076505065
Supply air flow area		
desired Mach	#	0.05
Mach associated speed	ft/sec	58.12863274
volumetric leakage	SCFM	10
mass flow rate	lbm/sec	0.012750844
req'd flow area	ft^2	0.000534802
	in^2	0.07701148
number of seals		1
effective dia.	in.	0.313135852

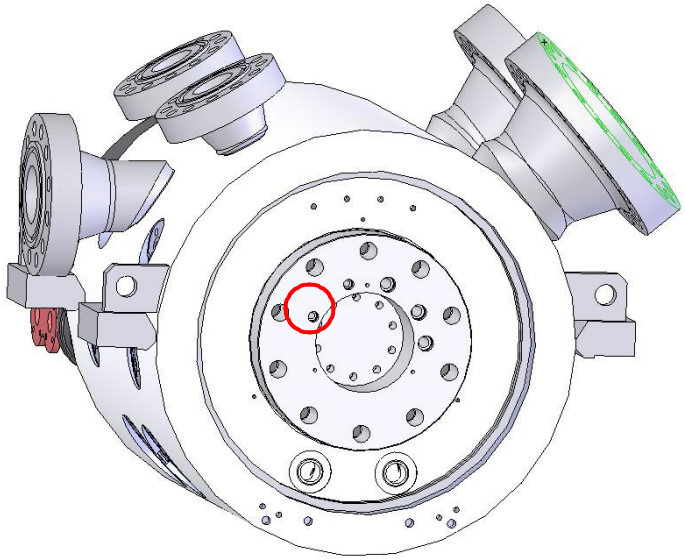

Mechanical Interfaces

- **Barrier seal supply gas, DE (common interior and exterior)**
  - **10 SCFM design point leakage per seal**
  - **Connection size: .75 dia. hole, TBD connection (1 in., MS fitting)**
  - **Location**
    - **Radial: 100 deg CW (viewed toward the drive end)**
    - **Axial: DE case end, ≈19.0 in. from rotor mid-plane**

Air		
gas temp	degF	100
	degR	559.67
purge gas pressure	psia	85
air density	lbm/ft^3	0.410162408
local speed of sound	ft/sec	1162.572655
stnd pressure	psia	14.7
stnd temp	degF	59
air standard density	lbm/ft^3	0.076505065
Supply air flow area		
desired Mach	#	0.05
Mach associated speed	ft/sec	58.12863274
volumetric leakage	SCFM	10
mass flow rate	lbm/sec	0.012750844
req'd flow area	ft^2	0.000534802
	in^2	0.07701148
number of seals		1
effective dia.	in.	0.313135852

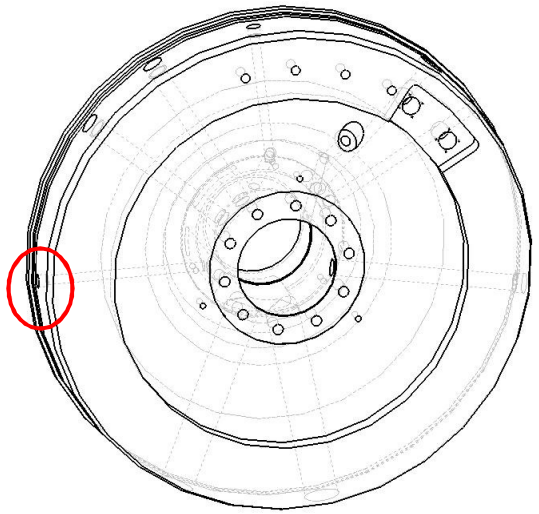

Mechanical Interfaces

- **Shaft seal leakage (mixed gas), NDE**
  - **Connection size: 2x 1.23 dia. holes, TBD connection (1.5 in., MS fitting)**
  - **Location**
    - **Radial: 10-80 deg CW (viewed toward the drive end)**
    - **Axial: Bearing housing face**

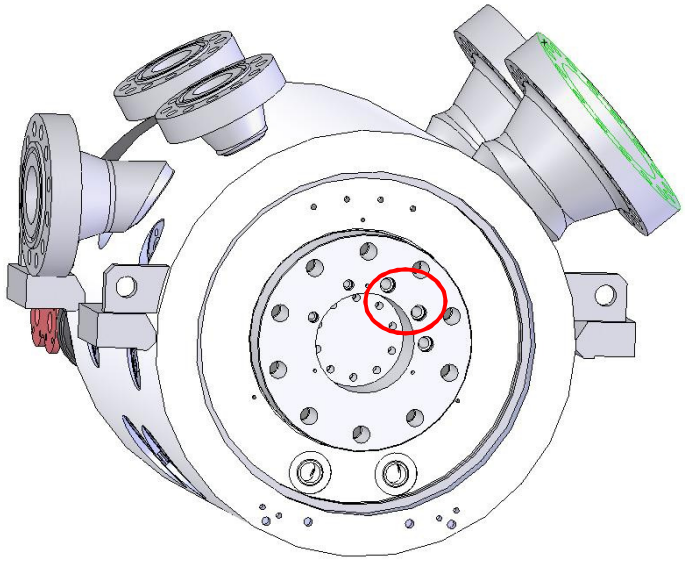

fluid co2
units e

intermediate shaft seal take-off

system		CO2	air	total		CO2	air	total
core flow	lbm/sec	0.078	0.15			0.078	0.15	
duct flow % core flow	%	100	100			100	100	
sizing mass flow	lbm/sec	0.078	0.15			0.078	0.15	
sizing pressure	psia	14.7	14.7			14.7	14.7	
sizing temp	degF	100	100			100	100	
density	lbm/ft^3	0.108188	0.070887			0.108188	0.070887	
local SOS	ft/sec	900.5859	1159.713			900.5859	1159.713	
Duct Mach number		0.1	0.1			0.17	0.17	
required area	ft^2	0.008006	0.018246	0.026252		0.004709	0.010733	0.015442
equiv. dia., 1 feed	in.	1.211522	1.829046	2.193899		0.929195	1.402814	1.682644
number of passages	#	1	1	1		1	1	1
passage dia., multiple	in.	1.211522	1.829046	2.193899		0.929195	1.402814	1.682644

Schedule 160 pipe diameters, nom.	ID, in.
1	1.16
2	1.689
3	2.626
4	3.438
5	4.313
6	5.189

Mechanical Interfaces

- **Shaft seal leakage (mixed gas), DE**
  - **Connection size: 2x 1.23 dia. holes, TBD connection (1.5 in., MS fitting)**
  - **Location**
    - **Radial: 40 & 60 deg CW (viewed toward the drive end)**
    - **Axial: DE case end, ≈19.0 in. from rotor mid-plane**

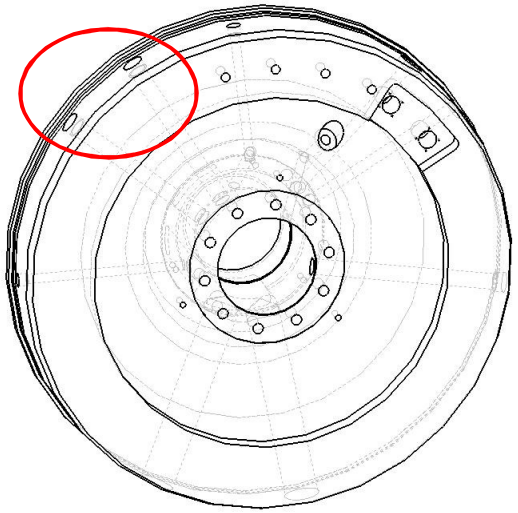

fluid co2
units e

intermediate shaft seal take-off

system		CO2	air	total		CO2	air	total
core flow	lbm/sec	0.078	0.15			0.078	0.15	
duct flow % core flow	%	100	100			100	100	
sizing mass flow	lbm/sec	0.078	0.15			0.078	0.15	
sizing pressure	psia	14.7	14.7			14.7	14.7	
sizing temp	degF	100	100			100	100	
density	lbm/ft^3	0.108188	0.070887			0.108188	0.070887	
local SOS	ft/sec	900.5859	1159.713			900.5859	1159.713	
Duct Mach number		0.1	0.1			0.17	0.17	
required area	ft^2	0.008006	0.018246	0.026252		0.004709	0.010733	0.015442
equiv. dia., 1 feed	in.	1.211522	1.829046	2.193899		0.929195	1.402814	1.682644
number of passages	#	1	1	1		1	1	1
passage dia., multiple	in.	1.211522	1.829046	2.193899		0.929195	1.402814	1.682644

Schedule 160 pipe diameters, nom.	ID, in.
1	1.16
2	1.689
3	2.626
4	3.438
5	4.313
6	5.189

Mechanical Interfaces

- **Dry gas seal, seal gas supply, DE**
  - **.073 lbm/sec flow requirement (2x clearance at 5 psid)**
  - **Connection size: 0.375 dia. hole, TBD connection (0.5 in., MS fitting)**
  - **Location**
    - **Radial: TBD**
    - **Axial: DE case end, ≈19.0 in. from rotor mid-plane**

fluid co2
units e

Bleed System

system		Jan10 dry gas seal, purge gas flowrate
core flow	lbm/sec	0.0000
duct flow % core flow	%	100
sizing mass flow	lbm/sec	0.075
sizing pressure	psia	145
sizing temp	degF	80
density	lbm/ft^3	1.160394
local SOS	ft/sec	860.7073
viscosity	lbm/ft-s	1.02E-05
dyn viscosity	ft^2/sec	8.75E-06
Duct Mach number		0.1
required area	ft^2	0.000751
equiv. dia., 1 feed	in.	0.371053
number of passages	#	1
passage dia., multiple	in.	0.371053

No model

Mechanical Interfaces

- **Oil supply, NDE**
  - **Connection size:**
    - **0.765 dia. hole, journal supply, TBD connection (1 in. pipe)**
    - **1.23 dia. hole, journal supply TBD connection (2 in. pipe)**
  - **Location**
    - **Radial: approx 10 deg CCW & 90 deg CW (viewed toward the drive end)**
    - **Axial: bearing housing face**

		air e SE01a case, journal bearing		air e SE01a case, thrust bearing		air e SE01a case, combined bearings	
Oil							
oil density	lbm/ft^3	53.69		53.69		53.69	
oil flow rate	gpm	20	flow for rep	70	flow for rep	90	combined
	lbm/sec	2.392478		8.373671		10.76615	
Sizing							
Oil (only) flow areas							
Supply							
mdot = A Cd sqrt(2 rho delP)							
delP	psid	3		3		3	
Cd (guess)		0.7		0.7		0.7	
A	ft^2	0.002798		0.009792		0.012589	
	in^2	0.402862		1.410017		1.812879	
Effective Feed Diameter	in.	0.716198		1.339884		1.519286	
Bearing Housing Oil Supply Rad	in	3.53		3.53		3.53	
Angle of Supply (from CL)	deg	30.00		30.00		30.00	
Slot Diameter	in	0.5		0.5		0.5	
Required Slot Angle	deg	9.580931		47.33324		62.43416	

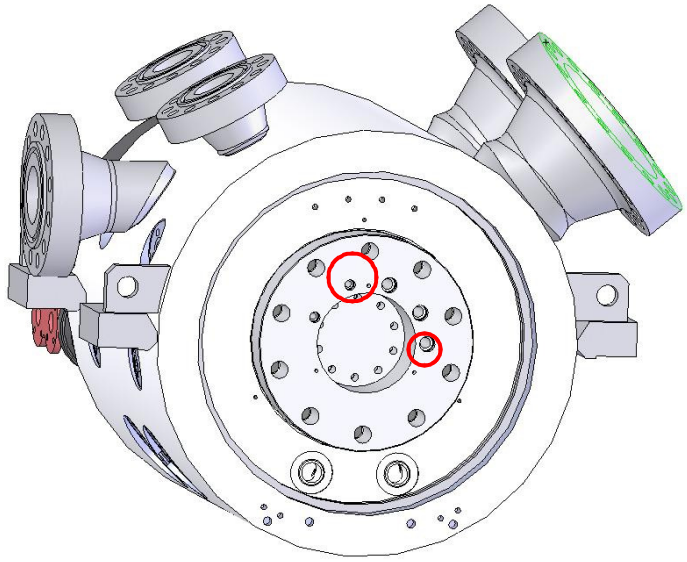

Mechanical Interfaces

- **Oil supply, NDE**
  - **Connection size: 2x 2.375 dia. hole, journal supply, TBD connection (3 in. pipe)**
  - **Location**
    - **Radial: +/- 18 deg from BDC**
    - **Axial: pressure head face**

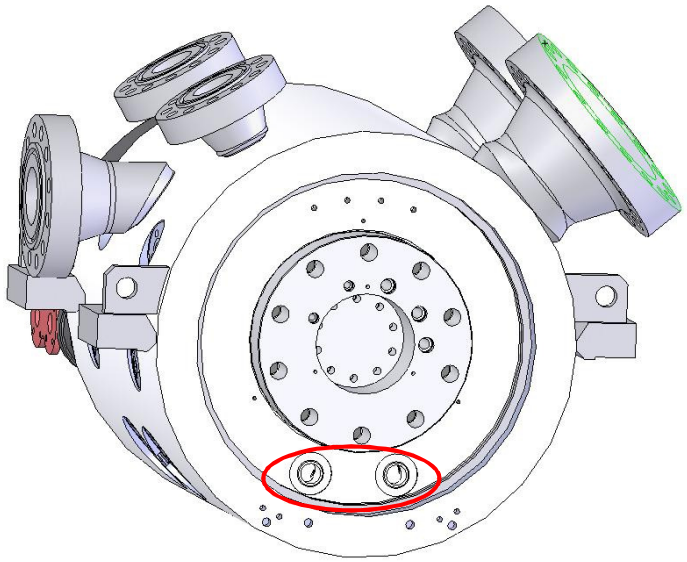

		air e SE01a case, journal bearing worst case	air e SE01a case, thrust bearing worst case	air e SE01a case, combined bearings worst case
Air				
air temp	degF	100	100	100
	degR	559.67	559.67	559.67
purge air pressure (lowest yields la	psia	14.7	14.7	14.7
air density	lbm/ft^3	0.07089	0.07089	0.07089
air speed of sound	ft/sec	1160.154	1160.154	1160.154
stnd pressure	psia	14.7	14.7	14.7
stnd temp	degF	59	59	59
air standard density	lbm/ft^3	0.076509	0.076509	0.076509
Oil				
oil density	lbm/ft^3	53.69	53.69	53.69
oil flow rate	gpm	20 flow for rep	70 flow for rep	90
	lbm/sec	2.392478	8.373671	10.76615
Drain				
mdot = rho V A				
velocity	ft/sec	2	2	2
	m/sec	0.6096	0.6096	0.6096
A	ft^2	0.02228	0.077982	0.100262
	in^2	3.208389	11.22936	14.43775
Effective Feed Diameter	in.	2.02115	3.781225	4.287507
Annulus Oil Take Off Radius	in	3.073	3.073	3.073
Required Annulus Width	deg	0.166167	0.581584	0.747751
Bearing Housing Oil Take Off Rad	in	3.53	3.53	3.53
Angle of Supply (from CL)	deg	30.00	30.00	30.00
Slot Diameter	in	0.50	0.50	0.50
Required Slot Angle	deg	114.7436	415.4027	535.6663
Air flow area				
desired Mach	#	0.05	0.05	0.05
Mach associated speed	ft/sec	58.0077	58.0077	58.0077
volumetric leakage	SCFM	0	118	118
mass flow rate	lbm/sec	0	0.150468	0.150468
req'd flow area	ft^2	0	0.036591	0.036591
	in^2	0	5.269111	5.269111
effective dia.	in.	0	2.590143	2.590143
Composite flow requirement				
Area_oil + Area_air	in^2	3.208389	16.49847	19.70686
effective dia. for single port	in.	2.02115	4.583286	5.009147
number of multiple ports		1	4	2
effective dia. for multiple port	in.	2.02115	2.291643	3.542002

Mechanical Interfaces

- **Oil supply, DE**
  - **Connection size:**
    - **0.76 dia. hole, journal supply, TBD connection (1 in. pipe)**
  - **Location**
    - **Radial: 15deg CW (viewed toward the drive end)**
    - **Axial: Axial: DE case end, ≈19.0 in. from rotor mid-plane**

			air e SE01a case, journal bearing		air e SE01a case, thrust bearing		air e SE01a case, combined bearings	
Oil								
oil density	lbm/ft^3		53.69		53.69		53.69	
oil flow rate	gpm		20	flow for rep	0	flow for rep	20	combined
	lbm/sec		2.392478		0		2.392478	
Sizing								
Oil (only) flow areas								
Supply								
mdot = A Cd sqrt(2 rho delP)								
delP	psid		3		3		3	
Cd (guess)			0.7		0.7		0.7	
A	ft^2		0.002798		0		0.002798	
	in^2		0.402862		0		0.402862	
effective dia.	in.		0.716198		0		0.716198	

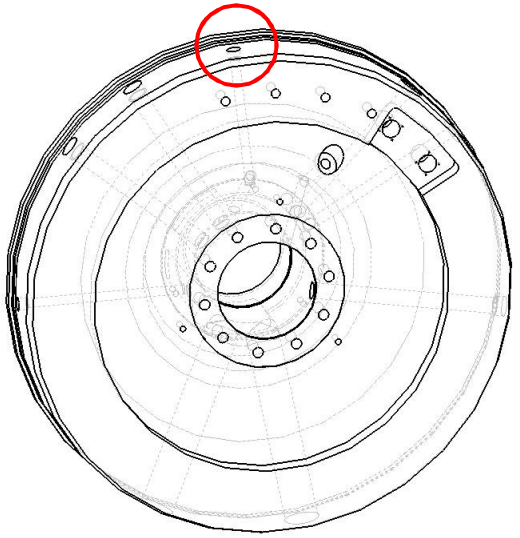

Mechanical Interfaces

- **Oil drain, DE**
  - **Connection size: 2x 2.5 dia. holes, TBD connection (3 in., case integral, rasied face flanges)**
  - **Location**
    - **Radial: +/- 16.8 deg from BDC**
    - **Axial: DE case end, ≈19.0 in. from rotor mid-plane**

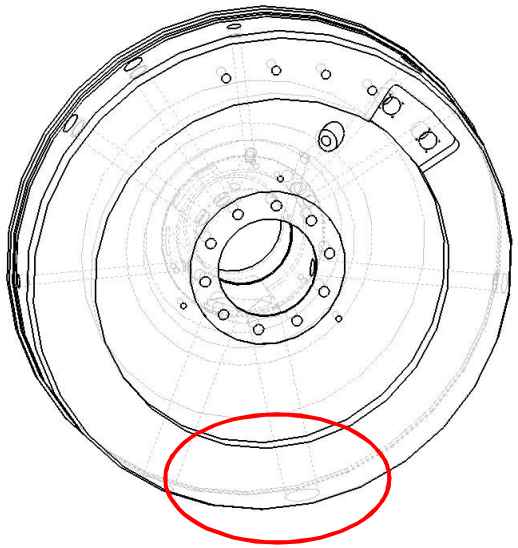

Air		
air temp	degF	100
	degR	559.67
purge air pressure (lowest yields	psia	14.7
air density	lbm/ft^3	0.07089
air speed of sound	ft/sec	1160.154
stnd pressure	psia	14.7
stnd temp	degF	59
air standard density	lbm/ft^3	0.076509
Oil		
oil density	lbm/ft^3	53.69
oil flow rate	gpm	20
	lbm/sec	2.392478
Sizing		
Oil (only) flow areas		
Supply		
mdot = A Cd sqrt(2 rho delP)		
delP	psid	3
Cd (guess)		0.7
A	ft^2	0.002798
	in^2	0.402862
effective dia.	in.	0.716198
delP=rho*g*h	psid	
h, drain height	ft	
Drain		
mdot = rho V A		
velocity	ft/sec	2
	m/sec	0.6096
A	ft^2	0.02228
	in^2	3.208389
effective dia.	in.	2.02115
Air flow area		
desired Mach	#	0.05
Mach associated speed	ft/sec	58.0077
volumetric leakage	SCFM	138
mass flow rate	lbm/sec	0.175971
req'd flow area	ft^2	0.042793
	in^2	6.162181
effective dia.	in.	2.801059
Composite flow requirement		
Area_oil + Area_air	in^2	9.37057
effective dia. for single port	in.	3.454125
number of multiple ports		2
effective dia. for multiple port	in.	2.442435

Mechanical Interfaces

- **Oil drain, DE**
  - **Connection size: 2x 2.5 dia. holes, TBD connection (3 in., case integral, rasied face flanges)**
  - **Location**
    - **Radial: +/- 16.8 deg from BDC**
    - **Axial: DE case end, ≈19.0 in. from rotor mid-plane**

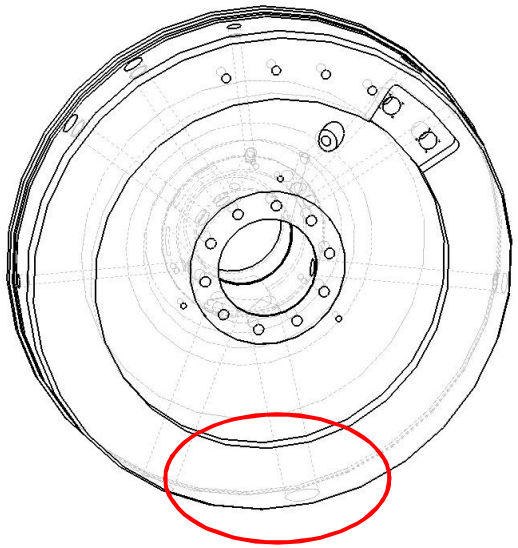

Air		
air temp	degF	100
	degR	559.67
purge air pressure (lowest yields	psia	14.7
air density	lbm/ft^3	0.07089
air speed of sound	ft/sec	1160.154
stnd pressure	psia	14.7
stnd temp	degF	59
air standard density	lbm/ft^3	0.076509
Oil		
oil density	lbm/ft^3	53.69
oil flow rate	gpm	20
	lbm/sec	2.392478
Sizing		
Oil (only) flow areas		
Supply		
mdot = A Cd sqrt(2 rho delP)		
delP	psid	3
Cd (guess)		0.7
A	ft^2	0.002798
	in^2	0.402862
effective dia.	in.	0.716198
delP=rho*g*h	psid	
h, drain height	ft	
Drain		
mdot = rho V A		
velocity	ft/sec	2
	m/sec	0.6096
A	ft^2	0.02228
	in^2	3.208389
effective dia.	in.	2.02115
Air flow area		
desired Mach	#	0.05
Mach associated speed	ft/sec	58.0077
volumetric leakage	SCFM	138
mass flow rate	lbm/sec	0.175971
req'd flow area	ft^2	0.042793
	in^2	6.162181
effective dia.	in.	2.801059
Composite flow requirement		
Area_oil + Area_air	in^2	9.37057
effective dia. for single port	in.	3.454125
number of multiple ports		2
effective dia. for multiple port	in.	2.442435

Mechanical Interfaces

- **HS coupling purge supply**
- **DE borescope access**

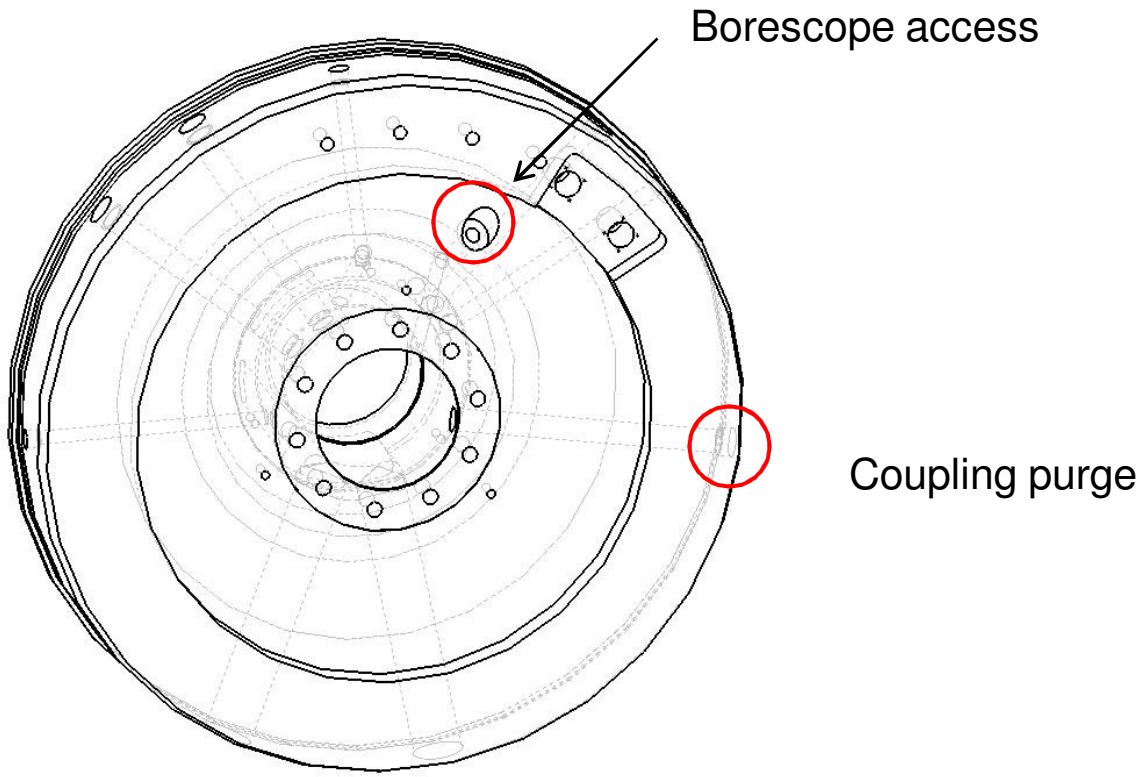

Mechanical Interfaces

- **DE and NDE damper supplies and drains not yet modeled**
  - **0.25 in. dia. ports**
  - **DE case end and Bearing housing locations**

Mechanical Interfaces

- **Coupling cavity purge vent**
  - **Connection size: gearbox internal**
  - **Location**
    - **Radial: BDC**
    - **Axial: gearbox internal**

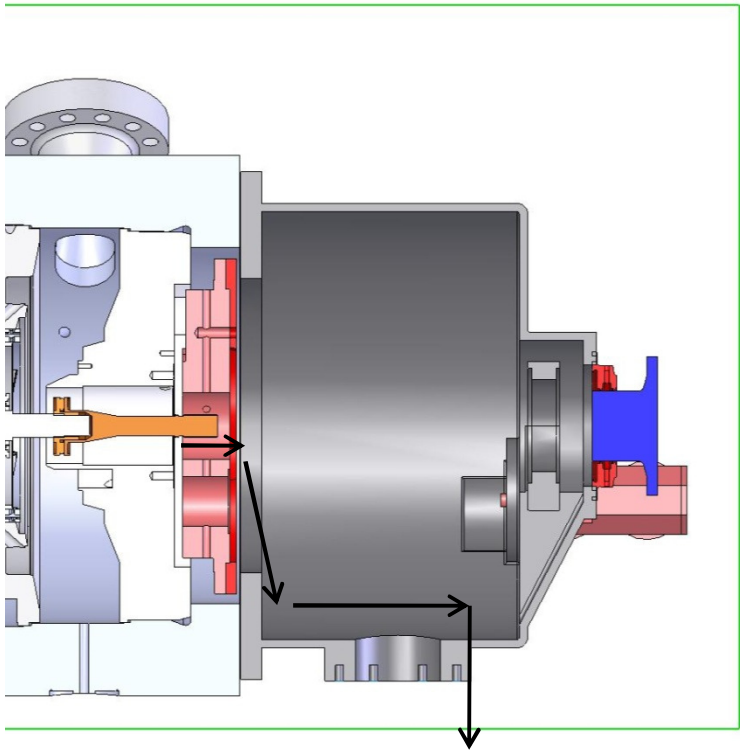

Mechanical Interfaces

- **Actuators**
  - **Connection size: custom, case-integral pad**
  - **Location**
    - **Radial:**
      - » **IGV actuators: ≈70 deg CCW from TDC (viewed toward the drive end)**
      - » **Bypass valve actuators: ≈20 deg CCW from TDC (viewed toward the drive end)**
    - **Axial: TBD**
      - » **IGV actuators: ≈11.5 in. from midplane**
      - » **Bypass valve actuators: ≈ 5.25 in. from midplane**

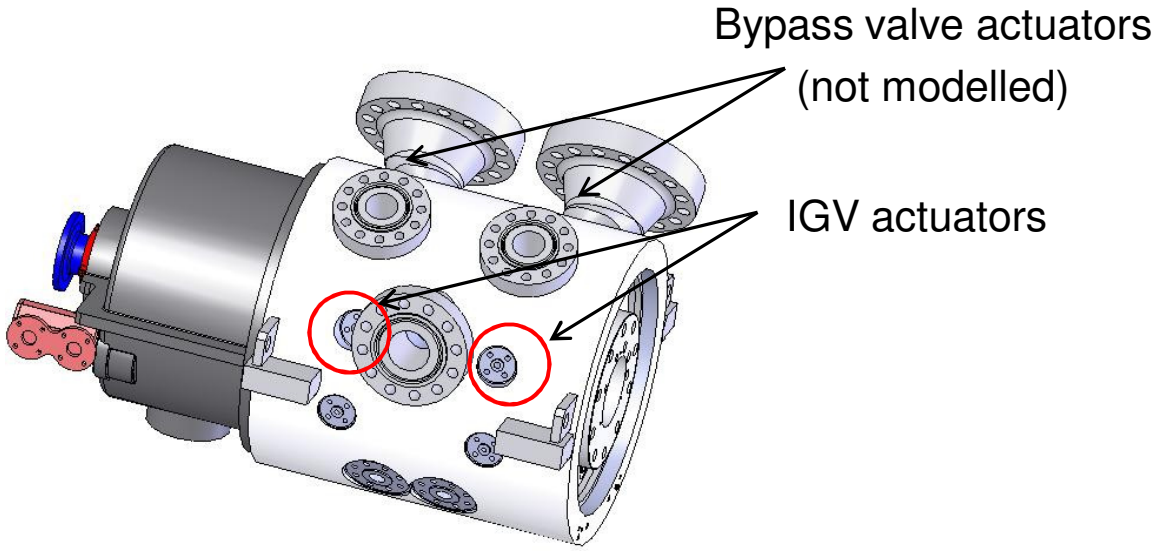

Mechanical Interfaces

- **Case drains**
  - **Connection size: 1 in., case integral, raised face, flange**
  - **Location**
    - **Radial: TBD**
    - **Axial: BDC**

Important Interfaces Cont'd

- **Fluid**
  - **Main Exhaust, currently modeling**
    - » **10" sch. 160 connection thru pressure vessel**
    - » **0.955" at diffuser discharge**
      - – **Assume no diffusion with maximum space utilized**
    - » **P=2200 psia, T = 650 deg. F**
  - **Aft Bleed,**
    - » **2X 3" sch. 160 connections thru pressure vessel**
    - » **7X R0.375" takeoffs thru volute plate**
    - » **P=220 psia, T=520 deg. F**
  - **HP leakage, 2X 3" sch. 160 connections thru pressure vessel**
    - » **6X R0.65" takeoff thru volute plate**
    - » **P=220 psia, T=520 deg. F**
  - **Bypass Valve Annular Slot**
    - » **Anticipated to open most of the inner vane space for fluid bypass**
    - » **P=486 psia, T = 212 deg. F, taken from 1-D starting model started un-backpressured**
    - » **P=2200 psia, T = 650 deg. F**

Work Plan / Analysis Tasks

- **Aerodynamic flowpath evaluation**
  - **Internal or Geminus evaluation**
    - **Geminus**
- **FEA/heat transfer**
  - **ASE/Agilis review of Ramgen internal work as required**

Budget and Schedule

- **PDR date**
  - **3rd week of March**
- **FDR date**
  - **3rd week of May**
- **Drawing Release date:**
  - **dependant on integrated part, nominally May with preceding material release and potentially roughing drawings (part release detail in assembly CDR)**
  - **Case nozzle definition Feb. 2010**
- **Estimated Manufacturing Time/Delivery date: September 1**
- **Is schedule achievable?**
  - **Schedule permits only single aero iteration. Practicality of this assumption is not validated.**
- **Current budget: $35,000 heat transfer ODCs + internal aero (no ODCs)**
- **Is current budget is adequate assuming single aero pass is adequate**

CO2 Rampressor Windage and Sealing

John Hinkey

January 12, 2010

Introduction

- **Why Windage And Sealing Together?**
  - They Are Intimately Related With Our High PR Rotor Design
- **Sealing – Primary Concern, Windage – Secondary**
  - If it doesn't seal well enough, then rotor performance will suffer greatly
  - If the windage is higher than desired – that's not as likely a fatal issue

Some First Cut CFD

- **1st Order Look At Flow Field Between Rotor & Shroud**
- **Looking For**
  - Amount Of Leakage w/o Any Bleed Through Static Hardware
  - Labirynth Seal Geometry Changes Effects on Leakage
  - Leakage Effect on Rotor Outflow
  - Effects of Rotor Leakage Into Primary Flow Path
    - *If this ever occurs (which it will at some point)*
- **Prelude To Using Full Non-Ideal CO2 Gas Model**
  - FINE/Turbo or Upgraded WindUS3

Conceptual Geometry Grid

- 2.5 deg. grid – 10 cells circumferential direction
- Wall Function Grid
- Spalart Turbulence Closure
- Aarnio #3 CO2 Ideal Gas Model
- Flow Computed In Stationary/Non-Rotating Reference Frame

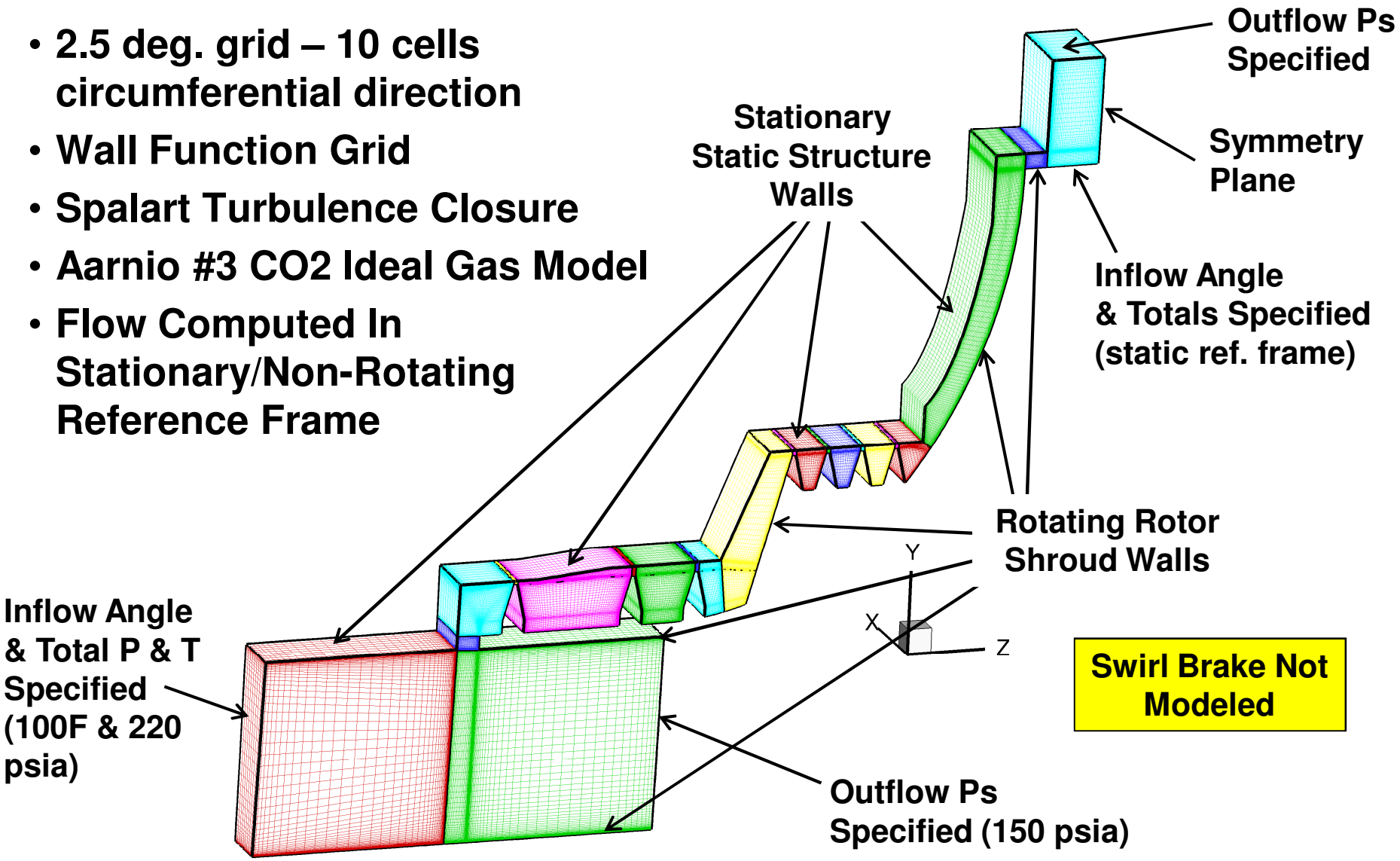

Baseline Conceptual Sealing Geometry

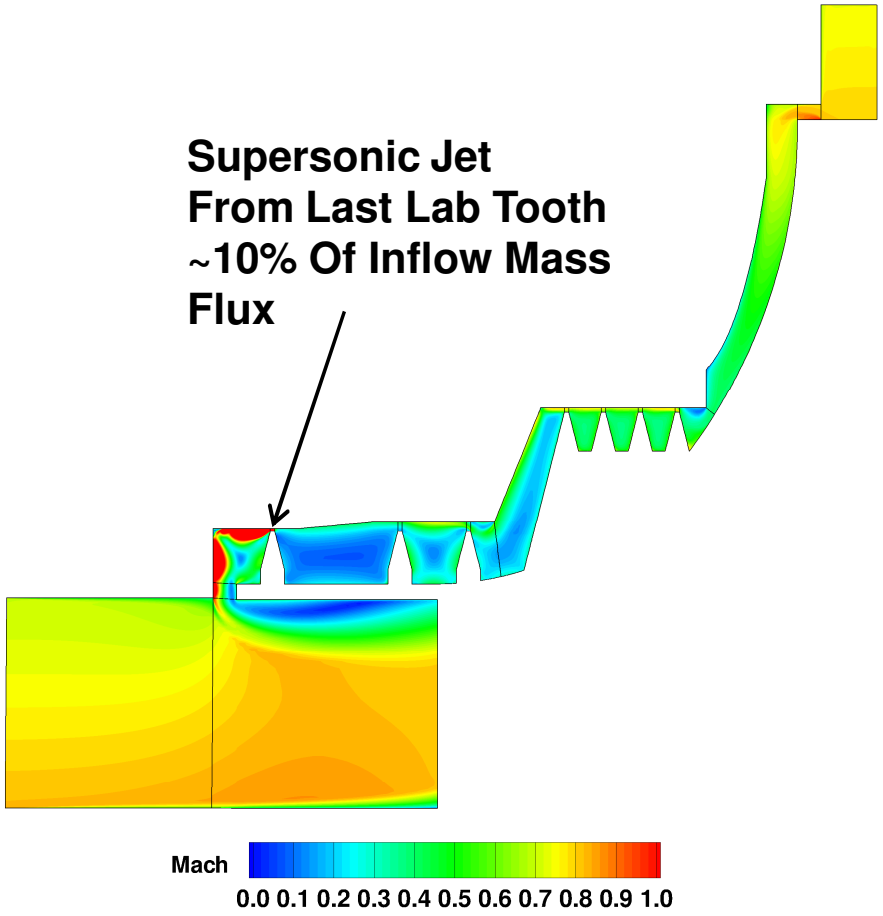

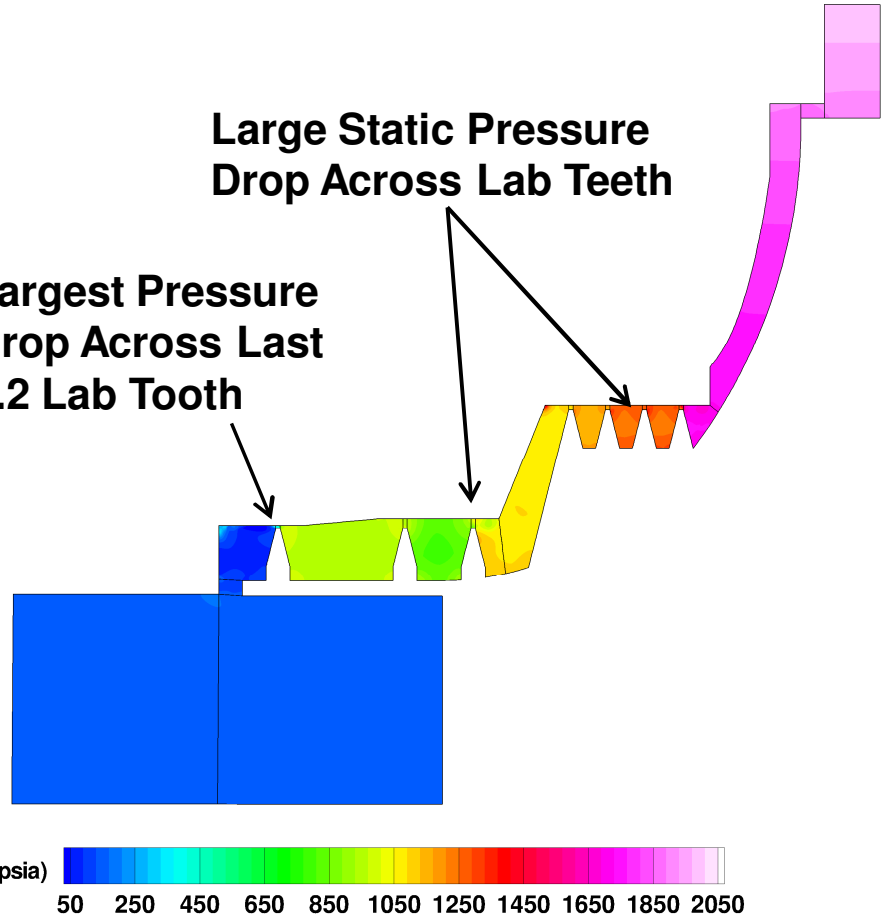

- Basic Conceptual Configuration
- 4 teeth at 15mil, 2 at 35 mil, 1 at 8.2 mil
- 150mil Rotor Outflow Gap

Modified Conceptual Geometry Grid

- 2.5 deg. grid – 10 cells circumferential direction
- Wall Function Grid
- Spalart Turbulence Closure
- Aarnio #3 CO2 Ideal Gas Model
- Flow Computed In Stationary/Non-Rotating Reference Frame

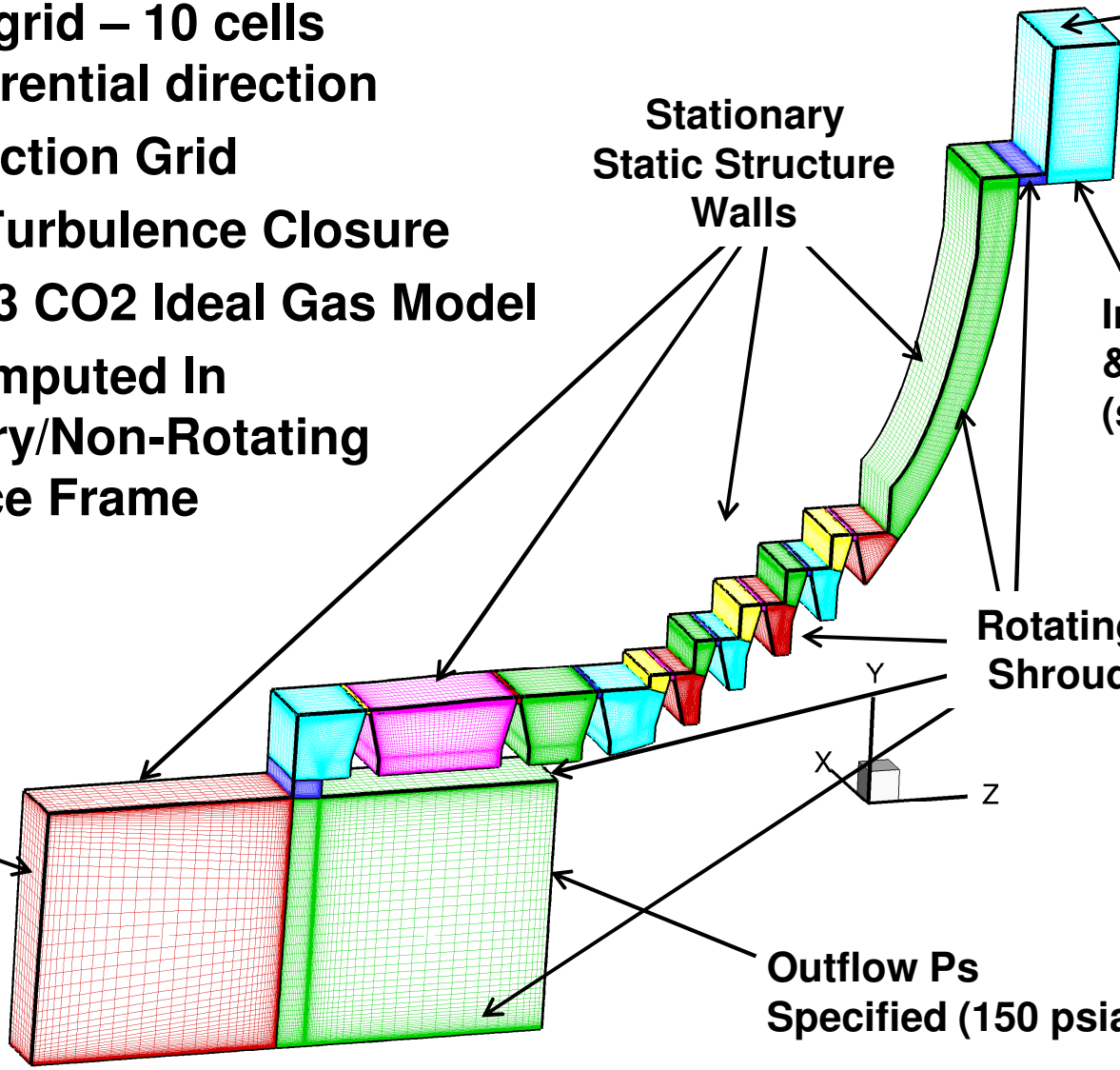

Modified Conceptual Geometry Grid

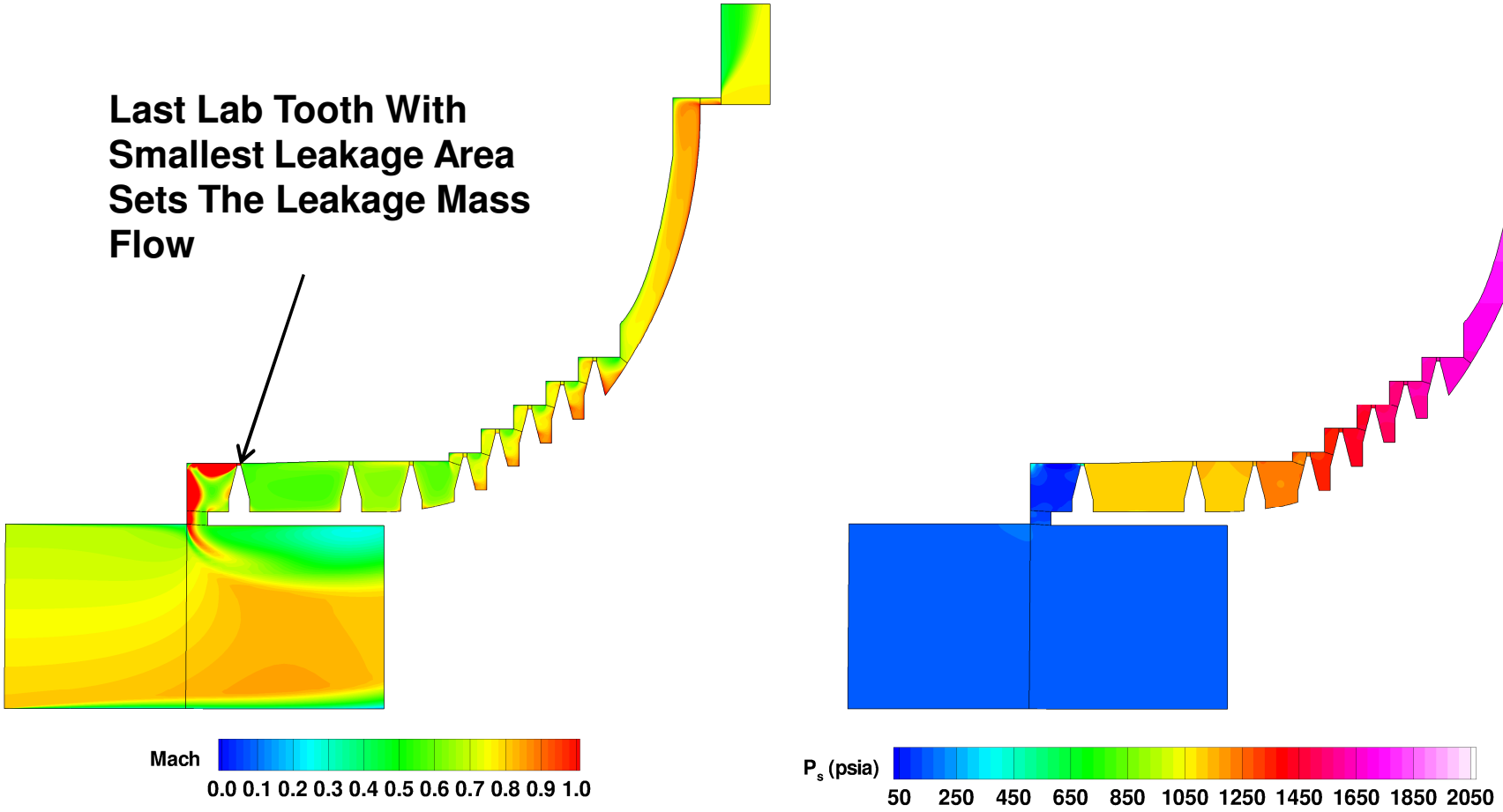

- High Pressure Labby Teeth Staggered and Gap Is Same
- 4 teeth at 15mil, 2 at 35 mil, 1 at 8.2 mil
- Leakage Largely Unaffected (~13.8%)

Modified Conceptual Geometry Grid: Staggered High P Teeth

- 2.5 deg. grid – 10 cells circumferential direction
- Wall Function Grid
- Spalart Turbulence Closure
- Aarnio #3 CO2 Ideal Gas Model
- Flow Computed In Stationary/Non-Rotating Reference Frame

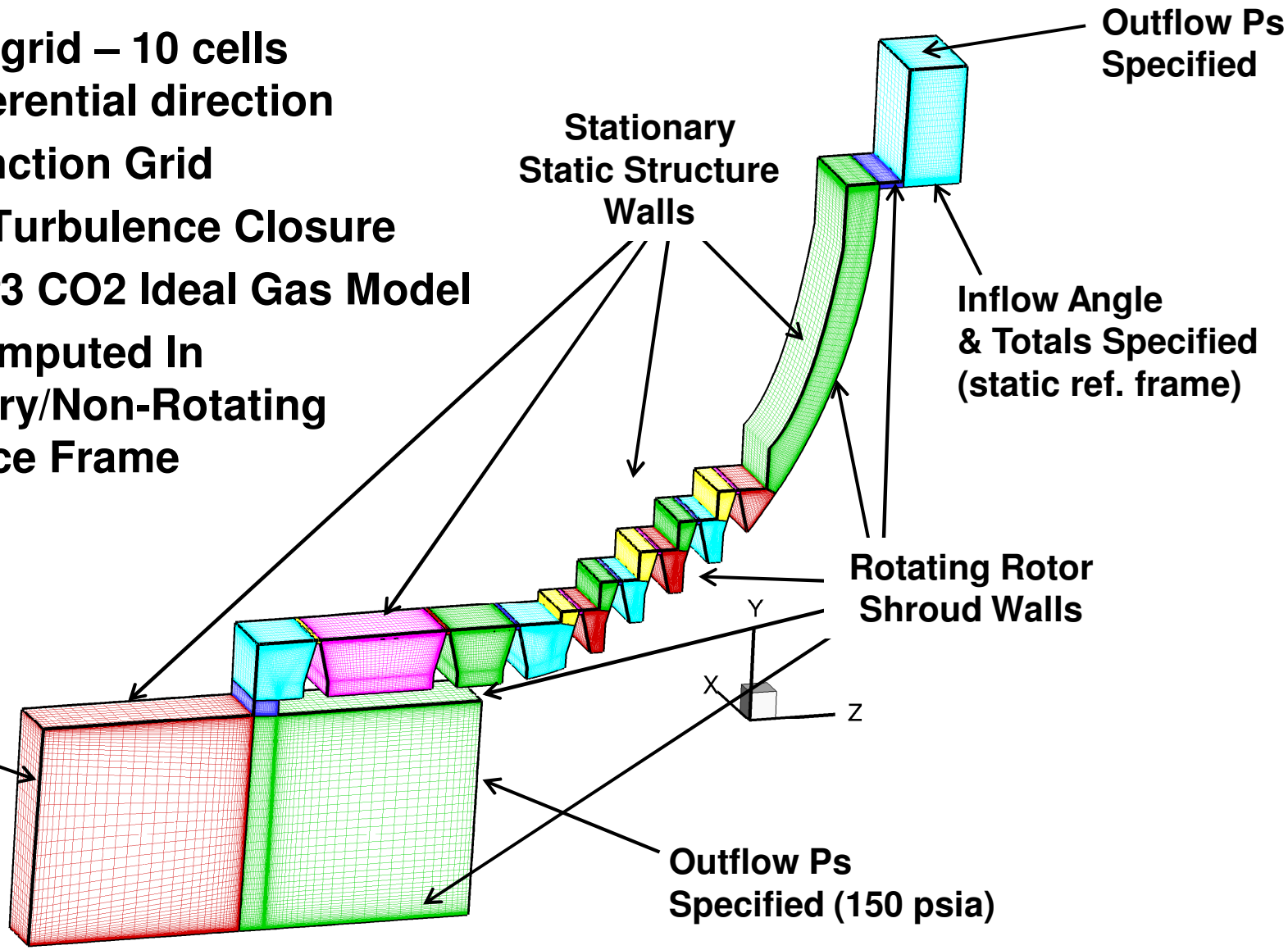

Modified Conceptual Geometry: High P Teeth – Gap Reduced

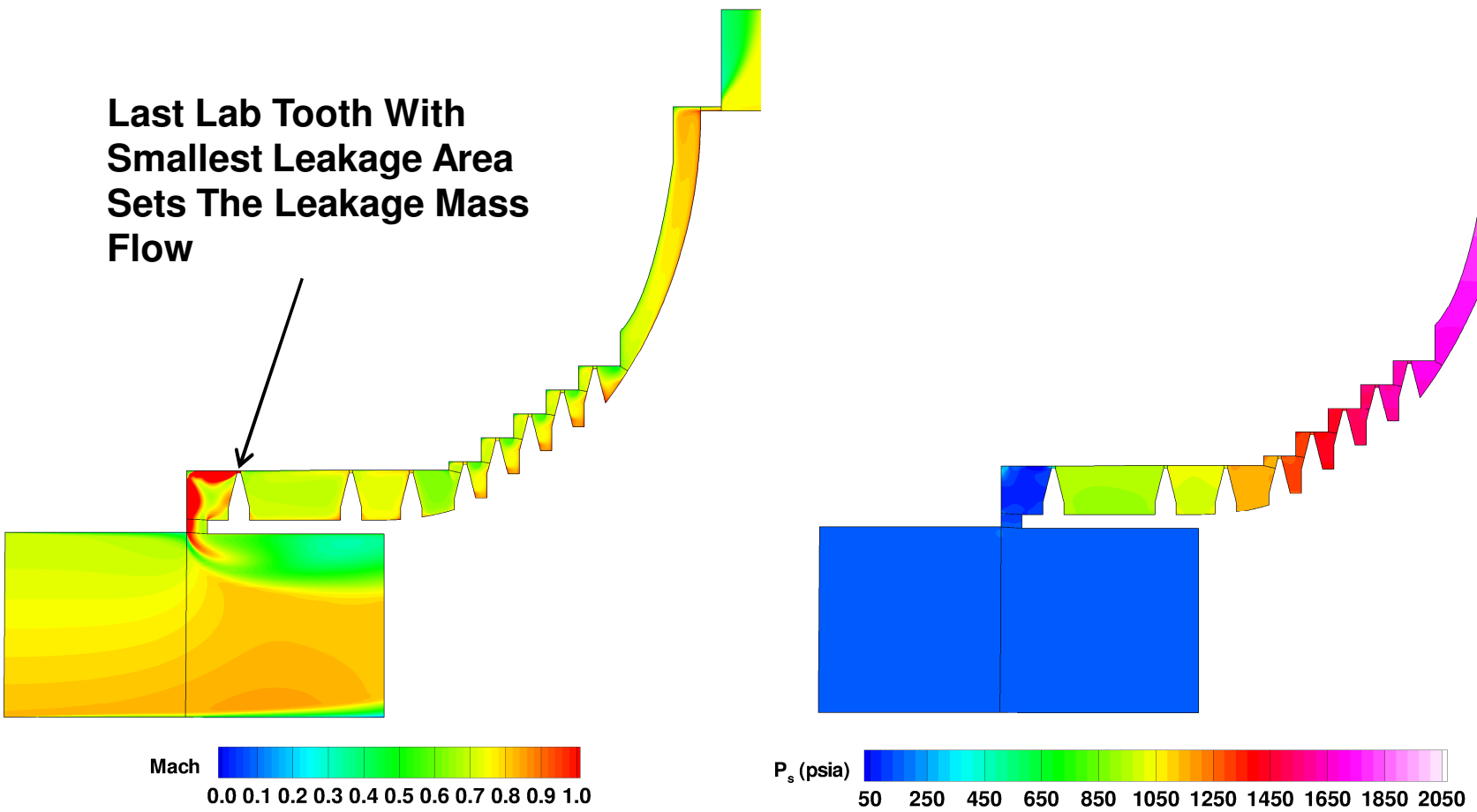

- All But Last Lab Tooth Gap Reduced to 10 mils
- 4 teeth at 10mil, 2 at 10 mil, 1 at 8.2 mil
- Leakage Still Largely The Same (~10.4%)

Modified Conceptual Geometry Grid: Staggered High P Teeth

- 2.5 deg. grid – 10 cells circumferential direction
- Wall Function Grid
- Spalart Turbulence Closure
- Aarnio #3 CO2 Ideal Gas Model
- Flow Computed In Stationary/Non-Rotating Reference Frame

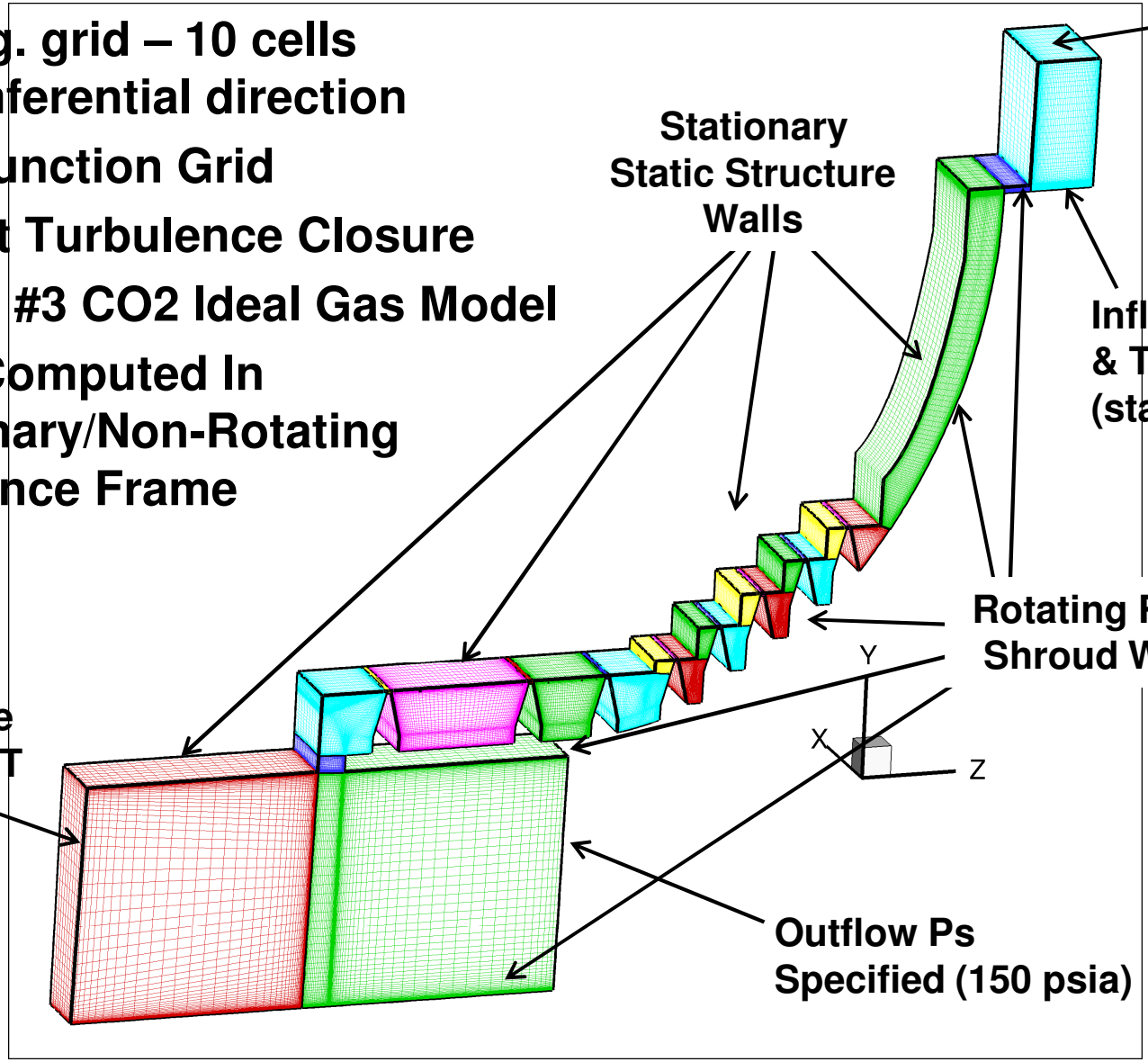

Version 4

Modified Conceptual Geometry: High P Teeth – All 5 mil Gaps

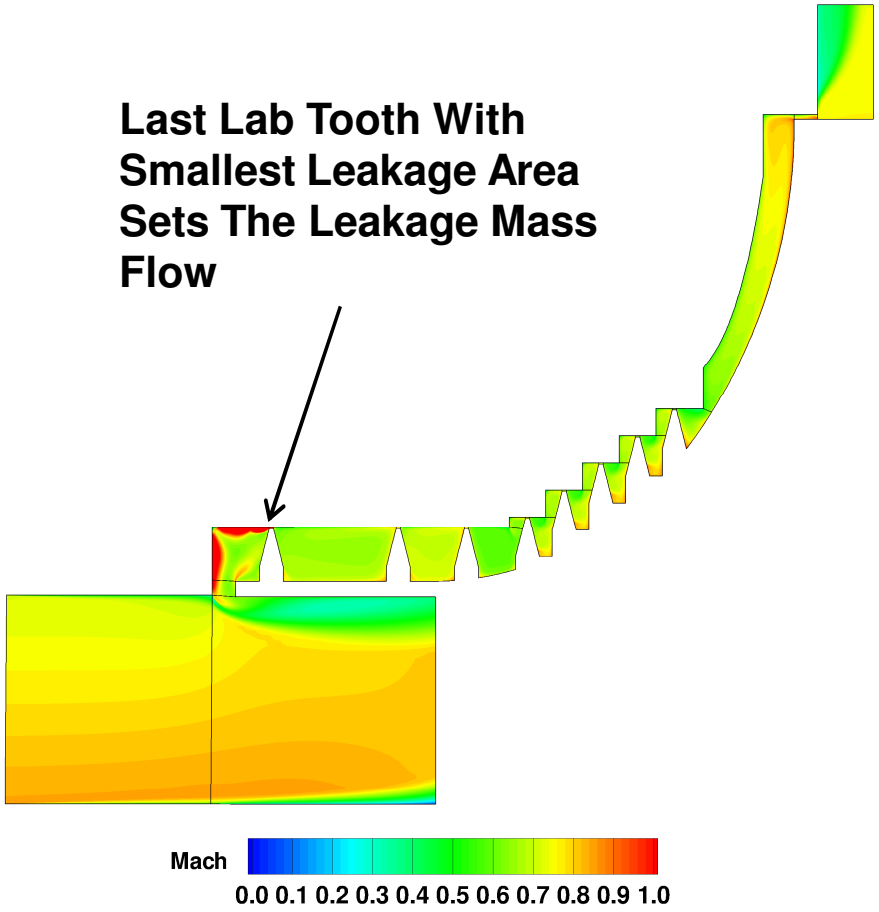

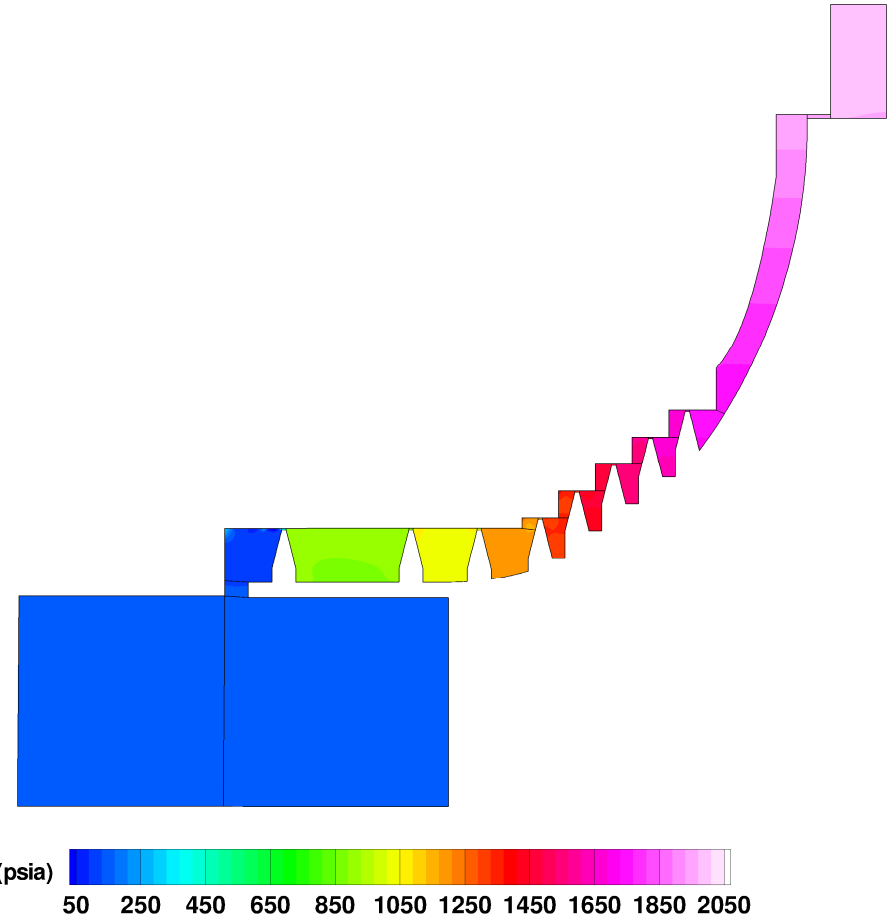

- All Lab Teeth Gaps Set To 5 mils
- Leakage Reduced by ~5/8ths (5mils/8mils)
- Last Lab Tooth Still Mostly Controls Leakage Rate (~5.8%)

So What Have We Learned (If We Didn't Know It Already)

- **An All Labyrinth Seal Design Looks Unlikely**
  - Smallest Radius High Pressure Seal Sets The Leakage Mass Flow
- **Want To Seal The High Pressure At The Smallest Radius With The Smallest Gap**
  - Seals At Larger Radius Need To Have Even A Better Seal Effectiveness (Gap for A Labyrinth Seal) Due To Large Total Leakage Area
  - Sealing At Lower Radius Also Has Smaller Static Pressure To Seal Against
    - *Flow In Gap Has Some Radial Pressure Gradient Set Up – So Take Advantage Of It*
    - *Lower Radius Also Has Lower Surface Speeds For Contact Seals*
  - BUT This Is Where The Least Mechanical Real Estate Exists
  - May Have Higher Windage
- **Leakage Flow Can Have Significant Effect On Stationary Diffuser Flow Characteristics**
  - Good or Bad?

Some Design Suggestions

- **Labyrinth Teeth – Need Smaller + More**

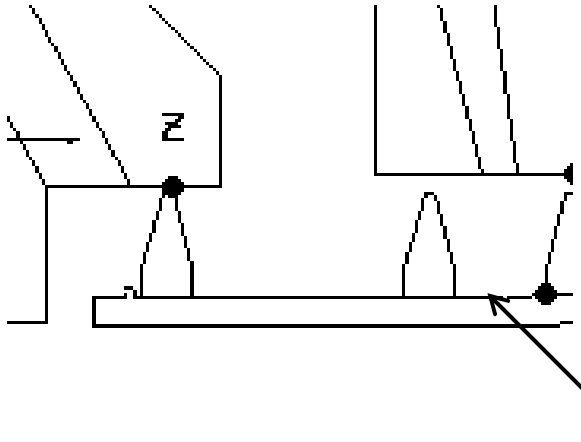

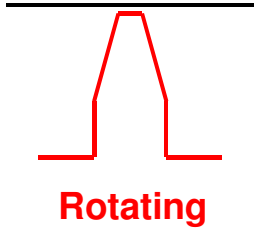

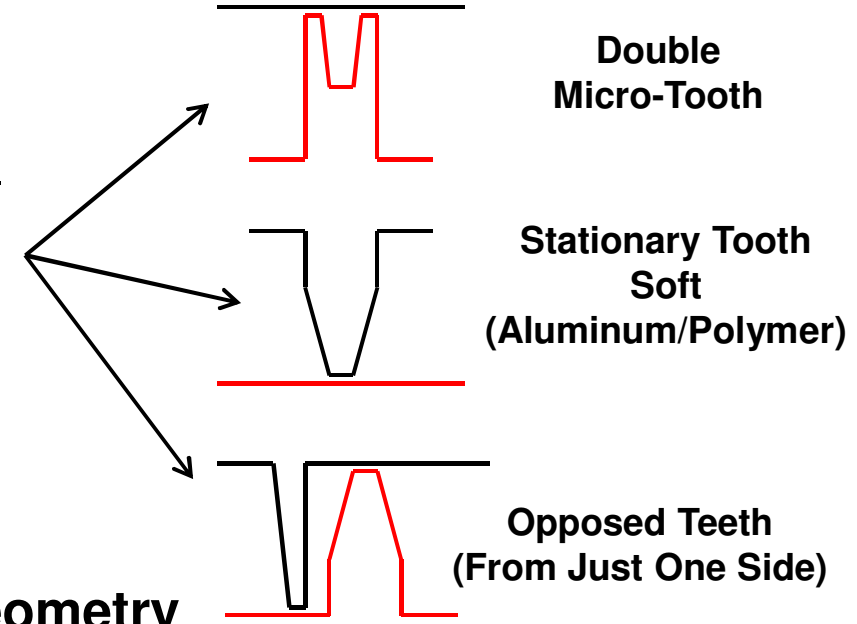

1250 ft/s or 376 m/s

- **Final Tooth Leakage "Catching" Geometry**

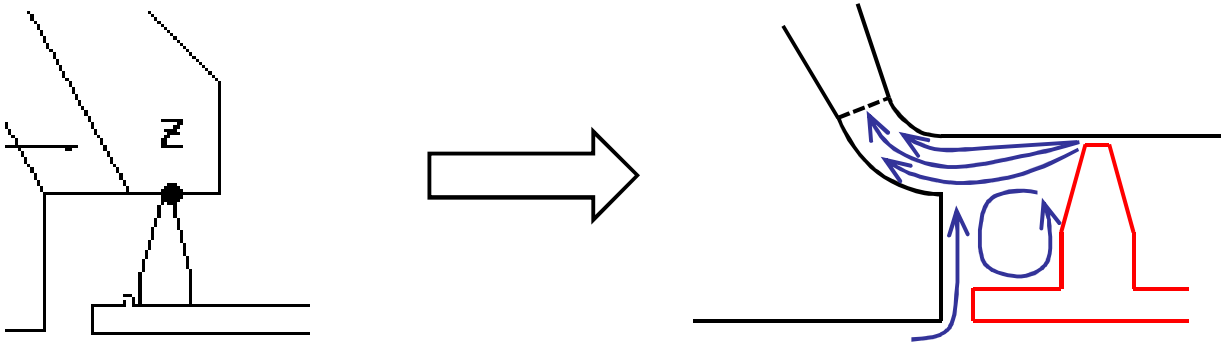

Goal Is To "Catch" The Leakage Jet So That It Has The Lease Pressure Loss From Turning To Get Out Of The Stationary Components

Labyrinth Tooth Types And Relative Leakage Characteristics

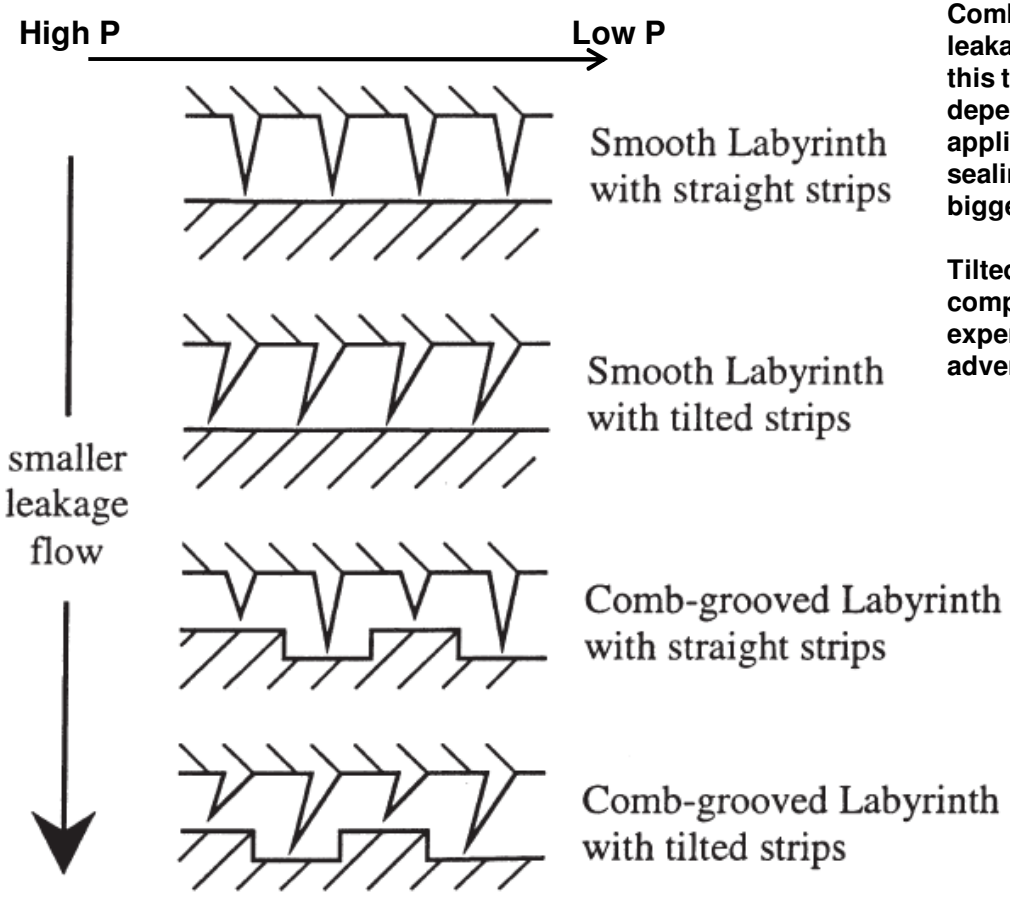

Figure 2. Labyrinth Seals Used in High Pressure Applications.

ROTORDYNAMIC STABILITY TESTS ON HIGH-PRESSURE RADIAL COMPRESSORS
By Urs Baumann
Proceedings of 28th Turbomachinery Symposium.

Comb-grooved labyrinths have a significantly lower leakage flow than smooth labyrinths. The biggest disadvantage of this type of seal is a certain risk of having thrust temperature dependent labyrinth coefficients (axial position). The main application of the comb-grooved labyrinth is the balance piston, sealing the highest differential pressure and therefore having the biggest impact on the efficiency.

Tilted labyrinth strips always reduce the leakage flow in comparison to straight strips. Unfortunately there are no experimental data available to show that the tilted surfaces do not adversely influence the seal coefficients

- **In General Rotation Produces Lower Leakages**
  - Swirling Flow In Cavities
- **Difference In Leakage Characteristics Not That Large**
  - i.e., maybe 20% less leakage from top to bottom

Labyrinth Tooth Types And Relative Leakage Characteristics

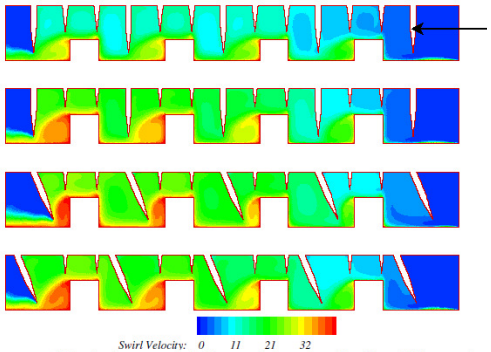

Figure 11. Axisymmetric swirl velocity in different designs (P_1/P_{14} = 10 – CFD)

Basic flow mechanisms that help in reducing leakage through a labyrinth seal were identified. They include

•The formation of turbulent vortices that require constant supply of energy to drive them,

• The process of stagnation of the flow,

• The turbulent throttling of fluid through narrow constrictions (which also contribute to the formation of vortices).

Other mechanisms identified are

• Turbulent viscous losses through various factors including forcing the fluid through a tortuous path.

• Axial location of the knife-edge in relation to the step was shown to have a significant effect on reducing leakage through the seal for studied pressure ratios.

Seal Discharge Coefficient

A particularly useful representation is the seal discharge coefficient, Cd_{seal}:

$$Cd_{seal} = \frac{massflow_{actual}}{massflow_{ideal}} \qquad (1)$$

As described by Waschka et al[11], the ideal flow is calculated (for the sub-critical flow case) using equation (2): the labyrinth clearance area is used as the cross sectional area of a hypothetical nozzle, and the seal overall pressure ratio as the nozzle pressure ratio.

$$\dot{m}_{ideal} = A_{cl}\left\{\frac{2k}{(k-1)}P_1\rho_1\left(\frac{P_2}{P_1}\right)^{\frac{2}{k}}\left[1-\left(\frac{P_2}{P_1}\right)^{\frac{k-1}{k}}\right]\right\}^{\frac{1}{2}} \qquad (2)$$

Flow Parameter

A dimensional parameter, ϕ, is used by Stocker[2,13] to correlate leakage performance of a labyrinth seal. This parameter is a correction factor on the mass flow and can be derived in the form below, using the ideal gas law[14]:

$$\dot{m} = \frac{\Phi P_1 A_{cl}}{\sqrt{T_1}} \qquad (3)$$

Lower values of ϕ and Cd represent less leakage in seals for similar operating conditions.

AN EXPERIMENTAL AND NUMERICAL STUDY OF LABYRINTH SEAL FLOW
A.D. Vakili, A.J. Meganathan, M. Michaud, S. Radhakrishnan
ASME GT2005-68224

Model	Reference	P_1/P_{14}	% Reduction
2D 60° knife	2D 90° knife	2	16.97
2D 60° knife	2D 90° knife	4	15.64
2D 60° knife	2D 90° knife	6	15.58
2D 60° knife	2D 90° knife	8	15.82
2D 60° knife	2D 90° knife	10	15.43
2D 90° knife High Step (40%)	2D 90° knife	10	2.06
2D 60° knife Tip at center	2D 90° knife	10	-0.53
Axisymmetric Rotation* 90° knife	Axisymmetric No rotation 90° knife	10	-2.93
Axisymmetric Rotation* 60° knife High Step (40%)	Axisymmetric No rotation 60° knife High Step 40%)	10	-0.0024
Axisymmetric No rotation 60° knife High Step (40%)	Axisymmetric No rotation 90° knife High Step (40%)	10	17.27
Axisymmetric Rotation* 60° knife High Step (40%)	Axisymmetric Rotation* 90° knife High Step (40%)	10	19.37

*All rotation at 60 Hz, All results from CFD
If not specified, position of knife tip is at X/L = 0.043, (figure 1).

Table 2. Comparison of leakage reduction

A Note On Flow Swirl And Rotor Stability

- ***Influence of Swirl on Stability***
  - The potentially destabilizing tangential forces are determined mainly by the relative circumferential speed of the gas within the labyrinth
  - A labyrinth seal is **stabilizing** if the shaft is driving the gas, and it is **destabilizing** if the gas is pushing (exciting) the shaft.
- ***Swirl Brakes***
  - The swirl frequency ratio based on the rotational speed of the shaft can also be defined as the ratio of the average swirl of the labyrinth flow to the rotational speed of the shaft (relative average swirl)

$$SFR_\Omega = \frac{K_{XY}}{C_{XX}} \cdot \frac{1}{\Omega} = \frac{swirl}{\Omega}$$

  - The installation of swirl brakes significantly reduces the swirl within the labyrinth. In some cases the swirl even becomes negative, causing the labyrinth to be a very strong source of damping.
  - The author's company uses two different types of swirl brakes.
    + *The first is a conventional type consisting of a certain number of radial slots placed directly in front of the labyrinth seal entrance.* ***This type ensures a zero preswirl to the seal.***
    + *The second type is called a thrust brake, again consisting of a certain number of radial slots, but placed on the outer diameter of the shroud sideroom. The thrust brake reduces the swirl in the sideroom and therefore also at the entrance to the labyrinth. This results in a higher pressure in the shroud sideroom, which compensates the impeller thrust and reduces the overall thrust of the compressor.* ***On the other hand, the higher pressure in the sideroom leads to an increased leakage flow and therefore to a lower performance of the compressor****.*

ROTORDYNAMIC STABILITY TESTS ON HIGH-PRESSURE RADIAL COMPRESSORS
By Urs Baumann
Proceedings of 28th Turbomachinery Symposium.

At the threshold of stability, the precessional speed of the shaft becomes equal to the lowest critical speed. This leads to the following definition of the swirl frequency ratio based on the critical speed (SFR_ω):

$$SFR_\omega = \frac{K_{XY}}{C_{XX} \cdot \omega} \quad (4)$$

Extending Equation (4) with the rotational speed (Ω) of the shaft leads to:

$$SFR_\omega = \frac{K_{XY}}{C_{XX} \cdot \Omega} \cdot \frac{\Omega}{\omega} = SFR_\Omega \cdot FR \quad (5)$$

where SFR_Ω is the swirl frequency ratio based on the rotational speed of the shaft and FR is the flexi ratio, which is a measure of the flexibility of the shaft at the speed of operation. Figure 4 visualizes the stability criterion given in Equation (3). A labyrinth seal is stabilizing if the shaft is driving the gas, and it is destabilizing if the gas is pushing (exciting) the shaft.

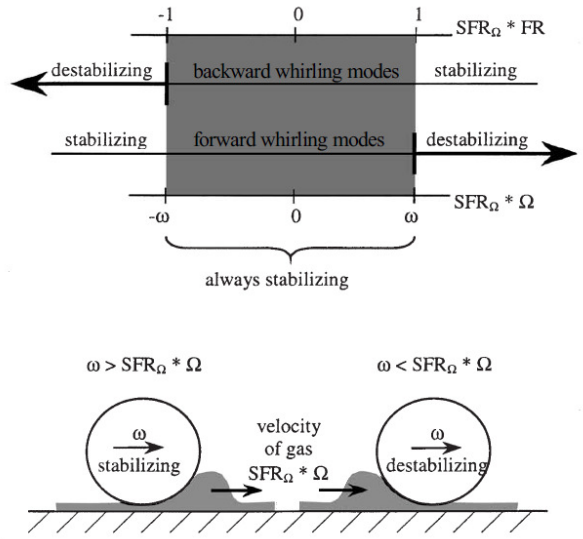

Figure 4. Stability Criterion of Labyrinth Seals.

A Note On Flow Swirl And Rotor Stability (Con't)

The author's company uses two different types of swirl brakes. The first is a conventional type consisting of a certain number of radial slots placed directly in front of the labyrinth seal entrance. This type ensures a zero preswirl to the seal.
The second type is called a thrust brake, again consisting of a certain number of radial slots, but placed on the outer diameter of the shroud sideroom. The thrust brake reduces the swirl in the sideroom and therefore also at the entrance to the labyrinth. This results in a higher pressure in the shroud sideroom, which compensates the impeller thrust and reduces the overall thrust of the compressor. On the other hand, the higher pressure in the sideroom leads to an increased leakage flow and therefore to a lower performance of the compressor.

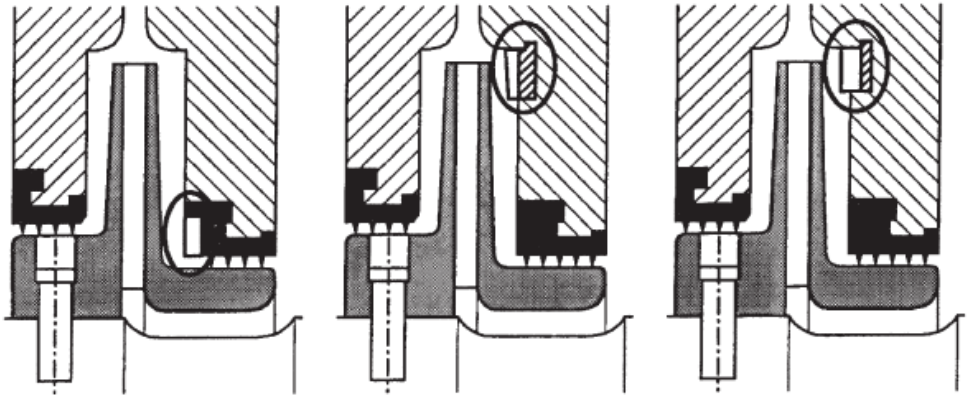

Figure 5. Swirl and Thrust Brakes Used in High Pressure Compressors.

- ***Some Conclusions***
  - Comb-Groove Lab Seals Are Sensitive To Axial Position of The Rotating and Non-Rotating Components
  - The critical frequency of the rotor can be significantly changed by the presence of lab teeth
  - The Radial Forces In The Seals Can Play As Significant A Role As The Tangential Forces

ROTORDYNAMIC STABILITY TESTS ON HIGH-PRESSURE RADIAL COMPRESSORS
By Urs Baumann
Proceedings of 28th Turbomachinery Symposium.

A Note On Flow Swirl And Rotor Stability (Con't)

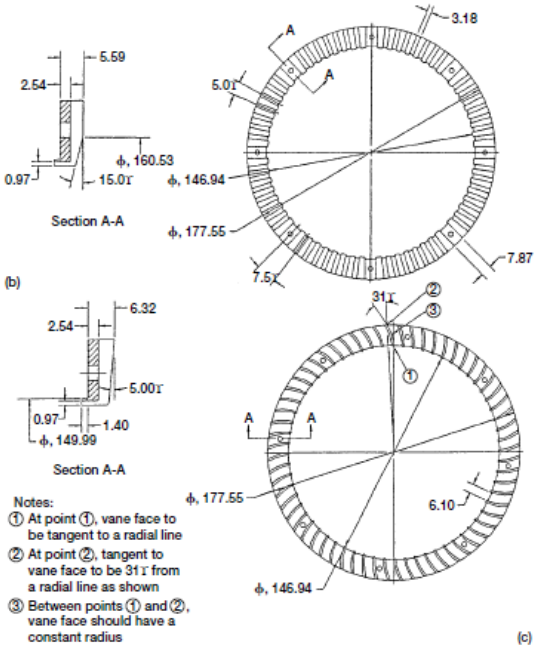

Figure 15.—Concluded. (b) Radial swirl brake. (c) Improved swirl brake. Dimensions in millimeters. (Childs et al., 1991.)

NASA/TM—2004-211991/PART2

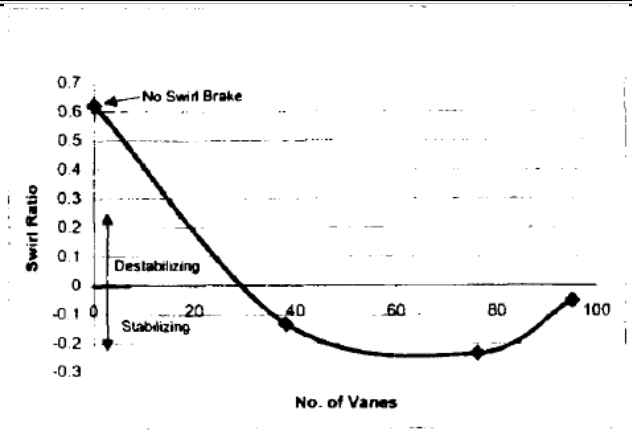

Figure 14 – Pitch-to-Chord Ratio Optimization Study

DESIGN OF SWIRL BRAKES FOR HIGH PRESSURE CENTRIFUGAL COMPRESSORS USING CFD TECHNIQUES
J. Jeffrey Moore and D. Lee Hill
Dresser-Rand Company, Olean, NY, USA

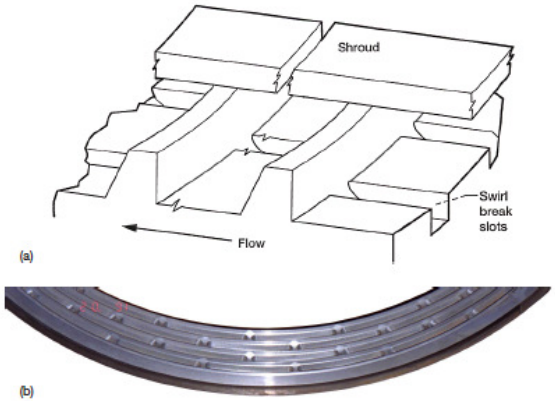

Figure 52.—Web seal. (a) Sketch of conceptual web seal. (b) Photograph of web seal or slotted labyrinth seal. (Camatti et al., 2003.) Courtesy ISCORMA–2.

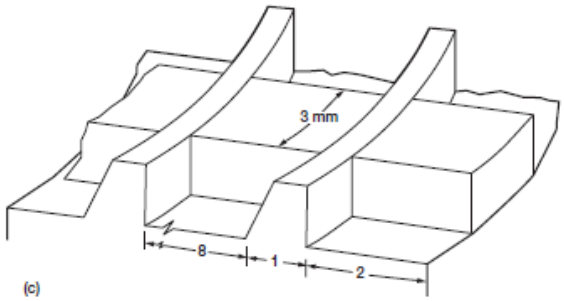

Figure 43.—Configuration of test seal. (a) Annular seal. (b) Labyrinth seal. (c) Flow blockers. Dimensions in millimeters. (Kanki et al., 2003.) Courtesy ISCORMA–2.

NASA/TM—2004-211991/PART2

- **Example Swirl Brakes**
- **NOTE: There Is Considerable Design Effort Involved In Designing An Effective Swirl Brake That Produces An Increase In The Log. Dec. As Pressure Increases**

Other Sealing Techniques

- **Gas Turbine and Compressor Sealing Technique Trends**
  - – Away From Conventional Labyrinth Seals
  - – Towards Different Materials:
    - + *Consumable Labyrinth Seals: Aluminum or Plastic (Polyimides, Aramids, etc.)*
  - – Different Sealing Techniques:
    - + *Finger Seals: Many Different Types*
    - + *Gas Film Seals: Radial & Face*
    - + *Brush Seals*
    - + *Carbon Ring Seals*
    - + *Hybrids of The Above*

Because:

- **They Can Have An Order Of Magnitude Less Leakage In Some Cases And Significantly Less Leakage In Most Other Cases Relative To Labyrinth Seals**
- **Can be compliant and withstand rotor radial excursions**
- **Have recently become commercially viable to manufacture**

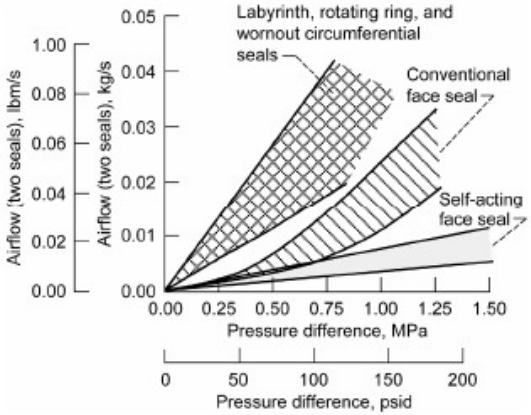

Figure 48.—Comparison of leakage characteristics for labyrinth, conventional (contact) face seal and self-acting face seals.[109]

Non-Conventional Seal Materials

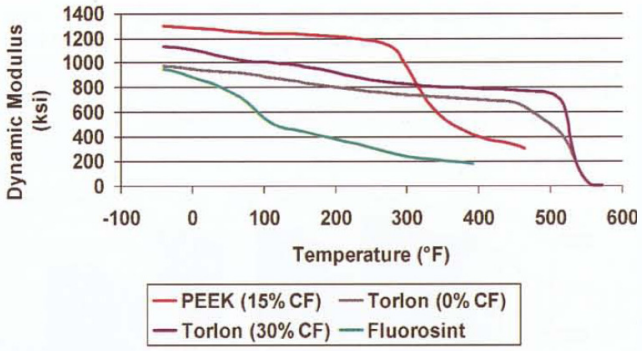

Figure 10. DMA Plot for Various Thermoplastic Materials.

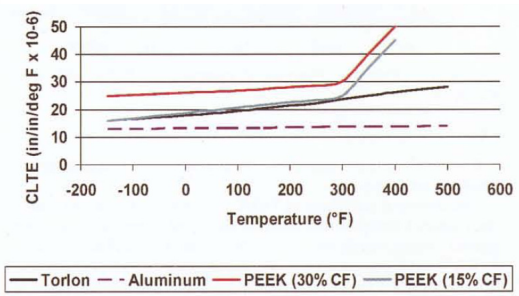

Figure 11. Coefficient of Linear Thermal Expansion (CLTE) Versus Temperature for TORLON®, PEEK™, and Aluminum. (Note the sharp knee in the PEEK™ curves, the start of this knee corresponds to the Tg of the material. Also note how the thermoplastic

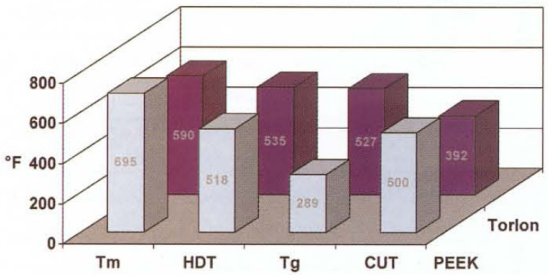

Figure 12. Relative Thermal Properties of TORLON® and PEEK™.

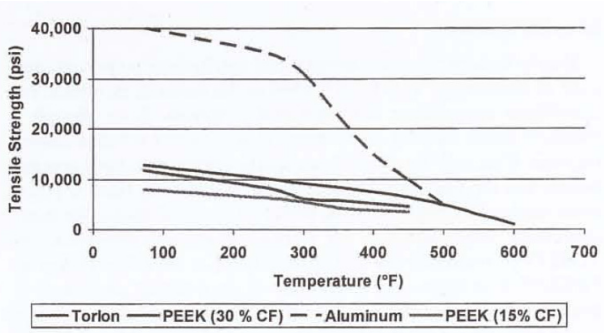

Figure 14. Material Tensile Strength Versus Temperature.

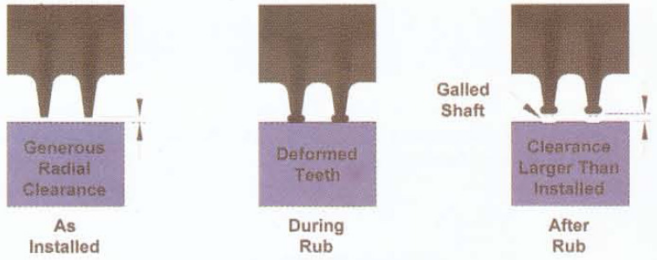

Figure 8. Typical Metallic Seal Prerub, During Rub, and Post Rub. (Note the permanent deformation of the metallic tooth and the possibility of galling damage to the rotating element.)

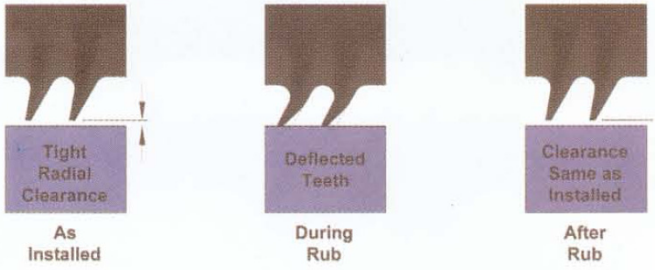

Figure 9. Typical Thermoplastic Seal Prerub, During Rub, and Post Rub. (Note the flexing of the tooth during contact and the damaged free rotating element after the rub.)

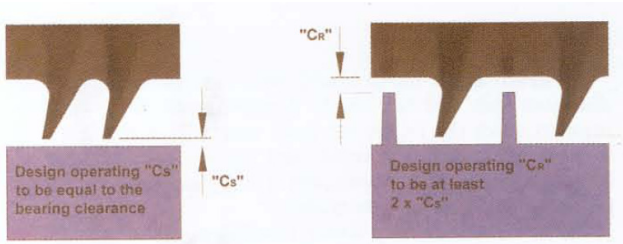

Figure 13. Drawing Illustrating Thermoplastic Seal Clearance Guidelines.

Thermoplastic Labyrinth Seals For Centrifugal Compressors
Whalen, Alvarez, & Palliser
PROCEEDINGS OF THE THIRTY-THIRD TURBOMACHINERY SYMPOSIUM' 2004

- **High Temp. Plastics Are An Option For Close Clearance Seals**

Non-Conventional Seal Materials

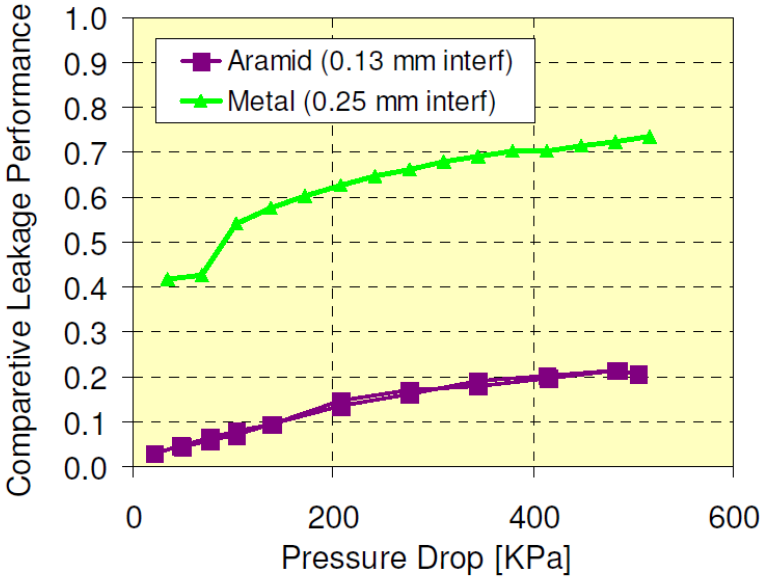

Fig. 8 Sample Aramid Seal Leakage Data

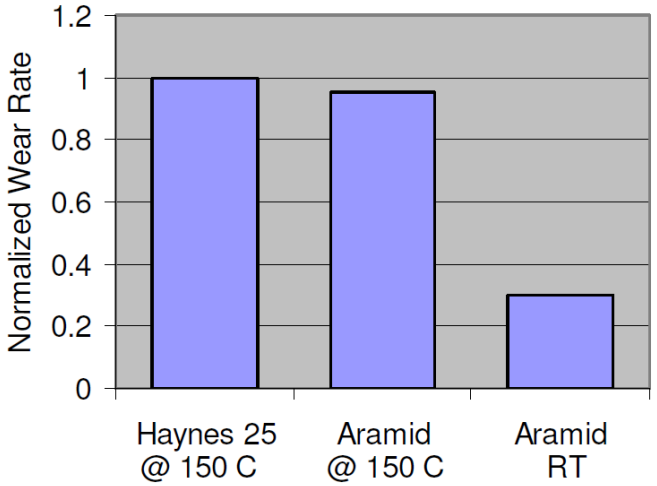

Fig. 5 Wear test results for aramid and Haynes 25 tufts against Ni-Cr-Mo-V. Data are normalized with wear rate of Haynes 25 bristles at 150 ^{0}C.

NON-METALLIC BRUSH SEALS FOR GAS TURBINE BEARINGS
Bhate, Thermos, & Aksit
GT2004-54296

- **Aramid Fibers For Brush Seals**
  - Lower Wear
  - Non-Metallic
  - Lower Temperature Capability
  - Better Sealing Performance

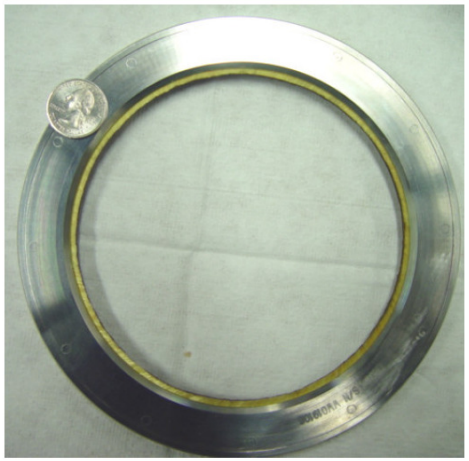

Fig. 6 Subscale aramid fiber brush seal.

Alternative Sealing Techniques: Brush Seals

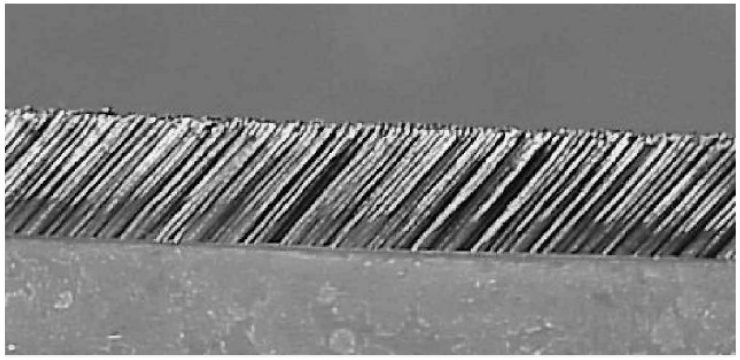

Fig. 4 HPP brush seal for 7EA gas turbine after 22,000 h of operation.

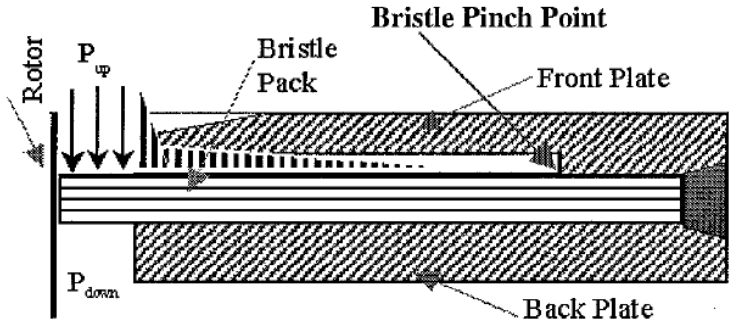

Fig. 5 Pressure forces acting on seal bristle pack.

Advanced Seals for Industrial Turbine Applications: Dynamic Seal Development
Raymond E. Chupp,¤ Farshad Ghasripoor, Norman A. Turnquist, Mehmet Demiroglu, & Mahmut F. Aksit¶
JOURNAL OF PROPULSION AND POWER
Vol. 18, No. 6, November–December 2002

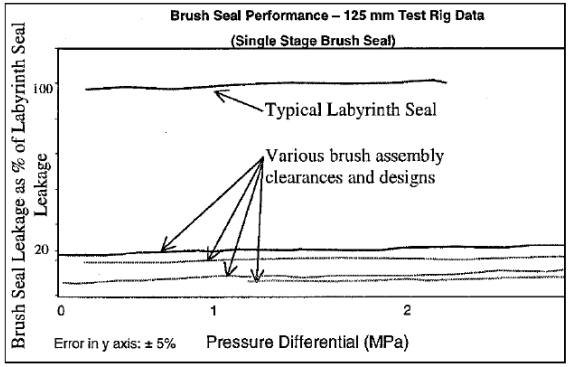

Fig. 3 Representative brush seal leakage data compared to a typical, 15-tooth, 0.5-mm (20-mil) clearance labyrinth seal.

Transient Capability/ Stable Brush Seals	To the engines3-5 times dynamically more aggressive than current engines
High Surface Speed	From 120 m/s (AE) and 244 m/s of (GT) to 500 m/s
High Pressure Loading	From 0.69 MPa two stage seals to 2.76 MPa single stage seal design. Now going for higher ΔP multi-stage designs.
High Swirl Flow Field	0.3 swirl ratio of current applications to 0.6 – 1.2 region.
Temperature	From 370 °C to 650 – 1000 °C
Seal Life and Durability	Gas Turbine fleet leader w/40,000 field hrs with acceptable degradation.
	Steam Turbine fleet leader 28,000 hrs with minimal degradation
Rotor Surface	Ceramic coated Aircraft engine rotors to uncoated Gas and Steam turbine rotors
	Interrupted surface at bucket tip seals

Fig. 9 Brush seal technology status.

Alternative Sealing Techniques: Finger Seals

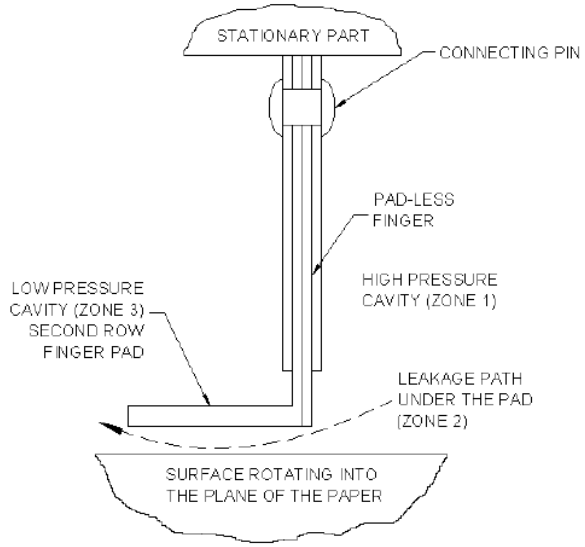

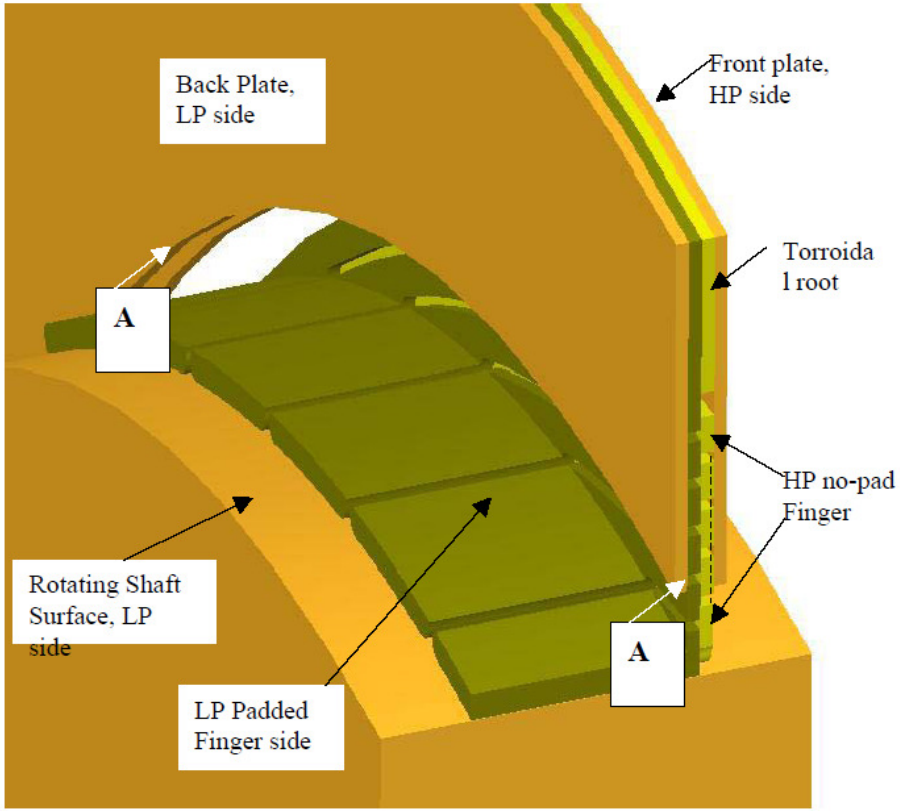

A STUDY OF NON-CONTACTING PASSIVE-ADAPTIVE TURBINE FINGER SEAL PERFORMANCE
VOLUME I
Hazel Marie
December, 2005
A Dissertation Presented to The Graduate Faculty of The University of Akron

Alternative Sealing Techniques: Finger Seals

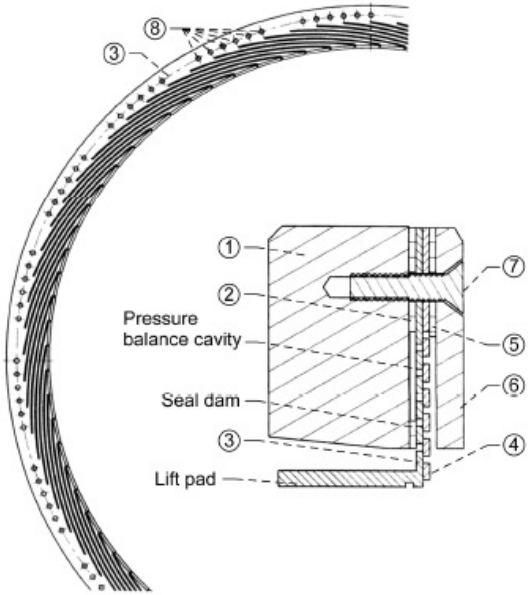

Figure 1.—Non-contacting finger seal design: 1, back plate; 2, aft spacer; 3, aft finger element; 4, forward finger element; 5, forward spacer; 6, front plate; 7, screw; 8, indexing and screw holes.

Figure 2.—Pre-test photo of non-contacting finger seal inner diameter.

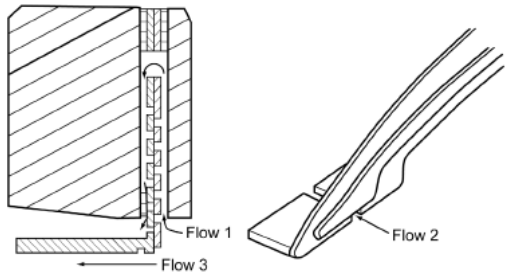

Figure 7.—Leakage flow paths included in non-contacting finger seal flow model.

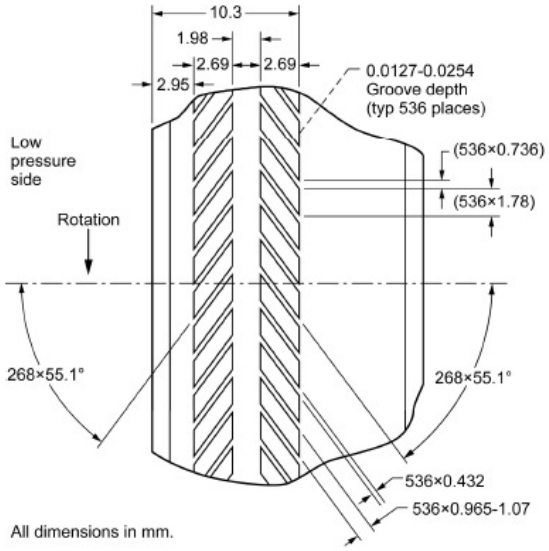

Figure 4.—Herringbone groove design.

- **1. After 93 min of rotation at 300 K and 5000 rpm there was no measurable wear.**
- **2. Non-contacting operation was achieved at 5000 rpm at pressures from 14 to 241 kPa.**
- **3. The measured flow factor of this non-contacting finger seal at 5000 rpm and 241 kPa was less than one third of the measured flow factor of a straight four-tooth labyrinth seal and less than one half of the measured flow factor of a contacting brush seal at static conditions.**
- **4. Rotation is required to properly seat the seal and results in lower flow factors.**
- **5. Non-contacting finger seal power loss is the same order of magnitude as brush and finger seals.**

Preliminary Test Results of a Non-Contacting Finger Seal on a Herringbone-Grooved Rotor
Margaret P. Proctor and Irebert R. Delgado
Glenn Research Center, Cleveland, Ohio
NASA/TM—2008-215475
AIAA–2008–4506

8.504” Diam. Rotor
185 ft/s Test

Alternative Sealing Techniques: Face Seals

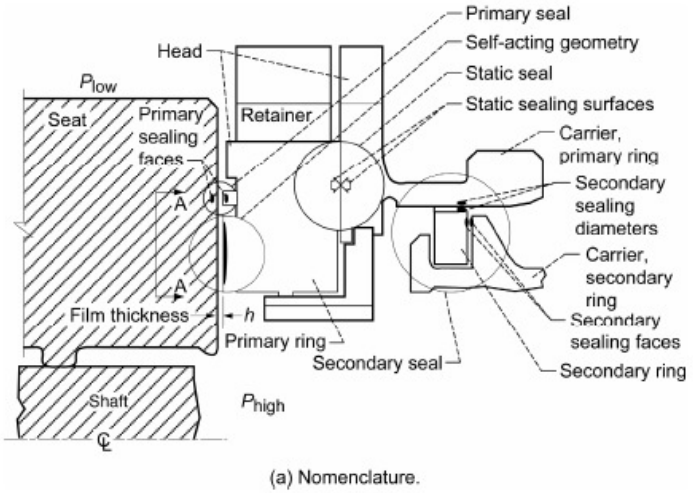

Figure 46.—Component schematic Rayleigh pad self-acting face seal.[109]

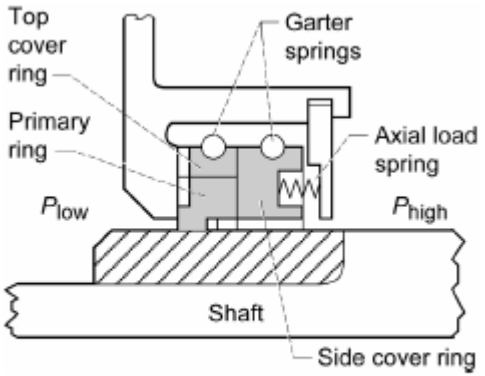

Figure 42.—Shaft riding or circumferential contact seal.[104]

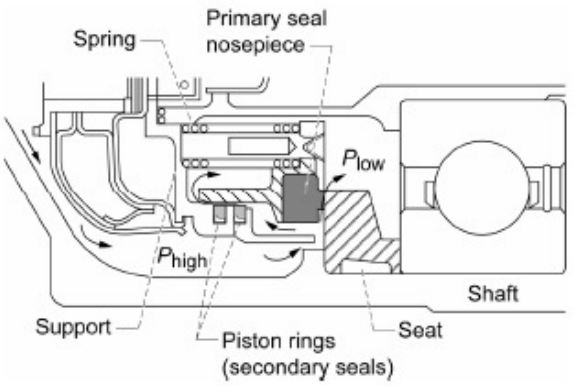

Figure 43.—Positive contact face seal.[106]

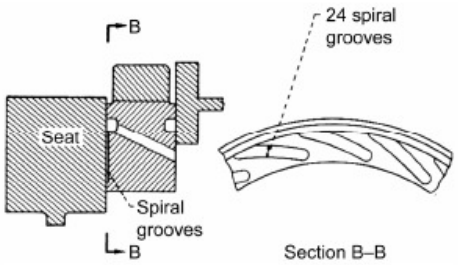

Figure 47.—Spiral groove sealing schematic.[109]

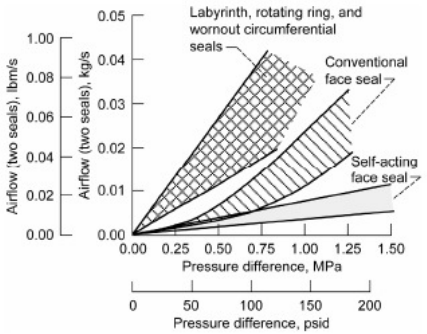

Figure 48.—Comparison of leakage characteristics for labyrinth, conventional (contact) face seal and self-acting face seals.[109]

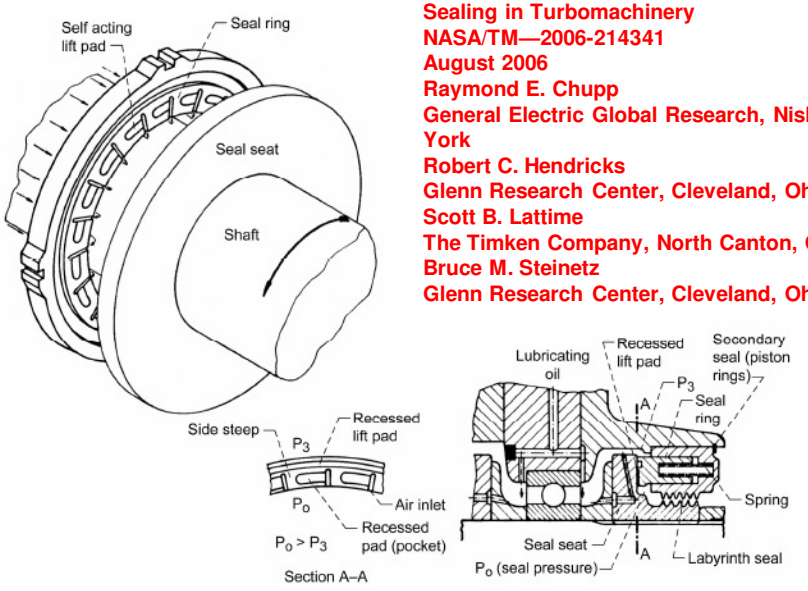

Figure 45.—Self-acting face seal with labyrinth seal presealing.[110]

Sealing in Turbomachinery
NASA/TM—2006-214341
August 2006
Raymond E. Chupp
General Electric Global Research, Niskayuna, New York
Robert C. Hendricks
Glenn Research Center, Cleveland, Ohio
Scott B. Lattime
The Timken Company, North Canton, Ohio
Bruce M. Steinetz
Glenn Research Center, Cleveland, Ohio

Alternative Sealing Techniques: Foil Seals

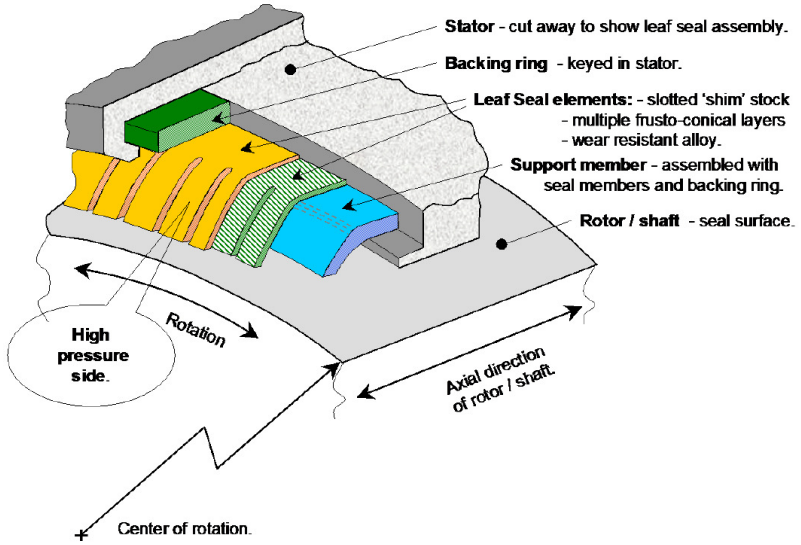

Figure 1. Pressure Actuated Leaf Seal Assembly.

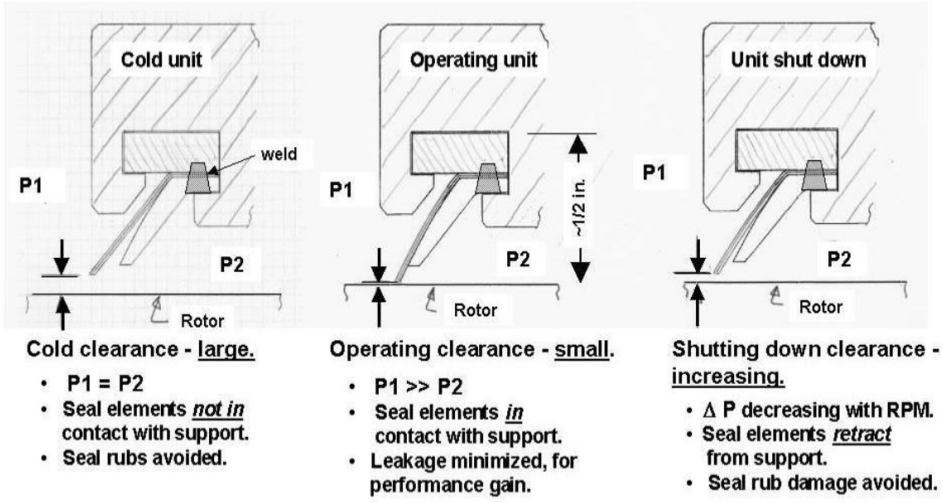

Figure 2. Pressure Actuated Leaf Seal Functional Characteristics.

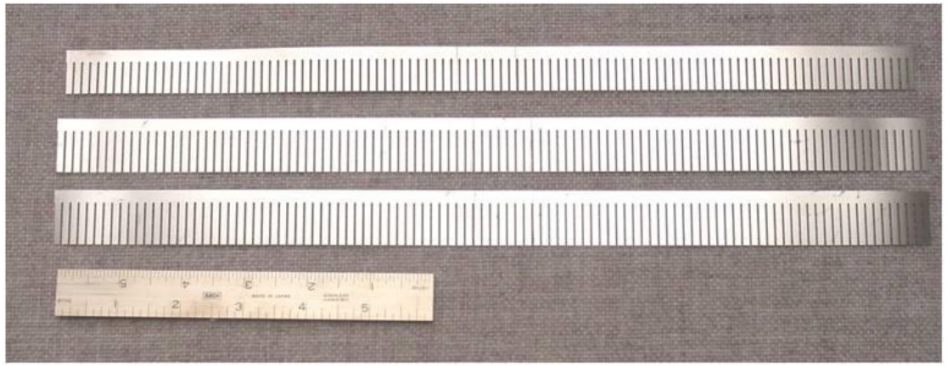

Figure 11. 3-D Strip Cut Seal Leaves.

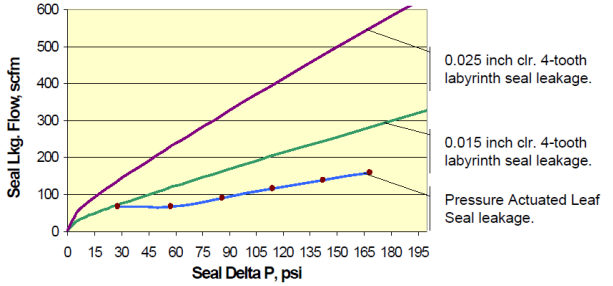

Figure3. Pressure Actuated Leaf Seal Leakage Compared.

Pressure Actuated Leaf Seal Feasibility Study and Demonstration, Clayton Grondahl, CMG Tech, LLC, AIAA 2009-5167

Alternative Sealing Techniques: Leaf Seals

Such seals are low leakage fluid film devices that are capable of operating at high surface velocities and temperature and pressure loadings limited by the foil materials used in the construction, for example, 365 m/s (1200 fps) and 600 ℃ (1100 ℉).

Pressure Actuated Leaf Seal Feasibility Study and Demonstration, Clayton Grondahl, CMG Tech, LLC, AIAA 2009-5167

- **Foil Seals Have High Temp and High Surface Speed Capability**

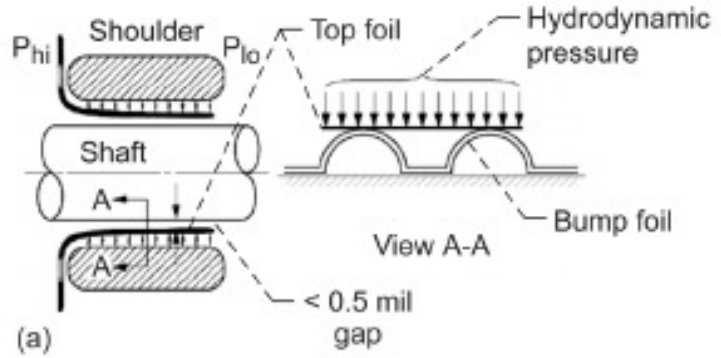

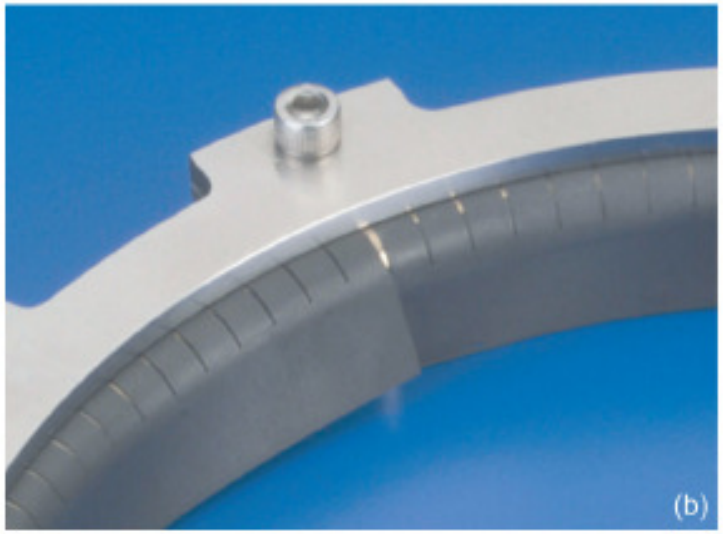

Figure 69.—Foil seal (a) schematic illustrating foil and bump-foil support [162, 163] (b) foil seal "Nozzle-inlet or L-shaped" interface at attached and free end.

Alternative Sealing Techniques: Leaf and Wafer Seals

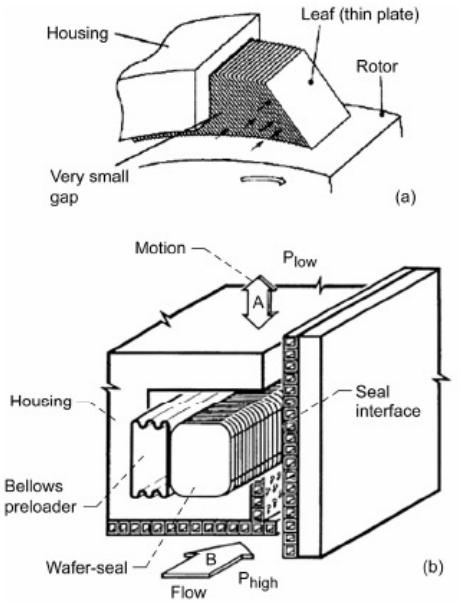

Figure 57.—Basic elements of leaf and wafer seals. (a) Leaf-seal.[137] (b) Wafer-seal.[139]

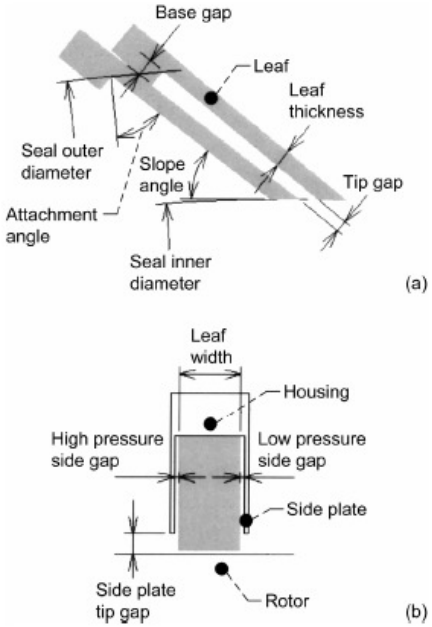

Figure 58.—Leaf seal configuration parameters. (a) Front view. (b) Side view.[138]

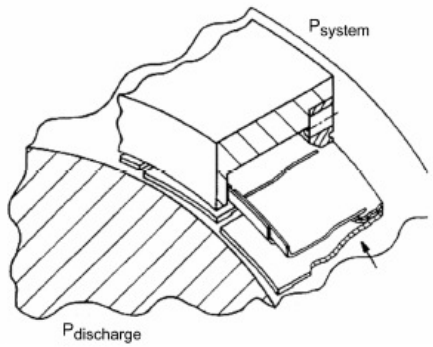

Figure 59.—Pressure balanced compliant film riding leaf-seal.[140]

Sealing in Turbomachinery
NASA/TM—2006-214341
August 2006
Raymond E. Chupp
General Electric Global Research, Niskayuna, New York
Robert C. Hendricks
Glenn Research Center, Cleveland, Ohio
Scott B. Lattime
The Timken Company, North Canton, Ohio
Bruce M. Steinetz
Glenn Research Center, Cleveland, Ohio

① Straight tooth labyrinth seal
2.751 diam., .125 pitch, 20 teeth,
.006 in. radial clearance

② Labyrinth seal, Teledyne
experimental data
30 000 rpm, 600 °F estimated
operating clearance – .006 in.

③ EG and G experimental brush seal
Surface speed – 900 ft/sec, 420°F

④ EG and G experimental "Triple-ply"
seal 45 fingers, 4 760 diam., 10 000 rpm

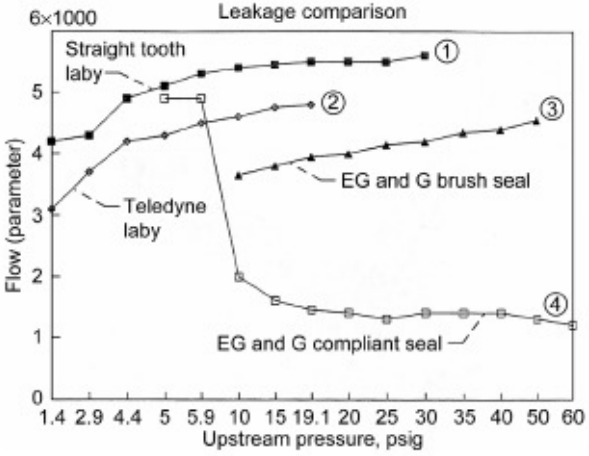

Figure 60.—Leaf-seal leakage comparison with labyrinth and brush seals.[140]

Alternative Sealing Techniques: Leaf and Wafer Seals (con't)

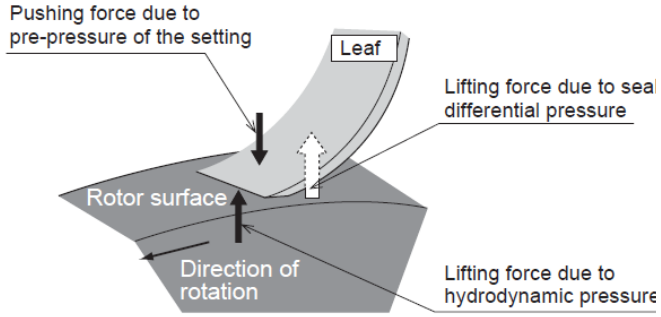

Fig. 7 Mechanism of leaf seal operation
The tip of the leaf is lifted-up by a balance of the pushing force due to pre-pressure of the setting, lifting force due to hydrodynamic pressure generated during rotation of the rotor, and lifting force due to the differential pressure of the seal.

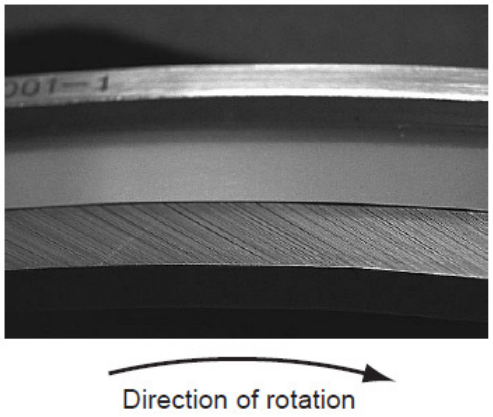

Fig. 6 Structure of leaf seal

Development of New
High Efficiency Steam Turbine
EIICHIRO WATANABE, YOSHINORI TANAKA,
TAKASHI NAKANO, HIROHARU OHYAMA,
KEIZO TANAKA, TOSHIHIRO MIYAWAKI,
MASANORI TSUTSUMI, TANEHIRO SHINOHARA
Mitsubishi Heavy Industries, Ltd.
Technical Review Vol.40 No.4 (Aug. 2003)

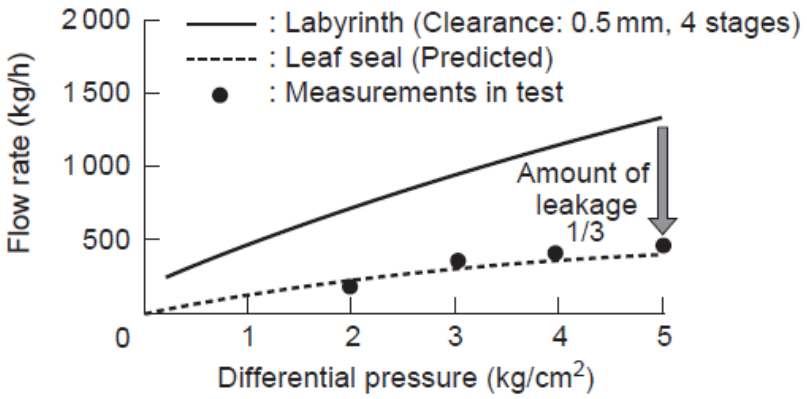

This seal consists of a number of thin metal plate (leaf) inclined in the circumferential direction so that the tip of the seal is kept in a non-contact state with negligibly small clearance when the rotor is rotating. This is done by a lifting force produced due to a hydrodynamic pressure effect acting between the tip of the leaf and the rotor. The result is that both the seal and rotor are prevented from wear and the durability of the seal is increased when the turbine is running, different from contact type seals such as brush seals. In addition, since the seal itself is in the shape of plate with axial width, it has a higher rigidity in the direction of the pressure difference and the sealing function can be kept up to a higher differential pressure compared with brush seals.

Alternative Sealing Techniques: Hybrid Seals

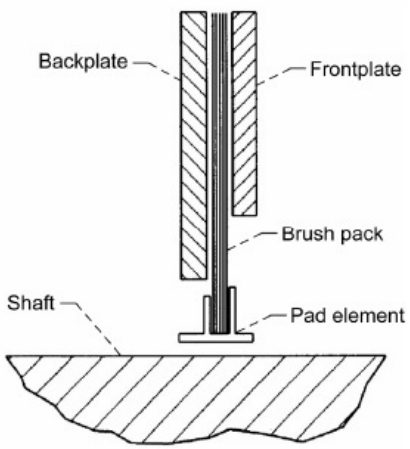

Figure 61.—Illustration of hydrodynamic brush seal (pad elements attached to bristles).[141]

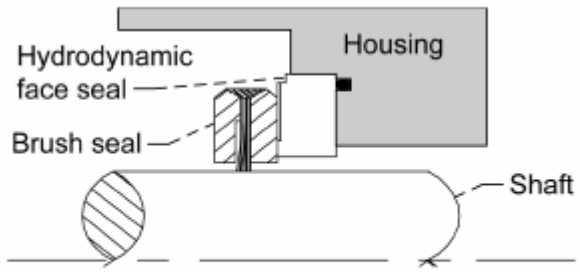

Figure 64.—The Hybrid Floating Brush Seal (HFBS).[146]

NASA/TM—2006-214341

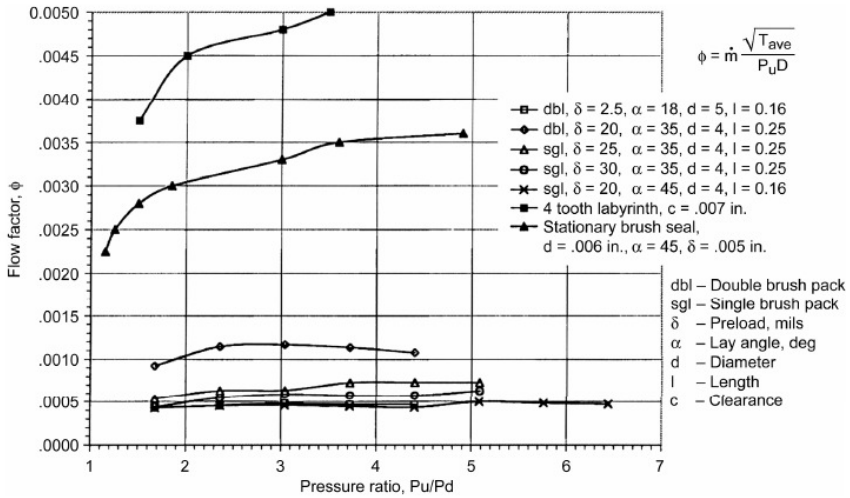

Figure 65.—HFBS performance compared to a stationary brush seal and a labyrinth seal. [$\dot{m}$ is the mass flow rate of air (pps), T_{ave} is the average upstream air temperature (°R), P_u is the average upstream air pressure (psia), D is the shaft outer diameter (in)].[146]

- **4 Tooth Lab Seal Has Substantially More Leakage Than Brush Seal**

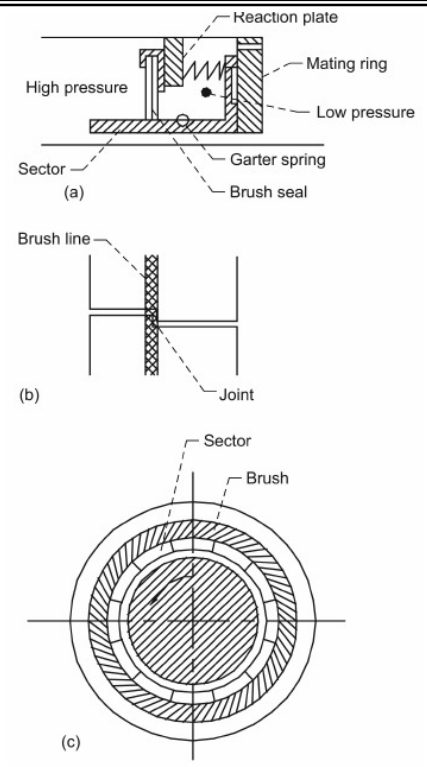

Figure 63.—Schematic of film riding brush seal. (a) Assembly. (b) Joint. (c) Installed.[143]

Figure 62.—Hydrodynamic brush seal (spring beam elements).[142]

Comparative Seal Performance & Capabilities

$$\phi = \frac{\dot{m}\sqrt{T_{avg}}}{P_u \times D_{seal}}, \mathrm{kg} - \sqrt{\mathrm{K}} / \mathrm{MPa} - \mathrm{m} - \mathrm{s}$$

The flow factor can be used to compare the leakage performance of seals with different diameters and with different operating conditions.

NASA/TM—2006-214420
Continued Investigation of Leakage and Power Loss Test Results for Competing Turbine Engine Seals
Irebert R. Delgado
Margaret P. Proctor

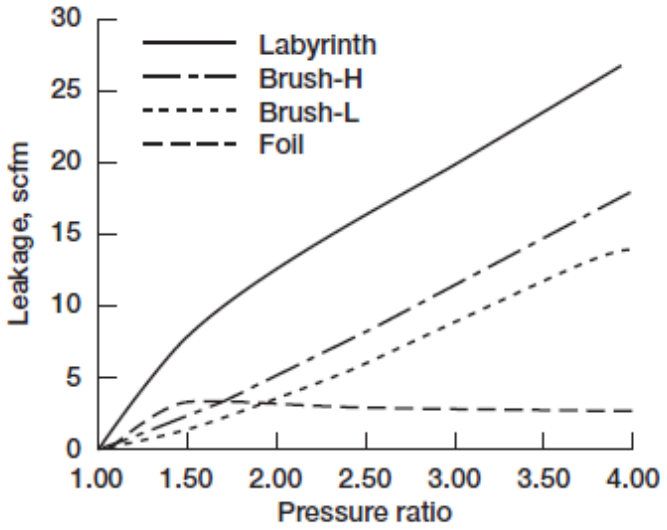

Figure 35.—Seal leakage comparison. (Munson et al., 2002.) Courtesy Rolls-Royce/Allison.

NASA/TM—2004-211991/PART1

- **Seal Performance/Design Metrics**
  - Leakage (absolute or using flow factor)
  - Power Loss
  - Pressure Ratio and Surface Speed Capability
  - Geometry Requirements: Space, Radial vs. Face
  - Radial Excursion Capability

Comparative Seal Performance & Capabilities

Leakage and seal power loss test data for annular and 4-knife labyrinth seals were obtained at various temperatures (297, 533, 700, 811, 922 K), seal pressure differentials (69, 138, 276, 345 kPa), and surface speeds (113, 183, 274 m/s) at NASA Glenn Research Center's High Temperature Turbine Seal Test Rig. The data were compared to previous brush and finger seal test results. The following conclusions are given for the seals tested:

- Seal leakage decreases with increasing surface speed due to reduced clearances from disk centrifugal growth.
- **Annular and labyrinth seal leakage is 2 to 3 times that of brush and finger seals.**
- Seal leakage rates increased with increasing temperature because of seal clearance growth due to different coefficients of thermal expansion between the seal and test disk.
- **Seal power loss is not strongly affected by inlet temperature.**
- **Seal power loss increases with increasing surface speed, seal pressure differential, mass flow rate or flow factor, and radial clearance.**
- **The brush and finger seals had nearly the same power loss.**
- **Annular and labyrinth seal power losses were higher than those of finger or brush seals. The brush seal power loss was the lowest and was 15 to 30 percent lower than annular and labyrinth seal power loss.**

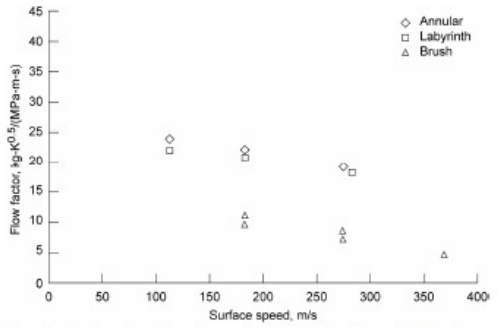

Figure 8.—Leakage flow factor for annular, 4-knife labyrinth and brush seals as a function of speed. Inlet air temperature = 297 K; Seal pressure differential = 276 kPa.

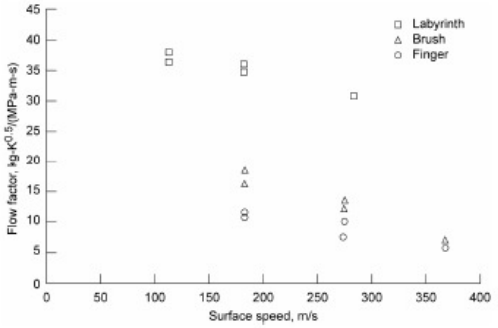

Figure 9.—Leakage flow factor for 4-knife labyrinth, brush, and finger seals as a function of speed. Inlet air temperature = 922 K; Seal pressure differential = 276 kPa.

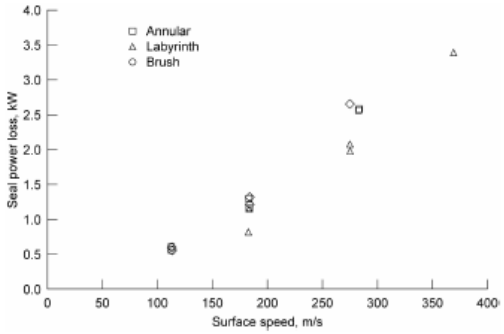

Figure 10.—Seal power loss for annular, 4-knife labyrinth and brush seals as a function of speed. Inlet air temperature = 297 K; Seal pressure differential = 276 kPa.

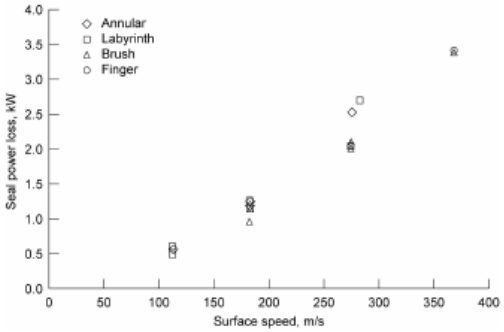

Figure 11.—Seal power loss for annular, 4-knife labyrinth, brush, and finger seals as a function of speed. Inlet air temperature = 700 K; Seal pressure differential = 276 kPa.

NASA/TM—2006-214420
Continued Investigation of Leakage and Power Loss Test Results for Competing Turbine Engine Seals
Irebert R. Delgado
Margaret P. Proctor

- **Brush and Finger Seals Have Substantially Lower Leakage Rate AND Lower Power Loss As Labyrinth Seals**

Some Final Seal Recommendations

- **Put The Seal Features On The Static Structure and Make The Rotor Shroud As Smooth A Surface As Possible**
  - Make the static structure the consumable/adjustable/replaceable part, not the rotor
- **Do Not Use Labyrinth Seals For The Shroud**
  - Need Better Sealing Capability Than They Can Produce
  - The Lowest Radius Lab Seal Basically Sets The Leakage Flow
  - Need Better Leakage Than Just 1 Lab Tooth Can Give Between Bleed Cavities
- **There Seems To Be A Variety of Advanced Seals That Can Probably Do Much Much Better Than (A) Labyrinth Seal(s)**
  - But They Will Require Much More Work To Design And Implement
- **Install Swirl Brakes Just Upstream of Seals**
  - Already in Conceptual Design
  - Swirl Brakes Need To Be Designed To Be Effective
  - Need Rotordynamic Coefficients of Seal For Input To Rotordynamics Calculations
- **Install Lab Seals On The Hub To Reduce Flow Into The Wheel Spaces**

People To Potentially Contact For Advice & Design

- **Seal Experts**
  - Bob Hendricks – NASA Glenn
  - Margaret Proctor – NASA Glenn
  - Irebert R. Delgado – NASA Glenn/U.S. Army Research Laboratory
  - Bruce M. Steinetz – NASA Glenn
  - A. Muszynska: A.M. Consulting, Minden, Nevada
  - Dresser-Rand for Seals And Swirl Brakes
  - Various University Professors:
    - *DW Childs Texas A&M*

- **Secondary Flow Design/Simulation**
  - Paul Vitt – ASE Technologies